

**Design, Synthesis and Biological
Evaluation of Small-Molecules
Targeting the Mdmx-p53 Interaction
and the Atad2 Bromodomain for
Cancer Therapy**

This thesis is submitted to Newcastle University for the degree of
Doctor of Philosophy

Santosh Adhikari

Northern Institute for Cancer Research

April 2016

Declaration

The work described in this thesis was carried out between September 2012 and November 2015 in the Northern Institute for Cancer Research Medicinal Chemistry Laboratories (Bedson Building, School of Chemistry, Newcastle University, Newcastle upon Tyne, UK, NE1 7RU) and in the Cancer Structural Biology Laboratories (Paul O’Gorman Building, Northern Institute for Cancer Research, Newcastle University, Newcastle upon Tyne, UK, NE2 4HH).

All the research described in this thesis is original and does not incorporate any material or ideas previously published or presented by other authors, except where acknowledged by references.

No part of this thesis is being, or has been previously, submitted for a degree, diploma or any qualification at any other university.

Acknowledgement

I would like to express my heartfelt gratitude to the late Professor Roger Griffin for his invaluable guidance and support. He was an exceptional medicinal chemist and a great human being, and it was a pleasure to be his student. I am forever indebted to my supervisor Dr Céline Cano for her constant belief in me, I could not have asked for a better supervisor. A special thank you must also go to Professor Bernard Golding and Dr Ian Hardcastle for their expertise and support throughout my PhD. Sincere thanks to Professor Herbie Newell for his encouragement and his infectious passion for drug discovery.

I would like to thank everyone at the NICR Medicinal Chemistry Laboratories, past and present; Mohammad Alyasiri, Dr Annalisa Bertoli, Dr Tim Blackburn, Dr Benoit Carbain, Dr Daniela Cortese, Dr Elena Costa, Dr Sarah Cully, Dr Stephen Hobson, Dr Lauren Molyneux, Dr Stephanie Myers, Dr Andrew Shouksmith, Dr Judith Unterlass and Dr Claire Wilson. Special acknowledgement goes to Dr Ruth Bawn and Dr Suzannah Harnor for helping me to develop practical organic chemistry skills during my first year. Special thanks to Dr Duncan Miller for teaching me the principles of medicinal chemistry. I also wish to thank Dr Karen Haggerty and Carlo Bawn for their technical support in the lab. Thanks to the members of “Tuesday Club”; Dr Bian Zhang, Dr Nick C Martin, James Pickles, Dr Tristan Reuillon, Dr Honorine Lebraud and Amy Heptinstall for creating a great environment in the lab and outside, you were the best colleagues one could wish for.

I also wish to thank all the members of NICR structural Biology team. Firstly, I would like to express my gratitude to Professor Jane Endicott and Professor Martin Noble for their supervision during my structural biology placement. Thanks to everyone working within their group for all the help and time, especially Dr Claire Jennings and Dr Judith Reeks for their patience, and teaching me fundamentals of structural biology. Thanks also to Dr Arnaud Basle, Dr Martin Day, Stephen Hallett, Dr Richard Heath, Svitlana Korolchuk, Dr Mathew Martin, Dr Bailey Massa, Dr Martyna Pastok and Dr Julie Tucker. I would also like to thank Dr Yan Zhao for running assays in the MDMX project.

There are many people outside of the lab who have made my time in Newcastle a pleasure; Steve Addison, Dr Arman Esfandiari, Hetansh Gala, Aishwarya Jay, Vivek Juthani, Federica Nicolini, Pratik Singh Parmar, Praveen Selvam, Shubhankar Sharma, Denise Sighel and Achint Soni. A special thanks to the members of “Lemon and Tequila”; Dr Daniela Cortese, Guillaume Derycke, Fran Luquin, Dr Nick C Martin, Dr Regina Mora and Monique Zangarini.

I am very thankful to my cousins Maina Adhikari, Naran Adhikari, “bhinaju” Tri Tuladhar, aunt Goma Neupane and uncle Kiran Neupane for being my local guardian in the UK and helping me in my difficult times.

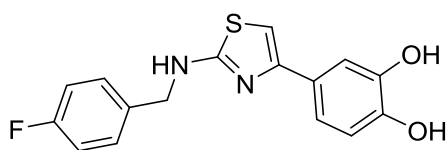
Biggest thanks in the world to my mum, dad, my sisters Sailu and Sofiya, and my wife Rakshya for their constant support and belief in me. This PhD would not have been possible without the encouragement and support I received from my family. I love you all.

I would like to dedicate this thesis to my parents Chhabilal Adhikari and Kamala Adhikari.

Abstract

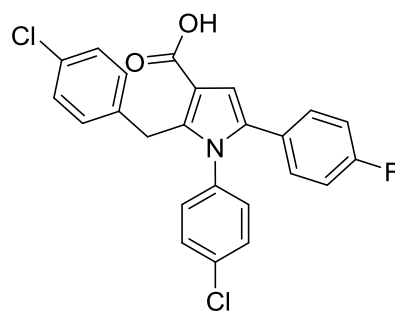
In this thesis small molecule inhibitors of MDMX-p53 interaction, and ATAD2 bromodomain are investigated.

In many human cancers, the function of the tumour suppressor protein p53 is inhibited by the overexpression of MDM2 or MDMX. Modulation of MDM2-p53 and MDMX-p53 interactions is therefore an attractive strategy for anticancer drug discovery. A number of small molecule inhibitors of the MDM2-p53 interaction have been reported to date and several have entered clinical trials. Although MDM2 and MDMX have a high sequence homology, most of the small molecule MDM2 inhibitors show significantly lower binding affinity towards MDMX. A series of 2,4-aminothiazoles including compound **1** with modest inhibitory activity against the MDM2-p53 and MDMX-p53 interactions has been reported. The series was extended to a pyrrole series, which led to the discovery of compound **2** with low micromolar dual inhibition of MDM2/MDMX and structure-activity relationship studies were conducted.



1

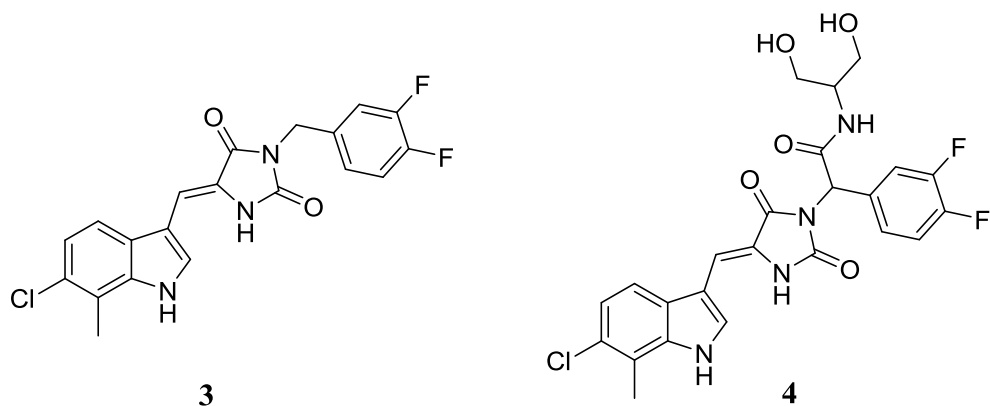
MDM2 IC₅₀ = 12 ± 9 μM
MDMX IC₅₀ = 24 ± 18 μM



2

MDM2 IC₅₀ = 11 ± 3 μM
MDMX IC₅₀ = 14 ± 3 μM

An ELISA was used to examine potency against MDM2-p53 and MDMX-p53. Although, the assay gave results in agreement with literature values for some inhibitors of the MDM2-p53 interaction, the potencies of the published dual inhibitors RO-2443 **3** and RO-5963 **4** were around 1000-fold lower than reported. Therefore, an HTRF assay was developed, which provided IC₅₀ values comparable to the reported values for inhibition of MDM2-p53 and MDMX-p53 by RO-5963. Co-crystallisation experiments, using three different constructs of MDMX, were attempted using 15 compounds.



Bromodomains are protein modules that function as epigenetic readers of histone lysine acetylation. ATAD2, a bromodomain containing protein, is overexpressed in a wide range of human cancers including breast, lung, prostate, ovarian, liver, osteosarcoma and gastrointestinal carcinomas. Due to the polar and flexible nature of the binding surface, ATAD2 has been considered as a challenging target for ligand discovery. Therefore, very few potent and selective inhibitors of ATAD2 bromodomains have been reported to date.

Extensive SAR studies around hit **5** obtained from a fragment screening led to the identification of a sub-millimolar inhibitor **6** of ATAD2 bromodomain. Co-crystal structures of ATAD2 were used to guide compound design and synthesis.

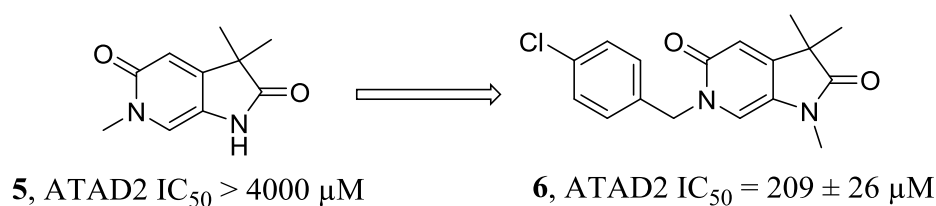


Table of Contents

Chapter 1. Introduction	1
1.1 Cancer	1
1.2 Cancer Chemotherapy.....	2
1.3 Protein-Protein Interaction.....	3
1.4 Stages of Drug Discovery	6
Chapter 2. Introduction to MDMX and Reported Inhibitors	8
2.1 p53, MDM2, and MDMX.....	8
2.1.1 Cell Cycle Arrest Mediated by p53	8
2.1.2 Apoptosis Mediated by p53	9
2.1.3 The Structure of p53 Protein	10
2.2 MDM2	11
2.3 MDMX and its Role in Cancer	12
2.4 Structure of MDMX: Comparison with MDM2.....	14
2.5 Reported Inhibitors of the MDMX-p53 Interaction	16
2.5.1 Peptides and Stapled Peptides	16
2.5.2 SJ-172550	18
2.5.3 Imidazole-Indoles	19
2.5.4 Pyrrolidones.....	20
2.5.5 Indolyhydantoins	21
2.5.6 Nutlin-3a Derivative	22
2.5.7 Pyrroles.....	23
2.6 MDMX Project Aim	24
Chapter 3. Development of Inhibitors of MDMX-p53 Interaction.....	25
3.1 Rationale	25
3.2 Synthesis of 1,2,5-trisubstituted pyrroles	28
3.3 Biological Evaluation	32
Chapter 4. Introduction of Water Solubilising Group.....	34

4.1	Rationale.....	34
4.2	Synthesis.....	34
4.3	Biological Evaluation	37
Chapter 5.	SAR Studies around Compound 2	38
5.1	Rationale.....	38
5.2	Synthesis.....	39
5.2.1	Synthesis of Tetra-Substituted and Penta-Substituted Pyrroles.....	39
5.2.2	Synthesis of pyrroles with succinimide ring at the 3/4-position.....	44
5.2.3	One-Carbon Homologation of 3-Carboxylic Acid.....	46
5.3	Biological Evaluation	48
Chapter 6.	SAR Studies around the Phenyl Rings at 2 and 5-Positions.....	50
6.1	Rationale.....	50
6.2	Synthesis.....	52
6.3	Biological Evaluation	54
Chapter 7.	Synthesis and Biological Evaluation of RO-2443 3 and RO-5963 4	55
7.1	Rationale.....	55
7.2	Synthesis.....	55
7.2.1	Synthesis of RO-2443 3	55
7.2.2	X-ray structure of RO-2443 3	58
7.2.3	Synthesis of RO-5963 4	59
7.3	Biological Evaluation	62
Chapter 8.	MDM2 and MDMX Structural Biology	63
8.1	Aims	63
8.2	Expression and Purification of MDM2 and MDMX.....	65
8.3	Co-Crystallisation of MDM2 and MDMX with Pyrrole Inhibitors	68
8.4	Co-Crystallisation of MDM2 and MDMX with Autoinhibitory domains	71
8.5	Development of Homogenous Time-Resolved FRET assay.....	73
Chapter 9.	Introduction to ATAD2 and Reported Small-Molecule Inhibitors.....	88

9.1	Introduction to Epigenetics	88
9.1.1	Chromatin Architecture	88
9.1.2	Post-Translational Modifications of Histones	89
9.2	Bromodomains	91
9.3	Bromodomain Inhibitors	93
9.3.1	BET-Bromodomain Inhibitors	93
9.3.2	Non-BET bromodomain Inhibitors	95
9.4	ATAD2 and its Role in Cancer	96
9.5	Structure and Druggability of ATAD2 Bromodomain	98
9.6	Reported ATAD2 Bromodomain Inhibitors	102
9.6.1	Fragments Targeting ATAD2 Bromodomains	102
9.6.2	Naphthyridone Series	106
Chapter 10.	Development of ATAD2 Inhibitors: SAR strategies	110
10.1	Fragment hits	110
10.2	Preliminary SARs around Fragment 157 , 158 and 160	112
10.2.1	Rationale	112
10.2.2	Synthesis	114
10.2.3	Biological Evaluation	117
Chapter 11.	SAR Studies around the N^1 -Position of Fragment 5	119
11.1	Rationale	119
11.2	Synthesis	120
11.3	Biological Evaluation	123
Chapter 12.	SAR Studies around the N^6 -Position of Fragment 5	125
12.1	Rationale	125
12.2	Synthesis	128
12.3	SAR and Biological Evaluation	130
Chapter 13.	Accessing the Region Occupied by Acetylated Histone	135
13.1	Rationale	135

13.2	Synthesis	136
13.2.1	Mono-alkylation at the 3-Position.....	136
13.2.2	Variation at the 3-Position using Knoevenagel Condensation.....	138
13.3	Biological Evaluation	140
Chapter 14.	Accessing the Bidentate Interaction with Asn1064	143
14.1	Rationale	143
14.2	Synthesis of Compound 252	144
14.3	Synthesis of Compound 253	147
14.4	Biological Evaluation	152
14.5	Investigation of Scaffold Hopping Approach.....	154
14.5.1	Synthesis of Compound 277	155
14.5.2	Biological Evaluation.....	156
14.6	Introduction of a H-bond Donor Heterocycle at 3-Position	159
14.6.1	Synthesis	160
14.6.2	Biological Evaluation.....	163
Chapter 15.	Conclusion and Future Directions	165
15.1	MDMX	165
15.2	ATAD2	166
Chapter 16.	Experimental	169
16.1	Summary of Generic Reactions, Analytical and Chromatographic Conditions..	169
16.1.1	Solvents and Reagents	169
16.1.2	Chromatography.....	169
16.1.3	Microwave Reactions.....	169
16.1.4	Analytical Techniques.....	169
16.2	Synthesis of MDMX Inhibitors-Experimental Procedures.....	170
16.2.1	MDMX Biology Procedures	170
16.2.2	Synthesis of MDMX Inhibitors: General Procedures	171
16.2.3	MDMX Inhibitors: Synthetic Procedures	175

16.2.4	Synthesis of RO-2443 (3) and RO-5963 (4).....	208
16.3	MDMX Structural biology experimental	216
16.3.1	General procedures	216
16.3.2	Expression from MDMX and MDM2 gene constructs	217
16.3.3	Protein purification	218
16.3.4	Protein preparation for crystallography	219
16.3.5	HTRF assay	219
16.4	Synthesis of ATAD2 Inhibitors-Experimental Procedures	221
16.4.1	ATAD2 Biology Procedures	221
16.4.2	Synthesis of ATAD2 Inhibitors: General Procedures	222
16.4.3	ATAD2 Inhibitors: Synthetic Procedures	223

ABBREVIATIONS

ANCAA	AAA nuclear co-regulator cancer-associated protein
AID	Auto-inhibitory domain
BET	Bromodomain and extra-terminal
CML	Chronic myelogenous leukaemia
DCM	Dichloromethane
DIBAL	Diisobutylaluminium hydride
DIC	<i>N,N'</i> -Diisopropylcarbodiimide
DMAP	4-Dimethylaminopyridine
DME	1,2-Dimethoxyethane
DMF	Dimethylformamide
DMP	Dess-Martin periodinane
DMSO	Dimethyl sulfoxide
DTT	Dithiothreitol
EDC	1-Ethyl-3-(3-dimethylaminopropyl)carbodiimide
ELISA	Enzyme linked immunosorbent assay
ELSD	Evaporative light scattering detector
ER	Estrogen receptor
(ES+)	Electrospray positive mode
(ES-)	Electrospray negative mode
EtOH	Ethanol
eq.	Number of molar equivalents
FDA	Food and drug administration

FRET	Fluorescence resonance energy transfer
FTIR	Fourier transform infrared
GIST	Gastrointestinal stromal tumour
GST	Glutathione S-transferase
HATU	1-[Bis(dimethylamino)methylene]-1H-1,2,3-triazolo[4,5-b]pyridinium 3-oxid hexafluorophosphate
HAT	Histone-acetyltransferase
HDAC	Histone deacetylase
HEPES	<i>N</i> -2-Hydroxyethylpiperazine- <i>N'</i> -2-ethanesulfonic acid
HPLC	High performance liquid chromatography
HRMS	High-resolution mass spectrometry
HTRF	Homogenous time-resolved FRET
HTS	High-throughput screening
IPTG	Isopropyl β -D-1-thiogalactopyranoside
Kac	Acetyllysine
KHMDS	Potassium bis(trimethylsilyl)amide
LC-MS	Liquid chromatography-mass spectrometry
LE	Ligand efficiency
LHMDS	Lithium bis(trimethylsilyl)amide
μ W	Microwave
MDM2	Murine double minute 2
MDMX	Murine double minute X
MeCN	Acetonitrile
MeOH	Methanol

mHBS	Modified HEPES-buffered saline
MOE®	Molecular operating environment
MPLC	Medium pressure liquid chromatography
m.p.	Melting point
MS	Mass spectrometry
NOE	Nuclear overhauser effect
NUT	Nuclear protein in Testis
LB	Luria-Bertani broth
PCC	Pyridinium chlorochromate
PEG	Polyethylene glycol
PDGFR	Platelet derived growth factor receptor
PTM	Post-translational modification
quant.	Quantitative
N/A	Not available
NaHMDS	Sodium bis(trimethylsilyl)amide
NES	Nuclear export sequence
NLS	Nuclear localization signal
PCNA	Proliferating cell nuclear antigen
PPI	Protein-protein interaction
RING	Really interesting new gene
Rb	Retinoblastoma
RT	Room temperature
Rt	Retention time (HPLC)

SAM	S-adenosylmethionine
SAR	Structure-activity relationship
SDS-PAGE	Dodecyl sulphate polyacrylamide gel electrophoresis
SEM	2-Trimethylsilylethoxymethyl
TAD	Transactivation domain
TB	Terrific broth
TBS	Tert-butyldimethylsilyl
THF	Tetrahydrofuran
TLC	Thin Layer Chromatography
TMSCN	Trimethylsilyl cyanide
TR-FRET	Time-resolved fluorescence resonance energy transfer
ν_{\max}	Maximum vibrational frequency
v/v	Volume for volume

Chapter 1. Introduction

1.1 Cancer

Cancer is a genetic disease caused by alterations in the genome such as point mutations, deletions, duplications, chromosome rearrangements and epigenetic changes.² The number of genetic alterations in a cancer can vary from tens to thousands.¹ A large number of mutations are known as ‘passengers’ that do not confer any growth advantage. The mutations that contribute to cancer development are known as ‘drivers’.^{1,3} A vast amount of research on the identification of ‘drivers’ has led to the discovery of various oncogenes and tumour suppressor genes.⁴ Oncogenes are dominant cancer genes that require only one of the two parental alleles present in the normal cell to be mutated, resulting in the activation of the encoded protein.⁵ Tumour suppressor genes are recessive genes that require mutations in both alleles resulting in the inactivation of the encoded protein.⁵

Cancer was first described as an evolutionary process analogous to Darwinian natural selection by Peter Nowell almost forty years ago.⁶ Genetic variations that confer growth advantage lead to the progression of normal cells into cancer cells.^{1, 6} An alternative to the Darwinian evolutionary model is the stem cell model, which proposes that a small population of cancer stem cells, irrespective of their origin, are responsible for cancer growth and progression.⁷⁻⁸ The stem cell model considers that a few sub-populations of cancer cells are tumorigenic, and responsible for cancer growth. The stem cell model and the evolutionary model are not mutually exclusive in cancers that follow stem cell model, in which stem cells can evolve by clonal evolution.⁸ Whereas, in cancers that do not follow stem cell model, the evolutionary model could explain the cancer growth. A better understanding of these models involved in various cancers will help to develop effective treatments.⁸

Cancer research over the past few decades has led to the identification of a large number of phenotypic and genotypic variations involved in cancer. In 2000, Hanahan and Weinberg proposed six hallmarks of cancer that comprised of physiological changes or capabilities acquired during cancer development (Figure 1.1).⁹ In an update in 2011, two new hallmarks were added: the avoidance of immune destruction and the reprogramming of energy metabolism.¹⁰

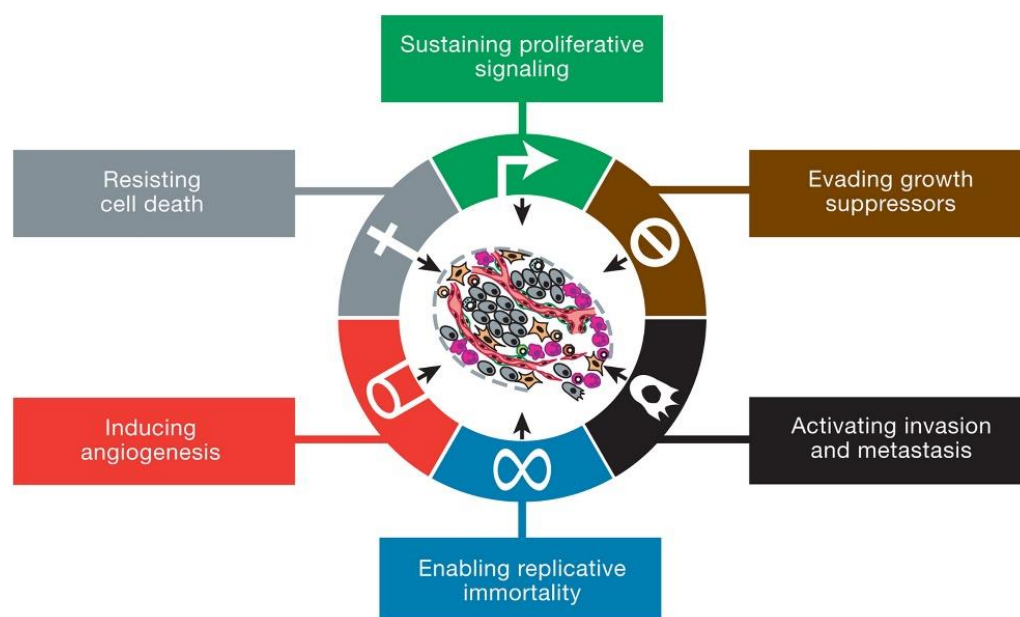
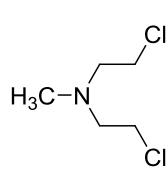


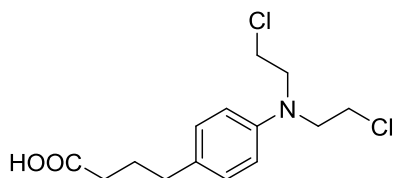
Figure 1.1: Hallmarks of cancer.¹⁰

1.2 Cancer Chemotherapy

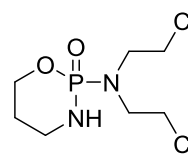
The era of chemotherapy began with the use of nitrogen mustards, including chlormethine **7**, for the treatment of lymphomas.¹¹ These agents act by cross-linking DNA. Several other DNA-alkylating agents were subsequently introduced including chlorambucil **8** and cyclophosphamide **9**.



7

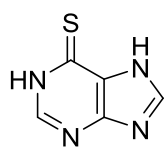


8

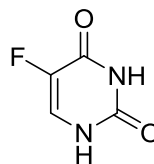


9

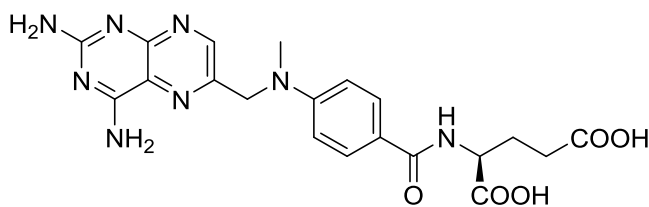
Over the next few decades, several chemotherapeutic agents including antimetabolites: 6-mercaptopurine **10**, 5-fluorouracil **11**, methotrexate **12**; antitumour antibiotics: doxorubicin; and antimitotic agents: *Vinca* alkaloids, taxanes were discovered.¹¹⁻¹² Antimetabolites mimic nitrogenous bases of DNA or other endogenous molecules and inhibit the synthesis of nucleic acids. Anti-mitotic agents act by inhibiting cell division of rapidly dividing cells. Conventional chemotherapy acts on the processes that contribute in the rapid division of cancer cells. However, many normal cells such as hair follicles, stomach epithelia, and bone-marrow cells are also rapidly replicating.¹³ Therefore, conventional chemotherapeutic agents also act on rapidly dividing non-cancerous cells causing serious side effects.



10



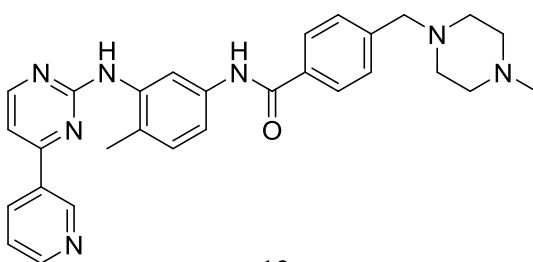
11



12

s

With the increase in the understanding of cancer biology at a molecular level, anti-cancer drug discovery transitioned from classical cytotoxic agents to targeted therapy. The new targets specific to cancer cells such as growth factors, signalling pathways, oncogenes, tumour suppressor genes, cell cycle proteins, apoptosis modulators and angiogenesis promoters were discovered. Imatinib (*Glivec*) **13**, a landmark anticancer drug (based on targeted therapy) is used for the treatment of chronic myeloid leukaemia (CML).¹⁴⁻¹⁵ Imatinib acts by inhibiting Bcr-Abl kinase which is a product of *bcr-abl* gene, formed by the fusion of a segment of the *bcr* gene from chromosome 22 to the part of *c-abl* gene on chromosome 9. Imatinib also inhibits c-KIT kinase and platelet derived growth factor receptor (PDGFR) kinase that are overexpressed in Gastrointestinal Stromal Tumour (GIST).¹⁶ Therefore, Imatinib is also used in the treatment of GIST.



13

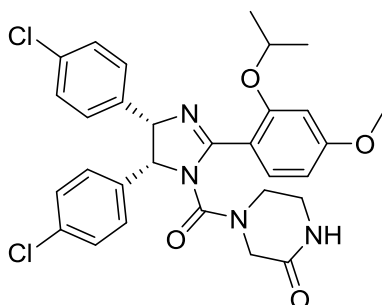
The clinical success of Imatinib was a breakthrough in the field of targeted anticancer therapy. To date, more than 30 small-molecules have been approved, and several are in various stages of clinical trials, as targeted therapy for the treatment of variety of cancers.¹⁷

1.3 Protein-Protein Interaction

Protein-protein interactions play an important role in most biological processes ranging from signal transduction to programmed cell death.¹⁸ Development of small molecules that modulate

protein-protein interactions involved in disease pathways has become an attractive strategy for drug discovery. However, there are several challenges in the discovery of small molecules that inhibit protein-protein interaction.

Protein-protein interfaces are generally flat with large surface areas around $1600 (\pm 400) \text{ \AA}^2$ on each protein.¹⁹ There are numerous interactions including electrostatic, hydrophobic, hydrogen bonds, involved in protein-protein interaction. It is not possible to interfere with all of the interactions using small molecules that typically have a very small surface area ($300\text{-}500 \text{ \AA}^2$) compared to the protein-protein interface.²⁰ Modulation of protein-protein interactions by small molecules can be successful by targeting ‘hot spots’ in the protein-protein interaction.¹⁸ Hot spots are the regions of key interactions at the protein-protein interface that contribute to the large component of the binding affinity. Therefore, even a molecule with a small surface area that can bind at hot spots can inhibit protein-protein interactions. For example, the p53-MDM2 interface area is approximately 1500 \AA^2 , whereas, the MDM2 inhibitor Nutlin 3a **14** has a surface area of approximately 800 \AA^2 .²¹⁻²² It is clear that Nutlin cannot cover the entire surface area; however, it is a strong inhibitor of the MDM2-p53 interaction, which suggests that interfering with all the interactions is not necessary.



Nutlin 3a **14**

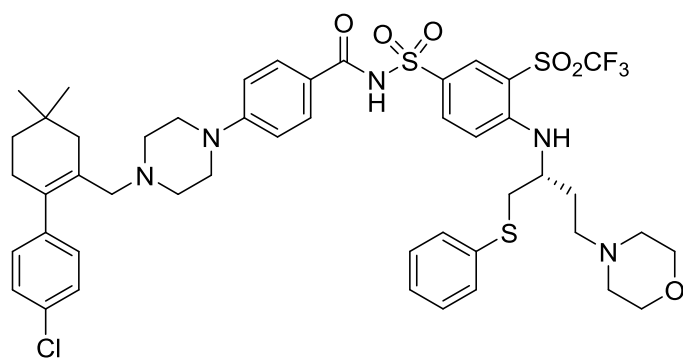
The other important examples of small molecule inhibitors of PPIs are inhibitors of Bcl-2 family proteins. These proteins play a major role in the regulation of apoptosis and are divided into three classes of proteins.²³

- The pro-apoptotic proteins Bax and Bak, which stimulates apoptosis.
- The anti-apoptotic proteins Bcl-2 and Bcl-xL, which inhibit the function of Bax and Bak.
- The BH3 only protein which inhibits Bcl-2 and Bcl-xL.

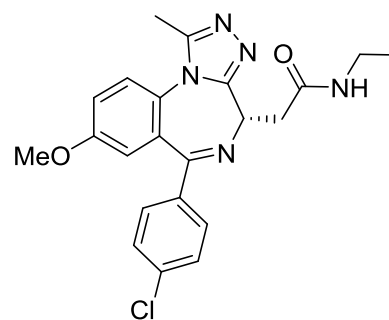
The Bcl-2 and Bcl-xL proteins contain a hydrophobic groove upon which Bax, Bak and BH3 only proteins bind.²⁴⁻²⁵ Bcl-2 and Bcl-xL are upregulated in cancer cells, and therefore, small

molecule inhibitors that can bind on the hydrophobic groove of the Bcl-2 and Bcl-xL proteins can induce apoptosis.^{23, 26}

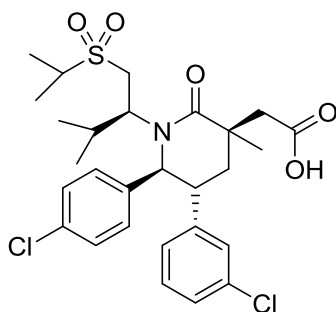
To date, several small molecule inhibitors have been identified for inhibiting protein-protein interactions. Some of the small-molecule PPI inhibitors which are in various stages of clinical development are shown in Figure 1.2.^{20, 27}



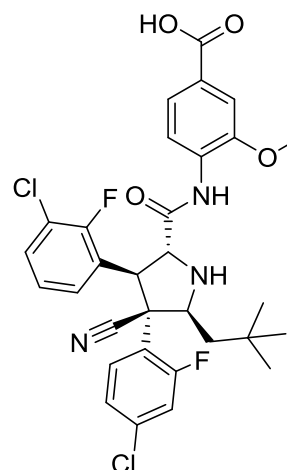
ABT-263 15
Bcl-XL/BAK inhibitor



I-BET762 16
BET bromodomain inhibitor



AMG-232 17
MDM2-p53 inhibitor



RG-7388 18
MDM2-p53 inhibitor

Figure 1.2: Small molecule PPI inhibitors under clinical development.²⁷

Although, binding at hot spots is often sufficient for inhibiting protein-protein interactions, identifying a hot spot is another challenge. Binding sites that could fit small molecules are sometimes not visible in crystal structures due to the flexibility and adaptivity of proteins.¹⁸

The drug leads developed by targeting the protein-protein interfaces often have high molecular weight and are hydrophobic. Inhibition of the protein-protein interaction is not enough for compound to become a drug. Small molecule PPI inhibitors should also possess drug-like

pharmacokinetic and pharmacodynamics properties. Therefore, besides being an attractive area for drug discovery, the development of small molecule inhibitors that can modulate protein-protein interactions has several challenges.

In this thesis, development of small molecules targeting two different protein-protein interactions are discussed: (a) MDMX-p53 interaction; (b) ATAD2-acetylated histone interaction.

1.4 Stages of Drug Discovery

The first stage in the drug discovery process involves the identification of a biological target, whose modulation might affect the disease progression (Figure 1.3). The target is then validated using data collected from bioinformatics, as well as several *in vivo* and *in vitro* experiments including genetically engineered knock-out animals, reducing the amount of target by short interfering siRNA experiments, or the target is modulated by a known small molecule or peptide inhibitor.²⁸⁻³⁰

Once a biological target is validated, a full drug discovery program can be commenced. The first step is the identification of a chemical starting point known as a ‘hit’, which is performed using various techniques like high-throughput screening (HTS), fragment screening, virtual screening, or structure based *de novo* design.³¹⁻³⁴

In the hit to lead phase, structure-activity relationships around the hit are studied in-order to identify the effect of different groups in a molecule on the potency, selectivity and pharmacokinetic properties.³⁴ A lead molecule, which has the potential to be developed as a drug is selected. In the lead optimisation stage, analogues of leads are synthesised by combining all of the desired properties in a molecule to achieve optimum potency, *in-vivo* pharmacokinetics, safety and pharmaceutical properties.³⁴ Then, a candidate is selected for pre-clinical evaluation.

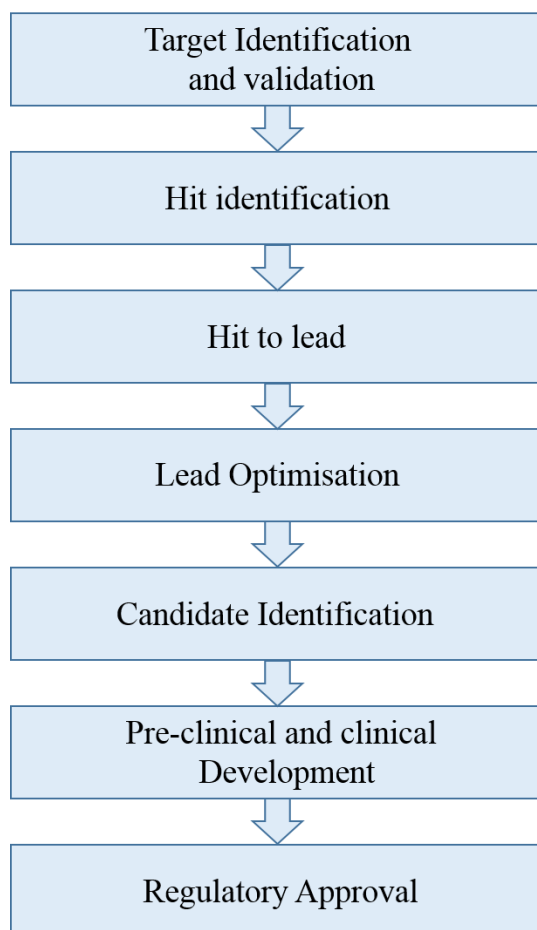


Figure 1.3: Various stages of drug discovery.

The two projects described in this thesis are in the target validation stage. The aim of the medicinal chemistry efforts was to develop chemical tools for use in *in vitro* and *in vivo* experiments to access the effect of inhibition of two protein-protein interactions: (a) MDMX-p53; (b) ATAD2 bromodomain-acetylated histone.

Chapter 2. Introduction to MDMX and Reported Inhibitors

2.1 p53, MDM2, and MDMX

The tumour suppressor gene *p53* is mutated in almost half of all human cancers.³⁵ In cancers with wild-type *p53*, the protein levels of p53 is controlled by its negative regulators, such as MDM2 and MDMX.³⁶ p53 functions as a transcription factor responsible for the regulation of expression of a variety of genes involved in various stages of cell growth and progression.³⁷ p53 is activated by DNA damage, abnormal growth signals, oncogene activation and other cellular stress, including hypoxia and nucleotide depletion (Figure 2.1).³⁷⁻³⁸ Following activation, tetrameric p53 binds to DNA,³⁹ and mediates the transcription of genes that express proteins to accomplish a number of functions including cell cycle arrest, DNA repair, apoptosis and inhibition of angiogenesis.⁴⁰ These responses either reverse potential mutagenic damage by cell cycle arrest and DNA repair, or signal the destruction of the damaged cells by apoptosis.³⁷⁻

38, 40-41

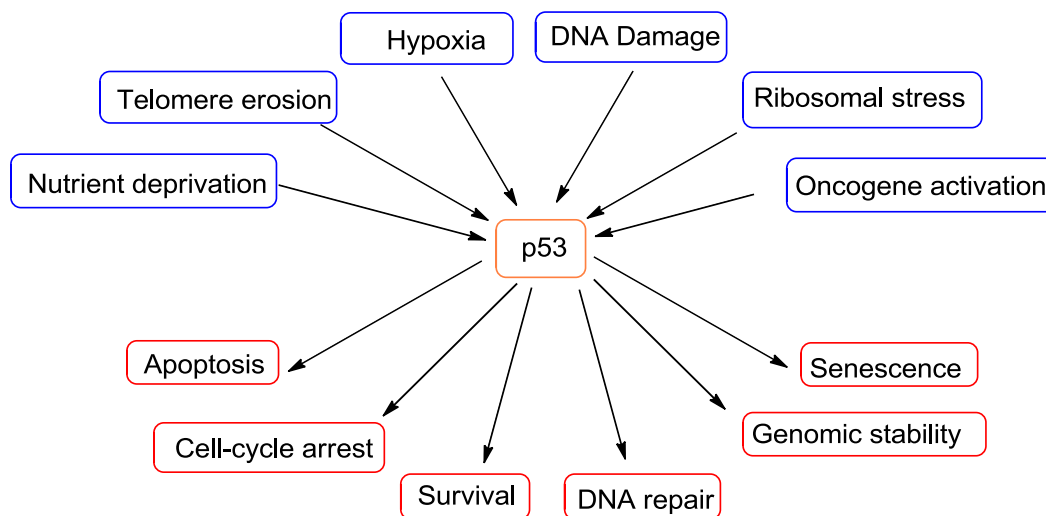


Figure 2.1: Upstream activators (blue) and downstream cellular effects (red) of p53.³⁷

2.1.1 Cell Cycle Arrest Mediated by p53

During G₁ to S phase transition of the cell cycle, four proteins, p16, cyclin D₁, CDK4 and Rb (Retinoblastoma protein) play a central role.⁴² p16 negatively regulates cyclin D₁ and CDK4 which activate Rb (Figure 2.2).⁴² After being activated by cyclin D₁ and CDK4, Rb protein releases several transcription factors responsible for the G₁ to S phase transition. In most

cancers, one of the four genes encoding for these four proteins is mutated. In response to upstream stress, p53 induces transcription of the *p21* gene which encodes for p21 protein. The p21 protein then binds to and inhibits several cyclin and CDK complexes, which inhibit progression of the cell cycle to S phase causing cell cycle arrest.⁴² The p21 protein is also involved in inhibiting DNA replication by binding with PCNA (Proliferating Cell Nuclear Antigen).⁴²

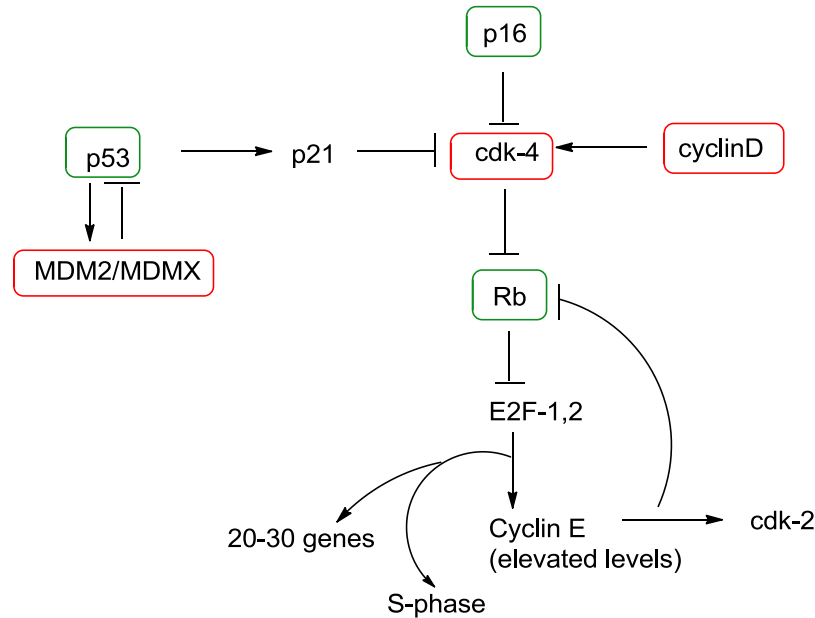


Figure 2.2: p53 mediated cell cycle arrest.

2.1.2 Apoptosis Mediated by p53

Apoptosis is a type of programmed cell death and is mediated by two main pathways, the intrinsic pathway and extrinsic pathway.⁴³ The extrinsic pathway is mediated by cell surface receptors, whereas, the intrinsic pathway is initiated by stress signals. The p53 protein is involved in induction of the proteins in both pathways, predominantly the intrinsic pathway. BAX and BH3-only proteins are apoptosis promoters involved in the intrinsic pathway, whereas, Bcl2 and Bcl-xL proteins are anti-apoptotic proteins.^{41, 44} The p53 protein induces apoptosis by transcriptionally regulating the genes encoding for apoptotic and anti-apoptotic proteins.⁴¹

2.1.3 The Structure of p53 Protein

Human p53 contains 393 amino acid residues divided into five domains (Figure 2.3):⁴⁵⁻⁴⁶

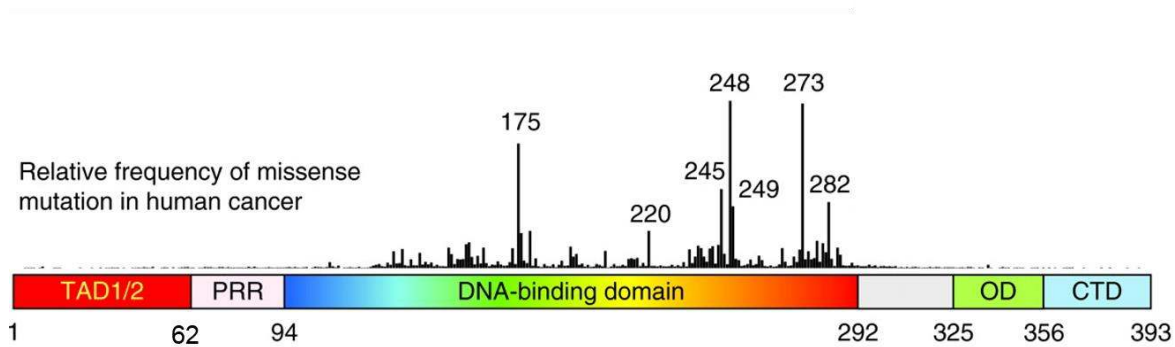


Figure 2.3: Schematic representation of p53 protein domains. The black columns indicate the mutational hotspots.⁴⁶

- (a) Transactivation domain: This domain is situated in the N-terminal region from residues 1 to 62 and can be divided into sub-domains TAD 1 and TAD 2.⁴⁶ The transactivation domain interacts with a number of regulators of p53 including MDM2 and MDMX.⁴⁷
- (b) Proline-rich domain: As the name suggests, this domain (residues 63-94) contains repeated proline residues. There are five repetitive sequence PXXP (P= Proline, X= any amino acid).⁴⁶ Although this domain is not essential for transcriptional activity, deletion from p53 inhibits p53's ability to reduce tumour cell growth in culture.⁴⁸
- (c) DNA binding domain: The DNA binding domain (residues 94-292) is the central core domain and contains mutational hotspots. This domain binds to DNA response elements that contain the repetitive sequence 5'-Pu-Pu-Pu-C-(A/T)-(T/A)-G-Py-Py-Py-3' (Pu represents A/G, Py represents T/C).⁴⁶ p53 forms a tetramer and other domains also cooperate in binding at these DNA response elements.³⁹
- (d) Tetramerization domain: This is present in the C-terminal region, residues 325-356, and regulates the formation of p53 tetramer.⁴⁶
- (e) Auto-regulatory domain: This is present in the C-terminal region, residues 356-393. This domain contains lysine residues that get acetylated by histone acetyltransferase

p300/CBP.⁴⁹ Acetylation plays critical role in DNA-binding to the central core domain, and is also important in the transcription activity of p53.⁵⁰

2.2 MDM2

MDM2, a negative regulator of p53, induces proteasomal degradation of p53 by modifying the carboxyl terminus *via* ubiquitination (Figure 2.4).⁵¹ MDM2 contains a RING (Really Interesting New Gene) domain⁵² in the C-terminal with an E3 ubiquitin ligase activity important for proteasomal degradation of p53. MDM2 has ubiquitin ligase activity following homo-dimerization as well as hetero-dimerization with MDMX.⁵³ In addition, MDM2 binds at the transactivation domain of p53 and inhibits its transcriptional activity.⁵⁴⁻⁵⁵ MDM2 contains nuclear export signal sequence that binds to p53, and exports it to the cytoplasm.⁵⁶ The transcriptional activity of p53 can only occur inside the nucleus, therefore, p53 can no longer act as a transcription factor.⁵⁷

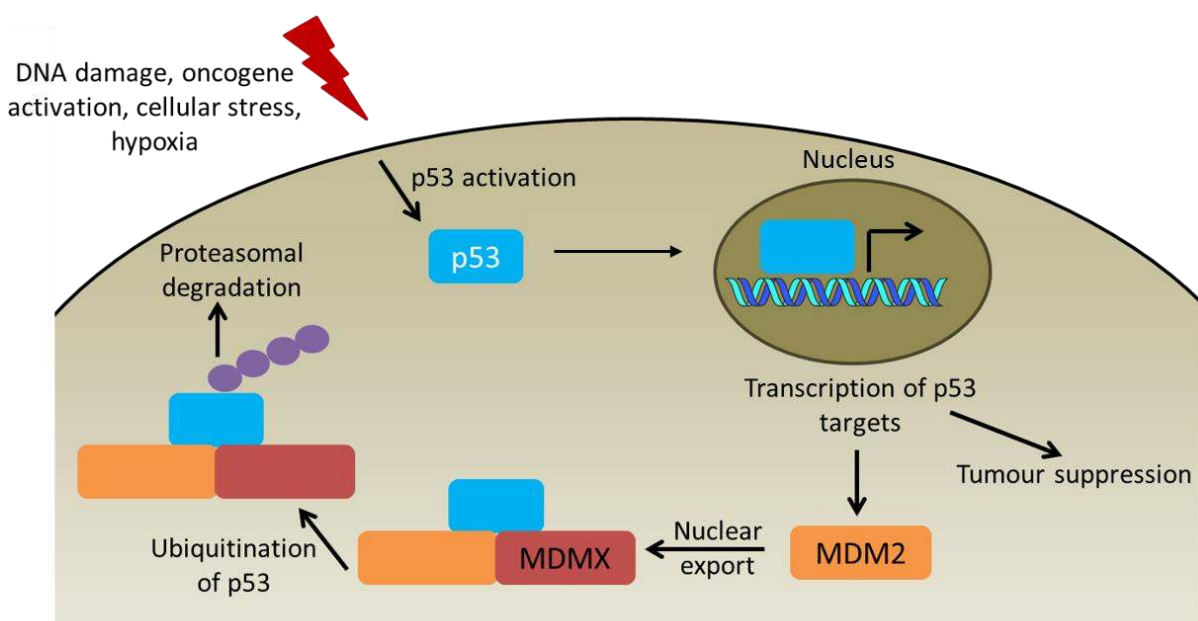
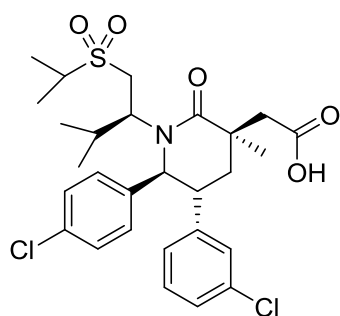


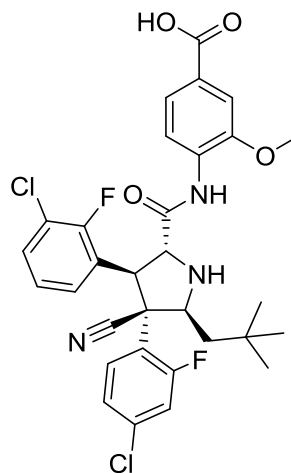
Figure 2.4: Regulation of p53 by MDM2 and MDMX.

MDM2 is a transcriptional target of p53; therefore, p53 increases the amount of MDM2, which in turn degrades p53. As a result, the level of p53 decreases which reduces the production of MDM2 that causes an increase in p53 activity forming an auto-regulatory feedback loop.⁵⁸⁻⁵⁹

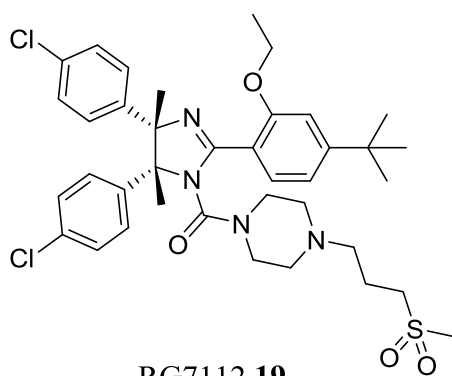
Inhibition of MDM2-p53 interaction is a well validated target, and several inhibitors (such as **17**, **18**, **19** and **20**) are currently under clinical evaluation.^{36, 60-61} However, these compounds do not inhibit MDMX-p53 interactions and therefore, fail to restore p53 activities in cancers overexpressing MDMX.⁶⁰



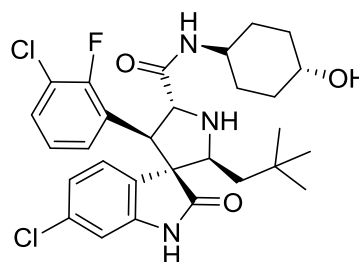
AMG-232 **17**



RG-7388 **18**



RG7112 **19**



MI-77301 **20**

2.3 MDMX and its Role in Cancer

In order to identify new cellular proteins that regulate p53 activity, Shvarts *et al.* screened a murine cDNA expression library with a radioactively labelled p53.⁶² A cDNA clone encoding MDMX was identified that had structural homology with MDM2. The human form, HDMX was identified by the same group a year later in 1997.⁶³

Like MDM2, MDMX also has a RING domain at its C-terminus but lacks intrinsic ubiquitin ligase activity. However, MDMX can mediate MDM2 ubiquitin ligase activity by hetero-oligomerisation with MDM2.⁵³ MDMX acts as a negative regulator of p53 primarily due to the inhibition of the transcriptional activity of p53.⁶²

MDMX is overexpressed in 15% of human cancers.⁶⁴ Elevated levels of *MDMX* mRNA are found in 65% of retinoblastoma, 65% of cutaneous melanoma, 19% of breast carcinoma, 19% of colon carcinoma and 18% of lung carcinoma (Table 2.1).⁶⁵⁻⁶⁷

Table 2.1: Analysis of primary tumour samples to study MDMX overexpression.⁶⁵⁻⁶⁷

Tumour Samples	Total Analysed	MDMX overexpressed
Retinoblastoma	49	32
Breast carcinoma	218	41
Colon carcinoma	27	5
Lung carcinoma	88	16
Prostate carcinoma	25	0
Stomach carcinoma	14	6
Testis carcinoma	11	3
Larynx carcinoma	13	3
Uterus carcinoma	13	2
Melanoma	14	2
Sarcoma	10	0

The deletion of *MDMX* in mice, despite having *MDM2*, causes embryonic lethality that can be rescued by loss of *Trp53*.⁶⁸⁻⁶⁹ This indicates that MDMX is a critical negative regulator of p53. The potent MDM2 inhibitor Nutlin 3 is inactive against MDMX-p53 interaction. Nutlin 3 failed to restore p53 activity in cancer cells overexpressing MDMX.⁷⁰ A combination of Nutlin with MDMX-siRNA increases p53 activity which suggests that inhibition of MDMX is also an attractive approach for restoring p53 activity.⁷⁰ It has been reported that dual inhibition of MDM2 and MDMX can increase the p53 activity more than the inhibitors of only MDM2-p53 interaction in cancer cells containing wild-type p53.⁷¹⁻⁷² Therefore, in order to achieve complete reactivation of p53 in cancers containing wild-type p53, inhibition of both MDM2 as well as MDMX is essential.

MDMX, independent of p53 and MDM2, is responsible for influencing genomic stability.^{64, 73} The overexpression of MDMX delayed DNA damage response signals and double strand DNA break repair.⁶⁴

2.4 Structure of MDMX: Comparison with MDM2

MDMX, containing 490 amino acids is structurally similar to MDM2 with 491 amino acids (Figure 2.5).⁷⁴ MDMX and MDM2 have a very similar N-terminal p53 binding domain with 54% sequence homology. MDMX lacks nuclear export sequence (NES) and nuclear localisation signal (NLS) to travel in and out from the nucleus.⁷⁵

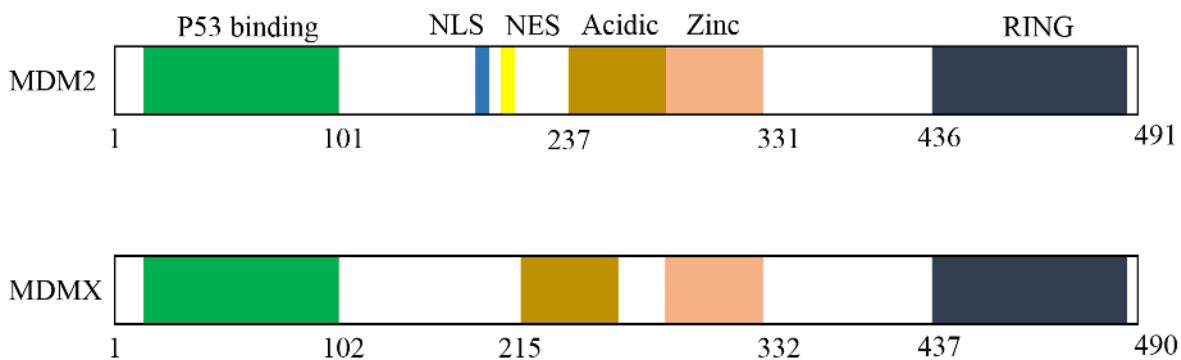


Figure 2.5: Domain structures of MDM2 and MDMX highlighting different domains. NLS: Nuclear Localisation Signal; NES: Nuclear Export Sequence. (Adapted from Lee *et al*)⁷⁵

N-terminal p53 binding domain of both MDM2 and MDMX have hydrophobic binding pockets into which the side-chains of three residues of p53; Phe19, Trp23 and Leu26 bind (Figure 2.6A/B).^{21, 76} The Trp23 nitrogen forms an H-bond with Leu54 in MDM2 (Figure 2.6 C), whereas, with Met53 in MDMX (Figure 2.6 D). The Leu26 pocket in MDMX is smaller and less-defined compared to MDM2 (Figure 2.6 E/F), and it is considered as the main hurdle to discovering a small-molecule inhibitor of MDMX-p53 interaction.⁷⁷

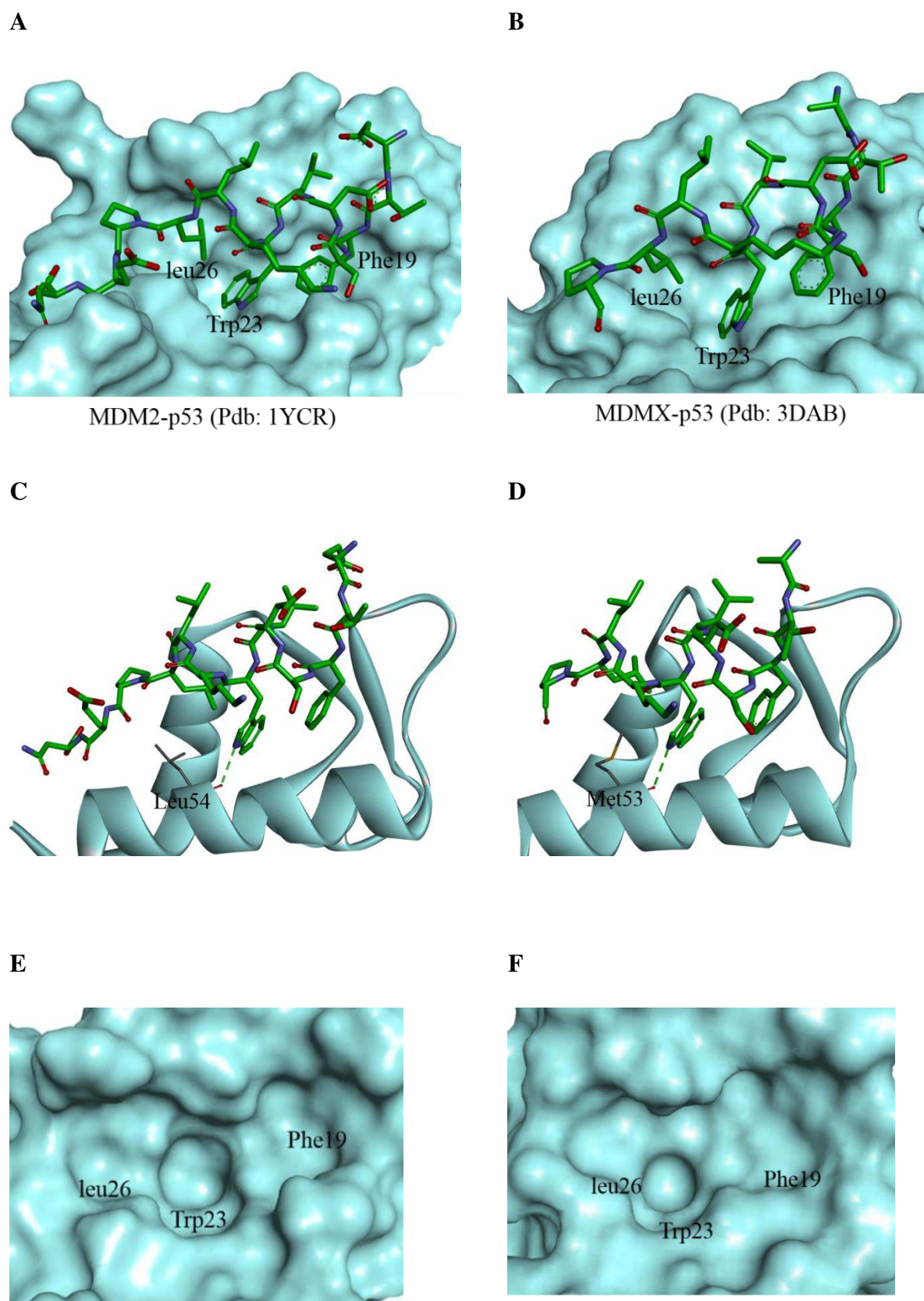


Figure 2.6: Crystal structure of p53-peptide (green) in complex with (A) MDM2,²¹ and (B) MDMX.⁷⁶ The H-bond interaction between the nitrogen of Trp23 with (C) MDM2, and (D) MDMX. The p53 binding surface of (E) MDM2, and (F) MDMX. The surface and secondary structures of both MDM2 and MDMX are coloured cyan.

2.5 Reported Inhibitors of the MDMX-p53 Interaction

2.5.1 Peptides and Stapled Peptides

Using structure-based design and phage display methods several peptide and peptidomimetics with nanomolar inhibitory activity against MDMX-p53 interactions have been identified.⁷⁸⁻⁷⁹ Despite having high potency against MDMX, peptides are less likely to become cancer therapeutics because of their instability *in vivo* and poor pharmacokinetic properties.⁸⁰ SAH-p53-8 is a stapled peptide with improved stability and pharmacokinetic properties (Figure 2.7).⁸¹ SAH-p53-8 acts as a dual inhibitor of MDM2-p53 and MDMX-p53 interactions *in vitro*. S20 and P27 residues in WT-p53 were replaced with synthetic olefinic residues, which were stapled using olefin metathesis. SAH-p53-8 showed nanomolar inhibitory activity against both MDM2- and MDMX-p53 interactions. The WT-p53 and mutant SAH-p53-8_{F19A} did not show any inhibition of MDMX at that dose range. However, SAH-p53-8 requires Nutlin-3a **14** for optimal inhibition of MDM2-p53 interactions in cells.⁸¹

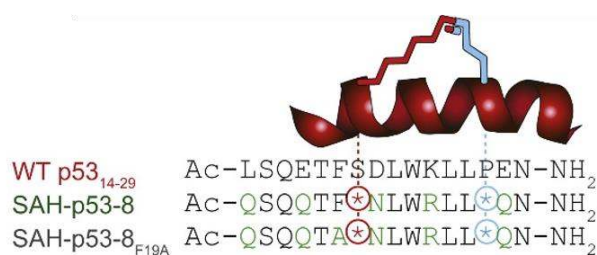


Figure 2.7: Composition of wild-type p53, SAH-p53-8 and SAH-p53-8_{F19A} peptides. The olefinic residues used for stapling are shown by stars.⁸¹

A stapled peptide ATSP-7041, which demonstrated p53 dependent tumour growth suppression in MDM2 or MDMX-overexpressing xenograft models was reported in 2013.⁷² ATSP-7041 binds with MDM2 and MDMX with nanomolar affinities *in vitro* and demonstrates sub-micromolar activities in cancer cells overexpressing MDM2 and MDMX.⁷² The stapled peptide also demonstrated favourable pharmacokinetic properties when tested *in vivo* in rat, mouse, and monkey.

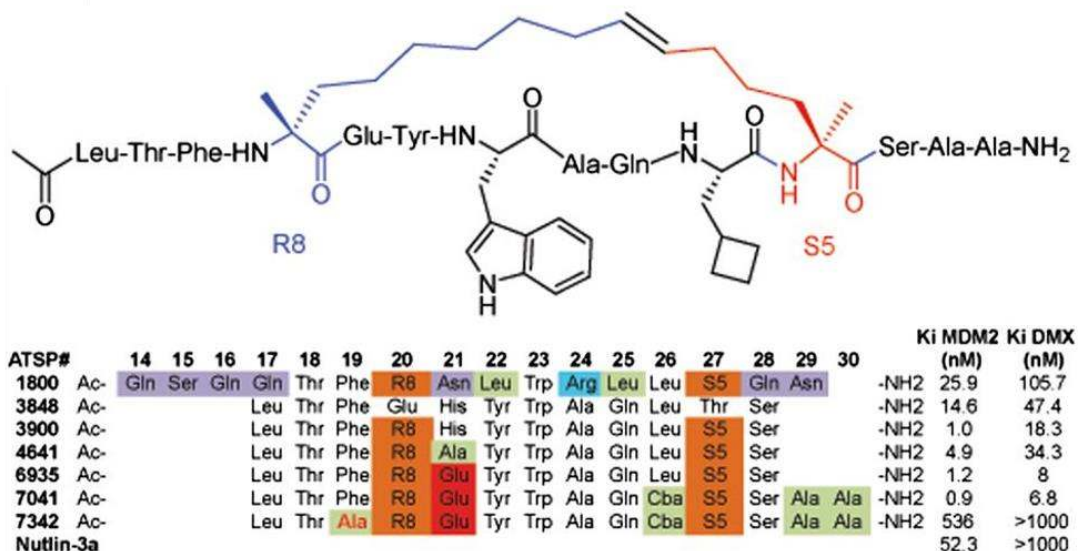


Figure 2.8: Sequences of a series of stapled peptides and their potency against MDM2 and MDMX. R8 and S5 are the olefinic residues stapled using olefin metathesis.⁷²

The crystal structure of ATSP-7041 in complex with MDMX (15-106) showed that Phe19, Trp23 and Cba26 were bound on the three hydrophobic pockets of MDMX (Figure 2.9).⁷² The Tyr²² of ATSP-7041 forms a water-mediated H-bond with His68 of MDMX. The staple group occupies a binding pocket on the surface of MDMX formed by Lys47, Met50, Gly54, Gln55 Ile57, and Met58.

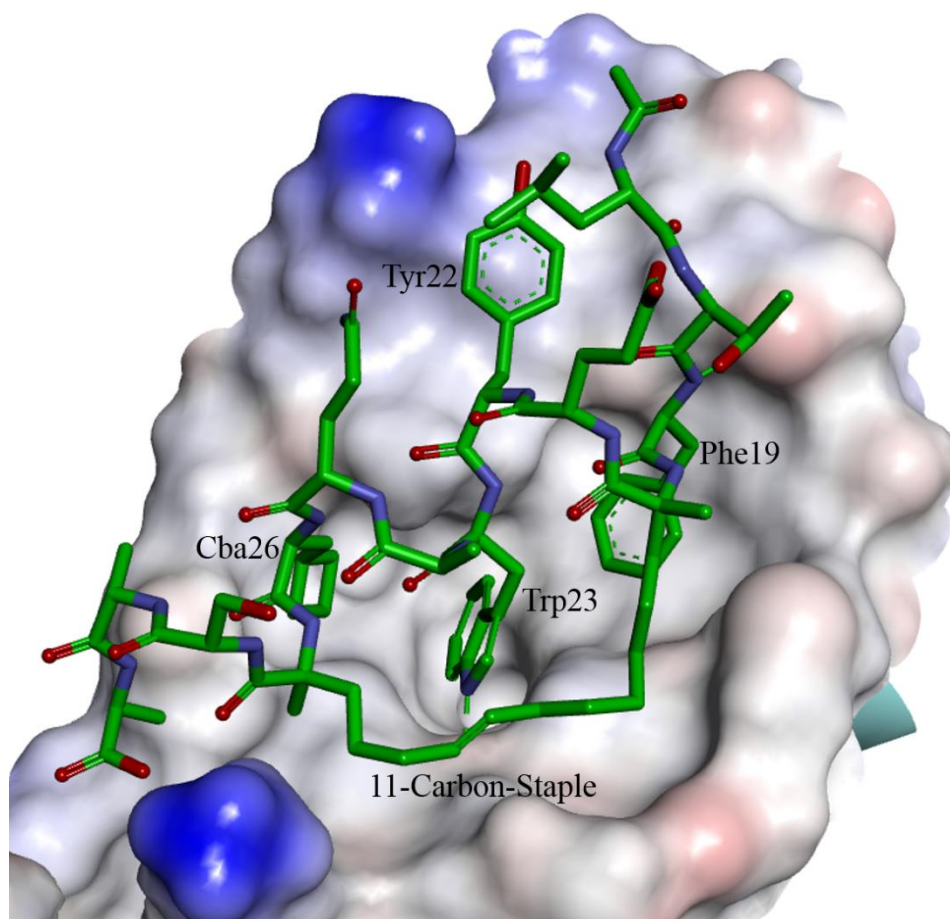
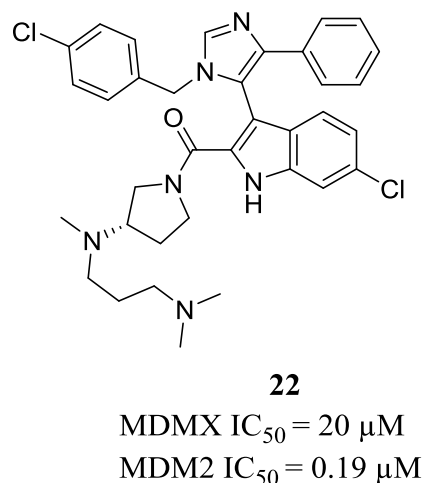
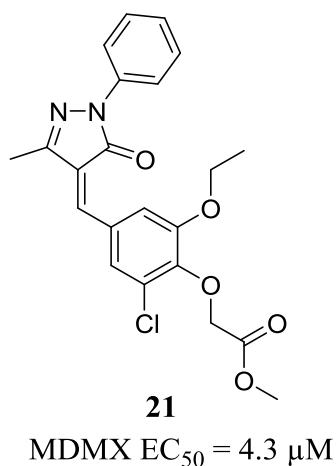


Figure 2.9: Crystal structure of ATSP-7041 (green) bound to MDMX (PDB: 4N5T). The MDMX surface is coloured based on the charge of amino acid residues: blue: positive; red: negative.

2.5.2 *SJ-172550*

SJ-172550 **21** was the first small-molecule inhibitor of MDMX discovered from the high-throughput screening of 295,848 unique compounds.⁸² It increased p53 activity in MDMX-amplified retinoblastoma cells. However, further studies on the compound showed that it forms a covalent adduct with cysteine residues of MDM2 and MDMX at the p53 binding domain.⁸³ Due to the reactivity of SJ-172550 with thiols, further development was discontinued.



2.5.3 Imidazole-Indoles

Imidazole-indoles are the class of MDM2-p53 interaction inhibitors developed by Novartis.⁸⁴⁻⁸⁵ WK298 **22**, an imidazole-indole is the first small-molecule whose crystal structure in complex with MDMX was solved (Figure 2.10).⁸⁶ The chloro-indole substituent binds at the Trp23 pocket. The nitrogen atom of the indole forms a hydrogen bond with Met53 in MDMX. The chlorine atom in the indole ring induces a conformational change in key residues including Leu54, Met53, Leu 98 and Leu102, which helps in enlargement of the central Trp23 binding pocket. The phenyl ring occupies the Phe19 pocket and the chlorobenzyl group, the Leu26 pocket in Mdmx. Although the compound was not a potent inhibitor of MDMX-p53 interaction, the crystal structure of WK298 bound to MDMX provided a basis for the structure based-design of small molecule MDMX inhibitors.

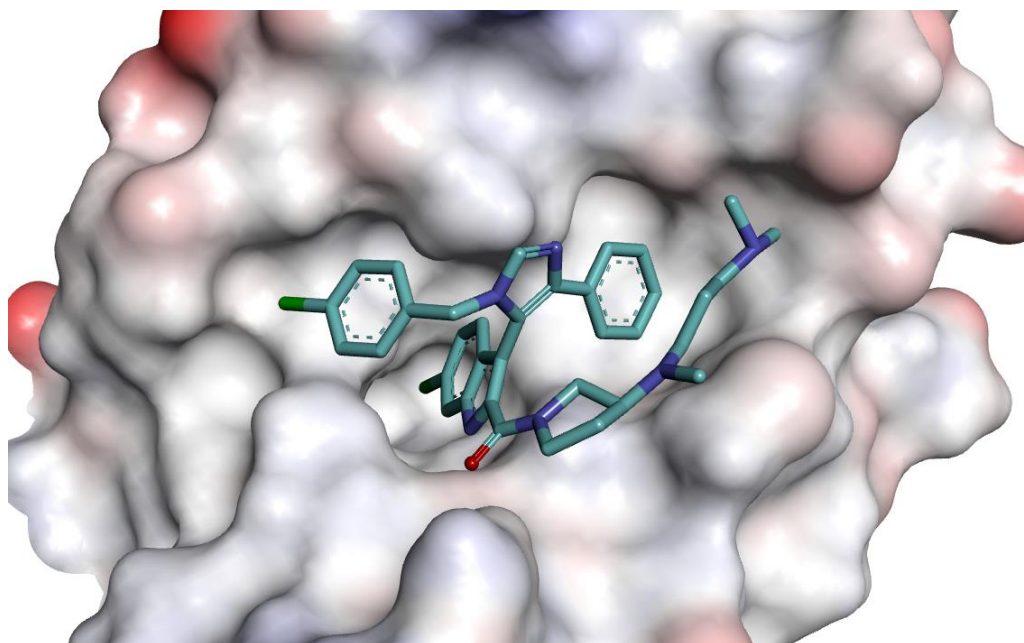
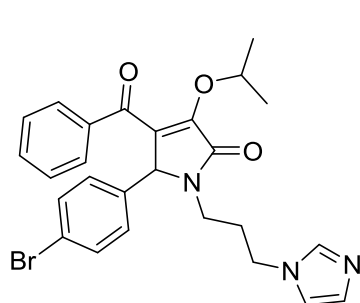


Figure 2.10: Crystal structure of WK298 (cyan) bound to MDMX (PDB: 3LBJ). The solvent accessible surface of MDMX is coloured based on the charge of the amino acid residues: positive: blue; negative: red.

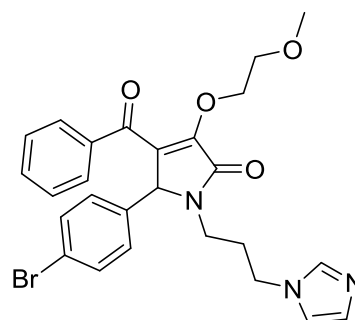
2.5.4 Pyrrolidones

Pyrrolidones are a class of compounds identified by structure-based virtual screening.⁸⁷ Structure based design led to the identification of compounds with low nanomolar activity against MDM2-p53 interaction. Several compounds (such as **23** and **24**) also showed low-micromolar binding affinity for MDMX.



23

MDMX $K_i = 2.6 \mu\text{M}$



24

MDMX $K_i = 2.1 \mu\text{M}$

2.5.5 Indolylhydantoin

Graves *et al* identified two compounds, RO-2443 (**3**) and RO-5963 (**4**), with low nanomolar potency against both MDM2 and MDMX.⁷¹ RO-5963 is an analogue of RO-2443 with improved solubility. RO-5963 restored p53 activity in MDMX overexpressing cell-lines SJSA-X and MCF-7. However, due to poor pharmacological characteristics, the compound did not progress for clinical development.⁷² The crystal structure of RO-2443 bound to MDMX showed that the compound forms a dimer, and MDMX also forms a dimer (Figure 2.11). The details of the crystal structure are discussed in detail in Chapter 8.

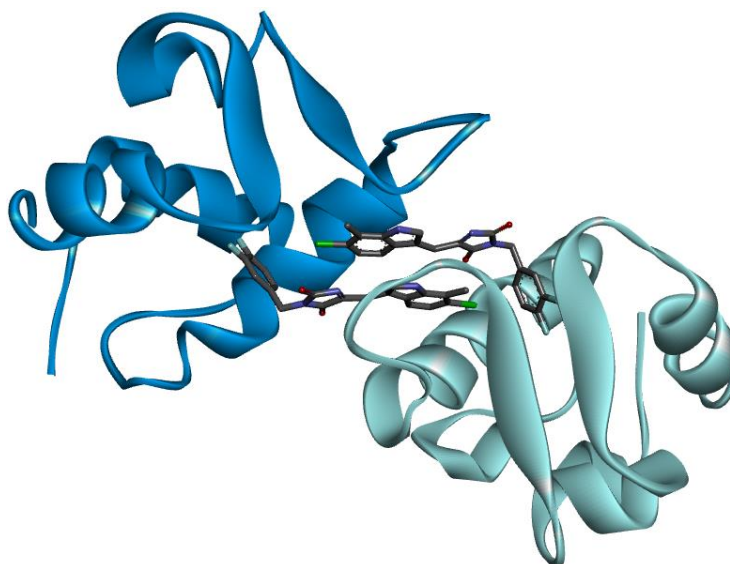
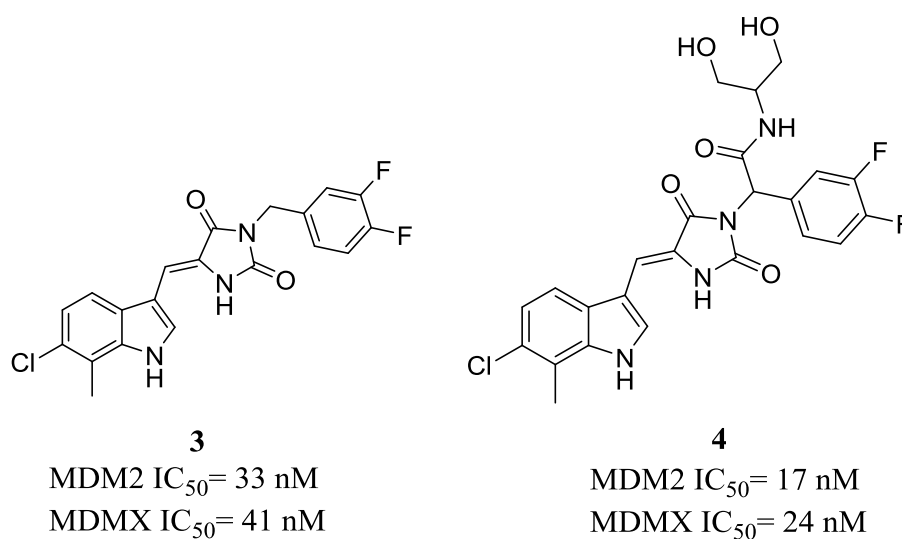
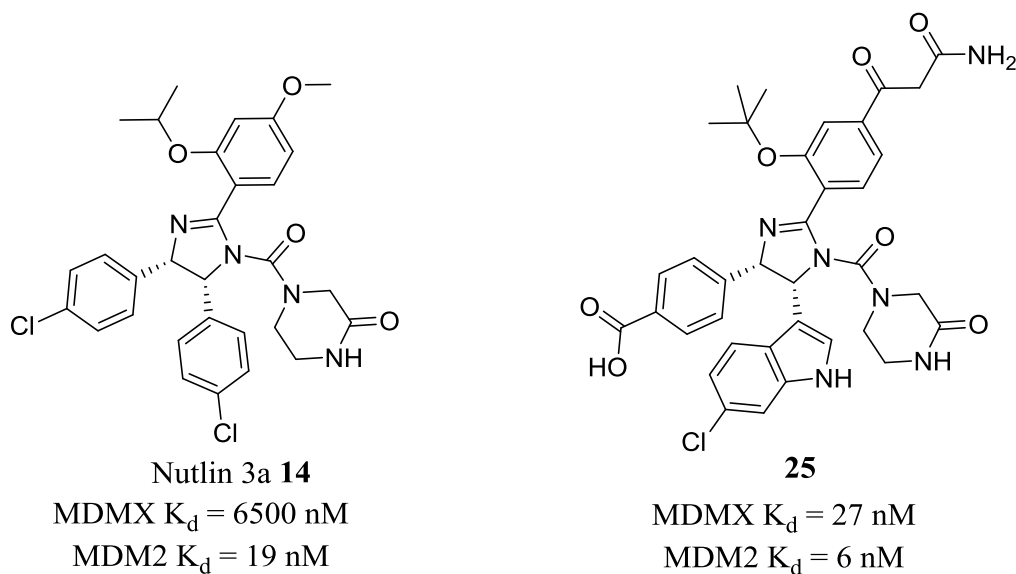


Figure 2.11: Crystal structure of RO-2443 (grey) bound to MDMX (PDB: 3U15). The two monomers of MDMX are coloured cyan and blue.

2.5.6 Nutlin-3a Derivative

Qin *et al* reported a Nutlin 3a derivative **25** as a dual inhibitor of MDM2- and MDMX-p53 interactions.⁸⁸ However, the paper was retracted recently (Oct 30, 2015) due to the intellectual property issues.⁸⁹ The compound was rationally designed using the crystal structure of Nutlin-3a bound to MDM2. The compound demonstrated p53-dependent activity on various cell lines.⁸⁸ After the withdrawal of RO-5963 from clinical evaluation, compound **25** is the only low-nanomolar inhibitor of MDMX reported to date with therapeutic potential.



The docking studies of compound **25** on p53 binding surface of MDMX revealed that the compound mimics the binding mode of p53 occupying the three key hydrophobic pockets.⁸⁸

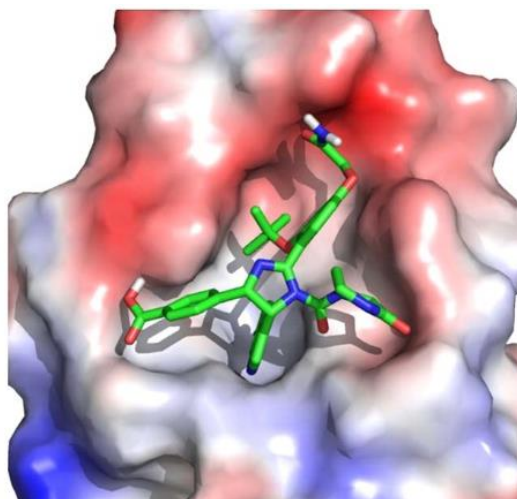
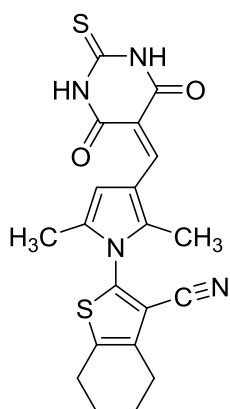


Figure 2.12: Docking of compound **25** (green) on the p53 binding surface of MDMX.⁸⁸

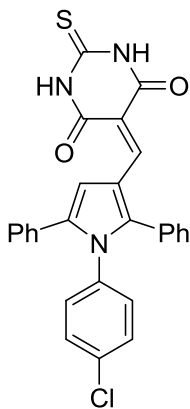
2.5.7 Pyrroles

The diaryl- and triaryl-pyrroles were identified within the group from a screening of 800 compounds using MDM2-p53 ELISA assay.⁹⁰ Compound **26** with an IC₅₀ of 12 μM against MDM2-p53 was identified as a hit. Extensive SAR studies around the hit were conducted to identify triaryl-pyrroles **27** and **28** as the most potent compounds in the series. SAR investigation revealed that the barbituric acid was important for the activity. However, the barbituric acid substituent is considered as a promiscuous binder in screening campaigns.⁹¹ Although, the compounds showed sub-micromolar potency against MDM2 and MDMX, the compounds were not selective on cancer cells with WT-p53 over cells containing mutant-p53. In this thesis, the structural features of the reported triaryl pyrroles were taken into consideration while designing compounds against MDMX-p53 interaction (discussed in detail in the next chapter).



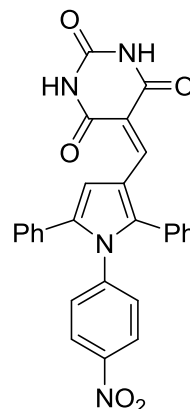
26

MDM2 IC₅₀ = 12 μM



27

MDM2 IC₅₀ = 0.11 μM
MDMX IC₅₀ = 4.2 μM



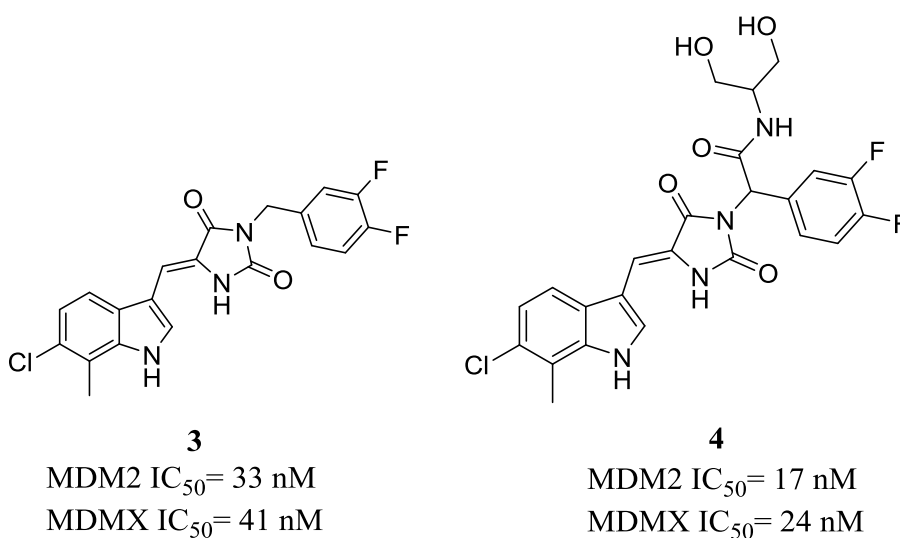
28

MDM2 IC₅₀ = 0.15 μM
MDMX IC₅₀ = 0.68 μM

2.6 MDMX Project Aim

As mentioned earlier, the MDM2-p53 interaction inhibitors cannot restore p53 activities in cancer cells overexpressing MDMX. The aim of the project was to design and develop small-molecule inhibitors of the MDMX-p53 interaction. The knowledge obtained from the SAR studies around the thiazole series and the pyrrole series (both series developed within the group) was utilised to design and synthesise a new set of compounds (details in next chapter).

The other aim of the project was to synthesise the reported dual inhibitors RO-2443 **3** and RO-5963 **4** to benchmark the in-house ELISA assay and develop a Homogenous Time Resolved FRET (HTRF) assay as an alternative assay.

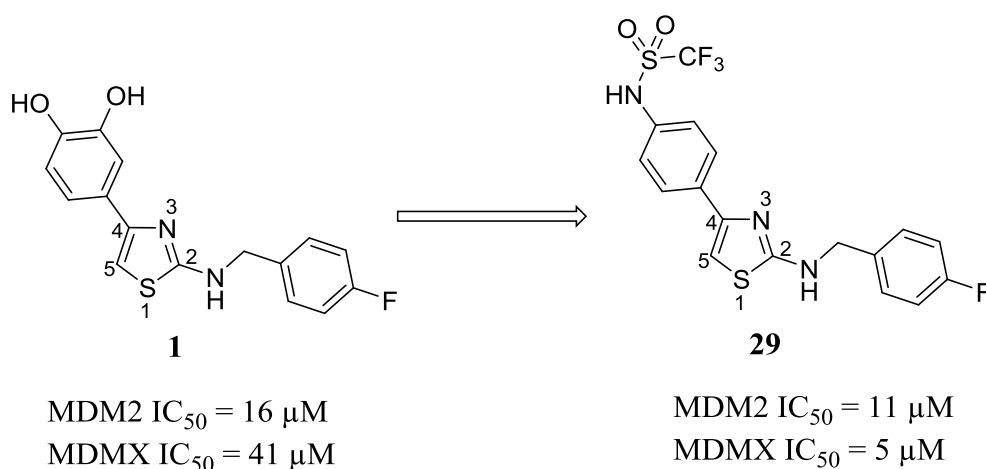


After almost 20 years since the discovery of MDMX, co-crystallisation of MDMX with small molecules has only been reported two times: one is with a micromolar inhibitor WK298 **22**,⁸⁶ and the other is with RO-2443 **3**,⁷¹ and the features of the co-crystal structure with RO-2443 could not be utilised in our series of compounds because it binds via a unique dimerization mode as discussed earlier. The final aim of the project was to co-crystallise MDMX with small-molecule inhibitors developed within the research group. A co-crystal structure would provide an insight into the binding mode of the molecules guiding the design of potent inhibitors of the MDMX-p53 interaction.

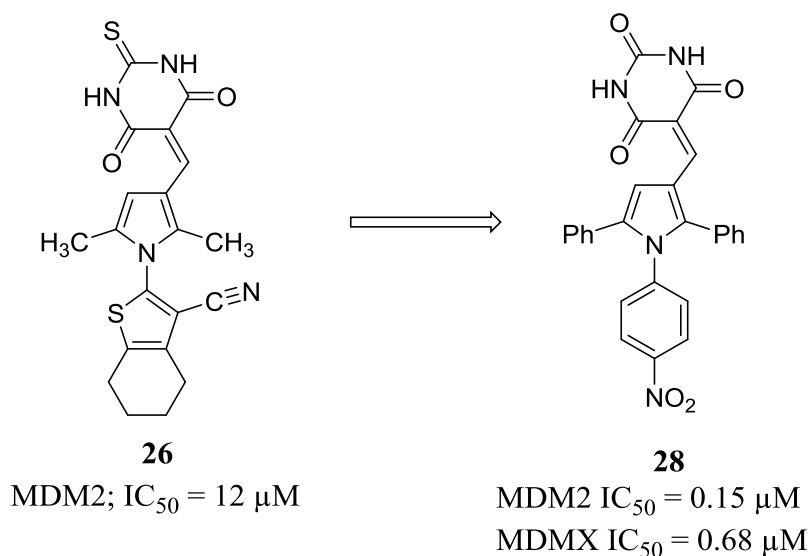
Chapter 3. Development of Inhibitors of MDMX-p53 Interaction

3.1 Rationale

The aminothiazole series was identified from virtual screening of a large library of compounds.⁹² SAR studies around hit **1** led to the identification of compound **29** with low-micromolar inhibitory activity against the MDMX-p53 interaction. However, due to the challenging chemistry at the 5-position of thiazoles, tri-substituted thiazoles that would be necessary to target the three hydrophobic pockets on the binding site of MDMX could not be synthesised. It was decided to change the scaffold from thiazole to pyrrole because the synthesis of tri-substituted pyrroles had been previously achieved within the group as described below.



The pyrrole scaffold had previously been used within the group for developing MDMX-p53 interaction inhibitors.⁹⁰ Tetra-substituted pyrrole **26** was identified as a hit from the screen of 800 compounds using Enzyme-Linked Immunosorbent Assay (ELISA).⁹⁰ Extensive SAR studies led to the identification of compound **28** that showed sub-micromolar inhibitory activity against MDMX-p53 interaction, but suffered from low solubility in both aqueous medium, as well as organic solvents.



It was decided to remove the barbituric acid group, which has been identified as a component of ‘frequent hitters’ in high-throughput screening campaigns.⁹¹ Compound **30** was designed and docked in the binding site of MDMX (PDB: 3DAC) using Molecular Operating Environment (MOE) software (Figure 3.1). The binding site was defined automatically by MOE around the region where p53 peptide was bound to MDMX. Ten different poses were generated by MOE using the default London dG and GBVI/WSA dG scoring systems,⁹³ and the top scoring pose was selected. The docking study suggested that a CH₂ linker provides a perfect angle for the phenyl ring to occupy the Phe19 pocket in the binding site of MDMX. Besides, it was identified later on that a CH₂ linker improved the organic solubility of the compounds. The 4-chlorophenyl group occupied the Trp23 pocket and the phenyl ring occupied the Leu26 pocket.

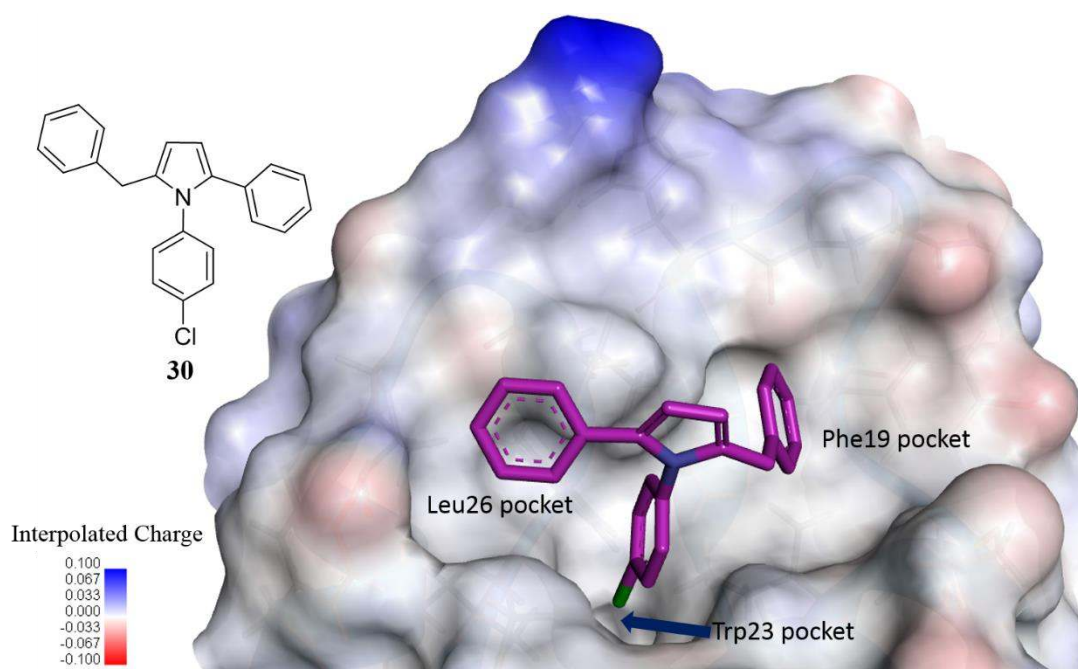


Figure 3.1: Compound **30** (carbons: magenta) docked on the binding site of MDMX (PDB: 3DAC) using Molecular Operating Environment (MOE) software. The binding surface is coloured based on the charge of the amino acid residue; positive: blue, negative: red.

The docked structure of compound **30** on MDMX was superimposed on the crystal structure of a p53 peptide in complex with MDMX (Figure 3.2). The superimposed image suggested that the substituents at 1,2,5-positions of the pyrrole ring occupied the same region as the three key amino acids in p53 (Leu26, Trp23 and Phe19).

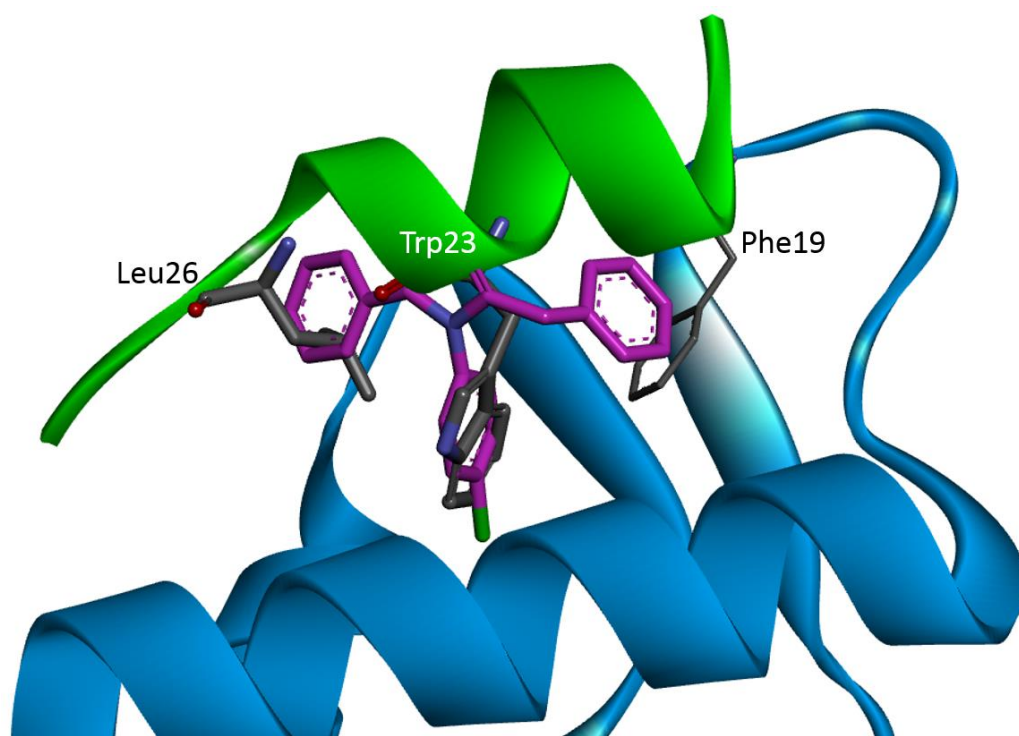


Figure 3.2: Superimposition of crystal structure of MDMX in complex with p53 peptide (PDB: 3DAC) and docked structure of compound **30** (carbons: magenta). MDMX secondary structure is coloured blue; p53 peptide is coloured green; three key amino acids in p53 are coloured grey.

Therefore, the first strategy was to access the three key hydrophobic pockets in the MDMX binding surface with aromatic substituents at 1,2, and 5-positions of pyrroles.

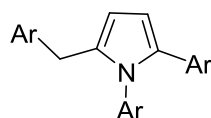
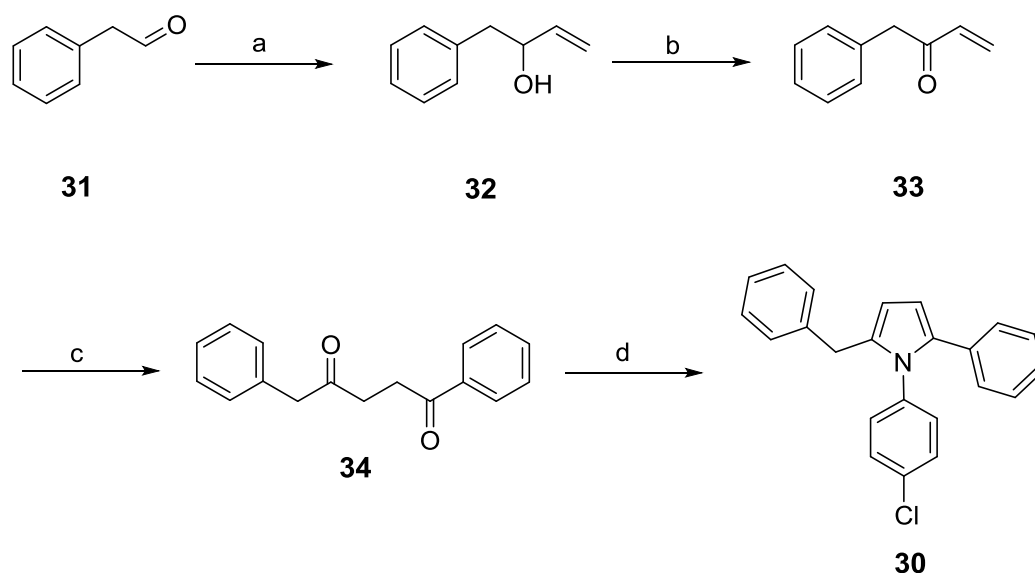


Figure 3.3: 1,2,5-trisubstituted pyrroles to be synthesised.

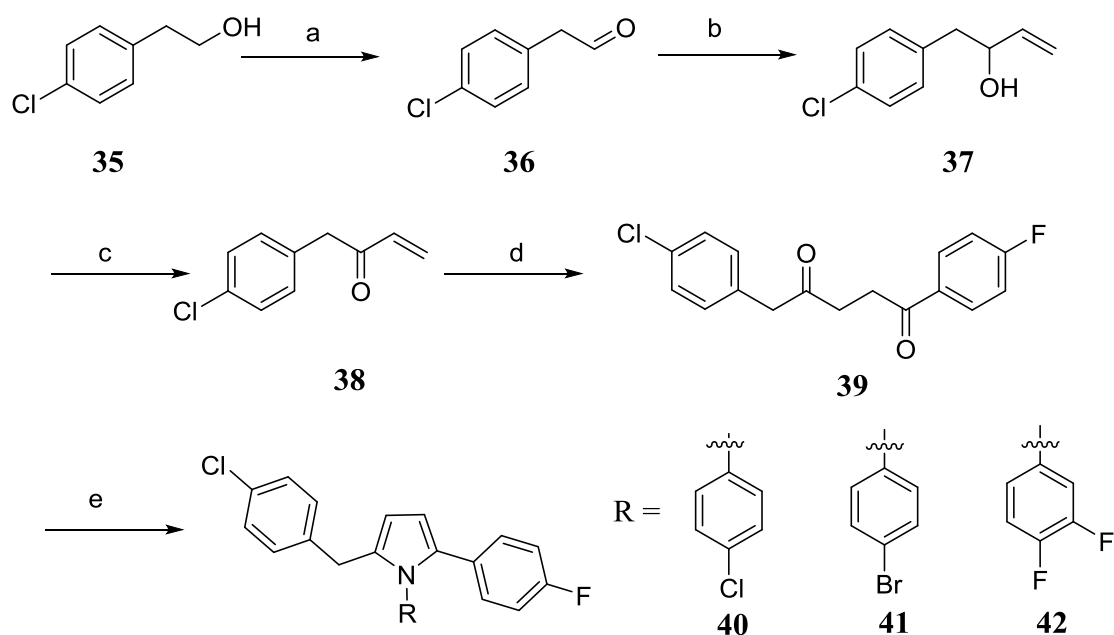
3.2 Synthesis of 1,2,5-trisubstituted pyrroles

Synthesis of compound **30** started with the Grignard reaction on commercially available phenylacetaldehyde **31** followed by oxidation to give α,β -unsaturated ketone **32** (Scheme 3.1). A Stetter reaction using a thiazolium salt provided the desired diketone **34**. Finally, the Paal-Knorr pyrrole synthesis afforded pyrrole **30**.



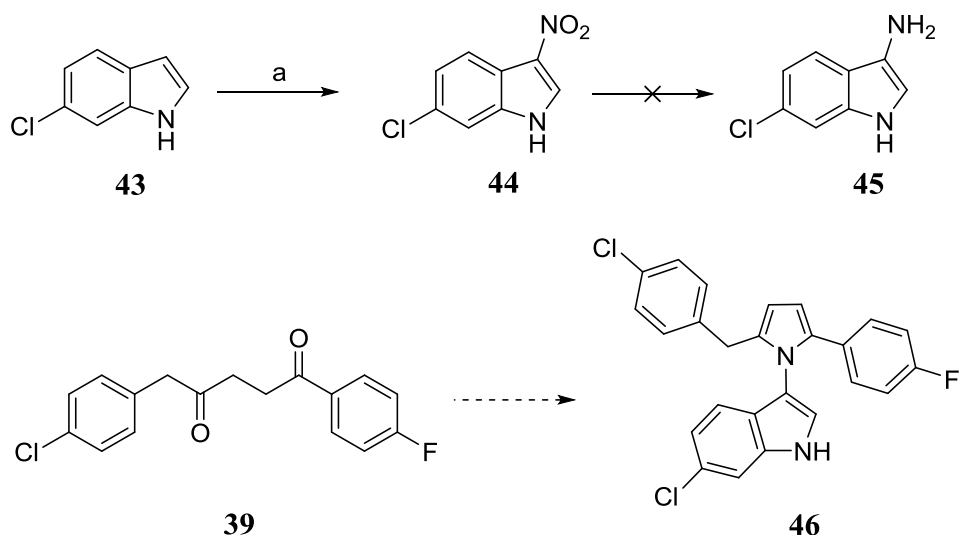
Scheme 3.1: *Reagents and conditions:* (a) vinyl magnesium chloride, THF, -78 °C, 30 min, then r.t., 2h, 61%; (b) DMP, DCM, 0 °C-r.t., 3.5 h, quant.; (c) 3-benzyl-5-(2-hydroxyethyl)-4-methylthiazolium chloride, benzaldehyde, NEt₃, EtOH, 80 °C, 19 h, 65%; (d) 4-chloroaniline, AcOH, reflux, 1.5 h, 30%.

Compounds **40**, **41**, and **42** were synthesized using the same route. The synthesis started with the oxidation of 4-chlorophenethyl alcohol **35** (Scheme 3.2). Subsequently, following the previously described reaction sequence, diketone **39** was obtained. Finally, the Paal-Knorr pyrrole synthesis afforded desired pyrroles **40**, **41** and **42**. The Paal-Knorr condensation condition used for synthesising compound **30**, **40** was low yielding, therefore, microwave conditions described by Minetto *et al* were employed.⁹⁴ Diketone **39** was heated with the corresponding amine under microwave irradiation for 10 min to obtain desired pyrroles **41** and **42** in good isolated yields.



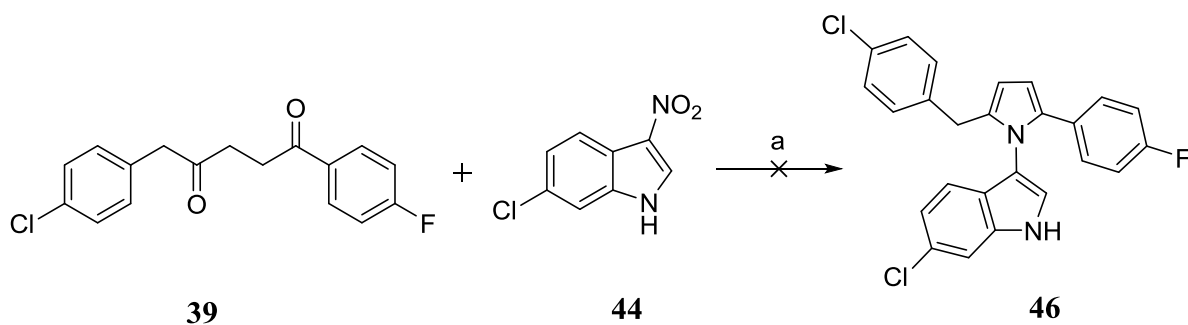
Scheme 3.2: Reagents and conditions: (a) DMP, DCM, 0 °C, 15 min, then r.t., 1 h, 66%; (b) vinyl magnesium chloride, THF, -78 °C, 30 min, then r.t., 2h, 39%; (c) DMP, DCM, 0 °C, 15 min, then r.t., 3.5 h; (d) 3-benzyl-5-(2-hydroxyethyl)-4-methylthiazolium chloride, benzaldehyde, NEt₃, EtOH, 80 °C, 19 h, 30% over 2 steps; (e) 4-chloroaniline, AcOH, reflux, 8 h, 31% (**40**); or, 4-bromoaniline or 3,4-difluoroaniline, AcOH, 170 °C μ W, 10 min, 83% (**41**), 77% (**42**).

Compound **46** with a 6-chloroindole at the pyrrole-*N*¹ position was designed based on the published inhibitor WK-298 **22**, which has a 6-chloroindole group to access the Trp23 pocket in MDMX. The proposed synthetic route for compound **46** is shown in Scheme 3.3. The synthesis started with the nitration of the commercially available indole **43**. There is literature precedent for nitration at multiple positions of indole under nitration conditions using nitric acid.⁹⁵ Therefore, milder conditions were attempted which provided desired 3-nitroindole **44** in 10% yield.⁹⁵ The low yield was due to the difficulty in purification of the tarry crude material as mentioned in the literature.⁹⁶ A thiol SPE cartridge was used to separate silver impurities generated in the reaction and the remaining material was purified by reverse phase chromatography which helped to increase the yield to 42%. The reduction of 3-nitroindole **44** was attempted with various reducing agents such as Zn/acetic acid, Zn/NH₄Cl in MeOH, and Pd/C and H₂, but resulted in a complex mixture of products.



Scheme 3.3: Reagents and conditions: (a) AgNO₃, benzoyl chloride, CH₃CN, 0 °C, 30 min., 42%.

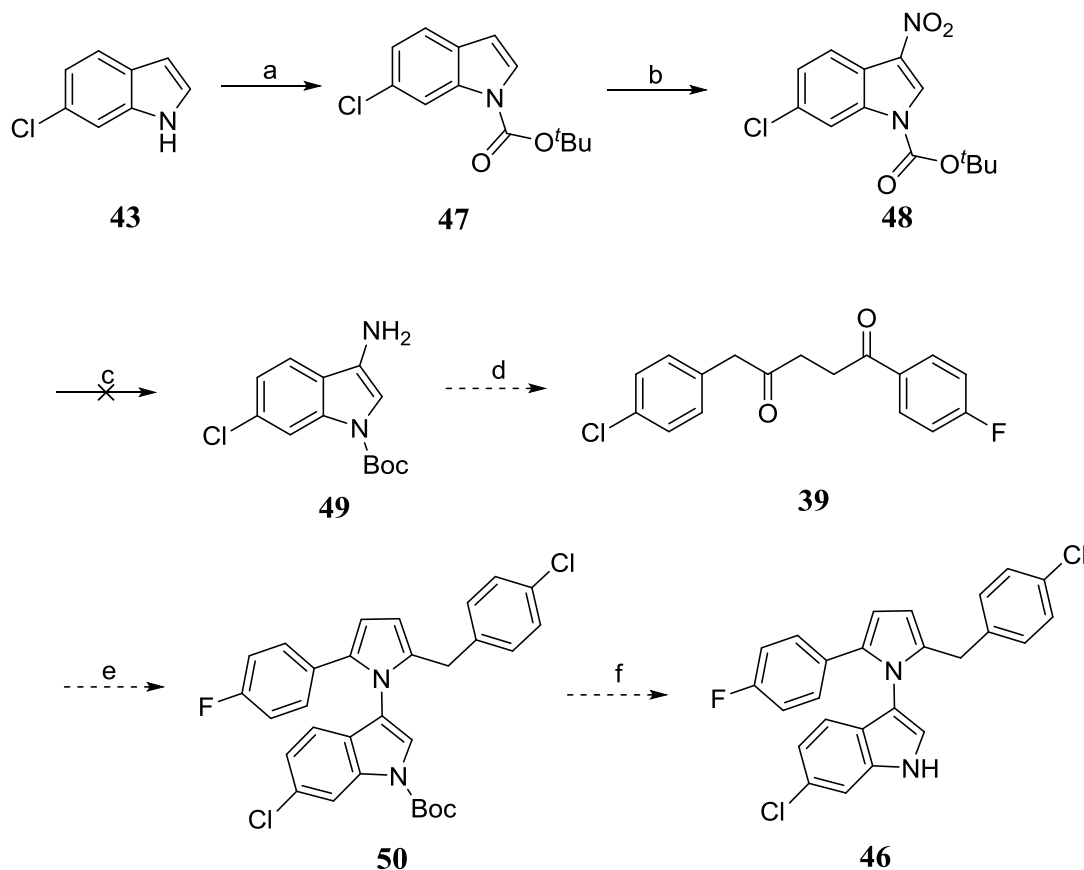
There is a literature precedent for the Paal-Knorr condensation using nitrobenzenes involving in-situ reduction of the nitrobenzene to anilines.⁹⁷ Using the literature conditions, the Paal-Knorr condensation using Zn/Acetic acid was attempted (Scheme 3.4) but the reaction provided complex mixture of products.



Scheme 3.4: Reagents and conditions: (a) Zn, AcOH, 90 °C, 20 h.

It was proposed that the 3-aminoindole **45**, due to its electron rich nature, would be involved in various side reactions. Therefore, the protection of indole **43** with an electron withdrawing protecting group was proposed (Scheme 3.5). The Boc protection of indole **43**, followed by nitration afforded compound **48**. Subsequent reduction of compound **48** using Zn/AcOH was unsuccessful. Following a literature procedure by Lee *et al*,⁹⁷ nitroindole **48** was used directly in the Paal-Knorr condensation using indium/acetic acid, however, a mixture of unidentified products was obtained. While this work was underway, it was determined that 1,2,5-

trisubstituted pyrroles (**30**, **40**, **41** and **42**) were not potent inhibitors of MDMX-p53 interaction as shown in Table 3.1. Therefore, the synthesis of compound **46** was abandoned. The focus was shifted towards other regions of the pyrroles with modifications designed to improve the solubility which will be discussed in detail in the next chapter.

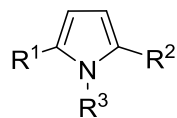


Scheme 3.5: Reagents and conditions: (a) Boc₂O, DMAP, MeCN, r.t., 2 h, 97%; (b) HNO₃, Ac₂O, -78 °C-0 °C, 17 h, 51%; (c) Zn, AcOH, r.t., 45 min.

3.3 Biological Evaluation

1,2,5-Trisubstituted pyrroles were tested against MDMX-p53 interaction using an Enzyme-Linked Immunosorbent Assay (ELISA). Compounds **30**, **40**, **41** and **42** demonstrated weak inhibition of the MDMX-p53 interaction (Table 3.1). The compounds were very lipophilic with average clogP around 9. Due to high lipophilicity, the compounds had low-solubility in assay buffer conditions resulting in weak inhibition of the MDMX-p53 interaction.

Table 3.1: Results of the ELISA for 1,2,5-trisubstituted pyrroles.

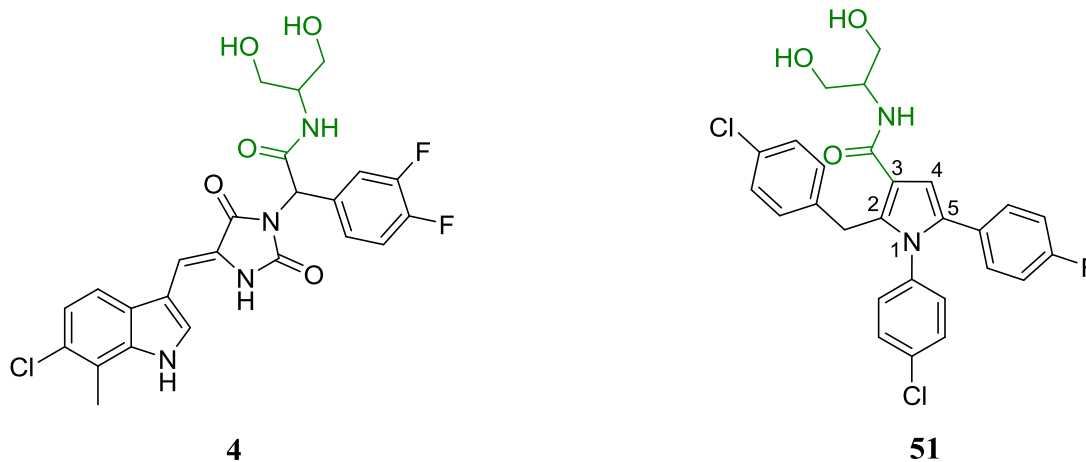


Compound	R ¹	R ²	R ³	MDMX IC ₅₀ (μM)
30	C ₆ H ₅ CH ₂	Ph	4-ClC ₆ H ₄	>200
40	4-ClC ₆ H ₄ CH ₂	4-FC ₆ H ₄	4-ClC ₆ H ₄	197
41	4-ClC ₆ H ₄ CH ₂	4-FC ₆ H ₄	4-BrC ₆ H ₄	168
42	4-ClC ₆ H ₄ CH ₂	4-FC ₆ H ₄	3,4-F ₂ C ₆ H ₃	281

Chapter 4. Introduction of Water Solubilising Group

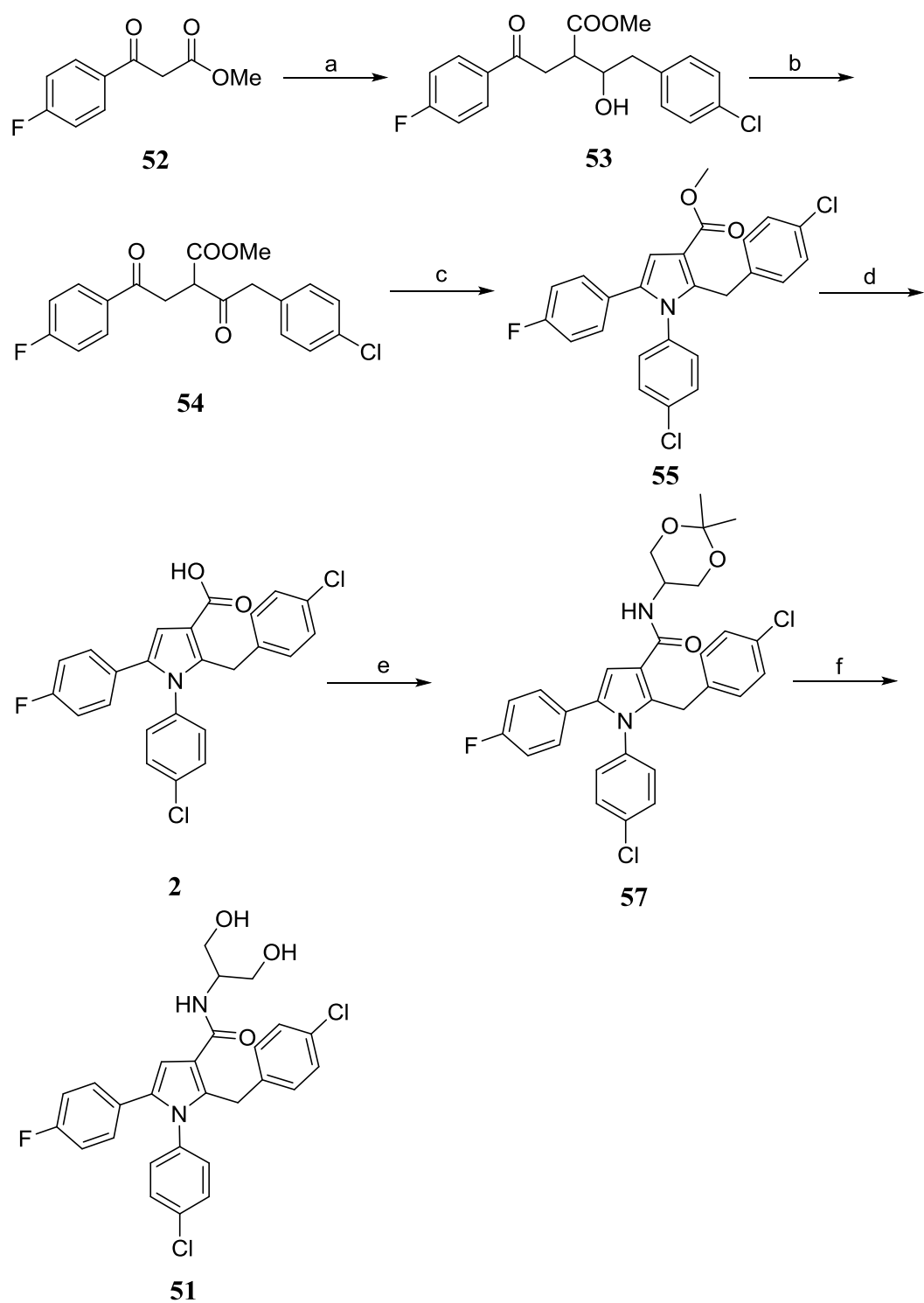
4.1 Rationale

It was postulated that 1,2,5-trisubstituted pyrroles were inactive against MDMX because of the poor solubility of the compounds in assay buffer conditions. Therefore, it was decided to introduce a water solubilising group in the molecule. The 3-position of the pyrrole was chosen for introducing a water solubilising group for reasons of synthetic accessibility. The water solubilising group in the published MDMX inhibitor RO-5963 **4** was chosen and compound **51** was designed.



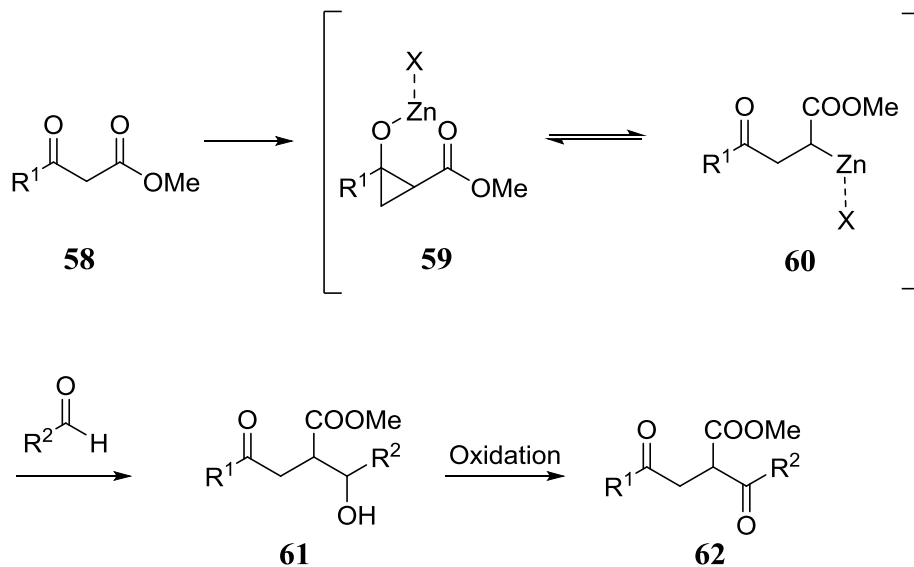
4.2 Synthesis

The synthesis of compound **51** started with the preparation of 1,4-diketone **54** following a route described by Minetto *et al* (Scheme 4.1).⁹⁴ 1,4-Diketone **54** was synthesised from the commercially available β -keto ester **52** using Et_2Zn and CH_2I_2 , followed by oxidation. Then, Paal-Knorr condensation of 1,4-diketone **54** with 4-chloroaniline provided pyrrole **55** which was hydrolysed to compound **2**. Subsequent amide coupling of the carboxylic acid **2** with the amine **115** produced compound **57**. The synthesis of amine **115** is discussed in detail in Chapter 7 (Scheme 7.2). Finally, the deprotection of acetal **57** using HCl provided desired target **51**.



Scheme 4.1: Reagents and conditions: (a) **36**, Et₂Zn, CH₂I₂, DCM, 0 °C, 1.5 h; (b) PCC, DCM, r.t., 41 h, 33% over 2 steps; (c) 4-chloroaniline, AcOH, 170 °C μW, 10 min, 48%; (d) LiOH, THF, MeOH, H₂O, r.t., 72 h, 91%; (e) **115**, DIC, DMAP, DCM, 0 °C, 15 min, then r.t., 16 h, 70%; (f) HCl, H₂O, THF, r.t., 3h, 94%.

Minetto *et al* proposed a mechanism for the formation of diketone using Et_2Zn and CH_2I_2 (Scheme 4.2).⁹⁴ The reaction proceeds via the formation of a cyclopropyl intermediate **59** which ring opens to intermediate **60**. The nucleophilic attack of intermediate **60** on the aldehyde affords alcohol **61**, which can be oxidised to give desired 1,4-diketone **62**.

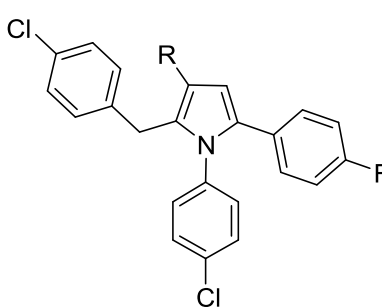


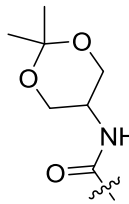
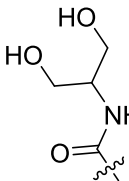
Scheme 4.2: Proposed mechanism for the conversion of β -Keto ester to 1,4-Diketone.^{94, 98}

4.3 Biological Evaluation

MDMX inhibitory activity of compound **51** along with the intermediates obtained during the synthesis were determined (Table 4.1). A significant increase in potency for MDM2 and MDMX, at least 12-fold, was observed upon the hydrolysis of ester **55** to carboxylic acid **2**. Amides **51** and **57** were at least 4-fold less potent than the carboxylic acid **2**. Interestingly, both the amides were more potent against MDMX than MDM2, compound **51** was the most MDMX selective compound. Compound **2** was considered as the lead in the pyrrole series and SAR studies around the compound were carried out, discussed in detail in following chapters.

Table 4.1: Results of the ELISA for tetra-substituted pyrroles.



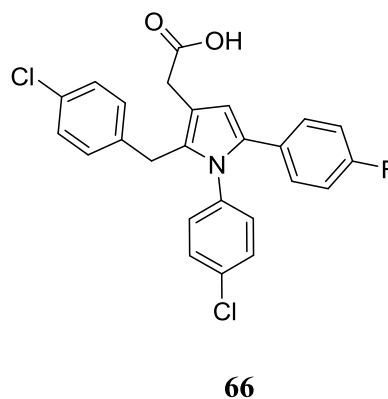
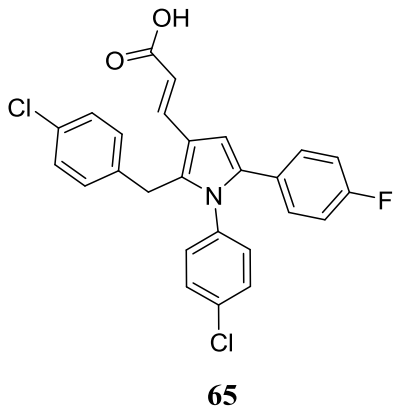
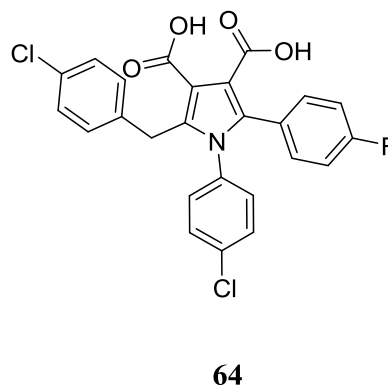
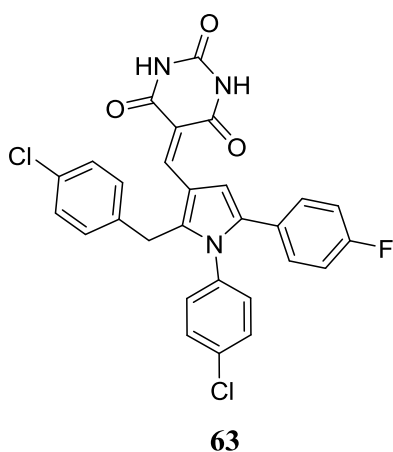
Compound	R	MDM2 IC ₅₀ (μM) ^a	MDMX IC ₅₀ (μM) ^a
30	H	>200	197
55	-COOMe	>200	188
2	-COOH	11 ^b	15 ^c
57		104	61
51		>200	40

^a Determinations (n = 1 unless otherwise stated); ^b n = 2; ^c n = 3

Chapter 5. SAR Studies around Compound 2

5.1 Rationale

The increase in potency due to a carboxylic acid at the 3-position, encouraged SAR studies around lead **2**. Compound **63** with a barbituric acid group at the 3-position could be used for direct comparison with the previously described pyrrole series.⁹⁰ Compound **64**, with two carboxylic acids was designed to study the effect of an additional acid at the 4-position. To understand the effect of homologation of carboxylic acid compound **65** and **66** were designed.



Introduction of a succinimide ring on the 3/4-positions could be accessible *via* dicarboxylic acid compound **67**. 3,4-Pyrroledicarboximides **68** has an unsubstituted nitrogen that could be used as a vector to introduce various water solubilising groups. Removal of fluorine is discussed in detail in Chapter 6.

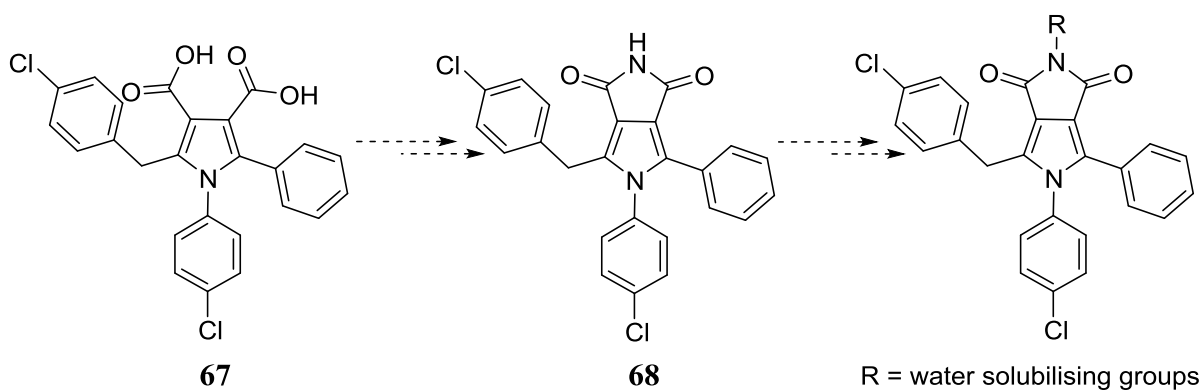


Figure 5.1: Design of 3,4-pyrroledicarboximides.

It was postulated that compound **69** with a CH₂ linker at the N¹-position would mimic the indole ring of Trp23 in p53 (Figure 5.2).

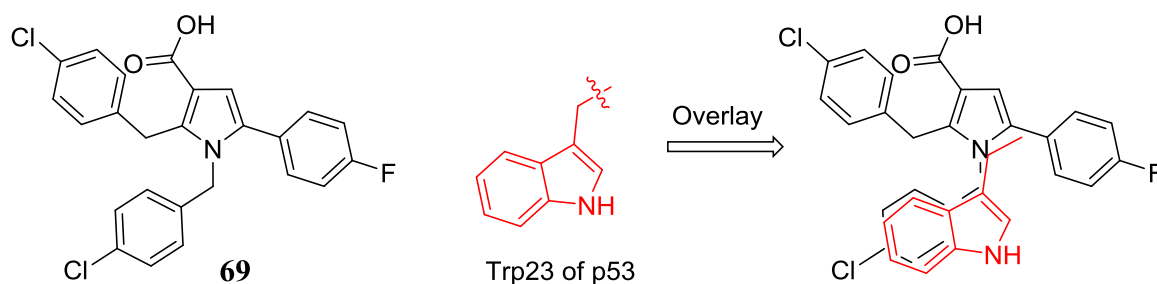


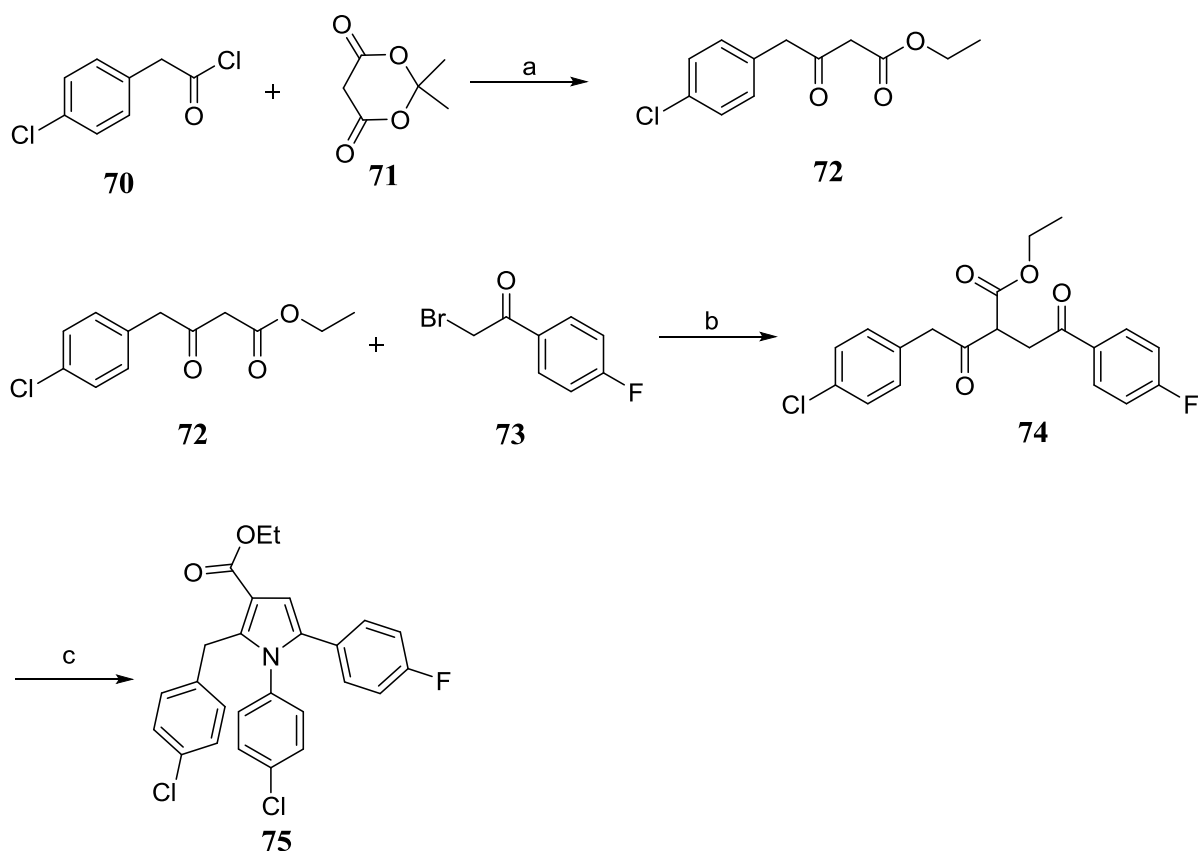
Figure 5.2: Overlay of compound **69** on the side chain of Trp23 of p53.

5.2 Synthesis

5.2.1 Synthesis of Tetra-Substituted and Penta-Substituted Pyrroles

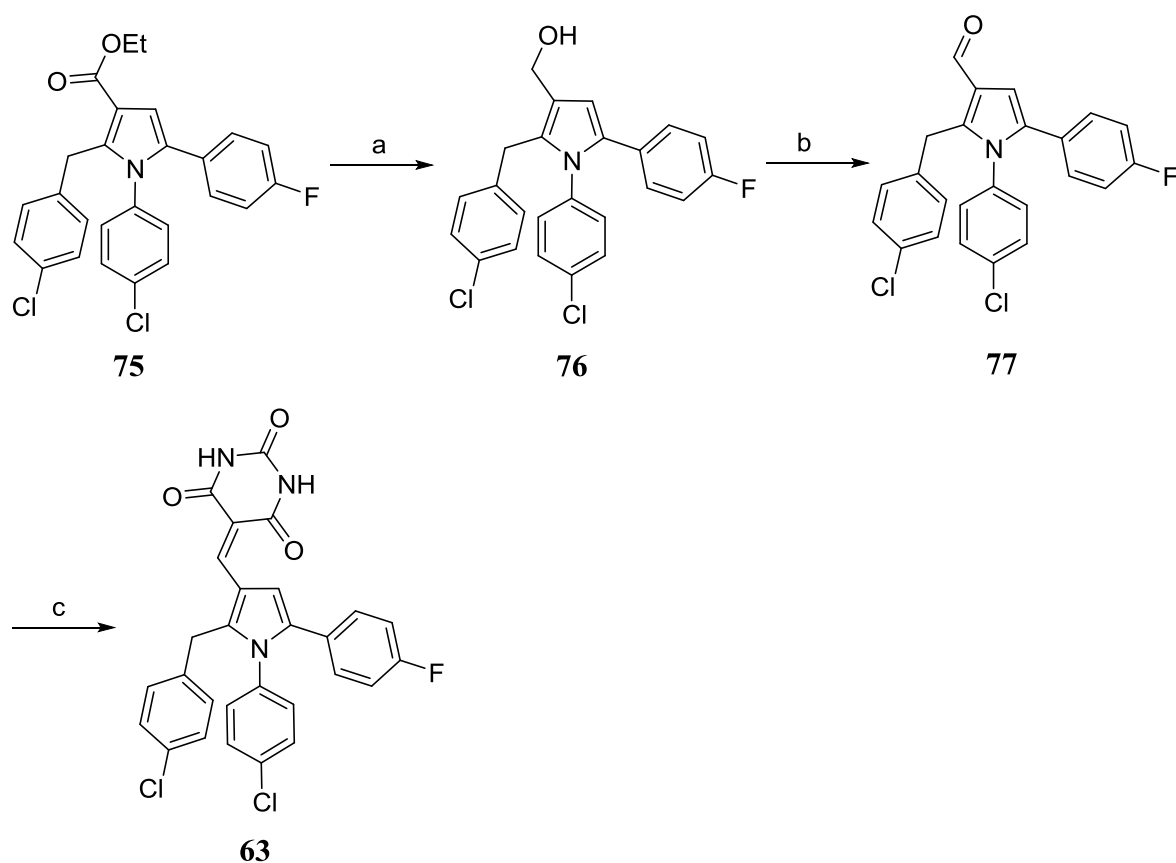
1,4-Diketone **74** and pyrrole **75** were synthesised in bulk quantities, and used for the synthesis of various compounds. The synthesis started with the preparation of β -keto ester **72** using acid chloride **70** and Meldrum's acid **71** (Scheme 5.1). The nucleophilic attack of the enolate of β -keto ester **71** on compound **73** afforded desired 1,4-diketone **74** in good isolated yield. Finally, the Paal-Knorr pyrrole synthesis using 4-chloroaniline provided pyrrole **75**. The scheme was high yielding, and the purification of the products was easier compared to the previously

described route (Scheme 4.1). In addition, this route was versatile in terms of synthesising different analogues of 1,4-diketone.



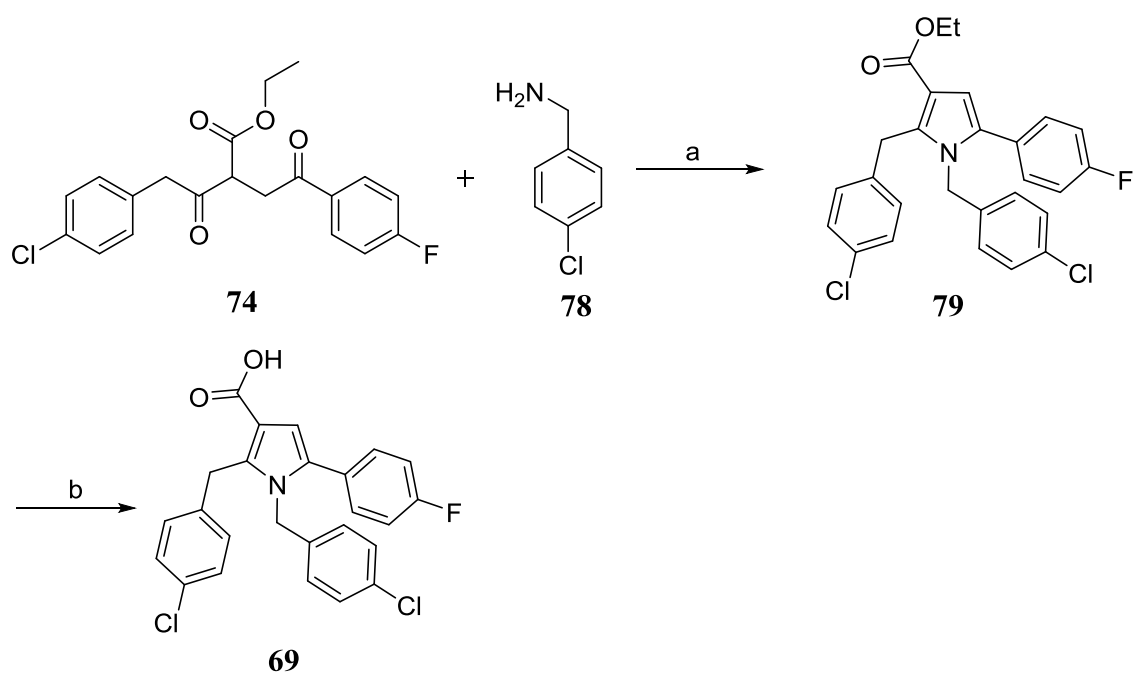
Scheme 5.1: *Reagents and Conditions:* (a) (i) pyridine, DCM, 0 °C, 1 h, then r.t., 2.5 h; (ii) EtOH, reflux, 2 h, then r.t., 16 h, 78% over 2 steps; (b) NaH, THF, r.t., 2.5 h. 91%; (c) 4-chloroaniline, AcOH, 170 °C μ W, 10 min, 67%.

Compound **63** was synthesised following a four-step reaction sequence starting from intermediate **75** (Scheme 5.2). DIBAL reduction of ester **75** gave alcohol **76**, and subsequent oxidation with Dess-Martin periodinane provided aldehyde **77**. Knoevenagel condensation of aldehyde **77** with barbituric acid in the presence of acetic acid afforded desired pyrrole **63**.



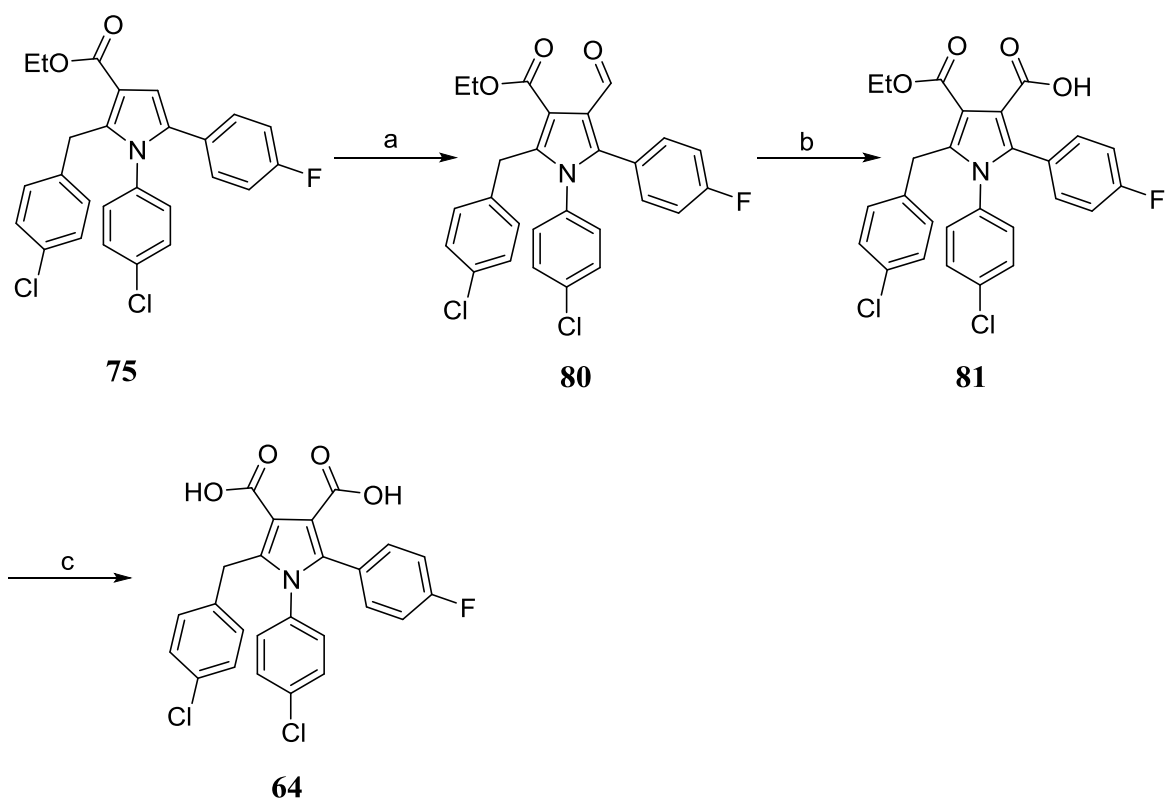
Scheme 5.2: Reagents and Conditions: (a) DIBAL, DCM, 0 °C, 2 h, 95%; (b) DMP, DCM, 0 °C-r.t., 2 h, 61%; (c) barbituric acid, AcOH, reflux, 2.5 h, 48%.

Compound **69** was synthesised following a two-step reaction sequence starting from intermediate diketone **74** (Scheme 5.3). Paal-Knorr condensation of diketone **74** with amine **78** afforded pyrrole **79**. Subsequent hydrolysis of the ester group provided desired pyrrole **69**.



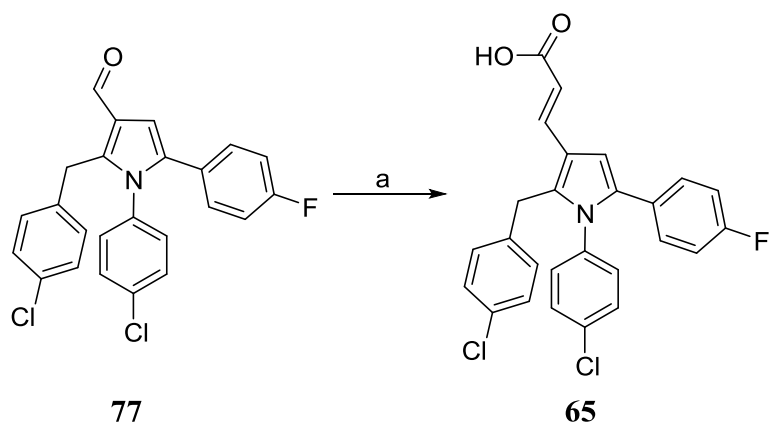
Scheme 5.3: Reagents and Conditions: (a) AcOH, 170 °C μ W, 10 min, 50%; (b) NaOH, THF, MeOH, H₂O, 75 °C, 18 h, 70%.

The synthesis of di-carboxylic acid compound **64** started with the formylation of intermediate **75** using Vilsmeier-Haack conditions (Scheme 5.4). Pinnick oxidation of aldehyde **80** provided mono-carboxylic acid **81**. Subsequent hydrolysis provided desired di-carboxylic acid **64**.



Scheme 5.4: Reagents and conditions: (a) POCl₃, DMF, 70 °C, 4 h, 71%; (b) NaClO₂, sulfamic acid, MeCN, H₂O, r.t., 2 h, quant.; (c) NaOH, MeOH, H₂O, reflux, 4 h, 97%.

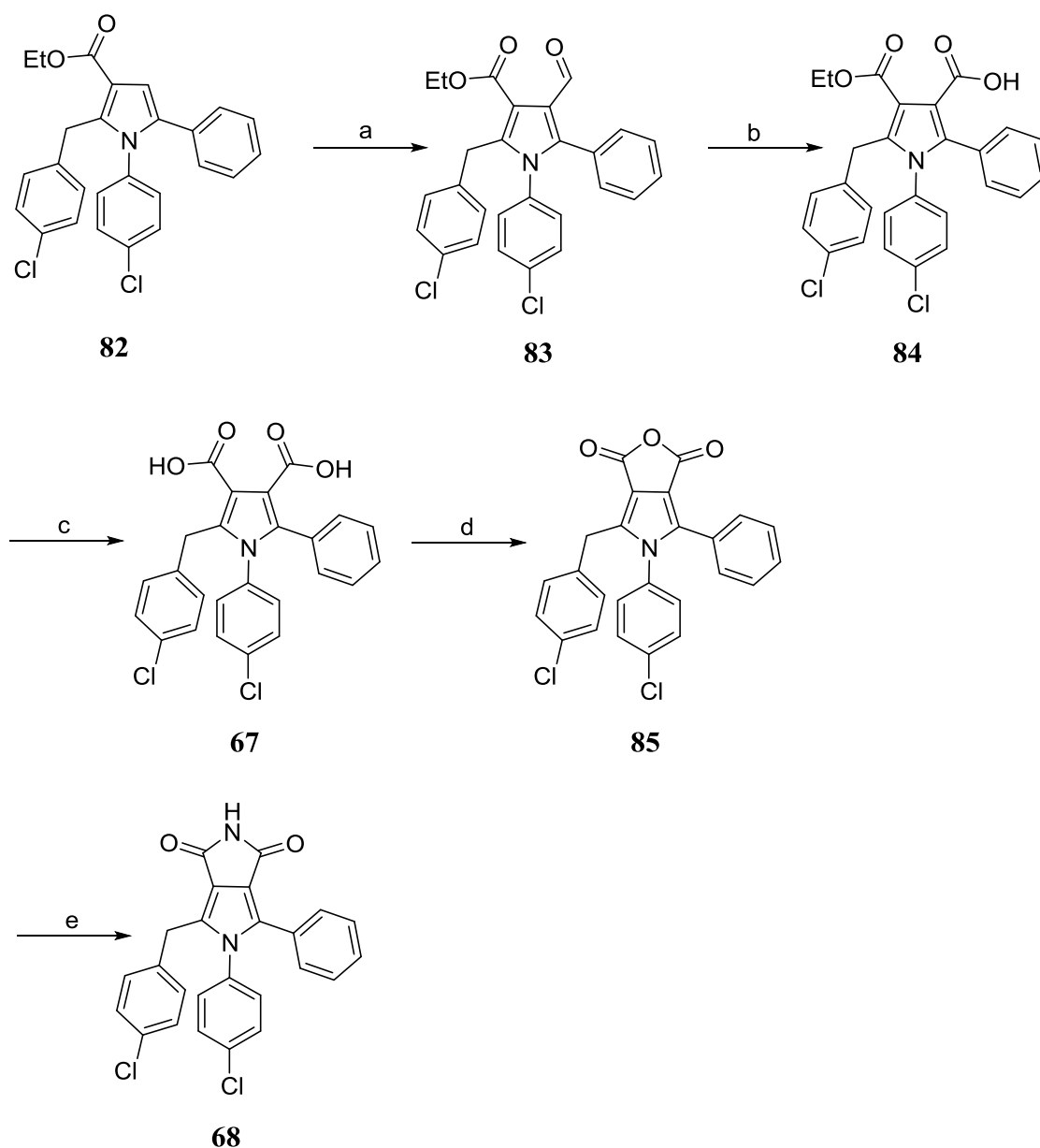
Compound **65** was synthesised by the condensation of aldehyde **77** and malonic acid using pyridine and piperidine (Scheme 5.5).



Scheme 5.5: Reagents and Conditions: (a) malonic acid, pyridine, piperidine, reflux, 2.5 h, 75%.

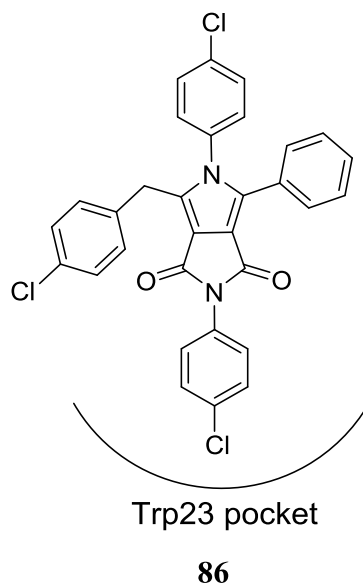
5.2.2 Synthesis of pyrroles with succinimide ring at the 3/4-position

Compound **68** was synthesised following a five step reaction sequence starting from intermediate **82** (Scheme 5.6). Di-carboxylic acid **67** was synthesised using the previously described chemistry. Acetic anhydride mediated ring closure afforded compound **85**. Nucleophilic attack of ammonia on anhydride **85** opens the ring producing an intermediate amide, which was converted to succinimide **68** upon thionyl chloride-mediated ring closure.

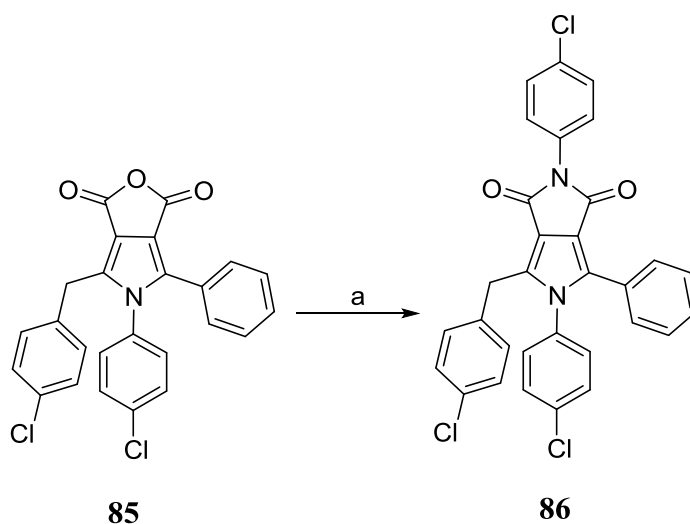


Scheme 5.6: Reagents and conditions: (a) POCl₃, DMF, 70 °C, 4 h, quant.; (b) NaClO₂, sulfamic acid, MeCN, H₂O, r.t., 2 h, 62%; (c) NaOH, MeOH, H₂O, reflux, 4 h, quant.; (d) Ac₂O, reflux, 2 h, 82%; (e) (i) NH₃, AcOH, 120 °C μW, 30 min; (ii) SOCl₂, THF, r.t., 1.5 h, 62%.

In order to examine the versatility of the reaction scheme, compound **86** was synthesised. Compound **86** has a 4-chlorophenyl ring at the N^1 -position of the succinimide ring that could flip the binding mode of the molecule such that the 4-chlorophenyl ring at the N^1 -position the succinimide ring would occupy the Trp23 pocket in MDMX.



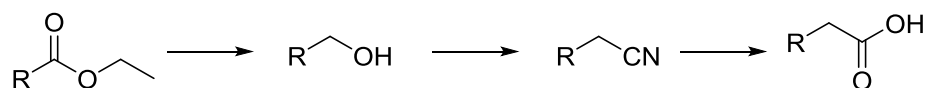
Compound **86** was synthesised in moderate isolated yield from anhydride **85** using 4-chloroaniline as a nucleophile (Scheme 5.7).



Scheme 5.7: *Reagents and Conditions:* (a) (i) 4-chloroaniline, AcOH, 120 °C μ W, 20 min; (ii) SOCl₂, THF, r.t., 18 h, 64%.

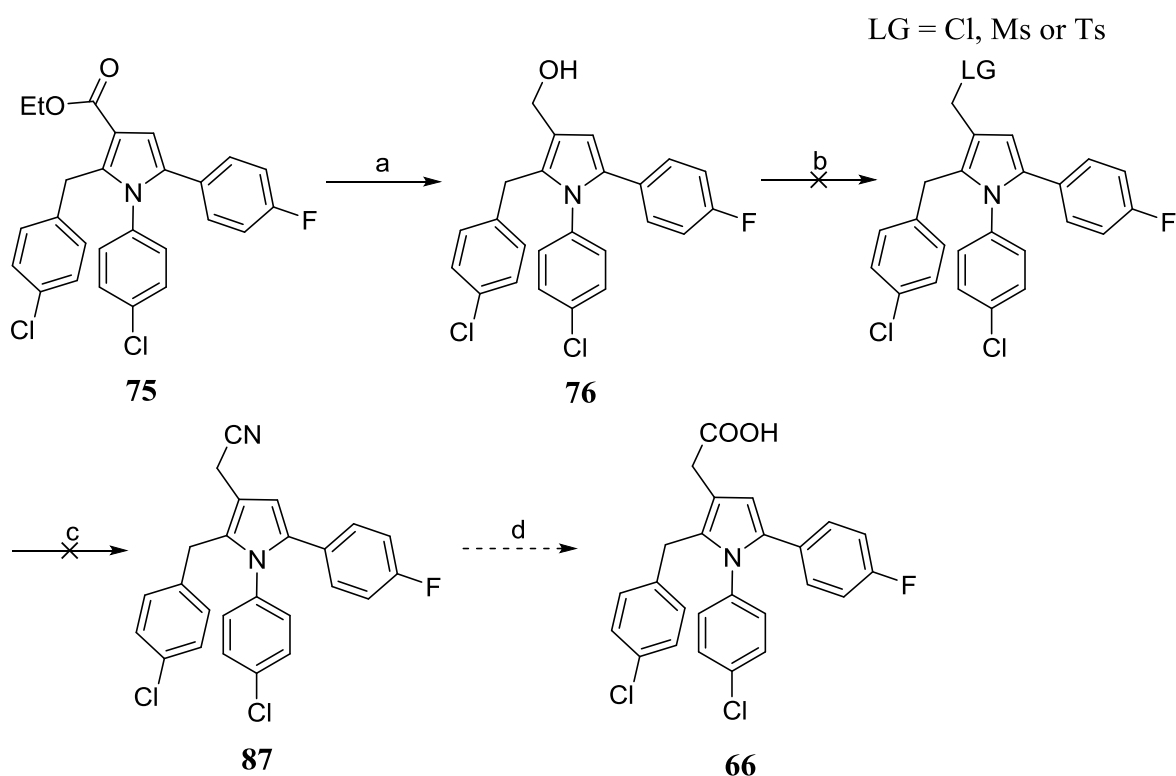
5.2.3 One-Carbon Homologation of 3-Carboxylic Acid

A classical route for one-carbon homologation of a carboxylic acid includes the conversion of the carbonyl compound to nitrile, which can be hydrolysed to get the desired homologated carboxylic acid (Scheme 5.8).



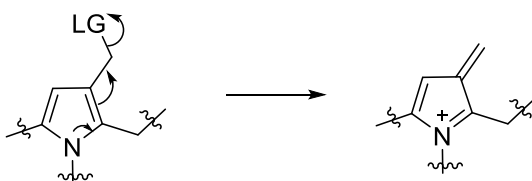
Scheme 5.8: One carbon homologation *via* nitrile.

Synthesis of homologated carboxylic acid analogue **66** started with the reduction of ester **75** to alcohol **76**. Conversion of alcohol **76** to nitrile **87** proved to be extremely challenging. Initial attempts to convert the alcohol group of **76** to a leaving group (LG) such as chloro, mesyl or tosyl resulted in a mixture of unidentified products.



Scheme 5.9: Reagents and conditions: (a) DIBAL, DCM, 0 °C, 2 h. (95%)

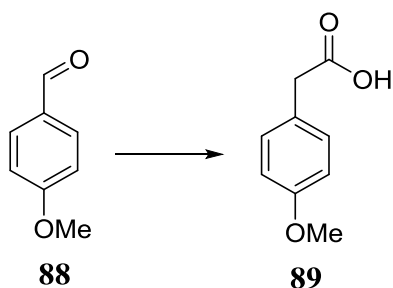
It was proposed that in the presence of a good leaving group, the lone pair of nitrogen pushes the electron density, eliminates the leaving group producing a reactive electrophile, which can be involved in unwanted side-reactions (Scheme 5.10).



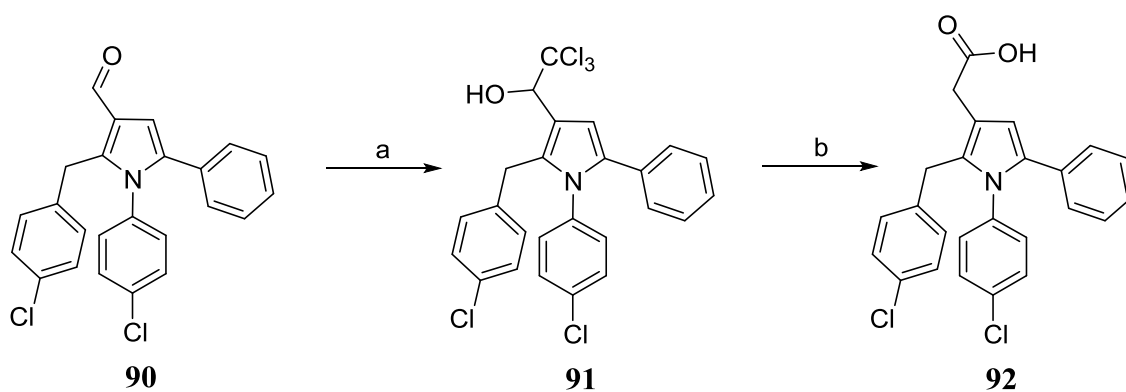
Scheme 5.10: Proposed mechanism for the formation of a reactive electrophile.

Simply heating alcohol **76** with various cyanide sources like $\text{Et}_4\text{N}^+\text{CN}^-$, NaCN , and TMSCN did not produce any reaction. Cheng *et al* have described the direct conversion of alcohols to nitriles using TMSCN and catalytic InBr_3 .⁹⁹ The reaction was attempted, but a complex mixture of products was obtained.

Cafiero *et al* has reported one-carbon homologation *via* an aldehyde.¹⁰⁰ One of the examples in the paper was aldehyde **88**, which has very similar electronic character to the pyrrole scaffold. The oxygen lone pair in methoxy group of compound **89** can push electron density, similar to the nitrogen of pyrroles (Scheme 5.10).



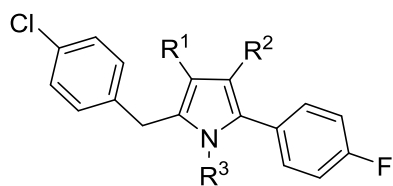
The procedure described by Cafiero *et al* (Scheme 5.11) was used for the synthesis of the one-carbon homologated carboxylic acid **92**.¹⁰⁰ The aldehyde **90** was trichloromethylated to afford compound **91**, which under sodium borohydride and diphenyldiselenide and sodium hydroxide provided desired acid **92** in good isolated yield. The diphenyldiselenide was important in the reaction. The reaction in the absence of diphenyldiselenide gave alcohol. Final compound **92** does not contain fluorine because it was identified simultaneously that the fluorine was not essential for potency (discussed in detail in next chapter).

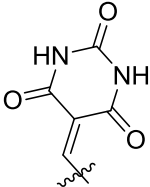
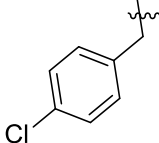


Scheme 5.11: Reagents and conditions: (a) (i) CHCl_3 , DMF, $-10\text{ }^\circ\text{C}$, 15 min; (ii) KOH, MeOH, $-10\text{ }^\circ\text{C}$, 3 h, 64%; (b) $(\text{PhSe})_2$, NaBH_4 , NaOH, EtOH, r.t., 24 h, 90%.

5.3 Biological Evaluation

Compounds along with the intermediates obtained during the synthesis were analysed by ELISA (Table 5.1). Compounds **76** and **80** without any acidic groups showed a significant loss in potency, suggesting that an acidic group at 3- or 4-position of pyrroles is essential for activity. Compound **81** with an acidic group as well as an ester group showed a reduction in potency against MDMX; however acidic groups at both 3- and 4-positions in compound **64** were tolerated. Interestingly, compound **69** with a CH_2 linker at the N^1 -position was at least 10-fold more potent against MDM2 than MDMX. A crystal structure of compound **69** in complex with MDMX would be beneficial to understand the selectivity observed.

Table 5.1: Results of the ELISA for tetra- and penta-substituted pyrrole derivatives.

Compound	R ¹	R ²	R ³	MDM2 IC ₅₀ (μM) ^a	MDMX IC ₅₀ (μM) ^a
2	COOH	H	4-ClC ₆ H ₄	11 ^b	15 ^c
63		H	4-ClC ₆ H ₄	3.5	4.5
69	COOH	H		4.9	53
80	COOEt	CHO	4-ClC ₆ H ₄	> 200	187
81	COOEt	COOH	4-ClC ₆ H ₄	15.8	55.9
64	COOH	COOH	4-ClC ₆ H ₄	8.1	13.4
76	CH ₂ OH	H	4-ClC ₆ H ₄	> 200	> 200

^a Determinations (n = 1 unless otherwise stated; ^b n = 2; ^c n = 3)

Before the biological evaluation of homologated carboxylic acid compounds **65** and **92**, the antibody used in the MDMX-ELISA was withdrawn from the market. Therefore, it was decided to develop an alternate Homogenous Time Resolved FRET (HTRF) assay (Chapter 8).

Chapter 6. SAR Studies around the Phenyl Rings at 2 and 5-Positions

6.1 Rationale

The docking studies with compound **30** suggested that there is not enough space (highlighted by red arrow in Figure 6.1) to accommodate any atoms in the *para*-position of the phenyl ring into the Leu26 pocket of MDMX.

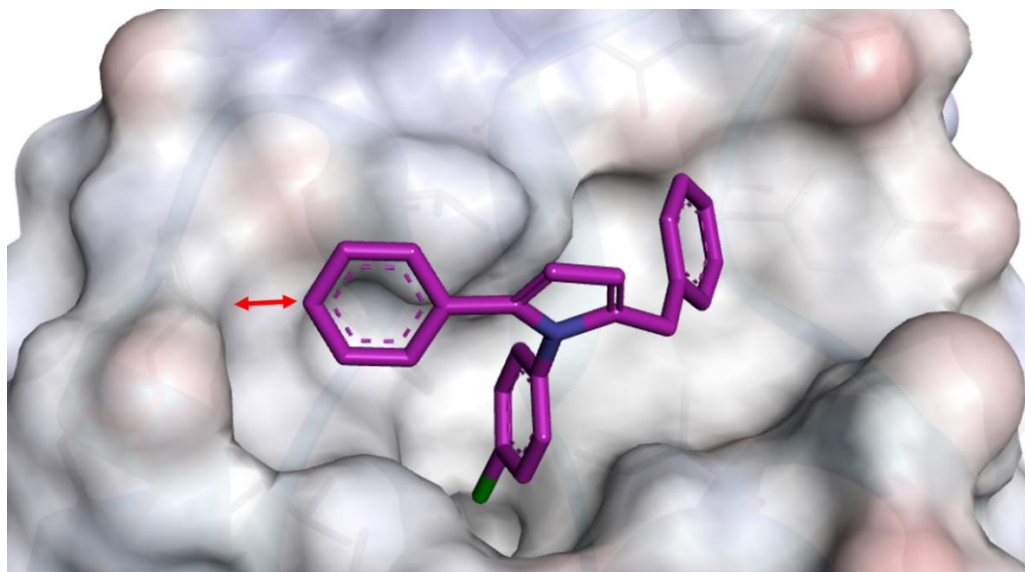
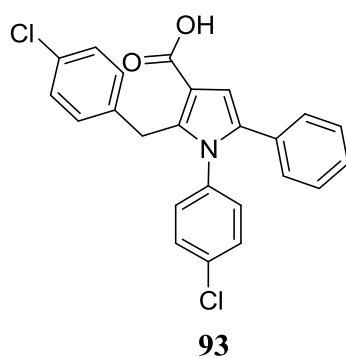


Figure 6.1: Compound **30** (carbons: magenta) docked on the binding site of MDMX (PDB: 3DAC) using Molecular Operating Environment (MOE) software. The binding surface is coloured based on the charge of the amino acid residue; positive: blue, negative: red. The space between the phenyl ring and Leu26 pocket is highlighted by a red arrow.

The role of the fluoro group from the *para* position of **2** was investigated, and compound **93** was designed.



The docking studies with compound **30** also suggested that the phenyl ring in the 5-position was close to the oxygen of Gln68 (Figure 6.2). It was postulated that an electron donating group might interact with Gln68 improving the potency.

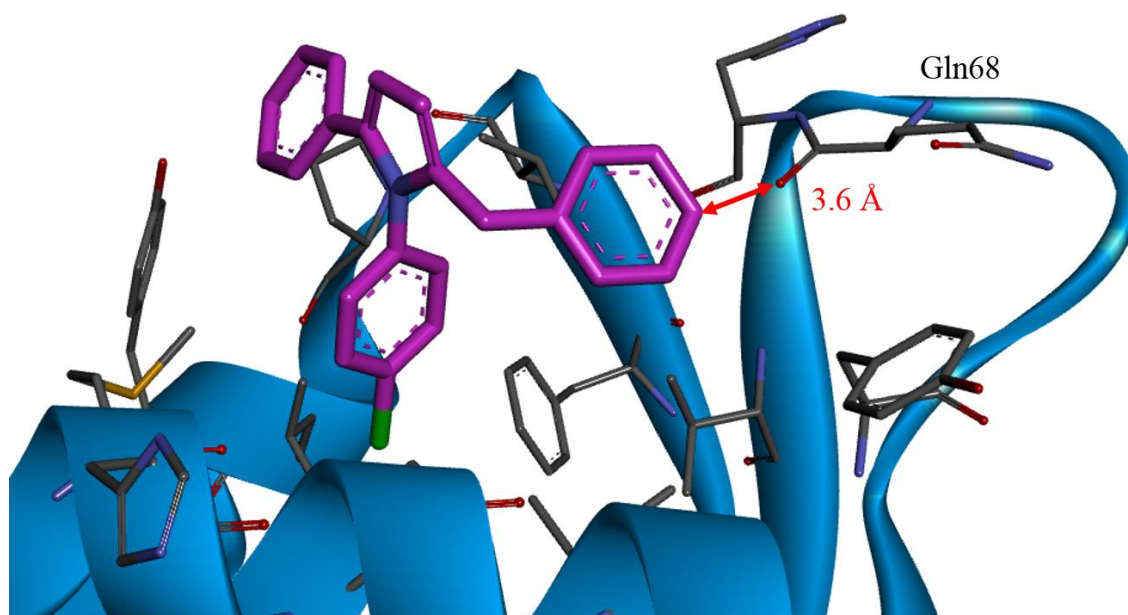
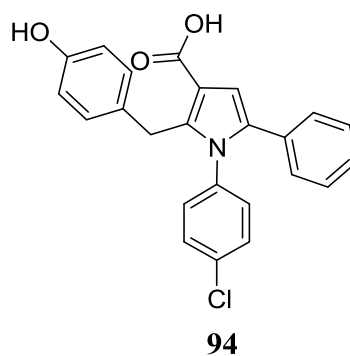


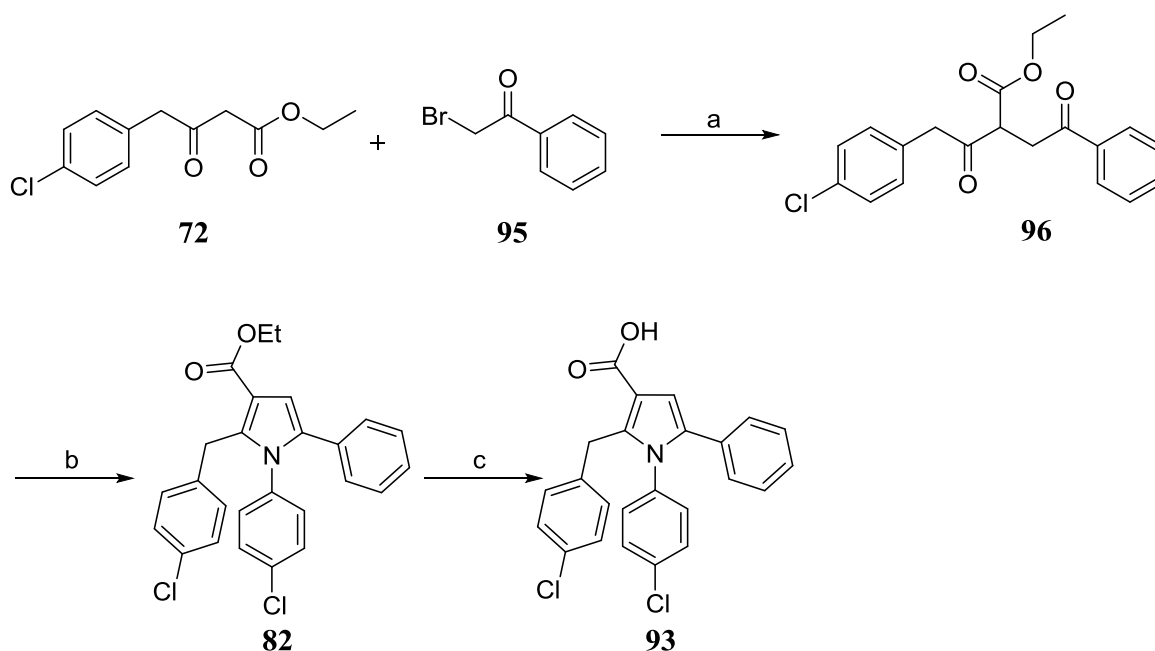
Figure 6.2: Compound **30** (carbons: magenta) docked on the binding site of MDMX using Molecular Operating Environment (MOE) software. The secondary structure of MDMX is coloured green. The carbons of key amino acids in the binding site are coloured grey. The red arrow highlights the distance between the phenyl ring and Gln68.

Compound **94** was designed replacing the chloro group with a hydroxyl group that might provide an H-bond interaction with Gln68. In addition, the hydroxyl group also reduced the lipophilicity of the molecule.



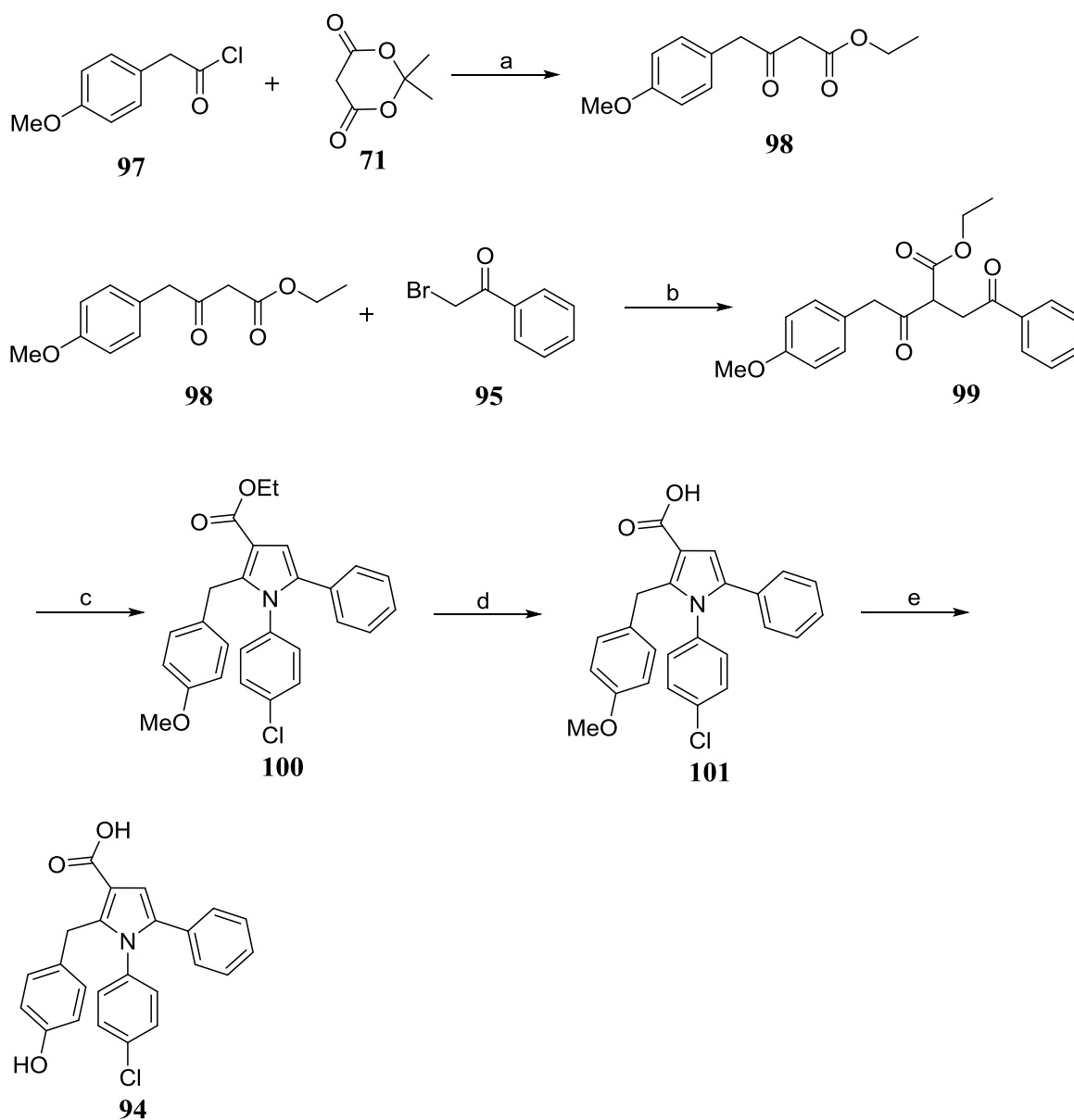
6.2 Synthesis

Compound **93** was synthesised using the previously described chemistry (Scheme 6.1). β -Keto ester was synthesised using acid chloride **70** and Meldrum's acid **71** (Scheme 5.1). The nucleophilic attack of the enolate of β -keto ester **72** on compound **95** afforded desired 1,4-diketone **96** in good isolated yield. The Paal-Knorr pyrrole synthesis using 4-chloroaniline provided pyrrole **82**, which was hydrolysed to desired pyrrole **93**.



Scheme 6.1: Reagents and Conditions: (a) NaH, THF, r.t., 2.5 h, 79%; (b) 4-chloroaniline, AcOH, 170 °C μ W, 10 min, 73%; (c) NaOH, MeOH, H₂O, 65 °C, 24 h, 98%.

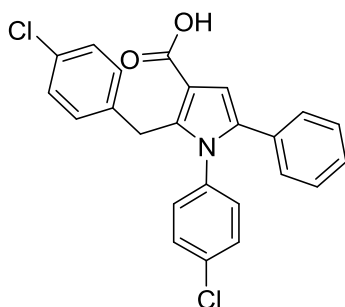
Similarly, compound **94** was synthesised following a five step reaction sequence (Scheme 6.2). The synthesis started with the formation of β -keto ester **98** from the commercially available acid chloride **97** and Meldrum's acid **71**. Following the chemistry described before, compound **101** was obtained. Finally, BBr₃-mediated removal of methyl group from compound **101** afforded desired target **94** in good isolated yield.



Scheme 6.2: Reagents and conditions: (a) (i) pyridine, DCM, 0 °C, 1 h, then r.t., 2.5 h; (ii) EtOH, reflux, 2 h, then r.t., 16 h, 72% over 2 steps; (b) NaH, THF, r.t., 2.5 h, 76%; (c) 4-chloroaniline, AcOH, 170 °C μ W, 10 min, 75%; (d) NaOH, MeOH, H₂O, 65 °C, 24 h, quant.; (e) BBr₃, DCM, 0 °C, 1 h, 88%.

6.3 Biological Evaluation

Compound **93**, retained the potency suggesting that the fluoro group at the *para*-position was not important for the inhibition of MDMX-p53 interaction.



93

MDM2 IC₅₀ = 15 μM

MDMX IC₅₀ = 8 μM

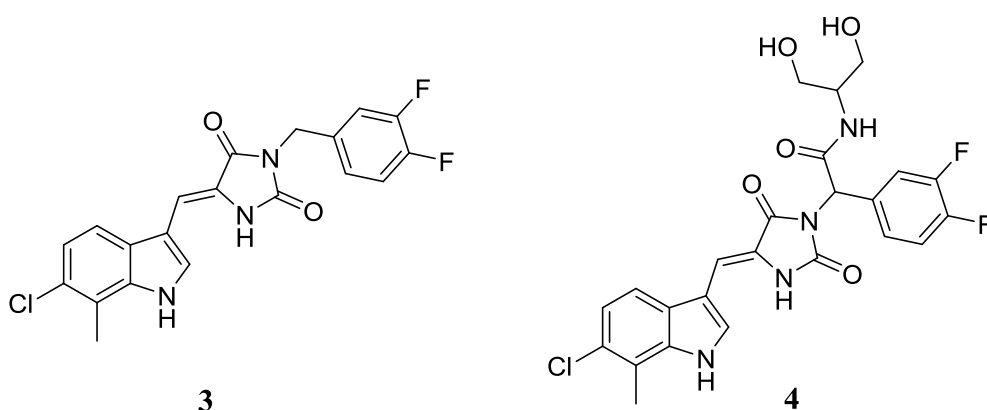
As mentioned in the last chapter, before the biological evaluation of compounds **94**, the antibody used in the MDMX-ELISA was withdrawn from the market. Therefore, it was decided to develop an alternate Homogenous Time Resolved FRET (HTRF) assay (Chapter 8).

Chapter 7. Synthesis and Biological Evaluation of RO-2443 **3** and RO-5963

4

7.1 Rationale

During the project work, RO-2443 **3** and RO-5963 **4** were the only reported dual small-molecule nanomolar inhibitors of MDM2 and MDMX. Therefore, in order to benchmark the biochemical assay ELISA, which was used for measuring the potency of in-house compounds, it was decided to synthesise RO-2443 **3** and RO-5963 **4**.⁷¹



7.2 Synthesis

7.2.1 Synthesis of RO-2443 **3**

The syntheses of RO-2443 **3** and RO-5963 **4** were not described in the paper by Graves *et al.*⁷¹ Initial retrosynthetic analysis of RO-2443 **3** suggested that the condensation of aldehyde **104** and substituted-hydantoin **107** could provide the desired target (Figure 7.1). The mono-alkylation of hydantoin **105** could be performed by K₂CO₃-mediated procedure reported by Fraile *et al.*¹⁰¹

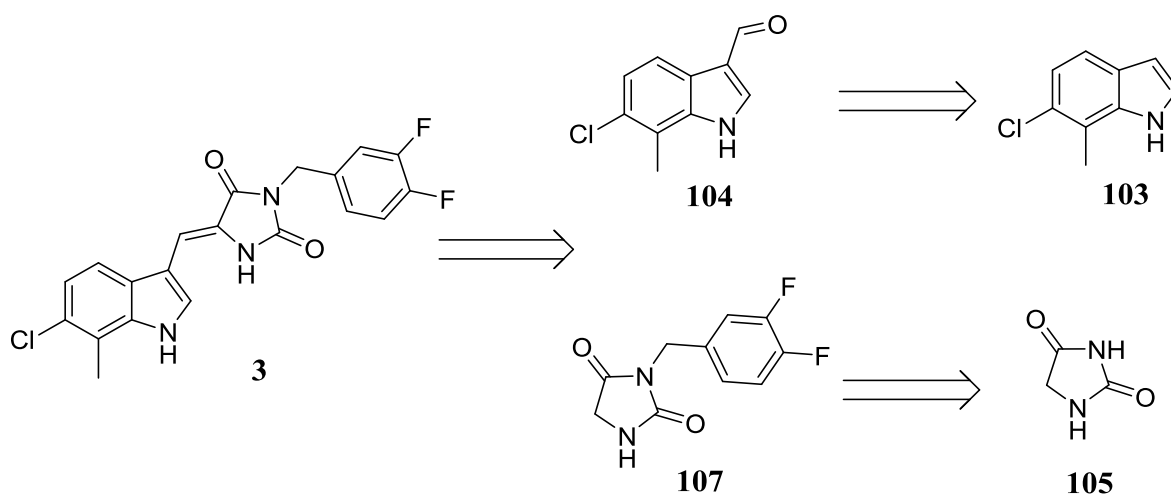
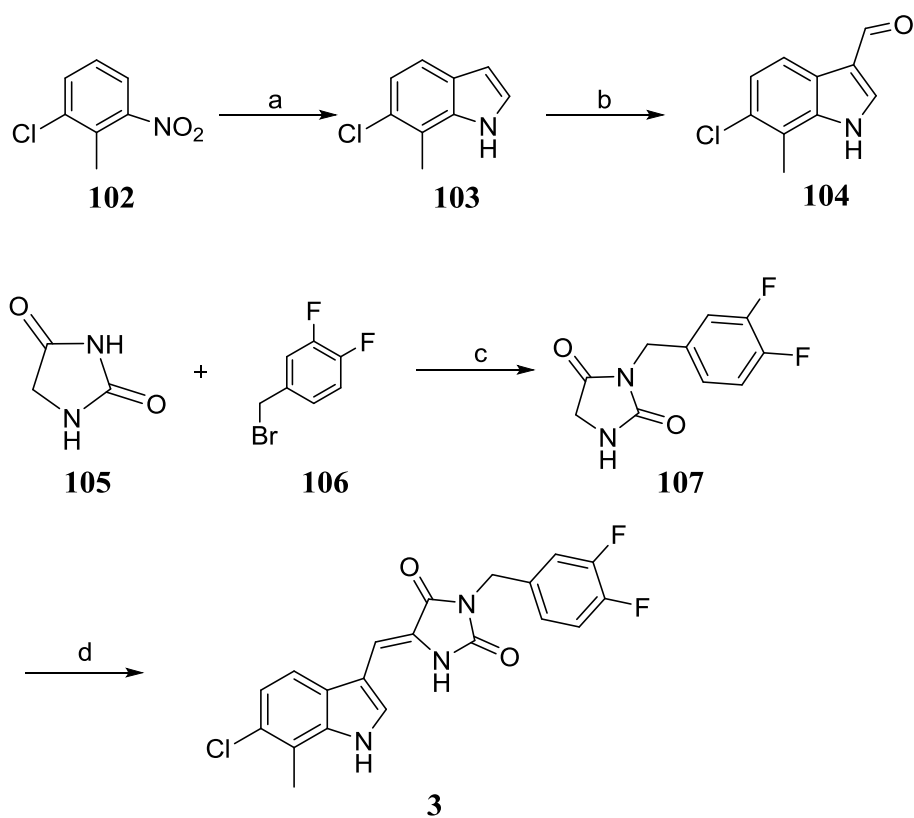


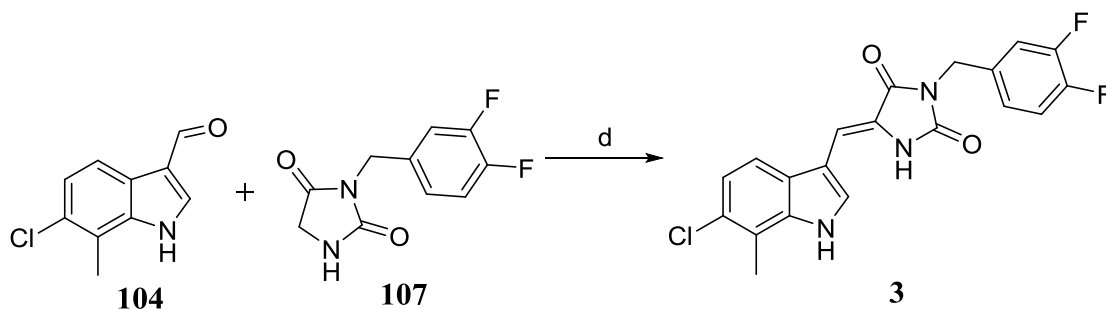
Figure 7.1: Retrosynthetic analysis of RO-2443.

The synthesis started with a Bartoli reaction on 1-chloro-2-methyl-3-nitrobenzene **102** to give indole **103**. Formylation under Vilsmeier-Haack conditions afforded aldehyde **104** in good yield. The monoalkylation of hydantoin **105** was achieved by using K_2CO_3 as a base to afford compound **107**. Di-alkylation was observed when NaH was used. The final condensation reaction with NH_4OAc in acetic acid was not successful. The condensation reaction was attempted with various reagents and conditions (Table 7.1). The desired target **3** was obtained in 24% yield using NH_4OAc in toluene. The best results were obtained with 3 equivalents of piperidine for condensation to give RO-2443 **3** in 92% isolated yield.



Scheme 7.1: Reagent and condition: (a) vinyl magnesium bromide, THF, -40 °C, 1 h, 43%; (b) POCl₃, DMF, 0 °C, then 70 °C μ W, 10 min, 93%; (c) K₂CO₃, CH₃CN, reflux, 6 h; r.t., 16 h, 57%; (d) piperidine, 130 °C, 30 min, 92%.

Table 7.1: Various reagents and conditions used in step d of Scheme 7.1 for the condensation of aldehyde **104** and hydantoin **107**.



Reagent	Solvent	Temperature (°C)	Time	Result
NH ₄ OAc	AcOH	180 μW	30 min	Complex mixture of products
NH ₄ OAc	Toluene	200 μW	30 min	24% isolated yield
NH ₄ OAc	DME	100 μW	30 min	Complex mixture of products
NH ₄ OAc	MeCN	100 μW	30 min	Complex mixture of products
Piperidine (excess)	-	Reflux	24 h	Complex mixture of products
Piperidine (3 eq)	-	Reflux	30 min	92 % yield

7.2.2 X-ray structure of RO-2443 **3**

A small molecule X-ray crystal structure of RO-2443 **3** was obtained (Figure 7.2). The torsion angle between the bond formed by C8 and C9 and the bond formed by C10 and C11 is 0.4° which suggests that the indolylhydantoin moiety is planar. The crystal structure, along with NMR and HRMS data confirmed that the compound synthesised was RO-2443 **3**.

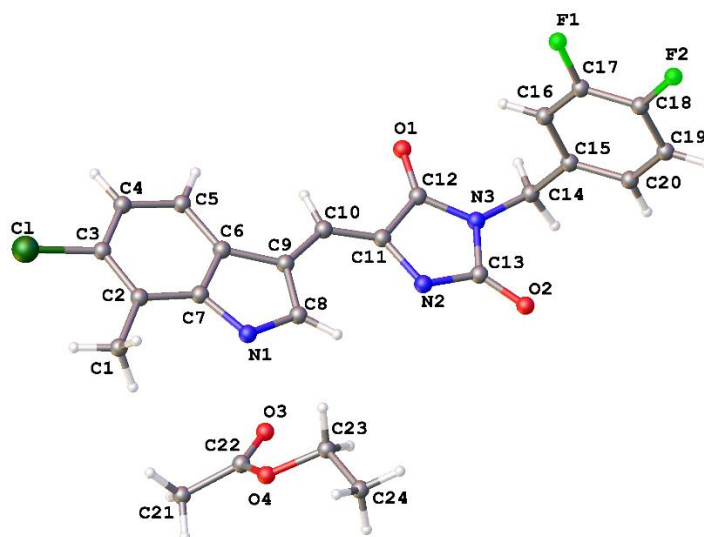


Figure 7.2: Crystal structure of RO-2443 **3**. Atoms are coloured as: carbon: grey, oxygen: red, nitrogen: blue, hydrogen: white; chlorine: green.

7.2.3 Synthesis of RO-5963 **4**

Initial retrosynthetic analysis of RO-5963 **4** suggested that the nucleophilic substitution reaction using indolyldantoin **118** and bromo-derivative **110** would provide the desired target (Figure 7.3). Indolyldantoin **118** could be prepared using the chemistry described for the synthesis of RO-2443 **3**. The bromo-compound **110** could be synthesised *via* the amide coupling of carboxylic acid **109** and 2-aminopropane-1,3-diol **112**.

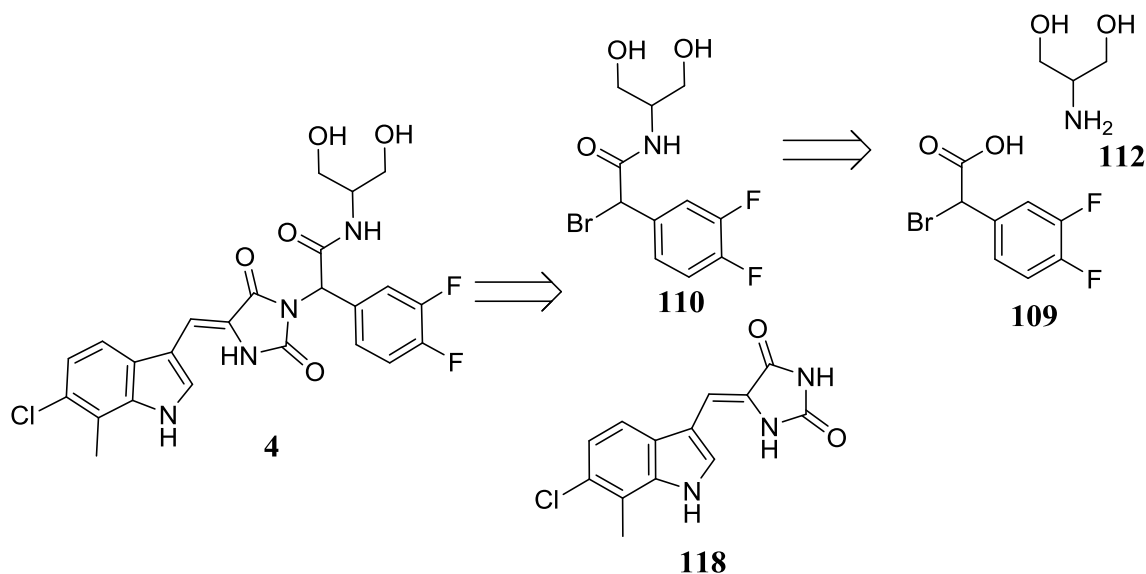
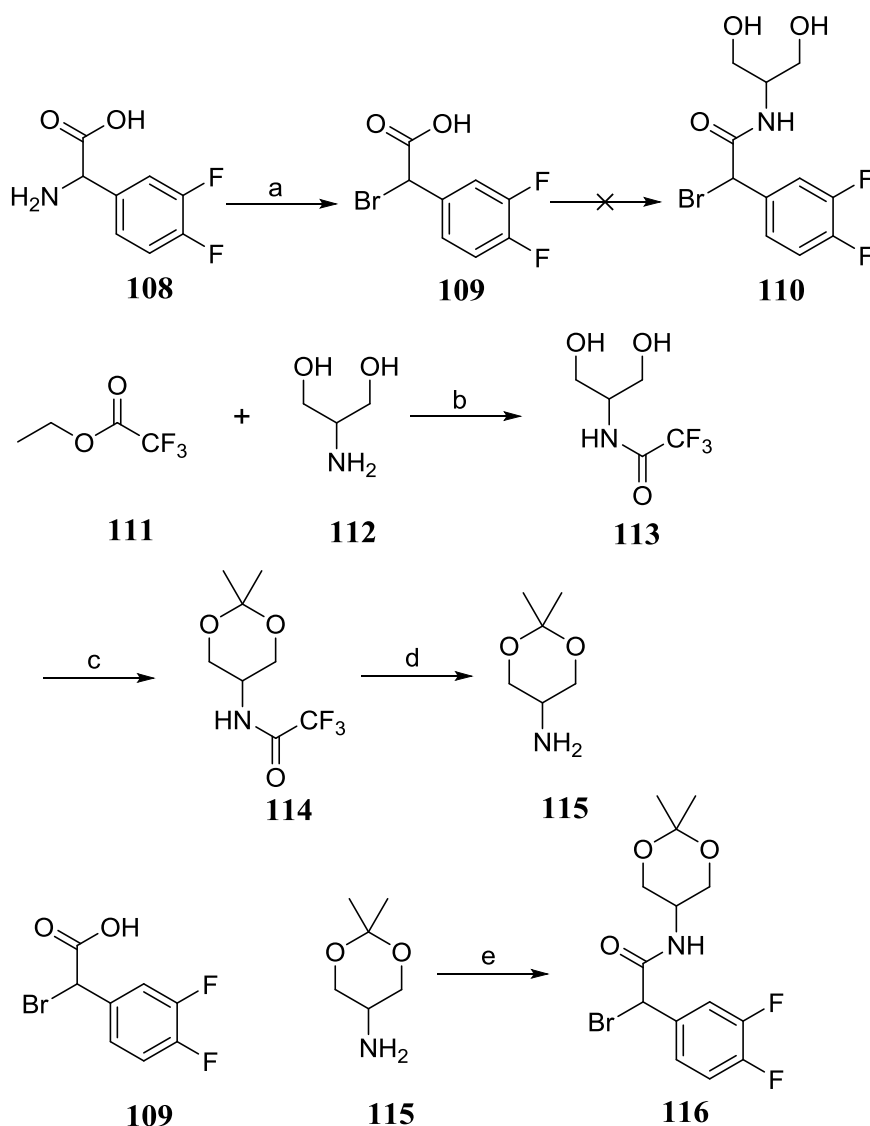


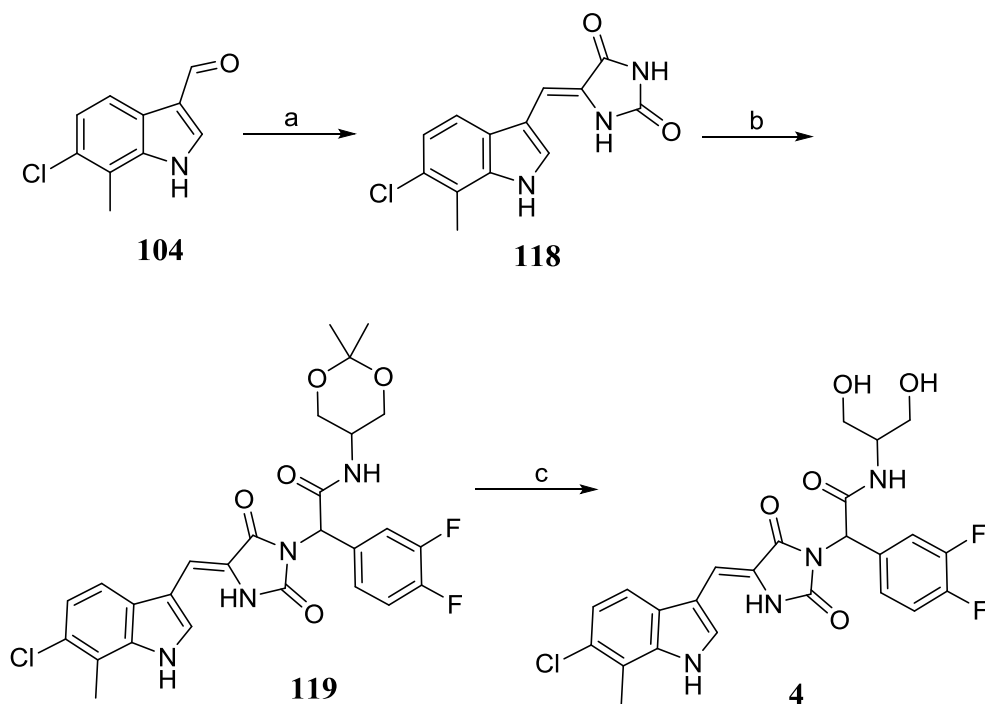
Figure 7.3: Retrosynthetic analysis of RO-5963 **4**.

The synthesis of RO-5963 **4** started with the preparation of bromo-compound **110** (Scheme 7.2). 3,4-Difluorophenylglycine **108**, was brominated *via* the formation of the diazonium salt, followed by a nucleophilic attack with bromide. The amide coupling of carboxylic acid **109** and 2-aminopropane-1,3-diol **112** in presence of DIC and EDC was unsuccessful. Therefore, it was decided to protect the diol. The amine group of 2-aminopropane-1,3-diol **112** was protected as a trifluoroacetate **113**. Subsequently, acetal protection afforded compound **114**. Finally, the trifluoroacetyl group was removed using LiOH to liberate the free amine **115**, which was used for amide coupling with carboxylic acid **109** to afford compound **116**.



Scheme 7.2: Reagents and condition: (a) HBr, KBr, NaNO₂, H₂O, 0 °C-r.t., 3 h, 36%; (b) THF, r.t., 48 h, 98%; (c) 2,2-dimethoxypropane, camphor-10-sulfonic acid, DCM, r.t., 96 h, 54%; (d) LiOH, THF, H₂O, r.t., 1.5 h, 54%; (e) DIC, DMAP, DCM, 0 °C-r.t., 16 h, 79%.

Condensation of aldehyde **104** with hydantoin afforded indolyldhydantoin **118** (Figure 7.3). The nucleophilic substitution reaction with indolyldhydantoin **118** and bromo-compound **116** was very slow, and desired product **119** was obtained in poor yield. Acid-catalysed acetal deprotection afforded RO-5963 **4**. Although, the scheme was low yielding in a few steps, the reactions were reproducible and was successfully repeated by a colleague (Dr Stephanie Myers).



Scheme 7.3: Reagents and condition: (a) hydantoin, piperidine, 130 °C, 1 h, 86%; (b) **116**, K₂CO₃, DMF, r.t., 96 h, 17%; (c) HCl, THF, H₂O, 0 °C-r.t., 3 h, 36%.

7.3 Biological Evaluation

Upon the biochemical evaluation by ELISA, RO-2443 **3** and RO-5963 **4** were at least 1000 fold less potent compared to the HTRF values reported by Graves *et al* (Table 7.2).⁷¹

Table 7.2: Comparison of the reported HTRF assay and in-house ELISA assay.

Compounds	Published HTRF IC ₅₀ (μM)		In-house ELISA IC ₅₀ (μM) ^a	
	MDM2	MDMX	MDM2	MDMX
RO-2443 3	0.033	0.041	7 ^c	14 ^d
RO-5963 4	0.019	0.024	17 ^b	20 ^b

^a Determinations (n = 1 unless otherwise stated);

^b n = 2; ^c n = 3; ^d n = 4

Although, the potencies of RO-2443 and RO-5963 were significantly lower in NCL-ELISA, the cellular data were in line with the published results. RO-2443 **3** and RO-5963 **4** were potent in MDMX overexpressing cell lines JEG3 and MCF-7. Although less potent, the compounds also exhibited growth inhibition in MDM2 overexpressing cell line SJSA-1. Therefore, in order to develop an alternative assay, a structural biology placement was undertaken (Chapter 8).

Chapter 8. MDM2 and MDMX Structural Biology

8.1 Aims

Although MDM2 and MDMX have high sequence homology, most of the small molecule MDM2 inhibitors show significantly lower binding affinity towards MDMX.^{70, 102-103} An extensive SAR on four different series (benzenoids, thiazoles, pyrroles and isoindolinones) did not produce any low nanomolar inhibitors of the MDMX-p53 interaction.^{92, 104-105} To guide rational drug design, a co-crystal structure of a small molecule bound to MDMX was essential.

To date, co-crystal structures of only two small molecules bound to MDMX have been reported. Compound WK298 **22** with low micromolar potency against MDMX is the first small molecule for which a structure bound to MDMX has been reported.⁸⁶ The co-crystal structure of WK-298 **22** bound to MDMX revealed many key features which are important for designing small molecule inhibitors of MDMX (Figure 8.1). The chloro-indole substituent binds in the Trp23 pocket. The nitrogen atom of the indole forms a hydrogen bond with Met53 in MDMX. The chlorine atom in the indole ring induces a conformational change in key residues including Leu54, Met53, Leu98 and Leu102 which helps to enlarge the Trp23 binding pocket. The phenyl ring occupies the Phe19 pocket and the chlorobenzyl group occupies a Leu23 pocket.

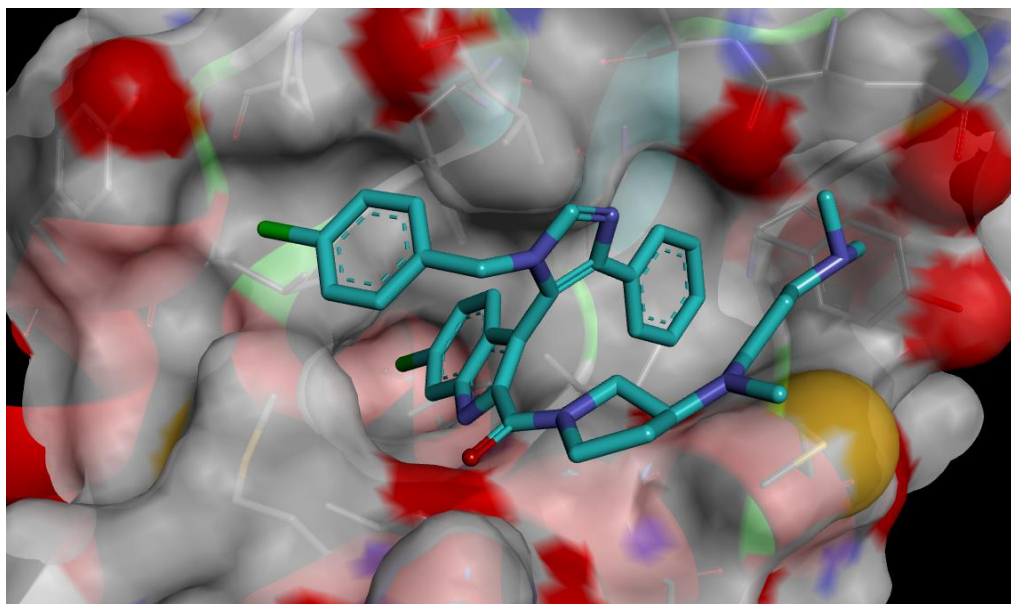


Figure 8.1: The X-ray co-crystal structure of WK-298 **22** bound to MDMX. WK-298 **22** is drawn in skeleton mode with carbon, nitrogen, oxygen and chlorine atoms coloured cyan, blue and red and green, respectively. The solvent accessible surface of MDMX (probe radius 1.5 Å) around WK-298 **22** is coloured based on the atoms; carbon: grey, oxygen: red, nitrogen blue, sulphur: yellow. The structure is taken from PDB code: 3LBJ.

Compound RO-2443 **3** developed by Roche is the other small molecule for which a co-crystal structure with MDMX has been reported and it is a potent inhibitor of MDMX with an IC_{50} of 41 nM.⁷¹ The compound interacts with MDM2 and MDMX by dimerization avoiding the challenging Leu26 pocket in both MDM2 and MDMX (Figure 8.2). The compound contains an indolyldihydroantoin and difluorophenyl groups. The indolyldihydroantoin moiety occupies the Phe19 pocket in one monomer of MDMX, and the difluorophenyl moiety occupies the Trp23 pocket of the other monomer of MDMX. The molecules also form aromatic stacking interactions between two indolyldihydroantoin moieties and two tyrosine residues from two MDMX monomers to generate a four level π -sandwich. The other key interaction is between the σ -hole of the chlorine substituent of one monomer of the small molecule with difluorophenyl ring of the other monomer of the small molecule. This interaction along with the aromatic stacking interaction helps in the dimerization of small molecule as well as MDMX protein.

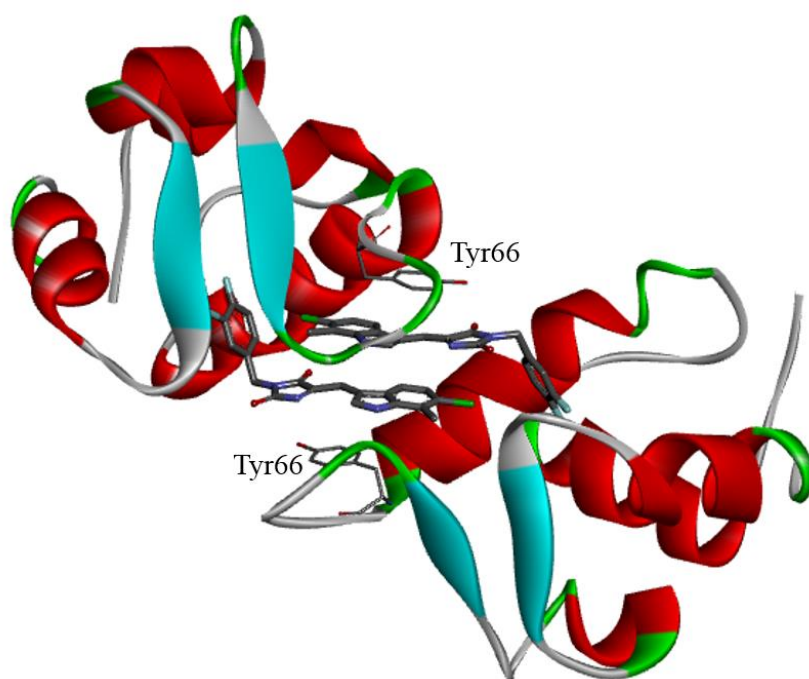


Figure 8.2: Co-crystal structure of RO-2443 **3** bound to MDMX. MDMX dimers are represented as ribbons and coloured based on secondary structure: helices are red, beta sheets are cyan, turns are green, and coils are white. Two molecules of RO-2443 **3** and two tyrosine residues from two MDMX monomers form a four level π -sandwich. The four-level sandwich is visible in this view holding the two MDMX molecules together. The chlorine atom is labelled green which forms an interaction via its σ -hole with the difluorophenyl ring of the other monomer of RO-2443 **3**. The structure is taken from PDB code: 3U15.

Due to the unique nature of the RO-2443 **3** binding mode, the key features of the crystal structure could not help rational drug design of the compound series developed at Newcastle. Therefore, a co-crystal structure of a small molecule inhibitor developed at Newcastle bound to MDMX would be valuable. To attempt to achieve this aim, a 5-month placement in structural biology at the Northern Institute for Cancer Research was completed.

8.2 Expression and Purification of MDM2 and MDMX

Three different constructs of MDM2 and MDMX encoding the N-terminal p53-binding domain were selected for co-crystallisation trials. This selection was based on the literature data as well as successes in protein expression experienced in-house.^{71, 86, 104-106} The constructs expressed and purified for co-crystallisation trials are listed in Table 8.1.

Table 8.1: Constructs of MDMX and MDM2 used for co-crystallisation trials.

Protein	Construct	Amino acid range	Mutations
MDMX	1	18-111	-
MDMX	2	22-111	-
MDMX	3	26-111	-
MDM2	1	17-125	K51A
MDM2	2	17-109	E69A/K70A
MDM2	3	17-125	E69A/K70A

The pre-cloned DNA coding for each construct of MDMX and MDM2 were inserted into the pGEX-6P-1 vector and expressed in *E. coli* Rosetta(DE3)pLys S and BL21(DE3) pLys S strains, respectively.

The pGEX-6P-1 plasmid contains several genes essential for the expression of the desired protein. The plasmid possesses genes encoding for ampicillin resistance, a glutathione-S-

transferase (GST) tag, a 3C viral protease cleavage site and the *lac* operon (Figure 8.3). The expression of N-GST tagged MDM2 and MDMX was induced by the addition of IPTG (isopropyl β -D-1-thiogalactopyranoside).

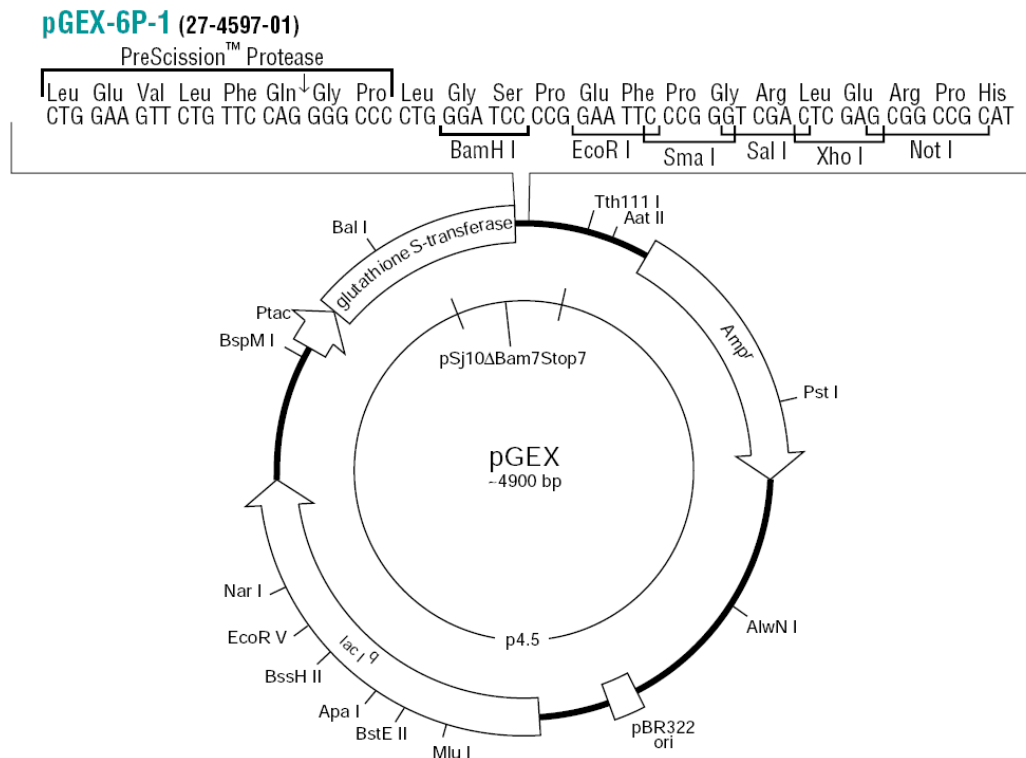


Figure 8.3: Map of the pGEX-6P-1 expression vector. The vector map shows the positions for the genes encoding ampicillin resistance (Amp^r), the GST protein tag, the cleavage codon (PreScissionTM Protease) and the *lac* operon (*lac* 1^q).¹⁰⁷

The expressed proteins were first purified by the addition of lysozyme, DNase and RNase followed by sonication and centrifugation. The addition of these three enzymes and sonication lyses the *E. coli* cells and subsequent centrifugation separates insoluble cell debris from soluble proteins, which include MDM2 or MDMX. To separate N-GST tagged MDMX or MDM2 from other undesired proteins, the supernatant obtained after centrifugation was incubated with glutathione-agarose and washed with mHBS buffer, pH 7.4 containing glutathione. SDS-PAGE analysis of the soluble cell lysate and the eluate from the glutathione column (Figure 8.4, lanes 2-7) confirmed the expression and purification of N-GST tagged MDMX or MDM2. Subsequent incubation with 3C protease successfully cleaved the GST tag from MDMX and MDM2 (Figure 8.4, lanes 8-10).

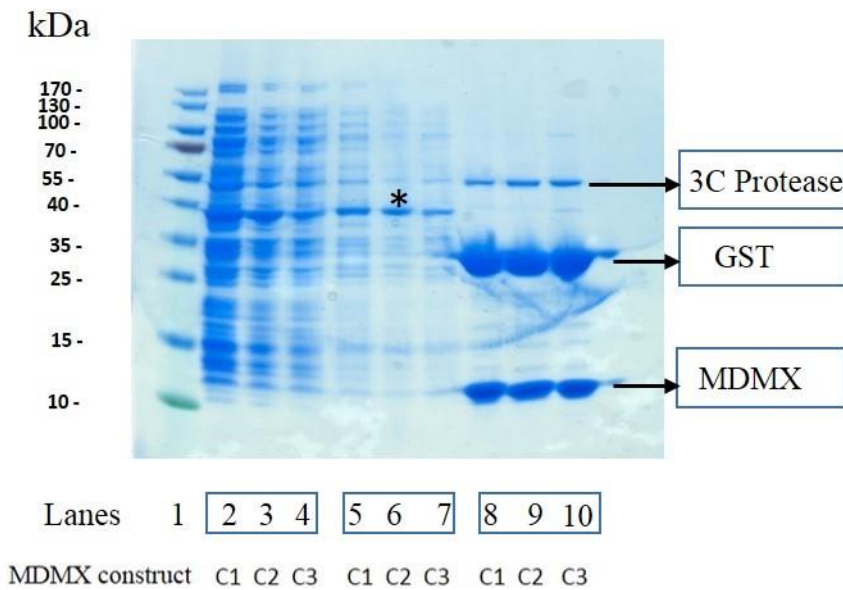


Figure 8.4: Purification of MDMX. SDS-PAGE (12% acrylamide) analysis of MDMX constructs 1, 2 and 3 at various stages during purification. Lanes 2-4, soluble cell lysate; lanes 5-7, glutathione elution; lanes 8-10, proteins post 3C digestion. Molecular weight markers, lane 1, uncleaved GST-MDMX (xkDa) is identified by a star.

The protein fractions containing MDMX obtained after elution from the glutathione column with mHBS buffer, pH 7.4 containing glutathione were pooled and incubated with 3C protease to cleave the GST tag from the desired protein. The protein was purified by size exclusion chromatography to separate the GST tag (Figure 8.5A). SDS-PAGE analysis of selected fractions confirmed the purity of the protein (Figure 8.5B). The pure protein fractions were concentrated by ultrafiltration and stored at -80 °C.

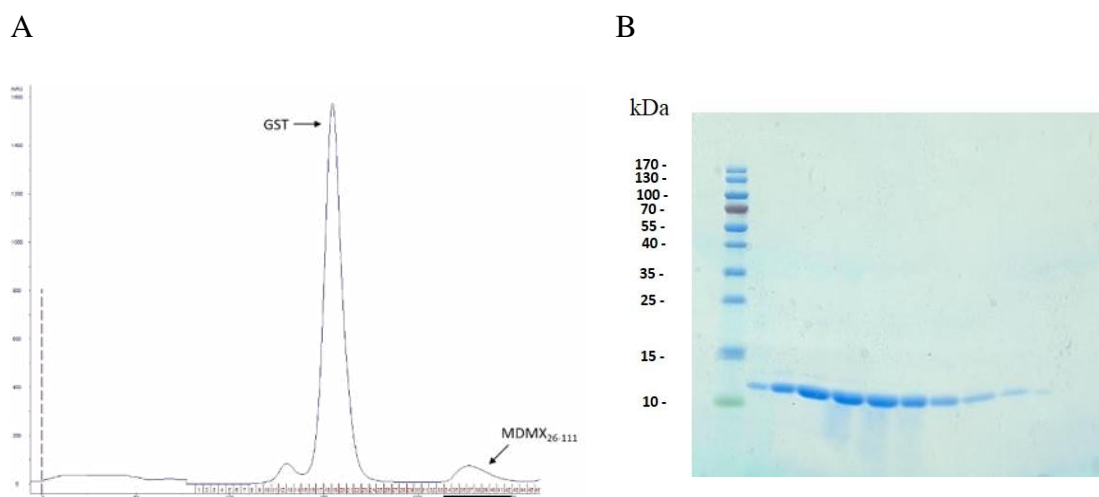
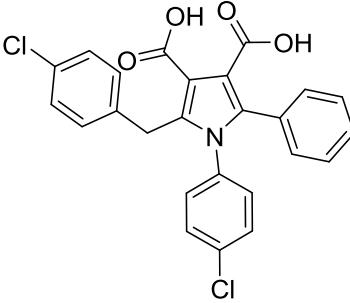
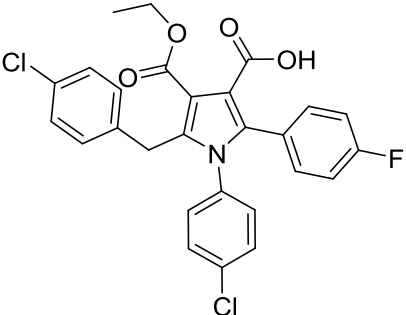
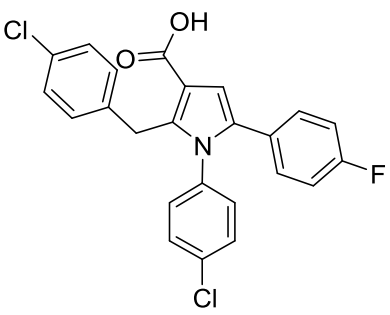
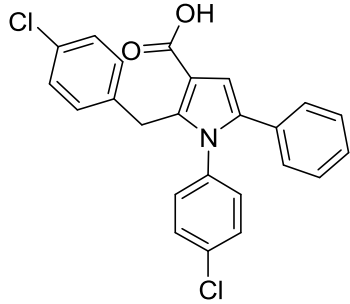
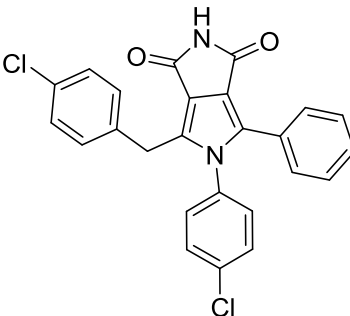


Figure 8.5: Purification of MDMX by size-exclusion chromatography. Construct C3 (MDMX₂₆₋₁₁₁) was subjected to size-exclusion chromatography as a final purification step. The sample was run on a Superdex HR 16/60 column (GE Healthcare) equilibrated in mHBS buffer. (A) Chromatogram, (B) SDS-PAGE of selected fractions. Fractions analysed in (B) are identified by the black line under the chromatogram in (A).

8.3 Co-Crystallisation of MDM2 and MDMX with Pyrrole Inhibitors

Compounds for co-crystallisation trials were selected based on the LogD values (calculated using Stardrop and the IC₅₀ values against MDMX measured by ELISA assay (Table 8.2). The compounds with LogD values greater than 4 showed visible precipitation in the presence of MDM2 or MDMX. Compound **68** has a logD value greater than 4 but it was selected for the co-crystallisation trials because of a unique molecular feature: It has a succinimide ring on the 3rd and 4th position of the pyrrole. The nitrogen of the succinimide ring would be a good vector to reach other favourable interactions or to introduce any water solubilising groups. A co-crystal structure of compound **68** bound to MDMX would be valuable to design a series of compounds with a fused ring system.

Table 8.2: Pyrrole MDMX inhibitors selected for co-crystallisation trials.

Compound	Structure	MDMX ELISA IC ₅₀ (μ M)	LogD
67		13.4	1.6
81		56	3.2
2		15	3.3
93		7.9	3.4
68		Not tested	5.5

The inhibitors were incubated with the concentrated proteins in a 3:2 molar ratio at 4 °C overnight. The inhibitor-protein complexes were concentrated to between 1.5 to 18 mg/ml (Table 8.3). The concentrations of the protein-inhibitor complexes with MDM2 were between 10-20 mg/ml, however, precipitation was observed with MDMX complexes at concentrations higher than 4-5 mg/ml. Precipitation was mostly observed with compounds **68** and **93** and as a result crystal trays were not set up for these inhibitors.

Table 8.3: Protein-inhibitor concentration for co-crystallisation trials.

Compound	Protein-Inhibitor Concentration (mg/ml)					
	MDMX constructs			MDM2 Constructs		
	1	2	3	1	2	3
2	3.7	3.1	2.3	23.0	10.0	17.3
68	3.5	-	-	19.0	7.2	-
67	2.9	2.7	2.1	19.0	4.0	15.8
81	2.9	2.9	2.2	23.0	5.7	16.8
93	-	-	-	22.0	5.5	15.0

In an attempt to identify novel crystallisation conditions, MDMX-inhibitor complexes were screened against three commercial crystallisation screens, JCSG+ (Molecular Dimensions), Index (Hampton Research) and ammonium sulfate (Qiagen) and MDM2-inhibitor complexes were screened against JCSG+ and ammonium sulfate. 2-subwell 96-well trays were used for co-crystallisation trials (Figure 8.6). Screening solutions were first added to the 96 wells by hand. The solutions were also mixed with protein-inhibitor complexes in 1:1 and 2:1 ratios (protein-inhibitor complex:screen) and the mixtures dispensed into the subwells using a Mosquito robot. Trays were stored at 4 °C in a Rikagu Minstrel tray hotel which also imaged the subwells at set time intervals. The images were observed for 8 weeks to monitor crystal formation.

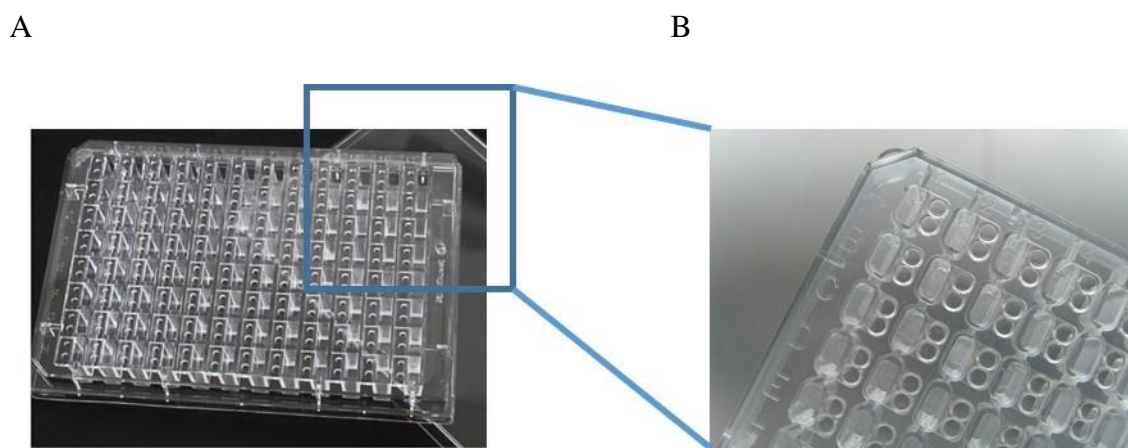


Figure 8.6: Crystallisation of MDM2 and MDMX with small molecule inhibitors. Complexes of MDM2 and MDMX bound to small molecule inhibitors were screened against selected commercial crystallisation screens in 96 well, 2 subwell plates. (A) The MRC crystallisation plate. (B) Close-up to show the juxtaposition of the two subwells and the screen well.

In total, 24 MDMX or MDM2-inhibitor complexes were subjected to crystallisation trials using three commercial screens for MDMX and two screens for MDM2. Overall, around 14,000 different conditions were used for co-crystallisation trials of MDMX and MDM2 with pyrrole-based inhibitors.

8.4 Co-Crystallisation of MDM2 and MDMX with Autoinhibitory domains

It was reported recently that MDMX contains an autoinhibitory sequence which interferes with its binding to p53.¹⁰⁸⁻¹⁰⁹ The autoinhibitory sequence is a tryptophan-rich segment within residues 190-210 of MDMX (¹⁹⁰FEEWDVAGLPWWFLGNLRSNY²¹⁰). The tandem tryptophan residues at positions 200 and 201 have been called the WW element. Bista *et al* (2013) performed isothermal titration calorimetry (ITC) experiments to measure the binding affinity (K_d) of MDMX with p53 in the presence or absence of the autoinhibitory sequence.¹⁰⁸ Full length MDMX (1-340) with an autoinhibitory sequence bound to p53 with a measured K_d of 2700 nM. MDMX (1-111) without the autoinhibitory sequence was 100-fold more tightly bound to p53 ($K_d = 30.3$ nM). MDMX without residues 193-210 had binding affinity of 92.6 nM with p53 (Table 8.4).

Table 8.4: Binding of different MDMX sequences to the transactivation domain of p53. The p53 transactivation domain is defined as residues 17-32.¹⁰⁸

Protein	K _d (nM)
MDMX 1-340	2700 ± 531
MDMX 1-111	30.3 ± 3.9
MDMX Δ193-210*	92.6 ± 11.7
MDMX W200D/201D	385 ± 43.5

*Residues 193-210 deleted.

Based on these findings reported by Bista *et al* (2013), it was hypothesised that the autoinhibitory sequence could stabilise MDMX and help in its crystallisation. Three autoinhibitory sequences (AID1, AID2 and AID3, Table 8.5) of different lengths were kindly supplied by Astex pharmaceuticals. All three autoinhibitory sequences contain the WW element which was reported as the most essential sequence for binding to the N-terminal domain of MDMX.

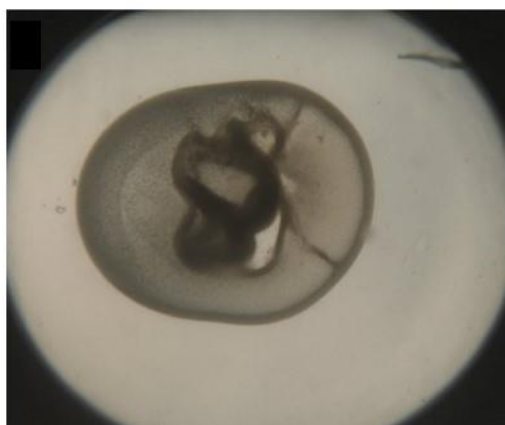
Co-crystallisation trials of AID with MDMX were set up using the JCSG+ and AmSO₄ screens (Table 8.5). Precipitation was observed when AID1 was incubated with MDMX construct 3. Similarly, AID3 showed precipitation with constructs 1 and 2.

Table 8.5: MDMX-AID co-crystallisation. Protein-autoinhibitory domain concentration for co-crystallisation trials.

Autoinhibitory Domain	Sequence	MDMX-Peptide concentration (mg/ml) MDMX constructs		
		1	2	3
AID1	FEEWDVAGLPWWFLGN	17.7	20.2	-
AID2	GLPWWFL	15	15	6
AID3	FEEWDVAGLPWWFLGNLRSNY	-	16	-

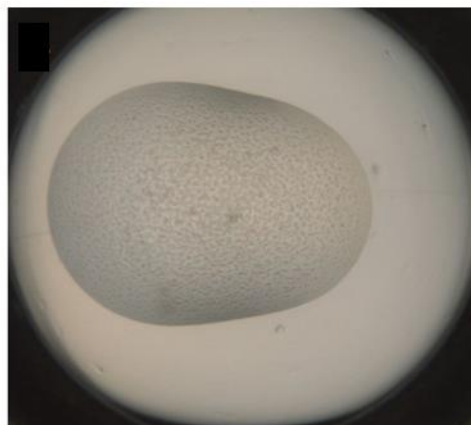
The images generated by the Rikagu Minstrel tray hotel were reviewed at irregular intervals for 8 weeks. Unfortunately, from more than 15,000 different conditions, crystal formation was not observed. In most of the cases, precipitation of the protein-inhibitor complex was observed (Figure 8.7A). In one case, a more promising precipitation was found (Figure 8.7B).

A



0.1 M Sodium citrate, 20% w/v PEG 3000

B



0.2 M LiSO₄, 50% v/v PEG 400, 0.1 M NaOAc

Figure 8.7: MDMX crystallisation trials. Images taken by the Rikagu Minstrel tray hotel. (A) MDMX C1 + **67**, (B) MDMX C2 + **81**.

Based on the most promising leads from the initial screen, an optimisation screen was prepared by altering the concentration of the Li₂SO₄ (0-0.3 M), PEG400 (30-100%), sodium acetate (0.1 M) and pH (4-5.5) of the final solution. The five pyrrole-based inhibitors, AID1 and AID2 were used for co-crystallisation trials with MDMX constructs 1, 2 and 3 using this optimised screen. However, crystal formation was not observed after 6 weeks of monitoring.

8.5 Development of Homogenous Time-Resolved FRET assay

RO-2443 **3** and RO-5963 **4** are reported as dual inhibitors of MDM2 and MDMX with low nanomolar IC₅₀ values against both MDM2 and MDMX.⁷¹ However, the IC₅₀ values generated using the in-house ELISA were around 500-1000 fold less than the reported IC₅₀ values (Table 8.6). To investigate the discrepancies in IC₅₀ values between Roche's homogenous time-resolved FRET (HTRF) assay and the NCL-ELISA assay, an HTRF assay was developed.

Table 8.6: IC₅₀ values of RO-2443 **3** and RO-5963 **4** obtained from ELISA assay and published HTRF values.

Inhibitors	Roche's HTRF assay		Newcastle ELISA assay	
	MDM2 IC ₅₀	MDMX IC ₅₀	MDM2 IC ₅₀	MDMX IC ₅₀
	(μ M)	(μ M)	(μ M)	(μ M)
RO-2443	0.033	0.041	6.9	13.7
RO-5963	0.019	0.024	16	26

The HTRF (Homogenous Time Resolved Fluorescence) assay relies on the Fluorescence Resonance Energy Transfer (FRET) from an excited donor molecule to an acceptor molecule.¹¹⁰⁻¹¹¹ The donor molecule absorbs energy and transfers it to an acceptor. FRET efficiency (E) is inversely proportional to the sixth power of the distance between the donor and acceptor as shown in the equation below.¹¹² E is the FRET efficiency, R₀ is the Förster distance at which half of the energy is transferred and r is the actual distance between the donor and acceptor. When the donor and acceptor are not in close proximity, the FRET efficiency is reduced (Figure 8.8).

$$E = \frac{R_0^6}{R_0^6 + r^6}$$

HTRF is a time resolved FRET in that there is a time delay of 50-150 μ s between the excitation of the donor and measurement of the FRET signal.¹¹¹ This time delay prevents measurement of any short-lived fluorescence which would otherwise interfere with measurement of the authentic signal.

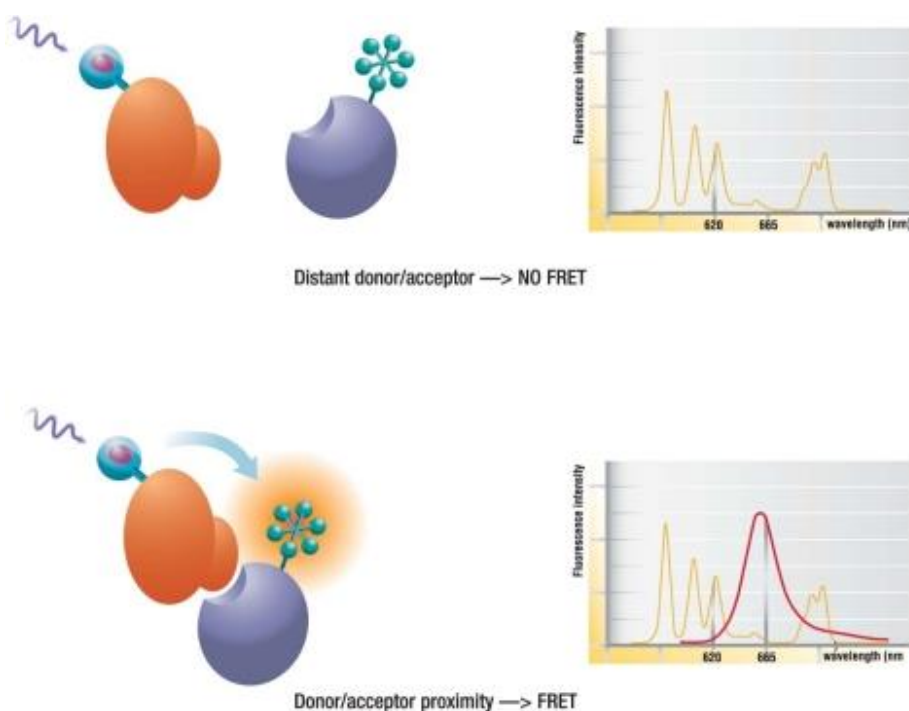


Figure 8.8: Principle of FRET (Fluorescence Resonance Energy Transfer).¹¹¹

In the HTRF assay established at Newcastle for measuring the potency of MDMX-p53 interaction inhibitors, GST-tagged MDMX (residues 22-111) was mixed with fluorescein-labelled IP3 peptide (Ac-16-MPRFMDYWQGLN-27-NH₂). IP3 peptide is a mutant form of p53 with high affinity for MDM2/MDMX.¹¹³ The fluorescein label on IP3 acts as an acceptor. A terbium-labelled anti-GST antibody which binds to GST-tagged MDMX was added to the mixture. The terbium label acts as a donor. Upon excitation, there is a transfer of FRET from donor to acceptor which can be measured (Figure 8.9A).

In the absence of an inhibitor, the donor (terbium) and the acceptor (fluorescein) are in close proximity. The donor terbium absorbs energy and transfers it to fluorescein. The transfer of energy is measured as a FRET signal. In the presence of an inhibitor, the donor and acceptor are separated which results in a decrease in the amount of FRET (Figure 8.9B).

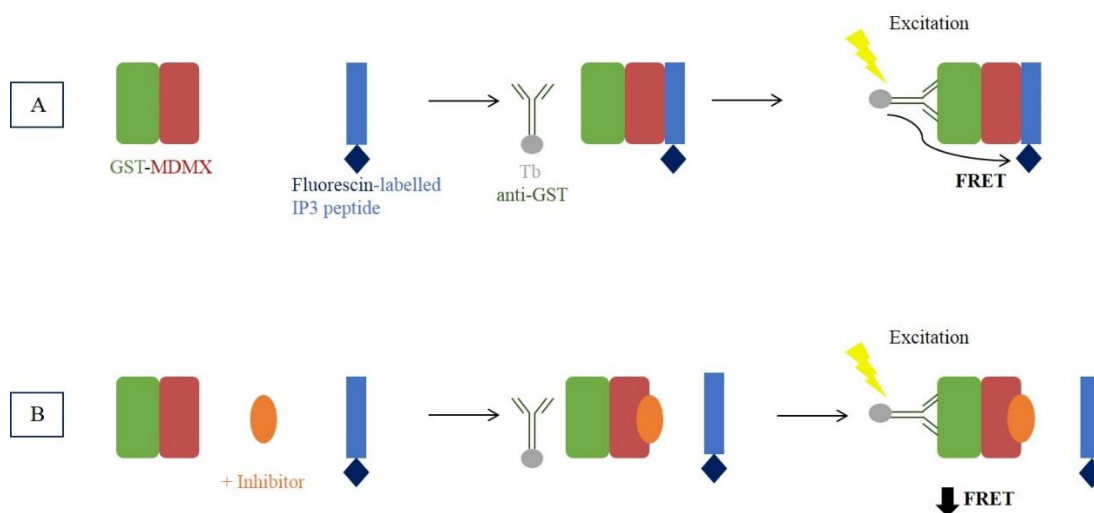


Figure 8.9: Schematic representation of MDMX-FRET assay. (A) Without inhibitor, (B) With inhibitor.

The ELISA was performed by Dr Yan Zhao. In the assay, biotinylated IP3 peptide was bound to streptavidin coated plate (Figure 8.10). MDM2 and MDMX were incubated with the compound being tested and added to the plate containing IP3 peptide. Then a primary mouse antibody that binds to MDM2 or MDMX was added. Subsequently, a secondary goat-antimouse antibody, conjugated to horseradish peroxidase (HRP) was bound to the primary antibody. The plate was analysed using a luminometer to detect signals from HRP (see chapter 16.2.1 for details). The data obtained from the luminometer were analysed and the IC_{50} values derived.

There were key differences between the protocols of the ELISA and HTRF assays. The major difference is the length of MDMX used, and it is believed to be the major cause of discrepancies between the IC_{50} s obtained from ELISA and HTRF assays. In the ELISA, full length MDMX was used, whereas, in the HTRF assay, the MDMX construct (residues 22-111) was used. The full length MDMX contains an autoinhibitory domain (described in section 8.3), which binds on the p53 binding domain of MDMX, thus, preventing the binding of p53 to MDMX. The MDMX construct used in the HTRF assay did not contain the autoinhibitory domain. The use of full length MDMX in HTRF assay development would require the optimisation of expression and purification of the desired protein, therefore, it was outside the scope of the structural biology placement undertaken. However, other differences in the assay protocols like the incubation order and times, different buffers were addressed during the HTRF assay development (described later in this chapter).

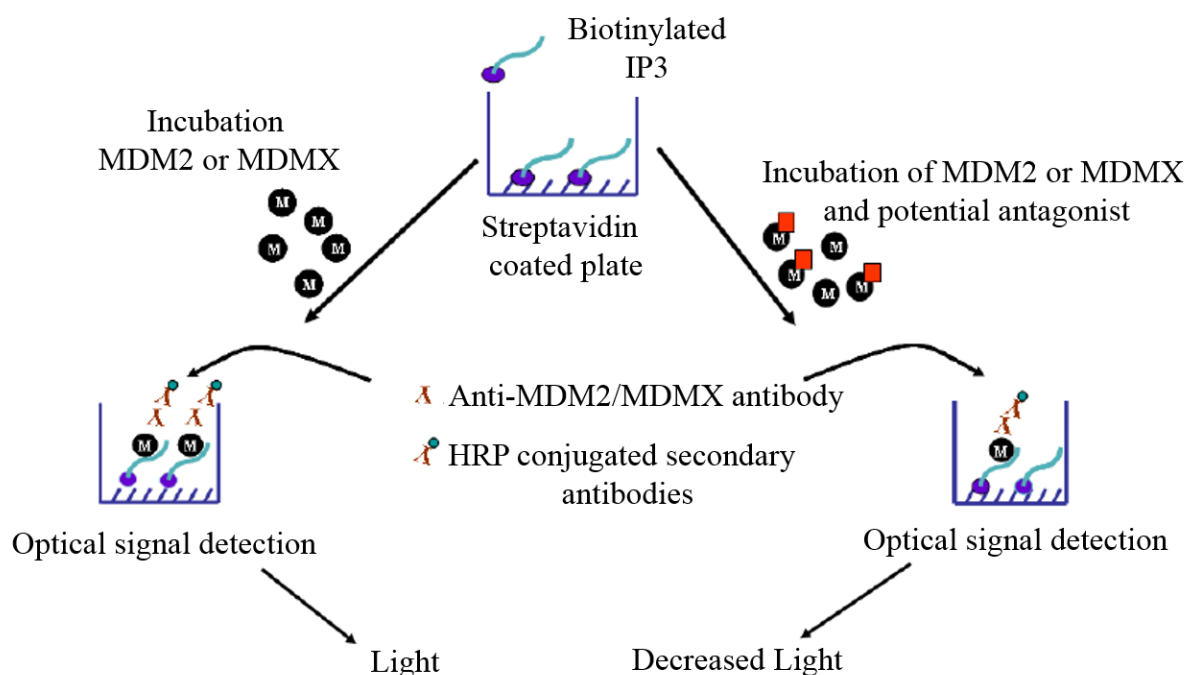


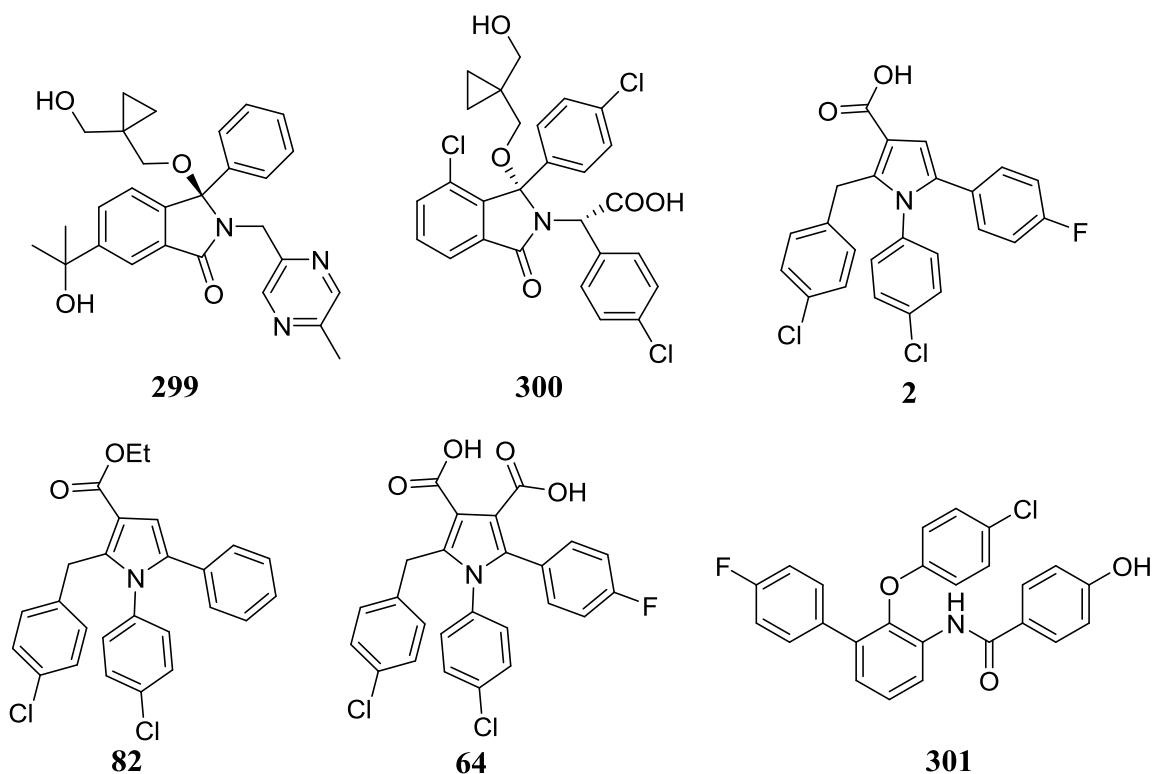
Figure 8.10: Schematic representation of ELISA.

The HTRF assay development was done by Dr Judith Reeks. In a typical HTRF experiment, the transfer of FRET signals were measured with the decreasing concentration of inhibitors. The maximum value (positive control) was obtained when p53 and MDMX formed a complex in the absence of inhibitors. The minimum value (negative control) was obtained in the absence of both MDMX and inhibitor. The values were converted to % inhibition using the formula given below and plotted against the concentration of the inhibitor to get a dose-response curve and IC_{50} value.

$$\% \text{ Inhibition} = \frac{\text{FRET(Average of positive control)} - \text{FRET (inhibitor)}}{\text{FRET(Average of positive control)} - \text{FRET(Average of negative control)}} \times 100$$

The assay had provided reasonable dose-response curves with stapled peptides and published small-molecule inhibitors, although the IC_{50} values obtained from the assay were not consistent (Figure 8.11A).¹¹⁴ RO-5963 showed greater than 50% inhibition at the lowest concentration used in the assay. However, the other Roche compound, RO-2443 was significantly less potent in our HTRF assay compared to the published data. The IC_{50} values from the assay were not reproducible, therefore, the data should not be over-interpreted. However, the discrepancies in the data may be due to the different constructs of MDMX used, but the construct of MDMX used in the assay was not disclosed by Roche. The investigation on the discrepancies observed,

and the development of other assay formats is currently ongoing. In favour of the assay, the signal to noise ratio of the assay was 25 and Z' of the assay was 0.61. The published inhibitors showed dose-response relationships, and the error bars were low. However, when the Newcastle small molecule inhibitors were tested in this assay, the measurements had associated high error bars (Figure 8.11B). Following assay optimisation, the final assay concentrations were MDMX-3nM, IP3 peptide-125 nM, 1 nM Tb-antibody and DMSO-2%.



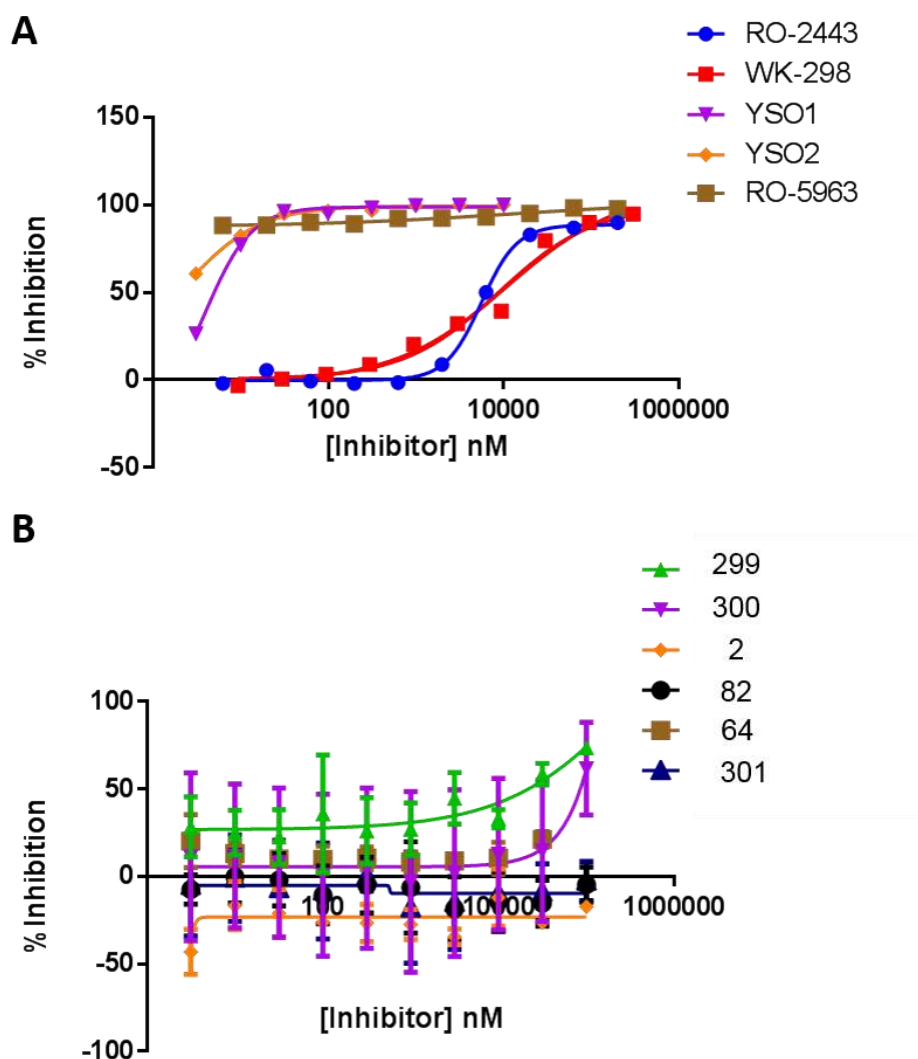


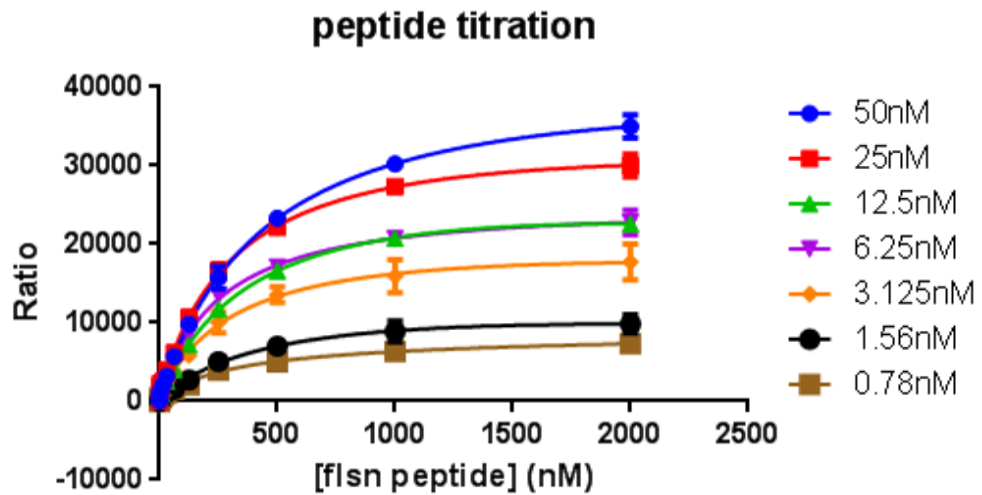
Figure 8.11: MDM2/X inhibitor evaluation by HTRF. HTRF assay results for (A) RO-2443 **3**, WK-298 **22**, and stapled peptides YSO1 and YSO2¹¹⁵, (B) Newcastle inhibitors. The assay was done in duplicates shown by the error bars.

The assay protocol required the inhibitor samples (provided in DMSO) to be diluted into assay buffer so that the final concentration of DMSO was 2%. Precipitation was observed with most of the Newcastle inhibitors when the DMSO solution of the inhibitors were added to the assay buffer. This resulted in high error bars and inhibition could not be observed with any Newcastle inhibitors.

In order to decrease precipitation of the inhibitors, the DMSO concentration was increased to 5%. However, this increase in the concentration of DMSO, decreased the Z' and signal to noise (S/N) ratio. Therefore, the assay had to be redeveloped to improve the Z' and S/N ratio. Initially,

MDMX at a range of concentrations was titrated against various concentrations of IP3 peptide to identify conditions that yielded a robust FRET readout at the lowest concentration of MDMX. The lowest concentration of MDMX and p53 after which the curve starts to flatten was chosen. Thus MDMX concentration was selected to be 10 nM as shown in Figure 8.12. The concentration of IP3 peptide was selected to be 300 nM as it was the rough average of the K_d values obtained.

A



B

	50nM	25nM	12.5nM	6.25nM	3.125nM	1.56nM	0.78nM
Bmax	46235	37129	33107	26453	22462	15292	7683
Kd	487.8	337.8	452.0	270.4	345.3	533.7	319.0

Figure 8.12: Titration of IP3 against different concentration of MDMX.¹¹⁴ (A), Graph showing the FRET values at different concentration of IP3 and MDMX, (B) Table associated with the figure A.

To determine the optimal concentration of Tb antibody, the S/N ratio was determined at various antibody concentrations with decreasing concentration of MDMX (Figure 8.13). At around 10 nM MDMX, 10 nM antibody provided maximum S/N ratio. Therefore the final concentration of the Tb antibody was selected to be 10 nM.

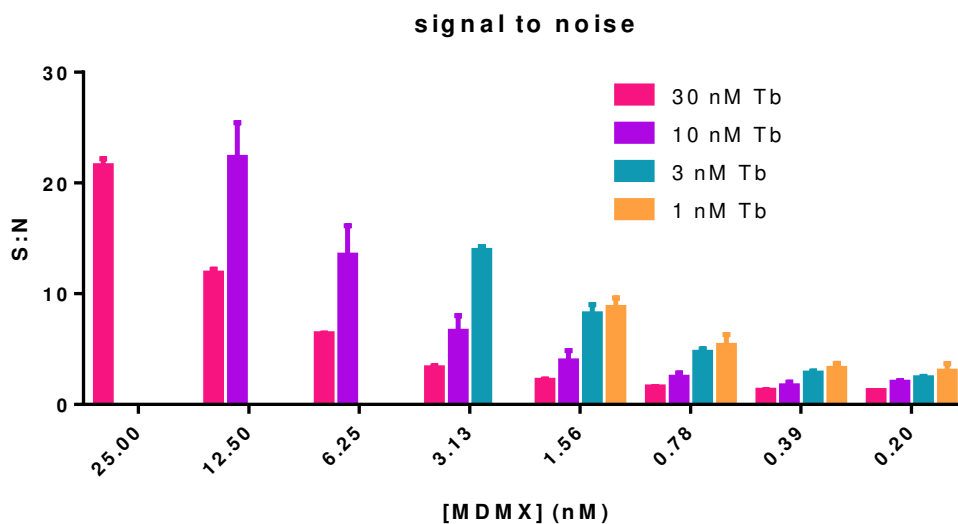
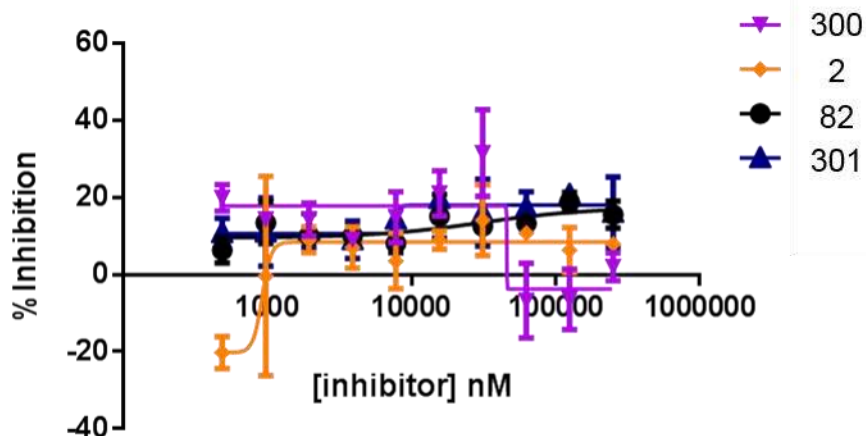


Figure 8.13: Signal to noise ratio at different concentrations of Tb antibody and MDMX.¹¹⁴

Based on these results, the final assay condition was changed to 10 nM MDMX, 300 nM IP3 peptide, 5% DMSO in buffer A. After 1 h incubation of MDMX, IP3 and inhibitor, the terbium-labelled antibody was added to a final concentration of 10 nM and the final assay volume was brought to 20 μ l. This new protocol provided good reproducible Z' values (0.5-0.7) and two inhibitors showed measurable inhibition (Figure 8.14).

A



B

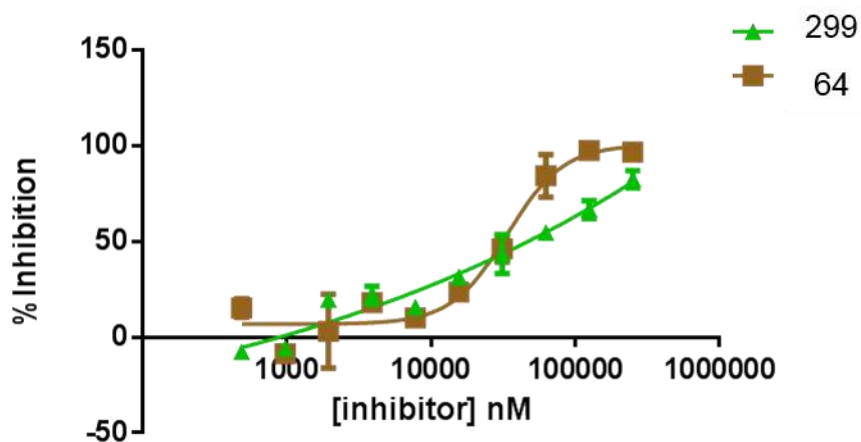
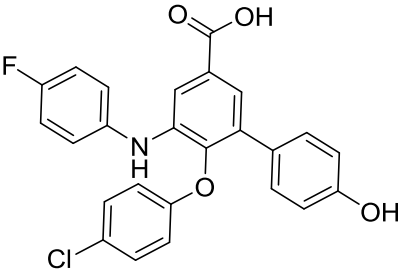
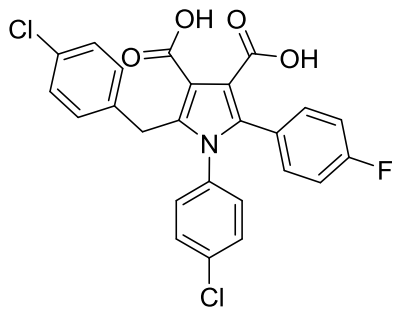
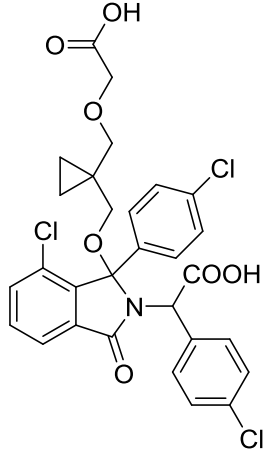
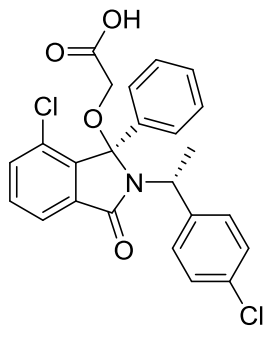


Figure 8.14: HTRF results for Newcastle small molecule inhibitors. (A) Compounds without any significant inhibition (B) Compounds that show inhibition.

The assay was repeated again with selected Newcastle inhibitors with low logD values (Table 8.7). The compounds with low logD values showed dose-response curves. The lipophilic compound **305** which was the most potent isoindolinone inhibitor of MDMX-p53 interaction in the ELISA showed no measurable inhibition in the HTRF assay (Figure 8.15).

Table 8.7: List of Newcastle inhibitors with their logD values and MDMX ELISA IC₅₀ values.

Compounds	Structures	LogD	MDMX IC ₅₀ (μM)
302		2.7	29
64		1.7	13
303		1.9	110
304		2.5	50% inhibition @ 200

305		6.1	6
306		2.1	Not tested
307		2.6	67

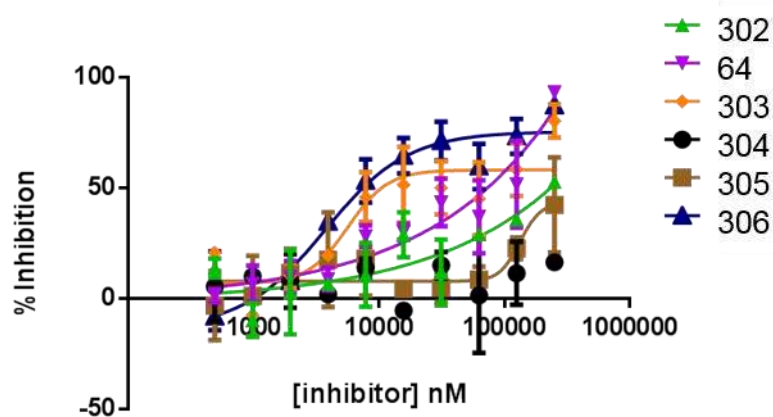


Figure 8.15: HTRF results for Newcastle small molecule inhibitors.

Although, hydrophilic compounds provided reasonable dose-response curves, the results were not reproducible and the derived IC_{50} values did not agree with the ELISA values. There were some major differences between the protocols of the ELISA and HTRF assay which are tabulated in Table 8.8.

Table 8.8: Protocol differences between the MDMX ELISA and HTRF assays.

S. No.	ELISA	HTRF
1.	PBS buffer was used.	Tris buffer was used.
2.	Inhibitors were incubated with MDMX for 45 min, then, p53 peptide was added.	Inhibitors, MDMX and p53 peptide were added to the final reaction plate and incubated for 1 h.
3.	Full length MDMX was used.	MDMX construct was used.
4.	Proteins are immobilised.	Proteins are in solution.

Following this comparative analysis, the buffer was changed to PBS and the incubation sequence was changed in the HTRF assay to make the two assay protocols similar. However, these changes did not improve the HTRF assay results (Figure 8.16).

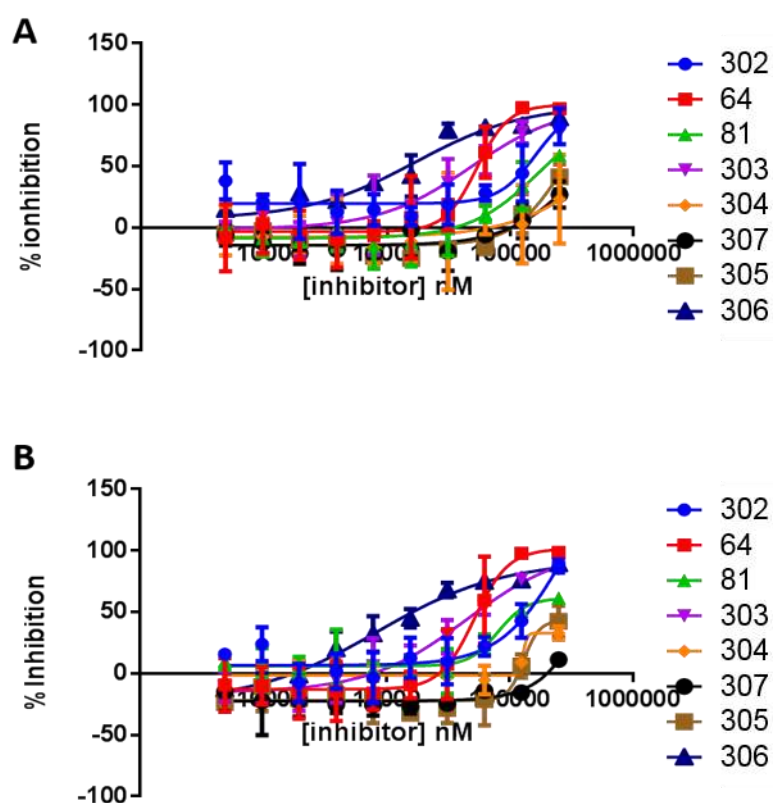


Figure 8.16: HTRF assay of Newcastle small molecule inhibitors. (A) With Tris buffer, (B) with PBS buffer. For both conditions, the order of addition of reagents was similar to that used in the ELISA as described in the 2nd point of Table 8.8.

The HTRF assay provided reasonable dose-response curves, with low error bars for literature inhibitors and peptides, but the IC_{50} values were inconsistent. Most of the Newcastle inhibitors did not return a measurable IC_{50} from the HTRF assay. Newcastle inhibitors provided high error bars and the results were not reproducible. The discrepancies in IC_{50} values obtained from the ELISA and HTRF assay may be because of the different constructs of MDMX used. The discrepancies in the IC_{50} values obtained for RO-2443 in the published HTRF assay and our HTRF assay might also be due to the difference in the length of MDMX used, but the MDMX construct was not disclosed by Roche. Further investigations on the different assay formats are ongoing. In order to get a good comparison between ELISA and HTRF assays, full length MDMX should be used in the HTRF assay. In addition, a label free assay such as Isothermal titration calorimetry (ITC) should be considered as an orthogonal assay. ITC does not rely on the fluorescence and depends on the change in enthalpy produced after the binding of the two

protein partners. Therefore, an assay with a different principle such as ITC might be beneficial to compare with the results obtained from ELISA and HTRF.

Chapter 9. Introduction to ATAD2 and Reported Small-Molecule Inhibitors

9.1 Introduction to Epigenetics

Every cells in an organism inherits the same genetic material, yet form structurally different tissues and organs with unique biological functions. This is due to the differences in the heritable epigenetic modifications, which include DNA methylation, histone modification and nucleosome positioning but do not include changes in the DNA sequence.¹¹⁶⁻¹¹⁸

To understand the role of epigenetic modifications in producing different phenotypes, and its disease linkage, it is important to understand the architecture of chromatin formed by DNA and several proteins, most importantly, histones.

9.1.1 Chromatin Architecture

The diploid human genome contains approximately 6 billion base pairs of DNA packaged into 23 pairs of chromosomes per cell.¹¹⁹⁻¹²⁰ Each base pair is around 0.34×10^{-9} metre long, therefore, each diploid cell contains approximately 2 meters of DNA ($(0.34 \times 10^{-9}) \times (6 \times 10^9)$).¹¹⁹ The histone proteins play an important role in the packaging of 2 meters of DNA into a small volume of cell nucleus. The dimers of four histone proteins H2A, H2B, H3 and H4 form an octamer which wraps approximately 147 base pairs of DNA to form nucleosomes which are the basic subunit of chromatin.¹²¹⁻¹²³

Nucleosomes are connected by short DNA segments known as 'linker DNA'. The linker DNA is either naked or bound to histone protein H1.¹²³ The nucleosomes assemble to form chromatin fibres, which are further packaged to form chromosomes (Figure 9.1).¹²⁰⁻¹²¹

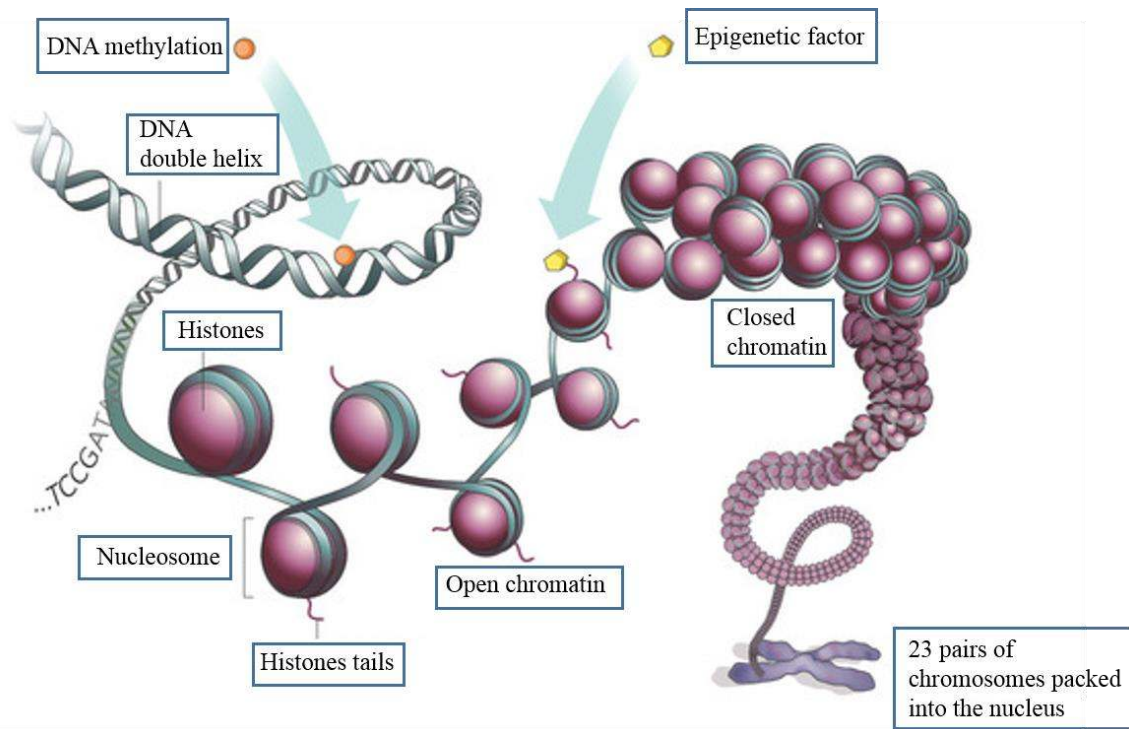


Figure 9.1: Packaging of DNA (adapted from Marx et al).¹²⁴

9.1.2 Post-Translational Modifications of Histones

The histone proteins undergo several post translational modifications which affect DNA centred processes, including DNA transcription, replication and repair as well as genomic architecture.¹²⁵ The histone post-translational modifications also known as ‘histone marks’ are regulated by three groups of proteins known as writers, erasers and readers (Figure 9.3).^{118, 126-127}

Although, there are several post-translational modifications of histones including phosphorylation and ubiquitylation, the most important and the most widely studied are acetylation and methylation.

9.1.2.1 Histone Acetylation

Histone acetyltransferases (HATs) are the writer proteins responsible for the acetylation of histones. Acetylation takes place at the amino group of the lysine side chain of the histone tail (Figure 9.2).¹²⁸⁻¹²⁹ Acetylation neutralises the positive charge on lysine reducing the affinity of the histone tail for DNA, resulting in a relaxed chromatin architecture.¹²⁹ Acetylation of histones has several effects depending on the site of acetylation. For example, acetylation of

H4K5 (means Histone H4, Lysine-5) and H4K12 are important for chaperone recognition during the formation of nucleosome core.¹¹⁸ Acetylation of H3K56 occurs on the histone within the nucleosome core and affects the interaction between histones and DNA.^{118, 130}

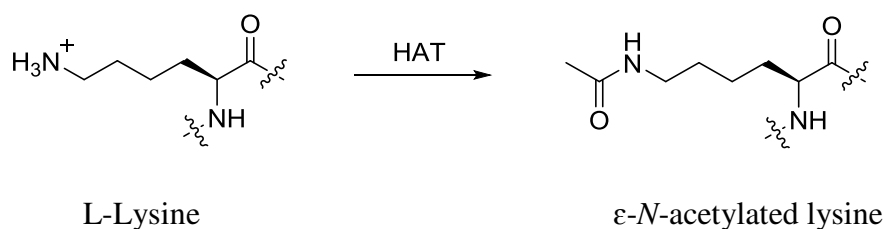


Figure 9.2: Neutralisation of the positive charge on lysine due to acetylation.

Histone deacetylases (HDACs) are the eraser proteins that help to remove the acetylation mark from the lysine residues of histones. HDACs are well-studied targets in the field of drug discovery and several clinically successful inhibitors of HDACs are reported to date (Table 9.1).¹³¹⁻¹³³

Table 9.1: Selected inhibitors of HDAC and their clinical status.¹³³

Drugs	Status
Vorinostat	Approved by FDA in 2006
Romidepsin	Approved by FDA in 2009
Panobinostat	Approved by FDA in 2015
Entinostat	Phase III
Mocetinostat	Phase II
Pracinostat	Phase III
Ricolinostat	Phase II
Resminostat	Phase II

9.1.2.2 Histone Methylation

There are different types of *S*-adenosylmethionine (SAM)-dependent methyl transferases that write one, two or three methyl marks mostly on the side chains of lysine and arginine residues

of histones.¹¹⁸ Methylation on glutamine and histidine residues of histones have also been reported.¹³⁴⁻¹³⁵ Unlike acetylation marks, methylation does not neutralise the charge on the positively charged amino acids in histones. Therefore, methylation of histones does not directly impact on the chromatin architecture, instead, the methyl marks are recognised by several other proteins.¹³⁶⁻¹³⁸

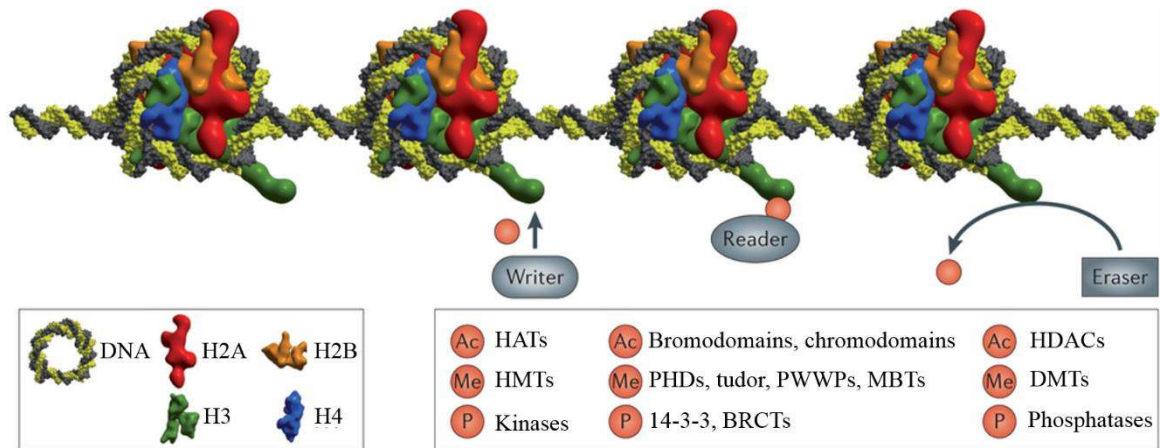


Figure 9.3: Representation of post-translational histone modifications.¹²⁶

9.2 Bromodomains

The post-translational modifications (PTMs) of histones are recognised and regulated by the reader proteins.¹²⁶ To date, several classes of readers have been identified with conserved domains that detect the modifications on histone.^{118, 127, 139}

One of the most important class of readers are bromodomains, which were first identified in the *brahma* gene of *Drosophila melanogaster* and named after it.¹⁴⁰ Bromodomains are the class of evolutionary conserved protein interaction modules which recognise the ϵ -*N*-acetylated lysines.¹²⁶ A total of 61 bromodomains in 46 diverse proteins have been identified in the human proteome. They are divided into eight structural classes (Figure 9.4).^{126, 141} Proteins containing bromodomains have been implicated in cancer, inflammation and viral diseases which make them one of the most studied targets currently in drug discovery.^{126, 142-145}

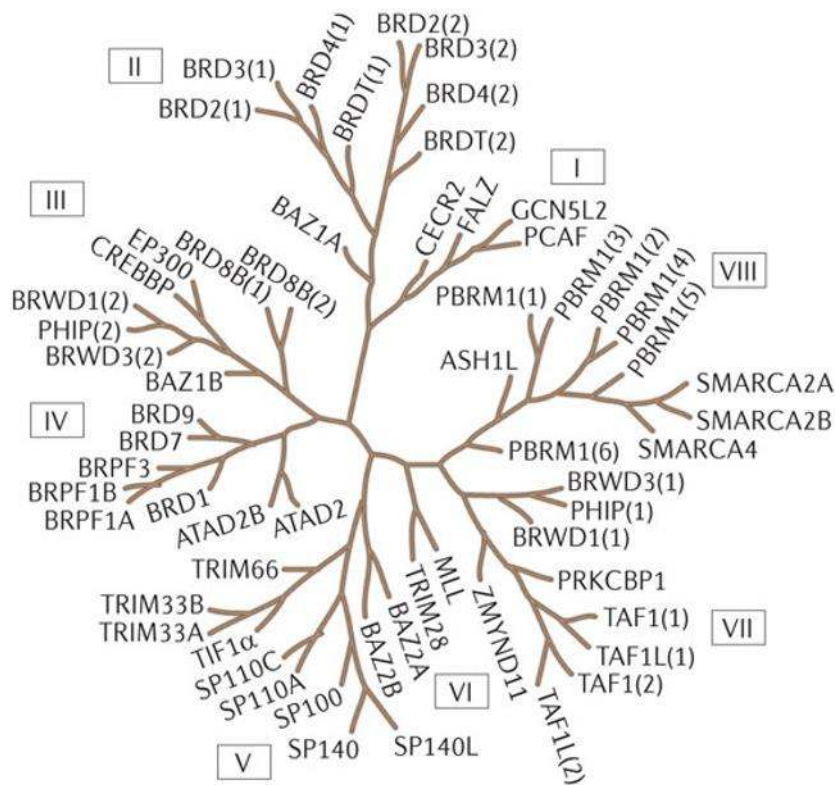


Figure 9.4: Structure based classification of bromodomains. The eight different classes are represented by Roman numerals.¹²⁶

Bromodomains contain an acetylated lysine binding site in a conserved fold containing four α helices (α_Z , α_A , α_B , α_C) and two loop regions ZA and BC loops (Figure 9.5). Structural studies with peptides have demonstrated that the acetylated lysine residue lies in the deep hydrophobic pocket where it forms hydrogen bond interactions with the conserved asparagine residue. In addition, there are several conserved water molecules which take part in the network of interactions with the acetylated histone.^{141, 146}

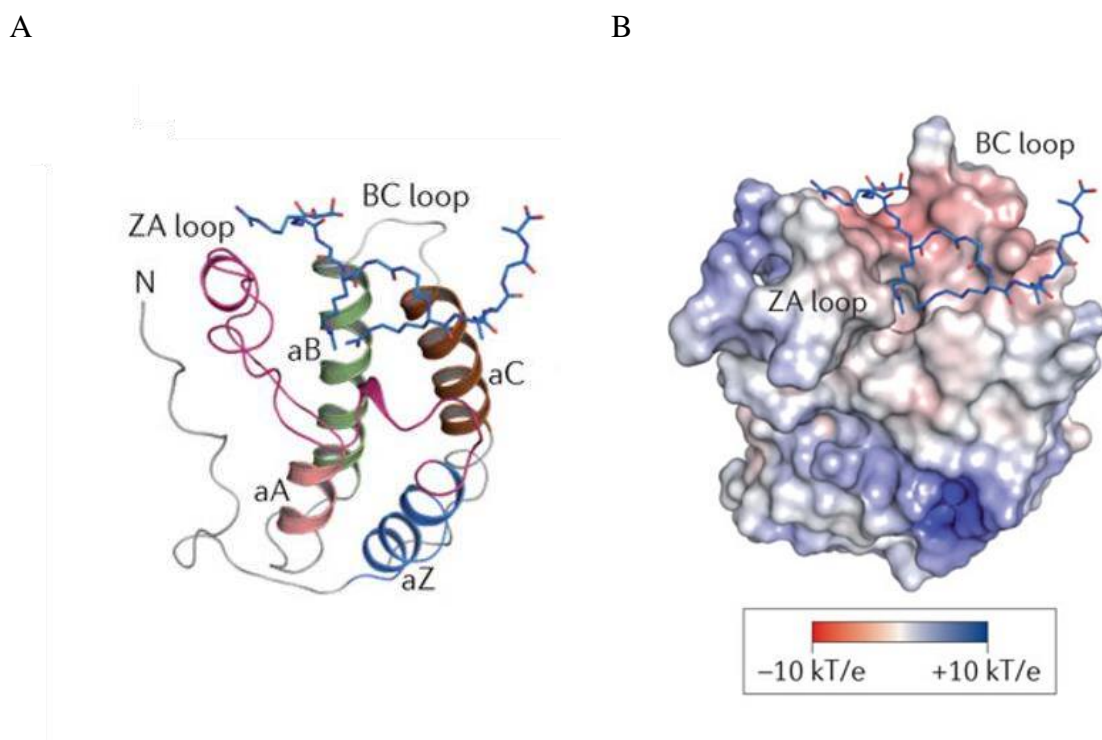


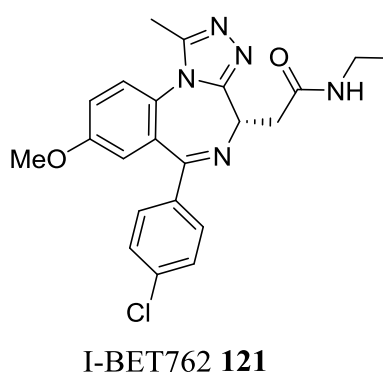
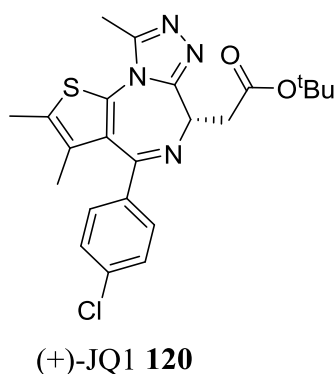
Figure 9.5: X-ray crystal structure of the first bromodomain of human BRD4 in complex with a diacetylated histone 4 peptide (PDB: 3UVW). (A) Helices and loops are highlighted by different colour codes. (B) The charged nature of the surface lining the KAc binding site is also coloured using electrostatic module ranging from -10 to +10 kT/e.¹²⁶

9.3 Bromodomain Inhibitors

9.3.1 *BET-Bromodomain Inhibitors*

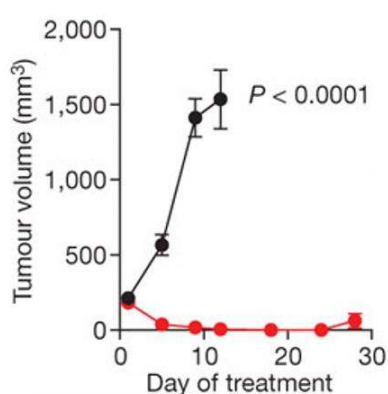
To date, different classes of bromodomain inhibitors have been identified. The BET family in the subfamily II of the structure-based tree (Figure 9.4) is one of the most studied classes of bromodomains with several known potent small molecule inhibitors.^{127, 147} BET family comprises of BRD2, BRD3, BRD4 and the testes specific BRDT. BET proteins contain two bromodomains and an extra terminal region.¹⁴¹

Although, few bromodomain inhibitors were reported in the literature,¹⁴⁸ it was in 2010 that two potent and selective inhibitors of BET bromodomains (+)-JQ1 (**120**)¹⁴⁹ and I-BET762 (**121**)¹⁵⁰ were disclosed, and provided the proof-of-principle that bromodomains can be selectively inhibited by small molecules. This sparked the field and led to the development of several potent and selective bromodomain inhibitors.^{126, 147, 151}



(+)-JQ1 **120** is the most widely studied bromodomain inhibitor which results in 179 hits in the scopus search field.¹⁵² The compound was developed by Filippakopoulos *et al.* after successful optimisation of a benzodiazepine core based on the several patents disclosed between 1998 and 2006.^{149, 153-154} The compound was selective for BET bromodomains over other classes of bromodomains when studied against a panel of 46 human bromodomains.¹⁴⁹ The first *in vivo* study that demonstrated the effect of bromodomain small-molecule inhibitors in cancer therapy was done with (+)-JQ1 on a mouse xenograft with NUT (Nuclear Protein in Testis) midline carcinoma. At minimal toxicity dose, the compound showed reduction in tumour volume and promoted survival (Figure 9.6).¹⁴⁹ Similarly, other studies with different BET bromodomain inhibitors have shown reduction in tumour volumes in various mouse models of tumours including acute myeloid leukaemia, glioblastoma, melanoma and prostate cancer.¹⁵⁵⁻¹⁵⁹

A



B

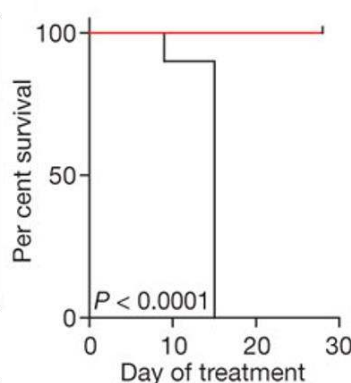
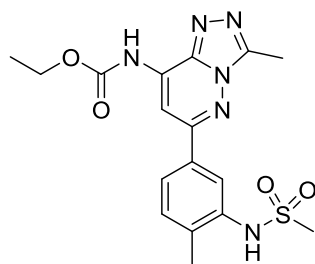


Figure 9.6: (+)-JQ1 (red line, 50 mg kg⁻¹, daily) on NUT midline carcinoma xenograft model produces (A) decrease in tumour volume, (B) prolonged survival. Vehicle is shown by black line.¹⁴⁹

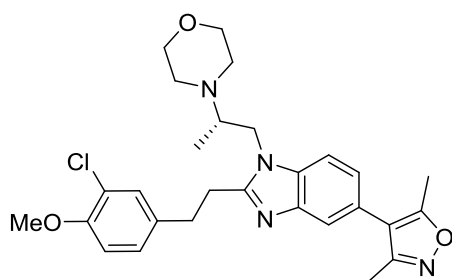
9.3.2 Non-BET bromodomain Inhibitors

After successful development of several small-molecule inhibitors of the BET bromodomains, drug discovery efforts were shifted towards the development of bromodomains outside the BET family. Structural Genomics Consortium (SGC) are aiming to develop a selective inhibitor for each bromodomain.¹⁶⁰ Bromosporine **122** was developed at SGC and is a pan-bromodomain inhibitor that inhibits various bromodomains, including BRD2(1), BRD3(1), BRD4(1), BRDT(1), CECR2, TAF1(2), BRD9, and CREBBP.¹⁶¹ The compound can be used as a chemical tool for identifying the biological role of the bromodomains for which selective inhibitor have not been developed.

Various selective small molecule inhibitors of non-BET bromodomains have been reported. SGC-CBP30 (**123**) for CREBBP, GSK2801 (**124**) for BAZ2A/B, PFI-3 (**125**) for SMARCA4 and PB1 are few examples of the selective non-BET bromodomain inhibitors.¹⁶²⁻¹⁶⁴

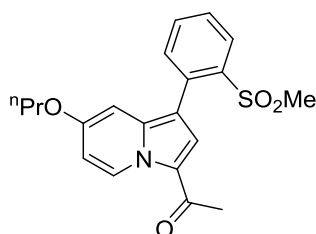


Bromosporine **122**



SGC-CBP30 **123**

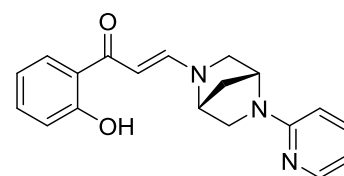
CREBBP IC = 79 nM



GSK2801 **124**

BAZ2A K_D = 257 nM

BAZ2B K_D = 136 nM



PFI-3 **125**

SMARCA4 K_D = 89 nM

PB1(5) K_D = 48 nM

9.4 ATAD2 and its Role in Cancer

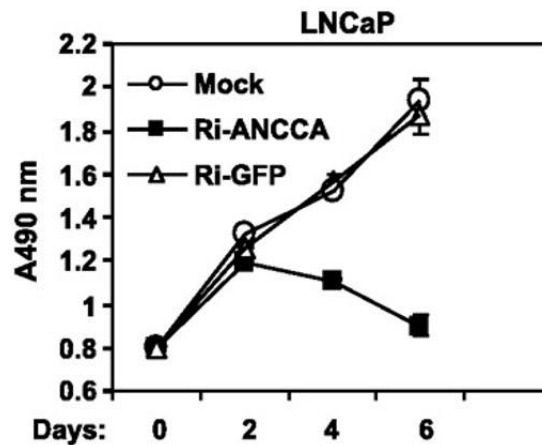
ATAD2 contains a double AAA+ ATPase domain¹⁶⁵ and a bromodomain. It is also known as ANCAA¹⁶⁶⁻¹⁶⁹ (AAA nuclear co-regulator cancer-associated protein), and belongs to subfamily IV in the structure-based classification of bromodomains (Figure 9.4). ATAD2 is overexpressed in a wide range of human cancers including breast, lung, prostate, ovarian, liver, osteosarcoma and gastrointestinal carcinomas, and it is present in low levels in normal non-tumour cells.^{167, 170-171} ATAD2 was overexpressed in 23% of 172 tumour specimens analysed by Ciró *et al* (Table 9.2).¹⁷¹ In a separate study by Kalashnikova *et al*, ATAD2 was shown to be overexpressed in around 70% of breast tumours.¹⁶⁶

Table 9.2: ATAD2 expression in primary tumours.¹⁷¹

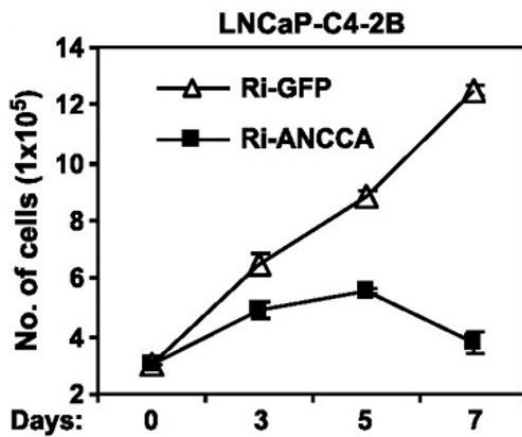
Tumour	No. of Samples	Highly expressed, n (%)
Breast carcinoma	25	9 (36)
Colon carcinoma	27	10 (37)
Lung carcinoma	22	5 (23)
Prostate carcinoma	24	0 (0)
Stomach carcinoma	21	9 (43)
Uterus carcinoma	20	4 (20)
Lymphoma	12	2 (17)
Melanoma	11	0 (0)
Sarcoma	10	1 (10)
Total	172	40 (23)

ATAD2 acts as a coactivator of various transcription factors including androgen receptor (AR), estrogen receptor (ER) and MYC. ATAD2 is crucial for the transcription of various androgen genes in prostate cancer.¹⁶⁷ Zou *et al*. showed that suppression of ATAD2 expression using ATAD2-RNAi inhibited the proliferation of androgen-dependent and androgen-independent or hormone refractory prostate cells (Figure 9.7).¹⁶⁷

A



B



C

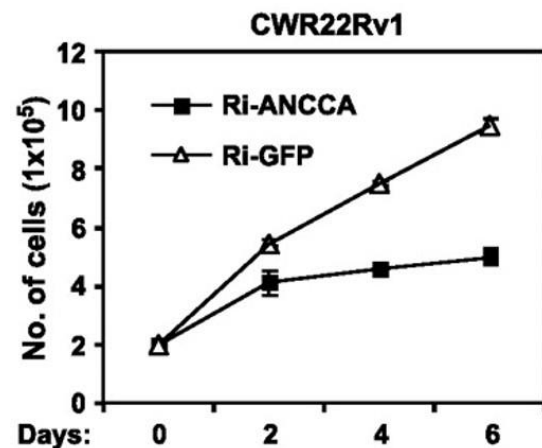


Figure 9.7: Suppression of ATAD2 expression in (A) androgen-dependent LNCaP cell lines (B) androgen-independent cell lines LNCaP-C4-2B, and (C) CW22Rv1. Cells were plated in hormone-deprived medium for 24 h before being infected with adeno-RNAi-ANCCA (ATAD2-RNAi) or adeno-RNAi-GFP control, or mock-infected (for LNCaP, also act as a control).¹⁶⁷

Similarly, ATAD2 is also a co-activator of estrogen receptor (ER), thus it is highly expressed in breast cancer.¹⁶⁸ ATAD2 is an important cofactor for MYC-dependent transcription. MYC is a critical regulator of cell proliferation, therefore, enhancement of MYC transcriptional activity by ATAD2 contributes to the development of many human cancers.¹⁷¹⁻¹⁷² Various knock-down studies using siRNA and shRNA technologies have confirmed the role of ATAD2 in apoptosis, cell growth and proliferation in several cancer cell lines.^{170, 172} Altogether, these studies suggest that ATAD2 is an important target for cancer drug discovery, and a small-

molecule inhibitor would provide an insight on the phenotypic response to the inhibition of ATAD2.

9.5 Structure and Druggability of ATAD2 Bromodomain

Similar to other bromodomain structures, ATAD2 has four left-handed helices (α_Z , α_A , α_B , α_C) and two loops (ZA and BC). The acetyllysine binding pocket is created by two helices (α_B , α_C), and ZA loop. The amino acids involved in the binding site are Val1008, Val1013, Val1018, Tyr1063 and Ile1074 (Figure 9.8A).

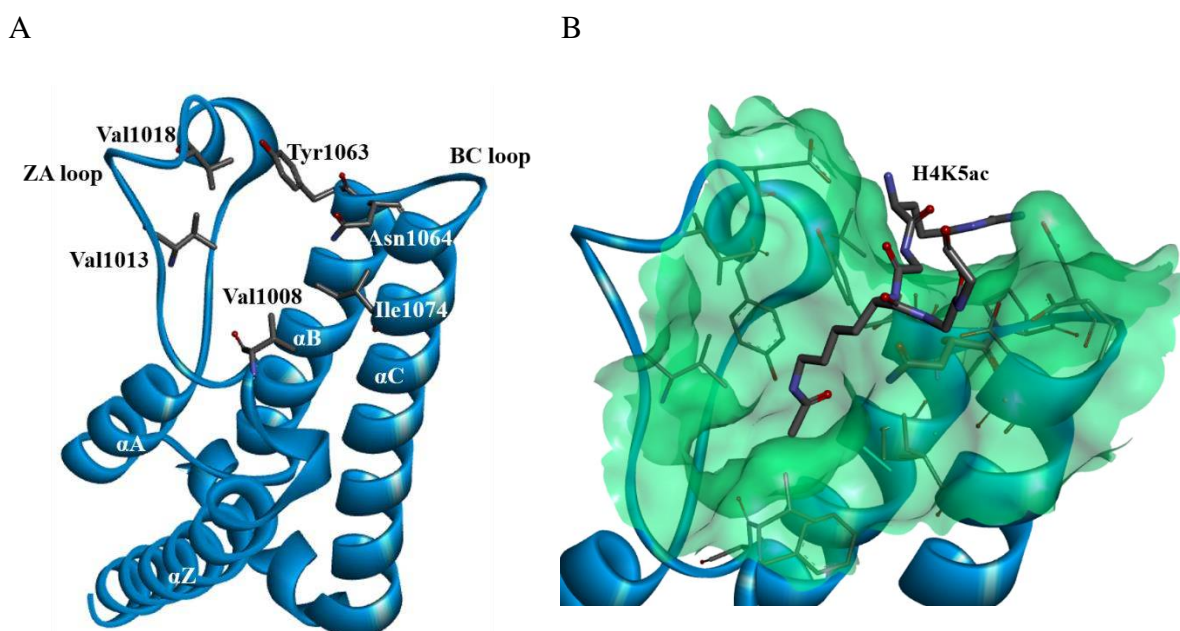


Figure 9.8: (A) Crystal structure of ATAD2 in apo form (PDB: 3DAI). The Asn1064 is evolutionarily conserved and is important for the histone recognition. The other highlighted amino acid residues form the acetyllysine binding pocket. (B) Acetyllysine binding surface of ATAD2 bound to H4K5ac (4QUU). The secondary structure of ATAD2 is coloured in blue. The acetyllysine binding surface of ATAD2 is coloured in green. The amino acid residues are coloured based on atoms; carbon: grey, oxygen: red, nitrogen: blue.

The crystal structure of ATAD2 bound to acetyllysine (PDB: 4QSP) shows the key hydrogen bond interaction that anchors the acetyllysine in the binding site (Figure 9.9).¹⁶⁹ The oxygen atom of the acetyl group forms two key hydrogen bond interactions, one with the Asn1064 and

the other with Tyr1021 *via* a water molecule. ATAD2, like other bromodomains, contains conserved water molecules which are important in the binding of acetyllysine.^{141, 169, 173}

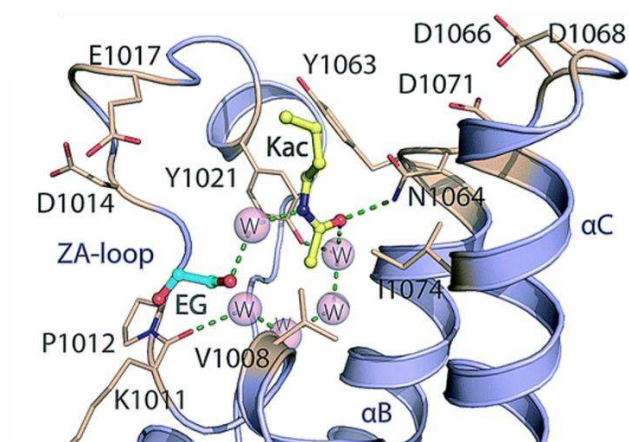


Figure 9.9: Interactions of ATAD2 with acetyllysine (PDB: 4QSP).¹⁶⁹ A bound ethylene glycol molecule (highlighted in cyan), water molecules (in pink spheres), Acetyllysine (carbons: yellow, oxygen: red, nitrogen: blue) are shown.

ATAD2 has some flexibility in its loops. Poncet-Montage *et al* studied the flexibility of ATAD2 using different conditions for crystallising ATAD2 in its apo form.¹⁷³ They obtained four crystal structures of apo-ATAD2 and compared with the published structures (PDB: 3DAI and 4QUU). Superimposition of the six structures demonstrates the flexibility in the ZA loop and the BC loop (Figure 9.10).

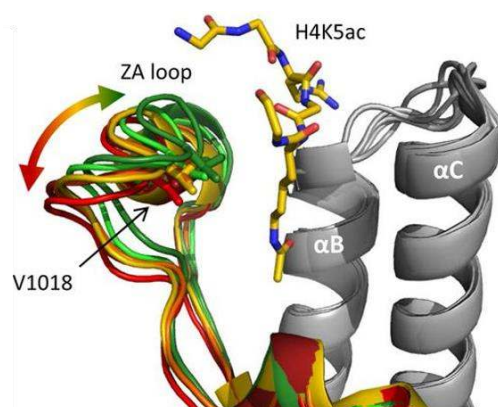
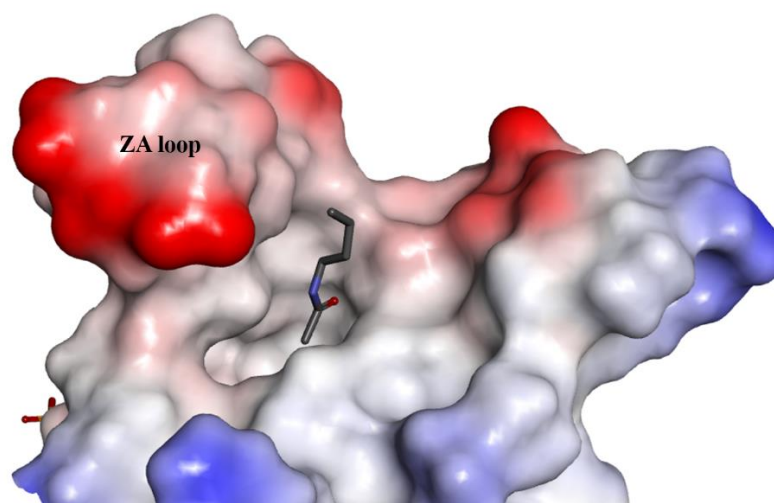


Figure 9.10: Superimposition of the 6 crystal structures of ATAD2. Red, yellow and green ZA loop represents the ATAD2 states from wide-open to closed state, respectively.¹⁷³

The acetyllysine binding site of ATAD2 is polar and shallow compared to several other bromodomains.¹⁶⁹ In Figure 9.11, the acetyllysine binding pocket of the bromodomain of ATAD2 is compared with the bromodomain of BRD4. The ZA loop of ATAD2 which forms a major part of the binding site is polar, whereas, the binding site in BRD4 is mostly hydrophobic.

A



B

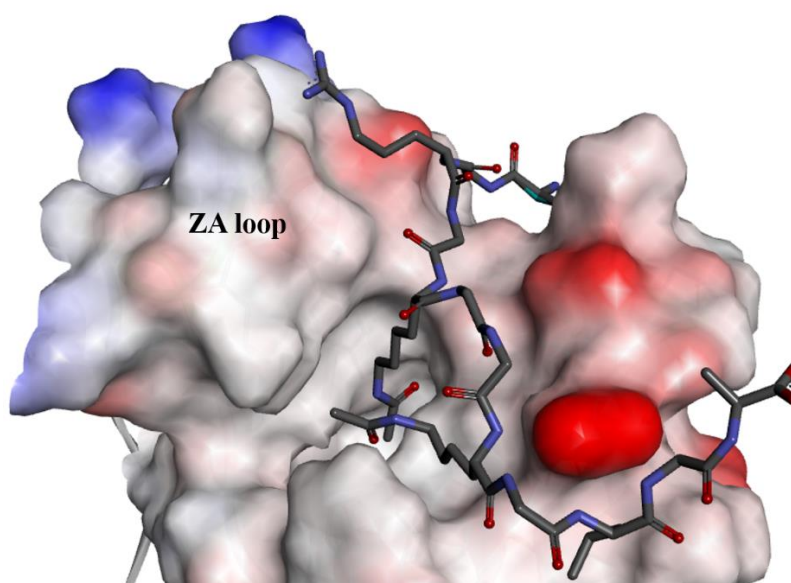


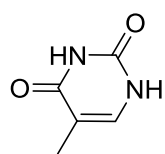
Figure 9.11: Comparison of the acetyllysine binding pocket of (A) ATAD2 (PDB: 4QUU) and, (B) BRD4 (PDB: 3UVW). The solvent accessible surface (probe radius 1.4) was coloured based on the charge; blue for positive charge and red for negative charge.

Altogether, due to the flexibility of the ZA loop, as well as, the shallow and polar nature of the binding site, ATAD2 bromodomain was grouped in the list of low-druggable bromodomains.^{169, 174} However, very recently a low nanomolar inhibitor of ATAD2 was reported by Bamborough *et al.* which is discussed in detail later in this chapter.¹⁷⁵

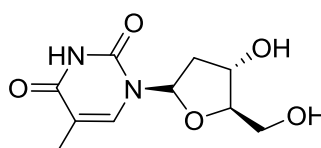
9.6 Reported ATAD2 Bromodomain Inhibitors

9.6.1 Fragments Targeting ATAD2 Bromodomains

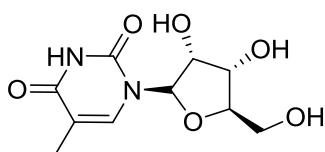
In 2014, Chaikuad *et al* used fragment based approach to identify thymine analogues (**126-130**) as a chemical starting point for the development of more potent inhibitors of ATAD2 bromodomain-acetylated histone interaction.¹⁶⁹ The optimisation of those fragments was reported as an on-going activity, and the results have not been published yet. Initial attempts to screen a library of acetyllysine mimetics using high-throughput screening methods revealed no potent hits. Therefore, co-crystallisation and NMR chemical shift perturbation experiments were used to identify the fragments. The binding affinities of the fragments were determined by the NMR chemical shift perturbation experiments where the chemical shifts of ¹³C-methyl-labelled ATAD2 was monitored. The fragments showed low millimolar binding affinities for ATAD2 bromodomain. As reported with apo-ATAD2,¹⁷³ the flexibility of the ZA loop was also observed in the presence of thymine based ligands.¹⁶⁹



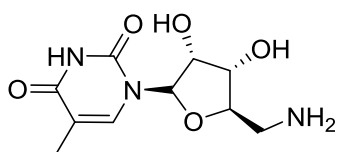
Thymine **126**
 $K_D = 10 \text{ mM}$



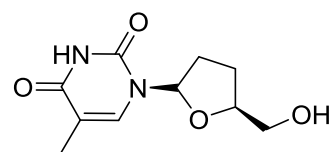
Thymidine **127**
 $K_D = 10 \text{ mM}$



128
 $K_D = 21 \text{ mM}$



129
 $K_D = 17 \text{ mM}$



130
 $K_D = 18 \text{ mM}$

Co-crystal structures of different thymine-based fragments bound to ATAD2 showed that the thymine ring formed the canonical acetyllysine mimetic H-bond with Asn1064 and the water mediated H-bond with Tyr1021 (Figure 9.12).

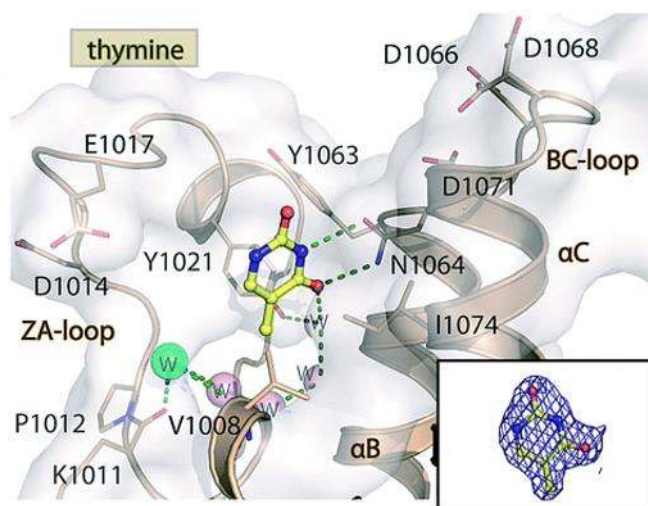
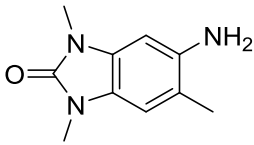
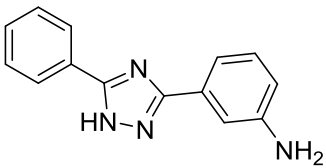
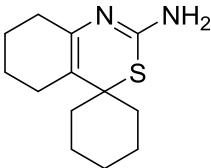
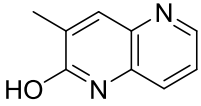
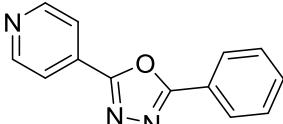
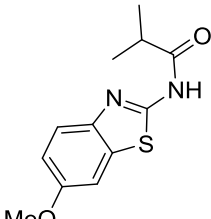
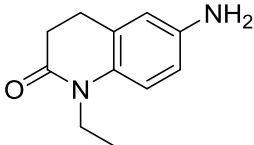
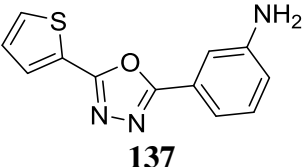
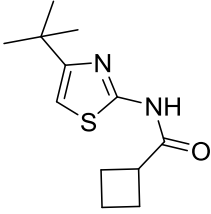
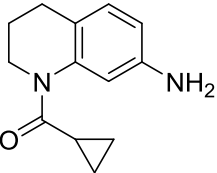
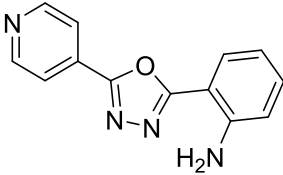
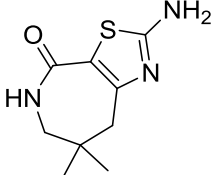


Figure 9.12: Crystal structure of ATAD2 bromodomain in complex with thymine (represented by yellow stick model).¹⁶⁹

Simultaneously, Harner *et al.* (2014) reported the results of a fragment-based screen using NMR against ATAD2 bromodomain.¹⁷⁶ A total of 65 hits were identified against ATAD2 bromodomain which were clustered into three chemical groups (Table 9.3). Cluster 1 contained the fragments with 5,6 and 6,6-fused ring systems that have been previously identified as acetyllysine mimetics. Cluster 2 contained fragments unique to ATAD2 bromodomains with tricyclic chemotypes. Cluster 3 also contained unique fragments with sulfur containing chemotypes.

Table 9.3: Representative ATAD2 bromodomain fragment hits identified by Harner *et al.*¹⁷⁶

Cluster 1	K _d (μ M)	Cluster 2	K _d (μ M)	Cluster 3	K _d (μ M)
 131	600	 135	350	 139	400
 132	600	 136	400	 140	450
 133	650	 137	450	 141	500
 134	650	 138	600	 142	500

Three fragments from different clusters were used for co-crystallisation studies. Out of the three fragment, two of them displaced conserved water molecules from the KAc binding site. Fragment **135** displaces four conserved water molecules which may account for the higher binding affinity. Fragment **142** displaces one conserved water molecule and the position of the water is occupied by an amine substituent (Figure 9.13).

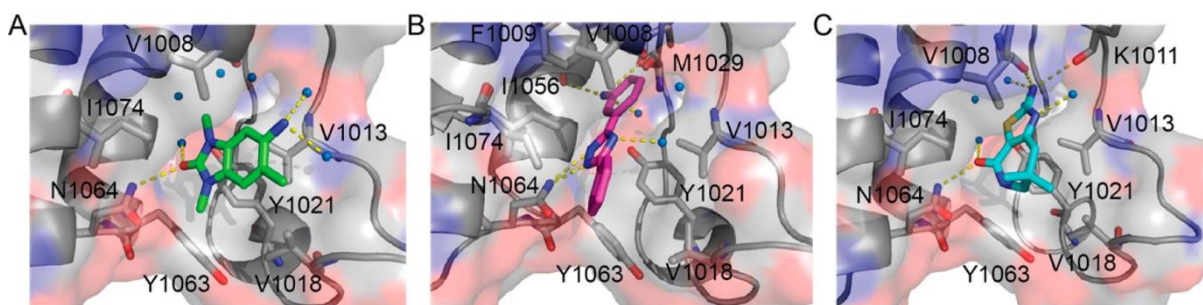
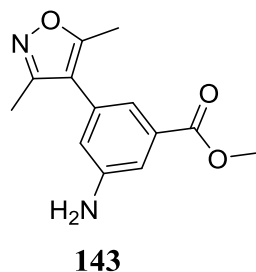


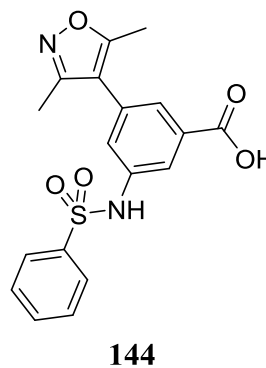
Figure 9.13: View of Kac binding site in presence of (A) fragment **131**, (B) fragment **135**, (C) fragment **142**. Fragment **131** does not displace any conserved waters, whereas, fragment **135** displaces four and fragment **142** displaces one conserved water.¹⁷⁶ PDB: 4TYL, 4TZ2, and 4TZ8, respectively.

Poncet-Montage *et al* (2015) reported two isoxazole based compounds **143** and **144** as ATAD2 bromodomain binders.¹⁷³ The compounds were identified from X-ray crystallography screen of fragments and known acetyllysine mimetic chemical scaffolds.

None of these compounds were potent enough to be used as a chemical tool to study the implications ATAD2 bromodomain inhibition in cells.



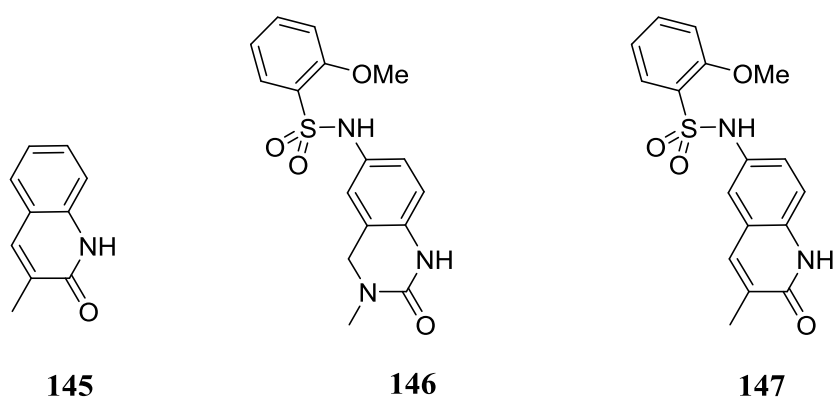
$IC_{50} = 96 \mu M$



$IC_{50} = 422 \mu M$

9.6.2 Naphthyridone Series

The first, and the only potent and selective small molecule inhibitor of the ATAD2 bromodomain reported to date was developed very recently.^{175,177} The small molecule inhibitor development started from a quinolone fragment **145** inspired from the dihydroquinazoline fragments known to bind the BET bromodomains, as seen in inhibitor PFI-1 **146** and its quinolin-2-one analogue **147**.¹⁷⁷



A crystal structure of fragment **145** bound to ATAD2 revealed that the carbonyl group mimics the acetyllysine binding mode. The carbonyl oxygen forms H-bond with Asn1064 and a water mediated H-bond with Tyr1021. The N-H forms an additional H-bond with the Asn1064. The methyl group points in the same pocket as occupied by the methyl group of the acetyllysine (Figure 9.14).

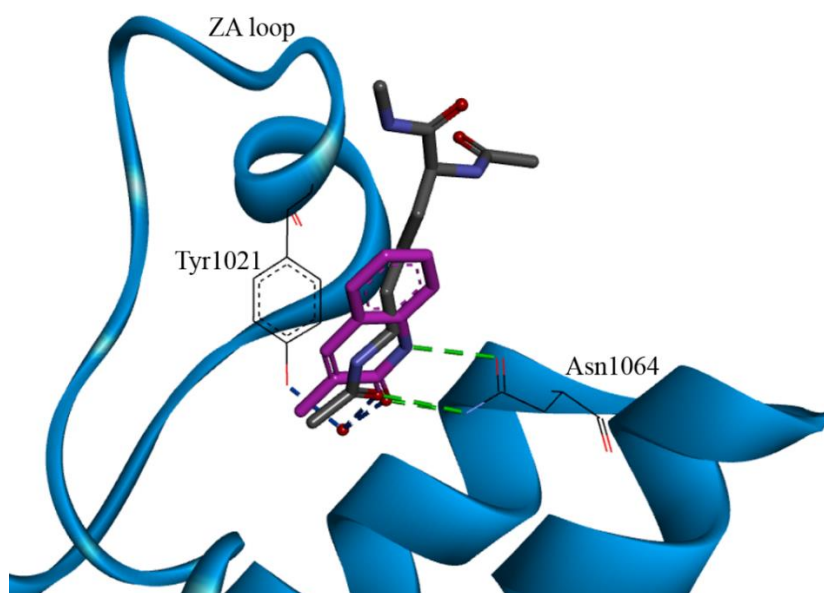


Figure 9.14: Overlay of the crystal structures of ATAD2 bromodomain bound to capped acetylated lysine (grey, PDB: 5a5n) and fragment **145** (magenta, PDB: 5a5o).

A focussed set of compounds based on quinolinone core were screened against ATAD2 bromodomain using time-resolved fluorescence resonance energy transfer (TR-FRET) assay. Compound **148** was considered as a ligand efficient starting point (LE = 0.3), and SAR studies at the C5-position resulted in the identification of a low micromolar inhibitor (**149**, ATAD2 IC₅₀ = 1.3 μM, Figure 9.15). Although, the compounds were the most potent inhibitors reported to date, they were not selective for ATAD2 over other BET bromodomains.¹⁷⁷

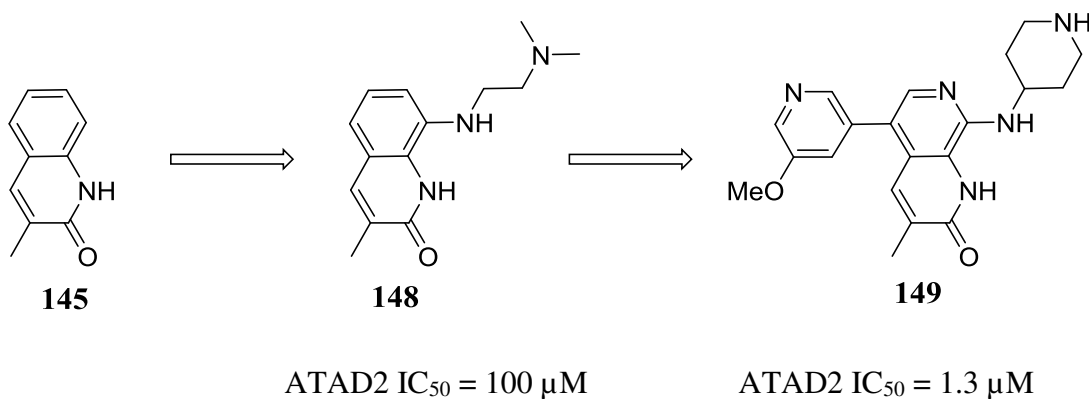


Figure 9.15: Development of the first low-micromolar inhibitor of ATAD2.¹⁷⁷

To improve the selectivity and potency of the inhibitor **149**, the RVF shelf of ATAD2 was targeted (Figure 9.16B).¹⁷⁵ The RVF shelf is formed by three amino acids Arg1007, Val1008 and Phe1009. It is in the same area as the WPF shelf (formed by Trp-Pro-Phe) in BET bromodomains. The WPF shelf has been exploited by potent BET inhibitors including (+)-JQ1 as well as I-BET762 (Figure 9.16A). RVF shelf in ATAD2 bromodomain is shallow and polar compared to the WPF shelf in BET bromodomains which was used as an advantage to get selectivity over BET bromodomains.

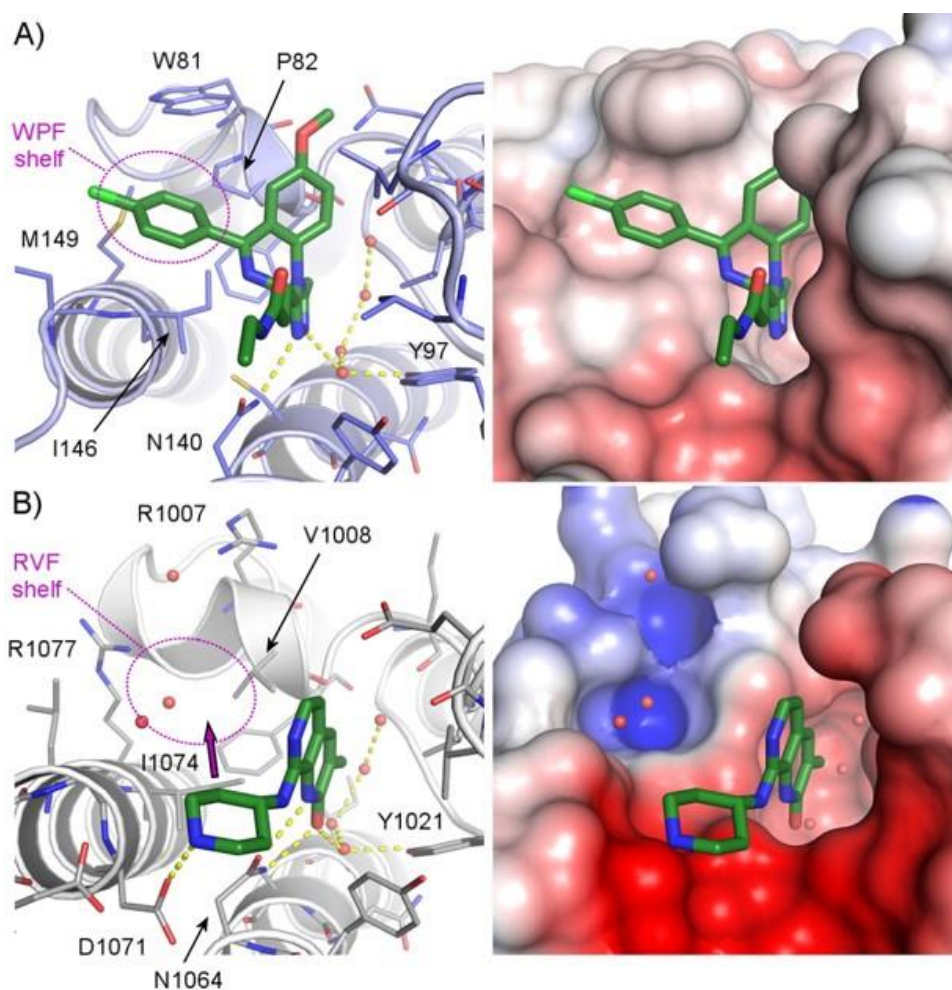
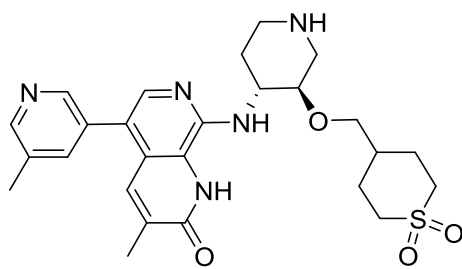


Figure 9.16: (A) BRD4 BD1 in complex to I-BET762 (PDB: 3p5o); (B) ATAD2 bromodomain in complex to a quinolone compound (PDB: 5a5q). The detailed interactions are on the left and protein surface coloured based on electrostatic charge on the right. A purple arrow head on (B) denotes the area of SAR investigation.¹⁷⁵

SAR studies at the 3'-position of the piperidine ring with the aim to target the RVF shelf gave compound **150** with desired potency and >100-fold selectivity for ATAD2 over other BET bromodomains (Figure 9.17). However, the compound was very hydrophilic with low cell-permeability. Attempts to increase cell permeability by reducing the polar surface area and the number of H-bond acceptors and donors resulted in reduced potency and selectivity. As described by Bamborough *et al*, the further optimisation of the series to obtain a cell permeable, potent and selective ATAD2 small molecule inhibitor is underway and will be published in the near future.¹⁷⁵



150

ATAD2 pIC ₅₀ (TR-FRET)	6.9
BRD2-4 BD1/2 pIC ₅₀ (TR-FRET)	4.3-5.3
Chemiluminescent nitrogen detection (CLND) solubility (μM)	179
Artificial membrane permeability (nm/s, pH 7.4)	<3

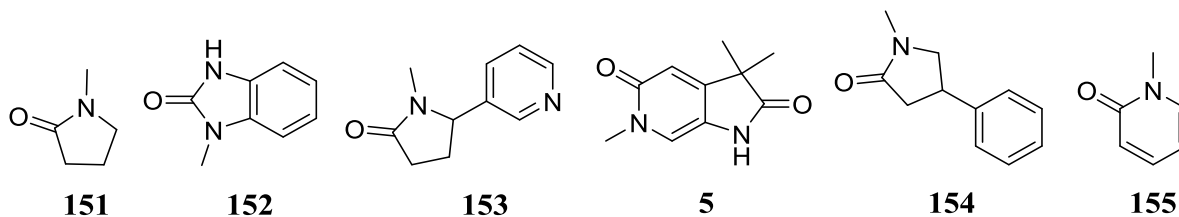
Figure 9.17: Summary of properties of compound **150**.¹⁷⁵

Chapter 10. Development of ATAD2 Inhibitors: SAR strategies

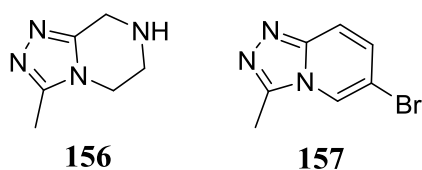
10.1 Fragment hits

Seventeen fragment hits bound in the acetyllysine binding site of ATAD2, were identified at Astex Pharmaceuticals by X-ray crystallographic focused screening. The fragments were clustered into five different classes based on their structures (Figure 10.1).

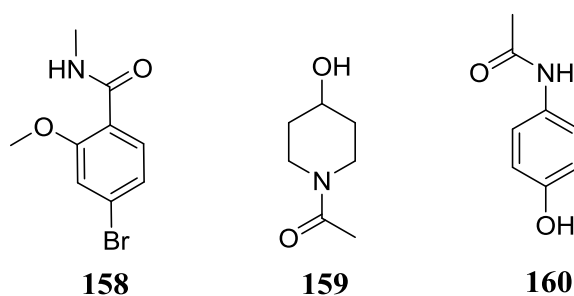
Cluster 1 (NMP-like)



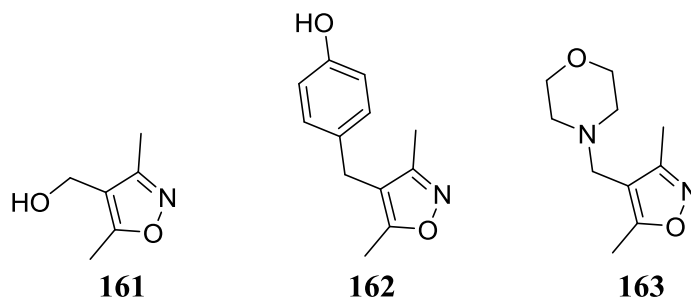
Cluster 2 (Triazoles)



Cluster 3 (Acetamides)



Cluster 4 (Isoxazoles)



Cluster 5 (Others)

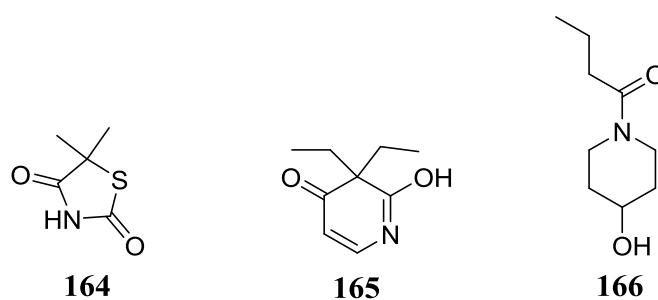


Figure 10.1: Structure-based classification of fragment hits identified at Astex Pharmaceuticals.

The initial strategy was to grow the fragments with subtle modifications including addition of alkyl or aryl groups in the lipophilic region of the binding surface, or adding H-bond donors or acceptors near the polar region of the binding surface. The work described in this thesis includes the SAR studies around four fragments **5**, **157**, **158** and **160**.

10.2 Preliminary SARs around Fragment 157, 158 and 160

10.2.1 Rationale

The crystal structure of ATAD2 in complex with fragment **158** revealed that the amide group mimics the acetyllysine binding mode (Figure 10.2). The oxygen atom of the amide group forms H-bond with Asn1064 and a water mediated H-bond with Tyr1021.

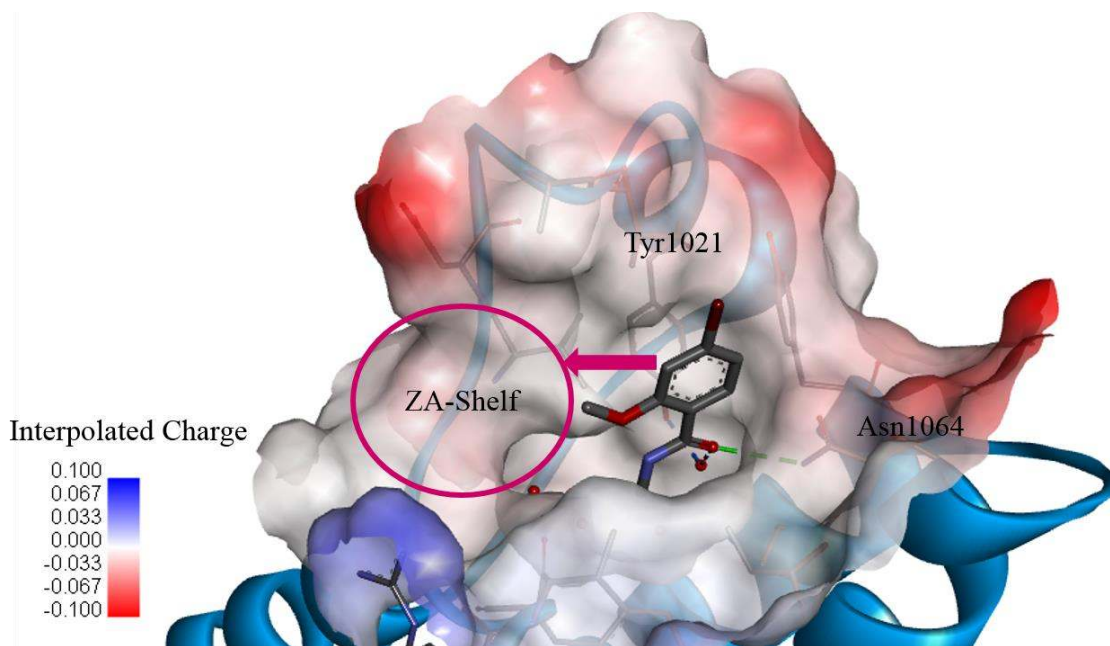


Figure 10.2: Crystal structure of fragment **158** (carbons: grey) bound to ATAD2. The binding surface is coloured based on the charge, positive: blue and negative: red. The ZA-shelf is shown by dark pink coloured circle. The pink arrow denotes the area of potential SAR investigation.

A shelf around the ZA loop (hereafter referred to as ZA-shelf) was identified from the crystal structure (Figure 10.2). Small alkyl substituents at the 3-position of fragment **158** were selected to exploit the ZA-shelf (Figure 10.3).

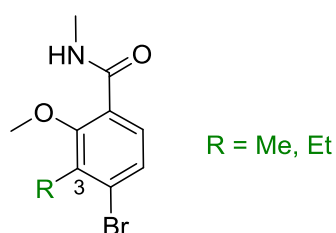


Figure 10.3: 3-Substituted benzamides to be synthesised.

Similarly, the crystal structure of fragment **160** bound to ATAD2 showed that the oxygen of amide forms H-bond with Asn1064, and a water mediated H-bond with Tyr1021 (Figure 10.4).

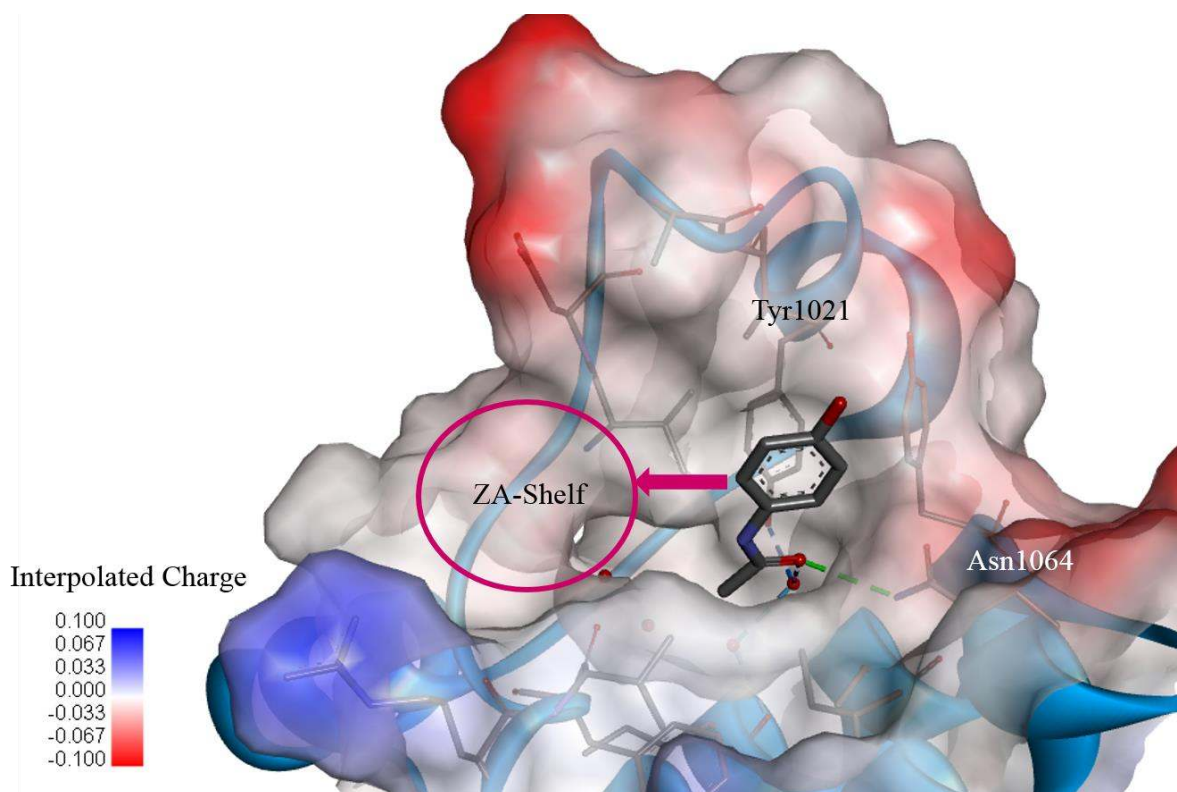


Figure 10.4: Crystal structure of fragment **160** (carbons: grey) bound to ATAD2. The binding surface is coloured based on the charge, positive: blue and negative: red. The ZA-shelf is shown by pink coloured circle. The pink arrow denotes the area of potential SAR investigation.

It was postulated that substitution at the 2-position of the phenyl ring could access the ZA-shelf. Alkyl and alkoxy substituents were selected for preliminary investigation (Figure 10.5).

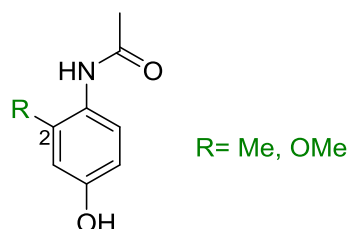


Figure 10.5: 2-Substituted phenylacetamides to be synthesised.

Crystal structure of triazole fragment **157** bound to ATAD2 showed that the compound adopted a different binding mode compared to other fragments (Figure 10.6). The H-bond with Asn1064 and water mediated H-bond with Tyr1021 was formed with two different nitrogen atoms in the

triazole ring, whereas, the two H-bonds were formed with one oxygen atom in fragments **158** and **160**.

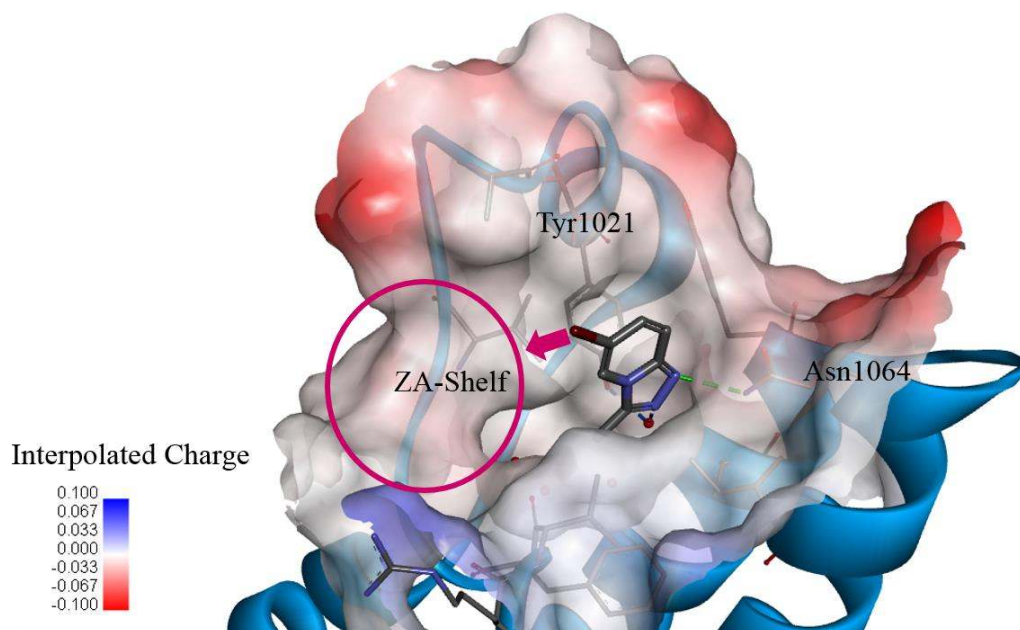


Figure 10.6: Crystal structure of fragment **157** (carbons: grey) bound to ATAD2. The binding surface is coloured based on the charge, positive: blue and negative: red. The ZA-shelf is shown by pink coloured circle. The pink arrow denotes the area of potential SAR investigation.

Interestingly, fragment **157** has a bromine atom on the pyridyl ring that could be utilised as a vector to exploit the ZA-shelf. Therefore, small alkyl substituents were selected for initial investigation (Figure 10.7).

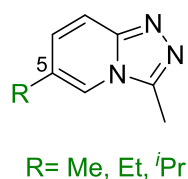
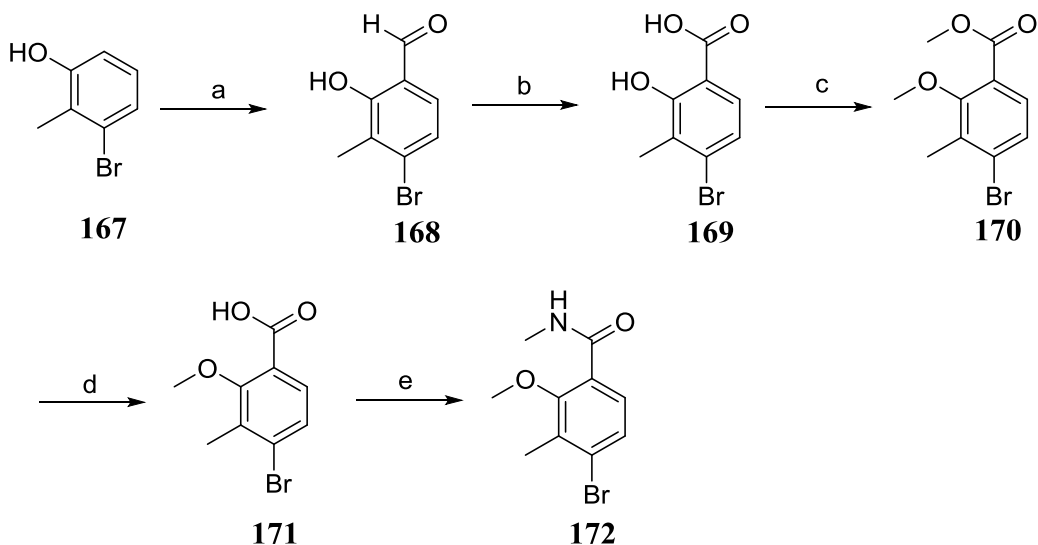


Figure 10.7: 5-substituted triazolopyridines to be synthesised.

10.2.2 Synthesis

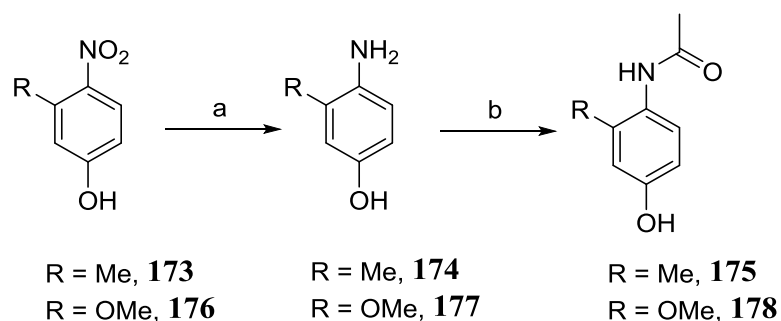
Synthesis of compound **172** began with formylation of the commercially available phenol **167** using magnesium chloride and paraformaldehyde (Scheme 10.1).¹⁷⁸ Subsequent Pinnick

oxidation of the aldehyde **168** gave carboxylic acid **169**, which was *bis*-methylated to obtain compound **170**. Hydrolysis of ester **170** followed by amide coupling with methylamine provided the target **172** in good yield.



Scheme 10.1: *Reagents and conditions:* (a) paraformaldehyde, NEt₃, MgCl₂, MeCN, reflux, 3 h, 93%; (b) NaClO₂, sulfamic acid, H₂O, MeCN, r.t., 8 h, 88%; (c) MeI, Cs₂CO₃, DMF, r.t., 18 h, 58%; (d) NaOH, H₂O, MeOH, 60 °C, 18 h, 95%; (e) MeNH₂, DIC, HATU, DMAP, THF, r.t., 18 h, 71%.

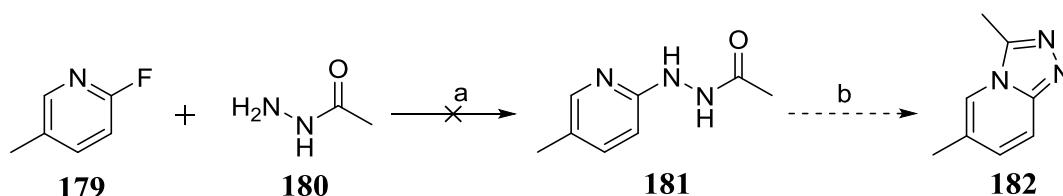
Compounds **175** and **178** were prepared following a two-step reaction sequence (Scheme 10.2). Reduction of commercially available nitrophenols **173** and **176** provided the corresponding amines, subsequent acetylation afforded targets **175** and **178**.



Scheme 10.2: *Reagents and conditions:* (a) H₂, 10% Pd/C, MeOH, r.t., 24 h; (b) Ac₂O, AcOH, r.t., 30 min, (**175**, 80%; **178**, 71%, over 2 steps).

To access triazolo[4,3-*a*]pyridine analogues, two different routes were employed. The first route involved S_NAr reaction on commercially available compound **179**. 2-Fluoro-5-methylpyridine **179** was resistant to S_NAr reaction with acethydrazide **180** at various conditions (Table 10.1).

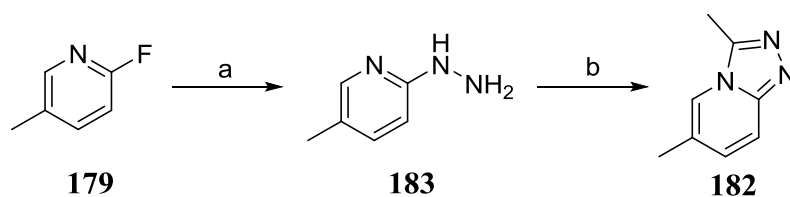
Table 10.1: Reagents and conditions used in step a



Solvent	Base	Temp °C	Time h	Result ^a
Ethanol	None	100	3	No conversion
Ethanol	None	100 under μ W	3	No conversion
Ethanol	NEt ₃	100	18	No conversion
Ethanol	DIPEA	100	18	No conversion

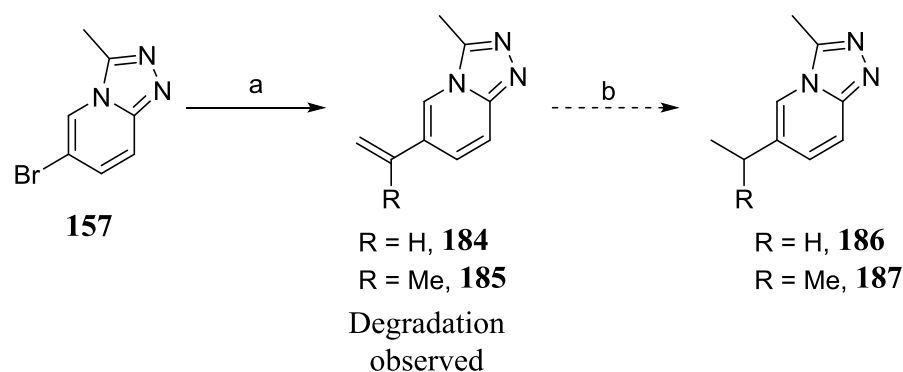
^a Observations from TLC and LCMS analyses

Failure of the S_NAr reaction might be due to the decrease in nucleophilicity of hydrazine in acethydrazide **180**, caused by the electron withdrawing acetyl group. Therefore, the S_NAr reaction was performed on commercially available compound **179** with unsubstituted hydrazine to get compound **183** (Scheme 10.3). Subsequent ring closure was performed in the presence of acetic acid and acetic anhydride, and gave target **182** in poor isolated yield.



Scheme 10.3: Reagents and conditions: (a) hydrazine, EtOH, reflux, 72 h, 43%; (b) Ac₂O, AcOH, reflux, 24 h, 16%.

The second route to access triazolo[4,3-*a*]pyridine analogues involved Suzuki-Miyaura coupling of compound **157** with alkyl boronic acids. Unfortunately, the coupling reaction with ethyl boronic acid was not successful. Further cross-coupling attempts were therefore performed with vinylboronic acid pinacol ester, followed by reduction (Scheme 10.4). However, the intermediate was found to be unstable with a noticeable colour change from beige to dark brown upon standing. A plausible explanation for the observed degradation is that the ring is very electron rich, therefore, susceptible to oxidation in presence of air. Literature searches of compound **186** and **187** were undertaken using Reaxys[®] and SciFinder[®] but with no success as the compounds had not been reported yet. Degradation of compounds with the triazolo[4,3-*a*]pyridine scaffold was also observed by our bioscientist colleague Dr Mathew Martin whilst performing the HTRF assay. Therefore, the series was not explored further due to the observed degradation of the intermediates **184** and **185**.



Scheme 10.4: *Reagents and conditions:* (a) vinylboronic acid pinacol ester, or isopropenylboronic acid pinacol ester, NaOH, *N,N*-dicyclohexylmethylamine, Pd(dppf)Cl₂.DCM, THF, 95 °C, 2.5 h, (**184**, 51%; **185**, 62%, over 2 steps); (b) H₂, 10% Pd/C, MeOH.

10.2.3 Biological Evaluation

A homogenous time resolved FRET assay (HTRF) was used to measure the ATAD2 inhibitory activity. GST-tagged ATAD2 was mixed with biotinylated acetylated ligand (Figure 10.8). Streptavidin labelled phycobiliprotein pigment purified from red algae (SA-XL665),¹¹¹ which binds to the biotinylated acetylated ligand, and a terbium-labelled anti-GST antibody that binds to GST-tagged ATAD2 was added to the mixture. The terbium label acts as a donor of FRET signal, and SA-XL665 acts as an acceptor of the FRET signal. Upon excitation, there is a

transfer of FRET from donor to acceptor which can be measured. In the absence of an inhibitor, the donor (terbium) and the acceptor (SA-XL665) are in close proximity. The donor terbium absorbs energy and transfers it to SA-XL665. The transfer of energy is measured as a FRET signal. In the presence of an inhibitor, the donor and acceptor are separated which results in a decrease in the amount of FRET. The experimental details of the HTRF assay are discussed in 16.4.1.

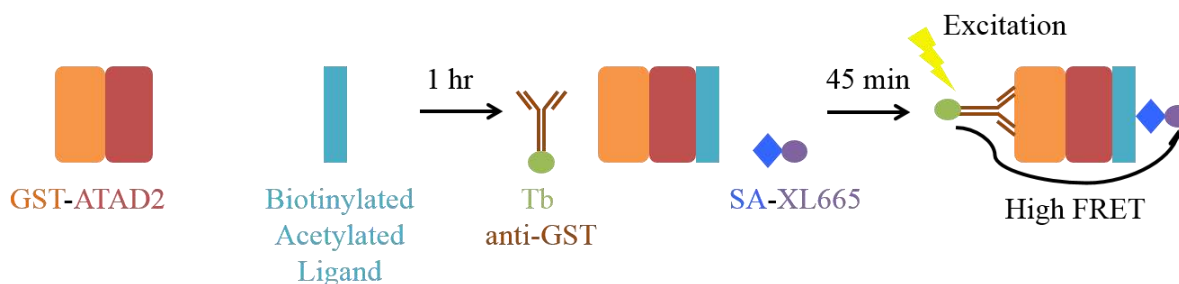
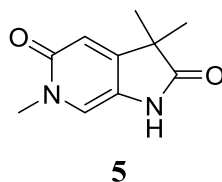


Figure 10.8: Schematic representation of ATAD2-HTRF assay.

Compounds **172**, **175**, **178** and **182** did not show measurable inhibition by Homogenous Time Resolved FRET assay (HTRF) at 4 mM concentration. In addition, co-crystallisation experiments of ATAD2 with the compounds had failed. Meanwhile, Dr Duncan Miller had demonstrated that subtle modifications in fragment **5** improved ATAD2 inhibition and the compounds were successfully co-crystallised with ATAD2. Besides, fragment **5** was a novel scaffold which had not been reported to date for bromodomain inhibition. Therefore, most of the medicinal chemistry effort was focussed in SAR studies around fragment **5** which will be discussed in detail in following chapters.



Chapter 11.SAR Studies around the N^1 -Position of Fragment 5

11.1 Rationale

Crystal structure of fragment **5** bound to ATAD2 showed that the oxygen atom of the pyridone ring formed two key H-bonds, one with Asn1064 and the other water mediated H-bond with Tyr1021 (Figure 11.1).

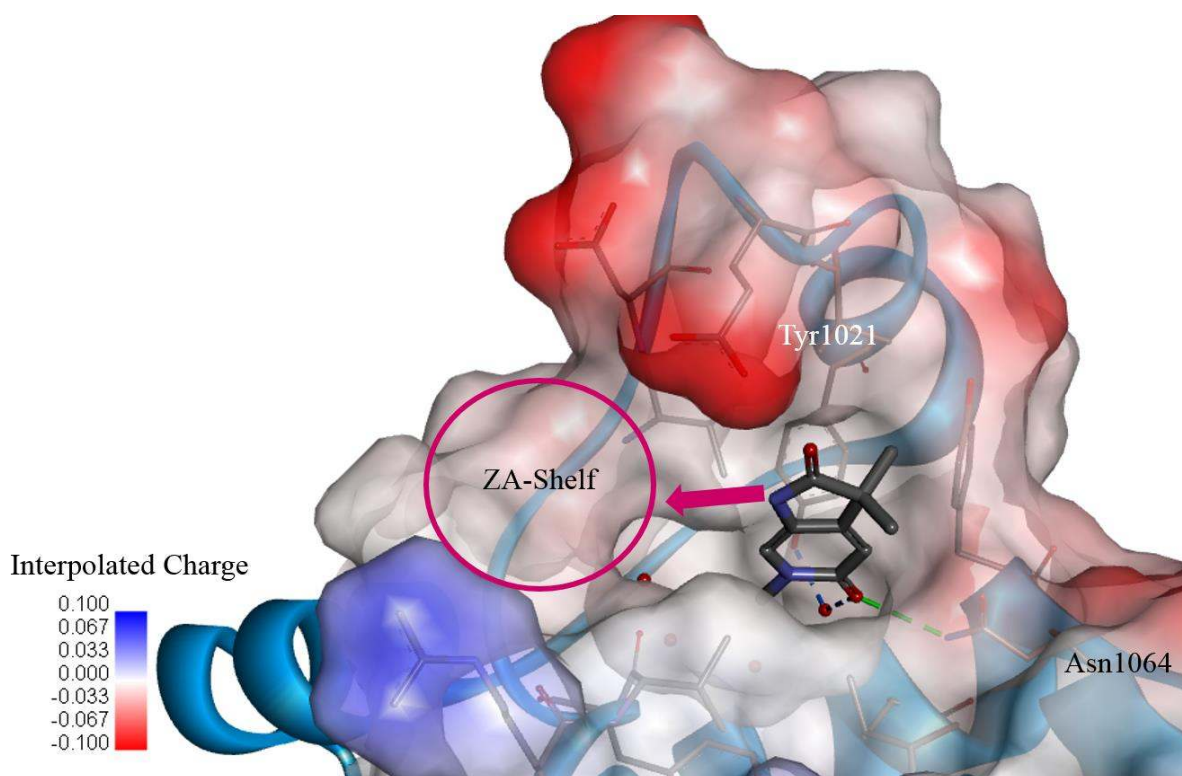


Figure 11.1: Crystal structure of fragment **5** (carbons: grey) bound to ATAD2. The binding surface is coloured based on the charge, positive: blue and negative: red. The ZA-shelf is shown by the dark pink coloured circle. The pink arrow denotes the area of potential SAR investigation. Water molecules are shown as red spheres.

The initial strategy was to explore SARs at the N^1 -position of the pyrrolidinone ring to access the ZA-shelf (Figure 11.1). A range of polar and lipophilic substituents were selected (Figure 11.2).

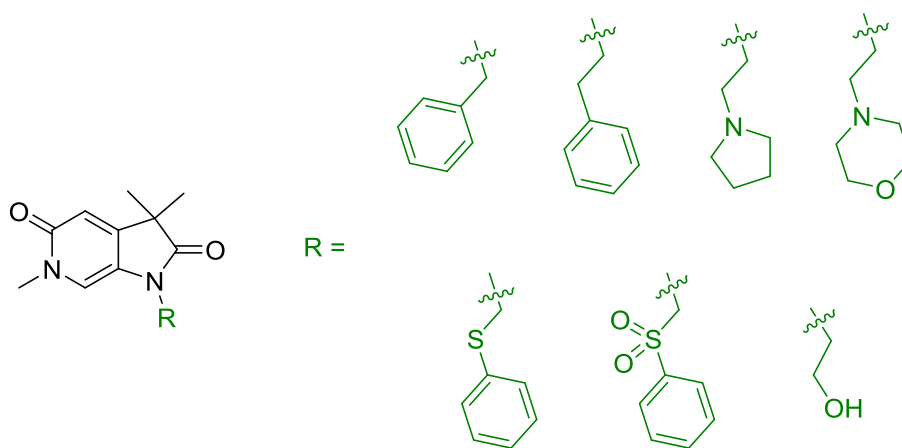
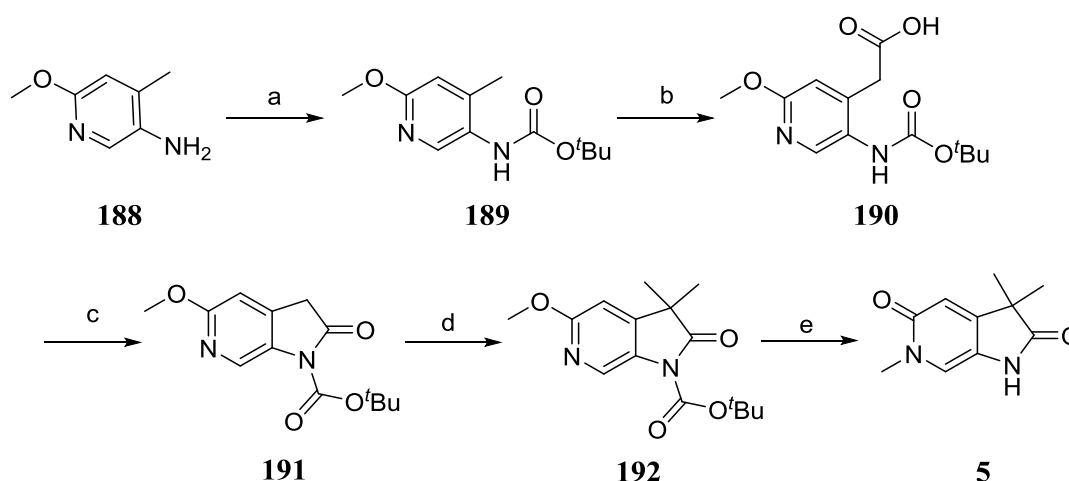


Figure 11.2: N^1 -substituted targets to be synthesised.

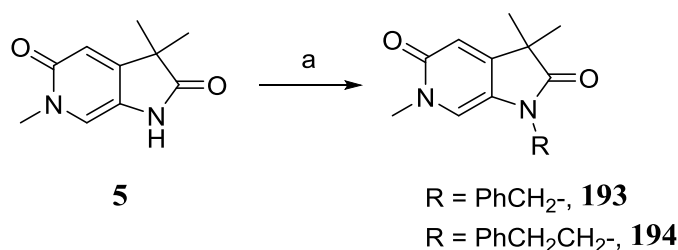
11.2 Synthesis

The strategy was to synthesise fragment **5** in bulk quantity, and subsequent alkylation reactions would provide the desired targets. The synthesis started with *N*-Boc protection of commercially available 6-methoxy-4-methylpyridin-3-amine **188** to get compound **189**, which was used in a carboxylation reaction to give compound **190** (Scheme 11.1). The ring closure was mediated by acetic anhydride in the presence of catalytic tetrabutylammonium acetate to give compound **191**. Subsequent *bis*-methylation provided compound **192**. The *N*-Boc deprotection, as well as formation of pyridone was achieved in a single step by heating in the presence of MeI and catalytic sodium iodide to get compound **5**. Formation of pyridone using MeI and sodium iodide is a widely used method to synthesise pyridones from 2-alkoxypyridines.¹⁷⁹⁻¹⁸² Interestingly, when the reaction was performed in the absence of sodium iodide, quantitative yield of the product was obtained.



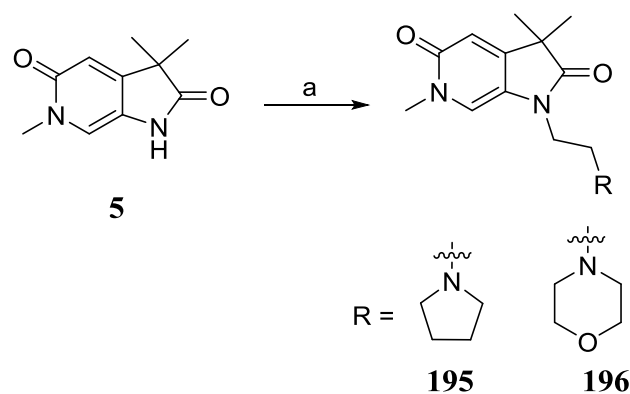
Scheme 11.1: *Reagents and conditions:* (a) Boc_2O , THF, Na_2CO_3 , THF, r.t., 42 h, 95%; (b) (i) *s*-BuLi, THF, $-78\text{ }^\circ\text{C}$, 15 min; (ii) CO_2 (dry ice), $-78\text{ }^\circ\text{C}$ to r.t., 45 min, 74%; (c) Ac_2O , tetrabutylammonium acetate, $65\text{ }^\circ\text{C}$, 1 h, 81%; (d) MeI, Cs_2CO_3 , MeCN, $60\text{ }^\circ\text{C}$, 3 h, 78%; (e) MeI, MeCN, $170\text{ }^\circ\text{C}$, μW , 1 h, quant.

Targets **193** and **194** were synthesised following NaH-mediated alkylation reactions (Scheme 11.2).



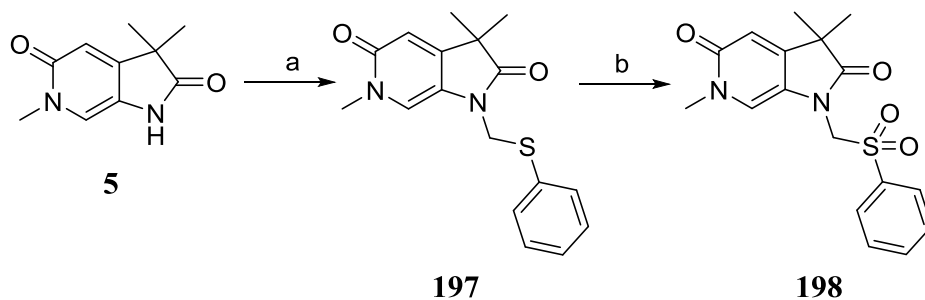
Scheme 11.2: *Reagents and conditions:* (a) (i) NaH, DMF, r.t., 15 min; (ii) benzyl bromide or (2-bromoethyl)benzene, r.t., 3 h, 61%; (**193**), 30% (**194**).

The isolated yields of NaH mediated alkylation reactions were low to moderate. Besides, isolation of the products was difficult due to close-running impurities. Therefore, in search of alternative alkylation conditions, the stronger base NaH was replaced by caesium carbonate. Caesium carbonate mediated alkylation reactions were faster, and isolation of the product easier (Scheme 11.3).



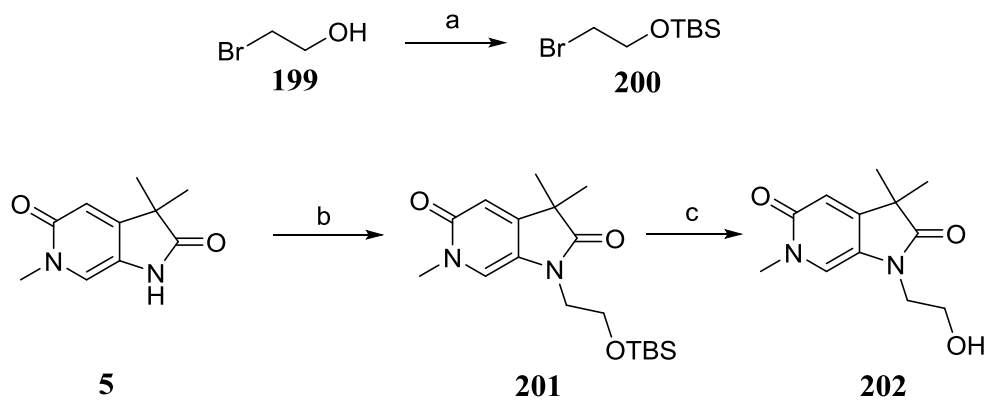
Scheme 11.3: *Reagents and conditions:* (a) 1-(2-chloroethyl)pyrrolidine hydrochloride or 4-(2-chloroethyl)morpholine hydrochloride, Cs_2CO_3 , DMF, 100 °C, μW , 30 min, 40% (**195**), 82% (**196**).

Target **198** was obtained from a two-step reaction sequence. Alkylation of compound **5** with chloromethyl phenyl sulphide gave sulphide **197**, which was subsequently oxidised using Oxone[®] to the corresponding sulfone **198** (Scheme 11.4).



Scheme 11.4: *Reagents and conditions:* (a) chloromethyl phenyl sulphide, Cs_2CO_3 , DMF, 100 °C, μW , 30 min, 75%; (b) Oxone[®], MeOH, H_2O , r.t., 18 h, 52%.

Initial attempt to synthesise target **202** by alkylation of compound **201** using 2-bromoethan-1-ol **199** was unsuccessful. Therefore, an alternate synthetic route was followed to prepare target **202** (Scheme 11.5). The synthesis started with TBS protection of commercially available alcohol **199** to get compound **200**, which was used for alkylation of compound **5** to obtain compound **201**. Finally, TBS-deprotection provided target **202** in good yield.

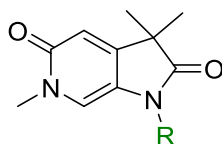


Scheme 11.5: Reagents and conditions: (a) TBSCl, NEt₃, DMAP, DCM, r.t., 18 h, quant.; (b) 200, Cs₂CO₃, DMF, 100 °C, μW, 30 min, 55%; (c) TBAF, THF, r.t., 18 h, 90%.

11.3 Biological Evaluation

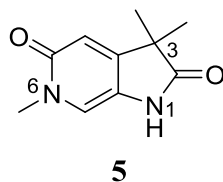
Diverse substitution at *N*¹-position of fragment **5** did not increase the ATAD2 inhibitory activity. The compounds did not show ATAD2 inhibition at 2 mM concentration using the HTRF assay (Table 11.1).

Table 11.1: ATAD2 inhibitory activity of derivatives with various substituents at N^1 -position.



Compound	R	ATAD2 IC ₅₀ (μ M)	Compound	R	ATAD2 IC ₅₀ (μ M)
193		>2000	197		>2000
194		>2000	198		>2000
195		>2000	202		>2000
196		>2000			

Therefore, focus was shifted towards the substitution on the other nitrogen (N^6) of the fragment **5**, and is discussed in detail in the next chapter.



Chapter 12. SAR Studies around the N^6 -Position of Fragment 5

12.1 Rationale

SAR studies conducted at the NICR by Dr Duncan Miller identified that methylation at the N^1 -position of fragment **5** to obtain fragment **203** changed the binding mode of the scaffold. The oxygen atom of the pyridone ring in the original fragment hit **5** forms key H-bonds with Asn1064 and a water-mediated H-bond with Tyr1021 (carbons coloured cyan in Figure 12.1A/B). However, upon N^1 -methylation, the pyridone ring in fragment **203** (carbons coloured green in Figure 12.1A/B) flips and points towards the ZA-shelf. Besides, the pyridone oxygen is involved in an additional water-mediated H-bond interaction with Asp1014 (Figure 12.1B).

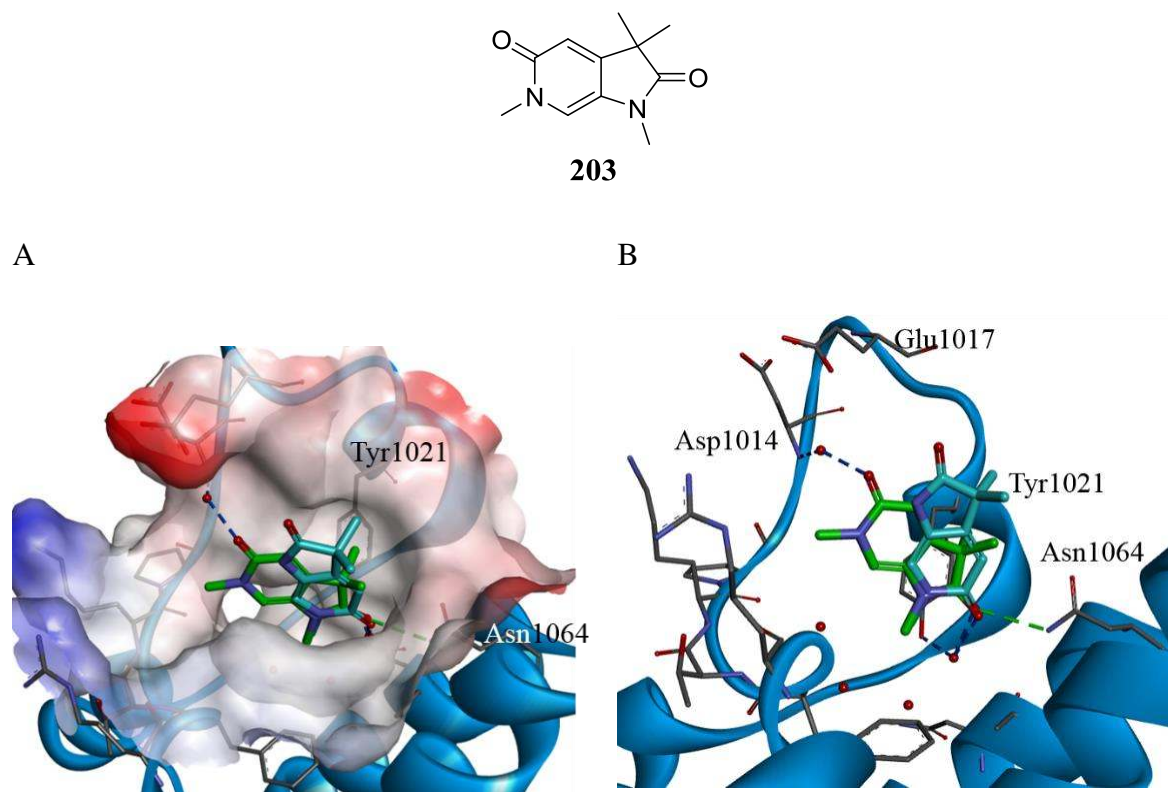
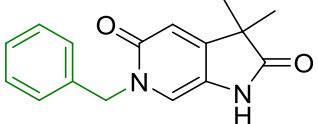
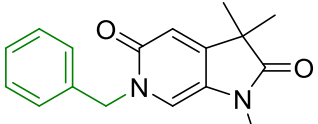
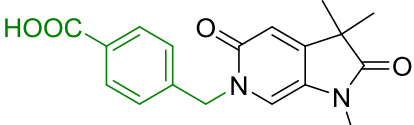


Figure 12.1: Overlay of the crystal structures of fragment **203** (green) bound to ATAD2 and the original fragment hit **5** (cyan) showing: (A) solvent accessible surface coloured based on charge, positive: blue, negative: red; (B) key H-bond interactions. Water molecules are shown as red spheres.

The flipped binding mode of fragment **203** encouraged us to explore SAR at the N^6 -position. Preliminary SAR studies at the N^6 -position proved that an increase in potency was achievable with the identification of compound **206**, which was the most potent in-house inhibitor to date (Table 12.1).

Table 12.1: ATAD2 inhibitory activities of N^6 -substituted analogues.

Compound	Structure	ATAD2 IC ₅₀ (μM) ^a	L.E
204		3000	0.17
205		716 ^b	0.21
206		247 ^c	0.21

^a Determinations (n = 1 unless otherwise stated); ^b n = 2; ^c n = 4

The crystal structure of compound **205** bound to ATAD2 suggested that H-bond donors or acceptors in the phenyl ring could interact with polar amino acids in the ZA loop including Arg1007 and Glu1017 (Figure 12.2).

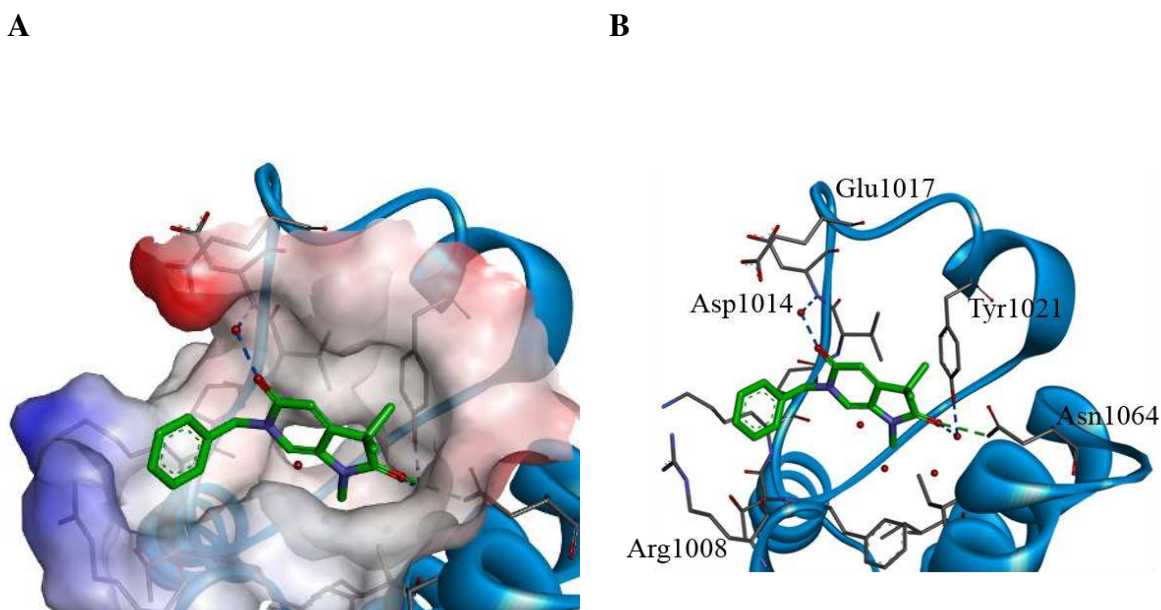


Figure 12.2: Crystal structure of ATAD2 in complex with compound **205** (green) showing (A) solvent accessible surface coloured based on the charge, positive: blue, negative: red; (B) Key H-bond interactions. Water molecules are shown as red spheres.

Various in-house crystal structures of ATAD2 in complex with different compounds suggested that the side chains of Glu1017 and Arg1008 were flexible, increasing the complexity of target design. SAR studies were carried out around the phenyl ring of compound **205** to obtain H-bond interactions with the polar residues in the ZA-shelf. It was decided to introduce a range of substituents including H-bond donors, acceptors, lipophilic groups, and halogens at the *ortho*-, *meta*- or *para*-positions of the phenyl ring of compound **205** (Figure 12.3).

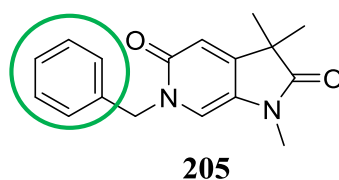
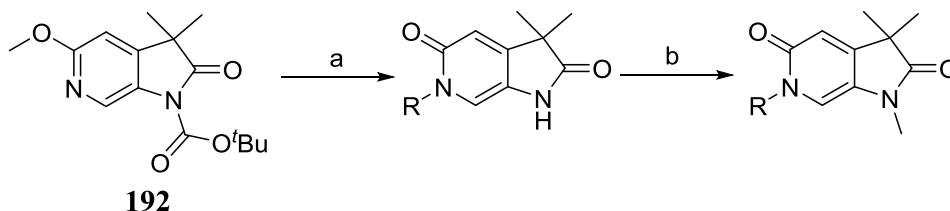


Figure 12.3: N^6 -substituted analogues to be synthesised. SAR studies to be carried out around the phenyl ring highlighted by a green circle.

12.2 Synthesis

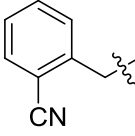
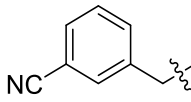
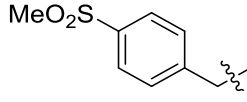
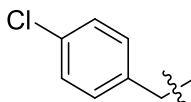
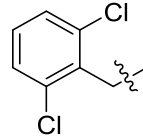
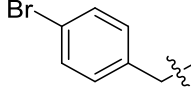
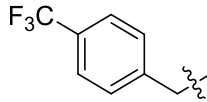
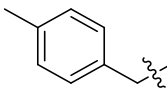
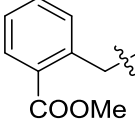
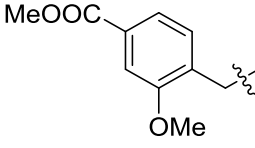
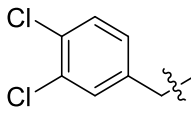
Intermediate **192** was synthesised in large quantity (Scheme 11.1) and used for the synthesis of various targets. Formation of pyridone using various alkylating agents, followed by *N*¹-methylation gave 10 targets (Scheme 12.1).



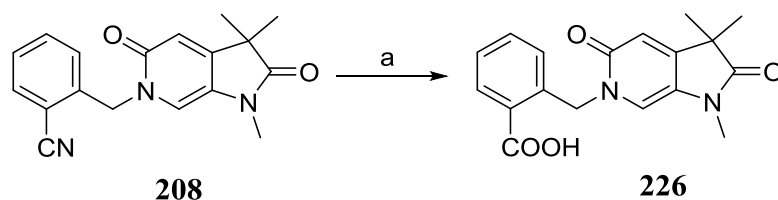
Scheme 12.1: Reagents and conditions: (a) R-Br, MeCN, 170 °C, μW, 45 min; (b) MeI, Cs₂CO₃, DMF, 100 °C, μW, 30 min.

The isolated yields obtained in step a and b for various targets are shown in Table 12.2. The pyridone formation reaction (step a, Scheme 12.1) provided the desired products in high yields except for compound **222**. The low yield for compound **222** might be due to the steric hindrance caused by the methyl ester in the *ortho*-position. The final methylation step provided the desired targets in moderate to good yields.

Table 12.2: Isolated yields of step a and step b in **Scheme 12.1**.

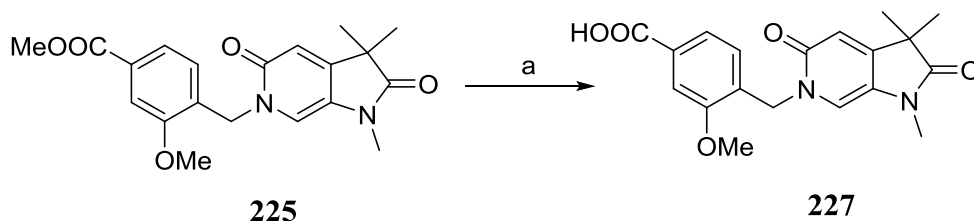
Compound	R	Step a	Step b
208		207, 63%	95%
210		209, 65%	91%
212		211, 53%	86%
6		213, 80%	90%
215		214, 82%	92%
217		216, 78%	95%
219		218, 71%	92%
221		220, 85%	92%
223		222, 22%	74%
225		224, 66%	80%
229		228, 93%	94%

Nitrile **208** was hydrolysed to get compound **226**.



Scheme 12.2: Reagents and conditions: (a) NaOH, EtOH, H₂O, 100 °C, 23 h, 32%.

Similarly compound **227** was obtained *via* ester-hydrolysis of compound **225**.

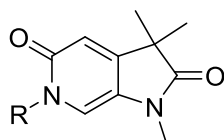


Scheme 12.3: Reagents and conditions: (a) NaOH, MeOH, H₂O, 70 °C, 2 h, 96%.

12.3 SAR and Biological Evaluation

A small library of compounds with different substituents on the phenyl ring were tested against ATAD2 (Table 12.3). Compounds **6** and **217** with a halogen at the *para*-position retained ATAD2 inhibitory activity. Compound **219** with a *para*-substituted trifluoromethyl group was also tolerated. However, compound **221** with a *para*-substituted methyl group showed a reduction in ATAD2 inhibitory activity by around 4-fold. The *para*-substituted methyl sulfone derivative **212**, which was synthesised to study the effect of an H-bond acceptor sulfone group in the proximity of polar amino acids in ZA-shelf, showed at least 2-fold reduction in potency. Substitution at the *ortho*-position resulted in a significant loss in ATAD2 inhibition as seen with compounds **208**, **215**, **223** and **226**. Compound **227** with a methoxy group at the *ortho*-position retained some activity, probably due to the presence of the carboxylic acid at the *para*-position. Compound **229** with an additional chloro substituent at the *meta*-position resulted in at least 2-fold loss in potency.

Table 12.3: ATAD2 inhibitory activity of *N*⁶-substituted analogues.



Compound	R	ATAD2 IC ₅₀ (μM) ^a	Compound	R	ATAD2 IC ₅₀ (μM) ^a
208		>2000	217		294 ^b
210		1393	219		354 ^d
212		565	221		815
6		209 ^c	223		>2000
215		>2000	225		>2000
229		469	227		734
226		>2000			

^a Determinations (n = 1 unless otherwise stated); ^b n = 2; ^c n = 3; ^d n = 6

Compound **6** with a chloro group at the *para*-position was the most potent inhibitor identified in this series. The crystal structure of compound **6** bound to ATAD2 showed that an additional water-mediated H-bond with the flexible side-chain of Glu1017 was formed (Figure 12.4). The

binding mode was very similar to the parent compound **205** where pyrrolidinone oxygen forms H-bond with Asn1064 and water mediated H-bond with Tyr1021.

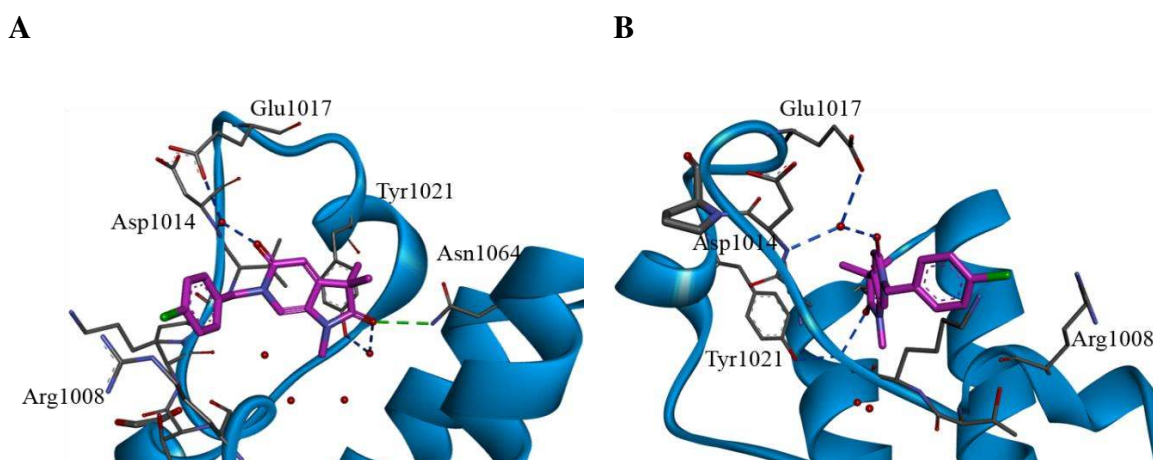


Figure 12.4: Crystal structure of ATAD2 in complex with compound **6** (magenta); (A) front view of the compound; (B) side view of the compound to highlight two water-mediated H-bonds with Asp1014 and Glu1017. Water molecules are shown as red spheres.

The crystal-structure of compound **226** showed that the *ortho*-substituted carboxylic acid twisted the phenyl ring, probably due to the intramolecular clash of the carboxylic acid with the pyridone oxygen atom, leading to reduced activity (Figure 12.5). In addition, the water-mediated H-bond with Asp1014 was not observed, due to the movement of the scaffold (Figure 12.5B).

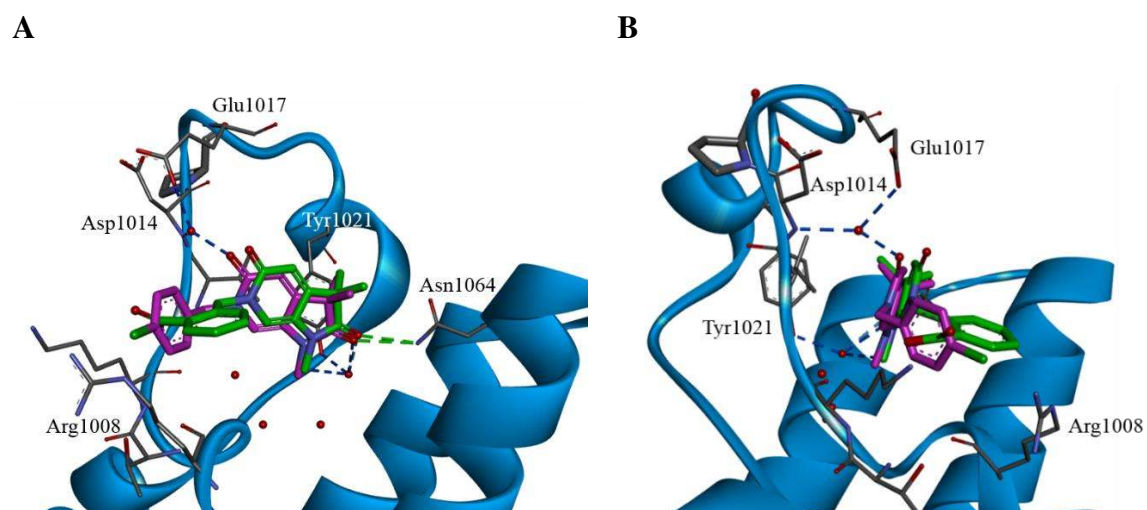


Figure 12.5: Overlay of crystal structure of compound **6** (magenta) and **226** (green) bound to ATAD2; (A) front view of the compounds, (B) side view of the compounds highlighting the movement of compound **226** (green).

As mentioned earlier the methyl sulfone substituted derivative **212** was synthesised to test the effect of 2 H-bond acceptors in the ZA-self. Although, the two oxygens of the sulfone group were in close proximity to Arg1008, H-bond interactions were not formed (Figure 12.6). The binding mode of compound **212** was same as that of compound **6**.

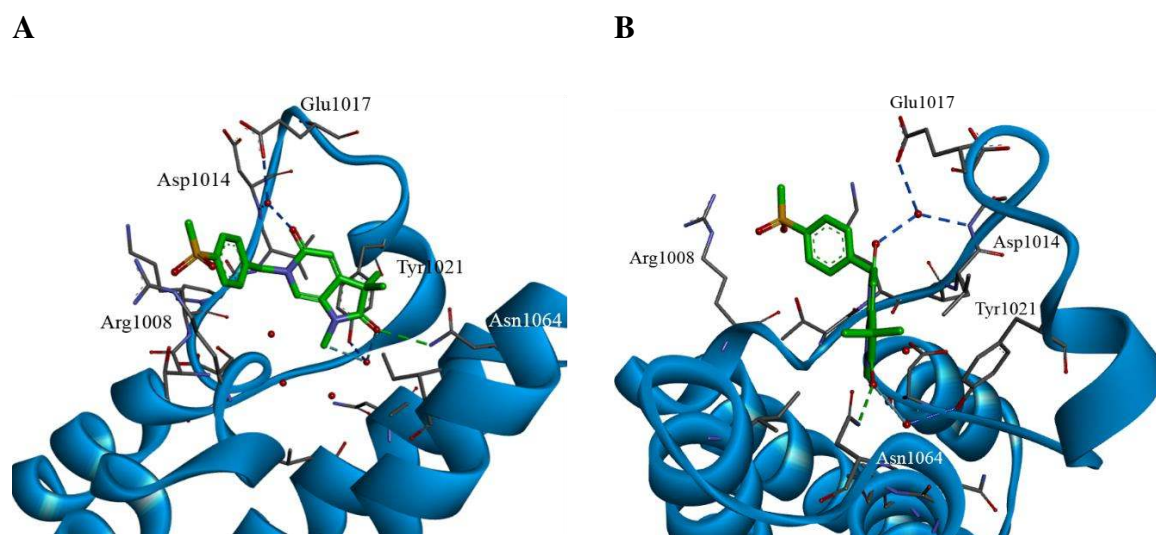


Figure 12.6: Crystal structure of ATAD2 in complex with compound **212** (green); (A) front view of the compound; (B) side view of the compound. Water molecules are shown as red spheres.

Various analogues bearing amines at the *para*-position were synthesised by other colleagues, with the hypothesis that H-bond donors might interact with the flexible side chain of Glu1017

leading to improvement in the ATAD2 inhibition. However, the compounds did not improve the activity, making the *para*-chloro substituted derivative **6**, the most potent compound to date. Therefore, the *para*-chlorobenzyl group was chosen as the optimum group to access the ZA-shelf and focus was shifted towards SAR studies at other positions of compound **6**.

Chapter 13. Accessing the Region Occupied by Acetylated Histone

13.1 Rationale

After identifying the *para*-chlorobenzyl as the optimum substituent at N^6 -position to access the ZA-shelf, new regions of the ATAD2 binding site were explored. A region around the BC loop was identified from the crystal structure of acetylated histone bound to ATAD2 (PDB: 4QUU, Figure 13.1). The acetylated histone occupies a region between the BC-loop and the ZA-loop. The lead compound **6** has two methyl groups pointing towards the same region (Figure 13.1).

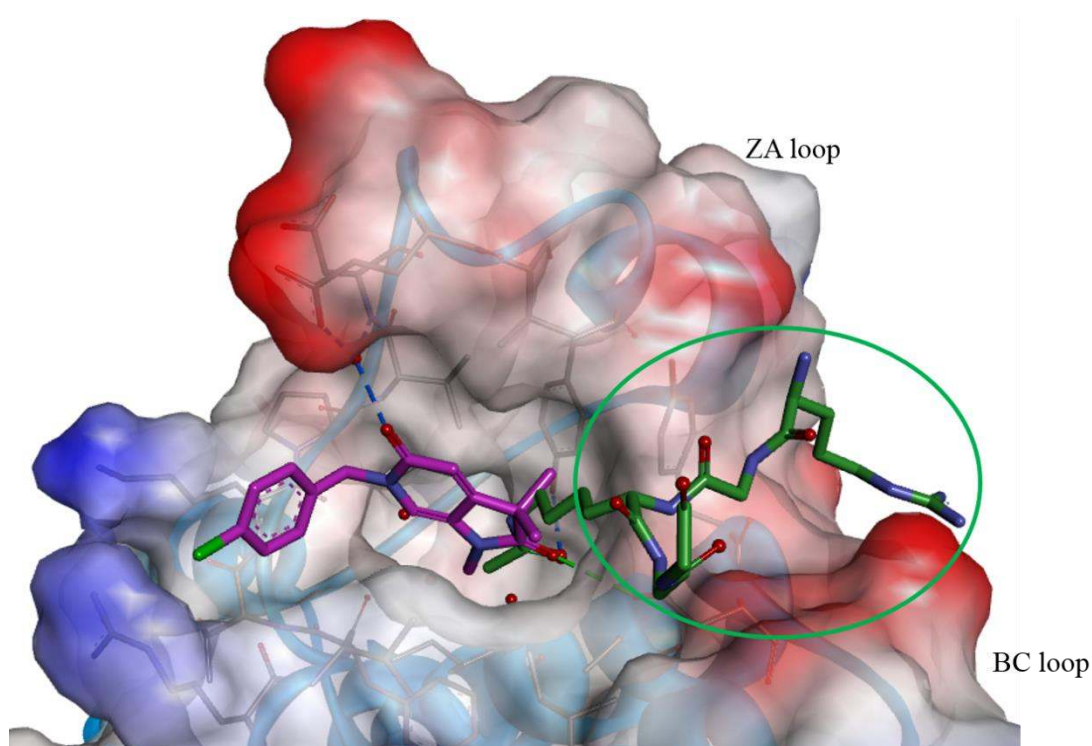


Figure 13.1: Overlay of crystal structures of ATAD2 in complex with compound **6** (magenta) and acetylated histone peptide (green, PDB: 4QUU). The binding surface is coloured based on the charge, positive: blue and negative: red. The region of interest is highlighted by a green circle.

It was decided to explore this region by using one of the methyl substituents as a vector for expansion. A series of 3-substituted pyrrolidinone derivatives were proposed (Figure 13.2).

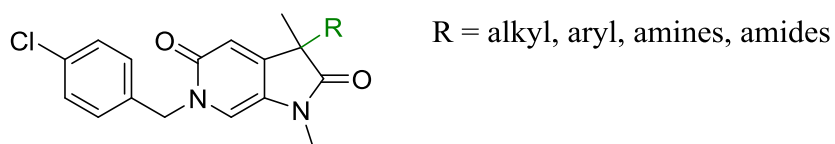
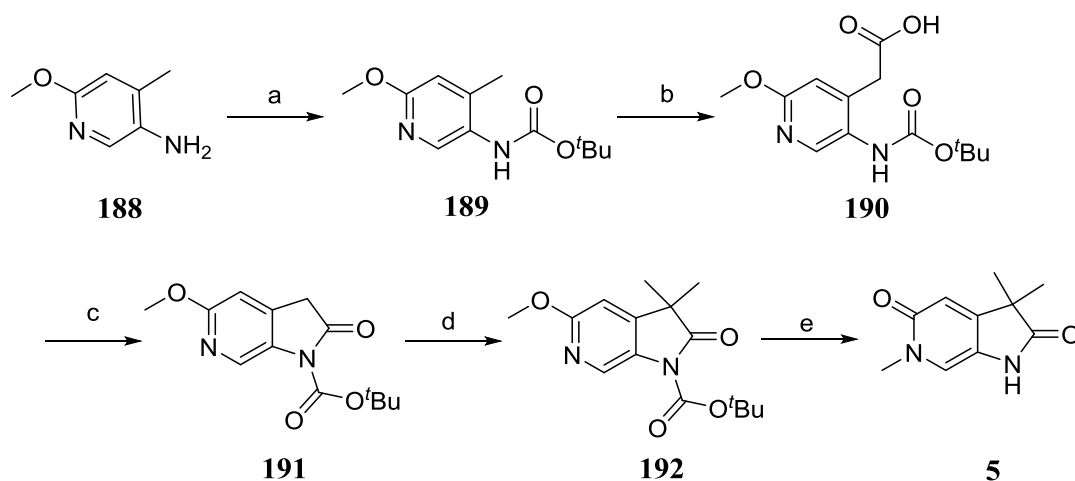


Figure 13.2: 3-substituted pyrrolidinone derivatives to be synthesised.

13.2 Synthesis

13.2.1 Mono-alkylation at the 3-Position

In the initial synthetic route to prepare intermediate **5** (Scheme 13.1), step d involved a *bis*-methylation at the 3-position. This route had to be modified to enable a mono-alkylation in step d.



Scheme 13.1: Reagents and conditions: (a) Boc_2O , THF, Na_2CO_3 , THF, r.t., 42 h, 95%; (b) (i) *s*-BuLi, THF, $-78\text{ }^\circ\text{C}$, 15 min; (ii) CO_2 (dry ice), $-78\text{ }^\circ\text{C}$ to r.t., 45 min, 74%; (c) Ac_2O , tetrabutylammonium acetate, $65\text{ }^\circ\text{C}$, 1 h, 81%; (d) MeI, Cs_2CO_3 , MeCN, $60\text{ }^\circ\text{C}$, 3 h, 78%; (e) MeI, MeCN, $170\text{ }^\circ\text{C}$, μW , 1 h, quant.

The mono-alkylation would provide a versatile intermediate which could be used to introduce a range of substituents at the 3-position (Figure 13.3).

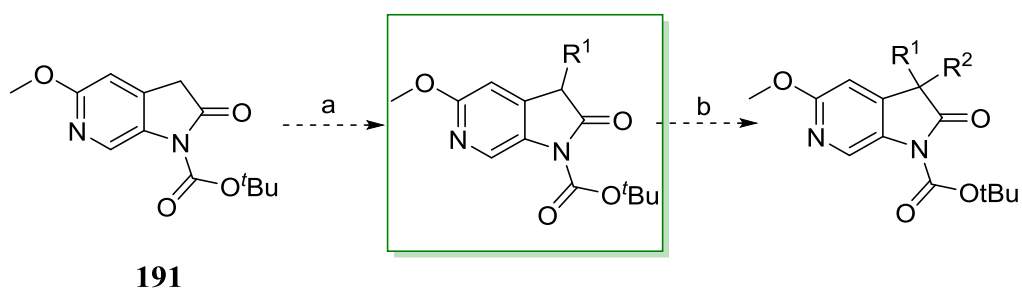
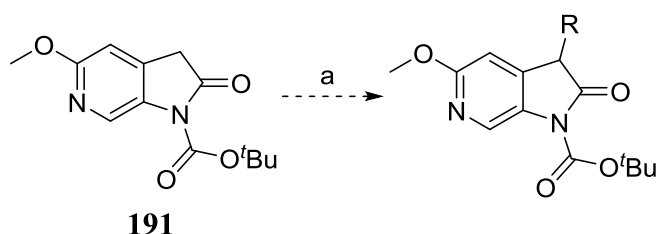


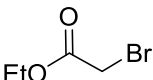
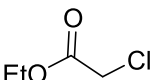
Figure 13.3: Proposed synthetic scheme to prepare a mono-alkylated intermediate.

As there were no literature precedent for mono-alkylating the 3-position of our scaffold, mono-alkylation at the 3-position of oxindoles was searched. There are numerous examples describing the mono-alkylation of the 3-position of oxindoles.¹⁸³⁻¹⁸⁶ The strategy was to deprotonate at the 3-position and use 1 equivalent of an electrophile to obtain the mono-alkylated product. However, various electrophiles and bases at different temperatures did not lead to mono-alkylated product. A significant amount of time was engaged to develop a chemistry that would allow mono-alkylation at the 3-position by three chemists within the group. Few examples are highlighted in Table 13.1.

Table 13.1: Summary of different conditions used for mono-alkylation at the 3-position.

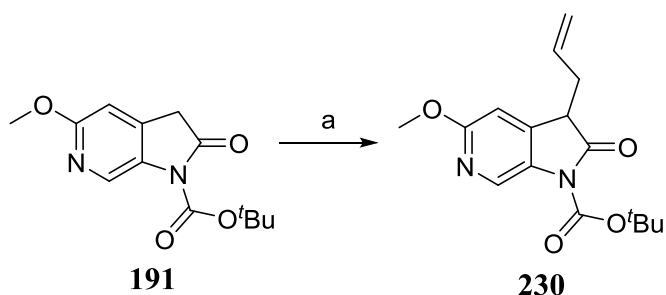


Electrophiles RX ^a	Bases ^a	Solvent	Temperature °C	Results
CH ₃ I	Cs ₂ CO ₃	MeCN	60	Significant <i>bis</i> -methylation
CH ₃ CH ₂ I	Cs ₂ CO ₃	MeCN	60	Complex mixture, significant <i>bis</i> -ethylation
CH ₃ CH ₂ I	Cs ₂ CO ₃ ^b	MeCN	r.t.	Complex mixture, significant <i>bis</i> -ethylation
CH ₃ CH ₂ I	LiHMDS	THF	-50	Starting material only

CH ₃ CH ₂ I	LiHMDS	THF	r.t.	Starting material only
CH ₃ I	KHMDS	THF	r.t.	Significant <i>bis</i> -methylated product
	LHMDS	THF	-78 to r.t.	Starting material only
	LHMDS	THF	-78 °C to r.t.	Starting material only

^a No. of equivalents used = 1; ^b No. of equivalents = 0.5

The mono-alkylation reaction worked with very low isolated yield when LHMDS was used as a base and allyl bromide as an electrophile (Scheme 13.2). The product was not stable in air, therefore, it had to be stored under nitrogen. Although, the reaction worked, the yield was poor, the reaction was not reproducible, and there were at least 4 additional steps towards the desired targets. Moreover, the scheme would not allow further functionalisation at the 3-position, therefore, the scheme was discarded.

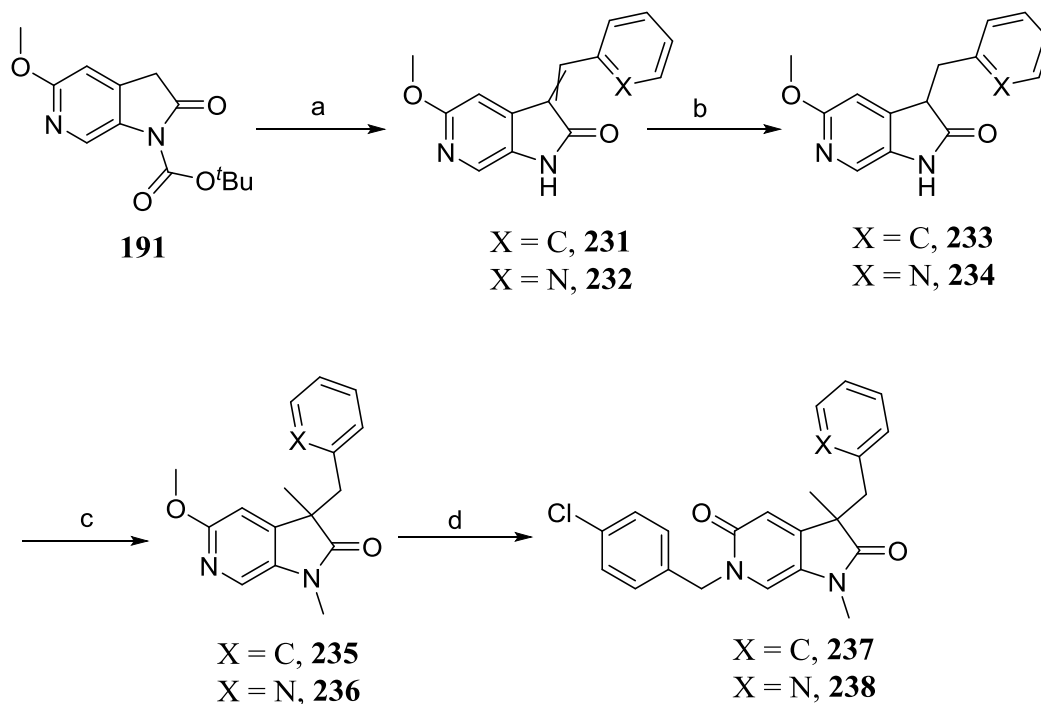


Scheme 13.2: *Reagents and conditions:* (a) (i) LHMDS, THF, -78 °C, 45 min; (ii) allyl bromide, -78 °C, 2 h, then, r.t., 20 h, 26%.

13.2.2 Variation at the 3-Position using Knoevenagel Condensation

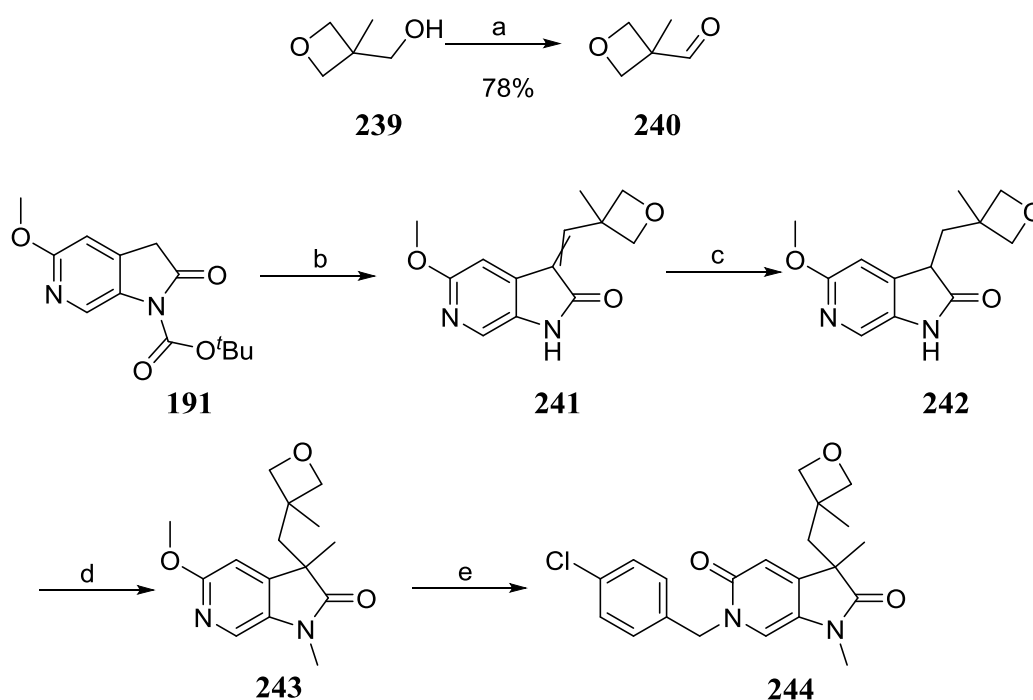
Whilst attempting various routes for mono-alkylating the 3-position, Knoevenagel condensation of compound **191** with acetaldehyde and formaldehyde was attempted, without any success. However, major breakthrough came from the Knoevenagel condensation of benzaldehyde with compound **191** which provided the desired compound **231** in high yield (Scheme 13.3). Subsequent reduction of the double bond, followed by methylation provided compound **235**. Treatment of pyridine **235** with 4-chlorobenzyl bromide at high temperature

provided the target pyridone **237** in moderate yield. Similarly, compound **238** was synthesised *via* Knoevenagel condensation of compound **191** and picolinaldehyde.



Scheme 13.3: Reagents and conditions: (a) benzaldehyde or picolinaldehyde, piperidine, THF, 100 °C, 30 min, 88% (X = C), 50% (X = N); (b) H₂, 10% Pd/C, THF, MeOH, r.t., 2 h; (c) MeI, Cs₂CO₃, DMF, 50 °C, 1.5 h, 55% (X = C), 56% (X = N) over 2 steps; (d) 4-chlorobenzyl bromide, MeCN, 170 °C μ W, 45 min, 64% (X = C), 50% (X = N).

It was decided to utilise the synthetic route *via* Knoevenagel condensation to synthesise more derivatives. The chemistry was performed with a variety of aldehydes. However, the condensation worked only in the absence of an enolisable proton at the α -position to the aldehyde carbon. Various aldehydes with different ring systems were used in the Knoevenagel condensation to explore SAR at the 3-position. Synthesis of compound **244** started with the oxidation of commercially available alcohol **239** to aldehyde **240**. The Knoevenagel condensation of compound **191** with aldehyde **240** provided compound **241**. Then, following the chemistry described before, target **244** was obtained.

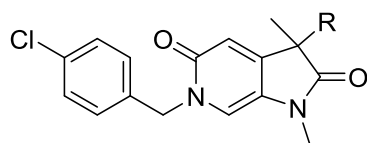


Scheme 13.4: Reagents and conditions: (a) DMP, DCM, 0 °C-r.t., 3 h, 78%; (b) **240**, piperidine, THF, 100 °C, 30 min, 50%; (c) H₂, 10% Pd/C, THF, MeOH, r.t., 2 h; (d) MeI, Cs₂CO₃, DMF, 50 °C, 1.5 h, 42% over 2 steps; (e) 4-chlorobenzyl bromide, MeCN, 170 °C μ W, 45 min, 83%.

13.3 Biological Evaluation

A small library of compounds were synthesised using the Knoevenagel condensation chemistry by three different chemists within the group. Compounds with different ring systems at 3-position were tested against ATAD2 inhibition (Table 13.2). The compounds with 6-membered aromatic rings at the 3-position were not tolerated. The 5-membered thiazole ring was tolerated, however, thiophene ring was detrimental to the ATAD2 inhibitory activity. Compounds with smaller substituents **244**, **247** and **251** retained activity.

Table 13.2: ATAD2 inhibitory activity of derivatives with various substituents at the 3-position.



Compound	R	ATAD2 IC ₅₀ (μM) ^a	Compound	R	ATAD2 IC ₅₀ (μM) ^a
237		>2000	248 ^e		352 ^c
238		1284	249 ^e		1633 ^b
245 ^e		>2000	244		214 ^c
246 ^e		>2000	250 ^f		1291 ^b
247 ^f		486 ^b	251 ^f		319 ^d

^a Determinations (n = 1 unless otherwise stated); ^b n = 2; ^c n = 3; ^d n = 4; ^e synthesised by Dr Stephen Hobson; ^f synthesised by Dr Duncan Miller.

The crystal structure of ATAD2 in complex with compound **238** showed that the 6-membered aromatic ring pointed towards solvent, rather than pointing towards the area where the acetylated histone binds, between the ZA and BC loops (Figure 13.4). The overall binding mode of the molecule was similar to the lead compound **6**.

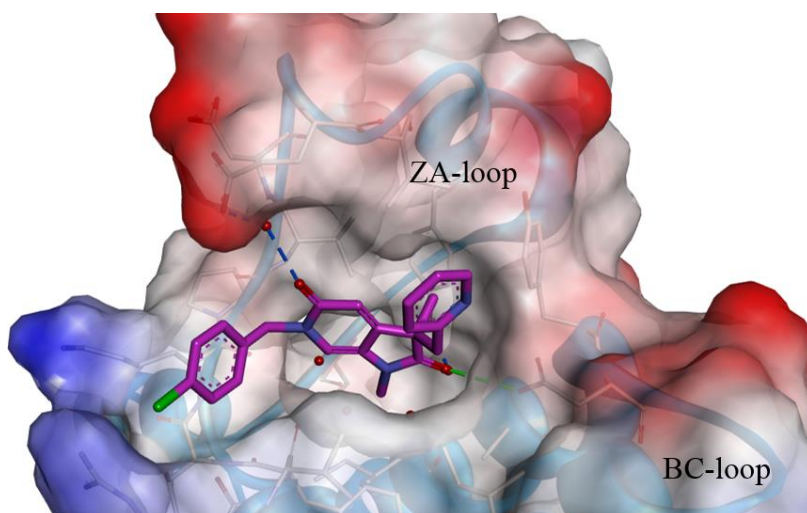


Figure 13.4: Crystal structure of ATAD2 in complex with compound **238** (magenta); the solvent accessible surface is coloured based on charge positive: blue, negative: red. Water molecules are shown as red spheres.

Similarly, the crystal structure of ATAD2 in complex with compound **244** showed that the 4-membered oxetane ring pointed towards solvent (Figure 13.5). The oxetane derivative **244** was at least 5-fold more potent than the pyridyl derivative **238**, suggesting that the 4-membered ring was tolerated in the binding site.

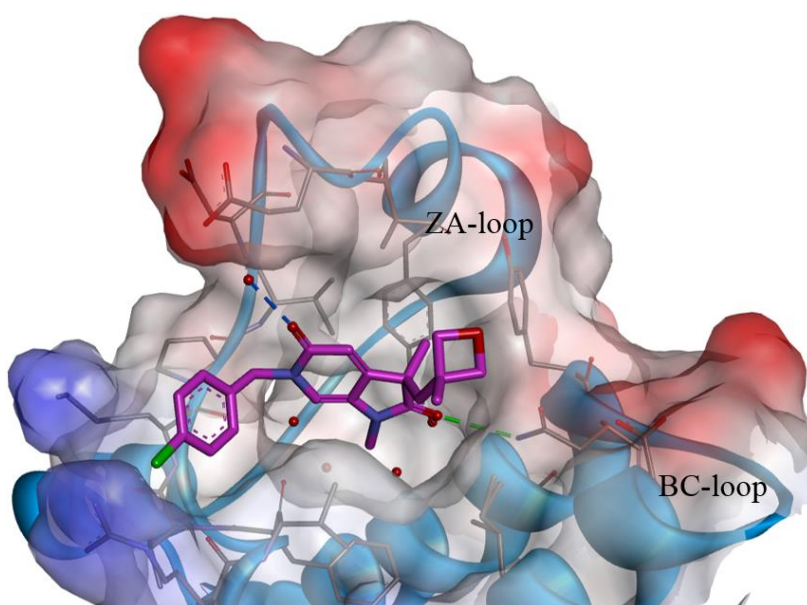


Figure 13.5: Crystal structure of ATAD2 in complex with compound **244** (magenta); the solvent accessible surface is coloured based on charge positive: blue, negative: red. Water molecules are shown as red spheres.

Chapter 14. Accessing the Bidentate Interaction with Asn1064

14.1 Rationale

It has been reported that the bidentate H-bond interaction with the conserved asparagine residue in bromodomains provided an increase in potency.^{147, 187-188} The crystal structure of compound **244** with ATAD2 revealed that the oxetane ring was in close proximity to Asn1064 (Figure 14.1). The carbon atom at the α -position to the oxygen atom of the oxetane ring was 3.2 Å away from the oxygen of Asn1064. It was hypothesised that an H-bond donor in the region near Asn1064 would form the additional H-bond interaction with Asn1064, improving the potency against ATAD2.

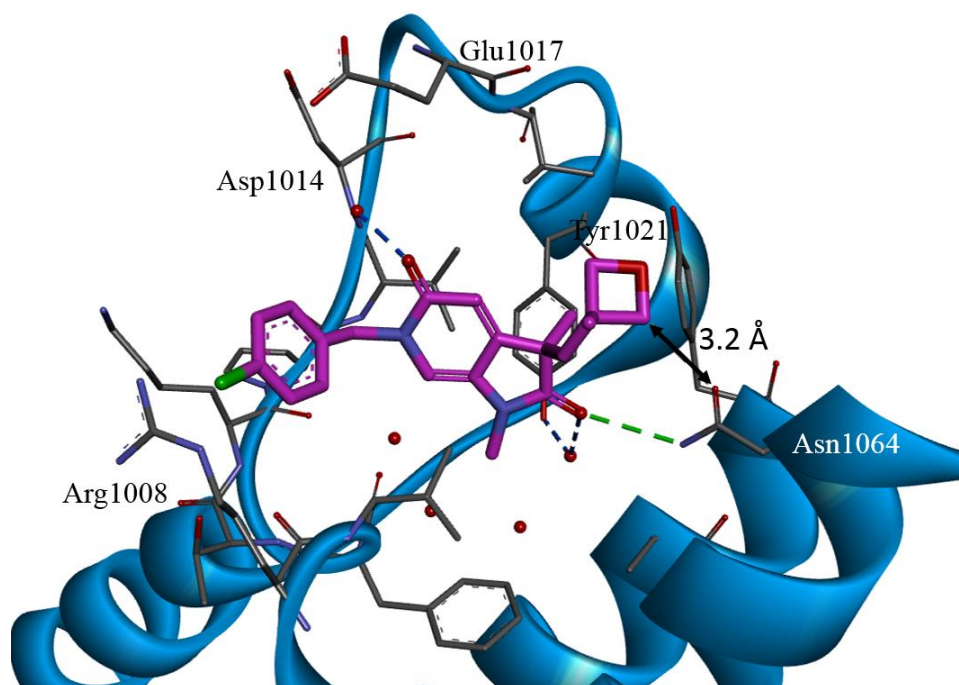


Figure 14.1: Crystal structure of compound **244** (magenta) bound to ATAD2 showing key H-bond interaction. The distance between the oxetane ring and Asn1064 is highlighted by a double headed black arrow.

The synthetic route used so far did not allow the introduction of desired H-bond donors including alcohols, amines and amides with variable linker lengths at the 3-position (Figure 14.2).

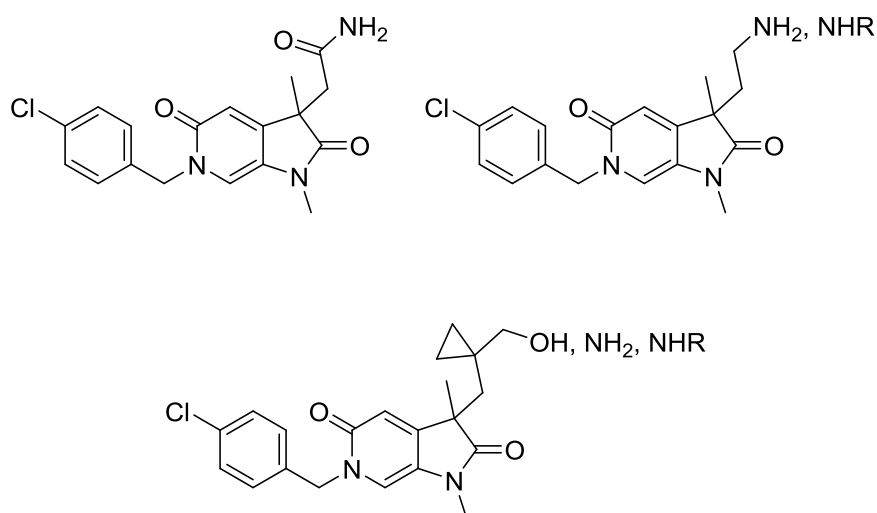


Figure 14.2: Compounds that were not accessible by the previously described synthetic route.

Therefore, a different strategy was taken to form the bidentate interaction with Asn1064. It was decided to synthesise spirocycles at the 3-position to introduce H-bond donors (Figure 14.3). Compound **253** with the pyrrolidine spirocycle was inspired from a natural product Horsfiline **254**, which was first isolated in 1991 from *Horsfieldia superba*, a tree whose extracts are used in local medicines in Malaysia.¹⁸⁹

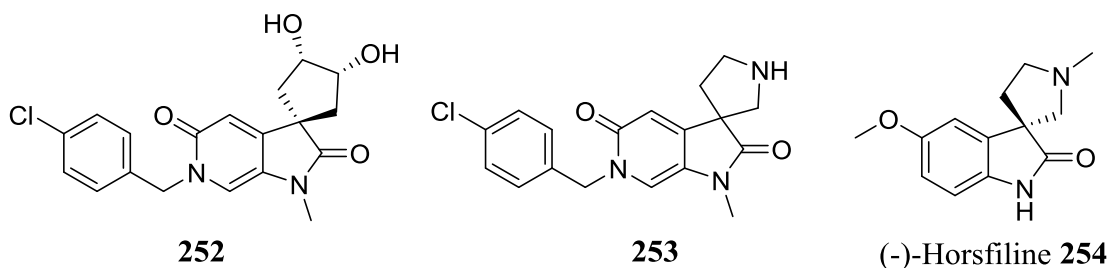
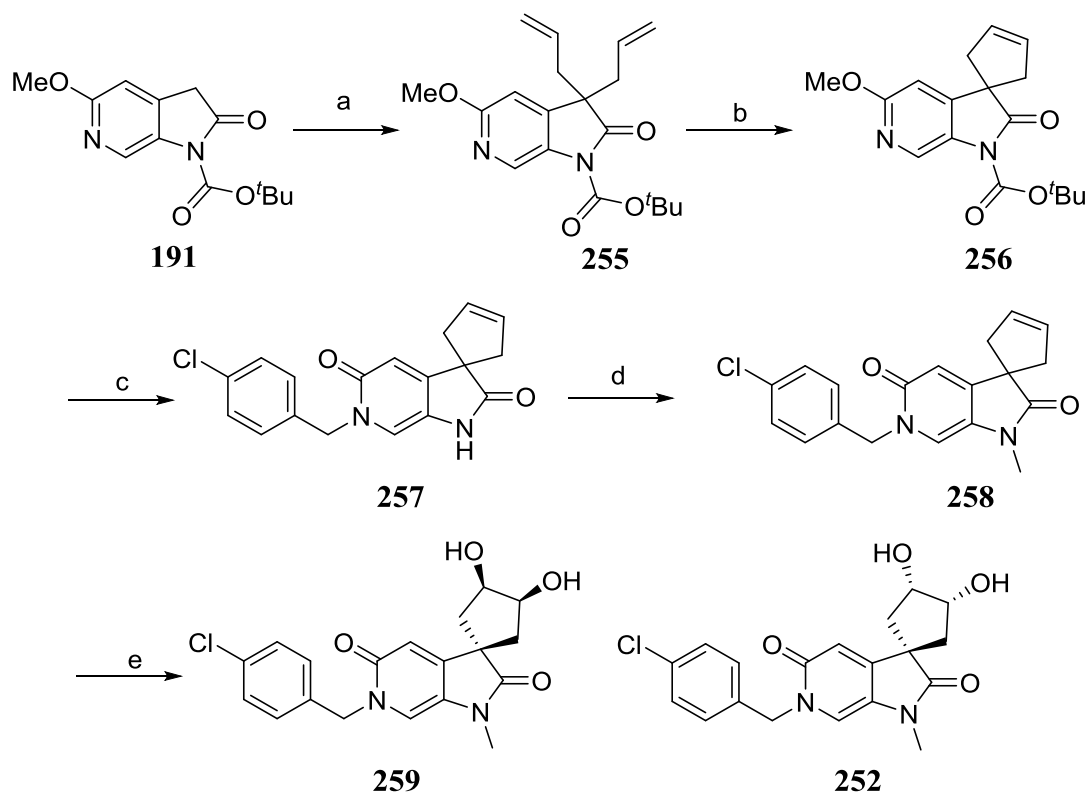


Figure 14.3: Proposed pyrrolidinone targets bearing a spirocycle at the 3-position.

14.2 Synthesis of Compound 252

Synthesis of compound **252** started with *bis*-allylation of intermediate **191** at the 3-position (Scheme 14.1). Olefin metathesis of compound **255** using Grubbs catalyst 2nd generation,¹⁹⁰⁻¹⁹¹ gave the desired spirocyclopropene **256** in 90% isolated yield. Compound **256** was converted to the pyridone **257** by heating with 4-chlorobenzyl bromide at 170 °C under microwave irradiation. Subsequent methylation gave compound **258**, which was subjected to osmium tetroxide-mediated *bis*-hydroxylation to get the desired target **252** in 59% yield and the diastereoisomer **259** in 18% yield.



Scheme 14.1: *Reagents and conditions:* (a) allyl bromide, Cs₂CO₃, MeCN, 40 °C, 2.5 h, 55%; (b) Grubbs catalyst 2nd generation, DCM, 80 °C μ W, 20 min, 90%; (c) 4-chlorobenzyl bromide, MeCN, 170 °C μ W, 45 min, 89%; (d) MeI, Cs₂CO₃, DMF, 100 °C μ W, 30 min, 87%; (e) OsO₄, NMO, THF, H₂O, r.t., 18 h, 59% (**252**), 18% (**259**).

The structures of the two diastereoisomers **252** and **259** were confirmed by NOE experiments. In case of compound **252**, the enhancement of both H₂ and H₃ signals were observed (Figure 14.4A). Enhancement of H₃ proton signal suggests that the H₃ protons are pointing upwards and the OH groups are pointing downwards.

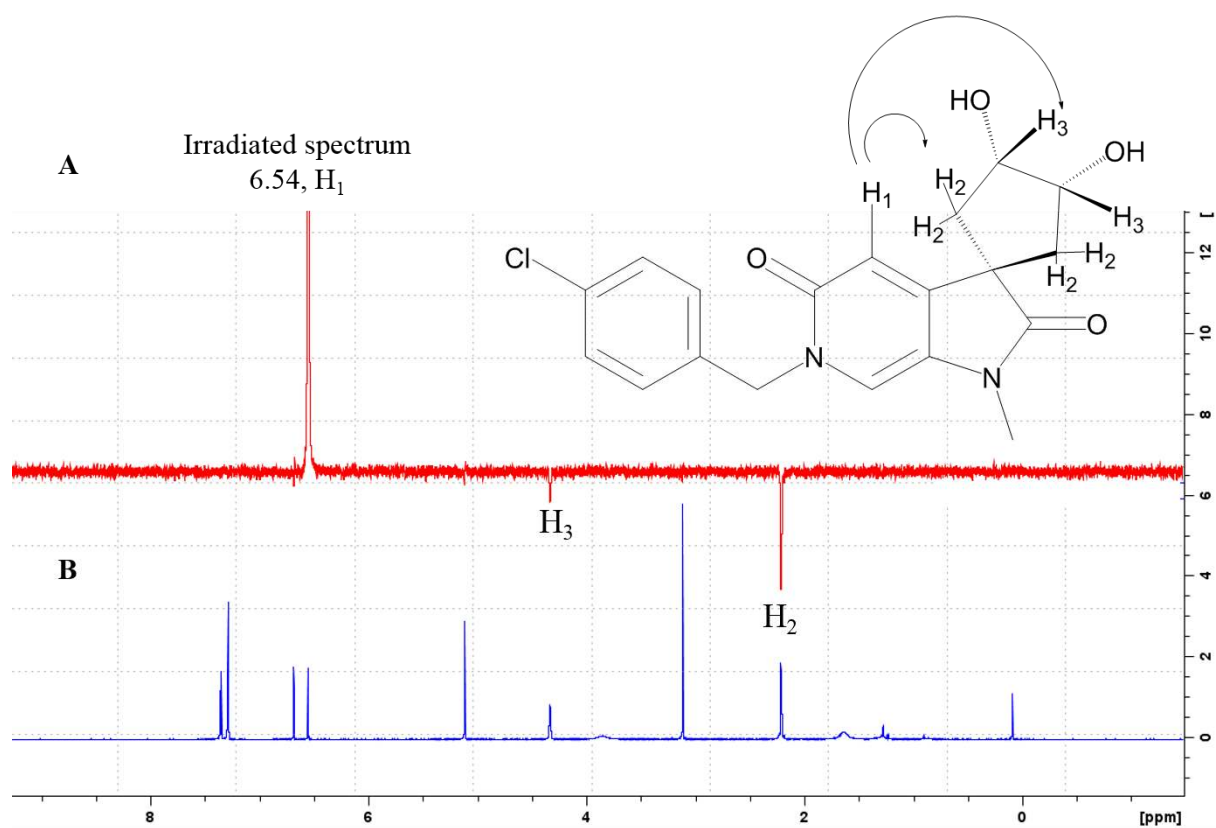


Figure 14.4: NOE difference spectrometry for compound **252**; (A) shows enhancement of H_2 and H_3 protons on irradiation of H_1 -proton; (B) shows the $^1\text{H-NMR}$ spectrum of compound **252**.

In the case of compound **259**, when H_1 proton was irradiated, only the H_2 proton signal was enhanced, confirming that the H_3 protons face downwards (Figure 14.5).

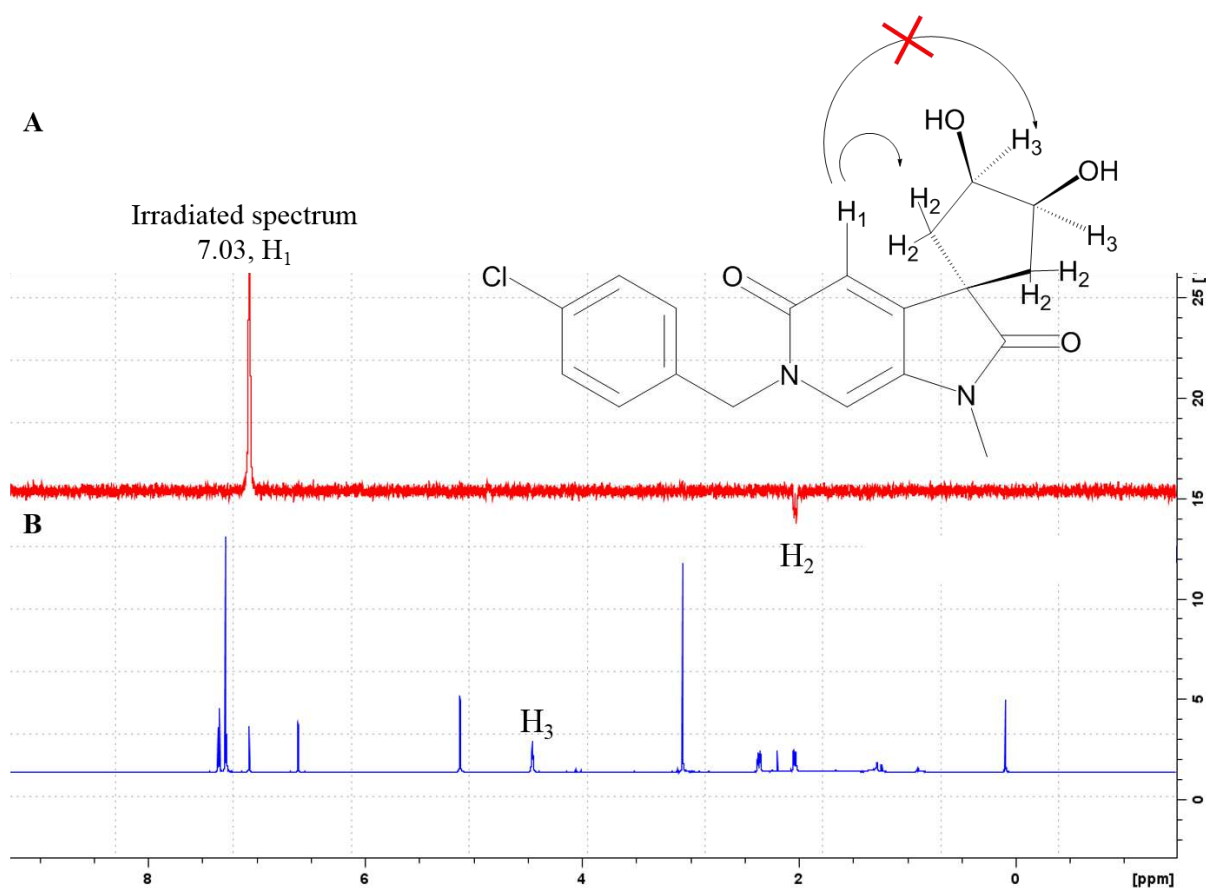
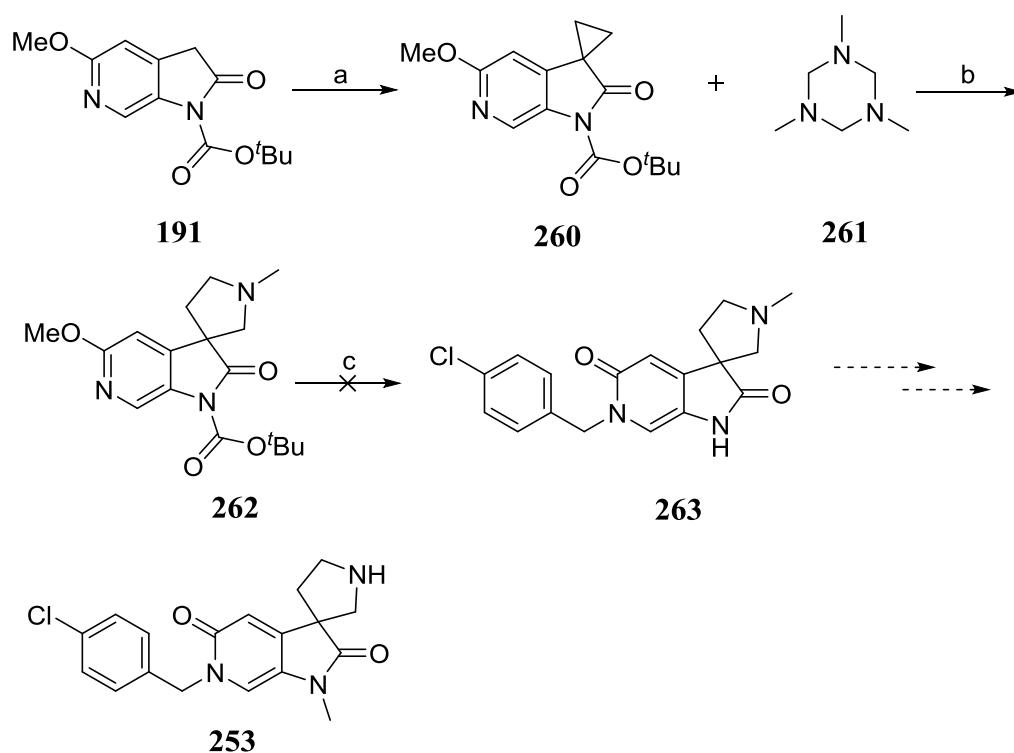


Figure 14.5: NOE difference spectrometry for compound **259**; (A) shows enhancement of the H₂ protons on irradiation of the H₁-proton; (B) shows the ¹H-NMR spectrum of compound **259**.

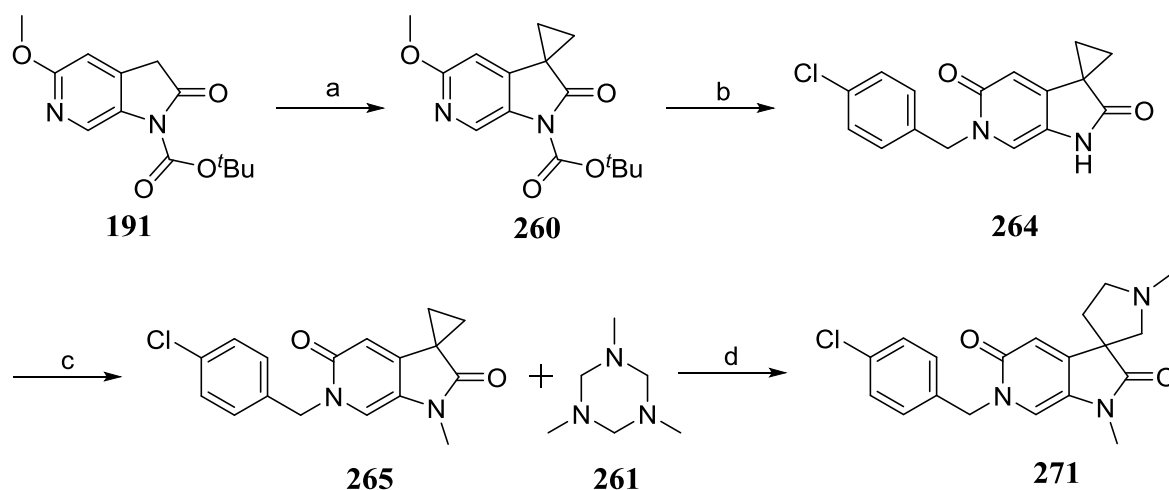
14.3 Synthesis of Compound 253

The synthetic route of compound **253** was designed based on the total synthesis of Horsfiline reported by Fischer *et al.* (Scheme 14.2).¹⁹² The synthesis started with the alkylation of intermediate **191** using 1,2-dibromoethane to get the spirocyclopropane **260**. Ring expansion of cyclopropane **260** using MgI₂ and triazinane **261** gave spiropyrrolidine **262** in moderate yield. However, the pyridone formation at 170 °C under microwave irradiation did not work, resulting in a complex mixture of products.



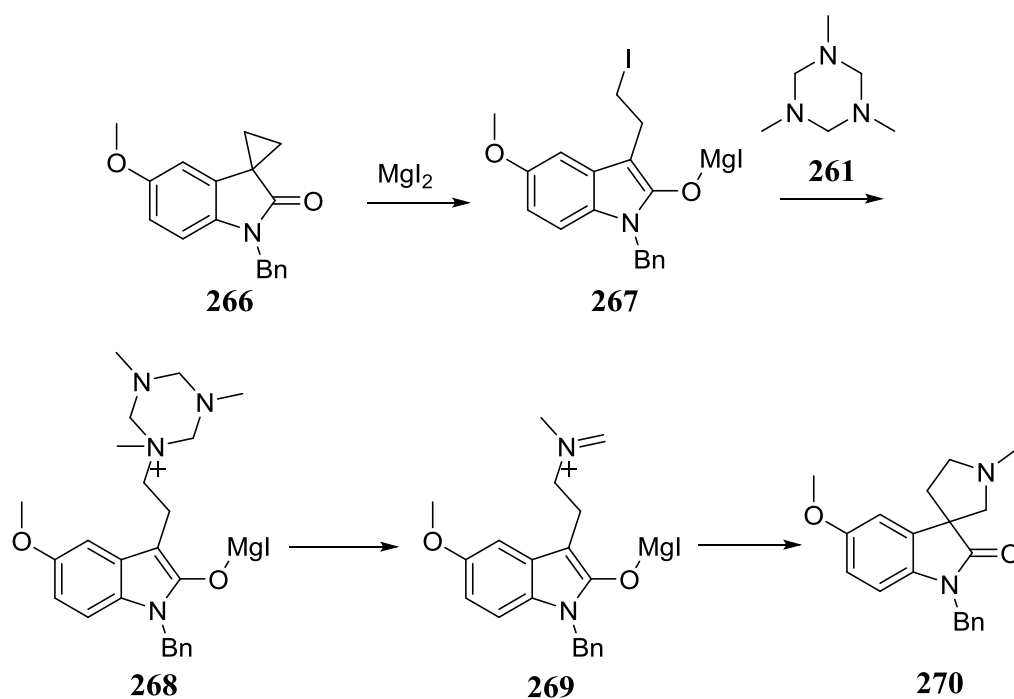
Scheme 14.2: Reagents and conditions: (a) 1,2-dibromoethane, Cs₂CO₃, MeCN, 40 °C, 3.5 h, 55%; (b) MgI₂ (10 mol%), THF, 50 °C, 26 h, 64%; (c) 4-chlorobenzyl bromide, MeCN, 170 °C μ W, 45 min.

The synthetic route was redesigned so that the ring-expansion of spirocyclopropane could be performed at a later stage (Scheme 14.3). The spirocyclopropane **260** was converted to compound **265** via pyridone formation and methylation as described before. Ring expansion of spirocyclopropane **265** was achieved using triazinane **261** and MgI₂ to get compound **271**.



Scheme 14.3: Reagents and conditions: (a) 1,2-dibromoethane, Cs₂CO₃, MeCN, 40 °C, 3.5 h, 55%; (b) 4-chlorobenzyl bromide, MeCN, 150 °C μ W, 45 min, 68%; (c) MeI, Cs₂CO₃, DMF, 100 °C μ W, 30 min, 53%; (d) MgI₂ (10 mol%), THF, 50 °C, 13 h, 90 °C, 20 h, 53%.

Fischer *et al.* proposed a mechanism for the ring expansion of spirocyclopropane, involving the formation of an intermediate enolate **267** (Scheme 14.4).¹⁹² Nucleophilic substitution of iodine by the triazinane **261** forms intermediate **268**, which upon fragmentation gives **269**. The enolate attack on the iminium ion provides the target pyrrolidine **270**. Fischer *et al.* also proposed a different mechanism in which the triazinane **261** undergoes fragmentation to form *N*-methylimine before attacking the electrophilic centre of C-I bond of the enolate **267**.¹⁹²



Scheme 14.4: Proposed mechanism of ring expansion of spirocyclopropane **266** to spiropyrolidine **270**.¹⁹²

The final step to get compound **253** was *N*-demethylation of compound **271**. However, various methods of *N*-demethylation using ACE-chloride and benzyl chloroformate did not provide the desired target **253**. Therefore, it was decided to incorporate a different group at the pyrrolidine nitrogen using the spirocyclopropane ring expansion approach. A benzyl derivative **272** or an allyl derivative **273** (Figure 14.6) were the first choice of targets because the corresponding triazinanes were either commercially available or the synthesis was reported.¹⁹³

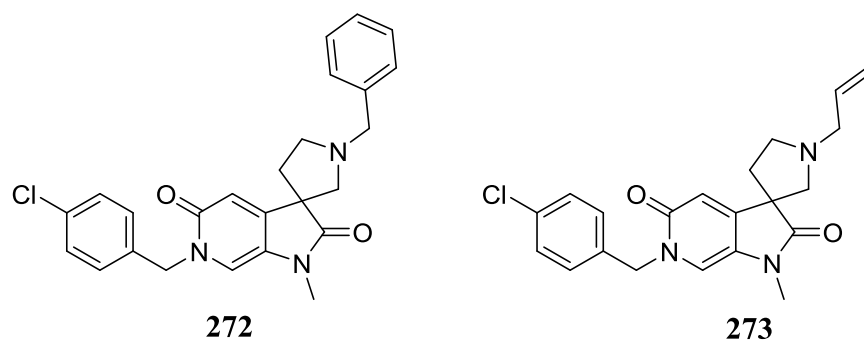
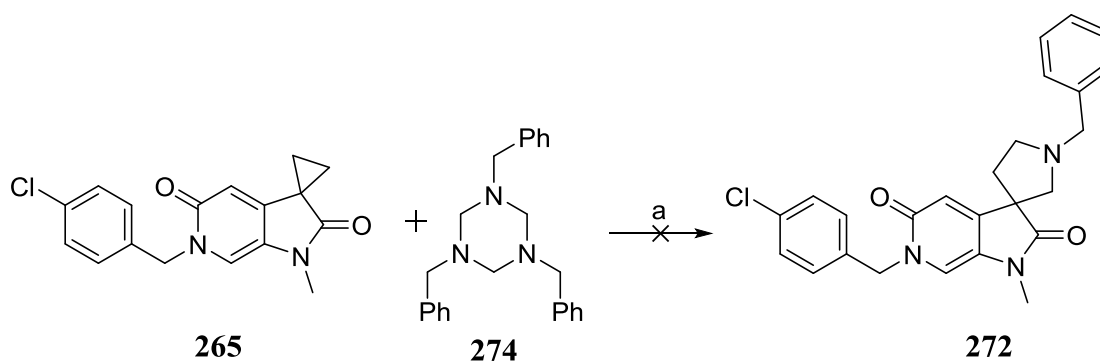


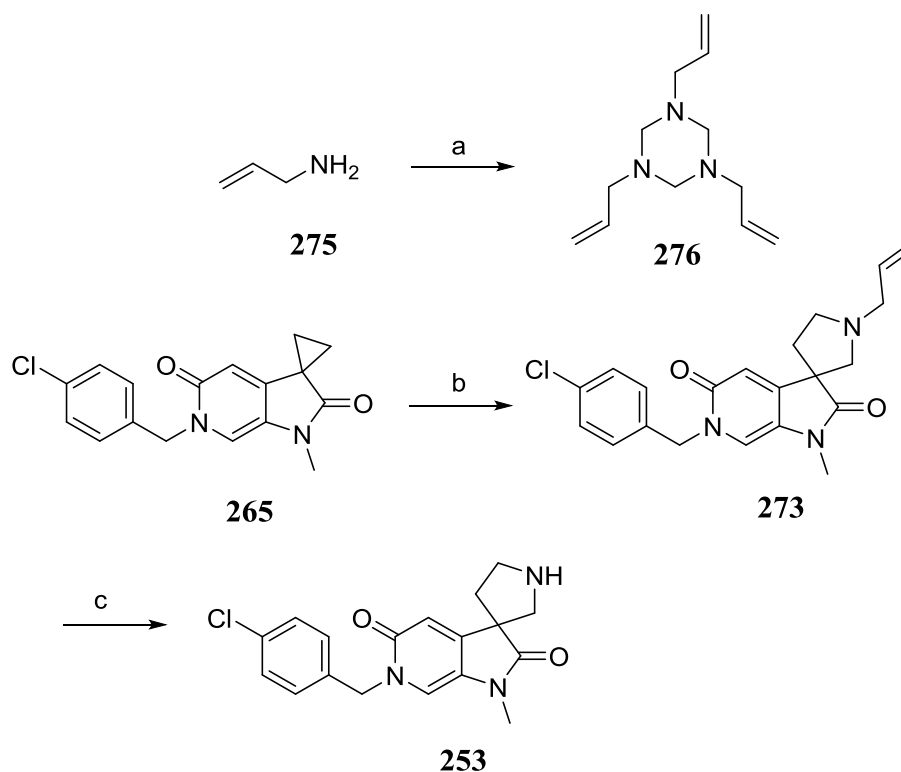
Figure 14.6: Compounds to be synthesised.

Ring expansion of spirocyclopropane **265** using commercially available triazinane **274** produced a mixture of unidentified products (Scheme 14.5).



Scheme 14.5: Reagents and conditions: (a) MgI₂ (10 mol%), THF, 50 °C, 13 h, 90 °C, 20 h.

Ring expansion of compound **265** with triazinane **276** provided the desired product **273** (Scheme 14.6). The triazinane **276** was prepared using allylamine **275** and paraformaldehyde following a procedure described by Jasiński *et al.*¹⁹³



Scheme 14.6: Reagents and conditions: (a) paraformaldehyde, MeOH, 0 °C-r.t., 20 h, quant.; (b) MgI₂ (10 mol%), THF, 90 °C, 20 h; (c) Pd(PPh₃)₄, *N,N*-dimethylbarbituric acid, DCM, 35 °C, 16 h, 22% over two steps.

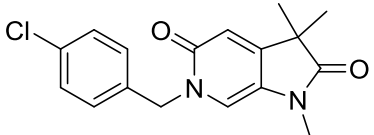
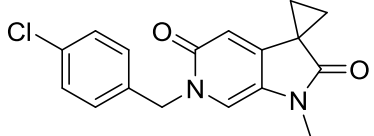
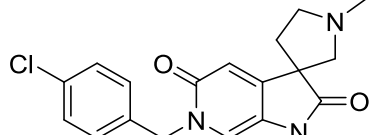
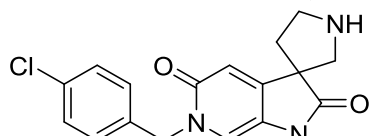
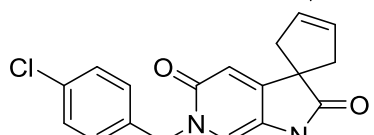
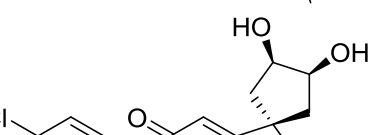
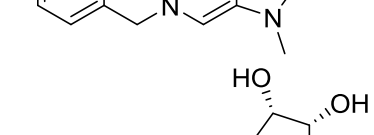
The compound **273** was not pure enough by ¹H-NMR, containing unidentified impurities, and a very small amount (16 mg) was remaining. Therefore, the compound was taken forward without further purification. Removal of the *N*-allyl group using Pd(PPh₃)₄ and *N,N*-

dimethylbarbituric acid following a protocol described by Garro-Helion *et al* (Scheme 14.6) to afforded desired target **253** in poor yield.¹⁹⁴

14.4 Biological Evaluation

The ATAD2 inhibitory activity of compounds **252** and **253** along with the intermediates obtained during the synthesis were determined (Table 14.1). Spirocyclopropane intermediate **265** was inactive, whereas, spirocyclopentene derivative **258** retained the potency. The *bis*-hydroxylated compounds **252** and **259** showed no ATAD2 inhibitory activity. The horsfiline analogue **271** showed a loss in potency by at least 7 fold compared to lead compound **6**. Removal of the *N*-methyl group was tolerated but did not improve the potency, although the desired bidentate H-bond interaction with Asn1064 was formed (Figure 14.7). Compound **253** was tested as a racemic mixture, therefore, the correct enantiomer might provide an increase in potency. In conclusion, the spirocycles with H-bond donors did not improve the activity against ATAD2, contradicting the initial hypothesis. A crystal structure of ATAD2 in complex with the *bis*-hydroxylated derivatives **252** and **259** would be beneficial to explain the loss in activity, despite having H-bond donors capable of forming the bidentate interaction with Asn1064.

Table 14.1: ATAD2 inhibitory activity of lead compound **6** compared with analogues bearing a spirocycle at the 3-position.

Compound	Structures	ATAD2 IC ₅₀ (μM) ^a
6		209 ^b
265		>2000
271		1571 ^b
253		234
258		339 ^c
259		1467 ^c
252		>2000 ^c

^a Determinations (n = 1 unless otherwise stated);

^b n = 3; ^c n = 4

A crystal structure of ATAD2 in complex with compound **253** was solved (Figure 14.7). The binding mode of compound **253** was very similar to that observed with the lead compound **6**.

The N-H of spiropyrrolidine ring forms a H-bond with Asn1064, making the bidentate interaction with Asn1064.

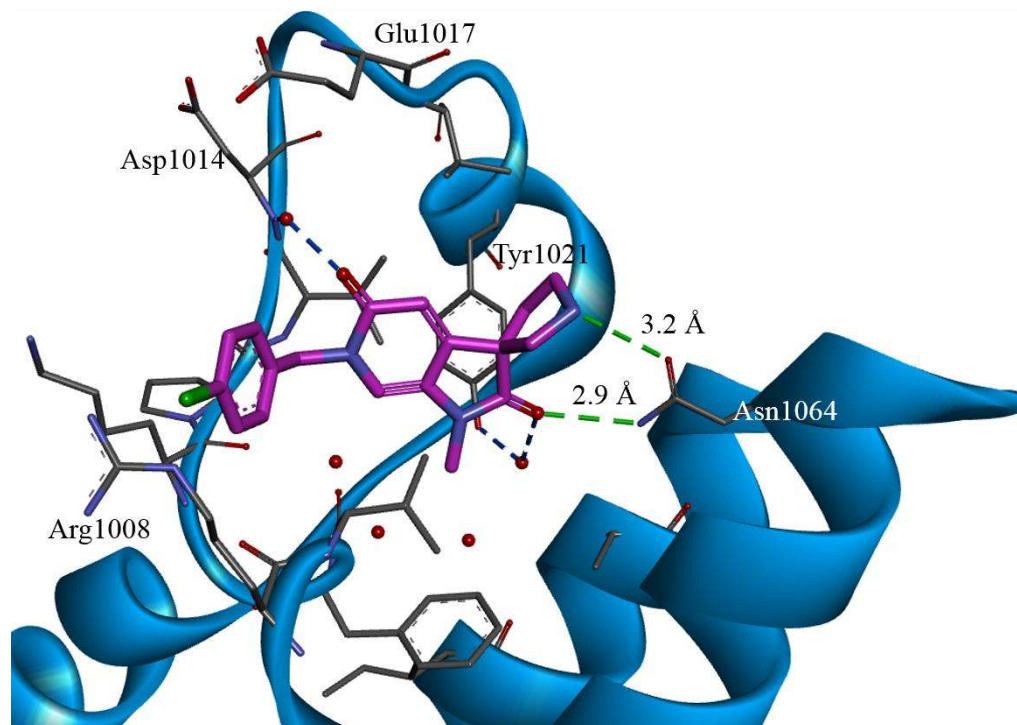


Figure 14.7: Crystal structure of ATAD2 in complex with compound **253** (magenta), showing the key H-bond interactions. Water molecules are shown as red spheres. The bidentate interaction with Asn1064 is shown as green dotted lines.

14.5 Investigation of Scaffold Hopping Approach

The bidentate interaction made by the spiropyrrolidine derivative **253** was not beneficial for increasing ATAD2 inhibition. The chemistry used so far did not allow the exploration of SAR at the 3-position with a range of H-bond donor substituents. Therefore, a scaffold hopping approach was used, changing the scaffold to oxindole, which was chosen because of its structural similarity to the current scaffold. In addition, the chemistry to introduce a range of substituents at 3-position of oxindoles has been reported.^{185, 195-196} Compound **277** with an amide at 3-position of the oxindole was modelled in the binding site of ATAD2 (Figure 14.8). The modelling suggested that the methylene linked amide group at 3-position would form an additional H-bond with Asn1064, providing the desired bidentate interaction.

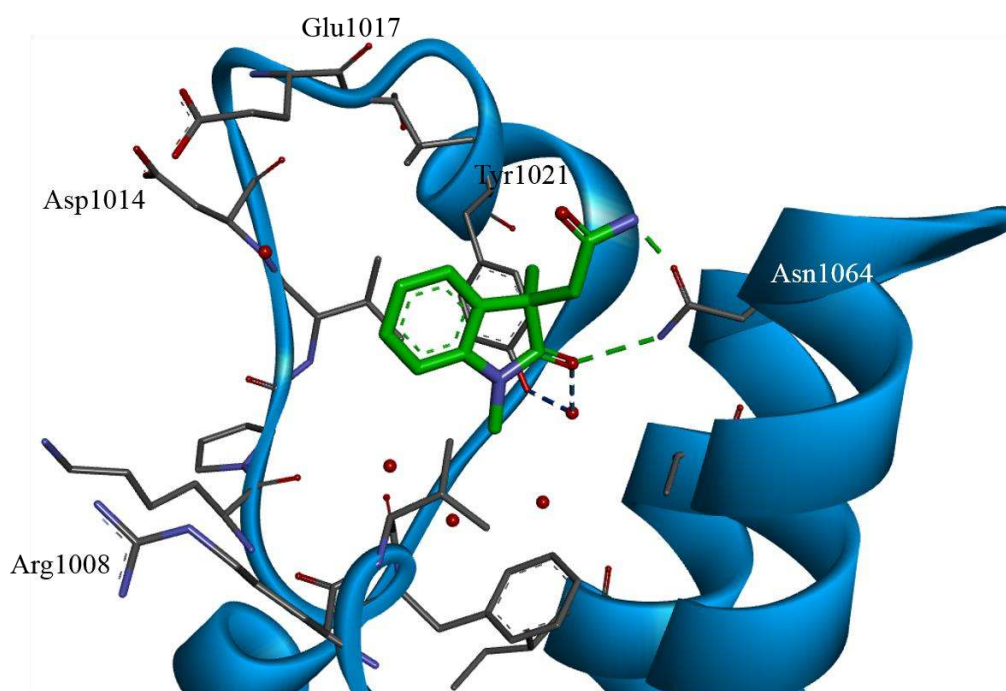


Figure 14.8: Modelling of compound **277** (green) on the ATAD2 binding site using Accelrys Discovery Studio.

Therefore, to examine the effect of a flexible H-bond donor, compound **277** was chosen as a target (Figure 14.9). Compound **278** was chosen to examine if scaffold hopping to oxindole retains the ATAD2 inhibition (Figure 14.9). The work load was shared with Dr Stephen Hobson, who undertook the synthesis of compound **278**.

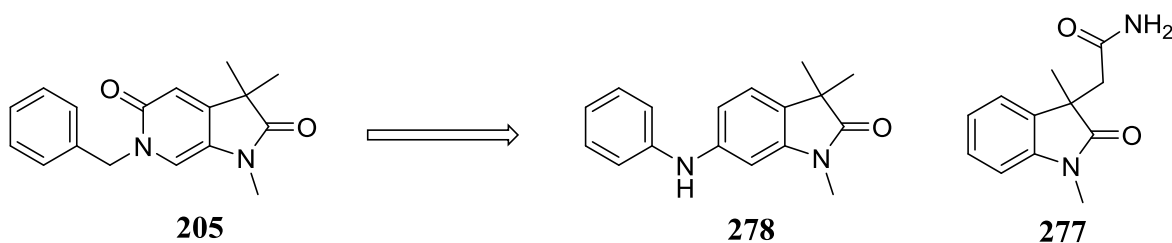
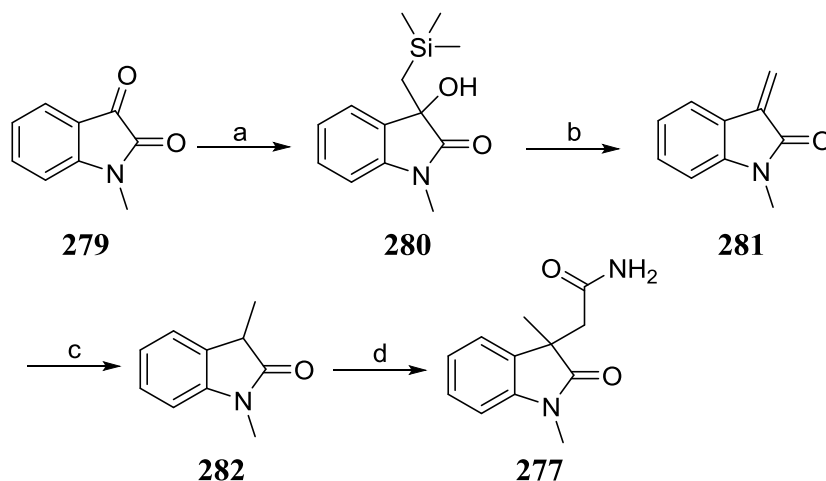


Figure 14.9: Targets to be synthesised based on scaffold hopping approach.

14.5.1 Synthesis of Compound 277

It was decided to synthesise intermediate **282**, which could be used with a range of electrophiles to explore the 3-position. Compound **281** was prepared following a literature procedure by Loreto *et al.*¹⁹⁷ Synthesis of compound **281** started with the Peterson olefination of *N*-

methylisatin **279** to give compound **281** (Scheme 14.7). Due to the reported instability,¹⁹⁷ compound **281** was reduced immediately to get intermediate **282** with a mono-methyl group at the 3-position. Nucleophilic attack of the enolate of compound **282** on 2-bromoacetamide gave the desired product in poor yield, but sufficient for co-crystallisation studies.

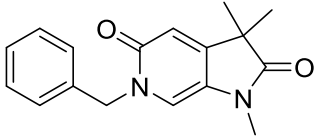
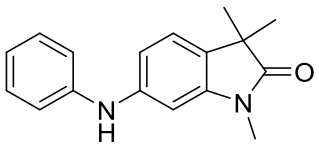
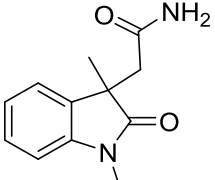


Scheme 14.7: Reagents and conditions: (a) (trimethylsilyl)methylmagnesium chloride (1M in Et_2O), THF, $-78\text{ }^\circ\text{C}$ to r.t., 1.5 h, 71%; (b) $\text{BF}_3 \cdot \text{Et}_2\text{O}$, DCM, $-78\text{ }^\circ\text{C}$, 1 h; (c) H_2 , 10% Pd/C, MeOH, Et_2O , r.t., 1 h, 50% over 2 steps; (d) 2-bromoacetamide, Cs_2CO_3 , DMF, $50\text{ }^\circ\text{C}$, 2 h, 12%.

14.5.2 Biological Evaluation

Compounds **277** and **278** did not show ATAD2 inhibitory activity at 4 mM concentration (Table 14.2). The inhibitory activity of compound **277** was expected to be low because it is a very small fragment, and it was intended for co-crystallisation studies. Compound **278** did not exhibit ATAD2 inhibition. These results suggested that the pyridone-pyrrolidinone scaffold was important for the ATAD2 inhibition.

Table 14.2: ATAD2 inhibitory activity of compounds **277** and **278** compared with compound **205**.

Compound	Structures	ATAD2 IC ₅₀ (μM) ^a
205		716 ^b
278^c		>4000
277		>4000

^a Determinations (n = 1 unless otherwise stated);

^b n = 2; ^c synthesised by Dr Stephen Hobson

A crystal structure of compound **277** bound to ATAD2 was solved (Figure 14.10). The *N*-methylpyrrolidinone ring mimics the acetyllysine, forming a key H-bond interaction with Asn1064 and a water-mediated H-bond with Tyr1021. The amide group flips away from the Asn1064 and did not form a H-bond interaction, contradicting the hypothesis based on modelling studies. Altogether, the compounds with an oxindole scaffold did not retain ATAD2 inhibitory activity, therefore, the series was not pursued further. However, the crystal structure of compound **277** bound to ATAD2 was helpful to demonstrate that a flexible methylene linked H-bond donor amide group at the 3-position would not be beneficial to get the bidentate interaction with Asn1064 (Figure 14.10).

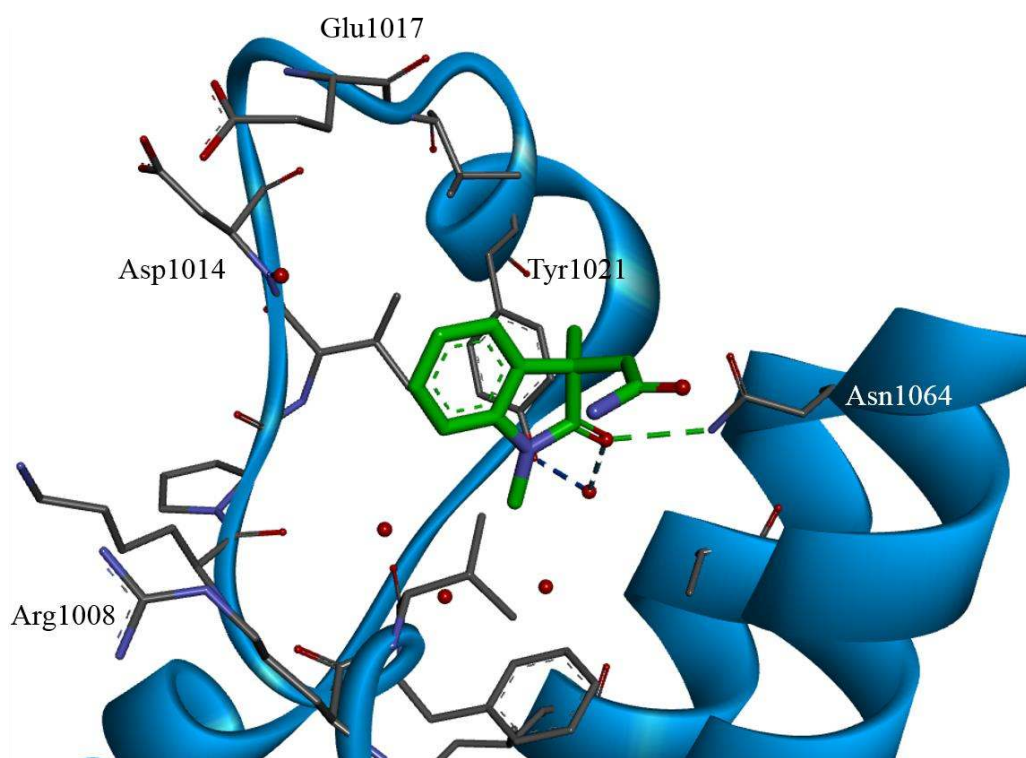


Figure 14.10: Crystal structure of ATAD2 in complex with compound **277** (green) showing the key H-bond interactions.

14.6 Introduction of a H-bond Donor Heterocycle at 3-Position

The crystal structure of compound **248** bound to ATAD2 showed that the 5-membered thiazole ring was close to the Asn1064 (Figure 14.11). It was hypothesised that a 5-membered heterocycle with a H-bond donor would interact with Asn1064.

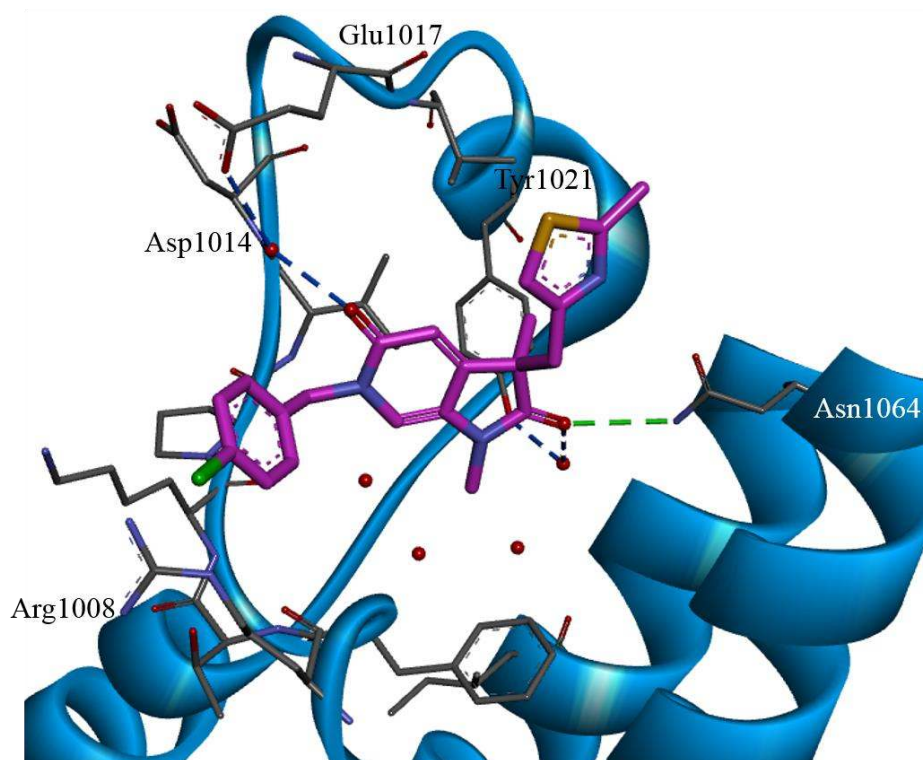
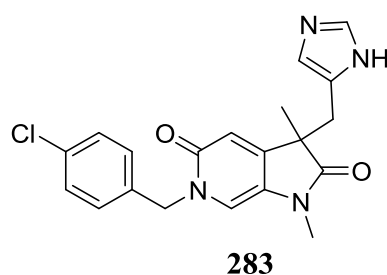


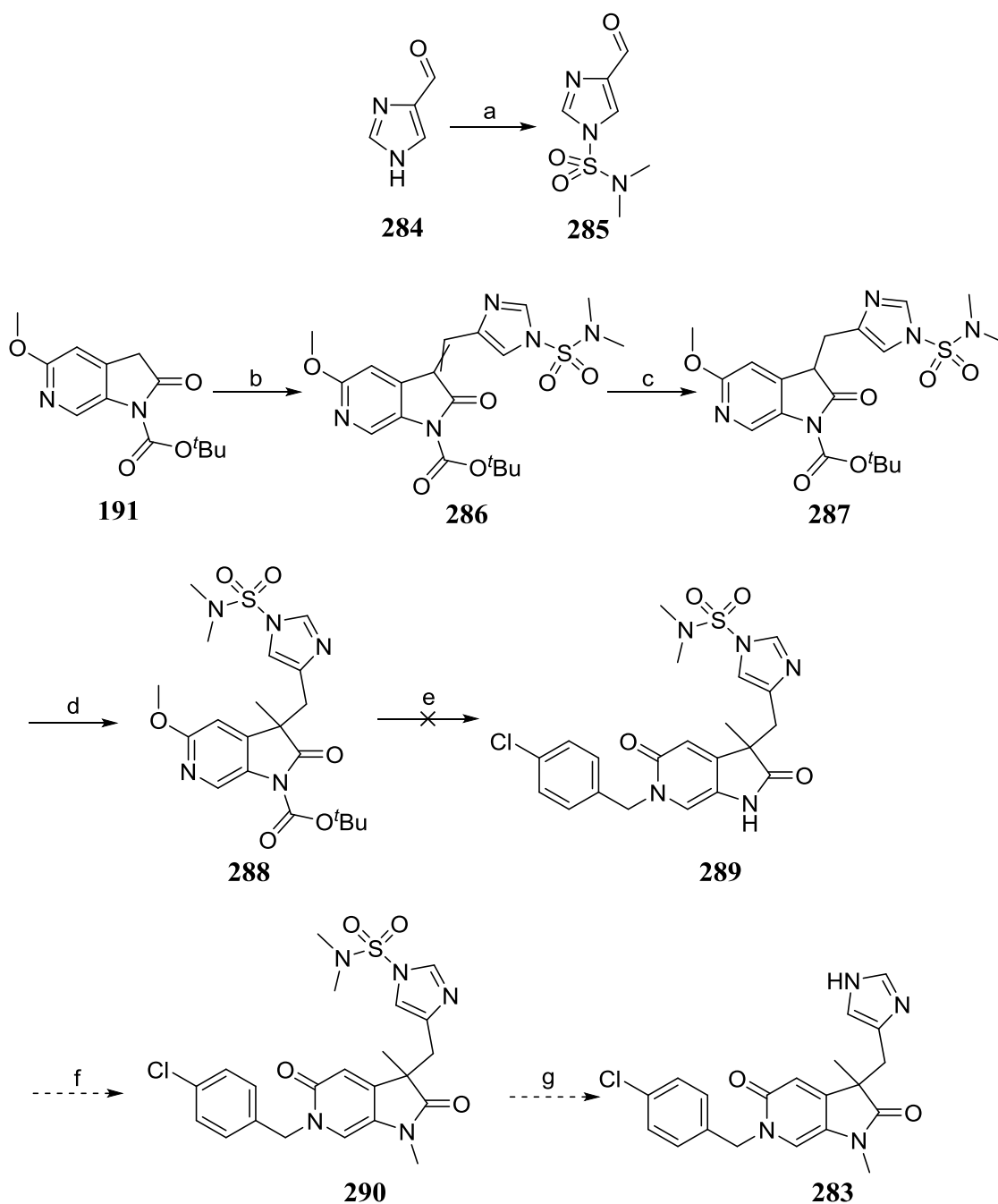
Figure 14.11: Crystal structure of ATAD2 in complex with compound **248** (green) showing the H-bond interactions.

In order to form the bidentate interaction with Asn1064, an imidazole derivative **283** was designed.



14.6.1 Synthesis

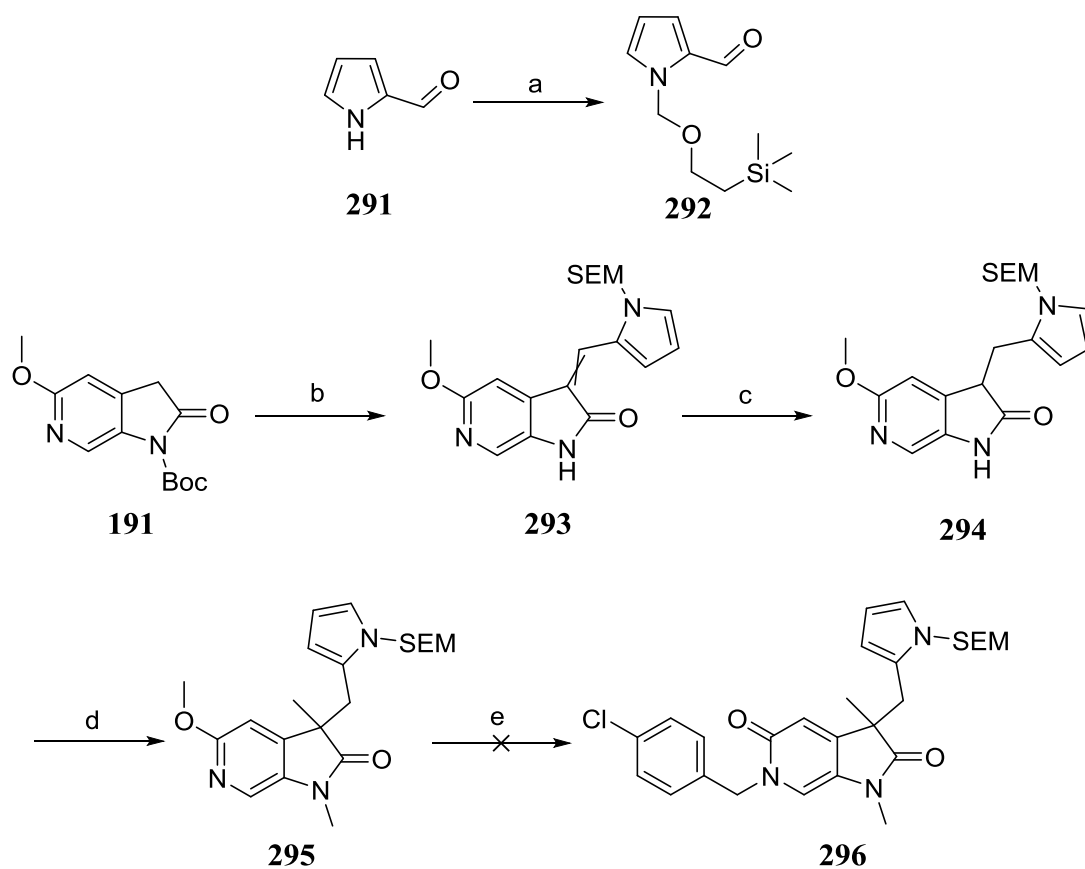
Previous work within the research group have suggested that the Knoevenagel condensation of unprotected heterocycles resulted in a complex mixture of products. Therefore, it was decided to protect 1*H*-imidazole-4-carbaldehyde **284**. The protecting group should withstand high temperatures up to 170 °C, mild acidic, and basic conditions. After an extensive literature search, *N,N*-dimethylsulfonic amide was selected as a protecting group as it was reported to withstand high temperatures, as well as, mild acidic and basic conditions.¹⁹⁸⁻¹⁹⁹ The protecting group could be cleaved by either strongly acidic or basic conditions. The synthesis started with the protection of 1*H*-imidazole-4-carbaldehyde **284** to get compound **285** (Scheme 14.8). Knoevenagel condensation of intermediate **191** and aldehyde **285** provided compound **286**. Surprisingly, the Boc group was not cleaved, unlike previous synthetic schemes. Compound **286** was then reduced, followed by methylation to get methoxypyridine **288**. The subsequent pyridone formation at 170 °C produced a mixture of complex products.



Scheme 14.8: Reagents and conditions: (a) *N,N*-dimethylsulfamoyl chloride, NEt_3 , DCM, r.t., 24 h, 85%; (b) **285**, piperidine, THF, 50 °C, 1 h, 30%; (c) H_2 , 10% Pd/C, THF, MeOH, r.t., 2 h; (d) MeI, Cs_2CO_3 , DMF, 50 °C, 1.5 h, 69% over 2 steps; (e) 4-chlorobenzyl bromide, MeCN, 170 °C μW , 45 min.

Concurrently, the synthesis of pyrrole derivative **296** was also undertaken, based on the same rationale as the imidazole derivative **283**. Synthesis of compound **296** started with a SEM-protection of *1H*-pyrrole-2-carbaldehyde **291** to get compound **292** (Scheme 14.9). The

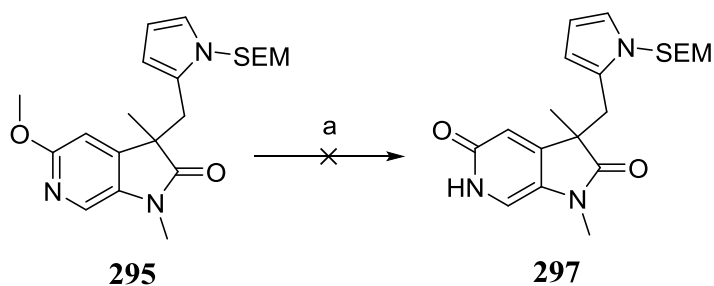
reduction of compound **293**, followed by *bis*-methylation gave compound **295**. The pyridone formation did not work as observed with the imidazole derivative **288** in Scheme 14.8.



Scheme 14.9: Reagents and conditions: (a) (i) NaH, THF, 0 °C, 30 min; (ii) SEMCl, r.t., 2.5 h, 85%; (b) **292**, piperidine, THF, 60 °C, 1 h, 79%; (c) H₂, 10% Pd/C, THF, MeOH, r.t., 2 h; (d) MeI, Cs₂CO₃, DMF, r.t., 1 h, 67% over 2 steps; (e) 4-chlorobenzyl bromide, MeCN, 170 °C μ W, 45 min.

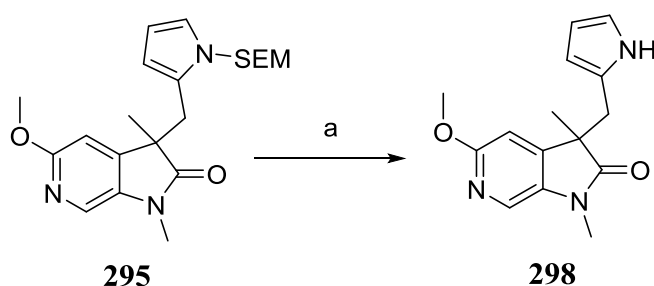
The pyridone formation reaction was performed at a very high temperature under microwave. Therefore, various milder conditions were attempted for the pyridone formation, however, a complex mixture of products were obtained in each case (Table 14.3).

Table 14.3: Reagents and conditions attempted for pyridone formation.



Entry	Reagents and conditions	Results
1	4M HCl, Dioxane, 80 °C, 18 h	Complex mixture of products
2	BBr ₃ , DCM, -78 °C, 2 h	Complex mixture of products
3	TMSI, MeCN, r.t., 1 h	Complex mixture of products

Due to the failure of several attempts of pyridone formation, it was decided to submit pyridine **298** for biological evaluation. The pyridine **298** would provide an answer to the design question, that is, whether an H-bond donor heterocycle would form an H-bond with Asn1064. The pyridine **298** was synthesised by TBAF-mediated removal of the SEM group from compound **295** (Scheme 14.10).



Scheme 14.10: Reagents and conditions: (a) TBAF, THF, 50 °C, 48 h, 51%.

14.6.2 Biological Evaluation

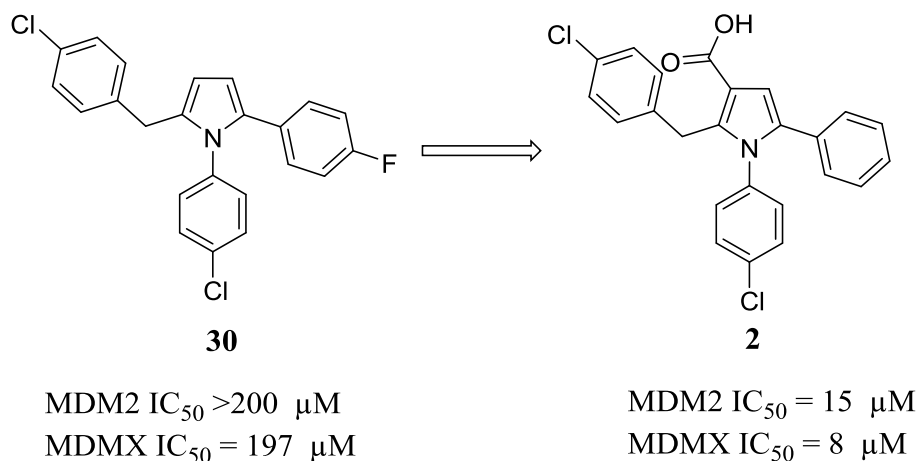
As expected, compound **298** did not show any ATAD2 inhibition at 2 mM in HTRF assay. A crystal structure of the compound bound to ATAD2 would be beneficial to understand if the

bidentate interaction with Asn1064 was achievable with H-bond donor heterocycles at 3-position. However, several attempts of co-crystallisation of the compound with ATAD2 have failed.

Chapter 15. Conclusion and Future Directions

15.1 MDMX

Based on the docking and modelling studies, a substituted-pyrrole series was identified. Introduction of an acidic group led to the identification of lead compound **2**.



A novel route to the synthesis of RO-2443 **3** and RO-5963 **4** was identified. The compounds were used to validate the in-house biochemical assay ELISA. There were at least 1000 fold discrepancies between the IC₅₀ values obtained from in-house ELISA and the published HTRF assay. Therefore, a structural biology placement was undertaken.

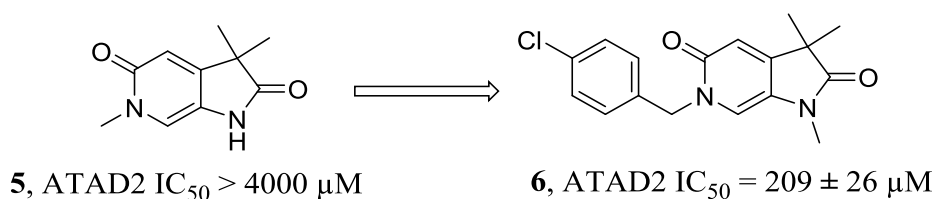
An HTRF assay was developed, which provided reasonable dose-response curves for published small molecules as well as peptides. The Newcastle small molecule inhibitors with logD < 3 yielded reasonable dose-response curves, but the lipophilic compounds with logD > 3 were completely inactive in the HTRF assay. The HTRF assay results for Newcastle small molecule inhibitors were not in line with the values obtained from the ELISA. The MDMX construct used in the HTRF assay does not include an autoinhibitory sequence. In contrast, a full length MDMX construct that includes the autoinhibitory sequence was used in the ELISA. This difference might be a major factor responsible for the discrepancies between the results obtained from the ELISA and HTRF assays. Therefore, development of HTRF assay with a full-length MDMX would be of interest.

Several MDMX and MDM2 constructs were expressed and purified. Co-crystallisation trials of MDM2 and MDMX with both small molecule inhibitors and autoinhibitory domains were

attempted. Around 20,000 different conditions were screened for co-crystallisation studies with MDMX but without any success. Future work will include the identification of a MDMX surface-entropy reduction mutant that could enhance crystallogenesis and might be used for the co-crystallisation of MDMX with small molecules, as reported for MDM2.²⁰⁰

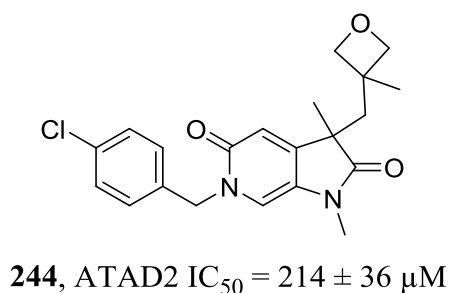
15.2 ATAD2

The ATAD2 project is in the hit to lead phase. Subtle modifications were undertaken around the fragment hits, obtained from Astex pharmaceuticals, with the aim to improve the ATAD2 inhibitory activity. Extensive SARs around fragment **5** led to the identification of compound **6**.



The SAR studies presented in this thesis have shown that substitution at *ortho*- or *meta*-position of the phenyl ring reduced the ATAD2 inhibition. SAR studies with different linkers between the phenyl ring and the N⁶-position would be of interest.

Based on the crystal structure of compound **6** bound to ATAD2, extensive SARs at the 3-position were performed. Chemistry to allow variations at the 3-position was challenging. The synthetic route involving a Knoevenagel condensation allowed rapid exploration of SARs around the 3-position. Compounds with methylene-linked 6-membered ring at the 3-position showed significant reduction in ATAD2 inhibition. Interestingly, methylene linked small sized rings, such as **244**, retained the potency.



In an attempt to form a bidentate interaction with Asn1064, several strategies were employed, including introduction of H-bond donor spirocycles, and flexible H-bond donor amides or heterocycles at the 3-position. Compound **253**, which was submitted as a racemic mixture, formed the desired bidentate interaction with Asn1064, and retained potency against ATAD2. The crystal structure of compound **253** bound to ATAD2 suggests that the substitution at the 2-position of the spiropyrrolidine ring would access the small RVF shelf, which was explored by Bamborough *et al.* to develop a potent ATAD2 inhibitor.¹⁷⁵ Therefore, SAR studies around spirocycles at the 3-position might provide the desired bidentate interaction, as well as access to the RVF shelf (Figure 15.1).¹⁷⁵

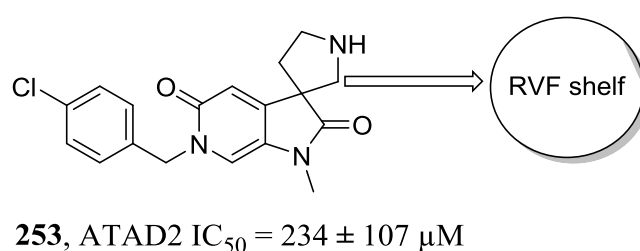


Figure 15.1: Possible future SAR studies around the spiropyrrolidine at the 3-position of compound **253** to access the RVF shelf.

Thus, the work presented in this thesis has enhanced our understanding of the binding site of ATAD2 bromodomain. Fragment based drug discovery and structure based drug design led to the identification of sub-millimolar inhibitors of ATAD2. The key SAR studies are summarised in Figure 15.2.

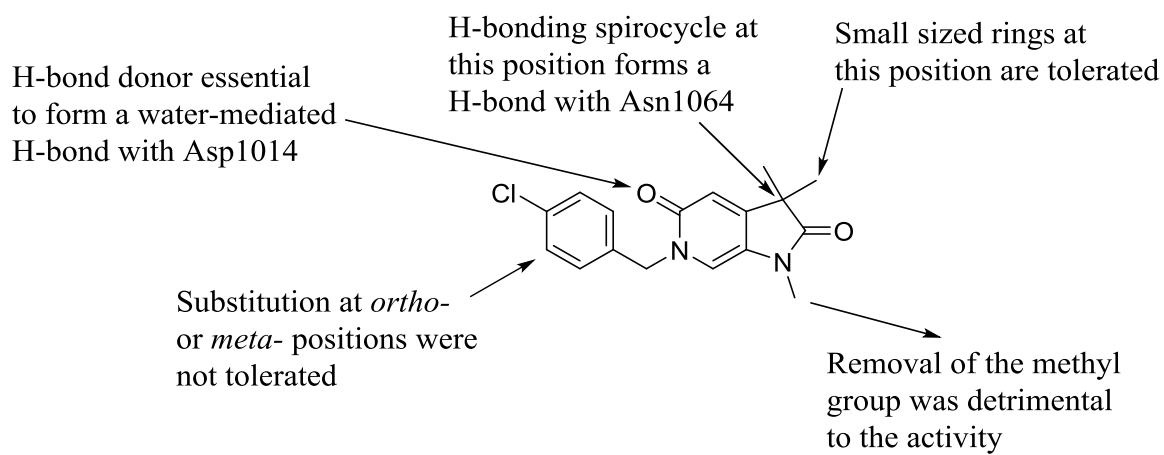


Figure 15.2: Summary of SARs around the pyridone-pyrrolidinone series.

Chapter 16. Experimental

16.1 Summary of Generic Reactions, Analytical and Chromatographic Conditions

16.1.1 Solvents and Reagents

All chemicals and reagents were purchased from Sigma Aldrich, Acros, Alfa Aesar, Apollo Scientific, Fisher Scientific, Fluorochem, Tokyo Chemical Industry or Strem Chemicals. The chemicals were of the highest available purity. Anhydrous solvents were stored in Aldrich Sure/Seal bottles and stored under an atmosphere of nitrogen. Petrol refers to the fraction with a boiling point between 40 and 60 °C.

16.1.2 Chromatography

Thin layer chromatography utilised to monitor reaction progress was conducted on plates pre-coated with silica gel (Merck 60F₂₅₄) or NH₂F_{254S}. The eluent was as stated (where this consisted of more than one solvent, the ratio is stated as volume:volume) and visualisation was either by short wave (254 nm) ultraviolet light, or by treatment with the visualisation reagent stated followed by heating. 'Flash' medium pressure liquid chromatography (MPLC) was carried out either on a Biotage SP4 automated purification system or a Varian 971-FP automated purification system, using pre-packed Varian or Grace silica or amino-bonded silica cartridges. Compounds were first loaded onto Biotage Isolute HM-N.

16.1.3 Microwave Reactions

All reactions carried out in a microwave were performed in a Biotage Initiator with Sixty robot.

16.1.4 Analytical Techniques

Melting points were determined using a VWR Stuart SMP40 apparatus and are uncorrected.

^1H , ^{13}C , ^{19}F and ^2D nuclear magnetic resonance (NMR) spectra were obtained as either CDCl_3 , CD_3OD or $\text{DMSO}-d_6$ solutions and recorded at 500 MHz, 125 MHz, 470 MHz and 76 MHz respectively, on a Bruker Avance III 500 spectrometer. Chemical shifts are quoted in parts per million (δ) referenced to the appropriate deuterated solvent employed. Multiplicities are indicated by s (singlet), d (doublet), t (triplet), q (quartet), m (multiplet), br (broad), ap (apparent) or combinations thereof. Coupling constant values are given in Hz. Homonuclear and heteronuclear two dimensional NMR experiments were used where appropriate to facilitate assignment of chemical shifts.

LC-MS was carried out on a Waters Acquity UPLC system with PDA and ELSD employing positive or negative electrospray modes as appropriate to the individual compound. High resolution mass spectrometry was performed by the EPSRC UK National Mass Spectrometry Facility, University of Wales Swansea, Singleton Park, Swansea, SA2 8PP.

FTIR spectra were recorded on either a Bio-Rad FTS 3000MX diamond ATR or an Agilent Cary 630 FTIR as a neat sample.

UV spectra were obtained using a U-2001 Hitachi Spectrophotometer with the sample dissolved in ethanol.

Data were compared with literature data for compounds which had been previously reported.

16.2 Synthesis of MDMX Inhibitors-Experimental Procedures

16.2.1 MDMX Biology Procedures

ELISA

To evaluate IC_{50} values of compounds, ELISA assay was undertaken by Dr Yan Zhao at the Northern Institute for Cancer Research (details taken from Hardcastle *et al*).²⁰¹ The 96-well black and white high binding luminometry isoplates (Wallac, Cat N0 140-155) were coated by overnight incubation at 35 °C with 200 μL per well of 5 $\mu\text{g mL}^{-1}$ streptavidin (Chemicon International) in coating buffer (0.1 M $\text{Na}_2\text{HPO}_4 \cdot 2\text{H}_2\text{O}$; 0.1 M citric acid; pH 5.0). The plates were washed five times in 1 \times dissociation enhanced lanthanide fluorescence immunoassay (DELFI) buffer (Wallac) and then incubated for 3 h at room temperature with saturation buffer (0.3 M D-sorbitol; 50 mM Tris; 150 mM NaCl; 0.1% BSA; 0.05% sodium azide; pH 7.0) to block nonspecific protein binding sites on the plate. After removal of the buffer from the plates, they were allowed to dry in a sterile laminar air flow hood at room temperature before incubation for 1 h at 4 °C with 200 μL per well of 100 $\mu\text{g mL}^{-1}$ biotinylated IP3 peptide (b-

IP3: Ac-Met-Pro-Arg-Phe19-Met-Asp-Tyr-Trp-Glu-Gly-Leu26- Asn-NH₂)₁₇ dissolved in 0.05% DMSO-PBS, pH 7.4 buffer. After washing the wells three times with PBS, the plates were ready to use for MDM2 binding.

For initial testing, the compounds and controls were plated out in triplicate into clear 96-well plates (Nunc) in 10- μ L aliquots to give final concentrations of 500 μ M, 100 μ M, and 20 μ M in the assay. Control samples consisted of 5% DMSO carrier alone as a negative control and 100 nM active peptide (AP-B: Ac-Phe19-MetAib-Pmp-6-Cl-Trp-Glu-Ac3-Leu26-NH₂) as a positive control peptide antagonist of the MDM2-p53 interaction (IC₅₀) 5 nM).¹⁸ Compounds and controls aliquoted in 96-well plates were preincubated at 20 °C for 20 min with 190 μ L aliquots of optimized concentrations of in vitro translated MDM2, before transfer of the MDM2-compound mixture to the b-IP3 streptavidin plates, and incubation at 4 °C for 90 min. After washing three times with PBS to remove unbound MDM2, each well was incubated at 20 °C for 1 h with a TBS-Tween (50 mM Tris pH 7.5; 150 mM NaCl; 0.05% Tween 20 nonionic detergent) buffered solution of primary mouse monoclonal anti-MDM2 antibody (Ab-5, Calbiochem, used at a 1/200 dilution), then washed three times with TBS-Tween before incubation for 45 min at 20 °C with a goat-anti-mouse horseradish peroxidase (HRP) conjugated secondary antibody (Dako, used at 1/2000). The unbound secondary antibody was removed by washing three times with TBS-Tween. The bound HRP activity was measured by enhanced chemiluminescence (ECL, Amersham Biosciences) using the oxidation of the diacylhydrazide substrate, luminol, to generate a quantifiable light signal. The luminol substrate together with enhancer was automatically injected into each well and the relative luminescence units (RLU) measured over a 30 s interval using a Berthold MicroLumat-Plus LB 96 V microplate luminometer. The percentage MDM2 inhibition at a given concentration is calculated as the (RLU detected in the compound treated sample \div RLU of DMSO controls) \times 100. The IC₅₀ was calculated using a plot of % MDM2 inhibition versus concentration and is the average of three independent experiments.

The same procedure was used for measuring MDMX inhibition.

16.2.2 Synthesis of MDMX Inhibitors: General Procedures

Except where water was included in the reaction mixture, all reactions were carried out under strict anhydrous conditions with glassware oven-dried and cooled under nitrogen. Temperatures quoted refer to bath temperatures.

General Procedure A: Grignard reaction

The relevant aldehyde (1 eq.) was dissolved in THF (1.2 mL/mmol) and cooled to -78 °C. A 1.6 M solution of vinylmagnesium chloride in THF (5 eq.) was added dropwise and the reaction mixture was stirred at -78 °C for 30 min and at r.t. until the starting material was completely consumed. The reaction was quenched with saturated aqueous NH₄Cl (20 mL), and extracted with ethyl acetate (3 × 20 mL). The organic layers were combined, washed with brine, dried over MgSO₄, and the solvent removed *in vacuo*.

General procedure B: Synthesis of β-keto ester

A solution of Meldrum's acid (1 eq.) in DCM (1.15 mL/mmol) was cooled to 0 °C and pyridine (2 eq.) was added dropwise followed by addition of the relevant acid chloride (1 eq.). The reaction mixture was stirred at 0 °C for 1 h and at r.t. for 2.5 h. The reaction mixture was poured into a mixture of ice and 2 M HCl (10 mL) and extracted with DCM (3 × 50 mL). The organic layers were combined, washed with brine (20 mL) and water (20 mL), dried over MgSO₄ and evaporated *in vacuo* to get an orange solid. The residue was suspended in ethanol, refluxed for 2 h and stirred at r.t. for 16 h. The mixture was cooled and the solvent was removed *in vacuo*.

General Procedure C: Synthesis of 1, 4-diketone

To a solution of the relevant β-keto ester (1 eq.) in THF (0.6 mL/mmol) was added NaH (60% in mineral oil, 1.3 eq) and stirred for 20 min at 0 °C. A solution of the relevant 2-bromoacetophenone (1.1 eq.) in THF (0.5 mL/mmol) was added dropwise and the mixture was stirred at r.t. for 2.5 h. The reaction was quenched with water (20 mL) and extracted with EtOAc (3 × 30 mL). The organic layers were combined, dried over MgSO₄ and the solvent removed *in vacuo*.

General Procedure D: Paal-Knorr pyrrole synthesis

A mixture of the relevant 1,4-diketone (1 eq.), the relevant amine (5 eq.) and acetic acid (3 mL/mmol) was heated under microwave irradiation to 170 °C for 10 min. The reaction was allowed to cool, neutralised with saturated aqueous NaHCO₃ and extracted with EtOAc (3 × 30 mL). The organic layers were combined, washed with brine, dried over MgSO₄ and the solvent removed *in vacuo*.

General Procedure E: Hydrolysis of esters

To a solution of the relevant ester (1 eq.), in MeOH:water (2:1) was added NaOH (30-50 eq.) and the mixture was stirred at 65 °C for 18 h. MeOH was added to the resulting suspension and stirred at 65 °C for 6 h. The reaction mixture was cooled and solvents removed *in vacuo*. The residue was dissolved in water (20 mL), acidified with 2M HCl and extracted with EtOAc (3 × 20 mL). The organic layers were combined, dried over MgSO₄ and the solvent removed *in vacuo*.

General procedure F: DIBAL reduction of esters to alcohols

The relevant pyrrole-ester (1 eq.) was dissolved in THF (1.6 mL/mmol) and cooled to 0 °C. 1M DIBAL in cyclohexane (2.5 eq.) was added dropwise and stirred at 0 °C until the starting material was completely consumed. The reaction mixture was warmed to r.t., MeOH (1.8 mL/mmol) was added and stirred for 10 min. A saturated aqueous solution of Rochelle's salt (6 mL/mmol) was added and stirred for 10 min. Water (20 mL), brine (10 mL) and EtOAc (30 mL) were added and the resulting mixture was stirred for 30 min. The aqueous layer was extracted with EtOAc (3 × 30 mL), organic layers were combined, dried over MgSO₄ and the solvent removed *in vacuo*.

General Procedure G: Oxidation of alcohols to aldehydes using Dess-Martin periodinane

The relevant alcohol (1 eq.) was dissolved in DCM (4 mL/mmol) and cooled to 0 °C. Dess-Martin periodinane (1.7 eq.) in DCM (6 mL/mmol) was added dropwise and the resulting mixture was stirred at 0 °C for 15 minutes, followed by stirring at r.t. until the starting material was completely consumed. Saturated aqueous NaHCO₃ (20 mL) and saturated aqueous Na₂S₂O₃ (25 mL) were added and stirred vigorously for 20 min. The aqueous layer was extracted with DCM (4 × 30 mL), dried over MgSO₄, and the solvent removed *in vacuo*.

General procedure H: Formylation of pyrroles

The relevant pyrrole (1 eq.) was dissolved in DMF (5 mL/mmol) and cooled to 0 °C. Phosphorous oxychloride (5 eq.) was added dropwise, warmed to 70 °C and stirred until the starting material was completely consumed. NaOH (1M in H₂O, 10 ml) and ice cubes were

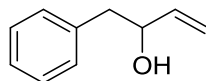
added to the reaction mixture and heated at 100 °C for 45 min. The reaction mixture was cooled to r.t. and extracted with EtOAc (3 × 30 mL). The organic layers were combined, washed with brine, dried over MgSO₄ and the solvent removed *in vacuo*.

General procedure I: Pinnick Oxidation

To a solution of the relevant pyrrole (1 eq.) in MeCN (11.8 mL/mmol), was added a solution of sodium chlorite (1.4 eq.) in water (1.12 mL/mmol of sodium chlorite). A solution of sulfamic acid (1.4 eq.) in water (1.12 mL/mmol of sodium chlorite) was added dropwise and the mixture was stirred at r.t. until the starting material was consumed. The solvent was removed *in vacuo* and water (30 mL) was added to the residue. The aqueous layer was extracted with EtOAc (3 × 30 mL), dried over MgSO₄ and the solvent removed *in vacuo*.

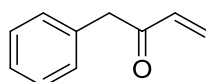
16.2.3 MDMX Inhibitors: Synthetic Procedures

1-Phenylbut-3-en-2-ol (**32**)²⁰²



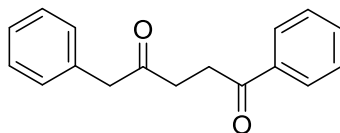
Prepared according to general procedure A using phenylacetaldehyde (1.4 mL, 12.48 mmol), 1.6 M solution of vinylmagnesium chloride in THF (11.7 mL, 18.72 mmol) and THF (15 mL). Purification by MPLC on SiO₂ (Petrol:EtOAc, 0-17%) gave a yellow liquid (1.12 g, 61%). R_f = 0.39 (15% EtOAc/Petrol); IR $\nu_{\text{max}}/\text{cm}^{-1}$ 3279 (OH), 3045, 2921, 2868; ¹H NMR (500 MHz, CDCl₃) δ_{H} 1.64 (1H, brs, OH), 2.81 (1H, dd, $J = 13.6$ and 8.0 Hz, ArCH₂), 2.88 (1H, dd, $J = 13.6$ and 5.4 Hz, 2 × ArCH₂), 4.33-4.37 (1H, m, CHOH), 5.15 (1H, app dt, $J = 10.5$ and 1.4 Hz, CH=CH_{cis}H), 5.27 (1H, app dt, $J = 17.2$ and 1.4 Hz, CH=CH_{trans}H), 5.95 (1H, ddd, $J = 17.2$, 10.5, 5.8 Hz, CH=CH₂), 7.24-7.27 (3H, m, 3 × ArH), 7.32-7.35 (2H, m, 2 × ArH); ¹³C NMR (125 MHz, CDCl₃) δ_{C} 43.8 (ArCH₂), 73.6 (CHOH), 114.9 (CH=CH₂), 126.5 (CH-Ar), 128.4 (2 × CH-Ar), 129.5 (2 × CH-Ar), 137.7 (C-Ar), 140.1 (CH=CH₂). LRMS (ES⁺) m/z 131.2 [(M-H₂O)+H]⁺.

1-Phenylbut-3-en-2-one (**33**)²⁰³



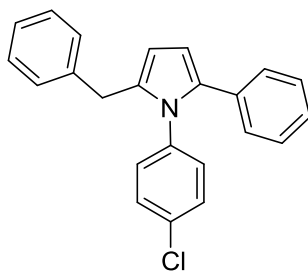
Prepared according to general procedure G using compound **32** (698 mg, 4.71 mmol) in DCM (17 ml) and Dess-Martin periodinane (3.99 g, 9.42 mmol) in DCM (25 mL). The product was used for next step without further purification (685 mg, quant.). R_f = 0.67 (15% EtOAc/Petrol); λ_{max} (EtOH)/nm 210, 256; IR $\nu_{\text{max}}/\text{cm}^{-1}$ 1670 (C=O); ¹H NMR (500 MHz, CDCl₃) δ_{H} 3.87 (2H, s, 2 × ArCH₂), 5.82 (1H, dd, $J = 10.3$ and 1.2 Hz, CH=CH_{cis}H), 6.30 (1H, dd, $J = 17.5$ and 1.2 Hz, CH=CH_{trans}H), 6.40 (1H, dd, $J = 17.5$ and 10.3 Hz, CH=CH₂), 7.20-7.22 (2H, m, 2 × ArH), 7.24-7.27 (1H, m, ArH), 7.31-7.35 (2H, m, 2 × ArH); ¹³C NMR (125 MHz, CDCl₃) δ_{C} (125 MHz, CDCl₃) δ 47.2 (ArCH₂), 127.0 (CH-Ar), 128.8 (2 × CH-Ar), 129.1 (CH=CH₂), 129.4 (2 × CH-Ar), 134.1 (C-Ar), 135.6 (CH=CH₂), 197.7 (C=O).

1,5-Diphenylpentane-1,4-dione (34)



Benzaldehyde (0.14 ml, 1.4 mmol) was dissolved in ethanol (0.8 mL), triethylamine (0.4 mL, 2.8 mmol), compound **33** (225 mg, 1.5 mmol), and 3-benzyl-5-(2-hydroxyethyl)-4-methylthiazolium chloride (94 mg, 0.35 mmol) were added and stirred at 80 °C for 19 h. The solvent was evaporated *in vacuo* and the residue was treated with 2M HCl (10 mL). The aqueous layer was extracted with DCM (3 × 20 ml). The organic layers were combined, washed with saturated aqueous NaHCO₃, dried over MgSO₄ and evaporated *in vacuo*. Purification by MPLC on SiO₂ (DCM:MeOH, 0-1%) gave a pale brown viscous liquid (230 mg, 65%). R_f = 0.40 (20% EtOAc/Petrol); λ_{max} (EtOH)/nm 240; IR ν_{max}/cm⁻¹ 1709 (C=O), 1686 (C=O); ¹H NMR (500 MHz, CDCl₃) δ_H 2.89 (2H, t, *J* = 6.3 Hz, 2 × CH₂CO), 3.26 (2H, t, *J* = 6.3 Hz, 2 × CH₂CO), 3.82 (2H, s, 2 × ArCH₂), 7.24-7.28 (3H, m, 3 × ArH), 7.32- 7.35 (2H, m, 2 × ArH), 7.43-7.46 (2H, m, 2 × ArH) 7.52-7.57 (1H, m, ArH), 7.95-7.97 (2H, m, 2 × ArH); ¹³C NMR (125 MHz, CDCl₃) δ_C 32.5 (CH₂CO), 35.6 (CH₂CO), 50.2 (ArCH₂), 127.1 (CH-Ar), 128.1 (2 × CH-Ar), 128.6 (2 × CH-Ar), 128.7 (2 × CH-Ar), 129.5 (2 × CH-Ar), 133.2 (C-Ar), 134.3 (C-Ar), 136.6 (C-Ar), 198.5 (C=O), 207.1 (C=O). LRMS (ES⁺) *m/z* 253.3 [M+H]⁺.

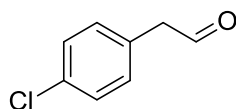
2-Benzyl-1-(4-chlorophenyl)-5-phenyl-1H-pyrrole (30)



A mixture of compound **34** (70 mg, 0.28 mmol), 4-chloroaniline (40 mg, 0.31 mmol) and acetic acid (2 mL) was refluxed for 1.5 h. After cooling to r.t., water (20 mL) was added and the mixture was neutralised with 1N NaOH. The aqueous layer was extracted with DCM (3 × 20 mL), the organic layers were combined, washed with water (30 mL), dried over MgSO₄ and evaporated *in vacuo*. Purification by MPLC on SiO₂ (Petrol:EtOAc, 0-20%) gave a white solid (29 mg, 30%). R_f = 0.83 (20% EtOAc/Petrol); m.p. 165 °C; λ_{max} (EtOH)/nm 286; IR ν_{max}/cm⁻¹ 3065, 2922, 2658, 1489.; ¹H NMR (500 MHz, CDCl₃) δ_H 3.73 (2H, s, 2 × CH₂), 6.00 (1H, d, *J*

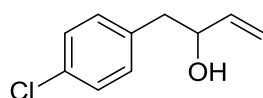
= 3.5 Hz, Pyrrole-*H*), 6.30 (1H, d, $J = 3.5$ Hz, Pyrrole-*H*), 6.87-6.89 (2H, m, $2 \times \text{ArH}$), 6.93-6.97 (4H, m, $4 \times \text{ArH}$), 7.00-7.03 (1H, m, *ArH*), 7.05-7.09 (3H, m, $3 \times \text{ArH}$), 7.11-7.18 (4H, m, $4 \times \text{ArH}$); ^{13}C NMR (125 MHz, CDCl_3) δ_{C} 33.6 (ArCH_2), 109.0 ($2 \times \text{CH-Pyrrole}$), 126.0 (C-Ar), 126.1 (C-Ar), 127.9 ($2 \times \text{C-Ar}$), 128.1 ($2 \times \text{C-Ar}$), 128.3 ($2 \times \text{C-Ar}$), 128.6 ($2 \times \text{C-Ar}$), 129.1 ($2 \times \text{C-Ar}$), 130.0 ($2 \times \text{C-Ar}$), 133.0 (C-Ar), 133.4 (C-Ar), 134.8 (C-Ar), 134.8 (C-Ar), 137.7 (C-Ar), 139.4 (C-Ar); LRMS (ES^+) m/z 344.3 [$\text{M}(^{35}\text{Cl})+\text{H}$] $^+$, 346.4 [$\text{M}(^{37}\text{Cl})+\text{H}$] $^+$.

2-(4-Chlorophenyl)acetaldehyde (36)



Prepared according to general procedure G using 2-(4-chlorophenyl) ethanol (244 mg, 1.56 mmol) in DCM (5 mL) and Dess-Martin periodinane (1 g, 2.35 mmol) in DCM (8 mL). Purification by MPLC on SiO_2 (Petrol:EtOAc, 0-20%) gave a colourless liquid (160 mg, 66%). $R_f = 0.70$ (15% EtOAc/Petrol); IR $\nu_{\text{max}}/\text{cm}^{-1}$ 3030, 2925, 1701 (C=O); ^1H NMR (500 MHz, CDCl_3) δ_{H} 3.68 (2H, d, $J = 2.1$ Hz, $2 \times \text{ArCH}_2$), 7.14-7.16 (2H, m, $2 \times \text{ArH}$), 7.33-7.35 (2H, m, $2 \times \text{ArH}$), 9.74 (t, $J = 2.1$ Hz, CHO); ^{13}C NMR (125 MHz, CDCl_3) δ_{C} 49.8 (CH_2), 129.1 ($2 \times \text{CH-Ar}$), 130.3 (C-Ar), 130.9 ($2 \times \text{CH-Ar}$), 133.5 (C-Ar), 198.6 (C=O).

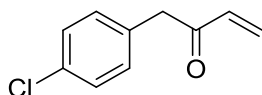
1-(4-Chlorophenyl)but-3-en-2-ol (37)



Prepared according to general procedure A using compound **36**, 1.6 M solution of vinylmagnesium chloride in THF (9.5 mL, 15.16 mmol) and THF (15 mL). Purification by MPLC on SiO_2 (Petrol:EtOAc, 0-20%) gave a colourless liquid (535 mg, 39%). $R_f = 0.38$ (15% EtOAc/Petrol); λ_{max} (EtOH)/nm 221, IR $\nu_{\text{max}}/\text{cm}^{-1}$ 3368 (OH), 3081, 2921, 2854, 1490; ^1H NMR (500 MHz, CDCl_3) δ_{H} 2.76 (1H, dd, $J = 13.6, 7.6$ Hz, ArCH_2), 2.82 (1H, dd, $J = 13.6, 5.2$ Hz, ArCH_2), 4.29-4.33 (1H, m, CHOH), 5.12 (1H, dt, $J = 10.4$ and 1.2 Hz, $\text{CH}=\text{CH}_{\text{cis}}\text{H}$), 5.22 (1H, dt, $J = 17.2$ and 1.2 Hz, $\text{CH}=\text{CH}_{\text{trans}}\text{H}$), 5.89 (1H, ddd, $J = 17.2, 10.4, 5.9$ Hz, $\text{CH}=\text{CH}_2$), 7.14-7.14 (2H, m, $2 \times \text{ArH}$), 7.25-7.28 (2H, m, $2 \times \text{ArH}$); ^{13}C NMR (125 MHz, CDCl_3) δ_{C} 43.0 (ArCH_2), 73.5 (CHOH), 115.3 ($\text{CH}=\text{CH}_2$), 128.6 ($2 \times \text{CH-Ar}$), 130.9 ($2 \times \text{CH-Ar}$), 132.4 (C-

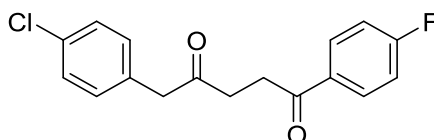
Ar), 136.3 (C-Ar), 139.9 (CH=CH₂). LRMS (ES⁺) *m/z* 165.2 [(M(³⁵Cl)-H₂O)+H]⁺, 167.2 [(M(³⁷Cl)-H₂O)+H]⁺.

1-(4-Chlorophenyl)but-3-en-2-one (**38**)²⁰⁴



Prepared according to general procedure G using compound **37** (100 mg, 0.547 mmol) in DCM (2 mL) and Dess-Martin periodinane (348 mg, 0.82 mmol) in DCM (4 mL). Purification (SP4, silica, EtOAc/Petrol, 0-10%) gave a colourless liquid; *R_f* = 0.70 (EtOAc/Petrol, 15%); λ_{max} (EtOH)/nm 218; IR ν_{max} /cm⁻¹ 3035, 2921, 1690 (C=O stretch); ¹H NMR (500 MHz, CDCl₃) δ 3.85 (2H, s, 2×ArCH₂), 5.86 (1H, dd, *J* = 10.3, 1.2 Hz, CH=CH_{cis}H), 6.30 (1H, dd, *J* = 17.5, 1.2 Hz, CH=CH_{trans}H), 6.40 (1H, dd, *J* = 17.5 and 10.3 Hz, CH=CH₂), 7.12-7.14 (2H, m, 2 × ArH), 7.28-7.31 (2H, m, 2 × ArH).

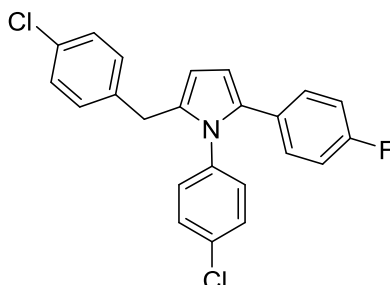
5-(4-Chlorophenyl)-1-(4-fluorophenyl)pentane-1,4-dione (**39**)



To a solution of 4-fluorobenzaldehyde (0.06 mL, 0.497 mmol) in ethanol (0.3 mL), was added triethylamine (0.14 mL, 0.25 mmol), compound **38** (crude product), and 3-benzyl-5-(2-hydroxyethyl)-4-methylthiazolium chloride (33 mg, 0.124 mmol) and stirred at 80 °C for 19 h. The solvent was evaporated *in vacuo* and the residue was treated with 2 M HCl (10 mL). The aqueous layer was extracted with DCM (3 × 20 mL), organic layers were combined, washed with saturated aqueous NaHCO₃, dried over MgSO₄ and evaporated *in vacuo*. Purification by MPLC on SiO₂ (Petrol:DCM, 0-80%) gave a colourless viscous liquid (50 mg, 30% in 2 steps). *R_f* = 0.42 (20% EtOAc/Petrol); λ_{max} (EtOH)/nm 240; IR ν_{max} /cm⁻¹ 3078, 2909, 1710 (C=O), 1689 (C=O); ¹H NMR (500 MHz, CDCl₃) δ_{H} 2.88 (2H, t, *J* = 6.1 Hz, CH₂CO), 3.23 (2H, t, *J* = 6.1 Hz, CH₂CO), 3.80 (2H, s, ArCH₂), 7.09-7.14 (2H, m, 2 × ArH), 7.15- 7.18 (2H, m, 2 × ArH), 7.29-7.31 (2H, m, 2 × ArH), 7.96-8.00 (2H, m, 2 × ArH); ¹³C NMR (125 MHz, CDCl₃) δ_{C} 32.5 (CH₂CO), 35.8 (CH₂CO), 49.3 (ArCH₂), 115.7 (2C, d, *J* = 21.5 Hz, 2 × ArCHCF), 128.8 (2 × CH-Ar), 130.7 (2C, d, *J* = 9.3 Hz, 2 × ArCHCHCF), 130.9 (2 × CH-Ar), 132.6 (C-Ar), 133.0 (d, *J* = 2.9 Hz, ArCCHCHCF), 133.1 (C-Ar), 165.8 (d, *J* = 254.9 Hz, ArCF), 196.8 (C=O),

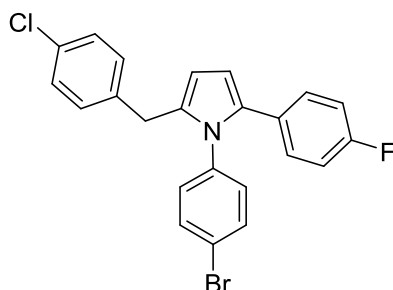
206.4 (C=O); ^{19}F NMR (470 MHz; CDCl_3) δ -105.0; HRMS calcd for $\text{C}_{17}\text{H}_{15}\text{ClFO}_2$ $[\text{M}(^{35}\text{Cl})+\text{H}]^+$ 305.0720, found 305.0721.

2-(4-Chlorobenzyl)-1-(4-Chlorophenyl)-5-(4-fluorophenyl)-1H-pyrrole (40)



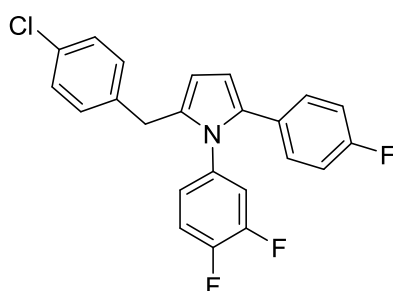
A mixture of compound **39** (35 mg, 0.115 mmol), 4-chloroaniline (15 mg, 0.115 mmol) and acetic acid (0.9 ml) were refluxed for 8 h. After cooling to r.t., water (20 mL) was added and the mixture was neutralised with 1M NaOH. The aqueous layer was extracted with DCM (3 \times 20 mL), the organic layers were combined, washed with water (30 mL), dried over MgSO_4 and evaporated *in vacuo*. Purification by MPLC on SiO_2 (Petrol:DCM, 0-15%) gave a white solid (14 mg, 31%) R_f = 0.56 (10% EtOAc/Petrol); m.p. 110-112 $^\circ\text{C}$; λ_{max} (EtOH)/nm 247; IR $\nu_{\text{max}}/\text{cm}^{-1}$ 2924, 2251, 1493; ^1H NMR (500 MHz, CDCl_3) δ_{H} 3.68 (2H, s, CH_2), 5.99 (1H, d, J = 3.5 Hz, Pyrrole- H), 6.24 (1H, d, J = 3.5 Hz, Pyrrole- H), 6.75-6.79 (2H, m, 2 \times Ar H), 6.83-6.85 (4H, m, 4 \times Ar H), 6.90-6.93 (2H, m, 2 \times Ar H), 7.08-7.11 (2H, m, 2 \times Ar H), 7.16-7.18 (2H, m, 2 \times Ar H). ^{13}C NMR (125 MHz, CDCl_3) δ_{C} 33.0 (CH_2), 108.9 (CH-Pyrrole), 109.1 (CH-Pyrrole), 115.1 (2C, d, J = 21.5 Hz, 2 \times ArCHCF), 128.4 (2 \times CH-Ar), 129.1 (d, J = 3.2 Hz, ArCCHCHCF) 129.2 (2 \times CH-Ar), 129.6 (2C, d, J = 7.8 Hz, 2 \times ArCHCHCF), 129.9 (2 \times CH-Ar), 129.9 (2 \times CH-Ar), 131.9 (C-Ar), 133.7 (C-Ar), 133.9 (C-Ar), 134.0 (C-Ar), 137.4 (C-Ar), 137.8 (C-Ar), 161.4 (d, J = 246.0 Hz, ArCF). ^{19}F NMR (470 MHz; CDCl_3) δ_{F} -116.0; HRMS calcd for $\text{C}_{23}\text{H}_{17}\text{Cl}_2\text{FN}$ $[\text{M}(^{35}\text{Cl}_2)+\text{H}]^+$ 396.0526, found 396.0523.

1-(4-Bromophenyl)-2-(4-chlorobenzyl)-5-(4-fluorophenyl)-1H-pyrrole (41)



Prepared according to general procedure D using compound **39** (50 mg, 0.164 mmol), 4-bromoaniline (141 mg, 0.82 mmol) and acetic acid (0.5 mL). Purification by MPLC on SiO₂ (Petrol:EtOAc, 0-20%) gave a white solid (60 mg, 83%) R_f = 0.56 (EtOAc/Petrol, 10%); m.p. 123-125 °C; λ_{max} (EtOH)/nm 248; IR ν_{max}/cm⁻¹ 3053, 2847, 2285, 1590, 1485; ¹H NMR (500 MHz, CDCl₃) δ_H 3.68 (2H, s, CH₂), 5.98 (1H, d, *J* = 3.5 Hz, Pyrrole-*H*), 6.24 (1H, d, *J* = 3.5 Hz, Pyrrole-*H*), 6.75-6.79 (4H, m, 4 × Ar*H*), 6.84-6.86 (2H, m, 2 × Ar*H*), 6.90-6.93 (2H, m, 2 × Ar*H*), 7.09-7.11 (2H, m, 2 × Ar*H*), 7.32-7.35 (2H, m, 2 × Ar*H*); ¹³C NMR (125 MHz, CDCl₃) δ_C 33.0 (CH₂), 108.9 (CH-Pyrrole), 109.1 (CH-Pyrrole), 115.1 (2C, d, *J* = 21.5 Hz, 2 × ArCHCF), 121.7 (C-Ar), 128.4 (2 × CH-Ar), 129.1 (d, *J* = 3.2 Hz, ArCCHCHCF) 129.6 (2C, d, *J* = 7.9 Hz, 2 × ArCHCHCF), 129.9 (2 × CH-Ar), 130.3 (2 × CH-Ar), 132.0 (C-Ar), 132.7 (C-Ar), 133.9 (C-Ar), 134.0 (C-Ar), 137.4 (C-Ar), 137.8 (C-Ar), 137.9 (C-Ar), 161.4 (d, *J* = 246.1 Hz, ArCF); ¹⁹F NMR (470 MHz; CDCl₃) δ_F -116.0; HRMS calcd for C₂₃H₁₆BrClFN [M(⁷⁹Br³⁵Cl)+H]⁺ 440.0025, found 440.0023.

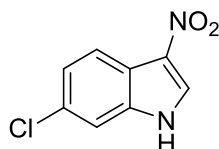
2-(4-Chlorobenzyl)-1-(3,4-difluorophenyl)-5-(4-fluorophenyl)-1H-pyrrole (42)



Prepared according to general procedure D using compound **39** (23 mg, 0.075 mmol), 3,4-difluoroaniline (0.04 ml, 0.375 mmol) and acetic acid (0.23 mL). Purification by MPLC on SiO₂ (Petrol:EtOAc, 0-20%) gave a white solid (60 mg, 77%). R_f = 0.52 (10% EtOAc/Petrol); m.p. 118-120 °C; λ_{max} (EtOH)/nm 277; IR ν_{max}/cm⁻¹ 2912, 2088, 1519; ¹H NMR (500 MHz, CDCl₃) δ_H 3.69 (2H, s, CH₂), 5.99 (1H, d, *J* = 3.5 Hz, Pyrrole-*H*), 6.23 (1H, d, *J* = 3.5 Hz,

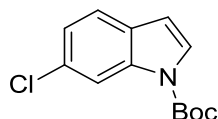
Pyrrole-*H*), 6.63-6.66 (1H, m, *ArH*), 6.73-6.76 (1H, m, *ArH*), 6.77-6.80 (2H, m, $2 \times \text{ArH}$), 6.83-6.85 (2H, m, $2 \times \text{ArH}$), 6.90-6.93 (2H, m, $2 \times \text{ArH}$), 6.98 (1H, q, $J = 18.4, 8.7$ Hz, *ArH*), 7.11 (2H, d, $J = 8.3$ Hz, $2 \times \text{ArH}$); ^{13}C NMR (125 MHz, CDCl_3) δ_{C} 33.0 (CH_2), 109.0 (CH-Pyrrole), 109.3 (CH-Pyrrole), 115.2 (2C, d, $J = 21.5$ Hz, $2 \times \text{ArCHCF}$), 117.4 (d, $J = 18.2$ Hz, ArCHCF), 118.1 (d, $J = 18.0$ Hz, ArCHCF), 125.1 (dd, $J = 6.1, 3.3$ Hz, ArCHCHCF), 128.5 ($2 \times \text{CH-Ar}$), 128.9 (d, $J = 3.3$ Hz, ArCCHCF), 129.6 (2C, d, $J = 7.9$ Hz, $2 \times \text{ArCHCF}$), 129.8 ($2 \times \text{CH-Ar}$), 132.1 (C-Ar), 134.0 (C-Ar), 134.2 (C-Ar), 135.2 (dd, $J = 7.4, 3.4$ Hz, ArCCHCF), 137.6 (C-Ar), 149.8 (dd, $J = 250.4, 12.5$ Hz, ArCF), 149.9 (dd, $J = 246.4$ Hz, ArCF), 161.5 (dd, $J = 246.4$ Hz, ArCF). ^{19}F NMR (470 MHz; CDCl_3) δ_{F} -137.2 (d, $J = 20.8$ Hz), -134 (d, $J = 20.8$ Hz), -115.7; HRMS calcd for $\text{C}_{23}\text{H}_{16}\text{ClF}_3\text{N}$ [$\text{M}(^{35}\text{Cl})+\text{H}$] $^+$ 398.0920, found 398.0918.

6-Chloro-3-nitro-1*H*-indole (44)



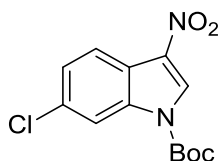
6-chloroindole (305 mg, 2.01 mmol) and silver nitrate (362 mg, 2.13 mmol) were suspended in MeCN (1.9 mL) and cooled to 0 °C. Benzoyl chloride (0.25 mL, 2.13 mmol) was added dropwise and the mixture was stirred at 0 °C for 30 min. The reaction mixture was treated with MeOH (5 mL) and filtered through PL-thiol cartridge. The filtrate was evaporated *in vacuo* and the residue was purified by MPLC ($\text{H}_2\text{O}:\text{MeOH}$, reversed phase with 0.1% HCOOH modifier, 0-85%) to get a yellow solid (165 mg, 42%). $R_f = 0.46$ (40% EtOAc/Petrol); m.p. 234-236 °C; IR $\nu_{\text{max}}/\text{cm}^{-1}$ 3191, 3144, 1456, 1368, 1199; ^1H NMR (500 MHz, $\text{DMSO-}d_6$) δ_{H} 7.37 (1H, dd, $J = 8.5$ and 1.8 Hz, H^5), 7.61 (1H, d, $J = 1.8$ Hz, H^7), 8.05 (1H, d, $J = 8.5$ Hz, H^4), 8.67 (1H, s, H^2), 12.74 (1H, br s, NH); ^{13}C NMR (125 MHz, $\text{DMSO-}d_6$): δ_{C} 113.6 (CH^7), 119.1 (C-Ar), 121.3 (CH^4), 124.5 (CH^5), 128.9 (C-Ar), 129.2 (C-Ar), 131.9 (CH^2), 135.9 (C-Ar). LRMS (ES $^-$) m/z 195.1 [$\text{M}(^{35}\text{Cl})-\text{H}$] $^-$, 197.1 [$\text{M}(^{37}\text{Cl})-\text{H}$] $^-$.

***tert*-Butyl 6-chloro-1*H*-indole-1-carboxylate (47)**



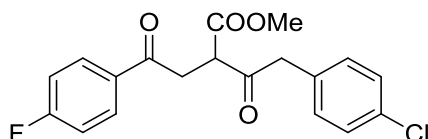
6-chloroindole (1 g, 6.59 mmol) and DMAP (402 mg, 3.29 mmol) were dissolved in MeCN (5 mL). A solution of di-*tert*-butyl dicarbonate (2.27 mL, 9.88 mmol) in MeCN (15 mL) was added dropwise and the mixture was stirred at r.t. for 2 h. The solvent was evaporated *in vacuo* to get brown coloured liquid. Purification by MPLC on SiO₂ (Petrol:EtOAc, 0-15%) gave a colourless liquid (1.6 g, 97%). R_f = 0.50 (20% EtOAc/Petrol); ¹H NMR (500 MHz, CDCl₃) δ_H 1.67 (9H, s, 3 × CH₃), 6.52 (1H, d, *J* = 3.3 Hz, *H*³), 7.19 (1H, dd, *J* = 8.3 and 1.9 Hz, *H*⁵), 7.44 (1H, d, *J* = 8.3 Hz, *H*⁴), 7.56 (1H, d, *J* = 3.3 Hz, *H*²), 8.19 (1H, s, *H*⁷); ¹³C NMR (125 MHz, CDCl₃) δ_C 28.2 (CH₃), 84.2 (C-CH₃), 107.0 (CH³), 115.5 (CH⁷), 121.6 (CH⁴), 123.2 (CH⁵), 126.4 (CH²), 129.0 (C-Ar), 130.2 (C-Ar), 135.6 (C-Ar), 149.4 (C=O). LRMS (ES⁺) *m/z* 252.3 [(M(³⁵Cl)+H)]⁺, 254.4 [(M(³⁷Cl)+H)]⁺.

***tert*-Butyl 6-chloro-3-nitro-1*H*-indole-1-carboxylate (48)**



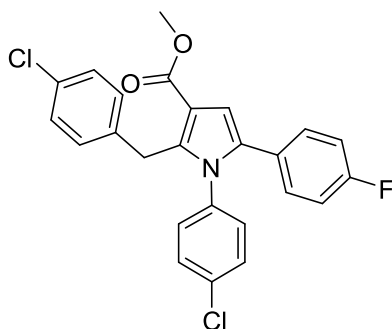
Acetyl nitrate was generated by the dropwise addition of fuming HNO₃ (0.15 mL, 3.57 mmol) to Ac₂O (2.4 mL) at 0 °C followed by standing at r.t. for 5 min and was used immediately. Compound **47** (300 mg, 1.19 mmol) was dissolved in Ac₂O (6 mL) and cooled to -78 °C and a solution of the acetyl nitrate was added dropwise. The mixture was warmed to 0 °C and stirred for 17 h. The reaction mixture was neutralised with saturated aqueous NaHCO₃ and stirred for 20 min. The aqueous layer was extracted with EtOAc (4 × 50 mL), the organic layers were combined, dried over MgSO₄ and the solvent was removed *in vacuo*. Purification by MPLC on SiO₂ (Petrol:EtOAc, 0-6%) gave a pale yellow solid (180 mg, 51%). R_f = 0.50 (5% EtOAc/Petrol); λ_{max} (EtOH)/nm 319, 250; IR ν_{max}/cm⁻¹ 3148, 3114, 2974, 2928, 1747 (C=O), 1542, 1493, 1326; ¹H NMR (500 MHz, CDCl₃) δ_H 1.70 (9H, s, 3×CH₃), 7.42 (1H, dd, *J* = 8.6 and 1.8 Hz, *H*⁵), 8.17 (1H, d, *J* = 8.6 Hz, *H*⁴), 8.28 (1H, d, *J* = 1.8 Hz, *H*⁷), 8.49 (1H, s, *H*²); ¹³C NMR (125 MHz, CDCl₃): δ_C 28.0 (3 × CH₃), 87.3 (C-CH₃), 115.9 (CH⁷), 120.0 (C-Ar), 121.6 (CH⁴), 126.2 (CH⁵), 128.1 (CH²), 132.3 (C-Ar), 132.9 (C-Ar), 134.6 (C-Ar), 147.8 (C-Ar); HRMS calcd for C₁₃H₁₄ClN₂O₄ [M(³⁵Cl)+H]⁺ 297.0637, found 297.0638.

Methyl 4-(4-chlorophenyl)-2-(2-(4-fluorophenyl)-2-oxoethyl)-3-oxobutanoate (54)



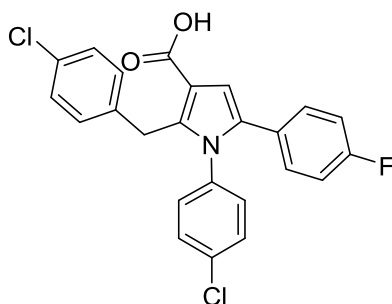
1M Diethylzinc in hexane (15 mL, 14.76 mmol) was dissolved in DCM (28 mL) and cooled to 0 °C. Diiodomethane (1.2 mL, 14.76 mmol) was added dropwise, and the mixture was stirred for 30 min. After the formation of a white precipitate, methyl 4-fluorobenzoyl acetate (0.57 mL, 3.6 mmol) was added dropwise, and the reaction mixture was stirred for 30 min. **Compound 36** (736 mg, 5 mmol) was added and the mixture was stirred at 0 °C for 1.5 h. Silica gel (10 g) was added and the mixture was stirred at r.t. for 30 min. The mixture was filtered and the solvent was evaporated *in vacuo*. The residue was dissolved in DCM (8 mL), PCC (853 mg, 3.96 mmol) was added, and the mixture was stirred at r.t. for 17 h. Then, additional PCC (776 mg, 3.6 mmol) was added and the reaction mixture was stirred at r.t. for 24 h. The mixture was passed through a short path of silica gel and eluted with DCM and concentrated *in vacuo*. Purification by MPLC on SiO₂ (Petrol:EtOAc, 0-20%) followed by another purification by MPLC (H₂O:MeOH, reversed phase with 0.1% HCOOH modifier, 0-100%) gave a pale yellow viscous liquid (436 mg, 33%). $R_f = 0.36$ (25% EtOAc/Petrol); λ_{\max} (EtOH)/nm 244, 225; IR $\nu_{\max}/\text{cm}^{-1}$ 3070, 2954, 2920, 1742 (C=O), 1719 (C=O), 1680 (C=O); ¹H NMR (500 MHz, CDCl₃) δ_H 3.51 (1H, dd, $J = 18.3$ and 4.8 Hz, 1 × CH₂), 3.70-3.75 (1H, m, peaks coincided with OMe singlet, 1 × CH₂), 3.75 (3H, s, CH₃), 4.05 (1H, d, $J = 16.9$ Hz, ArCH₂), 4.10 (1H, d, $J = 16.9$ Hz, ArCH₂), 4.30 (2H, dd, $J = 8.9$ and 4.8 Hz, CHCOOMe), 7.11-7.19 (4H, m, 4 × ArH), 7.29-7.31 (2H, m, 2 × ArH), 7.97-8.00 (2H, m, 2 × ArH); ¹³C NMR (125 MHz, CDCl₃) δ_C 37.7 (CH₂), 49.1 (ArCH₂), 52.4 (CHCOOMe), 52.9 (COOCH₃), 115.9 (2C, d, $J = 22.0$ Hz, 2 × ArCHCF), 128.7 (2 × CH-Ar), 130.9 (2C, d, $J = 9.4$ Hz, 2 × ArCHCHCF), 131.2 (2 × CH-Ar), 131.9 (C-Ar), 132.4 (d, $J = 2.9$ Hz, ArCCHCHCF), 133.1 (C-Ar), 166.1 (d, $J = 255.5$ Hz, ArCF), 169.1 (C=O), 195.5 (C=O), 201.7 (C=O); ¹⁹F NMR (470 MHz; CDCl₃) δ_F -104.1; HRMS calcd for C₁₉H₁₇ClFO₄ [M(³⁵Cl)+H]⁺ 363.0794, found 363.0787.

Methyl 2-(4-chlorobenzyl)-1-(4-chlorophenyl)-5-(4-fluorophenyl)-1H-pyrrole-3-carboxylate (55)



Prepared according to general procedure D using compound **54** (200 mg, 0.55 mmol), 4-chloroaniline (350 mg, 2.75 mmol) and acetic acid (1.6 ml). Purification by MPLC on SiO₂ (Petrol:EtOAc, 0-20%) gave a white solid (121 mg, 48%). $R_f=0.56$ (10% EtOAc/Petrol); m.p. 124-126 °C; λ_{max} (EtOH)/nm 263; IR ν_{max}/cm^{-1} 3068, 2946, 1700 (C=O); ¹H NMR (500 MHz, CDCl₃) δ_H 3.84 (3H, s, COOCH₃), 4.23 (2H, s, 2 × CH₂), 6.78-6.87 (7H, m, 7 × ArH), 6.96-6.99 (2H, d, 2 × ArH), 7.11-7.13 (2H, m, 2 × ArH), 7.23-7.25 (2H, m, 2 × ArH); ¹³C NMR (125 MHz, CDCl₃) δ_C 30.8 (CH₂), 51.2 (COOCH₃), 110.3 (CH-Pyrrole), 113.8 (C-Ar), 115.3 (2C, d, $J = 21.6$ Hz, 2 × ArCHCF), 127.9 (d, $J = 3.3$ Hz, ArCCHCHCF), 128.4 (2 × CH-Ar), 129.4 (2 × CH-Ar), 129.5 (2 × CH-Ar), 130.0 (2 × CH-Ar), 130.1 (2C, d, $J=8.05$ Hz, 2 × ArCHCHCF), 131.9 (C-Ar), 133.8 (C-Ar), 134.7 (C-Ar), 136.0 (C-Ar), 137.4 (C-Ar), 139.0 (C-Ar), 161.8 (d, $J = 247.5$ Hz, ArCF), 165.5 (COOMe). ¹⁹F NMR (470 MHz; CDCl₃) δ_F -114.5; HRMS calcd for C₂₅H₁₉Cl₂FNO₂ [M(³⁵Cl₂)+H]⁺ 454.0771, found 454.0763.

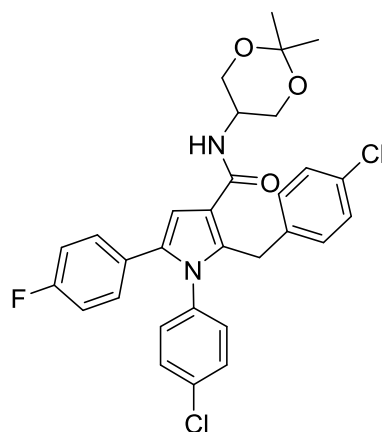
2-(4-Chlorobenzyl)-1-(4-chlorophenyl)-5-(4-fluorophenyl)-1H-pyrrole-3-carboxylic acid (2)



Compound **55** (70 mg, 0.15 mmol) was dissolved in THF (1 mL), 4 M LiOH in H₂O monohydrate (1 mL), and the mixture was stirred at r.t. for 15 h. To the resulting suspension, MeOH (1 mL) was added and the mixture was stirred at r.t. for 72 h. Then, the reaction mixture

was neutralised with 2 M HCl and extracted with EtOAc (3 × 20 mL). The organic layers were combined, dried over MgSO₄, and evaporated *in vacuo*. Purification by MPLC on SiO₂ (Petrol:EtOAc, 0-20%) gave a white solid (60 mg, 91%). The reaction repeated with 50 mg of the ester starting material to have enough material for the next step. R_f = 0.62 (2% MeOH/DCM); m.p. 184-186 °C; λ_{max} (EtOH)/nm 255; IR ν_{max}/cm⁻¹ 2300-3100 (very broad, O-H overlap with C-H), 1669 (C=O); ¹H NMR (500 MHz, CDCl₃) δ_H 4.24 (2H, s, CH₂), 6.79-6.88 (7H, m, 7 × ArH), 6.97-7.00 (2H, m, 2 × ArH), 7.12 (2H, d, *J* = 7.9 Hz, 2 × ArH), 7.25 (2H, d, *coincided with CDCl₃ peak*, 2 × ArH); ¹³C NMR (125 MHz, CDCl₃) δ_C 30.8 (CH₂), 110.8 (Pyrrole-CH), 115.3 (2C, d, *J* = 21.6 Hz, 2 × ArCHCF), 127.7 (d, *J* = 3.4 Hz, ArCCHCHCF), 128.4 (2 × CH-Ar), 129.4 (2 × CH-Ar), 129.5 (2 × CH-Ar), 130.0 (2 × CH-Ar), 130.1 (2C, d, *J* = 8.1 Hz, 2 × ArCHCHCF), 131.9 (C-Ar), 134.2 (C-Ar), 134.8 (C-Ar), 135.9 (C-Ar), 137.1 (C-Ar), 140.1 (C-Ar), 161.9 (d, *J* = 247.5 Hz, ArCF), 170.0 (COOH). ¹⁹F NMR (470 MHz; CDCl₃) δ_F -114.3; HRMS calcd for C₂₄H₁₇Cl₂FNO₂ [M(³⁵Cl₂)+H]⁺ 440.0615, found 440.0610.

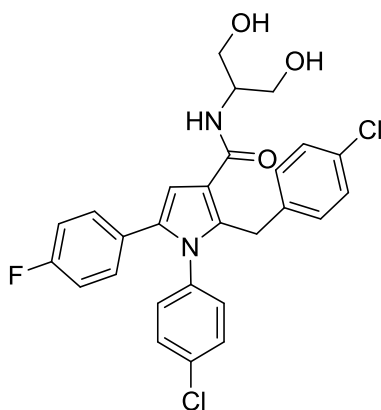
2-(4-Chlorobenzyl)-1-(4-chlorophenyl)-*N*-(2,2-dimethyl-1,3-dioxan-5-yl)-5-(4-fluorophenyl)-1*H*-pyrrole-3-carboxamide (57)



Compound **2** (98 mg, 0.22 mmol), amine **115** (34 mg, 0.26 mmol) and DMAP (2.5 mg, 0.02 mmol) were dissolved in DCM (2 mL) and the reaction mixture was stirred at 0 °C for 5 min. DIC (0.04 mL, 0.26 mmol) was added and the resulting solution was stirred at 0 °C for 15 min and at r.t. for 16 h. The reaction mixture was quenched with water (10 mL) and extracted with DCM (3 × 20 mL). The organic layers were combined, dried over MgSO₄, and concentrated *in vacuo*. Purification by MPLC on SiO₂ (Petrol:EtOAc, 0-50%) gave a white solid (85 mg, 70%). R_f = 0.17 (33% EtOAc/Petrol); m.p. 152-154 °C; λ_{max} (EtOH)/nm 240; IR ν_{max}/cm⁻¹ 3302 (NH), 2968, 2939, 2876, 1616 (C=O); ¹H NMR (500 MHz, CDCl₃) δ_H 1.43 (3H, s, CH₃), 1.51 (3H, s,

*CH*₃), 3.82 (2H, d, *J* = 11.3 Hz, *CH*₂OC), 4.05-4.08 (1H, m, CONHCHCH₂), 4.20-4.25 (2H, d, *J* = 11.3 Hz, *CH*₂OC), 4.25 (2H, s, 2 × *CH*₂), 6.56 (1H, s, pyrrole-*H*), 6.80-6.89 (7H, m, 6 × *ArH*, 1 × CONH), 6.98-7.01 (2H, m, 2 × *ArH*), 7.10-7.11 (2H, m, 2 × *ArH*), 7.23-7.24 (2H, m, 2 × *ArH*); ¹³C NMR (125 MHz, CDCl₃) δ_C 18.5 (*CH*₃), 29.1 (*CH*₃), 30.7 (*Ar-CH*₂), 43.3 (CONHCHCH₂), 64.0 (2C, 2 × *CH*₂OC), 98.6 (*C(CH*₃)₂), 107.3 (CH-Pyrrole), 115.3 (2C, d, *J* = 21.6 Hz, 2 × *ArCHCF*), 116.8 (C-*Ar*), 127.9 (d, *J* = 3.3 Hz, *ArCCHCHCF*), 128.3 (2 × CH-*Ar*), 129.3 (2 × CH-*Ar*), 129.6 (2 × CH-*Ar*), 130.0 (2 × CH-*Ar*), 130.1 (2C, d, *J* = 8.1 Hz, 2 × *ArCHCHCF*), 131.8 (C-*Ar*), 133.7 (C-*Ar*), 134.5 (C-*Ar*), 136.1 (C-*Ar*), 137.1 (C-*Ar*), 137.8 (C-*Ar*), 161.9 (d, *J* = 247.6 Hz, *ArCF*), 164.7 (COONH); ¹⁹F NMR (470 MHz; CDCl₃) δ_F -114.5; HRMS calcd for C₃₀H₂₆Cl₂FN₂O₃ [M(³⁵Cl₂)-H]⁻ 551.1310, found 551.1297.

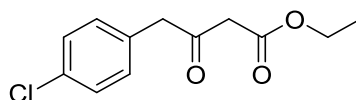
2-(4-Chlorobenzyl)-1-(4-chlorophenyl)-*N*-(1,3-dihydroxypropan-2-yl)-5-(4-fluorophenyl)-1*H*-pyrrole-3-carboxamide (58)



Compound **57** (60 mg, 0.108 mmol) was dissolved in THF (1.7 mL) and 2 M HCl (0.57 mL) was added dropwise and stirred at r.t. for 3 h. 2 M HCl (0.29 mL) was added again and the reaction was stirred for 15 min. The solvent was evaporated *in vacuo* and the residue was neutralised with 1 M NaOH and extracted with EtOAc (3 × 20 mL). The organic layers were combined, washed with H₂O, dried over MgSO₄ and evaporated *in vacuo* to get a white solid (52 mg, 94%). *R*_f = 0.34 (5% MeOH/DCM); m.p. 210-212 °C; λ_{max} (EtOH)/nm 239; IR ν_{max}/cm⁻¹ 3344 (broad, Amide N-H and O-Hs overlapped), 2922, 2852, 1600 (C=O stretch); ¹H NMR (500 MHz, DMSO-*d*₆) δ_H 3.52 (4H, t, *J* = 5.7 Hz, 2 × *CH*₂OC), 3.93-3.99 (1H, m, CONHCHCH₂), 4.29 (2H, s, 2 × *ArCH*₂), 4.65 (2H, t, *J* = 5.7 Hz, 2 × *CH*₂OH), 6.78-6.80 (2H, m, 2 × *ArH*), 6.99 (1H, s, Pyrrole-*H*), 7.01-7.03 (2H, m, 2 × *ArH*), 7.07 (4H, d, *J* = 7.2 Hz, 4 × *ArH*), 7.15-7.17 (2H, m, 2 × *ArH*), 7.46 (1H, d, *J* = 8.5 Hz, CONH); ¹³C NMR (125 MHz, DMSO-*d*₆) δ_C 29.6 (*CH*₂), 52.9 (CONHCHCH₂), 60.5 (2C, 2 × *CH*₂OC), 108.4 (CH-Pyrrole),

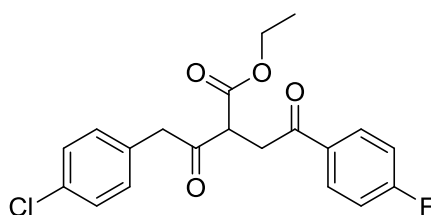
115.2 (2C, d, $J = 21.6$ Hz, $2 \times \text{ArCHCF}$), 116.7 (C-Ar), 127.8 ($2 \times \text{CH-Ar}$), 128.4 (d, $J = 3.3$ Hz, ArCCHCHCF), 129.2 ($2 \times \text{CH-Ar}$), 129.7 ($2 \times \text{CH-Ar}$), 129.8 (2C, d, $J = 8.1$ Hz, $2 \times \text{ArCHCHCF}$), 130.3 (C-Ar), 130.5 ($2 \times \text{CH-Ar}$), 132.2 (C-Ar), 133.0 (C-Ar), 136.1 (C-Ar), 136.5 (C-Ar), 138.3 (C-Ar), 160.9 (d, $J = 244.7$ Hz, ArCF), 164.3 (CONH). ^{19}F NMR (470 MHz; $\text{DMSO-}d_6$) δ_{F} -115.2; HRMS calcd for $\text{C}_{27}\text{H}_{22}\text{Cl}_2\text{FN}_2\text{O}_3$ [$\text{M}(^{35}\text{Cl}_2)\text{-H}$] 511.0997, found 511.0981.

Ethyl 4-(4-chlorophenyl)-3-oxobutanoate (72)



Prepared according to general procedure B using Meldrum's acid (1 g, 6.94 mmol), DCM (6 mL), pyridine (1.1 mL), 4-chlorophenylacetyl chloride (1 mL, 6.94 mmol) and ethanol (22 mL). Purification by MPLC on SiO_2 (Petrol:EtOAc, 0-20%) gave a colourless liquid (1.3 g, 78%). ^1H NMR (500 MHz, CDCl_3) δ_{H} 1.26 (3H, t, $J = 7.2$ Hz, $\text{COOCH}_2\text{CH}_3$), 3.45 (2H, s, CH_2), 3.81 (2H, s, CH_2), 4.17 (2H, q, $J = 7.2$ Hz, $\text{COOCH}_2\text{CH}_3$), 7.12-7.14 (2H, m, $2 \times \text{ArH}$), 7.30-7.32 (2H, m, $2 \times \text{ArH}$) ^{13}C NMR (125 MHz, CDCl_3) δ_{C} 14.1 ($\text{COOCH}_2\text{CH}_3$), 48.5 (CH_2), 49.0 (CH_2), 61.6 ($\text{COOCH}_2\text{CH}_3$), 129.0 ($2 \times \text{CH-Ar}$), 131.0 ($2 \times \text{CH-Ar}$), 131.6 (C-Ar), 133.4 (C-Ar), 167.0 (C=O), 199.9 (C=O).²⁰⁵

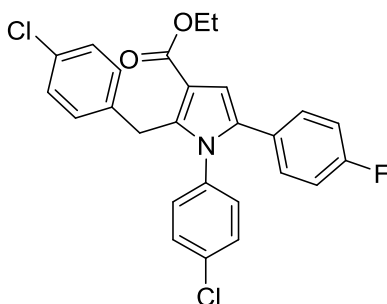
Ethyl 4-(4-chlorophenyl)-2-(2-(4-fluorophenyl)-2-oxoethyl)-3-oxobutanoate (74)



Prepared according to general procedure C using compound **72** (500 mg, 2.07 mmol) and NaH (60% in mineral oil, 107.6 mg, 2.69 mmol) in THF (1.3 mL) and 2-bromo-4'-fluoroacetophenone (492 mg, 2.27 mmol) in THF (1 mL). Purification by MPLC on SiO_2 (Petrol:EtOAc, 0-20%) gave a colourless viscous liquid which solidifies upon standing (709 mg, 91%). $R_{\text{f}} = 0.43$ (20% EtOAc/Petrol); λ_{max} (EtOH)/nm 244, 225; IR $\nu_{\text{max}}/\text{cm}^{-1}$ 3072, 2954, 1740 (C=O), 1718 (C=O), 1680 (C=O); ^1H NMR (500 MHz, CDCl_3) δ_{H} 1.28 (3H, t, $J = 7.1$ Hz, $\text{COOCH}_2\text{CH}_3$), 3.50 (1H, dd, $J = 18.3$ and 4.8 Hz, $1 \times \text{CH}_2$), 3.72 (1H, dd, $J = 18.3$ and 9.0 Hz,

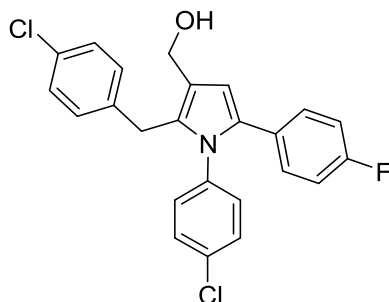
1 × CH₂), 4.08 (1H, d, *J* = 17.1 Hz, ArCH₂), 4.11 (1H, d, *J* = 17.1 Hz, ArCH₂), 4.20 (2H, q, *J* = 7.1 Hz, COOCH₂CH₃), 4.29 (2H, dd, *J* = 9.0 and 4.8 Hz, CHCOOEt), 7.11-7.18 (4H, m, 4 × ArH), 7.29-7.31 (2H, m, 2 × ArH), 7.97-8.00 (2H, m, 2 × ArH); ¹³C NMR (125 MHz, CDCl₃) δ_C 14.1 (COOCH₂CH₃), 37.7 (CH₂), 49.2 (ArCH₂), 52.6 (CHCOOMe), 62.0 (COOCH₂CH₃), 115.8 (2C, d, *J* = 22.0 Hz, 2 × ArCHCF), 128.7 (2 × CH-Ar), 130.9 (2C, d, *J* = 9.4 Hz, 2 × ArCHCHCF), 131.2 (2 × CH-Ar), 132.0 (C-Ar), 132.4 (d, *J* = 3.0 Hz, ArCCHCHCF), 133.1 (C-Ar), 166.0 (d, *J* = 255.5 Hz, ArCF), 168.6 (C=O), 195.6 (C=O), 201.9 (C=O); ¹⁹F NMR (470 MHz; CDCl₃) δ_F -104.2.

Ethyl 2-(4-chlorobenzyl)-1-(4-chlorophenyl)-5-(4-fluorophenyl)-1H-pyrrole-3-carboxylate (75)



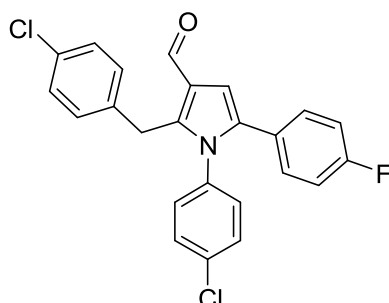
Prepared according to general procedure D using **74** (350 mg, 0.93 mmol), 4-chloroaniline (593 mg, 4.65 mmol) and acetic acid (2.8 mL). Purification by MPLC on SiO₂ (Petrol:EtOAc, 0-10%) gave a white solid (290 mg, 67%). The reaction was repeated to get enough material for next steps. *R*_f = 0.45 (10% EtOAc/Petrol); m.p. 132-134 °C; IR ν_{max}/cm⁻¹ 2985, 2927, 1702 (C=O); ¹H NMR (500 MHz, CDCl₃) δ_H 1.25 (3H, t, *J* = 7.1 Hz, COOCH₂CH₃), 4.15 (2H, s, ArCH₂), 4.24 (2H, q, *J* = 7.1 Hz, COOCH₂CH₃), 6.72-6.80 (6H, m, 6 × ArH), 6.90-6.93 (2H, m, 2 × ArH), 7.04-7.06 (2H, m, 2 × ArH), 7.15-7.18 (2H, m, 2 × ArH); ¹⁹F NMR (470 MHz, CDCl₃) δ_F -114.61; HRMS calcd for C₂₆H₂₁Cl₂NO₂F [M(³⁵Cl₂)+H]⁺ 468.0928, found 468.0915.

(2-(4-Chlorobenzyl)-1-(4-chlorophenyl)-5-(4-fluorophenyl)-1H-pyrrol-3-yl)methanol (76)



Prepared according to general procedure F using compound **75** (300 mg, 0.64 mmol), THF (1 mL), 1 M DIBAL in cyclohexane (1.53 mL, 1.53 mmol) and MeOH (1 mL). Purification by MPLC on SiO₂ (Petrol:EtOAc, 0-50%) gave a white solid (259 mg, 95%). $R_f = 0.20$ (25% EtOAc/Petrol); m.p. 124-126 °C; λ_{max} (EtOH)/nm 277; IR ν_{max}/cm^{-1} 3279 (O-H), 3045, 2921, 2868, 1525, 1488.; ¹H NMR (500 MHz, CDCl₃) δ_H 1.46 (1H, s, OH), 3.86 (2H, s, Ar-CH₂), 4.63 (2H, s, CH₂OH), 6.44 (1H, s, Pyrrole-H), 6.80-6.86 (6H, m, 6 × ArH), 6.96-6.99 (2H, m, 2 × ArH), 7.13-7.14 (2H, m, 2 × ArH), 7.20-7.21 (2H, m, 2 × ArH); ¹³C NMR (125 MHz, CDCl₃) δ_C 30.1 (Ar-CH₂), 57.9 (CH₂OH), 109.6 (CH-Pyrrole), 115.2 (2C, d, $J = 21.5$ Hz, 2 × ArCHCF), 121.9 (C-Ar), 128.5 (2 × CH-Ar), 128.7 (d, $J = 3.3$ Hz, ArCCHCHCF), 129.2 (2 × CH-Ar), 129.3 (2 × CH-Ar), 129.7 (2C, d, $J = 7.9$ Hz, 2 × ArCHCHCF), 130.0 (2 × CH-Ar), 131.0 (C-Ar), 131.9 (C-Ar), 133.6 (C-Ar), 133.9 (C-Ar), 137.1 (C-Ar), 138.0 (C-Ar), 161.5 (d, $J = 246.6$ Hz, ArCF). ¹⁹F NMR (470 MHz; CDCl₃) δ_F -115.6; HRMS calcd for C₂₄H₁₉Cl₂FNO [M(³⁵Cl₂)+H]⁺ 426.0822, found 426.0817.

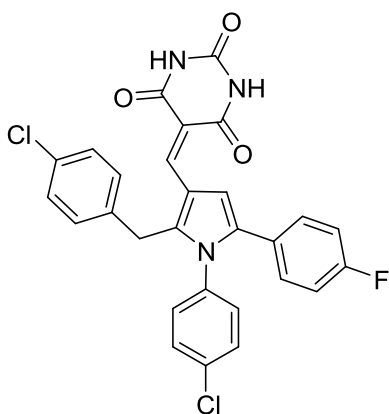
2-(4-Chlorobenzyl)-1-(4-chlorophenyl)-5-(4-fluorophenyl)-1H-pyrrole-3-carbaldehyde (77)



Prepared according to general procedure G using compound **76** (135 mg, 0.316 mmol) in DCM (3 ml) and Dess-Martin periodinane (268 mg, 0.632 mmol) in DCM (4 mL). Purification by MPLC on SiO₂ (Petrol:EtOAc, 0-50%) gave an off-white viscous liquid (82 mg, 61%). $R_f = 0.35$ (20% EtOAc/Petrol); λ_{max} (EtOH)/nm 247; IR ν_{max}/cm^{-1} 3057, 2922, 2852, 2731, 1664

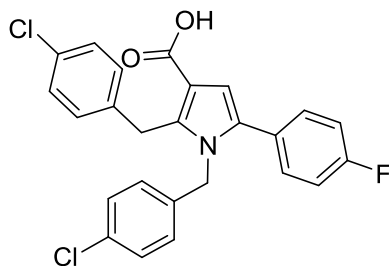
(C=O); ^1H NMR (500 MHz, CDCl_3) δ_{H} 4.17 (2H, s, Ar- CH_2), 6.78-6.89 (7H, m, $7 \times \text{ArH}$), 6.98-7.01 (2H, m, $2 \times \text{ArH}$), 7.14-7.15 (2H, m, $2 \times \text{ArH}$), 7.27-7.28 (1H, m, ArH), 10.01 (1H, s, CHO); ^{13}C NMR (125 MHz, CDCl_3) δ_{C} 30.3 (Ar- CH_2), 109.3 (CH-Pyrrole), 115.4 (2C, d, $J = 21.6$ Hz, $2 \times \text{ArCHCF}$), 123.5 (C-Ar), 127.4 (d, $J = 3.2$ Hz, ArCCHCHCF), 128.7 ($2 \times \text{CH-Ar}$), 129.4 ($2 \times \text{CH-Ar}$), 129.5 ($2 \times \text{CH-Ar}$), 129.8 ($2 \times \text{CH-Ar}$), 130.2 (2C, d, $J = 8.1$ Hz, $2 \times \text{ArCHCHCF}$), 132.4 (C-Ar), 135.0 (C-Ar), 135.4 (C-Ar), 135.4 (C-Ar), 136.5 (C-Ar), 140.2 (C-Ar), 162.0 (d, $J = 248.3$ Hz, ArCF), 186.0 (C=O). ^{19}F NMR (470 MHz; CDCl_3) δ_{F} -113.9. HRMS calcd for $\text{C}_{24}\text{H}_{17}\text{Cl}_2\text{FNO}$ [$\text{M}^{(35}\text{Cl}_2)+\text{H}$] $^+$ 424.0666, found 426.0660.

5-((2-(4-Chlorobenzyl)-1-(4-chlorophenyl)-5-(4-fluorophenyl)-1H-pyrrol-3-yl)methylene)pyrimidine-2,4,6(1H,3H,5H)-trione (63)



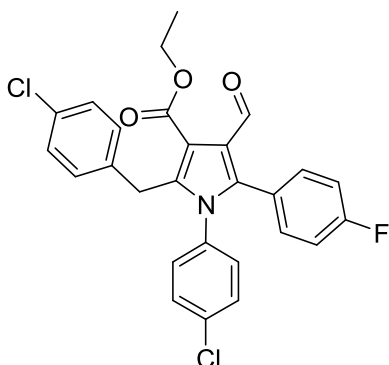
A mixture of compound **77** (48 mg, 0.11 mmol), barbituric acid (15 mg, 0.12 mmol) and acetic acid (1.2 mL) was refluxed for 2.5 h. The product precipitates on cooling which was filtered and washed with EtOAc to get yellow solid (28 mg, 48%). $R_f = 0.33$ (2% MeOH/DCM); m.p. 276 °C (degraded); λ_{max} (EtOH)/nm 398; IR $\nu_{\text{max}}/\text{cm}^{-1}$ 3198, 3054, 2924, 2848, 1737(C=O), 1690 (C=O), 1652(C=O); ^1H NMR (500 MHz, $\text{DMSO}-d_6$) δ_{H} 4.17 (2H, s, Ar CH_2), 6.84-6.85 (2H, m, $2 \times \text{ArH}$), 7.10-7.16 (4H, m, $4 \times \text{ArH}$), 7.19-7.20 (2H, m, $2 \times \text{ArH}$), 7.24-7.26 (2H, m, $2 \times \text{ArH}$), 7.45-7.47 (2H, m, $2 \times \text{ArH}$), 7.95 (1H, s, Pyrrole-H), 8.35 (1H, s, $\text{HC}=\text{C}(\text{CO})_2$), 11.05 (1H, s, NH), 11.15 (1H, s, NH).; ^{13}C NMR (125 MHz, $\text{DMSO}-d_6$) δ_{C} 29.4 (Ar CH_2), 110.8 (C-Ar), 113.1 (CH-Pyrrole), 115.4 (2C, d, $J = 21.7$ Hz, $2 \times \text{ArCHCF}$), 118.2 (C-Ar), 128.5 ($2 \times \text{CH-Ar}$), 129.4 ($2 \times \text{CH-Ar}$), 129.6 ($2 \times \text{CH-Ar}$), 130.1 ($2 \times \text{CH-Ar}$), 130.5 (2C, d, $J = 8.2$ Hz, $2 \times \text{ArCHCHCF}$), 131.1 (C-Ar), 133.7 (C-Ar), 135.2 (C-Ar), 135.5 (C-Ar), 136.8 (C-Ar), 145.8 (C-Ar), 146.5 (C-Ar), 150.3 (C-Ar), 160.4 (C=O), 161.4 (d, $J = 240.7$ Hz, ArCF), 162.5 (C=O), 164.4 (C=O). ^{19}F NMR (470 MHz; $\text{DMSO}-d_6$) δ_{F} -114.0; HRMS calcd for $\text{C}_{28}\text{H}_{19}\text{Cl}_2\text{FN}_3\text{O}_3$ [$\text{M}^{(35}\text{Cl}_2)+\text{H}$] $^+$ 534.0782, found 534.0776.

1,2-Bis(4-chlorobenzyl)-5-(4-fluorophenyl)-1H-pyrrole-3-carboxylic acid (69)



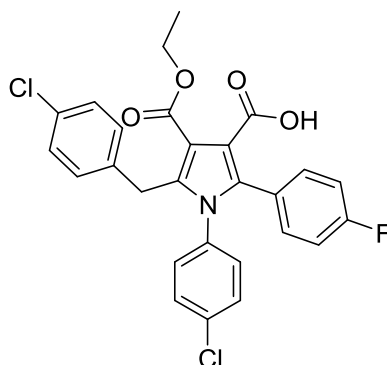
A mixture of **79** (38 mg, 0.078 mmol), NaOH (75 mg, 1.75 mmol), MeOH (3.5 mL) and water (1.5 mL) was heated at 75 °C for 18 h. The solvent was evaporated *in vacuo* and the remaining residue was acidified with 1 M HCl. The aqueous layer was extracted with EtOAc (3 × 30 mL). The organic layers were combined, dried over MgSO₄ and evaporated *in vacuo*. Purification by MPLC on SiO₂ (DCM:MeOH, 0-2%) gave a white solid (25 mg, 70%). $R_f = 0.56$ (2% MeOH/DCM); m.p. 215-217 °C; λ_{\max} (EtOH)/nm 398; IR $\nu_{\max}/\text{cm}^{-1}$ 2922, 2851, 2765, 2668, 2596, 1665 (C=O); ¹H NMR (500 MHz, DMSO-*d*₆) δ_H 4.29 (2H, s, ArCH₂), 5.06 (2H, s, ArCH₂-N), 6.59 (1H, s, Pyrrole-*H*), 6.64-6.66 (2H, m, 2 × Ar*H*), 7.06-7.07 (2H, m, 2 × Ar*H*), 7.14-7.18 (2H, m, 2 × Ar*H*), 7.20-7.22 (4H, m, 4 × Ar*H*), 7.28-7.31 (2H, m, 2 × Ar*H*), 12.10 (1H, br s, COOH); ¹³C NMR (125 MHz, DMSO-*d*₆) δ_C 29.5 (ArCH₂), 46.5 (ArCH₂-N), 110.5 (CH-Pyrrole), 113.6 (C-Ar), 115.5 (2C, d, $J = 21.4$ Hz, 2 × ArCHCF), 127.2 (2 × CH-Ar), 128.2 (2 × CH-Ar), 128.3 (d, $J = 4.1$ Hz, ArCCHCHCF), 128.4 (2 × CH-Ar), 129.8 (2 × CH-Ar), 130.7 (C-Ar), 130.9 (2C, d, $J = 8.2$ Hz, 2 × ArCHCHCF), 131.5 (C-Ar), 132.8 (C-Ar), 136.4 (C-Ar), 137.3 (C-Ar), 137.6 (C-Ar), 161.6 (d, $J = 245.4$ Hz, ArCF), 165.9 (COOH). ¹⁹F NMR (470 MHz; DMSO-*d*₆) δ_F -113.3; HRMS calcd for C₂₅H₁₉Cl₂FNO₂ [M(³⁵Cl₂)+H]⁺ 454.0771, found 454.0772.

Ethyl 2-(4-chlorobenzyl)-1-(4-chlorophenyl)-5-(4-fluorophenyl)-4-formyl-1H-pyrrole-3-carboxylate (80)



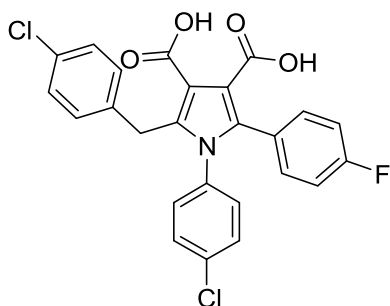
Prepared according to general procedure H using **75** (100 mg, 0.213 mmol), DMF (3 mL) phosphorus oxychloride (0.06 mL, 0.639 mmol) heated under microwave irradiation to 70 °C for 4 h. Purification by MPLC on SiO₂ (Petrol:EtOAc, 0-20%) gave a white solid (75 mg, 71%). *R*_f = 0.22 (20% EtOAc/Petrol); m.p. 132-134 °C; λ_{max} (EtOH)/nm 228; IR ν_{max}/cm⁻¹ 3050, 2962, 2849, 1679 (C=O); ¹H NMR (500 MHz, CDCl₃) δ_H 1.34 (3H, t, *J* = 7.1 Hz, COOCH₂CH₃), 4.14 (2H, s, ArCH₂), 4.38 (2H, q, *J* = 7.1 Hz, COOCH₂CH₃), 6.68-6.70 (2H, m, 2 × ArH), 6.77-6.79 (2H, m, 2 × ArH), 6.88-6.91 (2H, m, 2 × ArH), 7.06-7.09 (2H, m, 2 × ArH), 7.13-7.14 (2H, m, 2 × ArH), 7.17-7.19 (2H, m, 2 × ArH), 10.31 (1H, s, CHO); ¹³C NMR (125 MHz, CDCl₃) δ_C 14.3 (COOCH₂CH₃), 30.9 (ArCH₂), 60.9 (COOCH₂CH₃), 114.3 (C-Ar), 115.2 (2C, d, *J* = 21.7 Hz, 2 × ArCHCF), 121.4 (C-Ar), 128.5 (2 × CH-Ar), 129.4 (2 × CH-Ar), 129.5 (2 × CH-Ar), 129.9 (2 × CH-Ar), 132.3 (C-Ar), 132.8 (2C, d, *J* = 8.4 Hz, 2 × ArCHCHCF), 134.3 (C-Ar), 135.3 (C-Ar), 136.3 (C-Ar), 138.8 (C-Ar), 139.1 (C-Ar), 164.7 (C=O), 187.7 (C=O), ArCCHCHCF and ArCF was not seen. ¹⁹F NMR (470 MHz; CDCl₃) δ_F -111.52; HRMS calcd for C₂₇H₂₁Cl₂FNO₃ [M(³⁵Cl₂)+H]⁺ 496.0877, found 496.0878.

5-(4-Chlorobenzyl)-1-(4-chlorophenyl)-4-(ethoxycarbonyl)-2-(4-fluorophenyl)-1H-pyrrole-3-carboxylic acid (81)



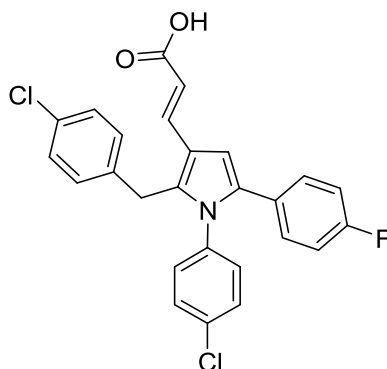
Prepared according to general procedure I using **80** (65 mg, 0.131 mmol), MeCN (2 mL), a solution of sodium chlorite (17 mg, 0.183 mmol) in H₂O (0.2 mL), a solution of sulfamic acid (18 mg, 0.183 mmol) in H₂O (0.2 mL). EtOAc extraction gave an off-white solid (68 mg, quant.) which did not require further purification; *R*_f = 0.56 (2% MeOH/DCM); m.p. 172-174 °C; λ_{max} (EtOH)/nm 223; IR ν_{max}/cm⁻¹ 2919, 2850, 2639, 1680 (broad, 2×C=O overlapped); ¹H NMR (500 MHz, DMSO-*d*₆) δ_H 1.18 (3H, t, *J* = 7.1 Hz, COOCH₂CH₃), 4.05 (2H, s, ArCH₂), 4.18 (2H, q, *J* = 7.1 Hz, COOCH₂CH₃), 6.81-6.83 (2H, m, 2 × ArH), 7.03-7.09 (4H, m, 4 × ArH), 7.18-7.22 (4H, m, 4 × ArH), 7.33-7.35 (2H, m, 2 × ArH), 12.39 (1H, s, COOH); ¹³C NMR (125 MHz, DMSO-*d*₆) δ_C 13.9 (COOCH₂CH₃), 29.9 (ArCH₂), 59.9 (COOCH₂CH₃), 113.0 (C-Ar), 114.7 (2C, d, *J* = 21.6 Hz, 2 × ArCHCF), 116.6 (C-Ar), 126.4 (d, *J* = 3.3 Hz, ArCCHCHCF), 128.1 (2 × CH-Ar), 129.0 (2 × CH-Ar), 129.6 (2 × CH-Ar), 130.7 (C-Ar), 130.7 (2 × CH-Ar), 132.8 (2C, d, *J* = 8.4 Hz, 2 × ArCHCHCF), 133.5 (C-Ar), 133.9 (C-Ar), 134.9 (C-Ar), 136.1 (C-Ar), 137.0 (C-Ar), 161.6 (d, *J* = 245.4 Hz, ArCF), 164.2 (C=O), 165.8 (C=O); ¹⁹F NMR (470 MHz; DMSO-*d*₆) δ_F -113.3; HRMS calcd for C₂₇H₂₁Cl₂FNO₄ [M(³⁵Cl₂)+H]⁺ 512.0826, found 512.0820.

2-(4-Chlorobenzyl)-1-(4-chlorophenyl)-5-(4-fluorophenyl)-1H-pyrrole-3,4-dicarboxylic acid (64)



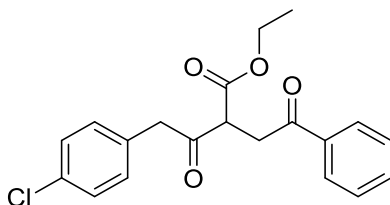
A mixture of **81** (55 mg, 0.107 mmol), NaOH (185 mg, 4.625 mmol), MeOH (3 mL), water (1.5 mL) was refluxed for 4 h. The solvent was evaporated *in vacuo* and the remaining residue was acidified with 2 M HCl. The aqueous layer was extracted with EtOAc (3 × 20 mL). The organic layers were combined, dried over MgSO₄ and evaporated *in vacuo* to obtain an off-white solid (50 mg, 97%) which did not require further purification. $R_f = 0.47$ (7.5% DCM/MeOH); m.p. 143-145 °C; λ_{max} (EtOH)/nm 224; IR ν_{max}/cm^{-1} 3506, 3048, 2919, 2849, 1687 (C=O), 1607 (C=O); ¹H NMR (500 MHz, DMSO-*d*₆) δ_H 4.16 (2H, s, 2 × ArCH₂), 6.81-6.83 (2H, m, 2 × ArH), 7.03-7.06 (4H, m, 4 × ArH), 7.19-7.21 (4H, m, 4 × ArH), 7.31-7.33 (2H, m, 2 × ArH), 13.2 (1H, br s, COOH), other COOH could not be seen.; ¹³C NMR (125 MHz, DMSO-*d*₆) δ_C 30.0 (ArCH₂), 114.5 (2C, d, $J = 21.4$ Hz, 2 × ArCHCF), 115.7 (2 × CH-Ar), 127.1 (d, $J = 4.0$ Hz, ArCCHCHCF), 128.0 (2 × CH-Ar), 129.9 (2 × CH-Ar), 129.6 (2 × CH-Ar), 130.6 (C-Ar), 130.7 (2 × CH-Ar), 132.8 (2C, d, $J = 8.3$ Hz, 2 × ArCHCHCF), 133.4 (C-Ar), 134.9 (C-Ar), 135.5 (C-Ar), 137.3 (C-Ar), 137.5 (C-Ar), 161.6 (d, $J = 245.7$ Hz, ArCF), 165.7 (COOH), 166.8 (COOH); ¹⁹F NMR (470 MHz; DMSO-*d*₆) δ_F -113.5; HRMS calcd for C₂₅H₁₇Cl₂FNO₄ [M(³⁵Cl₂)+H]⁺ 484.0507, found 484.0508.

(E)-3-(2-(4-Chlorobenzyl)-1-(4-chlorophenyl)-5-(4-fluorophenyl)-1H-pyrrol-3-yl)acrylic acid (65)



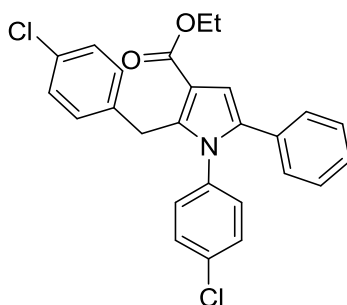
A mixture of aldehyde **77** (70 mg, 0.16 mmol), malonic acid (26 mg, 0.247 mmol), piperidine (1 drop), and pyridine (0.5 mL) was refluxed for 2.5 h. The reaction was acidified to pH 2 with 2M HCl and extracted with EtOAc (3 × 25 mL). The organic layers were combined, dried over MgSO₄, and evaporated *in vacuo*. Purification by MPLC on SiO₂ (DCM:MeOH, 0-10%) gave a yellow solid (58 mg, 71%); R_f = 0.24 (2% MeOH/DCM); m.p. 242-244 °C; λ_{max} (EtOH)/nm 264; IR ν_{max}/cm⁻¹ 3061, 2920, 2851, 1674 (C=O); ¹H NMR (500 MHz, DMSO-*d*₆) δ_H 4.01 (2H, s, CH₂), 6.24 (1H, d, *J* = 15.5 Hz, alkene-*H*), 6.79-6.81 (2H, m, 2 × Ar*H*), 6.91 (1H, s, Pyrrole-*H*), 7.06-7.13 (6H, m, 6 × Ar*H*), 7.23-7.24 (2H, m, 2 × Ar*H*), 7.40-7.41 (2H, m, 2 × Ar*H*), 7.59 (1H, d, *J* = 15.5 Hz, alkene-*H*); ¹³C NMR (125 MHz, DMSO-*d*₆) δ_C 28.9 (ArCH₂), 107.0 (Pyrrole-CH), 114.9 (Alkene-CH), 115.2 (2C, d, *J* = 21.4 Hz, 2 × ArCHCF), 118.6 (C-Ar), 128.2 (d, *J* = 3.5 Hz, ArCCHCHCF), 128.3 (2 × CH-Ar), 129.2 (2 × CH-Ar), 129.4 (2 × CH-Ar), 130.0 (2C, d, *J* = 8.1 Hz, 2 × ArCHCHCF), 130.3 (2 × CH-Ar), 130.7 (C-Ar), 133.0 (C-Ar), 134.6 (C-Ar), 135.8 (C-Ar), 136.2 (C-Ar), 136.5 (C-Ar), 137.7 (Alkene-CH), 161.1 (d, *J* = 244.6 Hz, ArCF), 168.2 (COOH); ¹⁹F NMR (470 MHz; DMSO-*d*₆) δ_F -115.0; LRMS (ES⁺) *m/z* 466.3 [M(³⁵Cl₂)+H]⁺, 468.3 [M(³⁵Cl³⁷Cl)+H]⁺.

Ethyl 4-(4-chlorophenyl)-3-oxo-2-(2-oxo-2-phenylethyl)butanoate, (96)



Prepared according to general procedure C using compound **72** (2.01 g, 8.35 mmol) and NaH (60% in mineral oil, 433 mg, 10.85 mmol) in THF (6 mL) followed by addition of 2-bromo-1-phenylethan-1-one (1.83 mg, 9.18 mmol) in THF (4 mL). The residue was purified by MPLC on SiO₂ (Petrol:EtOAc, 0-20%) to give a white solid (2.36 g, 79%). $R_f = 0.22$ (10% EtOAc/Petrol); m.p. 68-70 °C; λ_{max} (EtOH)/nm 241.8, 225.6; IR ν_{max}/cm^{-1} 3064, 3036, 2973, 2928, 2898, 1711 (C=O stretch), 1684 (C=O); ¹H NMR (500 MHz, CDCl₃) δ_H 1.28 (3H, t, $J = 7.1$ Hz, COOCH₂CH₃), 3.55 (1H, dd, $J = 18.4, 4.8$ Hz, 1 × CH₂), 3.76 (1H, dd, $J = 18.4, 9.1$ Hz, 1 × CH₂), 4.07 (1H, d, $J = 17.1$ Hz, ArCH₂), 4.12 (1H, d, $J = 17.1$ Hz, ArCH₂), 4.20 (2H, q, $J = 7.1$ Hz, COOCH₂CH₃), 4.29 (1H, dd, $J = 9.1$ and 4.8 Hz, CHCOOEt), 7.18-7.20 (2H, m, 2 × ArH), 7.29-7.31 (2H, m, 2 × ArH), 7.45-7.48 (2H, m, 2 × ArH), 7.56-7.59 (1H, m, 1 × ArH), 7.95-7.97 (2H, m, 2 × ArH); ¹³C NMR (125 MHz, CDCl₃) δ_C 14.1 (COOCH₂CH₃), 37.8 (CH₂), 49.2 (ArCH₂), 52.6 (CHCOOEt), 62.0 (COOCH₂CH₃), 128.2 (2 × C-Ar), 128.7 (2 × C-Ar), 128.7 (2 × C-Ar), 131.3 (2 × C-Ar), 132.0 (C-Ar), 133.1 (C-Ar), 133.6 (C-Ar), 135.9 (C-Ar), 168.7 (C=O), 197.2 (C=O), 202.0 (C=O); HRMS calcd for C₂₀H₁₈ClO₄ [M(³⁵Cl₂)-H]⁻ 357.0899, found 357.0890.

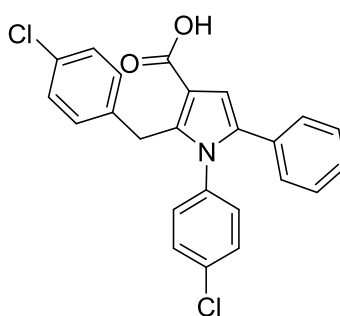
Ethyl 2-(4-chlorobenzyl)-1-(4-chlorophenyl)-5-phenyl-1H-pyrrole-3-carboxylate (82)



Prepared according to general procedure D using compound **96** (1.4 g, 3.90 mmol), 4-chloroaniline (2.5 g, 19.5 mmol) and acetic acid (11 mL). Purification by MPLC on SiO₂ (Petrol:EtOAc, 0-10%) gave a white solid (1.28 g, 73%). $R_f = 0.52$ (10% EtOAc/Petrol); m.p. 127-129 °C; IR ν_{max}/cm^{-1} 2985, 2927, 2657, 1702 (C=O); ¹H NMR (500 MHz, CDCl₃) δ_H 1.33

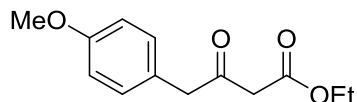
(3H, t, $J = 7.1$ Hz, $\text{COOCH}_2\text{CH}_3$), 4.23 (2H, s, $2 \times \text{ArCH}_2$), 4.31 (2H, q, $J = 7.1$ Hz, $\text{COOCH}_2\text{CH}_3$), 6.80-6.86 (5H, m, $5 \times \text{ArH}$), 7.01-7.04 (2H, m, $2 \times \text{ArH}$), 7.11-7.18 (5H, m, $5 \times \text{ArH}$), 7.22-7.26 (2H, m, $2 \times \text{ArH}$); ^{13}C NMR (125 MHz, CDCl_3) δ_{C} 14.5 ($\text{COOCH}_2\text{CH}_3$), 30.8 (ArCH_2), 59.8 ($\text{COOCH}_2\text{CH}_3$), 110.5 (C-Ar), 114.3 (C-Ar), 127.0 (C-Ar), 128.2 ($2 \times$ C-Ar), 128.3 ($2 \times$ C-Ar), 128.3 ($2 \times$ C-Ar), 129.3 ($2 \times$ C-Ar), 129.5 ($2 \times$ C-Ar), 130.0 ($2 \times$ C-Ar), 131.8 (C-Ar), 131.8 (C-Ar), 134.5 (C-Ar), 134.8 (C-Ar), 136.3 (C-Ar), 137.5 (C-Ar), 138.8 (C-Ar), 165.1 (C=O); HRMS calcd for $\text{C}_{26}\text{H}_{22}\text{Cl}_2\text{NO}_2$ [$\text{M}(^{35}\text{Cl}_2)+\text{H}$] $^+$ 450.1022, found 450.1012.

2-(4-Chlorobenzyl)-1-(4-chlorophenyl)-5-phenyl-1H-pyrrole-3-carboxylic acid (**93**)



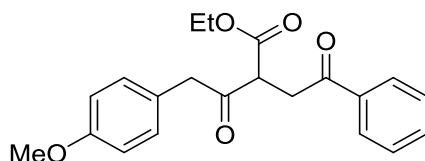
Prepared according to general procedure E using compound **82** (45 mg, 0.099 mmol), NaOH (143 mg, 3.56 mmol) in MeOH (2 ml) and water (1.5 ml) followed by addition of more MeOH (1 ml) after 18 h. Compound **93** was obtained as a white solid (41 mg, 98%) which did not require further purification. $R_f = 0.55$ (2% MeOH/DCM); m.p. 217-219 °C; λ_{max} (EtOH)/nm 264.6; IR $\nu_{\text{max}}/\text{cm}^{-1}$ 3300-2200 (broad COOH peak), 2936, 2851, 2591, 1665 (C=O); ^1H NMR (500 MHz, $\text{DMSO}-d_6$) δ_{H} 4.24 (2H, s, $2 \times \text{ArCH}_2$), 6.76 (1H, s, Pyrrole-H), 6.79 (2H, d, $J = 8.5$ Hz, $2 \times \text{ArH}$), 7.04-7.07 (4H, m, $4 \times \text{ArH}$), 7.13-7.21 (5H, m, $5 \times \text{ArH}$), 7.40 (2H, d, $J = 8.5$ Hz, $2 \times \text{ArH}$), 12.15 (1H, s, COOH); ^{13}C NMR (125 MHz, $\text{DMSO}-d_6$) δ_{C} 29.8 (ArCH_2), 110.3 (C-Ar), 114.0 (C-Ar), 126.9 (C-Ar), 128.0 ($2 \times$ C-Ar), 128.1 ($2 \times$ C-Ar), 128.2 ($2 \times$ C-Ar), 129.2 ($2 \times$ C-Ar), 129.5 ($2 \times$ C-Ar), 130.5 ($2 \times$ C-Ar), 131.5 (C-Ar), 133.2 (C-Ar), 133.9 (C-Ar), 136.1 (C-Ar), 137.7 (C-Ar), 138.5 (C-Ar), 165.8 (C=O); LRMS (ES^+) m/z 422.2 [$\text{M}(^{35}\text{Cl}_2)+\text{H}$] $^+$, 424.2 [$\text{M}(^{35}\text{Cl}^{37}\text{Cl})+\text{H}$] $^+$.

Ethyl 4-(4-methoxyphenyl)-3-oxobutanoate (**98**)



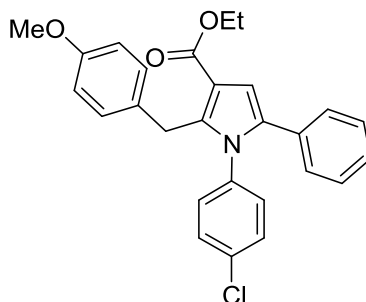
Prepared according to the procedure B using Meldrum's acid (1 g, 6.93 mmol), 4-methoxyphenylacetyl chloride (0.93 mL, 6.06 mmol), pyridine (1.1 mL, 13.21 mmol), DCM (6 mL), EtOH (21 mL). Purification by MPLC on SiO₂ (Petrol:EtOAc, 0-20%) gave a yellow oil (1.03 g, 72%). ¹H NMR (500 MHz, CDCl₃) δ_H 1.25 (3H, t, *J* = 7.2 Hz, COOCH₂CH₃), 3.45 (2H, s, CH₂), 3.75 (2H, s, CH₂Ar), 3.79 (3H, s, OCH₃), 4.16 (2H, q, *J* = 7.2 Hz, COOCH₂CH₃), 6.86-6.88 (2H, m, 2 × ArH), 7.11-7.13 (2H, m, 2 × ArH); ¹³C NMR (125 MHz, CDCl₃) δ_C 14.1 (COOCH₂CH₃), 48.2 (CH₂), 49.2 (CH₂Ar), 55.3 (OCH₃), 61.4 (COOCH₂CH₃), 114.3 (2 × CH-Ar), 125.2 (C-Ar), 130.6 (2 × CH-Ar), 131.6 (C-Ar), 158.9 (C-Ar), 167.2 (C=O), 201.0 (C=O).²⁰⁵

Ethyl 4-(4-methoxyphenyl)-3-oxo-2-(2-oxo-2-phenylethyl)butanoate (**99**)



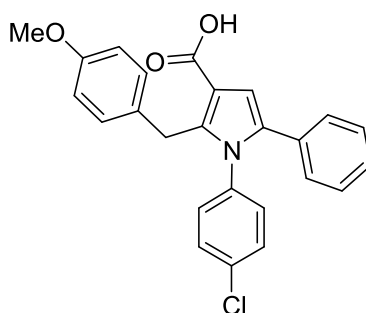
Prepared according to general procedure C using compound **98** (629 mg, 2.66 mmol) and NaH (60% in mineral oil, 138 mg, 3.45 mmol) in THF (1.7 mL) followed by addition of 2-bromo-1-phenylethan-1-one (582 mg, 2.92 mmol) in THF (1.3 mL). The residue was purified by MPLC on SiO₂ (Petrol:EtOAc, 0-20%) to give a yellow oil (715 mg, 76%). *R*_f = 0.33 (20% EtOAc/Petrol); λ_{max} (EtOH)/nm 241.2; IR ν_{max}/cm⁻¹ 2979, 2836, 1738 (C=O stretch), 1715 (C=O), 1681 (C=O); ¹H NMR (500 MHz, CDCl₃) δ_H 1.28 (3H, t, *J* = 7.1 Hz, COOCH₂CH₃), 3.54 (1H, dd, *J* = 18.3 and 5.5 Hz, 1 × CH₂), 3.69 (1H, dd, *J* = 18.3 and 8.5 Hz, 1 × CH₂), 3.79 (3H, s, OCH₃), 4.00 (1H, d, *J* = 16.6 Hz, ArCH₂), 4.04 (1H, d, *J* = 16.6 Hz, ArCH₂), 4.19 (2H, q, *J* = 7.1 Hz, COOCH₂CH₃), 4.31 (1H, dd, *J* = 8.5 and 5.5 Hz, CHCOOEt), 6.86-6.88 (2H, m, 2 × ArH), 7.16-7.18 (2H, m, 2 × ArH), 7.44-7.47 (2H, m, 2 × ArH), 7.55-7.59 (1H, m, 1 × ArH), 7.95-7.97 (2H, m, 2 × ArH); ¹³C NMR (125 MHz, CDCl₃) δ_C 14.1 (COOCH₂CH₃), 37.8 (CH₂), 49.0 (ArCH₂), 52.5 (CHCOOEt), 55.3 (CH₃), 61.8 (COOCH₂CH₃), 114.1 (2 × C-Ar), 125.6 (C-Ar), 128.2 (2 × C-Ar), 128.7 (2 × C-Ar), 130.9 (2 × C-Ar), 133.5 (C-Ar), 136.1 (C-Ar), 158.7 (C-Ar), 168.9 (C=O), 197.2 (C=O), 202.6 (C=O); HRMS calcd for C₂₁H₂₃O₅ [M+H]⁺ 355.1540, found 355.1536.

Ethyl 1-(4-chlorophenyl)-2-(4-methoxybenzyl)-5-phenyl-1*H*-pyrrole-3-carboxylate (**100**)



Prepared according to general procedure D using compound **99** (319 mg, 0.90 mmol), 4-chloroaniline (574 mg, 4.50 mmol) and acetic acid (2.7 mL). Purification by MPLC on SiO₂ (Petrol:EtOAc, 0-15%) gave a white solid (300 mg, 75%). $R_f = 0.56$ (20% EtOAc/Petrol); λ_{\max} (EtOH)/nm 274.8, 224.0; IR $\nu_{\max}/\text{cm}^{-1}$ 3110, 2996, 2936, 1701 (C=O); ¹H NMR (500 MHz, CDCl₃) δ_H 1.33 (3H, t, $J = 7.1$ Hz, COOCH₂CH₃), 3.74 (3H, s, OCH₃), 4.20 (2H, s, 2 × ArCH₂), 4.32 (2H, q, $J = 7.1$ Hz, COOCH₂CH₃), 6.68-6.71 (2H, m, 2 × ArH), 6.77-6.79 (2H, m, 2 × ArH), 6.84-6.86 (3H, m, 3 × ArH), 7.01-7.03 (2H, m, 2 × ArH), 7.13-7.17 (3H, m, 3 × ArH), 7.21-7.23 (2H, m, 2 × ArH); ¹³C NMR (125 MHz, CDCl₃) δ_C 14.5 (COOCH₂CH₃), 30.6 (ArCH₂), 55.2 (OCH₃), 59.8 (COOCH₂CH₃), 110.5 (C-Ar), 113.6 (C-Ar), 114.0 (C-Ar), 126.8 (2 × C-Ar), 128.2 (2 × C-Ar), 128.3 (2 × C-Ar), 129.1 (2 × C-Ar), 129.1 (2 × C-Ar), 130.1 (2 × C-Ar), 131.1 (C-Ar), 131.9 (C-Ar), 134.3 (C-Ar), 134.5 (C-Ar), 136.5 (C-Ar), 136.5 (C-Ar), 140.0 (C-Ar), 157.9 (C-Ar), 165.3 (C=O); HRMS calcd for C₂₇H₂₅ClNO₃ [M(³⁵Cl₂)+H]⁺ 446.1517, found 446.1511.

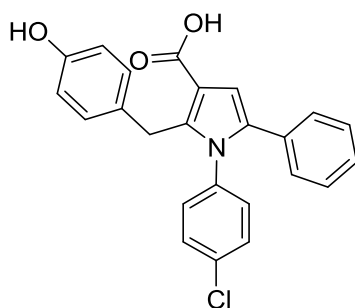
1-(4-Chlorophenyl)-2-(4-methoxybenzyl)-5-phenyl-1*H*-pyrrole-3-carboxylic acid (**101**)



Prepared according to general procedure E using compound **100** (31 mg, 0.069 mmol), NaOH (140 mg, 3.5 mmol) in MeOH (3 ml) and water (1.5 ml) followed by addition of more MeOH (1 ml) after 18 h. Purification by MPLC on SiO₂ (Petrol:EtOAc, 0-100%) gave a white solid (28 mg, quant.). $R_f = 0.40$ (2% MeOH/DCM); m.p. 214-216 °C; λ_{\max} (EtOH)/nm 275.4; IR

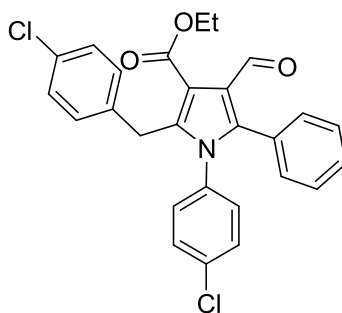
$\nu_{\max}/\text{cm}^{-1}$ 3005, 2996, 2922, 2828, 2576, 1654 (C=O); $^1\text{H NMR}$ (500 MHz, DMSO- d_6) δ_{H} 3.66 (3H, s, OCH₃), 4.19 (2H, s, 2 × ArCH₂), 6.67-6.71 (4H, m, 4 × ArH), 6.74 (1H, s, 1 × ArH), 7.01-7.06 (4H, m, 4 × ArH), 7.14-7.22 (3H, m, 3 × ArH), 7.40-7.42 (2H, m, 2 × ArH), 12.13 (1H, br s, COOH); $^{13}\text{C NMR}$ (125 MHz, DMSO- d_6) δ_{C} 29.5 (ArCH₂), 54.9 (OCH₃), 110.3 (C-Ar), 113.5 (C-Ar), 113.8 (C-Ar), 126.8 (2 × C-Ar), 127.9 (2 × C-Ar), 128.2 (2 × C-Ar), 128.7 (2 × C-Ar), 129.1 (2 × C-Ar), 130.5 (2 × C-Ar), 130.5 (C-Ar), 131.6 (C-Ar), 133.0 (C-Ar), 133.6 (C-Ar), 136.2 (C-Ar), 139.6 (C-Ar), 157.4 (C-Ar), 165.9 (C=O); LRMS (ES⁻) m/z 416.2 [M(³⁵Cl)-H]⁻, 418.3 [M(³⁷Cl)-H]⁻.

1-(4-Chlorophenyl)-2-(4-hydroxybenzyl)-5-phenyl-1H-pyrrole-3-carboxylic acid (94)



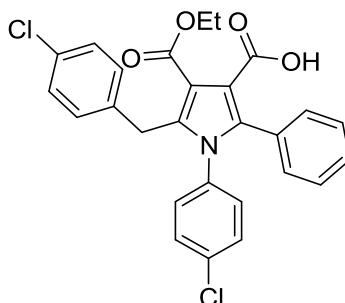
Compound **101** (20 mg, 0.048 mmol) was dissolved in DCM (2 mL) and cooled to 0 °C. Boron tribromide (1 M in DCM, 70 μL , 0.072 mmol) was added dropwise and the reaction mixture was stirred at 0 °C for 1 h. The mixture was quenched with water (20 mL) and extracted with EtOAc (3×30 mL). The organic layers were combined, washed with brine, dried over MgSO₄ and the solvent removed *in vacuo*. Purification by MPLC (H₂O:MeOH, reversed phase with 0.1% HCOOH modifier, 30-100%) gave a white solid (17 mg, 88%). R_f = 0.52 (8% MeOH/DCM); m.p. 230°C (degraded); IR $\nu_{\max}/\text{cm}^{-1}$ 3567 (OH), 3328-2325 (COOH), 3025, 2923, 2854, 1665 (C=O); $^1\text{H NMR}$ (500 MHz, DMSO- d_6) δ_{H} 4.19 (2H, s, 2 × ArCH₂), 6.48-6.49 (2H, m, 2 × ArH), 6.54-6.56 (2H, m, 2 × ArH), 6.70 (1H, s, Pyrrole-H), 6.99-7.02 (4H, m, 4 × ArH), 7.10-7.13 (1H, m, 1 × ArH), 7.16-7.19 (2H, m, 2 × ArH), 7.37-7.39 (2H, m, 2 × ArH); $^{13}\text{C NMR}$ was not be obtained; LRMS (ES⁻) m/z 402.2 [M(³⁵Cl)-H]⁻, 404.2 [M(³⁷Cl)-H]⁻.

Ethyl 2-(4-chlorobenzyl)-1-(4-chlorophenyl)-4-formyl-5-phenyl-1*H*-pyrrole-3-carboxylate (83)



Prepared according to general procedure H using compound **82** (940 mg, 2.08), phosphorous oxychloride (0.97 mL, 10.4 mmol) and DMF (10.5 mL). Purification by MPLC on SiO₂ (Petrol:EtOAc, 0-30%) gave a white solid (980 mg, quant.). R_f=0.38 (20% EtOAc/Petrol); m.p. 162-165 °C; IR $\nu_{\text{max}}/\text{cm}^{-1}$ 3060, 2972, 2928, 2846, 2767, 1697 (C=O), 1665 (C=O); ¹H NMR (500 MHz, DMSO-*d*₆) δ_{H} 1.22 (3H, t, *J* = 7.1 Hz, COOCH₂CH₃), 4.11 (2H, s, 2 × ArCH₂), 4.26 (2H, q, *J* = 7.1 Hz, COOCH₂CH₃), 6.85-6.87 (2H, m, 2 × ArH), 7.09-7.11 (2H, m, 2 × ArH), 7.20-7.26 (7H, m, 7 × ArH), 7.33-7.35 (2H, m, 2 × ArH) 10.11 (1H, s, CHO); ¹³C NMR (125 MHz, DMSO-*d*₆) δ_{C} 14.5 (COOCH₂CH₃), 30.6 (ArCH₂), 60.7 (COOCH₂CH₃), 113.8 (C-Ar), 121.2 (C-Ar), 128.2 (2×C-Ar), 128.6 (2×C-Ar), 129.0 (C-Ar), 129.4 (2×C-Ar), 129.7 (C-Ar), 130.1 (2×C-Ar), 131.2 (2×C-Ar), 131.3 (C-Ar), 131.5 (2×C-Ar), 134.2 (C-Ar), 134.9 (C-Ar), 137.3 (C-Ar), 138.5 (C-Ar), 140.6 (C-Ar), 164.7 (C=O) 187.1 (C=O); HRMS calcd for C₂₇H₂₂Cl₂NO₃ [M(³⁵Cl₂)+H]⁺ 478.0971, found 478.0967.

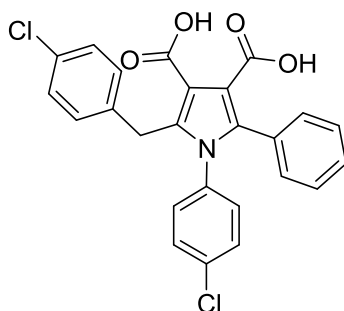
5-(4-Chlorobenzyl)-1-(4-chlorophenyl)-4-(ethoxycarbonyl)-2-phenyl-1*H*-pyrrole-3-carboxylic acid (84)



Prepared according to general procedure I using compound **83** (1.21 g, 2.52 mmol) in MeCN (30 ml), sodium chlorite (320 mg, 3.54 mmol) in water (4 mL), sulfamic acid (344 mg, 3.54 mmol) in water (4 ml). Purification by MPLC on SiO₂ (DCM:MeOH, 0-5%) gave a white solid

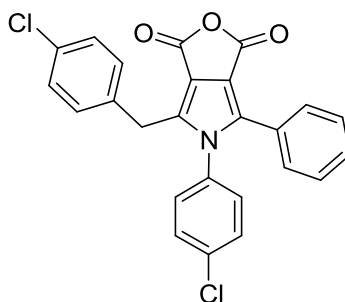
(780 mg, 62%). $R_f = 0.44$ (2% MeOH/DCM); m.p. 210-212 °C; λ_{\max} (EtOH)/nm 398; IR $\nu_{\max}/\text{cm}^{-1}$ 3031, 2984, 2921, 2903, 2628, 1709 (C=O), 1683 (C=O); ^1H NMR (500 MHz, DMSO- d_6) δ_{H} 1.20 (3H, t, $J = 7.1$ Hz, $\text{COOCH}_2\text{CH}_3$), 4.08 (2H, s, $2 \times \text{ArCH}_2$), 4.19 (2H, q, $J = 7.1$ Hz, $\text{COOCH}_2\text{CH}_3$), 6.82-6.84 (2H, m, $2 \times \text{ArH}$), 7.06-7.08 (2H, m, $2 \times \text{ArH}$), 7.14-7.16 (2H, m, $2 \times \text{ArH}$), 7.19-7.21 (4H, m, $4 \times \text{ArH}$), 7.33-7.34 (2H, m, $2 \times \text{ArH}$), 12.39 (1H, s, COOH); ^{13}C NMR (125 MHz, DMSO- d_6) δ_{C} 14.4 ($\text{COOCH}_2\text{CH}_3$), 30.4 (ArCH_2), 60.4 ($\text{COOCH}_2\text{CH}_3$), 113.4 (C-Ar), 117.2 (C-Ar), 128.2 ($2 \times \text{C-Ar}$), 128.4 (C-Ar), 128.6 ($2 \times \text{C-Ar}$), 129.4 ($2 \times \text{C-Ar}$), 130.1 ($2 \times \text{C-Ar}$), 130.5 (C-Ar), 130.9 ($2 \times \text{C-Ar}$), 131.2 (C-Ar), 131.2 ($2 \times \text{C-Ar}$), 133.9 (C-Ar), 135.1 (C-Ar), 135.5 (C-Ar), 136.7 (C-Ar), 137.6 (C-Ar), 164.6 (C=O), 166.5 (C=O); HRMS calcd for $\text{C}_{27}\text{H}_{22}\text{Cl}_2\text{NO}_4$ [$\text{M}(^{35}\text{Cl}_2)+\text{H}$] $^+$ 494.0920, found 494.0908.

2-(4-Chlorobenzyl)-1-(4-chlorophenyl)-5-phenyl-1H-pyrrole-3,4-dicarboxylic acid (67)



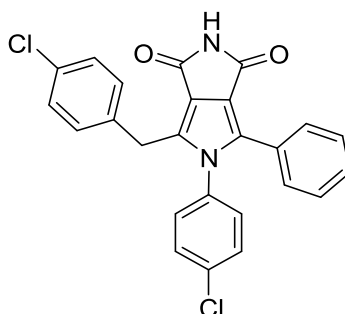
Compound **84** (735 mg, 1.48 mmol) was dissolved in MeOH (5 mL) and THF (5 mL) and 2 M NaOH (5 mL) was added. The reaction mixture was stirred at 80 °C for 3 h. After cooling to r.t., the solvent was removed *in vacuo*, residue was acidified with 2 M HCl and extracted with EtOAc (3×30 mL). The organic layers were combined, dried over MgSO_4 and the solvent removed *in vacuo*. Purification by MPLC on SiO_2 (DCM:MeOH, 0-20%) gave a beige solid (690 mg, quant.). $R_f = 0.13$ (8% MeOH/DCM); m.p. 184-188 °C; λ_{\max} (EtOH)/nm 270.0, 224.4; IR $\nu_{\max}/\text{cm}^{-1}$ 3031, 2984, 2921, 2903, 2767, 1709 (C=O), 1683 (C=O); ^1H NMR (500 MHz, DMSO- d_6) δ_{H} 4.21 (2H, s, $2 \times \text{ArCH}_2$), 6.82 (2H, d, $J = 8.4$ Hz, $2 \times \text{ArH}$), 7.01 (2H, d, $J = 8.4$ Hz, $2 \times \text{ArH}$), 7.12-7.18 (5H, m, $5 \times \text{ArH}$), 7.20 (2H, d, $J = 8.4$ Hz, $4 \times \text{ArH}$), 7.30 (2H, d, $J = 8.4$ Hz, $2 \times \text{ArH}$); ^{13}C NMR (125 MHz, DMSO- d_6) δ_{C} 30.5 (ArCH_2), 114.4 (C-Ar), 116.4 (C-Ar), 127.9 ($2 \times \text{C-Ar}$), 128.1 (C-Ar), 128.5 ($2 \times \text{C-Ar}$), 129.2 ($2 \times \text{C-Ar}$), 130.1 ($2 \times \text{C-Ar}$), 130.9 (C-Ar), 131.1 ($2 \times \text{C-Ar}$), 131.3 ($2 \times \text{C-Ar}$), 131.6 (C-Ar), 133.7 (C-Ar), 135.7 (C-Ar), 137.2 (C-Ar), 137.9 (C-Ar), 138.1 (C-Ar), 166.5 (C=O), 167.3 (C=O); HRMS calcd for $\text{C}_{25}\text{H}_{18}\text{Cl}_2\text{NO}_4$ [$\text{M}(^{35}\text{Cl}_2)+\text{H}$] $^+$ 466.0607, found 466.0598.

4-(4-Chlorobenzyl)-5-(4-chlorophenyl)-6-phenyl-1H-furo[3,4-c]pyrrole-1,3(5H)-dione
(85)



Compound **67** (520 mg, 1.11 mmol) was dissolved in acetic anhydride (8 mL) and refluxed for 2 h. After cooling to r.t., acetic anhydride was removed by filtration. The residue was washed with water (3×20mL) and petrol (3×20mL) and dried in vacuum oven at 40 °C to get an off-white solid (410 mg, 82%). $R_f=0.42$ (20% EtOAc/Petrol); m.p. 233-235 °C; λ_{max} (EtOH)/nm 275.4; IR ν_{max}/cm^{-1} 3092, 2649, 2376, 1816 (C=O), 1756 (C=O); 1H NMR (500 MHz, DMSO- d_6) δ_H 4.02 (2H, s, 2 × ArCH₂), 6.96 (2H, d, $J = 8.3$ Hz, 2 × ArH), 7.25-7.27 (4H, m, 4 × ArH), 7.30-7.34 (5H, m, 5 × ArH), 7.53 (2H, d, $J = 8.3$ Hz, 2 × ArH); ^{13}C NMR (125 MHz, DMSO- d_6) δ_C 31.0 (ArCH₂), 116.1 (C-Ar), 117.3 (C-Ar), 127.7 (C-Ar), 128.9 (2 × C-Ar), 129.0 (2 × C-Ar), 129.6 (2 × C-Ar), 129.9 (C-Ar), 130.2 (2 × C-Ar), 130.6 (2 × C-Ar), 130.8 (2 × C-Ar), 131.9 (C-Ar), 134.9 (C-Ar), 135.1 (C-Ar), 135.3 (C-Ar), 135.7 (C-Ar), 136.0 (C-Ar), 159.6 (C=O), 159.7 (C=O); HRMS calcd for C₂₅H₁₆Cl₂NO₃ [M(³⁵Cl₂)+H]⁺ 448.0502, found 448.0496.

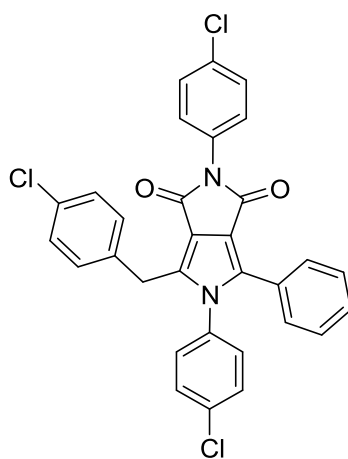
4-(4-Chlorobenzyl)-5-(4-chlorophenyl)-6-phenylpyrrolo[3,4-c]pyrrole-1,3(2H,5H)-dione
(68)



Compound **85** (65 mg, 0.14 mmol) was suspended in acetic acid (1 mL) and 0.5 M NH₃ in dioxane (4.2 mL, 2.1 mmol) was added. The mixture was heated at 120 °C under microwave irradiation for 30 min. After cooling to r.t., the solvent was removed *in vacuo*. The residue was

suspended in THF (3 mL) and thionyl chloride was added (70 μ L). The resulting solution was stirred at r.t. for 1.5 h and refluxed for 1.5 h. After cooling to r.t., the solvent was removed *in vacuo*. The residue was purified by MPLC on SiO₂ (Petrol:EtOAc, 0-50%) to give a beige solid (39 mg, 62%). $R_f = 0.52$ (2% MeOH/DCM); m.p. 274-276 °C; λ_{\max} (EtOH)/nm 322.8; IR $\nu_{\max}/\text{cm}^{-1}$ 3191 (NH), 3061, 2922, 2851, 2753, 1742 (C=O), 1701 (C=O); ¹H NMR (500 MHz, DMSO-*d*₆) δ_H 3.97 (2H, s, 2 \times ArCH₂), 6.88-6.90 (2H, m, 2 \times ArH), 7.22-7.29 (9H, m, 9 \times ArH), 7.48-7.50 (2H, m, 2 \times ArH), 10.59 (1H, s, NH); ¹³C NMR (125 MHz, DMSO-*d*₆) δ_C 30.6 (ArCH₂), 107.5 (C-Ar), 118.5 (C-Ar), 119.7 (C-Ar), 128.7 (2 \times C-Ar), 128.8 (2 \times C-Ar), 129.1 (C-Ar), 129.5 (2 \times C-Ar), 130.0 (2 \times C-Ar), 130.4 (2 \times C-Ar), 131.0 (2 \times C-Ar), 131.6 (C-Ar), 132.6 (C-Ar), 132.8 (C-Ar), 134.5 (C-Ar), 135.5 (C-Ar), 136.6 (C-Ar), 165.5 (C=O), 165.9 (C=O); HRMS calcd for C₂₅H₁₇Cl₂N₂O₂ [M(³⁵Cl₂)+H]⁺ 447.0662, found 447.0655.

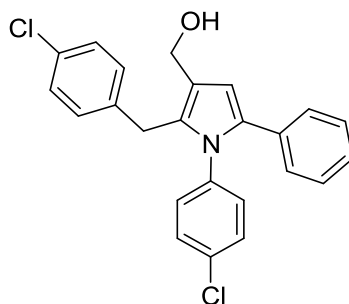
4-(4-Chlorobenzyl)-2,5-bis(4-chlorophenyl)-6-phenylpyrrolo[3,4-*c*]pyrrole-1,3(2*H*,5*H*)-dione (86)



Compound **85** (65 mg, 0.14 mmol) and 4-chloroaniline (90 mg, 0.70 mmol) were suspended in acetic acid (1.5 mL). The mixture was heated at 120 °C under microwave irradiation for 20 min. After cooling to r.t., the solvent was removed *in vacuo*. The residue was purified by MPLC on SiO₂ (DCM:MeOH, 0-10%) to give an off-white solid. The product was suspended in THF (5 mL) and thionyl chloride was added (200 μ L). The resulting solution was stirred at r.t. for 18 h. After cooling to r.t., the solvent was removed *in vacuo*. The residue was purified by MPLC on SiO₂ (DCM:MeOH, 0-10%) to give a beige solid (52 mg, 64%). $R_f = 0.52$ (20% EtOAc/Petrol); m.p. 256 °C (degraded); λ_{\max} (EtOH)/nm 246.8; IR $\nu_{\max}/\text{cm}^{-1}$ 3055, 2922, 2850, 1752 (C=O), 1700 (C=O); ¹H NMR (500 MHz, DMSO-*d*₆) δ_H 4.05 (2H, s, 2 \times ArCH₂), 6.94-6.96 (2H, m, 2 \times ArH), 7.24-7.27 (4H, m, 4 \times ArH), 7.30 (5H, s, 5 \times ArH), 7.44-7.46 (2H, m, 2 \times ArH), 7.51-7.53 (2H, m, 2 \times ArH), 7.57-7.59 (2H, m, 2 \times ArH); ¹³C NMR (125 MHz,

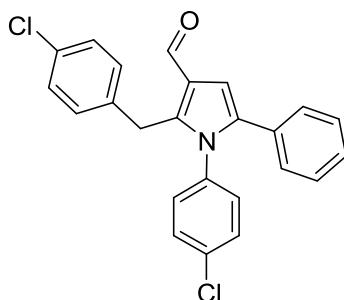
DMSO-*d*₆) δ_C 30.8 (ArCH₂), 116.9 (C-Ar), 118.1 (C-Ar), 128.5 (C-Ar), 128.8 (2 \times C-Ar), 128.8 (2 \times C-Ar), 129.2 (2 \times C-Ar), 129.4 (C-Ar), 129.6 (2 \times C-Ar), 129.7 (2 \times C-Ar), 130.1 (2 \times C-Ar), 130.6 (2 \times C-Ar), 131.0 (2 \times C-Ar), 131.7 (C-Ar), 132.1 (C-Ar), 132.5 (C-Ar), 133.9 (C-Ar), 134.2 (C-Ar), 134.7 (C-Ar), 135.3 (C-Ar), 136.3 (C-Ar), 163.0 (C=O), 163.3 (C=O); HRMS calcd for C₃₁H₂₀Cl₃N₂O₂ [M(³⁵Cl₃)+H]⁺ 557.0585, found 557.0585.

(2-(4-Chlorobenzyl)-1-(4-chlorophenyl)-5-phenyl-1*H*-pyrrol-3-yl)methanol (308)



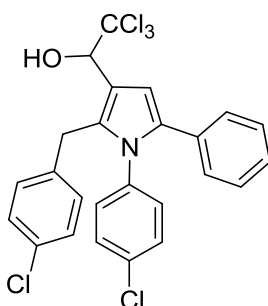
Prepared according to general procedure F using compound **82** (1.2 g, 2.66 mmol), 1 M DIBAL in THF (6.7 mL, 6.70 mmol) and THF (5 mL). Purification by MPLC on SiO₂ (Petrol:EtOAc, 0-30%) gave an off-white solid (1.06 g, 97%). *R*_f=0.25 (25% EtOAc/Petrol); m.p. 137-140 °C; λ_{\max} (EtOH)/nm 283.4; IR ν_{\max} /cm⁻¹ 3319 (OH), 3089, 2918, 2877, 2224; ¹H NMR (500 MHz, DMSO-*d*₆) δ_H 3.88 (2H, s, ArCH₂), 4.44 (2H, d, *J* = 5.3 Hz, ArCH₂OH), 4.84 (1H, t, *J* = 5.3 Hz, OH), 6.44 (1H, s, Pyrrole-*H*), 6.83-6.86 (2H, m, 2 \times Ar*H*), 6.95-6.98 (2H, m, 2 \times Ar*H*), 6.99-7.01 (2H, m, 2 \times Ar*H*), 7.07-7.11 (1H, m, 1 \times Ar*H*), 7.15-7.19 (4H, m, 4 \times Ar*H*), 7.34-7.37 (2H, m, 2 \times Ar*H*); ¹³C NMR (125 MHz, DMSO-*d*₆) δ_C 29.8 (ArCH₂), 56.4 (CH₂OH), 110.6 (C-Ar), 123.5 (C-Ar), 126.5 (C-Ar), 127.8 (2 \times C-Ar), 128.4 (2 \times C-Ar), 128.7 (2 \times C-Ar), 129.5 (2 \times C-Ar), 130.2 (2 \times C-Ar), 130.8 (C-Ar), 130.9 (2 \times C-Ar), 130.9 (C-Ar), 132.7 (C-Ar), 133.0 (C-Ar), 133.4 (C-Ar), 137.9 (C-Ar), 139.0 (C-Ar).

2-(4-Chlorobenzyl)-1-(4-chlorophenyl)-5-phenyl-1H-pyrrole-3-carbaldehyde (**90**)



Prepared according to general procedure G using compound **308** (1.05 g, 2.57 mmol) in DCM (10 mL) and Dess-Martin periodinane (1.85 g, 4.37 mmol) in DCM (15 mL). Purification by MPLC on SiO₂ (Petrol:EtOAc, 0-30%) gave an off-white viscous liquid (680 mg, 65%). $R_f = 0.50$ (25% EtOAc/Petrol); m.p. 132-135 °C; λ_{\max} (EtOH)/nm 250.8; IR $\nu_{\max}/\text{cm}^{-1}$ 3066, 2985, 2920, 2819, 2714, 1662 (C=O); ¹H NMR (500 MHz, CDCl₃) δ_H 4.18 (2H, s, 2 × ArCH₂), 6.79-6.80 (2H, m, 2 × ArH), 6.84-6.86 (3H, m, 3 × ArH), 7.01-7.03 (2H, m, 2 × ArH), 7.14-7.16 (2H, m, 2 × ArH), 7.17-7.19 (3H, m, 3 × ArH), 7.25-7.27 (2H, m, 2 × ArH), 10.01 (1H, s, CHO); ¹³C NMR (125 MHz, CDCl₃) δ_C 30.3 (ArCH₂), 109.4 (C-Ar), 123.5 (C-Ar), 127.4 (C-Ar), 128.3 (2 × C-Ar), 128.4 (2 × C-Ar), 128.6 (2 × C-Ar), 129.4 (2 × C-Ar), 129.4 (2 × C-Ar), 129.8 (2 × C-Ar), 131.3 (C-Ar), 132.4 (C-Ar), 134.9 (C-Ar), 135.6 (C-Ar), 136.5 (C-Ar), 136.6 (C-Ar), 140.2 (C-Ar), 186.1 (C=O); LRMS (ES⁺) m/z 406.2 [M(³⁵Cl₂)+H]⁺, 408.2 [M(³⁵Cl³⁷Cl)+H]⁺.

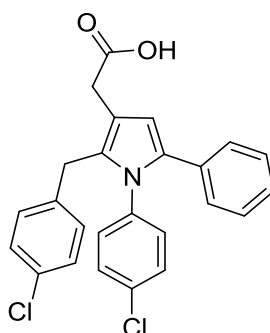
2,2,2-Trichloro-1-(2-(4-chlorobenzyl)-1-(4-chlorophenyl)-5-phenyl-1H-pyrrol-3-yl)ethan-1-ol (**91**)



Compound **90** (400 mg, 0.98 mmol) was dissolved in DMF (0.6 mL) and cooled to -10 °C. CHCl₃ (190 μ L, 2.35 mmol) was added dropwise and the mixture was stirred at -10 °C for 15 min. KOH (44 mg, 0.78 mmol) in MeOH (0.12 mL) was added and the mixture was stirred at -10 °C for 3 h. The reaction was quenched with 1 M HCl (2 mL) and toluene (2 mL) and stirred at -10 °C for 1 h. After warming to r.t., the aqueous layer was extracted with EtOAc (3×30 mL).

The organic layers were combined, dried over MgSO₄ and the solvent removed *in vacuo*. Purification by MPLC on SiO₂ (Petrol:EtOAc, 0-20%) gave an off-white solid (330 mg, 64%). R_f = 0.44 (20% EtOAc/Petrol); m.p. 84-87 °C; λ_{max} (EtOH)/nm 277.6; IR ν_{max}/cm⁻¹ 3550, 3035, 2920, 2850, 2656; ¹H NMR (500 MHz, CDCl₃) δ_H 3.88 (1H, d, *J* = 17.1 Hz, ArCH₂), 4.07 (1H, d, *J* = 17.1 Hz, ArCH₂), 5.20 (1H, s, CHOH), 6.69 (1H, br s, 1 × ArH), 6.75 (1H, s, 1 × ArH), 6.81-6.83 (2H, m, 2 × ArH), 6.98-7.05 (3H, m, 3 × ArH), 7.10-7.17 (6H, m, 6 × ArH), 7.24 (1H, br s, 1 × ArH); ¹³C NMR (125 MHz, CDCl₃) δ_C 30.6 (ArCH₂), 79.6 (CHOH), 104.0 (C-Ar), 108.0 (C-Ar), 117.5 (C-Ar), 126.6 (2 × C-Ar), 128.1 (2 × C-Ar), 128.5 (2 × C-Ar), 129.1 (2 × C-Ar), 129.3 (2 × C-Ar), 130.0 (2 × C-Ar), 132.0 (C-Ar), 132.1 (C-Ar), 133.0 (C-Ar), 134.0 (C-Ar), 135.0 (C-Ar), 137.0 (C-Ar), 137.2 (C-Ar); LRMS (ES⁺) *m/z* 524.0 [M(³⁵Cl₅)+H]⁺, 526.1 [M(³⁵Cl₄³⁷Cl)+H]⁺, 528.1 [M(³⁵Cl₃³⁷Cl₂)+H]⁺.

2-(2-(4-Chlorobenzyl)-1-(4-chlorophenyl)-5-phenyl-1H-pyrrol-3-yl)acetic acid (92)

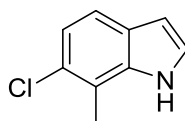


Diphenyl diselenide (76 mg, 0.24 mmol) was dissolved in ethanol (1 mL) and NaBH₄ (18 mg, 0.48 mmol) was added and the mixture was stirred at r.t. for 30 min. Compound **91** (122 mg, 0.23 mmol) was added, followed by the addition of NaOH (55 mg, 1.38 mmol) and the mixture was stirred at r.t. for 24 h. After cooling to r.t., the solvent was removed *in vacuo*. EtOAc (5 mL) and H₂O (5 mL) was added to the residue and acidified to pH 1 with 1 M HCl. The aqueous layer was extracted with EtOAc (3×30 mL). The organic layers were combined, dried over MgSO₄ and the solvent removed *in vacuo*. Purification by MPLC on SiO₂ (DCM:MeOH, 0-5%) gave a beige solid (90 mg, 90%). R_f = 0.47 (5% MeOH/DCM); m.p. 145-148 °C; λ_{max} (EtOH)/nm 252.8; IR ν_{max}/cm⁻¹ 3067, 2919, 2850, 2727, 2621, 1696 (C=O); ¹H NMR (500 MHz, DMSO-*d*₆) δ_H 3.44 (2H, s, CH₂COOH), 3.86 (2H, s, 2 × ArCH₂), 6.38 (1H, s, Pyrrole-H), 6.82-6.84 (2H, m, 2 × ArH), 6.98-7.02 (4H, m, 4 × ArH), 7.08-7.11 (1H, m, 1 × ArH), 7.16-7.19 (4H, m, 4 × ArH), 7.32-7.36 (2H, m, 2 × ArH), 12.22 (1H, s, COOH); ¹³C NMR (125 MHz, DMSO-*d*₆) δ_C 29.7 (ArCH₂), 32.5 (CH₂COOH), 111.3 (C-Ar), 115.8 (C-Ar), 126.5 (C-Ar), 127.8 (2 × C-Ar), 128.4 (2 × C-Ar), 128.7 (2 × C-Ar), 129.4 (2 × C-Ar), 130.1 (2 × C-Ar),

130.8 (2 × C-Ar), 130.8 (C-Ar), 131.3 (C-Ar), 132.7 (C-Ar), 132.9 (C-Ar), 133.5 (C-Ar), 138.0 (C-Ar), 138.8 (C-Ar), 173.5 (C=O); HRMS calcd for C₂₅H₂₀Cl₂NO₂ [M(³⁵Cl₂)+H]⁺ 436.0866, found 436.0857.

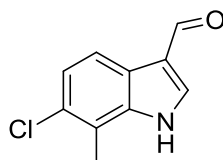
16.2.4 Synthesis of RO-2443 (3) and RO-5963 (4)

6-chloro-7-methyl-1H-indole (103)



2-Chloro-6-nitrotoluene (618 mg, 3.6 mmol) was dissolved in THF (25 mL) and cooled to -40 °C. 1 M vinylmagnesium bromide in THF (10.8 mL, 10.8 mmol) was added dropwise and the reaction mixture was stirred at -40 °C for 1 h. Saturated aqueous NH₄Cl (30 mL) was added and the aqueous layer was extracted with ethyl acetate (3 × 20 mL). The organic layers were combined, dried over MgSO₄, and evaporated *in vacuo*. Purification by MPLC on SiO₂ (Petrol:EtOAc, 0-20%) gave a dark brown viscous liquid (260 mg, 43%). R_f = 0.33 (20% EtOAc:Petrol); m.p. 116-119 °C. UV λ_{max} (EtOH)/nm 271, 220; IR ν_{max}/cm⁻¹ 3413 (NH), 1732, 1606; ¹H NMR (500 MHz; CDCl₃) δ_H 2.45 (3H, s, CH₃), 6.46 (1H, dd, *J* = 2.2 and 3.1 Hz, ArH), 7.05 (1H, d, *J* = 8.4 Hz, ArH), 7.13 (1H, dd, *J* = 2.2 and 3.1 Hz, ArH), 7.33 (1H, d, *J* = 8.4 Hz, ArH), 8.01 (1H, br s, NH); ¹³C NMR (125 MHz; CDCl₃) δ_C 13.9 (CH₃), 103.4 (CH-Ar), 118.1 (C-Ar), 118.9 (CH-Ar), 121.3 (CH-Ar), 124.5 (CH-Ar), 126.0 (C-Ar), 127.5 (C-Ar), 136.0 (C-Ar).

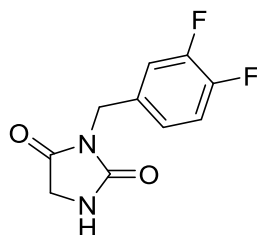
6-Chloro-7-methyl-1H-indole-3-carbaldehyde (104)



Prepared according to general procedure H using compound **103** (160 mg, 0.96 mmol), DMF (12 mL) and phosphorus oxychloride (0.25 mL, 2.89 mmol) heated under microwave irradiation at 70 °C for 10 min. EtOAc extraction gave a light brown solid (175 mg, 93%) which did not

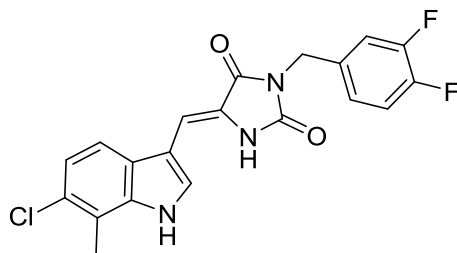
require further purification, $R_f = 0.35$ (2% MeOH/DCM); m.p. 239-241 °C; λ_{\max} (EtOH)/nm 263; IR $\nu_{\max}/\text{cm}^{-1}$ 1632 (C=O). ^1H NMR (500 MHz; DMSO- d_6) δ_{H} 2.54 (3H, s, CH_3), 7.26 (1H, d, $J = 8.5$ Hz, ArH), 7.91 (1H, d, $J = 8.5$ Hz, ArH), 8.36 (1H, s, 1×ArH), 9.94 (1H, s, CHO), 12.33 (1H, br s, NH). ^{13}C NMR (125 MHz; DMSO- d_6) δ_{C} 14.0 (CH_3), 118.4 (C-Ar), 119.3 (C-Ar), 119.8 (CH-Ar), 122.7 (CH-Ar), 123.1 (C-Ar), 127.8 (C-Ar), 137.1 (CH-Ar), 138.9 (C-Ar), 185.1 (C=O). HRMS calcd for $\text{C}_{10}\text{H}_7\text{ClNO}$ [$\text{M}^{(35}\text{Cl})\text{-H}$] $^-$ 192.0222, 192.0213.

3-(3,4-difluorobenzyl)imidazolidine-2,4-dione (107)



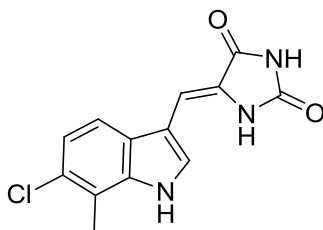
Hydantoin (500 mg, 5 mmol), 3,4-difluorobenzyl bromide (0.64 mL, 5 mmol) and K_2CO_3 (700 mg, 5mmol) were suspended in acetonitrile (12 mL). The reaction mixture was refluxed for 6 hours and stirred at 50 °C for 16 h. The reaction was cooled to r.t, quenched with ice and extracted with EtOAc (3×25 mL). The organic layers were combined, washed with brine, dried over MgSO_4 and evaporated *in vacuo*. Purification by MPLC on SiO_2 (Petrol:EtOAc, 0-20%) gave a white solid (643 mg, 57%). $R_f = 0.37$ (2% MeOH/DCM); m.p. 134-137 °C; λ_{\max} (EtOH)/nm 339, 268, 263; IR $\nu_{\max}/\text{cm}^{-1}$ 3259 (NH), 1771 (C=O), 1712 (C=O); ^1H NMR (500 MHz, CDCl_3) δ_{H} 3.92 (2H, s, CH_2), 4.54 (2H, s, CH_2), 6.15 (1H, br s, NH), 7.00-7.08 (2H, m, 2 × Ar-H), 7.15-7.20 (1H, m, Ar-H); ^{13}C NMR (125 MHz, CDCl_3) δ_{C} 41.3 (CH_2), 46.5 (CH_2), 117.5 (d, $J = 17.3$, CH-Ar), 118.0 (d, $J = 17.9$, CH-Ar), 125.0 (dd, $J = 3.7$ and 6.2 Hz, CH-Ar), 150.2 (dd, $J = 12.7$ and 249.3 Hz, ArCF), 150.2 (dd, $J = 12.7$ and 248.8 Hz, ArCF), 157.7 (C=O), 170.7 (C=O). ^{19}F NMR (470 MHz; CDCl_3) δ_{F} -138.5 (d, $J = 21.0$ Hz), -136.9 (d, $J = 21.0$ Hz). LRMS (ES^+) m/z 227.2 [$\text{M} + \text{H}$] $^+$.

(Z)-5-((6-chloro-7-methyl-1H-indol-3-yl)methylene)-3-(3,4-difluorobenzyl)imidazolidine-2,4-dione (3)



A mixture of compound **104** (50 mg, 0.26 mmol), **107** (68 mg, 0.30 mmol) and piperidine (0.08 mL) was heated at 130 °C for 30 min. The reaction mixture was cooled to 60 °C, water (2 mL) was added and the mixture was stirred for 1 hour and additional water (20 mL) was added, extracted with ethyl acetate (2 × 25 mL). The organic layers were combined, dried over MgSO₄ and evaporated *in vacuo* to get a yellow solid (96 mg, 92 %). $R_f = 0.39$ (4% MeOH/DCM); m.p. 278-280 °C (decomposed); λ_{max} (EtOH)/nm 368, 230. IR ν_{max}/cm^{-1} 3475 (NH), 3216, 3151, 3054, 1743 (C=O), 1699 (C=O). ¹H NMR (500 MHz, THF-d₈) δ_H 2.52 (3H, s, CH₃), 4.67 (2H, s, benzyl-CH₂), 6.92 (1H, s, CH=Hydantoin), 7.14 (1H, d, $J = 8.5$ Hz, Indole-H), 7.16-7.22 (2H, m, 2 × Phenyl-H), 7.31-7.35 (1H, m, Phenyl-H), 7.59 (1H, d, $J = 8.5$, indole-H), 7.82 (1H, d, $J = 2.4$ Hz, Indole-H₂), 9.27 (1H, br s, NH), 10.97 (1H, s, NH). ¹³C NMR (125 MHz, THF-d₈) δ_C 13.9 (CH₃), 40.4 (d, $J = 0.9$ Hz, Benzyl-CH₂), 103.5 (CH=Hydantoin), 111.2 (C-CO), 117.8 (CH-Indole), 118.0 (d, $J = 17.6$, Phenyl-CHCF), 118.4 (d, $J = 17.6$, Phenyl-CHCF), 119.7 (C-Ar), 122.5 (CH-Indole), 124.6 (C-Ar), 125.9 (dd, $J = 3.6$ and 6.5 Hz, Phenyl-CH), 126.8 (C-Ar), 126.9 (CH-Indole), 128.9 (C-Ar), 135.7 (dd, $J = 3.9$, 5.5 Hz, C-Ar), 137.4 (C-Ar), 150.8 (dd, $J = 30.8$ and 247.2 Hz, ArCF), 150.9 (dd, $J = 31.2$ and 247.2 Hz, ArCF), 155.2 (C=O), 164.3 (C=O). ¹⁹F NMR (470 MHz; THF-d₈) δ_F -141.4 (d, $J = 22.5$ Hz), -139.4 (d, $J = 20.7$ Hz). HRMS calcd for C₂₀H₁₃ClF₂N₃O₂ [M(³⁵Cl)-H]⁻ 400.0670, found 400.0655.

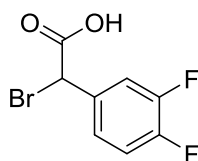
(Z)-5-((6-chloro-7-methyl-1H-indol-3-yl)methylene)imidazolidine-2,4-dione (118)



A mixture of compound **104** (100 mg, 0.52 mmol), hydantoin (47 mg, 0.47 mmol) and piperidine (0.16 mL) was heated at 130 °C for 1 h. The reaction mixture was cooled to 60 °C,

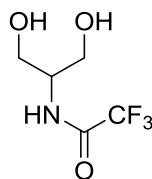
water (2 mL) was added and the mixture was stirred for 1 hour and additional water (20 mL) was added, extracted with ethyl acetate (2×25 mL). The organic layers were combined, dried over MgSO₄ and evaporated *in vacuo*. Purification by MPLC on SiO₂ (DCM:MeOH, 0-10%) gave a yellow solid (112 mg, 86 %). R_f = 0.29 (4% MeOH/DCM); m.p. 330-331 °C (decomposed); λ_{max} (EtOH)/nm 362, 267, 231; IR ν_{max}/cm⁻¹ 3047 (N-H), 3193, 2980, 2919, 1745 (C=O), 1703 (C=O). ¹H NMR (500 MHz, DMSO-*d*₆) δ_H 2.52 (3H, s, CH₃), 6.70 (1H, s, CH=CCO), 7.14 (1H, d, *J* = 8.4 Hz, indole-H), 7.62 (1H, d, *J* = 8.4 Hz, indole-H), 8.16 (1H, d, *J* = 2.1 Hz, indole-H₂), 10.17 (1H, s, NH), 11.00 (1H, br s, NH), 11.94 (1H, s, NH). ¹³C NMR (125 MHz, DMSO-*d*₆) δ_C 13.9 (CH₃), 101.1 (CH=CCO), 109.0 (indole-C), 116.8 (indole-CH), 119.0 (indole-C), 121.1 (indole-CH), 124.1, 125.5, 126.8 (indole-C), 127.2 (indole-CH), 135.9 (indole-C), 155.2 (C=O), 165.2 (C=O). HRMS calcd for C₁₃H₉ClN₃O₂ [M(³⁵Cl)-H]⁻ 274.0389, found 274.0382.

2-Bromo-2-(3,4-difluorophenyl)acetic acid (109)



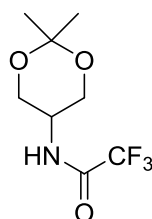
2-amino-2-(3,4-difluorophenyl)acetic acid (580 mg, 3.10 mmol) was added into a solution of 48% hydrobromic acid (2.8 mL, 24.8 mmol), KBr (1.48 g, 12.4 mmol) and water (6 mL). The mixture was stirred at 0°C for 15 min, then, a solution of NaNO₂ (684 mg, 9.92 mmol) in water (4 mL) was added dropwise and the mixture was stirred at r.t. for 3 hours. The aqueous layer was extracted with DCM (3×30 ml). The organic layers were combined, washed with water (30 mL), brine (20 mL), dried over MgSO₄, and evaporated *in vacuo*. Purification by MPLC on SiO₂ (Petrol:EtOAc, 0-100%, 0.5% Acetic acid) gave a white solid (281 mg, 36%). R_f = 0.66 (50% EtOAc/Petrol, 5 % AcOH); m.p. 89-90 °C; λ_{max} (EtOH)/nm 398; IR ν_{max}/cm⁻¹ 3060, 2920, 2669, 1728 (C=O); ¹H NMR (500 MHz, CDCl₃) δ_H 5.22 (1H, s, benzyl-CH), 7.06-7.11(1H, m, Ar-H), 7.14-7.21 (1H, m, Ar-H), 7.37-7.41(1H, m, Ar-H), 8.87 (1H, br s, COOH). ¹³C NMR (125 MHz, CDCl₃) δ_C 44.0 (benzyl-CH), 117.6 (d, *J* = 17.7 Hz, ArCH), 118.3 (d, *J* = 18.6 Hz, ArCH), 125.1 (dd, *J* = 3.7 and 6.6 Hz, ArC₆H), 131.8 (dd, *J* = 4.0, 5.8 Hz, ArC₁), 150.3 (dd, *J* = 11.6 and 249.0 Hz, ArCF), 151.0 (dd, *J* = 6.2 and 246.0 Hz, ArCF), 173.0 (COOH). ¹⁹F NMR (470 MHz; CDCl₃) δ_F -135.5 (d, *J* = 20.9 Hz), -131.5 (d, *J* = 20.9 Hz). LRMS (ES⁻) *m/z* 205.0 [(M(⁷⁹Br)-COOH)-H]⁻, 207.0 [(M(⁸¹Br)-COOH)-H]⁻.

***N*-(1,3-dihydroxypropan-2-yl)-2,2,2-trifluoroacetamide (113)**



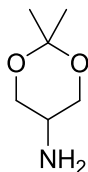
A mixture of 2-aminopropane-1,3-diol (562 mg, 6.17 mmol), ethyl trifluoroacetate (6 mL) and THF (2 mL) was stirred at r.t. for 48 h. The solvent was evaporated *in vacuo* and the residue was purified by filtering through silica to get a white solid (1.12 g, 98 %). $R_f = 0.57$ (10% MeOH/DCM); m.p. 61-62 °C; IR $\nu_{\max}/\text{cm}^{-1}$ 3289 (O-H), 1703 (C=O); ^1H NMR (500 MHz, CD_3OD) δ_{H} 3.52 (2H, dd, $J = 6.2$ and 11.3 Hz, CH_2), 3.58 (2H, dd, $J = 5.4$ and 11.3 Hz, CH_2), 3.91 (1H, m, NHCH); ^{13}C NMR (125 MHz, CD_3OD) δ_{C} 55.6 (NHCH), 61.5 (CH_2), 117.5 (d, $J = 286.7$ Hz, CF_3), 159.2 (d, $J = 36.8$ Hz, C=O). ^{19}F NMR (470 MHz, CD_3OD) δ_{F} -77.2 (s).

***N*-(2,2-dimethyl-1,3-dioxan-5-yl)-2,2,2-trifluoroacetamide (114)**



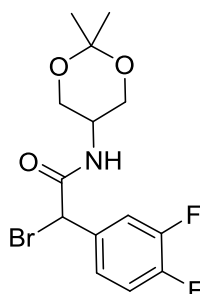
Compound **113** (721 mg, 3.9 mmol) was dissolved in DCM (7 mL), camphor-10-sulfonic acid (91 mg, 0.39 mmol) and 2,2-dimethoxypropane (3.84 mL, 31.2 mmol) were added, respectively. The reaction mixture was stirred at r.t. for 96 h. Saturated aqueous NaHCO_3 (20 mL) was added and stirred for 1 h. The aqueous layer was extracted with DCM (3×40 mL). The organic layers were combined, dried over MgSO_4 , and evaporated *in vacuo*. Purification by MPLC on SiO_2 (DCM:MeOH, 0-5%) gave a white solid (475 mg, 54%). $R_f = 0.81$ (2% MeOH/DCM); m.p. 73-75 °C; IR $\nu_{\max}/\text{cm}^{-1}$ 3283 (N-H), 1716 (C=O), 1550 (N-H); ^1H NMR (500 MHz, CD_3OD) δ_{H} 1.32 (3H, s, CH_3), 1.33 (1H, s, CH_3), 3.68 (2H, dd, $J = 5.6$ and 12.1 Hz, CH_2), 3.76-3.79 (1H, m, NHCH), 3.95 (2H, dd, $J = 3.8$ and 12.1 Hz, CH_2); ^{13}C NMR (125 MHz, CD_3OD) δ_{C} 23.1 (CH_3), 24.8 (CH_3), 46.0 (NHCH), 62.8 ($2\times\text{CH}_2$), 99.7 ($\text{CH}_2\text{OC}(\text{CH}_3)_2$), (d, $J = 286.5$ Hz, CF_3), 158.9 (d, $J = 37.3$ Hz, C=O). ^{19}F NMR (470 MHz, CD_3OD) δ_{F} -77.1 (s).

2,2-Dimethyl-1,3-dioxan-5-amine (115)



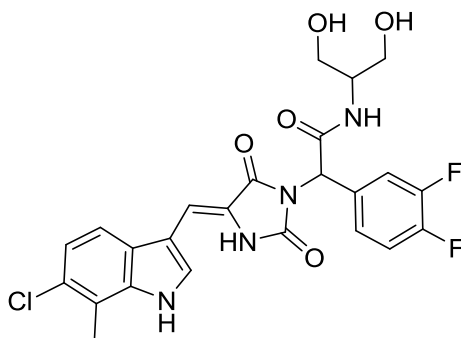
Compound **114** (500 mg, 2.2 mmol) was dissolved in THF (10 mL) and water (10 mL), LiOH monohydrate (184 mg, 4.4 mmol) was added and stirred at r.t. for 1.5 h. The solvent was evaporated *in vacuo*, the remaining residue was dissolved in water (20 mL) and extracted with DCM (5 × 15 mL). The organic layers were combined, dried over MgSO₄, and concentrated *in vacuo* to get a colourless liquid (157 mg, 54%) which was used for the next step without further purification. R_f = 0.18 (2% MeOH/DCM); IR ν_{max}/cm⁻¹ 3350 (NH₂ stretch), 2980, 2930; ¹H NMR (500 MHz, CDCl₃) δ_H 1.42 (3H, s, CH₃), 1.54 (2H, br s, 2×NH₂), 2.84(1H, br s, CH(CH₂)₂), 3.56 (2H, dd, J = 11.8 and 5.6 Hz, CH₂O), 4.01 (2H, dd, J = 11.8 and 3.5 Hz, CH₂O).

2-Bromo-2-(3,4-difluorophenyl)-N-(2,2-dimethyl-1,3-dioxan-5-yl)acetamide (116)



Compound **109** (130 mg, 0.517 mmol), **115** (68 mg, 0.517) and DMAP (6.3 mg, 0.05 mmol) were dissolved in DCM (2.6 mL) and the reaction mixture was stirred at 0 °C for 20 min. DIC (0.09 mL, 0.56 mmol) was added and the solution was stirred at 0 °C for 3 h and at r.t. for 13 h. The reaction mixture was quenched with water (10 mL) and extracted with DCM (3 × 20 mL). The organic layers were combined, dried over MgSO₄, and concentrated *in vacuo*. Purification by MPLC on SiO₂ (Petrol:EtOAc, 0-90%) gave a white solid (149 mg, 79%). R_f = 0.45 (50% EtOAc/Petrol); m.p. 145-147 °C; λ_{max} (EtOH)/nm 398; IR ν_{max}/cm⁻¹ 3279 (O-H stretch), 3045, 2921, 2868, 1525, 1488.; ¹H NMR (500 MHz, CDCl₃) δ_H 1.44 (3H, s, CH₃), 1.50 (3H, s, CH₃), 3.72-3.77(2H, m, CH₂O), 3.82-3.86 (1H, m, NHCH), 4.15 (2H, dd, J = 12.3, 2.0 Hz, CH₂O), 7.12-7.17 (1H, m, ArH), 7.20-7.23 (1H, m, ArH), 7.33-7.37 (1H, m, ArH), 7.51 (1H, br d, J = 7.7 Hz, NH); ¹³C NMR (125 MHz, CDCl₃) δ_C 18.3 (CH₃), 29.1 (CH₃), 44.8

(Z)-2-(4-((6-chloro-7-methyl-1H-indol-3-yl)methylene)-2,5-dioximidazolidin-1-yl)-2-(3,4-difluorophenyl)-N-(1,3-dihydroxypropan-2-yl)acetamide (4)



Compound **119** (18 mg, 0.032 mmol) was dissolved in THF (0.5 mL), 0.2 M HCl (0.17 mL) was added dropwise and stirred at 0 °C for 1 h and at r.t. for 2 h. The solvent was evaporated *in vacuo* and the remaining residue was neutralised with saturated aqueous NaHCO₃ and extracted with EtOAc (3 × 20 mL), dried over MgSO₄ and evaporated *in vacuo*. Purification by semi-preparative HPLC (C-18 silica, MeCN/formic acid aq., 65%) gave a yellow solid (6 mg, 36%). R_f = 0.36 (8% MeOH/DCM); m.p. 210 °C (degradation); λ_{max} (EtOH)/nm 371; IR ν_{max}/cm⁻¹ 3281 (O-H stretch), 2954, 1746 (C=O), 1700 (C=O), 1644 (C=O); ¹H NMR (500 MHz, THF-d₈) δ_H 2.41 (3H, s, CH₃), 3.43-3.52 (4H, m, 2×CH₂OH), 3.63 (1H, br s, OH), 3.72 (1H, br s, OH), 3.76-3.82 (1H, m, NHCH(CH₂OH)₂), 5.72 (1H, s, Benzyl-CH), 6.81 (1H, s, Indole-CHCCO), 6.89 (1H, d, J = 7.8 Hz, CONH), 7.02 (1H, d, J = 8.5, ArH), 7.07-7.13 (1H, m, ArH), 7.22-7.25 (1H, m, ArH), 7.43-7.48 (2H, m, 2 × ArH), 7.73 (1H, d, J = 2.5 Hz, ArH), 9.33 (1H, br s, Hydantoin-NH), 10.91 (1H, br s, Indole-NH). ¹³C NMR (125 MHz, THF-d₈) δ_C 12.9 (CH₃), 54.0 (CH(CH₂OH)₂), 56.7 (BenzylCH), 60.8 (CH(CH₂OH)₂), 103.1 (Indole-CHCCO), 110.2, 116.7 (ArCH, multiplicity not clear), 116.8 (Indole-CH), 118.8 (ArC), 118.9 (d, J = 18.4 Hz, ArCH), 121.5 (Indole-CH), 123.2 (ArC), 118.7 (ArC), 121.5 (ArCH), 123.6 (ArC), 124.9 (dd, J = 3.6, 6.5 Hz, ArCH), 125.8 (ArC), 126.1 (ArC), 126.5 (ArCH, multiplicity not clear), 137.2 (ArC), 154.0 (CO), 163.3 (CO), 165.9 (CO). The expected dd of 2×CF were not seen due to the dilute NMR sample. ¹⁹F NMR (470 MHz; THF-d₈) δ_F -140 (d, J = 21.8 Hz), -139.4 (d, J = 21.8 Hz); HRMS calcd for C₂₄H₂₁ClF₂N₄O₅ [M(³⁵Cl)+H]⁺ 519.1241, found 559.1226.

16.3 MDMX Structural biology experimental

16.3.1 General procedures

16.3.1.1 Media supplementation

All cultures were supplemented with an antibiotic, according to the antibiotic selectivity of the pGEX-6P-1 vector and *E. coli* strain used during recombinant protein expression. During IPTG-based induction of protein expression, the lactose analogue IPTG was added to the culture to induce protein expression. Appropriate amounts of IPTG (200 mM) and ampicillin (50 mg/mL) were dissolved in sterile 18.2 MΩ/cm H₂O, before storing at -20 °C until required. Chloramphenicol (34 mg/mL) was dissolved in 100% ethanol and stored at -20 °C.

16.3.1.2 mHBS buffer

To prepare the mHBS buffer, 20 mL of aq. NaCl (5 M), 5 mL of aq. DTT (1 M) and 20 mL of aq. HEPES (1 mM, pH 7.4) were used in 1 L of solution and the pH was brought to 7.4 by addition of aq. NaOH (10 M). The buffer was filtered and degassed before use and, if required, stored at 4 °C for no longer than one week.

16.3.1.3 Glutathione elution buffer

To prepare the glutathione elution buffer, glutathione (0.123g) was dissolved in mHBS (20 mL) and the pH was brought to 7.4 by addition of aq. NaOH (10 M). The buffer was stored at 4 °C and used immediately after preparation.

16.3.1.4 Polyacrylamide gel electrophoresis

SDS-PAGE was used for protein identification and semi-quantitative analysis. Pre-cast 12-well acrylamide gels (RunBlue; 12% for GST-MDMX/GST-MDM2 and 16% for MDMX/MDM2) were used with SDS run buffer (RunBlue). Samples were mixed with SDS loading buffer

(RunBlue) and denatured at 100 °C for 5 min before being loaded onto the gel. PageRuler pre-stained protein ladder (10-170 kDa, Thermo Scientific) was used. Electrophoresis was carried out at 180 V and gels were stained with InstantBlue™ protein stain.

16.3.2 Expression from MDMX and MDM2 gene constructs

1.1.1.1 Transformation of competent Rosetta™ BL21(DE3) pLysS E. coli

Recombinant MDMX pGEX-6P-1 expression vector plasmid were transformed into competent Rosetta™ (DE3)pLys S (Novagen), whilst recombinant MDM2 pGEX-6P-1 expression vector plasmid were transformed into competent BL21(DE3) pLys S *E. coli* (Novagen). Competent cells were mixed with 1 µL of plasmid and incubated on ice for 30 min. The cells were transferred to a water bath at 42 °C for 30 sec, before incubating on ice for 2 min. The cells were recovered through aseptic addition of 200 µL super optimal broth with catabolite repression (SOC) medium and incubated at 37 °C, 200 rpm for 1 h. The recovered cells were aseptically plated onto LB-agar plates supplemented with ampicillin and chloramphenicol and incubated overnight at 37 °C to allow growth of transformed bacterial colonies.

1.1.1.2 Recombinant MDMX expression following IPTG induction

Transformed Rosetta™ BL21(DE3) pLysS *E. coli* colonies were used to inoculate starter cultures containing 10 mL of Terrific Broth (TB), supplemented with ampicillin (20 µL) and chloramphenicol (10 µL). The starter cultures were incubated overnight at 37 °C, 200 rpm before aseptic transfer of a 1% (v/v) inoculum into an appropriate volume of expression media, supplemented with antibiotics. The culture was incubated at 37 °C, 160 rpm and the optical density (OD) of the culture was monitored by spectrometry during growth. Once an OD_{600 nm} of 0.6-1.0 was reached, 200 mM IPTG (1 mL) was added to the culture to induce protein expression. The culture was incubated at 20 °C, 160 rpm overnight.

1.1.1.3 Recombinant MDM2 expression following IPTG induction

BL21 (DE3) *E. coli* glycerol stocks for MDM2₁₇₋₁₂₅^{K51A} and MDM2₁₇₋₁₂₅^{E69K70A} were prepared previously by Judith Reeks and stored at -80 °C. A glycerol stock of BL21 (DE3) pLysS *E. coli* for MDM2₁₇₋₁₀₈^{E69K70A} was prepared and stored similarly. Transformed BL21 *E. coli* cells were

inoculated in starter cultures containing 10 mL of LB, supplemented with ampicillin (20 μ L) (BL21 (DE3)) or ampicillin (20 μ L) and chloramphenicol (10 μ L) (BL21 (DE3) pLysS). The starter cultures were incubated overnight at 37 °C, 200 rpm, before aseptic transfer of a 1% (v/v) inoculum into an appropriate volume of expression media, supplemented with chloramphenicol (1 mL) and/or ampicillin (1 mL). The culture was incubated at 37 °C, 160 rpm, whilst the optical density of the culture was monitored during growth. Once an OD_{600 nm} of 0.6-1.0 was reached, 200 mM IPTG (1 mL) was added to the culture to induce protein expression. The culture was incubated at 20 °C, 160 rpm overnight.

1.1.1.4 Cell harvesting

Following culture, the *E. coli* cells were harvested by centrifugation (5000 \times g, 15 min, 4°C) to give a pellet which was resuspended in mHBS supplemented with a protease inhibitor tablet (Roche; 1 tablet/40 mL), flash-frozen in dry ice and stored at -20 °C until further use.

16.3.3 Protein purification

The resuspended cell pellets were thawed under running water and lysozyme (400 μ L of 25 mg/mL stock), RNAase A (200 μ L of 10 mg/mL stock), DNAase I (200 μ L of 2 mg/mL stock) and MgCl₂ (100 μ L of 2 M stock) were added before sonication (30% amplitude; 20 sec on/40 sec off intervals for 15 min) whilst on ice. The lysed cells were centrifuged (45,000 \times g, 60 min, 4°C) and the supernatant (cell-free extract, CFE) was decanted from the pellet and retained. Diluted CFE samples were heated at 100 °C for 5 min and then analyzed by SDS-PAGE to establish whether the target protein had been overexpressed.

The supernatant was incubated overnight at 4 °C with glutathione Sepharose 4B resin (GE Healthcare, bed volume 2 mL). The mixture was loaded by gravity flow into a column and washed twice with mHBS (15 mL). The GST-MDMX (or GST-MDM2) was eluted with a fresh solution of glutathione in mHBS (20 mL). 3C protease (50:1 protein:3C protease by weight) was added to cleave MDMX or MDM2 from the GST tag and the mixture was incubated overnight at 4 °C. The desired protein was separated from the GST tag using gel filtration chromatography (Äkta Superdex 75 26/60, isocratic flow of mHBS, Äkta FPLC Chromatographic system, UV absorbance 280 nm).

The protein concentration was measured using a UV-vis spectrophotometer NanoDrop 2000 (Thermo Scientific).

16.3.4 Protein preparation for crystallography

The purified protein was incubated overnight at 4 °C with a 1.5× molar excess of inhibitor (20 mM stock in DMSO). Protein mixtures were concentrated using Amicon[®] Ultra-15 (Millipore) centrifugal filter devices (5000 × g, 4 °C) to a concentration between 1 and 20 mg/mL.

Crystallization trays were set up in 2-subwell 96-well plates by pipetting commercial screens (JCSG+ from Molecular Dimensions, Index (Hampton Research), and AmSO4 Suite from Qiagen) from deep well blocks prior to protein addition. Protein mixture and precipitant were mixed in the subwells by a Mosquito[®] robot (100 + 100 nL, 200 + 100 nL, precipitant:protein) using the sitting drop method. Plates were sealed and stored in the Minstrel (Rigaku) automated high-throughput monitoring system at 4 °C for up to five weeks. Crystals were transferred into a solution of 70% precipitant, 30% ethylene glycol, flash cooled in liquid nitrogen and shipped to Diamond Light Source (Oxford, UK) for data collection.

16.3.5 HTRF assay

The experimental detail described below is the final optimized procedure.

The inhibitor solutions (20 mM solution in DMSO) were dispensed in an Echo qualified 384-well low dead volume microplate source plate using a multi-channel pipette. Buffer A (50 mM Tris at pH 7.4, 100 mM NaCl, 100 µg/mL BSA, 1 mM DTT) and buffer B (50 mM Tris at pH 7.4, 100 mM NaCl, 100 µg/mL BSA) were prepared fresh. The inhibitors were dispensed into a 384-well black low-binding round bottom assay plate (Corning) using a Echo[®] Liquid Handler 550 (Labcyte), starting at 500 µM inhibitor (final assay concentration) and decreasing over a semi-log scale. Each well was backfilled with DMSO to a final volume of 250 nL and each condition was in duplicate.

IP3 peptide (300 µM in DMSO) was diluted in buffer A supplemented with 4.2 % DMSO to obtain a 500 nM solution and was added to all the wells on the assay plate (6 µL). GST-

MDMX₂₂₋₁₁₁ (107 μ M stock) was diluted with buffer A, first to 1.07 μ M and subsequently to 25 nM and was added to the plate (4 μ L). Positive (peptide, MDMX and DMSO; no inhibitor) and negative (peptide, buffer A and DMSO; no protein or inhibitor) controls were included. The plate was incubated on a shaking platform for 1 h. The final concentrations were as follows: 10 nM GST-MDMX, 300 nM IP3 peptide, 5 % DMSO. A solution of Tb-anti-GST-antibody (3.3 μ M stock) was prepared in buffer B (20 nM) and added to each well (10 μ L) of the assay plate followed by 45 min incubation on the shaker. The plate was read using PHERAstar FS (BMG Labtech) microplate reader.

16.4 Synthesis of ATAD2 Inhibitors-Experimental Procedures

16.4.1 ATAD2 Biology Procedures

HTRF assay protocol

The ATAD2 bromodomain 981-1108 was expressed with an N-terminal GST fusion from the pGEX-6P-1 plasmid. The plasmids were transformed into BL21 (DE3) pLysS *Escherichia coli* (Novagen) and then the cells grown in luria bertani (LB) media at 37 °C until an OD₆₀₀ of 0.6 was reached. The temperature was reduced to 20 °C and expression induced using 0.2 mM Isopropyl β-D-1-thiogalactopyranoside (IPTG). The cells were harvested after overnight incubation and resuspended in buffer A (20 mM HEPES pH 7.4, 100 mM NaCl, 5 mM Dithiothreitol (DTT)). The cells were lysed by sonication and the lysate cleared by centrifugation (50,000 x g, 4 °C, 1 hr). The protein was passed over 5ml of glutathione Sepharose 4B resin (GE Healthcare) at 4 °C. The resin was then washed with buffer A and the protein eluted with buffer A supplemented with 10 mM glutathione. The protein was then applied to a Superdex 200 26/60 gel filtration column (GE Healthcare) equilibrated in buffer A.

Compounds (dissolved to 100 mM in DMSO) were dispensed into black 384 well assay plates (Corning) over a final concentration range of 2000, 1350, 900, 600, 425, 300, 200, 100, 50, and 25 μM using an Echo 550 (Labcyte). Each well was backfilled to a final volume of 200 nl (for the MDM2 assay), resulting in final DMSO concentrations of 2 %. 5 μl of GST-ATAD2 was added to each well and incubated for 30mins resulting in a final concentration of 5 nM. 5μl of biotinylated-histone H4 peptide (SGRG-K(Ac)-GG-K(Ac)-GLG-K(Ac)-GGA-K(Ac)-RHRKVGG-K(Biotin)) was then added to each well at a final concentration of 500nM. Both GST-ATAD2 and peptide were diluted in buffer B (50 mM Tris pH 7.5, 100 nM NaCl, 1 mM DTT, 100 μg/ml bovine serum albumin (BSA)). The plate was then incubated at room temperature for 30mins and then 5 μl LanthaScreen® Tb-anti-GST Antibody (Life Technologies) at final concentration of 5 nM was added to each well and incubated for an additional 30mins. 5 μl of streptavidin-XLL65 (Cisbio Assay) at a final concentration of 62.5 μM was added to each assay well. Both dyes were diluted in buffer C (50 mM Tris pH 7.5, 100 nM NaCl, 100 μg/ml BSA). The plate was incubated at room temperature for a further 30mins

and then read using a PheraStar FS (BMG Labtech). The data were analysed using Graphpad Prism.

16.4.2 Synthesis of ATAD2 Inhibitors: General Procedures

General Procedure A: Substitution at N1

The relevant compound (1 eq.) and Cs₂CO₃ (3 eq.) were suspended in DMF. The relevant alkyl halide (2.5 eq.) was added and stirred at 100 °C under microwave irradiation for 30 min. The reaction was quenched with water (20 mL) and the aqueous layer was extracted with EtOAc (3×25 mL). The organic layers were combined, dried over MgSO₄ and the solvent removed *in vacuo*.

General Procedure B: Pyridone formation

The relevant pyridine (1 eq.) and alkyl halide (2 eq.) were dissolved in MeCN and the mixture was stirred at 170 °C under microwave irradiation for 1 h. The solvent was removed *in vacuo* and the residue was purified by MPLC.

General Procedure C: Knoevenagel condensation

The relevant compound (1 eq.) was dissolved in THF, the relevant aldehyde (1.1 eq.) and piperidine (1.5-3.1 eq.) were added. The reaction mixture was stirred at 100 °C until the starting material was completely consumed. The solvent was removed *in vacuo* and the residue was purified by MPLC.

General Procedure D: Reduction of an alkene and subsequent methylation

Step A: The relevant Knoevenagel product (1 eq.) was dissolved in THF and MeOH. 10% Pd/C was added and an atmosphere of hydrogen. The mixture was stirred at r.t. until the starting material was completely consumed. The mixture was filtered through a Celite plug using MeOH (3 × 20 mL). The solvent was removed *in vacuo* and the crude was taken forward without further purification.

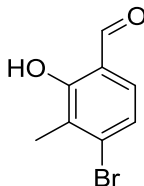
Step B: The crude was dissolved in DMF, Cs₂CO₃ (2-2.5 eq.) and MeI (1.8-2.1 eq.) were added and the mixture was stirred at 60 °C for 1 h. The reaction was quenched with water (20 mL) and the aqueous layer was extracted with EtOAc (3×25 mL). The organic layers were combined, dried over MgSO₄ and the solvent removed *in vacuo*.

General Procedure E: Synthesis of spiro-pyrrolidine derivatives

The relevant spirocyclopropane (1 eq.) and MgI₂ (0.1 eq.) were suspended in THF (1 mL). The relevant triazinane (1.5 eq.-3 eq.) was added and the reaction mixture was stirred at 90 °C until the SM was completely consumed. After cooling to r.t., solvent was removed *in vacuo* and the residue was purified by MPLC.

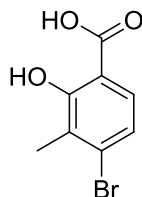
16.4.3 ATAD2 Inhibitors: Synthetic Procedures

4-Bromo-2-hydroxy-3-methylbenzaldehyde (168)



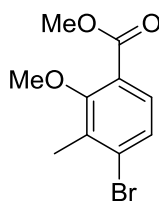
3-Bromo-2-methylphenol (500 mg, 2.67 mmol) was dissolved in MeCN (3.5 mL), MgCl₂ (381 mg, 4.00 mmol) and triethylamine (1.4 mL, 10.01 mmol) were added, respectively. To the solution, paraformaldehyde was added portion wise and the mixture was refluxed for 3 h. After cooling the reaction mixture to r.t., 5% HCl (6 mL) and Et₂O (10 mL) were added and stirred for 10 min. The aqueous layer was extracted with Et₂O (3×40 mL). The organic layers were combined, dried over MgSO₄ and the solvent removed *in vacuo* to get a light brown solid (535 mg, 93%) which did not require further purification. R_f = 0.76 (25% EtOAc/Petrol); m.p. 40-42 °C; λ_{max} (EtOH)/nm 330.2, 270.6; IR ν_{max}/cm⁻¹ 3099 (OH), 3019, 2872, 1635 (C=O); ¹H NMR (500 MHz, DMSO-*d*₆) δ_H 2.34 (3H, s, CH₃), 7.22 (1H, d, *J* = 8.4 Hz, Ar-*H*), 7.25 (1H, d, *J* = 8.4 Hz, Ar-*H*), 9.83 (1H, s, OH), 11.55 (1H, s, CHO); ¹³C NMR (125 MHz, CDCl₃) δ_C 14.8 (CH₃), 119.0 (C-Ar), 123.9 (CH-Ar), 127.5 (C-Ar), 131.4 (CH-Ar), 134.7 (C-Ar), 160.2 (C-Ar), 196.1 (CHO).

4-Bromo-2-hydroxy-3-methylbenzoic acid (169)



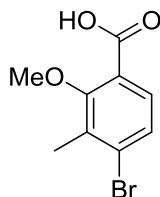
Compound **168** (480 mg, 2.23 mmol) was dissolved in MeCN (20 mL). A solution of sodium chlorite (344 mg, 3.80 mmol) in water (4 mL) and a solution of sulfamic acid (369 mg, 3.80 mmol) in water (4 mL) were added dropwise, respectively and the mixture was stirred at r.t. for 8 h. The solvent was evaporated *in vacuo*, water (30 mL) was added and the aqueous layer was extracted with EtOAc (3×30 mL). The organic layers were combined, dried over MgSO₄ and the solvent removed *in vacuo*. Purification by MPLC on SiO₂ (DCM:MeOH, 0-20%) gave a beige solid (450 mg, 88%). $R_f = 0.39$ (20% MeOH/DCM); m.p. 206-209 °C; λ_{\max} (EtOH)/nm 307.0, 248.4; ¹H NMR (500 MHz, DMSO-*d*₆) δ_H 2.27 (3H, s, CH₃), 7.17 (1H, d, $J = 8.5$ Hz, Ar-*H*), 7.57 (1H, d, $J = 8.5$ Hz, Ar-*H*), COOH and OH could not be seen; ¹³C NMR (125 MHz, DMSO-*d*₆) δ_C 15.6 (CH₃), 112.1 (C-Ar), 123.0 (CH-Ar), 126.1 (C-Ar), 128.9 (CH-Ar), 131.6 (C-Ar), 160.5 (C-Ar), 172.6 (COOH); LRMS (ES⁻) m/z 229.0 [(M(⁷⁹Br)-H)]⁻, 231.0 [(M(⁸¹Br)-H)]⁻.

Methyl 4-bromo-2-methoxy-3-methylbenzoate (170)



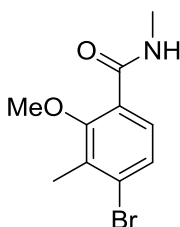
Compound **169** (190 mg, 0.83 mmol) was dissolved in DMF (6 mL), MeI (0.13 mL, 2.15 mmol) was added and stirred at r.t. for 18 h. Water (30 mL) was added and the aqueous layer was extracted with EtOAc (3×30 mL). The organic layers were combined, dried over MgSO₄ and the solvent removed *in vacuo*. Purification by MPLC on SiO₂ (DCM:MeOH, 0-7%) gave a light yellow oil (125 mg, 58%). $R_f = 0.76$ (5% MeOH/DCM); ¹H NMR (500 MHz, CDCl₃) δ_H 2.39 (3H, s, CH₃), 3.82 (3H, s, OCH₃), 3.90 (3H, s, COOCH₃), 7.37 (1H, d, $J = 8.4$ Hz, Ar-*H*), 7.52 (1H, dd, $J = 8.4$ Hz, Ar-*H*); ¹³C NMR (125 MHz, CDCl₃) δ_C 16.2 (CH₃), 52.3 (COOCH₃), 62.0 (OCH₃), 123.8 (C-Ar), 127.9 (CH-Ar), 129.4 (CH-Ar), 130.5 (C-Ar), 133.5 (C-Ar), 158.9 (C-Ar), 166.2 (C=O); LRMS (ES⁺) m/z 259.1 [(M(⁷⁹Br)+H)]⁺, 261.1 [(M(⁸¹Br)+H)]⁺.

4-bromo-2-methoxy-3-methylbenzoic acid (171)



Compound **170** (110 mg, 0.42 mmol) was dissolved in MeOH (4 mL) and 1 M NaOH in water (4 mL) was added and the mixture was stirred at 60 °C for 18 h. The solvent was evaporated *in vacuo*, water (30 mL) was added and the solution was acidified with 1 M HCl. The aqueous layer was extracted with EtOAc (3×30 mL). The organic layers were combined, dried over MgSO₄ and the solvent removed *in vacuo* to get a beige solid (97 mg, 95%). R_f = 0.26 (5% MeOH/DCM); m.p. 135-138 °C; ¹H NMR (500 MHz, DMSO-*d*₆) δ_H 2.32 (3H, s, CH₃), 3.75 (3H, s, OCH₃), 7.45 (1H, d, *J* = 8.4 Hz, Ar-*H*), 7.48 (1H, d, *J* = 8.4 Hz, Ar-*H*), 13.09 (1H, br s, COOH); ¹³C NMR (125 MHz, DMSO-*d*₆) δ_C 16.4 (CH₃), 62.2 (OCH₃), 125.9 (C-Ar), 128.1 (CH-Ar), 129.1 (C-Ar), 129.8 (C-Ar), 133.0 (C-Ar), 158.5 (C-Ar), 167.2 (COOH); HRMS calcd for C₉H₁₀BrO₃ [M(⁷⁹Br)+H]⁺ 244.9808, found 244.9812.

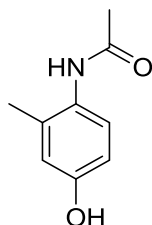
4-Bromo-2-methoxy-*N*,3-dimethylbenzamide (172)



Compound **171** (60 mg, 0.24 mmol), DIC (40 μL, 0.28 mmol) and DMAP (2.9 mg, 0.024 mmol) were dissolved in THF (2.5 mL). A 2 M solution of methylamine in THF (0.4 mL, 0.80 mmol) was added and the reaction mixture was stirred at r.t. for 18 h. The carboxylic acid (93% by LC-MS) was still remaining, therefore, HATU (182 mg, 0.48 mmol) was added and the mixture was stirred at 60 °C for 4 h and at r.t. for 18 h. Water (30 mL) was added and the aqueous layer was extracted with EtOAc (3×20 mL). The organic layers were combined, dried over MgSO₄ and the solvent removed *in vacuo*. Purification by MPLC on SiO₂ (DCM:MeOH, 0-5%) gave a white solid (50 mg, 71%). R_f = 0.71 (5% MeOH/DCM); m.p. 86-89 °C; λ_{max} (EtOH)/nm 242.4; IR ν_{max}/cm⁻¹ 3346 (NH), 2965, 2935, 2865, 1635 (C=O); ¹H NMR (500 MHz, CDCl₃) δ_H 2.39 (3H, s, CH₃), 3.02 (3H, d, *J* = 4.8 Hz, NHCH₃), 3.75 (3H, s, OCH₃), 7.43 (1H, d, *J* = 8.5 Hz, Ar-*H*), 7.66 (1H, br s, NH), 7.78 (1H, d, *J* = 8.5 Hz, Ar-*H*); ¹³C NMR (125 MHz, CDCl₃) δ_C

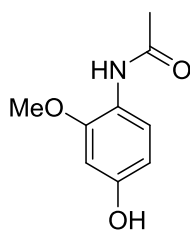
16.2 (CH₃), 26.7 (NHCH₃), 61.8 (OCH₃), 125.8 (C-Ar), 128.9 (CH-Ar), 129.3 (C-Ar), 129.8 (CH-Ar), 132.0 (C-Ar), 156.8 (C-Ar), 166.6 (C=O); HRMS calcd for C₁₀H₁₃BrNO₂ [M(⁷⁹Br)-H]⁻ 258.0124, found 258.0126.

***N*-(4-hydroxy-2-methylphenyl)acetamide (175)**



3-Methyl-4-nitrophenol (500 mg, 3.26 mmol) was dissolved in methanol (50 mL) and reduced using an H-Cube continuous flow reactor (Thalesnano Inc.) with a Pd/C CatCart (r.t., 1 mL/min). The solvent was removed *in vacuo* after 24 h and the residue was dissolved in AcOH (25 mL) and acetic anhydride (0.5 mL) and the mixture was stirred at r.t. for 30 min. The solvent was evaporated *in vacuo* and the residue was purified by MPLC on SiO₂ (DCM:MeOH, 0-15%) to give a brown solid (428 mg, 80%). R_f = 0.21 (5% MeOH/DCM); m.p. 85-90 °C; λ_{max} (EtOH)/nm 229.8; IR ν_{max}/cm⁻¹ 3239-3181 (NH and OH), 3059, 2922, 2817, 1623 (C=O); ¹H NMR (500 MHz, DMSO-*d*₆) δ_H 1.99 (3H, s, COCH₃), 2.08 (3H, s, CH₃), 6.53 (1H, dd, *J* = 8.5 and 2.6 Hz, Ar-*H*), 6.59 (1H, d, *J* = 2.6 Hz, Ar-*H*), 7.02 (1H, d, *J* = 8.5 Hz, Ar-*H*), 9.07 (1H, s, NH), 9.17 (1H, s, OH); ¹³C NMR (125 MHz, DMSO-*d*₆) δ_C 18.4 (CH₃), 23.4 (COCH₃), 113.0 (CH-Ar), 117.0 (CH-Ar), 127.5 (CH-Ar), 128.4 (C-Ar), 134.4 (C-Ar), 155.3 (C-Ar), 168.6 (COCH₃); HRMS calcd for C₉H₁₂NO₂ [M+H]⁺ 166.0863, found 166.0857.

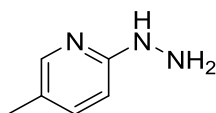
***N*-(4-hydroxy-2-methoxyphenyl)acetamide (178)**



3-Methoxy-4-nitrophenol (200 mg, 1.28 mmol) was dissolved in methanol (18 mL) and reduced using an H-Cube[®] continuous flow reactor (Thalesnano Inc.) with a Pd/C CatCart (r.t., 1 mL/min). The solvent was removed *in vacuo* after 24 h and the residue was dissolved in AcOH (9 mL) and acetic anhydride (0.18 mL) and the mixture was stirred at r.t. for 30 min. The solvent

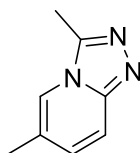
was evaporated *in vacuo* and the residue was purified by MPLC on SiO₂ (DCM:MeOH, 0-15%) which gave a brown solid (155 mg, 73%). $R_f=0.31$ (5% MeOH/DCM); λ_{\max} (EtOH)/nm 285.4, 250.4; IR $\nu_{\max}/\text{cm}^{-1}$ 3265 (OH), 2936, 2844, 1597 (C=O); ¹H NMR (500 MHz, DMSO-*d*₆) δ_H 1.99 (3H, s, COCH₃), 3.74 (3H, s, OCH₃), 6.28 (1H, dd, $J = 8.5$ and 2.5 Hz, Ar-*H*), 6.42 (1H, d, $J = 2.5$ Hz, Ar-*H*), 7.46 (1H, d, $J = 8.5$ Hz, Ar-*H*), 8.87 (1H, s, NH), 9.27 (1H, s, OH); ¹³C NMR (125 MHz, DMSO-*d*₆) δ_C 23.9 (COCH₃), 55.8 (OCH₃), 99.7 (CH-Ar), 106.5 (CH-Ar), 119.2 (C-Ar), 124.9 (CH-Ar), 152.2 (C-Ar), 155.4 (C-Ar), 168.4 (COCH₃); HRMS calcd for C₉H₁₂NO₃ [M+H]⁺ 182.0812, found 182.0808.

2-Hydrazinyl-5-methylpyridine (183)



2-Fluoro-5-methylpyridine (500 mg, 4.50 mmol) was dissolved in Ethanol (10 mL), hydrazine hydrate (2.2 mL, 45 mmol) was added and the reaction mixture was refluxed for 24 h. Starting material was still remaining, therefore, hydrazine hydrate (2.2 mL, 45 mmol) was added and the mixture was refluxed for 48 h. The solvent was removed *in-vacuo* and the residue was purified by MPLC on SiO₂ (DCM:MeOH, 0-5%) which gave a beige solid (240 mg, 43%); ¹H NMR (500 MHz, DMSO-*d*₆) δ_H 2.11 (3H, s, CH₃), 4.04 (2H, br s, NH₂), 6.63 (1H, d, $J = 8.5$ Hz, Ar-*H*), 7.11 (1H, br s, NH), 7.29 (1H, dd, $J = 8.5$ and 2.3 Hz, Ar-*H*), 7.81-7.83 (1H, m, Ar-*H*); ¹³C NMR (125 MHz, DMSO-*d*₆) δ_C 17.5 (CH₃), 106.7 (CH-Ar), 121.3 (C-Ar), 138.2 (CH-Ar), 147.1 (CH-Ar), 160.8 (C-Ar).

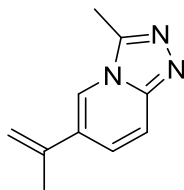
3,6-Dimethyl-[1,2,4]triazolo[4,3-*a*]pyridine (182)



Compound **183** (235 mg, 1.59 mmol) was dissolved in acetic acid (5 mL) and acetic anhydride (5 mL). The solution was refluxed for 48 h. After cooling to r.t., the solvent was removed *in vacuo* and the residue was purified by MPLC on SiO₂ (DCM:MeOH, 0-7%). The purification was repeated to get a white solid (45 mg, 16%). $R_f=0.35$ (5% MeOH/DCM); λ_{\max} (EtOH)/nm 289.0, 212.0; IR $\nu_{\max}/\text{cm}^{-1}$ 3033, 2925, 2868; ¹H NMR (500 MHz, DMSO-*d*₆) δ_H 2.30 (3H, d, J

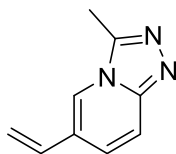
= 0.9 Hz, CH_3 -Pyridine), 2.64 (3H, s, CH_3 -Triazole), 7.20 (1H, dd, $J = 9.3$ and 1.3 Hz, Ar- H), 7.62 (1H, d, $J = 9.3$ Hz, Ar- H), 8.15-8.18 (1H, m, Ar- H); ^{13}C NMR (125 MHz, DMSO- d_6) δ_C 10.2 (CH_3 -Triazole), 17.9 (CH_3 -Pyridine), 114.9 (CH-Ar), 121.1 (CH-Ar), 122.9 (C-Ar), 130.7 (CH-Ar), 143.4 (C-Ar), 148.8 (C-Ar); HRMS calcd for $C_8H_{10}N_3$ $[M+H]^+$ 148.0869, found 148.0869.

3-Methyl-6-(prop-1-en-2-yl)-[1,2,4]triazolo[4,3-*a*]pyridine (185)



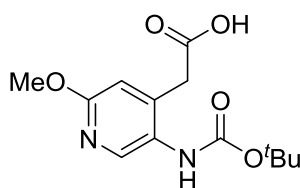
6-Bromo-3-methyl-[1,2,4]triazolo[4,3-*a*]pyridine (100 mg, 0.47 mmol), isopropenylboronic acid pinacol ester (0.13 mL, 0.71 mmol), NaOH (19 mg, 0.47 mmol), *N,N*-dicyclohexylmethylamine (0.1 mL, 0.47 mmol) were suspended in THF (2.6 mL). The reaction mixture was sparged for 30 min with nitrogen, [1,1'-*bis*(diphenylphosphino)ferrocene]dichloropalladium(II), complex with dichloromethane (38 mg, 0.047 mmol) was added and the suspension was sparged with nitrogen for a further 15 min. The reaction mixture was heated at 95 °C for 2.5 h, cooled to r.t, and filtered through a pad of Celite using MeOH. The solvent was removed *in vacuo* and the residue was purified by MPLC on SiO_2 (DCM:MeOH, 0-15%) which gave a white solid (50 mg, 62%). $R_f = 0.36$ (5% MeOH/DCM); λ_{max} (EtOH)/nm 282.6, 238.6; IR ν_{max}/cm^{-1} 2921, 2852, 2640; 1H NMR (500 MHz, DMSO- d_6) δ_H 2.18 (3H, s, CH_3), 2.71 (3H, s, CH_3 -Triazole), 5.25 (1H, s, $1 \times C=CH_2$), 5.63 (1H, s, $1 \times C=CH_2$), 7.64 (1H, dd, $J = 9.7$ and 1.6 Hz, $1 \times Ar-H$), 7.68 (1H, dd, $J = 9.7$ and 1.0 Hz, $1 \times Ar-H$), 8.23 (1H, ap s, Ar- H); ^{13}C NMR (125 MHz, DMSO- d_6) δ_C 10.3 (CH_3 -Triazole), 21.4 (CH_3), 115.0 (CH-Ar), 115.0 (C= CH_2), 120.4 (CH-Ar), 126.2 (CH-Ar), 126.3 (C-Ar), 138.9 (C= CH_2), 144.7 (C-Ar), 148.8 (C-Ar); LRMS (ES^+) m/z 174.2 $[(M+H)^+]$.

3-Methyl-6-vinyl-[1,2,4]triazolo[4,3-*a*]pyridine (184)



6-Bromo-3-methyl-[1,2,4]triazolo[4,3-*a*]pyridine (100 mg, 0.47 mmol), vinylboronic acid pinacol ester (0.12 mL, 0.71 mmol), NaOH (19 mg, 0.47 mmol), *N,N*-dicyclohexylmethylamine (0.1 mL, 0.47 mmol) were suspended in THF (3 mL). The reaction mixture was sparged for 30 min with nitrogen, [1,1'-*bis*(diphenylphosphino)ferrocene]dichloropalladium(II), complex with dichloromethane (38 mg, 0.047 mmol) was added and the suspension was sparged with nitrogen for a further 15 min. The reaction mixture was heated at 95 °C for 2.5 h, cooled to r.t, and filtered through a pad of celite using MeOH. The solvent was removed *in vacuo* and the residue was purified by MPLC on SiO₂ (DCM:MeOH, 0-10%) followed by another purification by MPLC (H₂O:MeCN, reversed phase with 0.1% HCOOH modifier, 0-80%) to give a beige solid (38 mg, 51%). R_f = 0.27 (5% MeOH/DCM); ¹H NMR (500 MHz, DMSO-*d*₆) δ_H 2.67 (3H, s, CH₃-Triazole), 5.40 (1H, br d, *J* = 10.9 Hz, 1×CH=CH₂), 5.96 (1H, br d, *J* = 17.5 Hz, 1×CH=CH₂), 6.77 (1H, dd, 17.5 and 10.9 Hz, CH=CH₂), 7.66 (1H, dd, *J* = 9.5 and 1.4 Hz, Ar-H), 7.70 (1H, d, *J* = 9.5 Hz, Ar-H), 8.40 (1H, s, Ar-H); ¹³C NMR (125 MHz, DMSO-*d*₆) δ_C 10.2 (CH₃-Triazole), 115.5 (CH-Ar), 116.3 (CH=CH₂), 122.6 (CH-Ar), 123.9 (C-Ar), 124.9 (CH-Ar), 132.6 (CH=CH₂), 144.5 (C-Ar), 149.1 (C-Ar); LRMS (ES⁺) *m/z* 160.2 [(M+H)⁺].

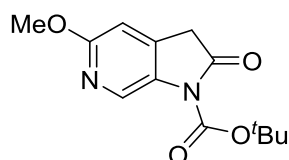
2-(5-((*Tert*-butoxycarbonyl)amino)-2-methoxypyridin-4-yl)acetic acid (190)



Compound **189** (4 g, 16.78 mmol) was dissolved in THF (71 mL) and cooled to -78 °C. 1.4 M *sec*-BuLi in cyclohexane (36 mL, 50.34 mmol) was added dropwise and the reaction mixture was stirred at -78 °C for 15 min. 5-6 Pellets of dry ice were added and the reaction mixture was cooled to r.t. over a period of 45 min. The reaction was quenched with water (50 mL) and saturated NaHCO₃ (50 mL). The aqueous layer was extracted with EtOAc (2 × 100 mL). The aqueous layer was collected and acidified with 2 M HCl, stirred for 15 min and extracted with

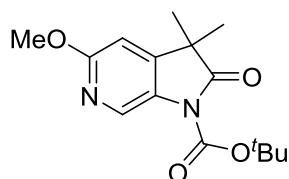
EtOAc (2 × 100 mL). The organic layers were combined, dried over MgSO₄ and the solvent removed *in vacuo* to get an off-white solid (3.5 g, 74%). R_f = 0.42 (20% MeOH/DCM); m.p. 116.120 °C; λ_{max} (EtOH)/nm 284.2, 234.6; IR ν_{max}/cm⁻¹ 3309, (NH), 2981, 2939, 2872, 2782, 1690 (C=O); ¹H NMR (500 MHz, DMSO-*d*₆) δ_H 1.43 (9H, s, C(CH₃)₃), 3.58 (2H, s, CH₂COOH), 3.82 (3H, s, OCH₃), 6.74 (1H, s, 1×Pyridine-*H*), 7.97 (1H, s, 1×Pyridine-*H*), 8.62 (1H, br s, NH), 12.44 (1H, br s, COOH); ¹³C NMR (125 MHz, DMSO-*d*₆) δ_C 28.6 (C(CH₃)₃), 36.9 (CH₂CO), 53.7 (OCH₃), 79.4 (C(CH₃)₃), 111.9 (CH-Pyridine), 128.4 (C-Pyridine), 143.7 (CH-Pyridine), 144.4 (C-Pyridine), 154.5 (COO^tBu), 161.6 (Pyridine-C-OMe), 171.6 (COOH); HRMS calcd for C₁₃H₁₉N₂O₅ [M+H]⁺ 283.1288, found 283.1288.

***Tert*-butyl 5-methoxy-2-oxo-2,3-dihydro-1*H*-pyrrolo[2,3-*c*]pyridine-1-carboxylate (191)**



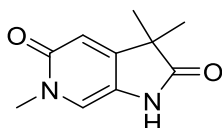
Compound **190** (1.47 g, 5.20 mmol), tetrabutylammonium acetate (50 mg, 0.16 mmol) were dissolved in acetic anhydride (27 mL) and the mixture was stirred at 65 °C for 1 h. The solvent was removed *in vacuo*, water (30 mL) was added and the aqueous layer was extracted with DCM (3×40 mL). The organic layers were combined, washed with NaHCO₃ (3×30 mL), dried over MgSO₄ and evaporated *in vacuo*. Purification by MPLC on SiO₂ (DCM:MeOH, 0-5%) gave a white solid (1.11 g, 81%). R_f = 0.71 (5% MeOH/DCM); m.p. 161-163 °C; λ_{max} (EtOH)/nm 338.2, 230.0; IR ν_{max}/cm⁻¹ 3309, (NH), 2981, 2939, 2872, 2782, 1690 (C=O), 1628 (C=O); ¹H NMR (500 MHz, DMSO-*d*₆) δ_H 1.57 (9H, s, C(CH₃)₃), 3.76 (2H, d, *J* = 1.0 Hz, CH₂CO), 3.83 (3H, s, OCH₃), 6.82 (1H, m, 1×Pyridine-*H*), 8.37 (1H, s, 1×Pyridine-*H*); ¹³C NMR (125 MHz, DMSO-*d*₆) δ_C 28.1 (C(CH₃)₃), 36.6 (CH₂CO), 53.8 (OCH₃), 84.2 (C(CH₃)₃), 106.9 (CH-Pyridine), 131.1 (CH-Pyridine), 133.4 (C-Pyridine), 138.4 (C-Pyridine), 148.9 (COO^tBu), 160.3 (Pyridine-C-OMe), 171.7 (C=O Pyrrolidinone); HRMS calcd for C₁₃H₁₇N₂O₄ [M+H]⁺ 265.1183, found 265.1187.

Tert-butyl 5-methoxy-3,3-dimethyl-2-oxo-2,3-dihydro-1H-pyrrolo[2,3-c]pyridine-1-carboxylate (192)



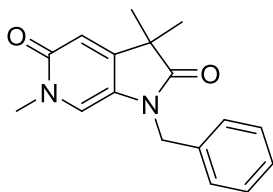
Compound **191** (1.10 g, 4.16 mmol) and Cs_2CO_3 (3 g, 9.15 mmol) were suspended in MeCN (29 mL). MeI (0.65 mL, 10.4 mmol) was added and stirred at 60 °C for 3 h. The insoluble solids were removed by filtration using EtOAc and the filtrate was evaporated *in vacuo*. The residue was purified by MPLC on SiO_2 (Petrol:EtOAc, 0-20%) to get a white solid (945 mg, 78%). $R_f = 0.77$ (5% MeOH/DCM); m.p. 175-178 °C; λ_{max} (EtOH)/nm 295.0, 233.0; IR $\nu_{\text{max}}/\text{cm}^{-1}$ 2983, 2936, 1785 (C=O), 1630 (C=O); ^1H NMR (500 MHz, CDCl_3) δ_{H} 1.41 (6H, s, $2\times\text{CH}_3$), 1.65 (9H, s, $\text{C}(\text{CH}_3)_3$), 3.92 (3H, s, OCH_3), 6.62 (1H, d, $J = 0.6$ Hz, $1\times\text{Pyridine-H}$), 8.54 (1H, d, $J = 0.6$ Hz, $1\times\text{Pyridine-H}$); ^{13}C NMR (125 MHz, CDCl_3) δ_{C} 24.8 ($2\times\text{CH}_3$), 28.1 ($\text{C}(\text{CH}_3)_3$), 44.7 ($\text{C}(\text{CH}_3)_2$), 53.7 (OCH_3), 84.8 ($\text{C}(\text{CH}_3)_3$), 104.8 (CH-Pyridine), 130.2 (C-Pyridine), 132.1 (CH-Pyridine), 147.3 (C-Pyridine), 148.9 (COO^tBu), 161.1 (Pyridine-C-OMe), 178.4 (C=O pyrrolidinone); HRMS calcd for $\text{C}_{15}\text{H}_{21}\text{N}_2\text{O}_4$ $[\text{M}+\text{H}]^+$ 293.1496, found 293.1497.

3,3,6-Trimethyl-1,6-dihydro-2H-pyrrolo[2,3-c]pyridine-2,5(3H)-dione (5)



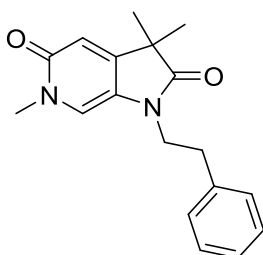
Compound **192** (630 mg, 2.15 mmol) was dissolved in MeCN (15 mL) and MeI (0.33 mL, 5.37 mmol) was added. The mixture was stirred at 170 °C under microwave irradiation for 1 h. The solvent was removed *in vacuo* and the residue was purified by MPLC on SiO_2 (DCM:MeOH, 0-10%) to get a white solid (148 mg, *quant.*). $R_f = 0.15$ (5% MeOH/DCM); m.p. 162-163 °C; λ_{max} (EtOH)/nm 336.2, 255.2, 218.6; IR $\nu_{\text{max}}/\text{cm}^{-1}$ 3455 (NH), 3081, 3019, 2960, 2926, 2705, 2663, 1705 (C=O), 1589 (C=O); ^1H NMR (500 MHz, $\text{DMSO-}d_6$) δ_{H} 1.24 (6H, s, $2\times\text{CH}_3$), 3.36 (3H, s, OCH_3), 6.48 (1H, s, $1\times\text{Pyridone-H}$), 7.14 (1H, s, $1\times\text{Pyridone-H}$), 10.25 (1H, s, NH); ^{13}C NMR (125 MHz, $\text{DMSO-}d_6$) δ_{C} 24.0 ($2\times\text{CH}_3$), 37.1 ($\text{C}(\text{CH}_3)_2$), 44.0 (NCH_3), 114.1 (CH-Pyridone), 116.9 (CH-Pyridone), 123.4 (C-Pyridone), 153.8 (C-Pyridone), 161.0 (C=O pyridone), 180.2 (C=O pyrrolidinone); HRMS calcd for $\text{C}_{10}\text{H}_{13}\text{N}_2\text{O}_2$ $[\text{M}+\text{H}]^+$ 193.0972, found 193.0968.

1-Benzyl-3,3,6-trimethyl-1,6-dihydro-2H-pyrrolo[2,3-c]pyridine-2,5(3H)-dione (193)



Compound **5** (50 mg, 0.26 mmol) was dissolved in DMF (3 mL). NaH (60% in mineral oil, 31 mg, 0.78 mmol) was added portion wise and the mixture was stirred at r.t. for 15 min. Benzyl bromide (62 μ L, 0.52 mmol) was added and the reaction was stirred at r.t. for 3 h. The reaction was quenched with water (20 mL) and the aqueous layer was extracted with EtOAc (3 \times 20 mL). The organic layers were combined, dried over MgSO₄, the solvent removed *in vacuo* and the residue was purified by MPLC on SiO₂ (DCM:MeOH, 0-5%) to get a beige solid (45 mg, 61%). R_f =0.35 (5% MeOH/DCM); m.p. 122-124°C; λ_{max} (EtOH)/nm 257.8, 236.8; IR ν_{max}/cm^{-1} 3090, 3056, 2972, 2924, 2852, 1703 (C=O), 1593 (C=O); ¹H NMR (500 MHz, DMSO-*d*₆) δ_H 1.32 (6H, s, 2 \times CH₃), 3.32 (3H, s, N-CH₃), 4.75 (2H, s, CH₂Ph), 6.57 (1H, s, 1 \times Pyridone-*H*), 7.28-7.37 (6H, m, 6 \times Ar*H*); ¹³C NMR (125 MHz, DMSO-*d*₆) δ_C 24.2 (2 \times CH₃), 37.3 (N-CH₃), 43.2 (CH₂-phenyl), 43.9 (C(CH₃)₂), 114.2 (CH-Pyridone), 117.2 (CH-Pyridone), 124.3 (C-Ar), 127.6 (2 \times C-Ar), 127.9 (C-Ar), 129.2 (2 \times C-Ar), 136.3 (C-Ar), 152.2 (C-Ar), 161.2 (C=O pyridone), 178.3 (C=O pyrrolidinone); HRMS calcd for C₁₇H₁₉N₂O₂ [M+H]⁺ 283.1441, found 283.1440.

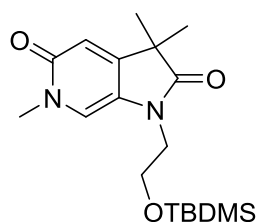
3,3,6-Trimethyl-1-phenethyl-1,6-dihydro-2H-pyrrolo[2,3-c]pyridine-2,5(3H)-dione (194)



Compound **5** (50 mg, 0.26 mmol) was dissolved in DMF (3 mL). NaH (60% in mineral oil, 31 mg, 0.78 mmol) was added portion wise and the mixture was stirred at r.t. for 15 min. (2-bromoethyl)benzene (90 μ L, 0.65 mmol) was added and the reaction was stirred at r.t. for 3 h. The reaction was quenched with water (20 mL) and the aqueous layer was extracted with EtOAc (3 \times 20 mL). The organic layers were combined, dried over MgSO₄, the solvent removed *in vacuo* and the residue was purified by MPLC on SiO₂ (DCM:MeOH, 0-5%) to get a beige solid (23 mg, 30%). R_f =0.36 (5% MeOH/DCM); λ_{max} (EtOH)/nm 337.0, 258.2; IR ν_{max}/cm^{-1} 3059,

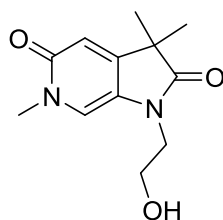
2967, 2926, 2866, 1706 (C=O), 1590 (C=O); ^1H NMR (500 MHz, CDCl_3) δ_{H} 1.28 (6H, s, $2\times\text{CH}_3$), 2.94 (2H, t, $J = 6.9$ Hz, $\text{CH}_2\text{CH}_2\text{Ph}$), 3.39 (3H, s, N- CH_3), 3.82 (2H, t, $J = 6.9$ Hz, $\text{CH}_2\text{CH}_2\text{Ph}$), 6.26 (1H, s, $1\times\text{Pyridone-H}$), 6.44 (1H, s, $1\times\text{Pyridone-H}$), 7.15-7.17 (2H, m, $2\times\text{ArH}$), 7.22-7.29 (3H, m, $3\times\text{ArH}$); ^{13}C NMR (125 MHz, CDCl_3) δ_{C} 24.0 ($2\times\text{CH}_3$), 33.7 ($\text{CH}_2\text{CH}_2\text{Ph}$), 37.6 (N- CH_3), 42.0 ($\text{CH}_2\text{CH}_2\text{Ph}$), 43.8 ($\text{C}(\text{CH}_3)_2$), 114.6 (CH-Pyridone), 114.7 (CH-Pyridone), 125.6 (C-Ar), 126.9 (C-Ar), 128.7 ($2\times\text{C-Ar}$), 129.0 ($2\times\text{C-Ar}$), 138.2 (C-Ar), 152.2 (C-Ar), 161.7 (C=O pyridone), 178.3 (C=O pyrrolidinone); HRMS calcd for $\text{C}_{18}\text{H}_{21}\text{N}_2\text{O}_2$ $[\text{M}+\text{H}]^+$ 297.1598, 297.1597.

1-(2-((*Tert*-butyldimethylsilyl)oxy)ethyl)-3,3,6-trimethyl-1,6-dihydro-2*H*-pyrrolo[2,3-*c*]pyridine-2,5(3*H*)-dione (201)



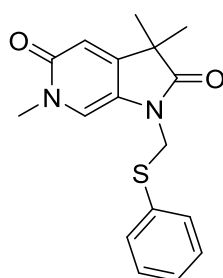
Prepared according to general procedure A using compound **5** (100 mg, 0.52 mmol), Cs_2CO_3 (508 mg, 1.56 mmol), compound **200** (311 mg, 1.30 mmol) and DMF (4.5 mL). Purification by MPLC on SiO_2 (DCM:MeOH, 0-5%) gave an orange viscous liquid (120 mg, 55%). $R_f = 0.20$ (5% MeOH/DCM); λ_{max} (EtOH)/nm 336.2, 257.6, 219.8; IR $\nu_{\text{max}}/\text{cm}^{-1}$ 2929, 2855, 1703 (C=O), 1589 (C=O); ^1H NMR (500 MHz, $\text{DMSO-}d_6$) δ_{H} 0.00 (6H, s, $2\times\text{CH}_3$ of TBDMS), 0.82 (9H, s, $\text{C}(\text{CH}_3)_3$ of TBDMS), 1.30 (6H, s, $2\times\text{CH}_3$), 3.42 (3H, s, N- CH_3), 3.71 (2H, t, $J = 5.3$ Hz, $\text{CH}_2\text{CH}_2\text{OTBDMS}$), 3.83 (2H, t, $J = 5.3$ Hz, $\text{CH}_2\text{CH}_2\text{OTBDMS}$), 6.56 (1H, s, $1\times\text{Pyridone-H}$), 7.48 (1H, s, $1\times\text{Pyridone-H}$); ^{13}C NMR (125 MHz, $\text{DMSO-}d_6$) δ_{C} -5.1 ($2\times\text{CH}_3$ of TBDMS), 18.2 ($\text{C}(\text{CH}_3)_3$ of TBDMS), 24.2 ($2\times\text{CH}_3$), 26.0 ($\text{C}(\text{CH}_3)_3$ of TBDMS), 37.2 (N- CH_3), 42.6 ($\text{CH}_2\text{CH}_2\text{OTBDMS}$), 43.7 ($\text{C}(\text{CH}_3)_2$), 60.0 ($\text{CH}_2\text{CH}_2\text{OTBDMS}$) 113.7 (CH-Pyridone), 117.6 (CH-Pyridone), 125.1 (C-Pyridone), 152.2 (C-Pyridone), 161.1 (C=O pyridone), 178.1 (C=O pyrrolidinone); HRMS calcd for $\text{C}_{18}\text{H}_{31}\text{N}_2\text{O}_3\text{Si}$ $[\text{M}+\text{H}]^+$ 351.2098, found 351.2100.

1-(2-Hydroxyethyl)-3,3,6-trimethyl-1,6-dihydro-2H-pyrrolo[2,3-c]pyridine-2,5(3H)-dione (202)



Compound **201** (98 mg, 0.28 mmol) was dissolved in THF (2.5 mL). 1 M TBAF in THF (2.5 mL) was added and the reaction mixture was stirred at r.t. for 18 h. The solvent was removed *in vacuo* and the residue was purified by MPLC on SiO₂ (DCM:MeOH, 0-20%) to get a white solid (56 mg, 90%). R_f = 0.30 (15% MeOH/DCM); m.p. 140-142°C; λ_{max} (EtOH)/nm 238.0, 258.6; IR ν_{max}/cm⁻¹ 3271 (OH), 3043, 2973, 2932, 2870, 1708, (C=O), 1571 (C=O); ¹H NMR (500 MHz, DMSO-*d*₆) δ_H 1.26 (6H, s, 2×CH₃), 3.39 (3H, s, CH₃), 3.57-3.60 (4H, m, CH₂), 4.82 (1H, t, *J* = 5.4 Hz, OH), 6.52 (1H, s, 1×Pyridone-*H*), 7.44 (1H, s, 1×Pyridone-*H*).; ¹³C NMR (125 MHz, DMSO-*d*₆) δ_C 24.2 (2×CH₃), 37.3 (N-CH₃), 42.9 (CH₂CH₂N), 43.7 (C(CH₃)₂), 58.0 (CH₂CH₂O), 113.7 (CH-Pyridone), 117.3 (CH-Pyridone), 125.2 (C-Pyridone), 152.4 (C-Pyridone), 161.1 (C=O pyridone), 178.2 (C=O pyrrolidinone); HRMS calcd for C₁₂H₁₇N₂O₃ [M+H]⁺ 237.1234, found 237.1232.

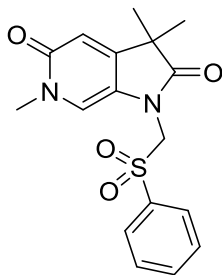
3,3,6-Trimethyl-1-((phenylthio)methyl)-1,6-dihydro-2H-pyrrolo[2,3-c]pyridine-2,5(3H)-dione (197)



Prepared according to general procedure A using compound **5** (50 mg, 0.26 mmol), Cs₂CO₃ (254 mg, 0.78 mmol), chloromethyl phenyl sulphide (0.09 mL, 0.65 mmol) and DMF (2 mL). Purification by MPLC on SiO₂ (DCM:MeOH, 0-5%) gave a white solid (61 mg, 75%). R_f = 0.35 (5% MeOH/DCM); m.p. 55-57 °C; λ_{max} (EtOH)/nm 335.2, 252.4; IR ν_{max}/cm⁻¹ 3422, 3055, 2968, 2927, 2866, 1712 (C=O), 1586 (C=O); ¹H NMR (500 MHz, DMSO-*d*₆) δ_H 1.09 (6H, s, 2×CH₃), 3.39 (3H, s, CH₃), 5.06 (2H, s, CH₂), 6.51 (1H, s, 1×Pyridone-*H*), 7.27-7.30 (3H, m, 3×ArH), 7.40-7.42 (2H, m, 2×ArH), 7.44 (1H, s, 1×Pyridone-*H*); ¹³C NMR (125 MHz, DMSO-

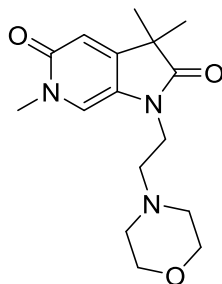
d_6) δ_C 24.0 (2 \times CH₃), 37.4 (N-CH₃), 43.8 (C(CH₃)₂), 44.3 (NCH₂S), 113.8 (CH-Pyridone), 118.8 (CH-Pyridone), 122.4 (C-Ar), 128.5 (C-Ar), 129.5 (2 \times C-Ar), 132.2 (C-Ar), 133.4 (2 \times C-Ar), 151.8 (C-Ar), 161.2 (C=O pyridone), 177.7 (C=O pyrrolidinone); HRMS calcd for C₁₇H₁₈N₂O₂S [M+H]⁺ 315.1162, found 315.1164.

3,3,6-Trimethyl-1-((phenylsulfonyl)methyl)-1,6-dihydro-2H-pyrrolo[2,3-c]pyridine-2,5(3H)-dione (198)



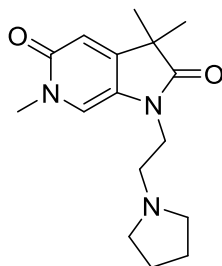
Compound **197** (35 mg, 0.11 mmol) was dissolved in MeOH (1 mL) and a solution of oxone (101 mg, 0.33 mL) in water (1 mL) was added. The reaction mixture was stirred at r.t. for 18 h. The solvent was removed *in vacuo*, water (20 mL) was added and the aqueous layer was extracted with EtOAc (3 \times 20 mL). The organic layers were combined, dried over MgSO₄, and the solvent removed *in vacuo* to get a white solid (20 mg, 52%). R_f = 0.35 (5% MeOH/DCM); m.p. 185-188 °C; λ_{\max} (EtOH)/nm 334.4, 256.0; IR ν_{\max} /cm⁻¹ 3053, 2970, 2920, 2865, 1718, (C=O), 1581 (C=O), 1309 (SO), 1134 (SO); ¹H NMR (500 MHz, DMSO-*d*₆) δ_H 1.12 (6H, s, 2 \times CH₃), 3.33 (3H, s, CH₃), 5.27 (2H, s, CH₂), 6.53 (1H, s, 1 \times Pyridone-*H*), 7.37 (1H, s, 1 \times Pyridone-*H*), 7.60-7.63 (2H, m, 2 \times Ar*H*), 7.74-7.78 (1H, m, 1 \times Ar*H*), 7.82-7.84 (2H, m, 2 \times Ar*H*); ¹³C NMR (125 MHz, DMSO-*d*₆) δ_C 24.0 (2 \times CH₃), 37.5 (N-CH₃), 43.6 (C(CH₃)₂), 61.0 (NCH₂SO₂), 113.8 (CH-Pyridone), 119.2 (CH-Pyridone), 122.5 (C-Ar), 129.3 (2 \times C-Ar), 130.0 (2 \times C-Ar), 135.1 (C-Ar), 137.5 (C-Ar), 151.3 (C-Ar), 161.1 (C=O pyridone), 177.5 (C=O pyrrolidinone); HRMS calcd for C₁₇H₁₉N₂O₄S [M - H]⁻ 347.1060, found 347.1056.

3,3,6-Trimethyl-1-(2-morpholinoethyl)-1,6-dihydro-2H-pyrrolo[2,3-c]pyridine-2,5(3H)-dione (196)



Prepared according to general procedure A using compound **5** (43 mg, 0.22 mmol), Cs₂CO₃ (287 mg, 0.88 mmol), 4-(2-chloroethyl)morpholine hydrochloride (102 mg, 0.55 mmol) and DMF (2.5 mL). The product is insoluble in EtOAc, therefore aqueous layer was collected and the solvent removed *in vacuo*. The residue was purified by MPLC (H₂O:MeCN, reversed phase with 0.1% HCOOH modifier, 0-50%) to get a white solid (55 mg, 82%). R_f = 0.15 (5% MeOH/DCM); m.p. 172-174°C; λ_{max} (EtOH)/nm 336.8, 258.2, 220.6; IR ν_{max}/cm⁻¹ 3034, 2939, 2852, 2811, 1712 (C=O), 1590 (C=O); ¹H NMR (500 MHz, CD₃OD) δ_H 1.27 (6H, s, 2×CH₃), 2.41 (4H, br s, 4×Morpholine-H), 2.52 (2H, t, J = 6.4 Hz, 2×CON-CH₂CH₂), 3.46 (3H, s, CH₃), 3.51 (4H, br t, J = 4.5 Hz, 4×Morpholine-H), 3.70 (2H, t, J = 6.4 Hz, 2×CON-CH₂), 6.47 (1H, s, 1×Pyridone-H), 7.34 (1H, s, 1×Pyridone-H); ¹³C NMR (125 MHz, CD₃OD) δ_C 22.8 (2×CH₃), 36.8 (CON-CH₂), 36.9 (N-CH₃), 44.0 (C(CH₃)₂), 53.2 (2×CH₂-Morpholine), 53.9 (CON-CH₂CH₂), 66.6 (2×CH₂-Morpholine), 113.0 (CH-Pyridone), 116.8 (CH-Pyridone), 126.1 (C-Pyridone), 153.5 (C-Pyridone), 162.5 (C=O pyridone), 179.4 (C=O pyrrolidinone); HRMS calcd for C₁₆H₂₄N₃O₃ [M+H]⁺ 306.1812, found 306.1812.

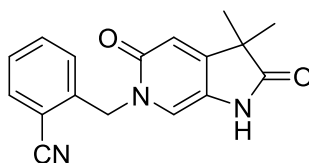
3,3,6-Trimethyl-1-(2-(pyrrolidin-1-yl)ethyl)-1,6-dihydro-2H-pyrrolo[2,3-c]pyridine-2,5(3H)-dione (195)



Prepared according to general procedure A using compound **5** (43 mg, 0.22 mmol), Cs₂CO₃ (287 mg, 0.88 mmol), 1-(2-chloroethyl)pyrrolidine hydrochloride (94 mg, 0.55 mmol) and DMF (2.5 mL). The product is insoluble in EtOAc, therefore aqueous layer was collected and

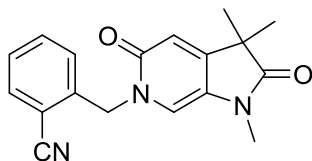
the solvent removed *in vacuo*. The residue was purified by MPLC (H₂O:MeCN, reversed phase with 0.1% HCOOH modifier, 0-50%) to get a white solid (25 mg, 40%). R_f = 0.15 (5% MeOH/DCM); λ_{max} (EtOH)/nm 336.0, 257.8, 220.0; IR ν_{max}/cm⁻¹ 3029, 2962, 2923, 2787, 1712 (C=O), 1587 (C=O); ¹H NMR (500 MHz, CD₃OD) δ_H 1.26 (6H, s, 2×CH₃), 1.69-1.72 (4H, m, 4×Pyrrolidine-*H*), 2.51-2.54 (4H, m, 4×Pyrrolidine-*H*), 2.65 (2H, t, *J* = 6.9 Hz, 2×CON-CH₂CH₂), 3.47 (3H, s, CH₃), , 3.70 (2H, t, *J* = 6.9 Hz, 2×CON-CH₂), 6.47 (1H, s, 1×Pyridone-*H*), 7.32 (1H, s, 1×Pyridone-*H*); ¹³C NMR (125 MHz, CD₃OD) δ_C 22.7 (2×CH₃), 22.9 (2×CH₂-Pyrrolidine), 36.9 (N-CH₃), 38.9 (CON-CH₂), 44.1 (C(CH₃)₂), 51.6 (CON-CH₂CH₂), 53.7 (2×CH₂-Pyrrolidine), 113.1 (CH-Pyridone), 116.6 (CH-Pyridone), 126.2 (C-Pyridone), 153.5 (C-Pyridone), 162.5 (C=O pyridone), 179.2 (C=O pyrrolidine); HRMS calcd for C₁₆H₂₄N₃O₂ [M+H]⁺ 290.1863, found 290.1865.

2-((3,3-Dimethyl-2,5-dioxo-1,2,3,5-tetrahydro-6*H*-pyrrolo[2,3-*c*]pyridin-6-yl)methyl)benzotrile (207)



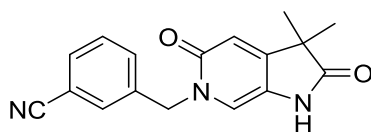
Prepared according to general procedure B using compound **192** (120 mg, 0.411 mmol), 2-(bromomethyl)benzotrile (162 mg, 0.824 mmol) and MeCN (3.8 mL). Purification by MPLC on SiO₂ (DCM:MeOH, 0-7%) gave a white solid (75 mg, 63%). R_f = 0.32 (5% MeOH/DCM); m.p. 315 °C (degraded); λ_{max} (EtOH)/nm 339.2, 224.0; IR ν_{max}/cm⁻¹ 3069, 3019, 2972, 2726, 2224 (CN), 1708 (C=O), 1588 (C=O); ¹H NMR (500 MHz, DMSO-*d*₆) δ_H 1.27 (6H, s, 2×CH₃), 5.24 (2H, s, CH₂), 6.58 (1H, s, 1×Pyridone-*H*), 7.12 (1H, d, *J* = 7.8 Hz, Ar*H*), 7.27 (1H, s, 1×Pyridone-*H*), 7.48 (1H, t, *J* = 7.6 Hz, Ar*H*), 7.67 (1H, td, *J* = 7.8 and 1.1 Hz, Ar*H*), 7.88 (1H, dd, *J* = 7.7 and 1.1 Hz, Ar*H*), 10.33 (1H, s, NH); ¹³C NMR (125 MHz, DMSO-*d*₆) δ_C 24.0 (2×CH₃), 44.1 (C(CH₃)₂), 50.4 (NCH₂Ar), 110.9 (C-Ar), 114.8 (CH-Pyridone), 116.2 (CH-Pyridone), 117.7 (CN), 124.1 (C-Ar), 127.8 (C-Ar), 128.5 (C-Ar), 133.5 (C-Ar), 134.1 (C-Ar), 141.5 (C-Ar), 154.7 (C-Ar), 160.7 (C=O pyridone), 180.1 (C=O pyrrolidinone); HRMS calcd for C₁₇H₁₆N₃O₂ [M+H]⁺ 294.1237, found 224.1240.

2-((1,3,3-Trimethyl-2,5-dioxo-1,2,3,5-tetrahydro-6H-pyrrolo[2,3-c]pyridin-6-yl)methyl)benzotrile (208)



Prepared according to general procedure A using compound **207** (50 mg, 0.17 mmol), Cs_2CO_3 (166 mg, 0.51 mmol), MeI (30 μL , 0.43 mmol) and DMF (1.5 mL). Purification by MPLC on SiO_2 (DCM:MeOH, 0-5%) gave a white solid (50 mg, 96%). $R_f = 0.42$ (5% MeOH/DCM); m.p. 195-197 $^\circ\text{C}$; λ_{max} (EtOH)/nm 258.4, 225.6; IR $\nu_{\text{max}}/\text{cm}^{-1}$ 3054, 2973, 2924, 2221 (CN), 1703 (C=O), 1599 (C=O); ^1H NMR (500 MHz, CD_3OD) δ_{H} 1.28 (6H, s, $2\times\text{CH}_3$), 3.03 (3H, s, N- CH_3), 5.28 (2H, s, CH_2), 6.51 (1H, s, $1\times\text{Pyridone-H}$), 7.17 (1H, d, $J = 7.9$ Hz, Ar- H), 7.35-7.38 (2H, m, Ar- H + Pyridone- H), 7.52 (1H, td, $J = 7.7, 1.2$ Hz, Ar- H), 7.67 (1H, dd, $J = 7.7, 1.0$ Hz, Ar- H); ^{13}C NMR (125 MHz, CD_3OD) δ_{C} 22.6 ($2\times\text{CH}_3$), 25.4 (N- CH_3), 44.2 ($\text{C}(\text{CH}_3)_2$), 51.2 (N CH_2Ar), 111.2 (C-Ar), 113.7 (CH-Pyridone), 115.7 (CH-Pyridone), 116.9 (CN), 127.5 (C-Ar), 127.7 (C-Ar), 128.1 (C-Ar), 132.9 (C-Ar), 133.1 (C-Ar), 139.9 (C-Ar), 154.0 (C-Ar), 162.2 (C=O pyridone), 179.0 (C=O pyrrolidine); HRMS calcd for $\text{C}_{18}\text{H}_{18}\text{N}_3\text{O}_2$ $[\text{M}+\text{H}]^+$ 308.1394, found 308.1396.

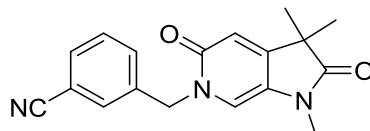
3-((3,3-Dimethyl-2,5-dioxo-1,2,3,5-tetrahydro-6H-pyrrolo[2,3-c]pyridin-6-yl)methyl)benzotrile (209)



Prepared according to general procedure B using compound **192** (100 mg, 0.342 mmol), 3-(bromomethyl)benzotrile (134 mg, 0.684 mmol) and MeCN (2.5 mL). Purification by MPLC on SiO_2 (DCM:MeOH, 0-7%) gave a white solid (65 mg, 65%). $R_f = 0.32$ (5% MeOH/DCM); m.p. 310 $^\circ\text{C}$ (degraded); λ_{max} (EtOH)/nm 338.4, 255.8, 223.0; IR $\nu_{\text{max}}/\text{cm}^{-1}$ 3059, 2964, 2925, 2723, 2227 (CN), 1709 (C=O), 1584 (C=O); ^1H NMR (500 MHz, $\text{DMSO}-d_6$) δ_{H} 1.25 (6H, s, $2\times\text{CH}_3$), 5.09 (2H, s, CH_2), 6.56 (1H, s, $1\times\text{Pyridone-H}$), 7.29 (1H, s, $1\times\text{Pyridone-H}$), 7.55-7.58 (1H, m, Ar H), 7.62-7.65 (1H, m, Ar H), 7.76-7.79 (2H, m, Ar H), 10.31 (1H, s, NH); ^{13}C NMR (125 MHz, $\text{DMSO}-d_6$) δ_{C} 24.0 ($2\times\text{CH}_3$), 44.1 ($\text{C}(\text{CH}_3)_2$), 50.9 (N CH_2Ar), 111.8 (C-Ar) 114.8 (CH-Pyridone), 115.8 (CH-Pyridone), 119.1 (CN), 124.1 (C-Ar), 130.3 (C-Ar), 131.8 (C-Ar),

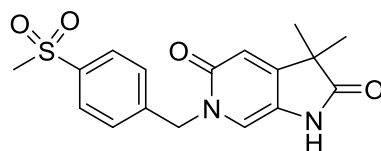
131.9 (C-Ar), 133.2 (C-Ar), 139.8 (C-Ar), 154.4 (C-Ar), 160.7 (C=O pyridone), 180.2 (C=O pyrrolidinone); HRMS calcd for $C_{17}H_{16}N_3O_2$ $[M+H]^+$ 294.1237, found 294.1242.

3-((1,3,3-trimethyl-2,5-dioxo-1,2,3,5-tetrahydro-6H-pyrrolo[2,3-c]pyridin-6-yl)methyl)benzonitrile (210)



Prepared according to general procedure A using compound **209** (40 mg, 0.136 mmol), CS_2CO_3 (133 mg, 0.408 mmol), MeI (21 μ L, 0.34 mmol) and DMF (1.5 mL). Purification by MPLC on SiO_2 (DCM:MeOH, 0-5%) gave a white solid (38 mg, 91%). $R_f=0.40$ (5% MeOH/DCM); m.p. 170-172 $^{\circ}C$; λ_{max} (EtOH)/nm 338.4, 259.4, 225.4; IR ν_{max}/cm^{-1} 3033, 2926, 2864, 2229 (CN), 1713 (C=O), 1579 (C=O); 1H NMR (500 MHz, CD_3OD) δ_H 1.26 (6H, s, $2\times CH_3$), 3.03 (3H, s, N- CH_3), 5.11 (2H, s, CH_2), 6.51 (1H, s, 1 \times Pyridone-*H*), 7.38 (1H, s, Ar-*H*), 7.43 (1H, app t, $J = 7.8$ Hz, Ar-*H*), 7.55-7.58 (2H, m, $2\times$ Ar-*H*), 7.63-7.65 (1H, m, Ar-*H*); ^{13}C NMR (125 MHz, CD_3OD) δ_C 22.6 ($2\times CH_3$), 25.5 (N- CH_3), 44.2 ($C(CH_3)_2$), 51.8 (N CH_2 Ar), 112.4 (C-Ar), 113.7 (CH-Pyridone), 115.2 (CH-Pyridone), 118.0 (CN), 127.7 (C-Ar), 129.5 (C-Ar), 131.2 (C-Ar), 131.3 (C-Ar), 132.3 (C-Ar), 138.5 (C-Ar), 153.8 (C-Ar), 162.1 (C=O pyridone), 179.0 (C=O pyrrolidinone); HRMS calcd for $C_{18}H_{18}N_3O_2$ $[M+H]^+$ 308.1394, found 308.1393.

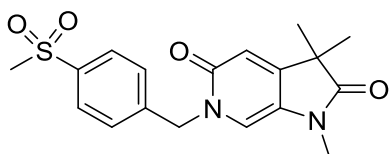
3,3-Dimethyl-6-(4-(methylsulfonyl)benzyl)-1,6-dihydro-2H-pyrrolo[2,3-c]pyridine-2,5(3H)-dione (211)



Prepared according to general procedure B using compound **192** (87 mg, 0.298 mmol), 1-(bromomethyl)-4-(methylsulfonyl)benzene (148 mg, 0.596 mmol) and MeCN (2.5 mL). Purification by MPLC on SiO_2 (DCM:MeOH, 0-7%) gave a white solid (55 mg, 53%). $R_f = 0.27$ (5% MeOH/DCM); m.p. 320 $^{\circ}C$ (degraded); λ_{max} (EtOH)/nm 339.4, 255.6, 223.2; IR ν_{max}/cm^{-1} 3083, 3008, 2973, 2926, 2731, 1717 (C=O), 1549, 1306 (SO), 1146 (SO); 1H NMR (500 MHz, $DMSO-d_6$) δ_H 1.26 (6H, s, $2\times CH_3$), 3.20 (1H, s, SO_2CH_3), 5.16 (2H, s, CH_2), 6.58 (1H, s, 1 \times Pyridone-*H*), 7.28 (1H, s, 1 \times Pyridone-*H*), 7.52-7.54 (2H, m, $2\times$ Ar-*H*), 7.89-7.91 (2H,

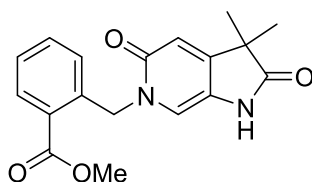
m, 2×Ar-*H*), 10.31 (1H, s, *NH*); ¹³C NMR (125 MHz, DMSO-*d*₆) δ_C 24.0 (2×CH₃), 44.0 (SO₂CH₃), 44.1 (C(CH₃)₂), 51.2 (NCH₂Ar), 114.8 (CH-Pyridone), 115.9 (CH-Pyridone), 124.0 (C-Ar), 127.8 (2×C-Ar), 128.9 (2×C-Ar), 140.3 (C-Ar), 144.1 (C-Ar), 154.4 (C-Ar), 160.7 (C=O pyridone), 180.2 (C=O pyrrolidinone); HRMS calcd for C₁₇H₁₉N₂O₄S [M+H]⁺ 347.1060, found 347.1062.

1,3,3-Trimethyl-6-(4-(methylsulfonyl)benzyl)-1,6-dihydro-2*H*-pyrrolo[2,3-*c*]pyridine-2,5(3*H*)-dione (212)



Prepared according to general procedure A using compound **211** (36 mg, 0.104 mmol), Cs₂CO₃ (102 mg, 0.312 mmol), MeI (16 μL, 0.260 mmol) and DMF (1 mL). Purification by MPLC on SiO₂ (DCM:MeOH, 0-5%) gave a white solid (32 mg, 86%). R_f = 0.35 (5% MeOH/DCM); m.p. 95-97 °C; λ_{max} (EtOH)/nm 338.8, 259.2, 224.6; IR ν_{max}/cm⁻¹ 3050, 2969, 2927, 1709 (C=O), 1587 (C=O), 1300 (SO), 1145 (SO); ¹H NMR (500 MHz, CD₃OD) δ_H 1.27 (6H, s, 2×CH₃), 2.99 (1H, s, SO₂CH₃), 3.03 (1H, s, N-CH₃), 5.19 (2H, s, CH₂), 6.52 (1H, s, 1×Pyridone-*H*), 7.37 (1H, s, 1×Pyridone-*H*), 7.46-7.48 (2H, m, 2×Ar-*H*), 7.82-7.84 (2H, m, 2×Ar-*H*); ¹³C NMR (125 MHz, CD₃OD) δ_C 22.6 (2×CH₃), 25.5 (N-CH₃), 42.9 (SO₂CH₃), 44.2 (C(CH₃)₂), 52.0 (NCH₂Ar), 113.7 (CH-Pyridone), 115.3 (CH-Pyridone), 127.5 (2×C-Ar), 127.7 (C-Ar), 128.3 (2×C-Ar), 140.1 (C-Ar), 143.1 (C-Ar), 153.9 (C-Ar), 162.1 (C=O pyridone), 179.0 (C=O pyrrolidinone); HRMS calcd for C₁₈H₂₁N₂O₄S [M+H]⁺ 361.1217, found 361.1215.

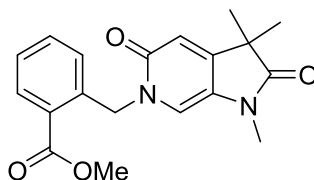
Methyl 2-((3,3-dimethyl-2,5-dioxo-1,2,3,5-tetrahydro-6*H*-pyrrolo[2,3-*c*]pyridin-6-yl)methyl)benzoate (222)



Prepared according to general procedure B using compound **192** (150 mg, 0.513 mmol), methyl 2-(bromomethyl)benzoate (235 mg, 1.02 mmol) and MeCN (4 mL). Purification by MPLC on SiO₂ (DCM:MeOH, 0-7%) gave a white solid (36 mg, 22%). R_f = 0.32 (5% MeOH/DCM); m.p.

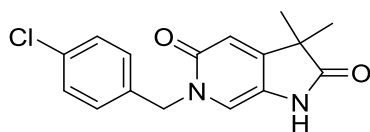
284-286 °C; λ_{\max} (EtOH)/nm 337.4, 256.4, 223.4; IR $\nu_{\max}/\text{cm}^{-1}$ 3085, 3015, 2964, 2783, 2739, 1711 (C=O), 1546 (C=O); ^1H NMR (500 MHz, DMSO- d_6) δ_{H} 1.28 (6H, s, 2 \times CH $_3$), 3.88 (3H, s, COOCH $_3$), 5.38 (2H, s, CH $_2$), 6.58 (1H, s, 1 \times Pyridone-*H*), 6.90 (1H, d, $J = 7.5$ Hz, Ar-*H*), 7.18 (1H, s, 1 \times Pyridone-*H*), 7.42 (1H, td, $J = 7.6, 0.8$ Hz, Ar-*H*), 7.55 (1H, td, $J = 7.6$ and 1.4 Hz, Ar-*H*), 7.93 (1H, dd, $J = 7.8$ and 1.2 Hz, Ar-*H*), 10.28 (1H, s, NH); ^{13}C NMR (125 MHz, DMSO- d_6) δ_{C} 24.1 (2 \times CH $_3$), 44.1 (C(CH $_3$) $_2$), 50.3 (NCH $_2$ Ar), 52.7 (COOCH $_3$), 114.8 (CH-Pyridone), 116.1 (CH-Pyridone), 124.0 (C-Ar), 127.4 (C-Ar), 127.7 (C-Ar), 129.0 (C-Ar), 130.8 (C-Ar), 133.2 (C-Ar), 139.2 (C-Ar), 154.4 (C-Ar), 160.8 (C=O pyridone), 167.4 (COOCH $_3$), 180.2 (C=O pyrrolidinone); HRMS calcd for C $_{18}$ H $_{19}$ N $_2$ O $_4$ [M+H] $^+$ 327.1339, found 327.1341.

Methyl 2-((1,3,3-trimethyl-2,5-dioxo-1,2,3,5-tetrahydro-6H-pyrrolo[2,3-*c*]pyridin-6-yl)methyl)benzoate (223)



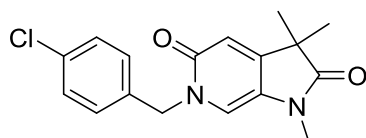
Prepared according to general procedure A using compound **222** (25 mg, 0.07 mmol), Cs $_2$ CO $_3$ (75 mg, 0.23 mmol), MeI (12 μL , 0.19 mmol) and DMF (3 mL). Purification by MPLC on SiO $_2$ (DCM:MeOH, 0-5%) gave a white solid (19 mg, 74%). $R_f = 0.40$ (5% MeOH/DCM); λ_{\max} (EtOH)/nm 337.0, 226.0; IR $\nu_{\max}/\text{cm}^{-1}$ 3062, 2968, 2924, 2863, 1716 (C=O), 1591 (C=O); ^1H NMR (500 MHz, CD $_3$ OD) δ_{H} 1.29 (6H, s, 2 \times CH $_3$), 3.00 (1H, s, N-CH $_3$), 3.84 (3H, s, COOCH $_3$), 5.49 (2H, s, CH $_2$), 6.54 (1H, s, 1 \times Pyridone-*H*), 6.88 (1H, d, $J = 7.8$ Hz, Ar-*H*), 7.28-7.31 (2H, m, 1 \times Ar-*H* + 1 \times Pyridone-*H*), 7.42 (1H, td, $J = 7.6, 0.8$ Hz, Ar-*H*), 7.92 (1H, dd, $J = 7.8$ and 1.2 Hz, Ar-*H*); ^{13}C NMR (125 MHz, CD $_3$ OD) δ_{C} 22.7 (2 \times CH $_3$), 25.4 (N-CH $_3$), 44.2 (C(CH $_3$) $_2$), 51.2 (NCH $_2$ Ar), 51.3 (COOCH $_3$), 113.6 (CH-Pyridone), 115.7 (CH-Pyridone), 126.8 (C-Ar), 127.2 (C-Ar), 127.6 (C-Ar), 128.7 (C-Ar), 130.6 (C-Ar), 132.5 (C-Ar), 138.0 (C-Ar), 153.7 (C-Ar), 162.4 (C=O pyridone), 167.4 (COOCH $_3$), 179.1 (C=O pyrrolidinone); HRMS calcd for C $_{19}$ H $_{20}$ N $_2$ O $_4$ [M+H] $^+$ 341.1496, found 341.1497.

6-(4-Chlorobenzyl)-3,3-dimethyl-1,6-dihydro-2H-pyrrolo[2,3-c]pyridine-2,5(3H)-dione
(213)



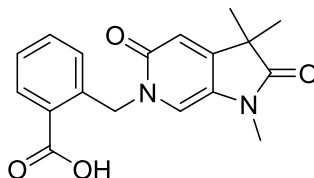
Prepared according to general procedure B using compound **192** (75 mg, 0.25 mmol), 4-chlorobenzyl bromide (105 mg, 0.51 mmol) and MeCN (2 mL). Purification by MPLC on SiO₂ (DCM:MeOH, 0-7%) gave a white solid (62 mg, 80%). $R_f=0.30$ (5% MeOH/DCM); m.p. 255-257 °C; λ_{max} (EtOH)/nm 338.8, 256.6, 221.4; IR ν_{max}/cm^{-1} 3071, 3022, 2967, 2930, 2864, 2734, 1711 (C=O), 1559 (C=O); ¹H NMR (500 MHz, DMSO-*d*₆) δ_H 1.24 (6H, s, 2×CH₃), 5.04 (2H, s, CH₂), 6.55 (1H, s, 1×Pyridone-*H*), 7.22 (1H, d, *J* = 0.4 Hz, 1×Pyridone-*H*), 7.32-7.34 (2H, m, 2×Ar-*H*), 7.40-7.42 (2H, m, 2×Ar-*H*), 10.27 (1H, s, NH); ¹³C NMR (125 MHz, DMSO-*d*₆) δ_C 24.0 (2×CH₃), 44.0 (C(CH₃)₂), 50.7 (NCH₂Ar), 114.8 (CH-Pyridone), 115.7 (CH-Pyridone), 123.9 (C-Ar), 129.0 (2×C-Ar), 130.2 (2×C-Ar), 132.6 (C-Ar), 137.3 (C-Ar), 154.2 (C-Ar), 160.6 (C=O pyridone), 180.2 (C=O pyrrolidinone); HRMS calcd for C₁₆H₁₆ClN₂O₂ [M(³⁵Cl)+H]⁺ 303.0895, found 303.0901.

6-(4-Chlorobenzyl)-1,3,3-trimethyl-1,6-dihydro-2H-pyrrolo[2,3-c]pyridine-2,5(3H)-dione
(6)



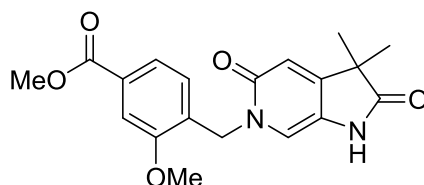
Prepared according to general procedure A using compound **213** (34 mg, 0.11 mmol), Cs₂CO₃ (110 mg, 0.33 mmol), MeI (17 μ L, 0.28 mmol) and DMF (1.2 mL). Purification by MPLC on SiO₂ (DCM:MeOH, 0-5%) gave a white solid (32 mg, 90%). $R_f=0.37$ (5% MeOH/DCM); m.p. 181-183 °C; λ_{max} (EtOH)/nm 338.4, 259.4, 221.2; IR ν_{max}/cm^{-1} 3061, 3018, 2973, 2927, 2864, 1713 (C=O), 1597 (C=O); ¹H NMR (500 MHz, CD₃OD) δ_H 1.26 (6H, s, 2×CH₃), 3.01 (1H, s, N-CH₃), 5.06 (2H, s, CH₂), 6.50 (1H, s, 1×Pyridone-*H*), 7.24 (4H, s, 4×Ar-*H*) 7.31 (1H, s, 1×Pyridone-*H*); ¹³C NMR (125 MHz, CD₃OD) δ_C 22.6 (2×CH₃), 25.4 (N-CH₃), 44.1 (C(CH₃)₂), 51.6 (NCH₂Ar), 113.6 (CH-Pyridone), 115.1 (CH-Pyridone), 127.6 (C-Ar), 128.4 (2×C-Ar), 129.2 (2×C-Ar), 133.4 (C-Ar), 135.6 (C-Ar), 153.5 (C-Ar), 162.1 (C=O pyridone), 179.0 (C=O pyrrolidinone); HRMS calcd for C₁₇H₁₈ClN₂O₂ [M(³⁵Cl)+H]⁺ 317.1051, found 317.1056.

2-((1,3,3-Trimethyl-2,5-dioxo-1,2,3,5-tetrahydro-6H-pyrrolo[2,3-c]pyridin-6-yl)methyl)benzoic acid (226)



Compound **208** (32 mg, 0.10 mmol) was dissolved in ethanol (4 mL), 1 M NaOH in water (2 mL) was added and the mixture was stirred at 80 °C for 16 h. The reaction did not go into completion, therefore, 1 M NaOH (1 mL) was added and the reaction mixture was stirred at 100 °C for 7 h. Ethanol was evaporated *in vacuo* and the residue was acidified to pH 1 using 1 M HCl. The aqueous layer was extracted with EtOAc (4×20 mL), the organic layers were combined, dried over MgSO₄ and the solvent removed *in vacuo* (11 mg, 32%). $R_f = 0.29$ (5% MeOH/DCM); m.p. 268 °C (degraded); λ_{max} (EtOH)/nm 339.0, 258.8; IR ν_{max}/cm^{-1} 3071-2180 (broad spectrum), 2919, 2851, 1713 (C=O), 1545 (C=O); ¹H NMR (500 MHz, CD₃OD) δ_H 1.29 (6H, s, 2×CH₃), 2.99 (1H, s, N-CH₃), 5.52 (2H, s, CH₂), 6.54 (1H, s, 1×Pyridone-H), 6.88 (1H, d, $J = 7.8$ Hz, Ar-H), 7.26-7.29 (1H, m, 1×Ar-H), 7.31 (1H, s, 1×Pyridone-H), 7.37 (1H, td, $J = 7.8$ and 1.3 Hz, Ar-H), 7.93 (1H, dd, $J = 7.8$ and 1.0 Hz, Ar-H); ¹³C NMR (125 MHz, CD₃OD) δ_C 22.7 (2×CH₃), 25.4 (N-CH₃), 44.2 (C(CH₃)₂), 51.1 (NCH₂Ar), 113.6 (CH-Pyridone), 115.8 (CH-Pyridone), 126.9 (C-Ar), 127.1 (C-Ar), 127.6 (C-Ar), 130.8 (C-Ar), 132.0 (C-Ar), 135.8 (C-Ar), 137.7 (C-Ar), 153.6 (C-Ar), 162.4 (C=O pyridone), 169.4 (COOCH₃), 179.1 (C=O pyrrolidinone); HRMS calcd for C₁₈H₁₉N₂O₄ [M+H]⁺ 327.1339, found 327.1343.

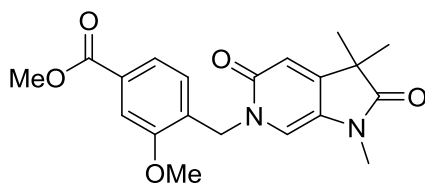
Methyl 4-((3,3-dimethyl-2,5-dioxo-1,2,3,5-tetrahydro-6H-pyrrolo[2,3-c]pyridin-6-yl)methyl)-3-methoxybenzoate (224)



Prepared according to general procedure B using compound **192** (115 mg, 0.39 mmol), methyl 4-(bromomethyl)-3-methoxybenzoate (168 mg, 0.65 mmol) and MeCN (2.5 mL). Purification by MPLC on SiO₂ (DCM:MeOH, 0-7%) gave a white solid (92 mg, 66%). $R_f = 0.31$ (5% MeOH/DCM); m.p. 308-310 °C; λ_{max} (EtOH)/nm 247.0, 211.2; IR ν_{max}/cm^{-1} 3076, 3004, 2964, 2735, 1715 (C=O), 1556 (C=O); ¹H NMR (500 MHz, DMSO-*d*₆) δ_H 1.27 (6H, s, 2×CH₃), 3.85

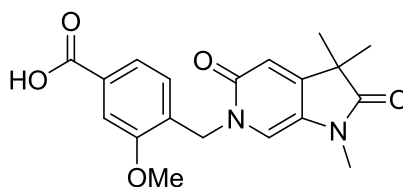
(3H, s, COOCH₃), 3.92 (3H, s, OCH₃), 5.04 (2H, s, CH₂), 6.56 (1H, s, 1×Pyridone-H), 6.98 (1H, d, *J* = 8.0 Hz, Ar-H), 7.15 (1H, s, 1×Pyridone-H), 7.52-7.54 (2H, m, 2×Ar-H), 10.23 (1H, s, NH); ¹³C NMR (125 MHz, DMSO-*d*₆) δ_C 24.0 (2×CH₃), 44.1 (C(CH₃)₂), 47.4 (NCH₂Ar), 52.7 (COOCH₃), 56.2 (OCH₃), 111.1 (C-Ar), 114.7 (CH-Pyridone), 116.3 (CH-Pyridone), 122.0 (C-Ar), 123.8 (C-Ar), 128.3 (C-Ar), 130.4 (C-Ar), 131.3 (C-Ar), 154.3 (C-Ar), 157.1 (C-Ar), 160.7 (C=O pyridone), 166.4 (COOCH₃), 180.1 (C=O pyrrolidinone); HRMS calcd for C₁₉H₂₁N₂O₅ [M+H]⁺ 357.1445, found 357.1448.

Methyl 3-methoxy-4-((1,3,3-trimethyl-2,5-dioxo-1,2,3,5-tetrahydro-6H-pyrrolo[2,3-c]pyridin-6-yl)methyl)benzoate (225)



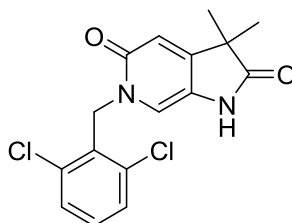
Prepared according to general procedure A using compound **224** (66 mg, 0.18 mmol), Cs₂CO₃ (180 mg, 0.55 mmol), MeI (28 μL, 0.46 mmol) and DMF (1.5 mL). Purification by MPLC on SiO₂ (DCM:MeOH, 0-5%) gave a white solid (55 mg, 80%). R_f = 0.36 (5% MeOH/DCM); m.p. 195-198°C; λ_{max} (EtOH)/nm 247.4, 212.0; IR ν_{max}/cm⁻¹ 2963, 2933, 1715 (C=O), 1606 (C=O); ¹H NMR (500 MHz, DMSO-*d*₆) δ_H 1.29 (6H, s, 2×CH₃), 3.01 (N-CH₃), 3.85 (3H, s, COOCH₃), 3.94 (3H, s, OCH₃), 5.05 (2H, s, CH₂), 6.62 (1H, s, 1×Pyridone-H), 6.91-6.92 (1H, m, Ar-H), 7.44 (1H, s, 1×Pyridone-H), 7.52-7.54 (2H, m, 2×Ar-H); ¹³C NMR (125 MHz, DMSO-*d*₆) δ_C 24.1 (2×CH₃), 26.7 (N-CH₃), 43.9 (C(CH₃)₂), 47.8 (NCH₂Ar), 52.7 (COOCH₃), 56.2 (OCH₃), 111.0 (C-Ar), 114.5 (CH-Pyridone), 116.3 (CH-Pyridone), 122.0 (C-Ar), 126.1 (C-Ar), 127.8 (C-Ar), 130.3 (C-Ar), 131.1 (C-Ar), 152.8 (C-Ar), 157.0 (C-Ar), 161.0 (C=O pyridone), 166.4 (COOCH₃), 177.9 (C=O pyrrolidinone); HRMS calcd for C₂₀H₂₃N₂O₅ [M+H]⁺ 371.1601, found 371.1600.

3-Methoxy-4-((1,3,3-trimethyl-2,5-dioxo-1,2,3,5-tetrahydro-6H-pyrrolo[2,3-c]2,4,5-triazine-6-yl)methyl)benzoic acid (227)



Compound **225** (26 mg, 0.07 mmol) was dissolved in MeOH (1.5 mL), 1 M NaOH (1.5 mL) was added and the reaction mixture was stirred at 70 °C for 2 h. The solvent was removed *in vacuo* and water (2 mL) was added to the residue and the mixture was acidified to pH 1 with 1 M HCl. The aqueous layer was extracted with EtOAc (4×20 mL), the organic layers were combined, dried over MgSO₄ and the solvent removed *in vacuo* (24 mg, 96%). $R_f = 0.56$ (15% MeOH/DCM); m.p. 246-248 °C; λ_{max} (EtOH)/nm 236.8, 209.6; IR ν_{max}/cm^{-1} 3049-2200 (broad stretch), 1707 (C=O), 1688 (C=O), 1581 (C=O); ¹H NMR (500 MHz, DMSO-*d*₆) δ_H 1.29 (6H, s, 2×CH₃), 3.01 (N-CH₃), 3.93 (3H, s, OCH₃), 5.04 (2H, s, CH₂), 6.62 (1H, s, 1×Pyridone-H), 6.90 (1H, d, $J = 7.8$ Hz, Ar-H), 7.43 (1H, s, 1×Pyridone-H), 7.49-7.52 (2H, m, 2×Ar-H), 13.03 (1H, s, COOH); ¹³C NMR (125 MHz, DMSO-*d*₆) δ_C 24.1 (2×CH₃), 26.7 (N-CH₃), 43.9 (C(CH₃)₂), 47.8 (NCH₂Ar), 56.1 (OCH₃), 111.2 (C-Ar), 114.5 (CH-Pyridone), 116.3 (CH-Pyridone), 122.1 (C-Ar), 126.1 (C-Ar), 127.7 (C-Ar), 130.6 (C-Ar), 131.6 (C-Ar), 152.7 (C-Ar), 156.9 (C-Ar), 161.0 (C=O pyridone), 167.5 (COOH), 177.9 (C=O pyrrolidinone); HRMS calcd for C₁₉H₂₁N₂O₅ [M+H]⁺ 357.1445, found 357.1449.

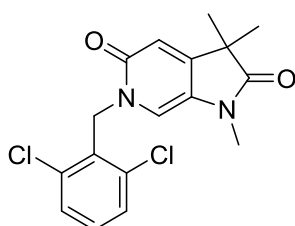
6-(2,6-dichlorobenzyl)-3,3-dimethyl-1,6-dihydro-2H-pyrrolo[2,3-c]pyridine-2,5(3H)-dione (214)



Prepared according to general procedure B using compound **192** (76 mg, 0.26 mmol), 2-(bromomethyl)-1,3-dichlorobenzene (187 mg, 0.78 mmol) and MeCN (2.5 mL). Purification by MPLC on SiO₂ (DCM:MeOH, 0-7%) gave a white solid (72 mg, 82%). $R_f = 0.32$ (5% MeOH/DCM); m.p. 310 °C (degraded); λ_{max} (EtOH)/nm 338.6, 256.6; IR ν_{max}/cm^{-1} 3078, 3012, 2962, 2924, 2735, 1712 (C=O), 1550 (C=O); ¹H NMR (500 MHz, DMSO-*d*₆) δ_H 1.24 (6H, s,

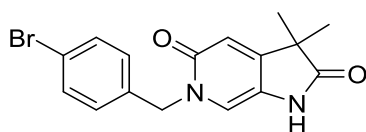
2×CH₃), 5.25 (2H, s, CH₂), 6.50 (1H, d, *J* = 0.5 Hz, 1×Pyridone-*H*), 6.57 (1H, d, *J* = 0.5 Hz, 1×Pyridone-*H*), 7.49 (1H, dd, *J* = 7.5 and 8.5 Hz, 1×Ar-*H*), 7.61 (2H, ap d, *J* = 8.1 Hz, 2×Ar-*H*), 9.87 (1H, s, NH); ¹³C NMR (125 MHz, DMSO-*d*₆) δ_C 24.0 (2×CH₃), 44.1 (C(CH₃)₂), 46.3 (NCH₂Ar), 112.8 (CH-Pyridone), 114.6 (CH-Pyridone), 124.0 (C-Ar), 129.6 (2×C-Ar), 131.9 (2×C-Ar), 136.6 (2×C-Ar), 153.7 (C-Ar), 160.5 (C=O pyridone), 179.8 (C=O pyrrolidinone); HRMS calcd for C₁₆H₁₅Cl₂N₂O₂ [M(³⁵Cl₂)+H]⁺ 337.0505, found 337.0509.

6-(2,6-dichlorobenzyl)-1,3,3-trimethyl-1,6-dihydro-2*H*-pyrrolo[2,3-*c*]pyridine-2,5(3*H*)-dione (215)



Prepared according to general procedure A using compound **214** (50 mg, 0.148 mmol), Cs₂CO₃ (145 mg, 0.44 mmol), MeI (23 μL, 0.37 mmol) and DMF (1.5 mL). Purification by MPLC on SiO₂ (DCM:MeOH, 0-5%) gave a white solid (48 mg, 92%). R_f = 0.37 (5% MeOH/DCM); m.p. 153-155°C; λ_{max} (EtOH)/nm 338.0, 258.8; IR ν_{max}/cm⁻¹ 3027, 2970, 2926, 2867, 1711 (C=O), 1578 (C=O); ¹H NMR (500 MHz, CD₃OD) δ_H 1.25 (6H, s, 2×CH₃), 5.36 (2H, s, CH₂), 6.50 (1H, s, 1×Pyridone-*H*), 6.64 (1H, s, 1×Pyridone-*H*), 7.29-7.32 (1H, m, Ar-*H*), 7.40-7.42 (2H, m, 2×Ar-*H*); ¹³C NMR (125 MHz, CD₃OD) δ_C 22.6 (2×CH₃), 25.2 (N-CH₃), 44.0 (C(CH₃)₂), 47.1 (NCH₂Ar), 112.6 (CH-Pyridone), 113.5 (CH-Pyridone), 127.4 (C-Ar), 128.8 (2×C-Ar), 130.9 (C-Ar), 130.9 (C-Ar), 136.7 (2×C-Ar), 153.1 (C-Ar), 162.1 (C=O pyridone), 178.9 (C=O pyrrolidinone); HRMS calcd for C₁₇H₁₇Cl₂N₂O₂ [M(³⁵Cl₂)+H]⁺ 351.0662, found 351.0665.

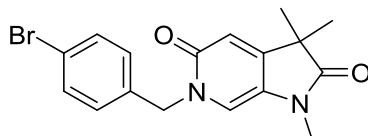
6-(4-Bromobenzyl)-3,3-dimethyl-1,6-dihydro-2*H*-pyrrolo[2,3-*c*]pyridine-2,5(3*H*)-dione (216)



Prepared according to general procedure B using compound **192** (80 mg, 0.27 mmol), 1-bromo-4-(bromomethyl)benzene (135 mg, 0.54 mmol) and MeCN (2 mL). Purification by MPLC on

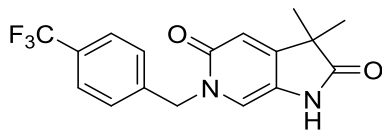
SiO₂ (DCM:MeOH, 0-7%) gave a white solid (73 mg, 78%). R_f=0.32 (5% MeOH/DCM); m.p. 269-271 °C; λ_{max} (EtOH)/nm 339.4, 259.4, 221.6; IR ν_{max}/cm⁻¹ 3025, 2965, 2928, 2860, 2734, 1705 (C=O), 1545 (C=O); ¹H NMR (500 MHz, DMSO-*d*₆) δ_H 1.24 (6H, s, 2×CH₃), 5.02 (2H, s, CH₂), 6.55 (1H, s, 1×Pyridone-*H*), 7.22 (1H, s, 1×Pyridone-*H*), 7.26-7.28 (2H, m, 2×Ar-*H*), 7.53-7.55 (2H, m, 2×Ar-*H*), 10.27 (1H, s, NH); ¹³C NMR (125 MHz, DMSO-*d*₆) δ_C 24.0 (2×CH₃), 44.0 (C(CH₃)₂), 50.7 (NCH₂Ar), 114.8 (CH-Pyridone), 115.7 (CH-Pyridone), 121.1 (C-Ar), 123.9 (C-Ar), 130.5 (2×C-Ar), 131.9 (2×C-Ar), 137.7 (C-Ar), 154.2 (C-Ar), 160.6 (C=O pyridone), 180.2 (C=O pyrrolidinone); HRMS calcd for C₁₆H₁₆BrN₂O₂ [M(⁷⁹Br)+H]⁺ 347.0390, found 347.0390.

6-(4-bromobenzyl)-1,3,3-trimethyl-1,6-dihydro-2*H*-pyrrolo[2,3-*c*]pyridine-2,5(3*H*)-dione (217)



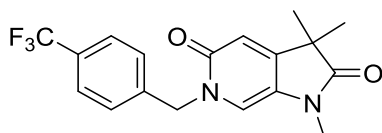
Prepared according to general procedure A using compound **216** (50 mg, 0.14 mmol), Cs₂CO₃ (137 mg, 0.42 mmol), MeI (22 μL, 0.35 mmol) and DMF (1.4 mL). Purification by MPLC on SiO₂ (DCM:MeOH, 0-5%) gave a white solid (48 mg, 95%). R_f=0.40 (5% MeOH/DCM); m.p. 198-200 °C; λ_{max} (EtOH)/nm 338.2, 259.4, 222.4; IR ν_{max}/cm⁻¹ 3063, 3019, 2977, 2933, 2870, 1715 (C=O), 1598 (C=O); ¹H NMR (500 MHz, CD₃OD) δ_H 1.26 (6H, s, 2×CH₃), 3.01 (1H, s, N-CH₃), 5.04 (2H, s, CH₂), 6.50 (1H, s, 1×Pyridone-*H*), 7.16-7.18 (2H, m, 2×Ar-*H*), 7.31 (1H, s, 1×Pyridone-*H*), 7.38-7.40 (2H, m, 2×Ar-*H*); ¹³C NMR (125 MHz, CD₃OD) δ_C 22.6 (2×CH₃), 25.4 (N-CH₃), 44.1 (C(CH₃)₂), 51.7 (NCH₂Ar), 113.6 (CH-Pyridone), 115.1 (CH-Pyridone), 121.3 (C-Ar), 127.6 (C-Ar), 129.5 (2×C-Ar), 131.4 (2×C-Ar), 136.0 (C-Ar), 153.5 (C-Ar), 162.1 (C=O pyridone), 179.0 (C=O pyrrolidinone); HRMS calcd for C₁₇H₁₇BrN₂O₂ [M(⁷⁹Br)+H]⁺ 361.0546, found 361.0544.

3,3-Dimethyl-6-(4-(trifluoromethyl)benzyl)-1,6-dihydro-2H-pyrrolo[2,3-c]pyridine-2,5(3H)-dione (218)



Prepared according to general procedure B using compound **192** (80 mg, 0.27 mmol), 1-(bromomethyl)-4-(trifluoromethyl)benzene (129 mg, 0.54 mmol) and MeCN (2 mL). Purification by MPLC on SiO₂ (DCM:MeOH, 0-7%) gave a white solid (67 mg, 71%). *R*_f = 0.30 (5% MeOH/DCM); m.p. 275-277 °C; λ_{max} (EtOH)/nm 338.0, 257.0, 217.4; IR ν_{max} /cm⁻¹ 3073, 3008, 2973, 2932, 2867, 2735, 1716 (C=O), 1562 (C=O); ¹H NMR (500 MHz, DMSO-*d*₆) δ_{H} 1.25 (6H, s, 2×CH₃), 5.13 (2H, s, CH₂), 6.57 (1H, s, 1×Pyridone-*H*), 7.26 (1H, s, 1×Pyridone-*H*), 7.49 (2H, d, *J* = 8.1 Hz, 2×Ar-*H*), 7.72 (2H, d, *J* = 8.1 Hz, 2×Ar-*H*); ¹³C NMR (125 MHz, DMSO-*d*₆) δ_{C} 24.0 (2×CH₃), 44.1 (C(CH₃)₂), 51.1 (NCH₂Ar), 114.8 (CH-Pyridone), 115.9 (CH-Pyridone), 124.0 (C-Ar), 124.7 (CF₃, q, *J* = 127.9 Hz), 125.9 (2×CF₃CCH-Ar, q, *J* = 3.6 Hz), 128.4 (CF₃C-Ar, q, *J* = 31.9 Hz), 128.8 (2×CF₃CCHCH-Ar), 143.0 (2×C-Ar), 154.4 (C-Ar), 160.7 (C=O pyridone), 180.2 (C=O pyrrolidinone); ¹⁹F NMR (470 MHz, DMSO-*d*₆) δ -60.92 (3F, s, CF₃); HRMS calcd for C₁₇H₁₆F₃N₂O₂ [M+H]⁺ 337.1158, found 337.1155.

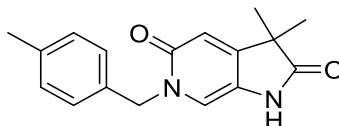
1,3,3-Trimethyl-6-(4-(trifluoromethyl)benzyl)-1,6-dihydro-2H-pyrrolo[2,3-c]pyridine-2,5(3H)-dione (219)



Prepared according to general procedure A using compound **218** (42 mg, 0.13 mmol), Cs₂CO₃ (122 mg, 0.38 mmol), MeI (20 μ L, 0.31 mmol) and DMF (1.2 mL). Purification by MPLC on SiO₂ (DCM:MeOH, 0-5%) gave a white solid (40 mg, 92%). *R*_f = 0.40 (5% MeOH/DCM); m.p. 172-174 °C; λ_{max} (EtOH)/nm 338.8, 258.8, 218.8; IR ν_{max} /cm⁻¹ 3035, 2970, 2928, 2865, 1706 (C=O), 1580 (C=O); ¹H NMR (500 MHz, CD₃OD) δ_{H} 1.27 (6H, s, 2×CH₃), 3.02 (1H, s, N-CH₃), 5.16 (2H, s, CH₂), 6.52 (1H, s, 1×Pyridone-*H*), 7.33 (1H, s, 1×Pyridone-*H*), 7.41 (2H, d, *J* = 8.1 Hz, 2×Ar-*H*), 7.54 (2H, d, *J* = 8.1 Hz, 2×Ar-*H*); ¹³C NMR (125 MHz, CD₃OD) δ_{C} 22.6 (2×CH₃), 25.4 (N-CH₃), 44.1 (C(CH₃)₂), 51.9 (NCH₂Ar), 113.7 (CH-Pyridone), 115.2 (CH-Pyridone), 125.2 (2×CF₃CCH-Ar, q, *J* = 3.6 Hz), 127.6 (C-Ar), 127.9 (2×CF₃CCHCH-Ar), 129.6 (CF₃C-Ar, q, *J* = 32.2 Hz), 141.2 (C-Ar), 153.7 (C-Ar), 162.2 (C=O pyridone), 179.0

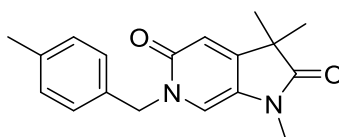
(C=O pyrrolidinone), CF₃ quartet was not observed; ¹⁹F NMR (470 MHz, CD₃OD) δ -64.10 (3F, s, CF₃); HRMS calcd for C₁₈H₁₈F₃N₂O₂ [M+H]⁺ 551.1310, found 551.1297.

3,3-Dimethyl-6-(4-methylbenzyl)-1,6-dihydro-2H-pyrrolo[2,3-c]pyridine-2,5(3H)-dione (220)



Prepared according to general procedure B using compound **192** (80 mg, 0.27 mmol), 1-(bromomethyl)-4-methylbenzene (75 mg, 0.54 mmol) and MeCN (2.7 mL). Purification by MPLC on SiO₂ (DCM:MeOH, 0-7%) gave a white solid (66 mg, 85%). R_f = 0.30 (5% MeOH/DCM); m.p. 252-254 °C; λ_{max} (EtOH)/nm 339.4, 256.8, 217.6; IR ν_{max}/cm⁻¹ 3021, 2968, 2922, 2863, 2736, 1719 (C=O), 1586 (C=O); ¹H NMR (500 MHz, DMSO-*d*₆) δ_H 1.24 (6H, s, 2×CH₃), 2.27 (3H, s, CH₃-Ar), 5.00 (2H, s, CH₂), 6.53 (1H, s, 1×Pyridone-*H*), 7.12-7.15 (2H, m, 2×Ar-*H* + 1×Pyridone-*H*), 7.20-7.22 (2H, m, 2×Ar-*H*), 10.18 (1H, s, NH); ¹³C NMR (125 MHz, DMSO-*d*₆) δ_C 21.2 (CH₃-Ar), 24.0 (2×CH₃), 44.0 (C(CH₃)₂), 50.8 (NCH₂Ar), 114.7 (CH-Pyridone), 115.6 (CH-Pyridone), 123.7 (C-Ar), 128.4 (2×C-Ar), 129.6 (2×C-Ar), 135.3 (C-Ar), 137.2 (C-Ar), 153.9 (C-Ar), 160.6 (C=O pyridone), 180.2 (C=O pyrrolidinone); HRMS calcd for C₁₇H₁₉N₂O₂ [M+H]⁺ 283.1441, found 283.1440.

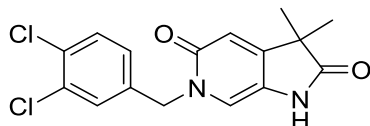
1,3,3-Trimethyl-6-(4-methylbenzyl)-1,6-dihydro-2H-pyrrolo[2,3-c]pyridine-2,5(3H)-dione (221)



Prepared according to general procedure A using compound **220** (50 mg, 0.18 mmol), Cs₂CO₃ (173 mg, 0.53 mmol), MeI (22 μL, 0.35 mmol) and DMF (1.7 mL). Purification by MPLC on SiO₂ (DCM:MeOH, 0-5%) gave a white solid (48 mg, 92%). R_f=0.42 (5% MeOH/DCM); m.p. 180-182 °C; λ_{max} (EtOH)/nm 337.8, 256.0, 218.2; IR ν_{max}/cm⁻¹ 3056, 2973, 2928, 2865, 1713 (C=O), 1601 (C=O); ¹H NMR (500 MHz, CD₃OD) δ_H 1.25 (6H, s, 2×CH₃), 2.20 (3H, s, CH₃-Ar), 3.00 (1H, s, N-CH₃), 5.04 (2H, s, CH₂), 6.49 (1H, d, *J* = 0.3 Hz, 1×Pyridone-*H*), 7.04-7.06 (2H, m, 2×Ar-*H*), 7.12-7.14 (2H, m, 2×Ar-*H*), 7.24 (1H, d, *J* = 0.3 Hz, 1×Pyridone-*H*); ¹³C

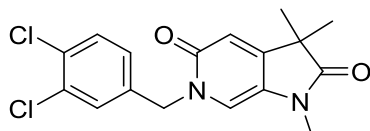
NMR (125 MHz, CD₃OD) δ_C 21.1 (CH₃-Ar), 24.1 (2×CH₃), 26.8 (N-CH₃), 45.5 (C(CH₃)₂), 53.3 (NCH₂Ar), 115.0 (CH-Pyridone), 116.6 (CH-Pyridone), 128.9 (C-Ar), 129.0 (2×C-Ar), 130.4 (2×C-Ar), 135.2 (C-Ar), 138.9 (C-Ar), 154.7 (C-Ar), 163.6 (C=O pyridone), 180.5 (C=O pyrrolidinone); HRMS calcd for C₁₈H₂₁N₂O₂ [M+H]⁺ 297.1598, found 297.1596.

6-(3,4-Dichlorobenzyl)-3,3-dimethyl-1,6-dihydro-2H-pyrrolo[2,3-*c*]pyridine-2,5(3H)-dione (228)



Prepared according to general procedure B using compound **192** (80 mg, 0.27 mmol), 4-(bromomethyl)-1,2-dichlorobenzene (132 mg, 0.54 mmol) and MeCN (2 mL). Purification by MPLC on SiO₂ (DCM:MeOH, 0-7%) gave a white solid (85 mg, 93%). R_f = 0.39 (5% MeOH/DCM); m.p. 248-250 °C; λ_{\max} (EtOH)/nm 339.0, 256.8, 220.0; IR ν_{\max} /cm⁻¹ 2961, 2870, 2789, 2729, 1703 (C=O), 1546 (C=O); ¹H NMR (500 MHz, DMSO-*d*₆) δ_H 1.25 (6H, s, 2×CH₃), 5.04 (2H, s, CH₂), 6.55 (1H, s, 1×Pyridone-*H*), 7.27 (1H, s, 1×Pyridone-*H*), 7.30 (1H, dd, *J* = 8.2 and 2.0 Hz, 1×Ar-*H*), 7.60-7.63 (2H, m, 2×Ar-*H*), 10.27 (1H, s, NH); ¹³C NMR (125 MHz, DMSO-*d*₆) δ_C 24.0 (2×CH₃), 44.0 (C(CH₃)₂), 50.4 (NCH₂Ar), 114.8 (CH-Pyridone), 115.7 (CH-Pyridone), 124.1 (C-Ar), 128.8 (C-Ar), 130.5 (C-Ar), 131.3 (C-Ar), 131.4 (C-Ar), 139.4 (2×C-Ar), 154.4 (C-Ar), 160.6 (C=O pyridone), 180.2 (C=O pyrrolidinone); HRMS calcd for C₁₆H₁₅Cl₂N₂O₂ [M(³⁵Cl₂)+H]⁺ 337.0505, found 337.0505.

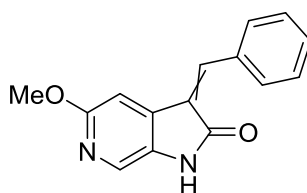
6-(3,4-Dichlorobenzyl)-1,3,3-trimethyl-1,6-dihydro-2H-pyrrolo[2,3-*c*]pyridine-2,5(3H)-dione (229)



Prepared according to general procedure A using compound **228** (50 mg, 0.15 mmol), Cs₂CO₃ (145 mg, 0.44 mmol), MeI (23 μ L, 0.37 mmol) and DMF (1.5 mL). Purification by MPLC on SiO₂ (DCM:MeOH, 0-5%) gave a white solid (49 mg, 94%). R_f = 0.41 (5% MeOH/DCM); m.p. 151-153 °C; λ_{\max} (EtOH)/nm 340.2, 259.6, 220.6; IR ν_{\max} /cm⁻¹ 3063, 3022, 2974, 2929, 2866, 1712 (C=O), 1595 (C=O); ¹H NMR (500 MHz, CD₃OD) δ_H 1.26 (6H, s, 2×CH₃), 3.02 (1H, s,

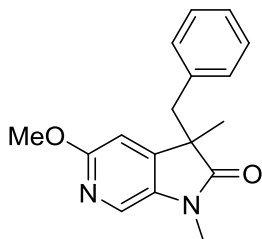
N-CH₃), 5.04 (2H, s, CH₂), 6.50 (1H, s, 1×Pyridone-H), 7.18 (1H, dd, *J* = 8.3 and 2.0 Hz, Ar-H), 7.33 (1H, s, 1×Pyridone-H), 7.39 (1H, d, *J* = 8.3 Hz, Ar-H), 7.44 (1H, d, *J* = 2.0 Hz, Ar-H); ¹³C NMR (125 MHz, CD₃OD) δ_C 24.0 (2×CH₃), 26.9 (N-CH₃), 45.5 (C(CH₃)₂), 52.7 (NCH₂Ar), 115.1 (CH-Pyridone), 116.5 (CH-Pyridone), 128.9 (C-Ar), 129.1 (C-Ar), 131.1 (C-Ar), 131.8 (C-Ar), 132.8 (C-Ar), 133.5 (C-Ar), 138.9 (C-Ar), 155.1 (C-Ar), 163.5 (C=O pyridone), 180.4 (C=O pyrrolidinone); HRMS calcd for C₁₇H₁₇Cl₂N₂O₂ [M(³⁵Cl₂)+H]⁺ 351.0662, found 351.0661.

3-Benzylidene-5-methoxy-1,3-dihydro-2H-pyrrolo[2,3-c]pyridin-2-one (231)



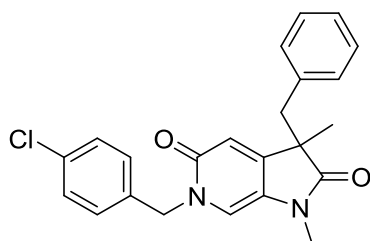
Prepared according to general procedure C using compound **191** (250 mg, 0.95 mmol), benzaldehyde (0.10 mL, 1.04 mmol), piperidine (0.29 mL, 2.93 mmol) and THF (2 mL). Purification by MPLC on SiO₂ (DCM:MeOH, 0-10%) gave an orange solid (210 mg, 88%, E:Z = 1:4 by ¹H NMR). R_f = 0.36 (5% MeOH/DCM); m.p. 221-224 °C; λ_{max} (EtOH)/nm 323.2, 260.6; IR ν_{max}/cm⁻¹ 3161, 2978, 2938, 2345, 1694 (C=O); ¹H NMR (500 MHz, DMSO-*d*₆) δ_H 3.76 (3H, s, OCH₃, Z-isomer), 3.83 (3H, s, OCH₃, E-isomer), 6.84 (1H, s, 1×Pyridine-H, Z-isomer), 7.26 (1H, s, 1×Pyridine-H, E-isomer), 7.50-7.59 (3H, m 3×Ar-H, E and Z-isomers), 7.64 (1H, s, 1×Pyridine-H, E-isomer), 7.71-7.74 (3H, m, 2×Ar-H + 1×Pyridine-H, Z-isomer), 7.90 (1H, s, CHAr, Z-isomer), 8.09 (1H, s, CHAr, E-isomer), 8.43-8.45 (2H, m, 2×Ar-H, E-isomer), 10.67 (1H, s, NH, E and Z isomers); ¹³C NMR (125 MHz, DMSO-*d*₆) δ_C 53.7 (OCH₃, Z-isomer), 53.7 (OCH₃, E-isomer), 101.8 (CH-Pyridine, E-isomer), 104.0 (CH-Pyridine, Z-isomer), 125.5 (CH-Pyridine, E-isomer), 125.8 (C-Ar), 126.4 (CH-Pyridine, Z-isomer), 126.9 (C-Ar), 128.8 (C-Ar), 129.4 (C-Ar), 130.0 (C-Ar), 131.1 (C-Ar), 132.0 (C-Ar), 132.4 (C-Ar), 132.8 (C-Ar), 133.1 (C-Ar), 133.8 (C-Ar), 134.2 (C-Ar), 137.7 (C-Ar), 142.1 (CH-Ar, Z-isomer), 142.3 (CHAr, E-isomer), 159.4 (C-Ar), 159.7 (C-Ar), 167.0 (C=O, E-isomer), 168.2 (C=O, Z-isomer); HRMS calcd for C₁₅H₁₃N₂O₂ [M+H]⁺ 551.1310, found 551.1297.

3-Benzyl-5-methoxy-1,3-dimethyl-1,3-dihydro-2H-pyrrolo[2,3-c]pyridin-2-one (235)



Prepared according to general procedure D using compound **231** (122 mg, 0.483 mmol), 10% Pd/C (40 mg), THF (18 mL) and MeOH (9 mL) in step A and Cs₂CO₃ (315 mg, 0.97 mmol), MeI (55 μL, 0.88 mmol), DMF (7.5 mL) in Step B. Purification by MPLC on SiO₂ (DCM:MeOH, 0-5%) gave a colourless sticky solid (75 mg, 55%). R_f=0.70 (5% MeOH/DCM); m.p. 73-76 °C; λ_{max} (EtOH)/nm 305.0, 251.0; IR ν_{max}/cm⁻¹ 2927, 2655, 1708 (C=O); ¹H NMR (500 MHz, CD₃Cl) δ_H 1.45 (3H, s, CH₃), 2.97 (1H, d, *J* = 13.2 Hz, CH₂Ar), 3.00 (3H, s, N-CH₃), 3.14 (1H, d, *J* = 13.2 Hz, CH₂Ar), 3.89 (3H, s, OCH₃), 6.55 (1H, d, *J* = 0.6 Hz, 1×Pyridine-*H*), 6.88-6.90 (2H, m, 2×Ar-*H*), 7.09-6.10 (3H, m, 3×Ar-*H*), 7.41 (1H, d, *J* = 0.6 Hz, 1×Pyridine-*H*); ¹³C NMR (125 MHz, CD₃Cl) δ_C 22.6 (2×CH₃), 26.2 (N-CH₃), 44.0 (CH₂Ar), 50.3 (C(CH₃)CH₂Ar), 53.7 (OCH₃), 106.8 (CH-Pyridine), 123.5 (CH-Pyridine), 126.8 (C-Ar), 127.8 (2×C-Ar), 129.8 (2×C-Ar), 134.8 (C-Ar), 135.4 (C-Ar), 146.5 (C-Ar), 160.2 (C=O pyridone), 178.4 (C=O pyrrolidinone); HRMS calcd for C₁₇H₁₈N₂O₂ [M+H]⁺ 253.0972, found 253.0971.

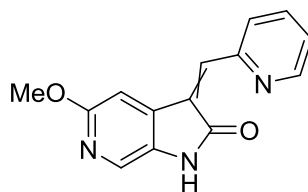
3-Benzyl-6-(4-chlorobenzyl)-1,3-dimethyl-1,6-dihydro-2H-pyrrolo[2,3-c]pyridine-2,5(3H)-dione (237)



Prepared according to general procedure B using compound **235** (60 mg, 0.21 mmol), 1-(bromomethyl)-4-chlorobenzene (87 mg, 0.42 mmol) and MeCN (2 mL). Reaction time: 30 min. Purification by MPLC on SiO₂ (DCM:MeOH, 0-6%) gave a white solid (53 mg, 64%). R_f = 0.45 (5% MeOH/DCM); m.p. 175-178 °C; λ_{max} (EtOH)/nm 340.4, 260.0; IR ν_{max}/cm⁻¹ 3049, 2971, 2926, 1718 (C=O), 1594 (C=O); ¹H NMR (500 MHz, CD₃Cl) δ_H 1.48 (3H, s, CH₃), 2.81 (3H, s, N-CH₃), 2.90 (1H, d, *J* = 13.1 Hz, CH₂Ar), 3.22 (1H, d, *J* = 13.1 Hz, CH₂Ar), 5.01 (1H,

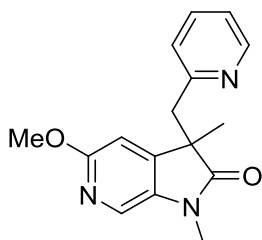
d, $J = 14.9$ Hz, 1×4-Chlorophenyl- CH_2), 5.06 (1H, d, $J = 14.9$ Hz, 1×4-Chlorophenyl- CH_2), 6.33 (1H, s, 1×Pyridone- H), 6.58 (1H, s, 1×Pyridone- H), 6.95-6.96 (2H, m, 2×4-Chlorophenyl- H), 7.09-7.12 (5H, m, 5×Ph- H), 7.29-7.31 (2H, m, 2×4-Chlorophenyl- H); ^{13}C NMR (125 MHz, CD_3Cl) δ_C 22.6 (2× CH_3), 26.2 (N- CH_3), 44.7 (CH_2Ar), 50.3 ($C(CH_3)CH_2Ar$), 51.6 (4-Chlorophenyl- CH_2N), 112.4 (CH-Pyridone), 116.3 (CH-Pyridone), 127.1 (C-Ar), 127.6 (C-Ar), 128.0 (2×C-Ar), 129.1 (2×C-Ar), 129.2 (2×C-Ar), 129.9 (2×C-Ar), 134.0 (C-Ar), 135.0 (C-Ar), 135.4 (C-Ar), 150.5 (C-Ar), 161.3 (C=O pyridone), 177.0 (C=O pyrrolidinone); HRMS calcd for $C_{23}H_{22}ClN_2O_2$ [$M(^{35}Cl)+H$] $^+$ 393.1364, found 393.1359.

5-Methoxy-3-(pyridin-2-ylmethylene)-1,3-dihydro-2H-pyrrolo[2,3-*c*]pyridin-2-one (232)



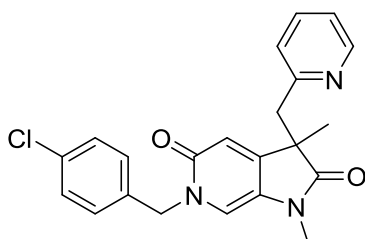
Prepared according to general procedure C using compound **191** (250 mg, 0.95 mmol), picolinaldehyde (99 μ L, 1.04 mmol), piperidine (291 μ L, 2.95 mmol) and THF (2 mL). Purification by MPLC on SiO_2 (DCM:MeOH, 0-10%) gave an orange solid (120 mg, 50%). $R_f = 0.39$ (5% MeOH/DCM); m.p. 217-230 $^{\circ}C$; λ_{max} (EtOH)/nm 333.2, 263.6, 210.2; IR ν_{max}/cm^{-1} 3163, 3105, 2992, 2943, 2851, 1717 (C=O); 1H NMR (500 MHz, $DMSO-d_6$) δ_H 3.83 (3H, s, OCH_3), 7.52-7.55 (1H, m, Pyridine- H), 7.71 (1H, s, 1×Methoxypyridine- H), 7.80 (1H, s, $CHAr$), 7.97-8.02 (2H, m, 2×Pyridine- H), 8.47 (1H, s, 1×Methoxypyridine- H), 8.93-8.95 (2H, m, 2×Ar- H), 10.68 (1H, s, NH); ^{13}C NMR (125 MHz, $DMSO-d_6$) δ_C 53.7 (OCH_3), 109.6 (CH-Methoxypyridine), 125.5 (CH-Methoxypyridine), 125.8 (C-Ar), 128.3 (C-Ar), 130.1 (C-Ar), 133.1 (C=CH), 134.2 (C-Ar), 138.0 (C-Ar), 139.4 (C=CH), 150.3 (C-Ar), 152.9 (C-Ar), 160.0 (C-Ar), 168.8 (C=O); HRMS calcd for $C_{14}H_{11}N_3O_2$ [$M+H$] $^+$ 254.0924, found 254.0927.

5-Methoxy-1,3-dimethyl-3-(pyridin-2-ylmethyl)-1,3-dihydro-2H-pyrrolo[2,3-c]pyridin-2-one (236)



Prepared according to general procedure D using compound **232** (95 mg, 0.37 mmol), 10% Pd/C (30 mg), THF (12 mL) and MeOH (6 mL) in step A and Cs₂CO₃ (257 mg, 0.79 mmol), MeI (47 μL, 0.75 mmol), DMF (4 mL) in Step B. Purification by MPLC on SiO₂ (DCM:MeOH, 0-5%) gave a beige solid (60 mg, 56%). R_f = 0.48 (5% MeOH/DCM); m.p. 105-108 °C; λ_{max} (EtOH)/nm 306.2, 252.2, 205.0; IR ν_{max}/cm⁻¹ 3005, 3009, 2976, 2937, 1700 (C=O); ¹H NMR (500 MHz, CD₃Cl) δ_H 1.46 (3H, s, CH₃), 3.14 (3H, s, N-CH₃), 3.22 (1H, d, J = 13.8 Hz, CH₂Ar), 3.41 (1H, d, J = 13.8 Hz, CH₂Ar), 3.85 (3H, s, OCH₃), 6.54 (1H, s, 1×Methoxypyridine-H), 6.98-7.03 (2H, m, 2×Ar-H), 7.45-7.49 (2H, m, 2×Ar-H), 8.30-8.32 (2H, m, 2×Ar-H); ¹³C NMR (125 MHz, CD₃Cl) δ_C 23.4 (2×CH₃), 26.5 (N-CH₃), 45.0 (CH₂Ar), 48.9 (C(CH₃)CH₂Ar), 53.5 (OCH₃), 106.9 (CH-Methoxypyridine), 121.7 (C-Ar), 123.5 (CH-Methoxypyridine), 123.8 (C-Ar), 134.9 (C-Ar), 136.1 (C-Ar), 146.4 (C-Ar), 148.7 (C-Ar), 156.3 (C-Ar), 160.3 (C-Ar), 178.8 (C=O); HRMS calcd for C₁₆H₁₈N₃O₂ [M+H]⁺ 284.1394, found 284.1393.

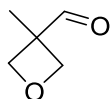
6-(4-Chlorobenzyl)-1,3-dimethyl-3-(pyridin-2-ylmethyl)-1,6-dihydro-2H-pyrrolo[2,3-c]pyridine-2,5(3H)-dione (238)



Prepared according to general procedure B using compound **236** (46 mg, 0.16 mmol), 1-(bromomethyl)-4-chlorobenzene (67 mg, 0.32 mmol) and MeCN (1 mL). Reaction time: 30 min. Purification by MPLC on SiO₂ (DCM:MeOH, 0-6%) gave a brown solid (32 mg, 50%). R_f = 0.30 (5% MeOH/DCM); m.p. 182-185 °C; λ_{max} (EtOH)/nm 340.6, 260.8, 222.0; IR ν_{max}/cm⁻¹ 3187, 3044, 2966, 2927, 1711 (C=O), 1586 (C=O); ¹H NMR (500 MHz, CD₃OD) δ_H 1.48 (3H, s, CH₃), 3.02 (3H, s, N-CH₃), 3.26 (1H, d, J = 14.1 Hz, CH₂-Pyridine), 3.41 (1H, d,

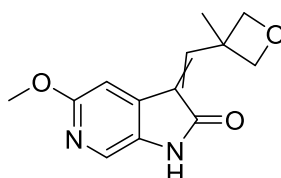
$J = 14.1$ Hz, CH_2 -Pyridine), 5.04 (1H, d, $J = 14.8$ Hz, 1×4-Chlorophenyl- CH_2), 5.12 (1H, d, $J = 14.8$ Hz, 1×4-Chlorophenyl- CH_2), 6.51 (1H, s, 1×Pyridone- H), 7.09-7.14 (2H, m, 2×Pyridine- H), 7.16 (1H, s, 1×Pyridone- H), 7.18-7.19 (2H, m, 2×4-Chlorophenyl- H), 7.30-7.32 (2H, m, 2×4-Chlorophenyl- H), 7.57 (1H, td, $J = 11.5$ and 1.9 Hz, 1×Pyridine- H), 8.22-8.23 (1H, m, 1×Pyridine- H); ^{13}C NMR (125 MHz, CD_3OD) δ_{C} 23.5 (2× CH_3), 26.8 (N- CH_3), 45.8 (CH_2 -Pyridine), 50.0 ($\text{C}(\text{CH}_3)\text{CH}_2\text{Ar}$), 52.8 (4-Chlorophenyl- CH_2N), 116.0 (CH-Pyridone), 116.1 (CH-Pyridone), 123.2 (C-Ar), 125.3 (C-Ar), 129.7 (C-Ar), 129.8 (2×C-Ar), 130.2 (2×C-Ar), 134.7 (C-Ar), 137.0 (C-Ar), 137.8 (C-Ar), 149.6 (C-Ar), 152.6 (C-Ar), 157.5 (C-Ar), 163.2 (C=O pyridone), 179.5 (C=O pyrrolidinone); HRMS calcd for $\text{C}_{22}\text{H}_{21}\text{ClN}_3\text{O}_2$ [$\text{M}^{(35}\text{Cl})+\text{H}$] $^+$ 394.1311, found 394.1311.

3-Methyloxetane-3-carbaldehyde (240)



(3-methyloxetan-3-yl)methanol (0.49 mL, 4.89 mmol) was dissolved in DCM (15 mL) and cooled to 0 °C. Dess-Martin periodinane (3.11 g, 7.34 mmol) in DCM (30 mL) was added and the solution was stirred at 0 °C for 30 min and at r.t. for 3 h. The reaction mixture was poured into a solution of saturated aqueous $\text{Na}_2\text{S}_2\text{O}_3$ (30 mL) and saturated aqueous NaHCO_3 (30 mL) and stirred for 30 min. The aqueous layer was extracted with DCM (3×40 mL), the organic layers were combined, dried over MgSO_4 and the solvent removed *in vacuo* to get a colourless oil (380 mg, 78%). ^1H NMR (500 MHz, CD_3Cl) δ_{H} 1.47 (3H, s, CH_3), 4.49 (2H, d, $J = 6.3$ Hz, CH_2), 4.86 (2H, d, $J = 6.3$ Hz, CH_2), 9.94 (1H, s, CHO); ^{13}C NMR (125 MHz, CD_3Cl) δ_{C} 17.5 (CH_3), 49.3 (Cq), 76.7 (2× CH_2), 200.6 (C=O).

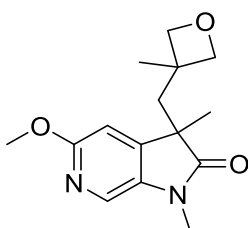
5-Methoxy-3-((3-methyloxetan-3-yl)methylene)-1,3-dihydro-2H-pyrrolo[2,3-*c*]pyridin-2-one (241)



Prepared according to general procedure C using compound **191** (200 mg, 0.76 mmol), compound **240** (121 mg, 1.21 mmol), piperidine (150 μL , 1.51 mmol) and THF (0.7 mL).

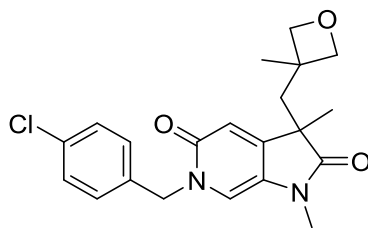
Purification by MPLC on SiO₂ (DCM:MeOH, 0-10%) gave an light-orange solid (120 mg, 50%). R_f = 0.27 (5% MeOH/DCM); m.p. 154-156 °C; λ_{max} (EtOH)/nm 255.8; IR ν_{max}/cm⁻¹ 3157, 3069, 3023, 2955, 2855, 1715 (C=O); Ratio of diastereoisomers by ¹H NMR = 3:5; ¹H NMR (500 MHz, DMSO-*d*₆) δ_H 1.59 (3H, s, CH₃-Oxetane, isomer 1), 1.60 (3H, s, CH₃-Oxetane, isomer 2), 3.80 (3H, s, OCH₃, isomer 1), 3.80 (3H, s, OCH₃, isomer 2), 4.48 (1H, d, *J* = 6.1 Hz, 2×Oxetane-H, isomer 1), 4.67-4.69 (4H, m, 2×Oxetane-H, isomer 1 and 2), 4.76 (1H, d, *J* = 5.8 Hz, 1×Oxetane-H, isomer 2), 6.38 (1H, s, 1×Methoxypyridine-*H*, isomer 2), 7.06 (1H, s, 1×Methoxypyridine-*H*, isomer 1), 7.34 (1H, s, CH=CCO, isomer 2), 7.60 (1H, s, CH=CCO, isomer 2), 7.63 (1H, s, 1×Methoxypyridine-*H*, isomer 1), 7.70 (1H, s, 1×Methoxypyridine-*H*, isomer 2), 10.53 (1H, s, NH, isomer 1), 10.62 (1H, s, NH, isomer 2); ¹³C-NMR was not be obtained; HRMS calcd for C₁₃H₁₄N₃O₂ [M+H]⁺ 247.1077, found 247.1080.

5-Methoxy-1,3-dimethyl-3-((3-methyloxetan-3-yl)methyl)-1,3-dihydro-2*H*-pyrrolo[2,3-*c*]pyridin-2-one (243)



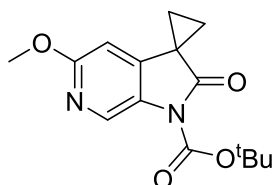
Prepared according to general procedure D using compound **241** (58 mg, 0.24 mmol), 10% Pd/C (20 mg), THF (10 mL) and MeOH (5 mL) in step A and Cs₂CO₃ (176 mg, 0.54 mmol), MeI (30 μL, 0.48 mmol), DMF (4.7 mL) in Step B. Purification by MPLC on SiO₂ (DCM:MeOH, 0-5%) gave an off-white solid (30 mg, 42%). R_f=0.40 (5% MeOH/DCM); m.p. 98-101 °C; λ_{max} (EtOH)/nm 305.6, 249.8, 205.2; IR ν_{max}/cm⁻¹ 3060, 2931, 2866, 1715 (C=O); ¹H NMR (500 MHz, CD₃Cl) δ_H 0.96 (3H, s, CH₃-Oxetane), 1.34 (3H, s, CH₃), 2.32 (1H, d, *J* = 14.5 Hz, CH₂-Oxetane), 2.39 (1H, d, *J* = 14.5 Hz, CH₂-Oxetane), 3.20 (3H, s, N-CH₃), 3.78 (1H, d, *J* = 5.8 Hz, 1×Oxetane-H₂), 3.90 (3H, s, OCH₃), 4.05 (1H, d, *J* = 5.8 Hz, 1×Oxetane-H₂), 4.37 (1H, d, *J* = 5.8 Hz, 1×Oxetane-H₂), 4.46 (1H, d, *J* = 5.8 Hz, 1×Oxetane-H₂), 6.64 (1H, s, 1×Methoxypyridine-*H*), 7.65 (1H, s, 1×Methoxypyridine-*H*); ¹³C NMR (125 MHz, CD₃Cl) δ_C 22.9 (CH₃-Oxetane), 26.6 (N-CH₃), 27.0 (CH₃), 39.2 (C-Oxetane), 45.5 (Pyrrolidinone-CH₂-Oxetane), 47.3 (C(CH₃)CH₂Oxetane), 53.7 (OCH₃), 83.5 (CH₂-Oxetane), 83.8 (CH₂-Oxetane), 106.8 (CH-Methoxypyridine), 124.1 (CH-Methoxypyridine), 134.6 (C-Ar), 146.6 (C-Ar), 160.4 (C-Ar), 178.7 (C=O); HRMS calcd for C₁₅H₂₁N₂O₃ [M+H]⁺ 277.1547, found 277.1544.

6-(4-Chlorobenzyl)-1,3-dimethyl-3-((3-methyloxetan-3-yl)methyl)-1,6-dihydro-2H-pyrrolo[2,3-c]pyridine-2,5(3H)-dione (244)



Prepared according to general procedure B using compound **243** (18 mg, 0.065 mmol), 1-(bromomethyl)-4-chlorobenzene (27 mg, 0.13 mmol) and MeCN (1 mL). Reaction time: 45 min. Purification by MPLC on SiO₂ (DCM:MeOH, 0-6%) gave an off-white solid (21 mg, 83%). *R*_f = 0.32 (5% MeOH/DCM); m.p. 167-170 °C; IR $\nu_{\text{max}}/\text{cm}^{-1}$ 3049, 2964, 2923, 2863, 1709 (C=O) 1598 (C=O); ¹H NMR (500 MHz, CD₃Cl) δ_{H} 1.05 (3H, s, CH₃-Oxetane), 1.35 (3H, s, CH₃), 2.22 (1H, d, *J* = 14.5 Hz, CH₂-Oxetane), 2.40 (1H, d, *J* = 14.5 Hz, CH₂-Oxetane), 3.04 (3H, s, N-CH₃), 3.93 (1H, d, *J* = 5.8 Hz, 1×Oxetane-H₂), 4.05 (1H, d, *J* = 5.8 Hz, 1×Oxetane-H₂), 4.44 (1H, d, *J* = 5.8 Hz, 1×Oxetane-H₂), 4.48 (1H, d, *J* = 5.8 Hz, 1×Oxetane-H₂), 4.98 (1H, d, *J* = 14.6 Hz, 1×4-Chlorophenyl-CH₂), 5.21 (1H, d, *J* = 14.6 Hz, 1×4-Chlorophenyl-CH₂), 6.54 (1H, s, 1×Pyridone-H), 6.64 (1H, s, 1×Pyridone-H), 7.23-7.24 (2H, m, 2×4-Chlorophenyl-H₂), 7.31-7.33 (2H, m, 2×4-Chlorophenyl-H₂); ¹³C NMR (125 MHz, CD₃Cl) δ_{C} 23.4 (CH₃-Oxetane), 26.7 (N-CH₃), 27.1 (CH₃), 39.4 (C-Oxetane), 45.7 (Pyrrolidinone-CH₂-Oxetane), 46.9 (C(CH₃)CH₂Oxetane), 51.7 (NCH₂-Ar), 83.6 (CH₂-Oxetane), 83.6 (CH₂-Oxetane), 113.0 (CH-Methoxypyridine), 116.3 (CH-Methoxypyridine), 127.0 (C-Ar), 129.3 (2×C-Ar), 129.5 (2×C-Ar), 134.3 (C-Ar), 135.0 (C-Ar), 150.6 (C-Ar), 161.1 (C-Ar), 177.3 (C=O); HRMS calcd for C₂₁H₂₄ClN₂O₃ [M(³⁵Cl)+H]⁺ 387.1470, found 387.1465.

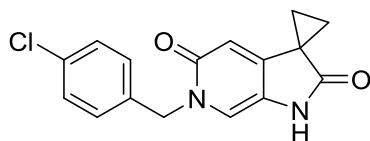
***Tert*-butyl 5'-methoxy-2'-oxospiro[cyclopropane-1,3'-pyrrolo[2,3-c]pyridine]-1'(2'*H*)-carboxylate (260)**



Compound **191** (600 mg, 2.27 mmol) and Cs₂CO₃ (1.62 g, 4.99 mmol) were suspended in MeCN (15 mL). 1,2-dibromoethane (0.22 mL, 2.50 mmol) was added and the mixture was stirred at 40 °C for 3.5 h. The starting material was not completely consumed, therefore, 1,2-

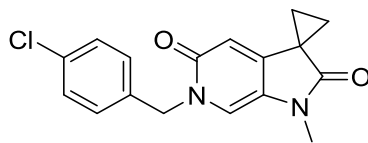
dibromoethane (50 μ L, 0.57 mmol) was added and stirred at 40 $^{\circ}$ C for 1.5 h. The reaction mixture was filtered using EtOAc (3 \times 30 mL) and the filtrate was evaporated *in vacuo*. Water (30 mL) was added to the residue and the aqueous layer was extracted with EtOAc (3 \times 25 mL). The organic layers were combined, dried over MgSO₄ and the solvent removed *in vacuo*. Purification by MPLC on SiO₂ (Petrol:EtOAc, 0-10%) gave a white solid (360 mg, 55%). R_f = 0.75 (5% MeOH/DCM); m.p. 146-149 $^{\circ}$ C; λ_{max} (EtOH)/nm 293.8; IR ν_{max}/cm^{-1} 3085, 2977, 1767 (C=O), 1720 (C=O); ¹H NMR (500 MHz, CDCl₃) δ_H 1.59 (2H, q, J = 4.2 Hz, CH₂-spirocyclopropane), 1.65 (9H, s, C(CH₃)₃), 1.92 (2H, q, J = 4.2 Hz, CH₂-spirocyclopropane), 3.92 (3H, s, OCH₃), 6.23 (1H, d, J = 0.6 Hz, 1 \times Pyridine-*H*), 8.55 (1H, d, J = 0.6 Hz, 1 \times Pyridine-*H*); ¹³C NMR (125 MHz, CDCl₃) δ_C 22.5 (CH₂-spirocyclopropane), 27.8 (C(CH₂)₃), 28.1 (C(CH₃)₃), 53.7 (OCH₃), 84.7 (C(CH₃)₃), 100.3 (CH-Pyridine), 131.5 (C-Pyridine), 131.6 (CH-Pyridine), 143.1 (C-Pyridine), 148.7 (COO^tBu), 160.8 (Pyridine-C-OMe), 174.3 (C=O pyrrolidinone); HRMS calcd for C₁₅H₁₉N₂O₄ [M+H]⁺ 291.1339, found 291.1337.

6'-(4-Chlorobenzyl)-1',6'-dihydrospiro[cyclopropane-1,3'-pyrrolo[2,3-*c*]pyridine]-2',5'-dione (264)



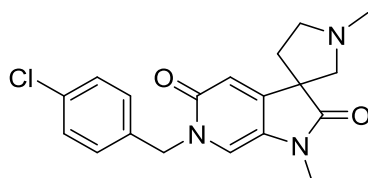
Prepared according to general procedure B using compound **260** (100 mg, 0.34 mmol), 1-(bromomethyl)-4-chlorobenzene (141 mg, 0.69 mmol) and MeCN (3.4 mL). Reaction time: 45 min. Purification by MPLC on SiO₂ (DCM:MeOH, 0-10%) gave a white solid (70 mg, 68%). R_f = 0.24 (5% MeOH/DCM); m.p. 298 $^{\circ}$ C; λ_{max} (EtOH)/nm 339.4, 230.6; IR ν_{max}/cm^{-1} 3073, 3026, 2997, 2936, 2876, 2735, 1714 (C=O), 1554 (C=O); ¹H NMR (500 MHz, DMSO-*d*₆) δ_H 1.53-1.61 (4H, m, 2 \times CH₂), 5.06 (2H, s, CH₂-Ar), 6.19 (1H, s, 1 \times Pyridone-*H*), 7.25 (1H, s, 1 \times Pyridone-*H*), 7.28-7.30 (2H, m, 2 \times Ar-*H*), 7.39-7.41 (2H, m, 2 \times Ar-*H*), 10.42 (1H, s, NH); ¹³C NMR (125 MHz, DMSO-*d*₆) δ_C 20.5 (2 \times CH₂), 27.1 (C(CH₂)₂), 50.7 (NCH₂Ar), 109.8 (CH-Pyridone), 115.7 (CH-Pyridone), 124.8 (C-Ar), 128.9 (2 \times C-Ar), 130.0 (2 \times C-Ar), 132.4 (C-Ar), 137.4 (C-Ar), 150.1 (C-Ar), 160.3 (C=O pyridone), 176.0 (C=O pyrrolidinone); HRMS calcd for C₁₆H₁₄ClN₂O₂ [M(³⁵Cl)+H]⁺ 301.0738, found 301.0738.

6'-(4-Chlorobenzyl)-1'-methyl-1',6'-dihydrospiro[cyclopropane-1,3'-pyrrolo[2,3-c]pyridine]-2',5'-dione (265)



Prepared according to general procedure A using compound **264** (60 mg, 0.199 mmol), Cs₂CO₃ (130 mg, 0.398 mmol), MeI (25 μL, 0.398 mmol) and DMF (4 mL). Purification by MPLC on SiO₂ (DCM:MeOH, 0-5%) gave a white solid (50 mg, 80%). R_f = 0.32 (5% MeOH/DCM); m.p. 155-157 °C; λ_{max} (EtOH)/nm 339.4, 231.2; ¹H NMR (500 MHz, CD₃Cl) δ_H 1.51 (2H, q, *J* = 4.1 Hz, CH₂-spirocyclopropane), 1.83 (2H, q, *J* = 4.1 Hz, CH₂-spirocyclopropane), 3.12 (1H, s, N-CH₃), 5.11 (2H, s, CH₂-Ar), 6.13 (1H, s, 1×Pyridone-*H*), 6.67 (1H, s, 1×Pyridone-*H*), 7.23-7.25 (2H, m, 2×Ar-*H*), 7.30-7.32 (2H, m, 2×Ar-*H*); ¹³C NMR (125 MHz, CD₃Cl) δ_C 21.0 (2×CH₂), 26.9 (N-CH₃), 51.6 (NCH₂Ar), 109.9 (CH-Pyridone), 112.6 (CH-Pyridone), 128.0 (C-Ar), 129.2 (2×C-Ar), 129.4 (2×C-Ar), 134.1 (C-Ar), 135.3 (C-Ar), 148.8 (C-Ar), 161.3 (C=O pyridone), 174.3 (C=O pyrrolidinone); HRMS calcd for C₁₇H₁₆ClN₂O₂ [M(³⁵Cl)+H]⁺ 315.0895, found 315.0893.

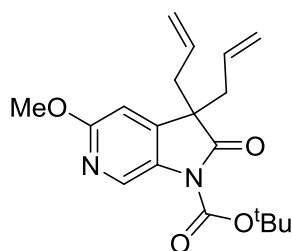
6'-(4-Chlorobenzyl)-1,1'-dimethyl-1',6'-dihydrospiro[pyrrolidine-3,3'-pyrrolo[2,3-c]pyridine]-2',5'-dione (271)



Prepared according to general procedure E using Compound **265** (150 mg, 0.476 mmol), MgI₂ (13 mg, 0.047 mmol), 1,3,5-trimethyl-1,3,5-triazinane (0.17 mL, 1.19 mmol) and THF (1.6 mL). Purification by MPLC on SiO₂ (DCM:MeOH, 0-12%) gave a beige solid (92 mg, 53%). R_f = 0.27 (5% MeOH/DCM); m.p. 78-80 °C; λ_{max} (EtOH)/nm 339.4, 259.8; IR ν_{max}/cm⁻¹ 3047, 2936, 2844, 2783, 1707 (C=O), 1588 (C=O); ¹H NMR (500 MHz, CD₃Cl) δ_H 2.00 (1H, dt, *J* = 12.9, 7.5 Hz, CH-spiropyrrrolidine), 2.35-2.40 (1H, m, CH-spiropyrrrolidine), 2.40 (3H, s, N-CH₃), 2.65 (1H, dd, *J* = 16.3 and 8.4 Hz, CH-spiropyrrrolidine), 2.78 (2H, s, CH₂-Spiropyrrrolidine), 2.99-3.03 (1H, m, CH-spiropyrrrolidine), 3.05 (3H, s, N-CH₃), 5.09 (2H, s, CH₂-Ar), 6.59 (1H, s, 1×Pyridone-*H*), 6.81 (1H, s, 1×Pyridone-*H*), 7.25-7.27 (2H, m, 2×Ar-*H*), 7.30-7.33 (2H, m, 2×Ar-*H*); ¹³C NMR (125 MHz, CD₃Cl) δ_C 26.6 (N-CH₃), 37.9 (CH₂-

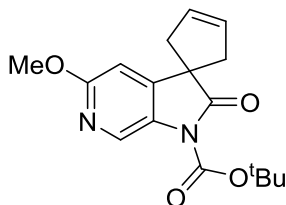
Spiropyrrolidine), 41.4 (N-CH₃), 51.5 (NCH₂Ar), 53.0 (C-Spiropyrrolidine), 56.0 (CH₂-Spiropyrrolidine), 66.1 (CH₂-Spiropyrrolidine), 112.1 (CH-Pyridone), 115.9 (CH-Pyridone), 127.1 (C-Ar), 129.1 (2×C-Ar), 129.4 (2×C-Ar), 134.0 (C-Ar), 135.1 (C-Ar), 152.7 (C-Ar), 161.7 (C=O pyridone), 177.0 (C=O pyrrolidinone); LRMS (ES⁺) *m/z* 358.3 [M(³⁵Cl)+H]⁺, 360.3 [M(³⁷Cl)+H]⁺.

***Tert*-butyl 3,3-diallyl-5-methoxy-2-oxo-2,3-dihydro-1*H*-pyrrolo[2,3-*c*]pyridine-1-carboxylate (255)**



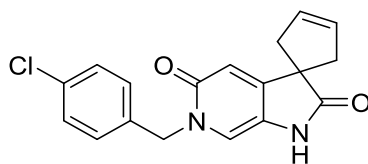
Compound **191** (493 mg, 1.865 mmol) and Cs₂CO₃ (1.40 g, 4.289 mmol) were suspended in MeCN (12.5 mL). Allyl bromide (0.4 mL, 4.662 mmol) was added and the mixture was stirred at 40 °C for 2.5 h. The reaction mixture was filtered using EtOAc (3×30 mL) and the filtrate was evaporated *in vacuo*. Water (40 mL) was added to the residue and the aqueous layer was extracted with EtOAc (3×25 mL). The organic layers were combined, dried over MgSO₄ and the solvent removed *in vacuo*. Purification by MPLC on SiO₂ (Petrol:EtOAc, 0-20%) gave a white solid (350 mg, 55%). R_f = 0.56 (20% EtOAc/Petrol); m.p. 84-87 °C; λ_{max} (EtOH)/nm 295.2, 230.6; IR ν_{max}/cm⁻¹ 3084, 2980, 2947, 2908, 1759 (C=O), 1719 (C=O); ¹H NMR (500 MHz, CD₃Cl) δ_H 1.63 (9H, s, C(CH₃)₃), 2.49-2.53 (2H, m, CH₂CH=CH₂), 2.60-2.64 (2H, m, CH₂CH=CH₂), 3.93 (3H, s, OCH₃), 4.98-5.05 (4H, m, 2×CH₂CH=CH₂), 5.40-5.49 (2H, m, 2×CH₂CH=CH₂), 6.61 (1H, d, *J* = 0.7 Hz, 1×Pyridine-*H*), 8.51 (1H, d, *J* = 0.7 Hz, 1×Pyridine-*H*); ¹³C NMR (125 MHz, CDCl₃) δ_C 28.1 (C(CH₃)₃), 41.6 (2×CH₂CH=CH₂), 53.4 (C(CH₂CH=CH₂)₂), 53.7 (OCH₃), 84.7 (C(CH₃)₃), 105.7 (CH-Pyridine), 120.2 (2×CH=CH₂), 130.9 (2×CH=CH₂), 131.4 (C-Pyridine), 132.0 (CH-Pyridine), 143.2 (C-Pyridine), 148.5 (COO^tBu), 160.8 (Pyridine-C-OMe), 176.3 (C=O pyrrolidinone); HRMS calcd for C₁₉H₂₅N₂O₄ [M+H]⁺ 345.1809, found 345.1804.

Tert-butyl 5'-methoxy-2'-oxospiro[cyclopentane-1,3'-pyrrolo[2,3-*c*]pyridin]-3-ene-1'(2'*H*)-carboxylate (256)



Compound **255** (329 mg, 0.955 mmol) was dissolved in DCM (19.5 mL). Grubbs catalyst 2nd generation (41 mg, 5 mol%) was added and the reaction mixture was stirred at 80 °C under microwave irradiation for 20 min. The solvent was removed *in vacuo* and the residue was purified by MPLC on SiO₂ (Petrol:EtOAc, 0-20%) to get a white solid (272 mg, 90%). R_f = 0.48 (20% EtOAc/Petrol); m.p. 163-166 °C; ¹H NMR (500 MHz, CD₃Cl) δ_H 1.65 (9H, s, C(CH₃)₃), 2.60-2.63 (2H, m, CH₂CH=CHCH₂), 3.08-3.11 (2H, m, CH₂CH=CHCH₂), 3.91 (3H, s, OCH₃), 5.79 (2H, s, CH₂CH=CHCH₂), 6.68 (1H, d, J = 0.7 Hz, 1×Pyridine-*H*), 8.51 (1H, d, J = 0.7 Hz, 1×Pyridine-*H*); ¹³C NMR (125 MHz, CDCl₃) δ_C 28.1 (C(CH₃)₃), 46.2 (2×CH₂CH=CHCH₂), 52.7 (CCH₂CH=CH), 53.7 (OCH₃), 84.8 (C(CH₃)₃), 103.8 (CH-Pyridine), 128.5 (2×CH=CH), 130.1 (C-Pyridine), 131.9 (CH-Pyridine), 148.4 (C-Pyridine), 148.7 (COO^tBu), 161.4 (Pyridine-C-OMe), 178.7 (C=O pyrrolidinone); HRMS calcd for C₁₇H₂₁N₂O₄ [M+H]⁺ 317.1496, found 317.1493.

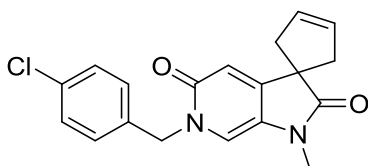
6'-(4-Chlorobenzyl)-1',6'-dihydrospiro[cyclopentane-1,3'-pyrrolo[2,3-*c*]pyridin]-3-ene-2',5'-dione (257)



Prepared according to general procedure B using compound **256** (257 mg, 0.81 mmol), 1-(bromomethyl)-4-chlorobenzene (334 mg, 1.63 mmol) and MeCN (5.4 mL). Reaction time: 45 min. Purification by MPLC on SiO₂ (DCM:MeOH, 0-10%) gave a white solid (237 mg, 89%). R_f = 0.29 (5% MeOH/DCM); m.p. 274-277 °C; λ_{max} (EtOH)/nm 343.0, 258.4, 221.4; IR ν_{max}/cm^{-1} 3021, 2933, 2844, 2792, 2734, 1718 (C=O), 1588 (C=O); ¹H NMR (500 MHz, DMSO-*d*₆) δ_H 2.55-2.59 (2H, m, CH₂CH=CHCH₂), 2.79-2.82 (2H, m, CH₂CH=CHCH₂), 5.04 (2H, s, CH₂-Ar), 5.78 (2H, s, CH₂CH=CHCH₂), 6.29 (1H, s, 1×Pyridone-*H*), 7.21 (1H, s, 1×Pyridone-*H*), 7.31-7.33 (2H, m, 2×Ar-*H*), 7.39-7.41 (2H, m, 2×Ar-*H*), 10.31 (1H, s, NH);

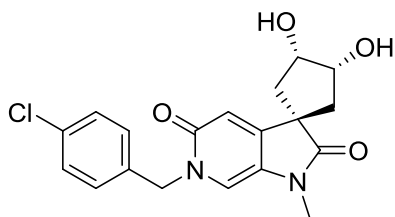
^{13}C NMR (125 MHz, $\text{DMSO-}d_6$) δ_{C} 45.2 ($2\times\text{CH}_2\text{CH}=\text{CHCH}_2$), 50.7 (NCH_2Ar), 51.9 ($\text{CCH}_2\text{CH}=\text{CH}$), 113.1 (CH-Pyridone), 115.7 (CH-Pyridone), 124.1 (C-Ar), 129.0 ($2\times\text{C-Ar}$), 129.1 ($2\times\text{CH}=\text{CH}$), 130.2 ($2\times\text{C-Ar}$), 132.6 (C-Ar), 137.2 (C-Ar), 155.5 (C-Ar), 160.8 ($\text{C}=\text{O}$ pyridone), 180.1 ($\text{C}=\text{O}$ pyrrolidinone); HRMS calcd for $\text{C}_{18}\text{H}_{16}\text{ClN}_2\text{O}_2$ [$\text{M}(^{35}\text{Cl})+\text{H}$] $^+$ 327.0895, found 327.0895.

6'-(4-Chlorobenzyl)-1'-methyl-1',6'-dihydrospiro[cyclopentane-1,3'-pyrrolo[2,3-c]pyridin]-3-ene-2',5'-dione (258)



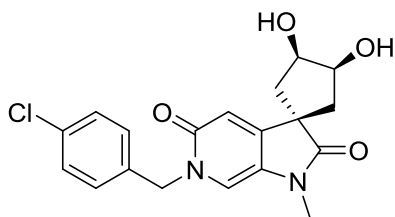
Prepared according to general procedure A using compound **257** (225 mg, 0.69 mmol), Cs_2CO_3 (673 mg, 2.07 mmol), MeI (110 μL , 1.72 mmol) and DMF (7 mL). Purification by MPLC on SiO_2 ($\text{DCM}:\text{MeOH}$, 0-10%) gave an off-white solid (205 mg, 87%). $R_f = 0.48$ (5% MeOH/DCM); m.p. 56-58 $^\circ\text{C}$; λ_{max} (EtOH)/nm 339.6, 261.0, 221.6; IR $\nu_{\text{max}}/\text{cm}^{-1}$ 3058, 2918, 2844, 1704 ($\text{C}=\text{O}$), 1582 ($\text{C}=\text{O}$); ^1H NMR (500 MHz, CD_3Cl) δ_{H} 2.56-2.62 (2H, m, $\text{CH}_2\text{CH}=\text{CHCH}_2$), 2.98-3.03 (2H, m, $\text{CH}_2\text{CH}=\text{CHCH}_2$), 3.06 (3H, s, N-CH_3), 5.08 (2H, s, $\text{CH}_2\text{-Ar}$), 5.78 (2H, s, $\text{CH}_2\text{CH}=\text{CHCH}_2$), 6.60 (1H, s, 1 \times Pyridone-*H*), 6.62 (1H, s, 1 \times Pyridone-*H*), 7.25-7.27 (2H, m, 2 \times Ar-*H*), 7.31-7.33 (2H, m, 2 \times Ar-*H*); ^{13}C NMR (125 MHz, CD_3Cl) δ_{C} 25.6 (N-CH_3), 44.0 ($2\times\text{CH}_2\text{CH}=\text{CHCH}_2$), 50.5 (NCH_2Ar), 50.9 ($\text{CCH}_2\text{CH}=\text{CH}$), 111.3 (CH-Pyridone), 113.1 (CH-Pyridone), 126.0 (C-Ar), 127.6 ($2\times\text{CH}=\text{CH}$), 128.1 ($2\times\text{C-Ar}$), 128.4 ($2\times\text{C-Ar}$), 133.0 (C-Ar), 134.0 (C-Ar), 152.7 (C-Ar), 160.8 ($\text{C}=\text{O}$ pyridone), 177.2 ($\text{C}=\text{O}$ pyrrolidinone); HRMS calcd for $\text{C}_{19}\text{H}_{18}\text{ClN}_2\text{O}_2$ [$\text{M}(^{35}\text{Cl})+\text{H}$] $^+$ 341.1051, found 341.1050.

**(1*s*,3*R*,4*S*)-6'-(4-Chlorobenzyl)-3,4-dihydroxy-1'-methyl-1',6'-
dihydrospiro[cyclopentane-1,3'-pyrrolo[2,3-*c*]pyridine]-2',5'-dione (252)**



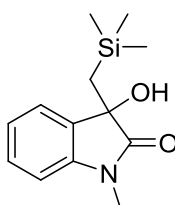
Compound **258** (25 mg, 0.073 mmol) was dissolved in THF:water (3:1, 2.4 mL) and cooled to 0 °C. *N*-methylnmorpholine (12 mg, 0.099 mmol) and 2.5 wt% OsO₄ in *t*BuOH (30 μL, 4 mol%) were added, respectively and the mixture was stirred at r.t. for 18 h. The starting material was not completely consumed, therefore, 2.5 wt% OsO₄ in *t*BuOH (70 μL, 9.3 mol%) was added and the reaction was stirred at r.t. for 24 h. The mixture was quenched with saturated Na₂SO₃ (30 mL) and stirred for 30 min. The aqueous layer was extracted with EtOAc (3×20 mL), the organic layers were combined, dried over MgSO₄ and the solvent removed *in vacuo*. Purification by MPLC on SiO₂ (DCM:MeOH, 0-10%) gave a white solid (16 mg, 59%) and other isomer **259** (5 mg, 18%). R_f = 0.18 (5% MeOH/DCM); m.p. 68-71 °C; λ_{max} (EtOH)/nm 339.4, 260.8, 221.6; IR ν_{max}/cm⁻¹ 3355 (OH), 3049, 2925, 2853, 1698 (C=O), 1582 (C=O); ¹H NMR (500 MHz, CD₃Cl) δ_H 2.17-2.20 (4H, m, 2×CH₂CHOH), 3.09 (3H, s, N-CH₃), 3.81 (2H, d, *J* = 9.8 Hz, 2×OH), 4.28-4.33 (2H, m, 2×CHOH), 5.08 (2H, s, CH₂-Ar), 6.52 (1H, s, 1×Pyridone-*H*), 6.65 (1H, s, 1×Pyridone-*H*), 7.25-7.27 (2H, m, 2×Ar-*H*), 7.31-7.33 (2H, m, 2×Ar-*H*); ¹³C NMR (125 MHz, CD₃Cl) δ_C 26.5 (N-CH₃), 42.2 (2×CH₂CHOH), 51.1 (NCH₂Ar), 51.2 (CCH₂CHOH), 74.4 (2×CHOH), 112.9 (CH-Pyridone), 114.8 (CH-Pyridone), 126.4 (C-Ar), 128.7 (2×C-Ar), 129.0 (2×C-Ar), 133.8 (C-Ar), 134.2 (C-Ar), 151.0 (C-Ar), 160.9 (C=O pyridone), 179.9 (C=O pyrrolidinone); HRMS calcd for C₁₉H₂₀ClN₂O₄ [M(³⁵Cl)+H]⁺ 375.1106, found 375.1103.

(1r,3R,4S)-6'-(4-Chlorobenzyl)-3,4-dihydroxy-1'-methyl-1',6'-dihydrospiro[cyclopentane-1,3'-pyrrolo[2,3-*c*]pyridine]-2',5'-dione (259)



Obtained as a white solid from the reaction above (5 mg, 18%). R_f = 0.11 (5% MeOH/DCM); λ_{\max} (EtOH)/nm 339.4, 260.8, 221.8; IR $\nu_{\max}/\text{cm}^{-1}$ 3374 (OH), 2924, 2853, 1700 (C=O), 1567 (C=O); ^1H NMR (500 MHz, CD_3Cl) δ_{H} 2.00 (2H, dd, J = 13.7 and 5.2 Hz, CH_2CHOH), 2.34 (2H, dd, J = 13.7 and 6.0 Hz, CH_2CHOH), 3.04 (3H, s, N- CH_3), 3.31 (2H, br s, 2 \times OH), 4.43 (2H, br s, 2 \times CHOH), 5.09 (2H, s, CH_2 -Ar), 6.58 (1H, s, 1 \times Pyridone- H), 7.03 (1H, s, 1 \times Pyridone- H), 7.24-7.26 (2H, m, 2 \times Ar- H), 7.31-7.33 (2H, m, 2 \times Ar- H); ^{13}C NMR (125 MHz, CD_3Cl) δ_{C} 26.6 (N- CH_3), 42.6 (2 \times CH_2CHOH), 50.5 (N CH_2 Ar), 51.6 (C CH_2CHOH), 74.2 (2 \times CHOH), 112.1 (CH-Pyridone), 116.8 (CH-Pyridone), 127.9 (C-Ar), 129.2 (2 \times C-Ar), 129.5 (2 \times C-Ar), 134.1 (C-Ar), 134.8 (C-Ar), 153.5 (C-Ar), 162.2 (C=O pyridone), 179.1 (C=O pyrrolidinone); HRMS calcd for $\text{C}_{19}\text{H}_{20}\text{ClN}_2\text{O}_4$ [$\text{M}^{(35}\text{Cl})+\text{H}$] $^+$ 375.1106, found 375.1102.

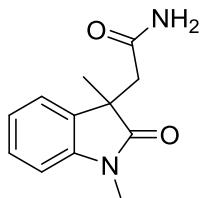
3-Hydroxy-1-methyl-3-((trimethylsilyl)methyl)indolin-2-one (280)



N-methylisatin (200 mg, 1.24 mmol) was dissolved in THF (6.2 mL) and cooled to -78°C . 1 M (trimethylsilyl)methylmagnesium chloride in Et_2O (2.5 mL, 2.5 mmol) was added dropwise and the solution was stirred at r.t. for 1.5 h. The solvent was removed *in-vacuo* and the residue was purified by MPLC on SiO_2 (Petrol:EtOAc, 0-20%) to get a light yellow solid (220 mg, 71%). R_f = 0.31 (5% MeOH/DCM); m.p. 143-145 $^\circ\text{C}$; λ_{\max} (EtOH)/nm 256.8, 209.4; IR $\nu_{\max}/\text{cm}^{-1}$ 3352 (OH), 3057, 2950, 2899, 2871, 1690 (C=O), 1609 (C=O); ^1H NMR (500 MHz, CDCl_3) δ_{H} -0.31 (9H, s, 3 \times CH_3), 1.53 (1H, d, J = 13.5 Hz, 1 \times CH_2), 1.56 (1H, d, J = 13.5 Hz, 1 \times CH_2), 2.80 (1H, s, OH), 3.18 (3H, s, N CH_3), 6.83 (1H, d, J = 7.7 Hz, 1 \times Ar- H), 7.09 (1H, td, J = 7.5 and 0.9 Hz, 1 \times Ar- H), 7.32 (1H, td, J = 7.7 and 1.3 Hz, 1 \times Ar- H), 7.36 (1H, dd, J = 7.5 and 0.9 Hz, 1 \times Ar- H), 8.54 (1H, d, J = 0.6 Hz, 1 \times Pyridine- H); ^{13}C NMR (125 MHz, CDCl_3) δ_{C} 0.0 (3 \times CH_3), 27.4

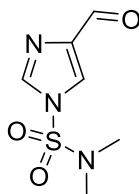
(N-CH₃), 29.9 (CH₂), 76.9 (COH), 109.7 (CH-Ar), 124.4 (CH-Ar), 125.4 (CH-Ar), 131.0 (CH-Ar), 132.3 (C-Ar), 144.2 (C-Ar), 179.5 (C=O pyrrolidinone); HRMS calcd for C₁₃H₂₀NO₂Si [M+H]⁺ 250.1258, found 250.1257.

2-(1,3-Dimethyl-2-oxoindolin-3-yl)acetamide (277)



To a solution of compound **282** (60 mg, 0.37 mmol) in DMF (4 mL), Cs₂CO₃ (182 mg, 0.55 mmol) and 2-bromoacetamide (77 mg, 0.55 mmol) were added, respectively. The reaction mixture was stirred at 50 °C for 2 h. The reaction was quenched with water (20 mL) and the aqueous layer was extracted with EtOAc (3×20 mL). The organic layers were combined, dried over MgSO₄ and the solvent removed *in vacuo*. Purification by MPLC on SiO₂ (DCM:MeOH, 0-7%) gave a white solid (10 mg, 12%). R_f = 0.28 (5% MeOH/DCM); m.p. 177-178 °C; λ_{max} (EtOH)/nm 252.8, 205.6; IR ν_{max}/cm⁻¹ 3371 (NH), 3189, 3052, 2920, 1674 (C=O), 1609 (C=O); ¹H NMR (500 MHz, CDCl₃) δ_H 1.42 (3H, s, CH₃), 2.66 (1H, d, *J* = 14.9 Hz, 1×CH₂), 2.78 (1H, d, *J* = 14.9 Hz, 1×CH₂), 3.21 (3H, s, NCH₃), 5.30 (1H, br s, 1×NH₂), 6.40 (1H, br s, 1×NH₂), 6.83 (1H, d, *J* = 7.7 Hz, 1×Ar-*H*), 7.05 (1H, td, *J* = 7.7 and 0.9 Hz, 1×Ar-*H*), 7.23-7.28 (2H, m, 2×Ar-*H*); ¹³C NMR (125 MHz, CDCl₃) δ_C 23.5 (CH₃), 26.4 (N-CH₃), 43.4 (CH₂), 46.0 (C(CH₃)), 108.4 (CH-Ar), 122.7 (CH-Ar), 122.9 (CH-Ar), 128.3 (CH-Ar), 133.3 (C-Ar), 142.8 (C-Ar), 171.3 (CONH₂), 180.6 (C=O pyrrolidinone); HRMS calcd for C₁₂H₁₅N₂O₂ [M+H]⁺ 219.1128, found 219.1125.

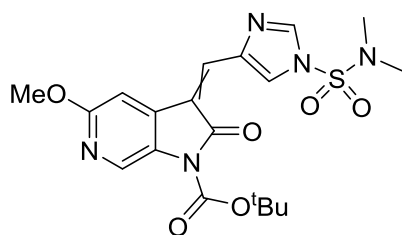
4-Formyl-N,N-dimethyl-1H-imidazole-1-sulfonamide (285)



1*H*-imidazole-4-carbaldehyde (200 mg, 2.08 mmol) was suspended in DCM (7 mL), trimethylamine (0.32 mL, 2.29 mmol) and *N,N*-dimethylsulfamoyl chloride (0.25 mL, 2.29 mmol) were added, respectively. The reaction mixture was stirred at r.t. for 24 h. *N,N*-

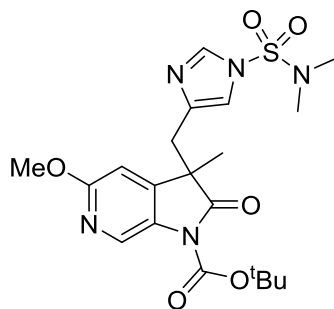
dimethylsulfamoyl chloride (0.12 mL, 1.14 mmol) and the reaction mixture was stirred at 40 °C for 24 h. The reaction was quenched with water (30 mL) and the aqueous layer was extracted with EtOAc (3×30 mL). The organic layers were combined, dried over MgSO₄ and the solvent removed *in vacuo*. Purification by MPLC on SiO₂ (DCM:MeOH, 0-5%) gave colourless crystals (360 mg, 85%). *R*_f = 0.36 (5% MeOH/DCM); m.p. 99-101 °C; λ_{max} (EtOH)/nm 245.8; IR ν_{max}/cm⁻¹ 3134, 3092, 3032, 2951, 2838, 1692 (C=O), 1387 (SO), 1174 (SO); ¹H NMR (500 MHz, CDCl₃) δ_H 2.91 (6H, s, 2×CH₃), 7.88 (1H, d, *J* = 1.3 Hz, 1×Ar-*H*), 7.95 (1H, d, *J* = 1.3 Hz, 1×Ar-*H*), 9.93 (1H, s, CHO); ¹³C NMR (125 MHz, CDCl₃) δ_C 38.2 (2×CH₃), 121.8 (CH-Ar), 137.5 (CH-Ar), 142.3 (C-Ar), 185.8 (C=O pyrrolidinone); HRMS calcd for C₆H₁₀N₃O₃S [M+H]⁺ 204.0437, found 204.0433.

***Tert*-butyl 3-((1-(*N,N*-dimethylsulfamoyl)-1*H*-imidazol-4-yl)methylene)-5-methoxy-2-oxo-2,3-dihydro-1*H*-pyrrolo[2,3-*c*]pyridine-1-carboxylate (286)**



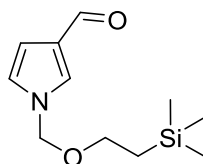
Compound **191** (275 mg, 1.04 mmol) and compound **285** (275 mg, 1.35 mmol) were dissolved in THF (0.5 mL), piperidine (0.2 mL, 2.08 mmol) was added and the reaction mixture was stirred at 50 °C for 1 h. The reaction mixture was filtered using Et₂O (5×20 mL) and water (2×10 mL) to get a yellow solid (140 mg, 30%). *R*_f = 0.63 (5% MeOH/DCM); m.p. 197-200 °C; λ_{max} (EtOH)/nm 339.4, 213.2; IR ν_{max}/cm⁻¹ 3108, 3019, 2971, 2927, 1773 (C=O), 1636 (C=O), 1118 (SO); ¹H NMR (500 MHz, DMSO-*d*₆) δ_H 1.60 (9H, s, C(CH₃)₃), 2.91 (6H, s, N(CH₃)₂), 3.88 (3H, s, OCH₃), 7.81 (1H, s, Pyrrole-*H*), 8.51 (1H, s, 1×Pyridine-*H*), 8.63 (1H, s, Pyrrole-*H*), 8.65 (1H, s, C=CH), 8.87 (1H, s, 1×Pyridine-*H*); ¹³C NMR (125 MHz, DMSO-*d*₆) δ_C 28.2 (C(CH₃)₃), 38.3 (N(CH₃)₂), 53.9 (OCH₃), 84.4 (C(CH₃)₃), 107.6 (C-Ar), 121.5 (C-Ar), 128.8 (C-Ar), 130.5 (C-Ar), 131.3 (C-Ar), 132.2 (C-Ar), 133.0 (C-Ar), 138.2 (C=CH), 139.6 (C=CH), 148.7 (COO^tBu), 160.9 (C-OMe), 166.0 (C=O pyrrolidinone); HRMS calcd for C₁₉H₂₄N₅O₆S [M+H]⁺ 450.1442, found 450.1430.

Tert-butyl 3-((1-(*N,N*-dimethylsulfamoyl)-1*H*-imidazol-4-yl)methyl)-5-methoxy-3-methyl-2-oxo-2,3-dihydro-1*H*-pyrrolo[2,3-*c*]pyridine-1-carboxylate (288)



Prepared according to general procedure D using compound **286** (75 mg, 0.16 mmol), 10% Pd/C (20 mg), THF (12 mL) and MeOH (6 mL) in step A and Cs₂CO₃ (81 mg, 0.25 mmol), MeI (20 μL, 0.25 mmol), DMF (4.5 mL) in Step B. Purification by MPLC on SiO₂ (DCM:MeOH, 0-5%) gave a white solid (53 mg, 69%). R_f = 0.51 (5% MeOH/DCM); λ_{max} (EtOH)/nm 229.4; IR ν_{max}/cm⁻¹ 3112, 2972, 2935, 1792 (C=O), 1385 (SO), 1144 (SO); ¹H NMR (500 MHz, CD₃Cl) δ_H 1.52 (3H, s, CH₃), 1.63 (9H, s, C(CH₃)₃), 2.67 (6H, s, N(CH₃)₂), 2.99 (1H, d, *J* = 14.3 Hz, CH₂), 3.21 (1H, d, *J* = 14.3 Hz, CH₂), 3.88 (3H, s, OCH₃), 6.54 (1H, d, *J* = 0.5 Hz, 1×Pyridine-*H*), 6.78 (1H, s, 1×Pyrrole-*H*), 7.62 (1H, d, *J* = 1.2 Hz, 1×Pyrrole-*H*), 8.43 (1H, d, *J* = 0.5 Hz, 1×Pyridine-*H*); ¹³C NMR (125 MHz, CD₃Cl) δ_C 23.6 (CH₃), 28.1 (C(CH₃)₃), 36.9 (CH₂), 38.0 (N(CH₃)₂), 49.3 (C(CH₃)), 53.6 (OCH₃), 84.7 (C(CH₃)₃), 105.6 (C-Ar), 115.3 (C-Ar), 130.9 (C-Ar), 131.8 (C-Ar), 136.1 (C-Ar), 138.5 (C-Ar), 145.0 (C-Ar), 148.8 (COOtBu), 160.8 (C-OMe), 177.2 (C=O pyrrolidinone); HRMS calcd for C₂₀H₂₈N₅O₆S [M+H]⁺ 466.1755, found 466.1743.

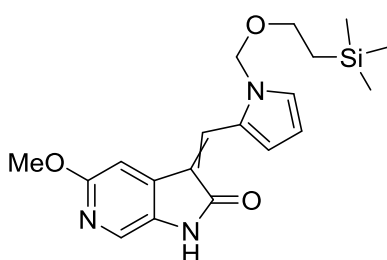
1-((2-(Trimethylsilyloxy)methyl)-1*H*-pyrrole-3-carbaldehyde (292)



1*H*-pyrrole-3-carbaldehyde (500 mg, 5.25 mmol) was dissolved in THF (21 mL) and cooled to 0 °C. NaH (60% in mineral oil, 252 mg, 6.30 mmol) was added portion wise and the mixture was stirred at 0 °C for 30 min. 2-(chloromethoxy)ethyltrimethylsilane (1.02 mL, 5.78 mmol) was added and the reaction mixture was stirred at r.t. for 2.5 h. The reaction was quenched with saturated NH₄Cl (30 mL) and the aqueous layer was extracted with EtOAc (3×50 mL). The organic layers were combined, dried over MgSO₄ and the solvent removed *in vacuo*.

Purification by MPLC on SiO₂ (Petrol:EtOAc, 0-20%) gave colourless oil (1 g, 85%). ¹H NMR (500 MHz, CD₃Cl) δ_H 0.00 (9H, s, Si(CH₃)₃), 0.91-0.95 (2H, m, CH₂), 3.56-3.59 (2H, m, CH₂), 5.74 (2H, s, NCH₂O), 6.33 (1H, dd, *J* = 3.9 and 2.6 Hz, Ar-*H*), 7.01 (1H, dd, *J* = 3.9 and 1.7 Hz, Ar-*H*), 7.17-7.18 (1H, m, 1×Ar-*H*), 9.62 (1H, d, *J* = 1.0 Hz, CHO); ¹³C NMR (125 MHz, CD₃Cl) δ_C 0.0 (Si(CH₃)₃), 19.3 (CH₂), 67.6 (CH₂), 78.1 (NCH₂O), 112.0 (C-Ar), 126.7 (C-Ar), 132.5 (C-Ar), 133.3 (C-Ar), 181.1 (C=O).

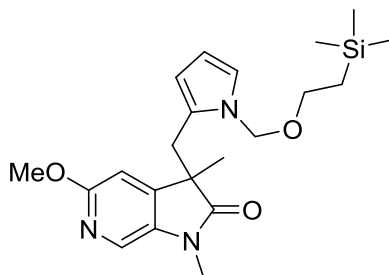
5-Methoxy-3-((1-((2-(trimethylsilyl)ethoxy)methyl)-1*H*-pyrrol-2-yl)methylene)-1,3-dihydro-2*H*-pyrrolo[2,3-*c*]pyridin-2-one (293)



Prepared according to general procedure C using compound **191** (335 mg, 1.26 mmol), compound **292** (343 mg, 1.52 mmol), piperidine (250 μL, 2.53 mmol) and THF (250 μL), except temperature was 60 °C. Purification by MPLC on SiO₂ (DCM:MeOH, 0-5%) gave an orange solid (372 mg, 79%), ratio of diastereomers = 4:3; R_f = 0.32 (5% MeOH/DCM); m.p. 142-145 °C; λ_{max} (EtOH)/nm 399.8, 260.4, 209.0; IR ν_{max}/cm⁻¹ 3137, 3085, 2946, 2888, 1688 (C=O); ¹H NMR (500 MHz, DMSO-*d*₆) δ_H -0.12 (9H, s, Si(CH₃)₃, isomer 1), -0.10 (9H, s, Si(CH₃)₃, isomer 2), 0.78-0.83 (2H, m, CH₂, isomer 1 and 2), 3.43-3.47 (2H, m, CH₂, isomer 1 and 2), 3.80 (3H, s, OCH₃, isomer 1), 3.81 (3H, s, OCH₃, isomer 2), 5.50 (2H, s, NCH₂O, isomer 1), 5.67 (2H, s, NCH₂O, isomer 2), 6.35 (1H, dd, *J* = 4.1 and 2.7 Hz, Ar-*H*, isomer 2), 6.42 (1H, dd, *J* = 3.7 and 2.7 Hz, Ar-*H*, isomer 1), 7.12 (1H, s, Ar-*H*, isomer 2), 7.15 (1H, d, *J* = 3.3 Hz, Ar-*H*, isomer 1), 7.29 (1H, s, Ar-*H*, isomer 1), 7.45 (1H, dd, *J* = 2.5 and 1.4 Hz, Ar-*H*, isomer 1), 7.46 (1H, dd, *J* = 2.5 and 1.7 Hz, Ar-*H*, isomer 2), 7.60 (1H, s, Ar-*H*, isomer 2), 7.68 (1H, s, Ar-*H*, isomer 1), 7.79 (1H, s, Ar-*H*, isomer 1), 7.84 (1H, s, Ar-*H*, isomer 2), 8.42 (1H, dd, *J* = 4.0 and 1.5 Hz, Ar-*H*, isomer 2), 10.43 (1H, s, NH, isomer 2), 10.49 (1H, s, NH, isomer 2); ¹³C NMR (125 MHz, DMSO-*d*₆) δ_C -0.6 (Si(CH₃)₃, isomer 1), -0.5 (Si(CH₃)₃, isomer 2), 17.9 (CH₂, isomer 1 and 2), 54.0 (OCH₃, isomer 1 and 2), 65.9 (CH₂, isomer 1), 66.0 (CH₂, isomer 2), 76.2 (NCH₂O, isomer 1), 76.7 (NCH₂O, isomer 2), 100.5, 103.5, 111.1, 111.2, 117.3, 119.2, 120.5, 124.0, 125.3, 126.1, 127.5, 128.0, 128.9, 129.2, 130.8, 132.0, 132.1, 133.5, 133.8, 138.6,

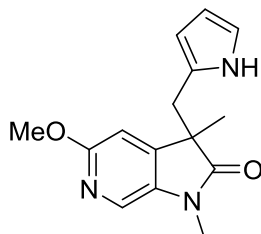
159.7 (C-OMe, isomer 1), 160.0 (C-OMe, isomer 2), 167.8 (C=O, isomer 1), 169.6 (C=O, isomer 2); HRMS calcd for C₁₉H₂₆N₃O₃Si [M+H]⁺ 372.1738, found 372.1732.

5-Methoxy-1,3-dimethyl-3-((1-((2-(trimethylsilyl)ethoxy)methyl)-1H-pyrrol-2-yl)methyl)-1,3-dihydro-2H-pyrrolo[2,3-c]pyridin-2-one (295)



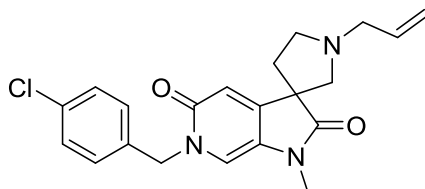
Prepared according to general procedure D using compound **293** (100 mg, 0.27 mmol), 10% Pd/C (20 mg), THF (15 mL) and MeOH (7.5 mL) in step A and Cs₂CO₃ (202 mg, 0.62 mmol), MeI (40 μL, 0.62 mmol), DMF (5 mL) in Step B; reaction done at r.t.. Purification by MPLC on SiO₂ (DCM:MeOH, 0-5%) gave a beige sticky liquid (72 mg, 67%). R_f = 0.57 (5% MeOH/DCM); λ_{max} (EtOH)/nm 305.4, 250.0; IR ν_{max}/cm⁻¹ 2949, 2892, 1708 (C=O); ¹H NMR (500 MHz, CD₃Cl) δ_H -0.047 (9H, s, SiC(CH₃)₃), 0.77-0.87 (2H, m, CH₂), 1.43 (3H, s, CH₃), 3.11 (1H, d, *J* = 15.2 Hz, Pyrrolidinone-CH₂-Pyrrole), 3.11 (3H, s, NCH₃), 3.19 (1H, d, *J* = 15.2 Hz, CH₂-Pyrrole), 3.27-3.35 (2H, m, CH₂), 3.88 (3H, s, OCH₃), 4.90 (1H, d, *J* = 11.2 Hz, NCH₂O), 5.10 (1H, d, *J* = 11.2 Hz, NCH₂O), 5.59 (1H, dd, *J* = 3.4 and 1.6 Hz, Pyrrole-*H*), 5.89 (1H, app t, Pyrrole-*H*), 6.44 (1H, d, *J* = 0.6 Hz, 1×Pyridine-*H*), 6.52 (1H, dd, *J* = 2.7 and 1.7 Hz, Pyrrole-*H*), 7.54 (1H, d, *J* = 0.6 Hz, 1×Pyridine-*H*); ¹³C NMR (125 MHz, CD₃Cl) δ_C 0.0 (SiC(CH₃)₃), 19.1 (CH₂), 24.4 (CH₃), 27.9 (N(CH₃)₂), 34.5 (Pyrrolidinone-CH₂-Pyrrole), 50.8 (C(CH₃)), 55.0 (OCH₃), 66.7 (CH₂), 77.4 (NCH₂O), 108.0 (C-Ar), 108.7 (C-Ar), 111.0 (C-Ar), 123.2 (C-Ar), 125.2 (C-Ar), 128.3 (C-Ar), 161.9 (C-OMe), 180.1 (C=O pyrrolidinone), 2 aromatic carbons not observed due to dilute NMR sample; HRMS calcd for C₂₁H₃₂N₃O₃Si [M+H]⁺ 402.2207, found 402.2203.

3-((1*H*-Pyrrol-2-yl)methyl)-5-methoxy-1,3-dimethyl-1,3-dihydro-2*H*-pyrrolo[2,3-*c*]pyridin-2-one (298)



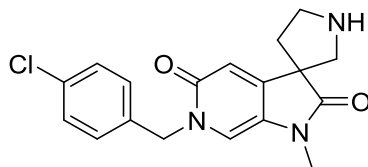
Compound **295** (55 mg, 0.13 mmol) was dissolved in THF (0.25 mL), 1 M TBAF in THF (0.7 mL, 0.7 mmol) was added and the reaction mixture was stirred at 50 °C for 48 h. THF (20 mL) and TBAF scavenger (1 g) were added to the reaction and the mixture was stirred at r.t. for 48 h. The reaction mixture was filtered and the filtrate was evaporated *in vacuo* to get an off-white solid (19 mg, 51%). $R_f = 0.42$ (5% MeOH/DCM); m.p. 146-149 °C; λ_{\max} (EtOH)/nm 249.4; IR $\nu_{\max}/\text{cm}^{-1}$ 3348 (NH), 2976, 2928, 2863, 1706 (C=O); $^1\text{H NMR}$ (500 MHz, CD_3Cl) δ_{H} 1.30 (3H, s, CH_3), 2.91 (1H, d, $J = 14.5$ Hz, CH_2), 3.03 (1H, d, $J = 14.5$ Hz, CH_2), 3.06 (3H, s, N- CH_3), 3.79 (3H, s, OCH_3), 5.40-5.42 (1H, m, Pyrrole-*H*), 5.77 (1H, dd, $J = 5.6$ and 2.6 Hz, Pyrrole-*H*), 6.44-6.46 (1H, m, Pyrrole-*H*), 6.59 (1H, d, $J = 0.7$ Hz, 1×Pyridone-*H*), 7.69 (1H, d, $J = 0.7$ Hz, 1×Pyridone-*H*), 10.3 (1H, s, NH); $^{13}\text{C NMR}$ (125 MHz, CD_3Cl) δ_{C} 23.0 (CH_3), 26.6 (N- CH_3), 35.3 (CH_2), 49.2 (C(CH_3)), 53.6 (OCH_3), 106.2 (C-Ar), 106.8 (C-Ar), 107.8 (C-Ar), 116.7 (C-Ar), 124.3 (C-Ar), 126.3 (C-Ar), 135.4 (C-Ar), 147.1 (C-Ar), 159.9 (C-Ar), 178.5 (C=O pyrrolidinone); HRMS calcd for $\text{C}_{15}\text{H}_{18}\text{N}_3\text{O}_2$ $[\text{M}+\text{H}]^+$ 272.1394, found 272.1394.

1-Allyl-6'-(4-chlorobenzyl)-1'-methyl-1',6'-dihydrospiro[pyrrolidine-3,3'-pyrrolo[2,3-*c*]pyridine]-2',5'-dione (273)



Prepared according to general procedure E using Compound **265** (30 mg, 0.095 mmol), MgI_2 (5 mg), compound **276** (118 mg, 0.57 mmol) and THF (0.3 mL). The residue was purified by MPLC on SiO_2 (DCM:MeOH, 0-7%) gave a sticky beige solid (16 mg). The compound was not pure enough by $^1\text{H-NMR}$. However, to avoid the loss of any material, the compound was taken forward without further purification and characterisation.

6'-(4-Chlorobenzyl)-1'-methyl-1',6'-dihydrospiro[pyrrolidine-3,3'-pyrrolo[2,3-c]pyridine]-2',5'-dione (253)



To a mixture of tetrakis(triphenylphosphine) palladium (2 mg, 4.4 mol%) and N,N-dimethylbarbituric acid (15 mg, 0.097 mmol), a solution of compound **273** (15 mg, 0.039 mmol) in DCM (1 mL) purged with N₂ was added and the mixture was stirred at 35 °C for 16 h. The solvent was removed *in vacuo* and the residue was treated with saturated NaHCO₃ (10 mL) and Et₂O (10 mL) and the mixture was stirred for 30 min. The aqueous layer was collected and the residue was purified by eluting through a pad of amine silica (DCM:MeOH, 10%) to get beige sticky solid (7 mg, 22% over 2 steps). R_f=0.48 (15% MeOH/DCM); λ_{max} (EtOH)/nm 339.4, 221.2; IR ν_{max}/cm⁻¹ 3415 (NH), 3045, 2921, 2851, 1705 (C=O), 1585 (C=O); ¹H NMR (500 MHz, CD₃Cl) δ_H 2.00-2.06 (1H, m, Pyrrolidine-*H*), 2.29-2.35 (1H, m, Pyrrolidine-*H*), 2.92-2.96 (1H, m, Pyrrolidine-*H*), 3.06 (1H, s, N-CH₃), 3.14-3.19 (1H, m, Pyrrolidine-*H*), 3.36-3.39 (2H, m, Pyrrolidine-*H*), 5.09 (2H, s, CH₂-Ar), 6.55 (1H, s, 1×Pyridone-*H*), 6.62 (1H, s, 1×Pyridone-*H*), 7.25-7.27 (2H, m, 2×Ar-*H*), 7.31-7.33 (2H, m, 2×Ar-*H*); ¹³C NMR (125 MHz, CD₃Cl) δ_C 26.5 (N-CH₃), 39.6 (C-Pyrrolidine), 49.0 (C-Pyrrolidine), 51.5 (NCH₂Ar), 54.2 (C), 60.7 (C-Pyrrolidine), 112.4 (CH-Pyridone), 114.8 (CH-Pyridone), 127.4 (C-Ar), 129.1 (2×C-Ar), 129.4 (2×C-Ar), 134.1 (C-Ar), 135.0 (C-Ar), 150.9 (C-Ar), 161.4 (C=O pyridone), 178.0 (C=O pyrrolidinone); HRMS calcd for C₁₈H₁₉ClN₃O₂ [M(³⁵Cl)+H]⁺ 344.1160, found 344.1160.

Appendices

Crystal data and structure refinement for RO2443 3.

Identification code	rjg130001	
Chemical formula (moiety)	C ₂₄ H ₂₀ ClF ₂ N ₃ O ₄	
Chemical formula (total)	C ₂₄ H ₂₀ ClF ₂ N ₃ O ₄	
Formula weight	487.88	
Temperature	150(2) K	
Radiation, wavelength	MoK α , 0.71073 Å	
Crystal system, space group	triclinic, P $\bar{1}$	
Unit cell parameters	a = 8.8755(5) Å	$\alpha = 78.372(6)^\circ$
	b = 10.4934(7) Å	$\beta = 81.700(5)^\circ$
	c = 13.5493(9) Å	$\gamma = 69.763(6)^\circ$
Cell volume	1155.88(13) Å ³	
Z	2	
Calculated density	1.402 g/cm ³	
Absorption coefficient μ	0.218 mm ⁻¹	
F(000)	504	
Crystal colour and size	0.40 × 0.02 × 0.02 mm ³	
Reflections for cell refinement	2773 (θ range 3.8 to 28.5°)	
Data collection method	Xcalibur, Atlas, Gemini ultra thick-slice ω scans	
θ range for data collection	3.0 to 26.0°	
Index ranges	h -10 to 10, k -12 to 12, l -16 to 16	
Completeness to $\theta = 25.0^\circ$	99.8 %	
Reflections collected	10284	
Independent reflections	4441 ($R_{\text{int}} = 0.0335$)	
Reflections with $F^2 > 2\sigma$	3486	
Absorption correction	semi-empirical from equivalents	
Min. and max. transmission	0.9180 and 0.9957	
Structure solution	direct methods	
Refinement method	Full-matrix least-squares on F^2	
Weighting parameters a, b	0.0624, 0.5323	
Data / restraints / parameters	4441 / 0 / 311	
Final R indices [$F^2 > 2\sigma$]	R1 = 0.0478, wR2 = 0.1155	
R indices (all data)	R1 = 0.0669, wR2 = 0.1293	
Goodness-of-fit on F^2	1.030	
Extinction coefficient	0.0031(16)	
Largest and mean shift/su	0.005 and 0.000	
Largest diff. peak and hole	0.77 and -0.26 e Å ⁻³	

References

1. Greaves, M.; Maley, C. C., Clonal evolution in cancer. *Nature* **2012**, *481* (7381), 306-313.
2. Gillies, R. J.; Verduzco, D.; Gatenby, R. A., Evolutionary dynamics of carcinogenesis and why targeted therapy does not work. *Nat. Rev. Cancer* **2012**, *12* (7), 487-493.
3. Greenman, C.; Stephens, P.; Smith, R.; Dalgliesh, G. L.; Hunter, C.; Bignell, G.; Davies, H.; Teague, J.; Butler, A.; Stevens, C.; Edkins, S.; O'Meara, S.; Vastrik, I.; Schmidt, E. E.; Avis, T.; Barthorpe, S.; Bhamra, G.; Buck, G.; Choudhury, B.; Clements, J.; Cole, J.; Dicks, E.; Forbes, S.; Gray, K.; Halliday, K.; Harrison, R.; Hills, K.; Hinton, J.; Jenkinson, A.; Jones, D.; Menzies, A.; Mironenko, T.; Perry, J.; Raine, K.; Richardson, D.; Shepherd, R.; Small, A.; Tofts, C.; Varian, J.; Webb, T.; West, S.; Widaa, S.; Yates, A.; Cahill, D. P.; Louis, D. N.; Goldstraw, P.; Nicholson, A. G.; Bressan, F.; Looijenga, L.; Weber, B. L.; Chiew, Y.-E.; deFazio, A.; Greaves, M. F.; Green, A. R.; Campbell, P.; Birney, E.; Easton, D. F.; Chenevix-Trench, G.; Tan, M.-H.; Khoo, S. K.; Teh, B. T.; Yuen, S. T.; Leung, S. Y.; Wooster, R.; Futreal, P. A.; Stratton, M. R., Patterns of somatic mutation in human cancer genomes. *Nature* **2007**, *446* (7132), 153-158.
4. Vogelstein, B.; Kinzler, K. W., Cancer genes and the pathways they control. *Nat. Med.* **2004**, *10* (8), 789-799.
5. Stratton, M. R., Exploring the genomes of cancer cells: Progress and promise. *Science* **2011**, *331* (6024), 1553-1558.
6. Nowell, P. C., The clonal evolution of tumor cell populations. Acquired genetic lability permits stepwise selection of variant sublines and underlies tumor progression. *Science* **1976**, *194* (4260), 23-28.
7. Dick, J. E., Stem cell concepts renew cancer research. *Blood* **2008**, *112* (13), 4793-4807.
8. Shackleton, M.; Quintana, E.; Fearon, E. R.; Morrison, S. J., Heterogeneity in Cancer: Cancer Stem Cells versus Clonal Evolution. *Cell* **2009**, *138* (5), 822-829.
9. Hanahan, D.; Weinberg, R. A., The hallmarks of cancer. *Cell* **2000**, *100* (1), 57-70.
10. Hanahan, D.; Weinberg, R. A., Hallmarks of cancer: The next generation. *Cell* **2011**, *144* (5), 646-674.
11. DeVita Jr, V. T.; Chu, E., A history of cancer chemotherapy. *Cancer Res.* **2008**, *68* (21), 8643-8653.
12. Chabner, B. A.; Roberts Jr, T. G., Chemotherapy and the war on cancer. *Nat. Rev. Cancer* **2005**, *5* (1), 65-72.

13. Hurley, L. H., DNA and its associated processes as targets for cancer therapy. *Nat. Rev. Cancer* **2002**, 2 (3), 188-200.
14. Druker, B. J.; Tamura, S.; Buchdunger, E.; Ohno, S.; Segal, G. M.; Fanning, S.; Zimmermann, J.; Lydon, N. B., Effects of a selective inhibitor of the Ab1 tyrosine kinase on the growth of Bcr-Ab1 positive cells. *Nat. Med.* **1996**, 2 (5), 561-566.
15. Druker, B. J.; Sawyers, C. L.; Kantarjian, H.; Resta, D. J.; Reese, S. F.; Ford, J. M.; Capdeville, R.; Talpaz, M., Activity of a Specific Inhibitor of the BCR-ABL Tyrosine Kinase in the Blast Crisis of Chronic Myeloid Leukemia and Acute Lymphoblastic Leukemia with the Philadelphia Chromosome. *New Engl. J. Med.* **2001**, 344 (14), 1038-1042.
16. Capdeville, R.; Buchdunger, E.; Zimmermann, J.; Matter, A., Glivec (STI571, imatinib), a rationally developed, targeted anticancer drug. *Nat. Rev. Drug Discov.* **2002**, 1 (7), 493-502.
17. Tsimberidou, A.-M., Targeted therapy in cancer. *Cancer Chemother. Pharmacol.* **2015**, 76 (6), 1113-1132.
18. Arkin, M. R.; Wells, J. A., Small-molecule inhibitors of protein-protein interactions: progressing towards the dream. *Nat. Rev. Drug Discov.* **2004**, 3 (4), 301-17.
19. Conte, L. L.; Chothia, C.; Janin, J., The atomic structure of protein-protein recognition sites1. *J. Mol. Biol.* **1999**, 285 (5), 2177-2198.
20. Arkin, M. R.; Tang, Y.; Wells, J. A., Small-molecule inhibitors of protein-protein interactions: Progressing toward the reality. *Chem. Biol.* **2014**, 21 (9), 1102-1114.
21. Kussie, P. H.; Gorina, S.; Marechal, V.; Elenbaas, B.; Moreau, J.; Levine, A. J.; Pavletich, N. P., Structure of the MDM2 oncoprotein bound to the p53 tumor suppressor transactivation domain. *Science* **1996**, 274 (5289), 948-953.
22. Fischer, P. M.; Lane, D. P., Small-molecule inhibitors of the p53 suppressor HDM2: Have protein-protein interactions come of age as drug targets? *Trends Pharmacol. Sci.* **2004**, 25 (7), 343-346.
23. Lessene, G.; Czabotar, P. E.; Colman, P. M., BCL-2 family antagonists for cancer therapy. *Nat. Rev. Drug Discov.* **2008**, 7 (12), 989-1000.
24. Petros, A. M.; Olejniczak, E. T.; Fesik, S. W., Structural biology of the Bcl-2 family of proteins. *Biochim. Biophys. Acta* **2004**, 1644 (2-3), 83-94.
25. Sattler, M.; Liang, H.; Nettlesheim, D.; Meadows, R. P.; Harlan, J. E.; Eberstadt, M.; Yoon, H. S.; Shuker, S. B.; Chang, B. S.; Minn, A. J.; Thompson, C. B.; Fesik, S. W., Structure of Bcl-x(L)-Bak peptide complex: Recognition between regulators of apoptosis. *Science* **1997**, 275 (5302), 983-986.

26. Vogler, M.; Dinsdale, D.; Dyer, M. J. S.; Cohen, G. M., Bcl-2 inhibitors: small molecules with a big impact on cancer therapy. *Cell Death Differ.* **2008**, *16* (3), 360-367.
27. Sheng, C.; Dong, G.; Miao, Z.; Zhang, W.; Wang, W., State-of-the-art strategies for targeting protein-protein interactions by small-molecule inhibitors. *Chem. Soc. Rev.* **2015**, *44* (22), 8238-8259.
28. Wang, S.; Sim, T. B.; Kim, Y.-S.; Chang, Y.-T., Tools for target identification and validation. *Curr. Opin. Chem. Biol.* **2004**, *8* (4), 371-377.
29. Schenone, M.; Dancik, V.; Wagner, B. K.; Clemons, P. A., Target identification and mechanism of action in chemical biology and drug discovery. *Nat. Chem. Biol.* **2013**, *9* (4), 232-240.
30. Whittaker, P. A., The role of bioinformatics in target validation. *Drug Discovery Today: Technologies* **2004**, *1* (2), 125-133.
31. Erlanson, D. A.; McDowell, R. S.; O'Brien, T., Fragment-based drug discovery. *J. Med. Chem.* **2004**, *47* (14), 3463-3482.
32. Bohacek, R. S.; McMartin, C.; Guida, W. C., The art and practice of structure-based drug design: A molecular modeling perspective. *Medicinal Research Reviews* **1996**, *16* (1), 3-50.
33. Hughes, J. P.; Rees, S.; Kalindjian, S. B.; Philpott, K. L., Principles of early drug discovery. *Br. J. Pharmacol.* **2011**, *162* (6), 1239-1249.
34. Bleicher, K. H.; Bohm, H.-J.; Muller, K.; Alanine, A. I., Hit and lead generation: beyond high-throughput screening. *Nat. Rev. Drug Discov.* **2003**, *2* (5), 369-378.
35. Vogelstein, B.; Lane, D.; Levine, A. J., Surfing the p53 network. *Nature* **2000**, *408* (6810), 307-310.
36. Hoe, K. K.; Verma, C. S.; Lane, D. P., Drugging the p53 pathway: understanding the route to clinical efficacy. *Nat. Rev. Drug Discov.* **2014**, *13* (3), 217-236.
37. Vousden, K. H.; Lane, D. P., p53 in health and disease. *Nat. Rev. Mol. Cell Biol.* **2007**, *8* (4), 275-83.
38. Vazquez, A.; Bond, E. E.; Levine, A. J.; Bond, G. L., The genetics of the p53 pathway, apoptosis and cancer therapy. *Nat. Rev. Drug Discov.* **2008**, *7* (12), 979-987.
39. Weinberg, R. L.; Veprintsev, D. B.; Fersht, A. R., Cooperative Binding of Tetrameric p53 to DNA. *J. Mol. Biol.* **2004**, *341* (5), 1145-1159.
40. Riley, T.; Sontag, E.; Chen, P.; Levine, A., Transcriptional control of human p53-regulated genes. *Nat. Rev. Mol. Cell Biol.* **2008**, *9* (5), 402-412.

41. Villunger, A.; Michalak, E. M.; Coultas, L.; Müllauer, F.; Böck, G.; Ausserlechner, M. J.; Adams, J. M.; Strasser, A., p53- and Drug-Induced Apoptotic Responses Mediated by BH3-Only Proteins Puma and Noxa. *Science* **2003**, *302* (5647), 1036-1038.
42. Levine, A. J., p53, the cellular gatekeeper for growth and division. *Cell* **1997**, *88* (3), 323-331.
43. Fulda, S.; Debatin, K. M., Extrinsic versus intrinsic apoptosis pathways in anticancer chemotherapy. *Oncogene* **2006**, *25* (34), 4798-4811.
44. Cory, S.; Adams, J. M., The BCL2 family: Regulators of the cellular life-or-death switch. *Nat. Rev. Cancer* **2002**, *2* (9), 647-656.
45. Joerger, A. C.; Fersht, A. R., The tumor suppressor p53: from structures to drug discovery. *Cold Spring Harbor perspectives in biology* **2010**, *2* (6).
46. Joerger, A. C.; Fersht, A. R., Structure-function-rescue: The diverse nature of common p53 cancer mutants. *Oncogene* **2007**, *26* (15), 2226-2242.
47. Marine, J. C.; Francoz, S.; Maetens, M.; Wahl, G.; Toledo, F.; Lozano, G., Keeping p53 in check: essential and synergistic functions of Mdm2 and Mdm4. *Cell Death Differ.* **2006**, *13* (6), 927-934.
48. Walker, K. K.; Levine, A. J., Identification of a novel p53 functional domain that is necessary for efficient growth suppression. *Proc. Natl. Acad. Sci. USA* **1996**, *93*, 15335-15340.
49. Prives, C.; Manley, J. L., Why is p53 acetylated? *Cell* **2001**, *107* (7), 815-818.
50. Friedler, A.; Veprintsev, D. B.; Freund, S. M.; von Glos, K. I.; Fersht, A. R., Modulation of binding of DNA to the C-terminal domain of p53 by acetylation. *Structure* **2005**, *13* (4), 629-36.
51. Kubbutat, M. H. G.; Jones, S. N.; Vousden, K. H., Regulation of p53 stability by Mdm2. *Nature* **1997**, *387* (6630), 299-303.
52. Fang, S.; Jensen, J. P.; Ludwig, R. L.; Vousden, K. H.; Weissman, A. M., Mdm2 Is a RING Finger-dependent Ubiquitin Protein Ligase for Itself and p53. *J. Biol. Chem.* **2000**, *275* (12), 8945-8951.
53. Huang, L.; Yan, Z.; Liao, X.; Li, Y.; Yang, J.; Wang, Z.-G.; Zuo, Y.; Kawai, H.; Shadfan, M.; Ganapathy, S.; Yuan, Z.-M., The p53 inhibitors MDM2/MDMX complex is required for control of p53 activity in vivo. *Proc. Natl. Acad. Sci.* **2011**, *108* (29), 12001-12006.
54. Momand, J.; Zambetti, G. P.; Olson, D. C.; George, D.; Levine, A. J., The mdm-2 oncogene product forms a complex with the p53 protein and inhibits p53-mediated transactivation. *Cell* **1992**, *69* (7), 1237-1245.
55. Chen, J.; Marechal, V.; Levine, A. J., Mapping of the p53 and mdm-2 interaction domains. *Mol. Cell. Biol.* **1993**, *13* (7), 4107-4114.

56. Roth, J.; Dobbelstein, M.; Freedman, D. A.; Shenk, T.; Levine, A. J., Nucleocytoplasmic shuttling of the hdm2 oncoprotein regulates the levels of the p53 protein via a pathway used by the human immunodeficiency virus rev protein. *The EMBO Journal* **1998**, *17* (2), 554-564.
57. Tao, W.; Levine, A. J., Nucleocytoplasmic shuttling of oncoprotein Hdm2 is required for Hdm2-mediated degradation of p53. *Proc. Natl. Acad. Sci.* **1999**, *96* (6), 3077-3080.
58. Wu, X.; Bayle, J. H.; Olson, D.; Levine, A. J., The p53-mdm-2 autoregulatory feedback loop. *Genes and Development* **1993**, *7* (7), 1126-1132.
59. Picksley, S. M.; Lane, D. P., The p53-mcdm2 autoregulatory feedback loop: A paradigm for the regulation of growth control by p53? *Bioessays* **1993**, *15* (10), 689-690.
60. Zhao, Y.; Aguilar, A.; Bernard, D.; Wang, S., Small-Molecule Inhibitors of the MDM2–p53 Protein–Protein Interaction (MDM2 Inhibitors) in Clinical Trials for Cancer Treatment. *J. Med. Chem.* **2015**, *58* (3), 1038-1052.
61. Zhang, B.; Golding, B. T.; Hardcastle, I. R., Small-molecule MDM2-p53 inhibitors: Recent advances. *Future. Med. Chem.* **2015**, *7* (5), 631-645.
62. Shvarts, A.; Steegenga, W. T.; Riteco, N.; Van Laar, T.; Dekker, P.; Bazuine, M.; Van Ham, R. C. A.; Van Der Houven Van Oordt, W.; Hateboer, G.; Van Der Eb, A. J.; Jochemsen, A. G., MDMX: A novel p53-binding protein with some functional properties of MDM2. *EMBO Journal* **1996**, *15* (19), 5349-5357.
63. Shvarts, A.; Bazuine, M.; Dekker, P.; Ramos, Y. F. M.; Steegenga, W. T.; Merckx, G.; Van Ham, R. C. A.; Van Der Houven Van Oordt, W.; Van Der Eb, A. J.; Jochemsen, A. G., Isolation and identification of the human homolog of a new p53-binding protein, Mdmx. *Genomics* **1997**, *43* (1), 34-42.
64. Carrillo, A. M.; Bouska, A.; Arrate, M. P.; Eischen, C. M., Mdmx promotes genomic instability independent of p53 and Mdm2. *Oncogene* **2015**, *34* (7), 846-856.
65. Laurie, N. A.; Donovan, S. L.; Shih, C.-S.; Zhang, J.; Mills, N.; Fuller, C.; Teunisse, A.; Lam, S.; Ramos, Y.; Mohan, A.; Johnson, D.; Wilson, M.; Rodriguez-Galindo, C.; Quarto, M.; Francoz, S.; Mendrysa, S. M.; Kiplin Guy, R.; Marine, J.-C.; Jochemsen, A. G.; Dyer, M. A., Inactivation of the p53 pathway in retinoblastoma. *Nature* **2006**, *444* (7115), 61-66.
66. Danovi, D.; Meulmeester, E.; Pasini, D.; Migliorini, D.; Capra, M.; Frenk, R.; de Graaf, P.; Francoz, S.; Gasparini, P.; Gobbi, A.; Helin, K.; Pelicci, P. G.; Jochemsen, A. G.; Marine, J.-C., Amplification of Mdmx (or Mdm4) Directly Contributes to Tumor Formation by Inhibiting p53 Tumor Suppressor Activity. *Mol. Cell. Biol.* **2004**, *24* (13), 5835-5843.
67. Gembarska, A.; Luciani, F.; Fedele, C.; Russell, E. A.; Dewaele, M.; Villar, S.; Zwolinska, A.; Haupt, S.; de Lange, J.; Yip, D.; Goydos, J.; Haigh, J. J.; Haupt, Y.; Larue, L.;

Jochemsen, A.; Shi, H.; Moriceau, G.; Lo, R. S.; Ghanem, G.; Shackleton, M.; Bernal, F.; Marine, J.-C., MDM4 is a key therapeutic target in cutaneous melanoma. *Nat. Med.* **2012**, *18* (8), 1239-1247.

68. Parant, J.; Chavez-Reyes, A.; Little, N. A.; Yan, W.; Reinke, V.; Jochemsen, A. G.; Lozano, G., Rescue of embryonic lethality in Mdm4-null mice by loss of Trp53 suggests a nonoverlapping pathway with MDM2 to regulate p53. *Nat. Genet.* **2001**, *29* (1), 92-95.

69. Migliorini, D.; Denchi, E. L.; Danovi, D.; Jochemsen, A.; Capillo, M.; Gobbi, A.; Helin, K.; Pelicci, P. G.; Marine, J.-C., Mdm4 (Mdmx) Regulates p53-Induced Growth Arrest and Neuronal Cell Death during Early Embryonic Mouse Development. *Mol. Cell. Biol.* **2002**, *22* (15), 5527-5538.

70. Hu, B.; Gilkes, D. M.; Farooqi, B.; Sebti, S. M.; Chen, J., MDMX overexpression prevents p53 activation by the MDM2 inhibitor nutlin. *J. Biol. Chem.* **2006**, *281* (44), 33030-33035.

71. Graves, B.; Thompson, T.; Xia, M.; Janson, C.; Lukacs, C.; Deo, D.; Di Lello, P.; Fry, D.; Garvie, C.; Huang, K. S.; Gao, L.; Tovar, C.; Lovey, A.; Wanner, J.; Vassilev, L. T., Activation of the p53 pathway by small-molecule-induced MDM2 and MDMX dimerization. *Proc. Natl. Acad. Sci. USA* **2012**, *109* (29), 11788-11793.

72. Chang, Y. S.; Graves, B.; Guerlavais, V.; Tovar, C.; Packman, K.; To, K.-H.; Olson, K. A.; Kesavan, K.; Gangurde, P.; Mukherjee, A.; Baker, T.; Darlak, K.; Elkin, C.; Filipovic, Z.; Qureshi, F. Z.; Cai, H.; Berry, P.; Feyfant, E.; Shi, X. E.; Horstick, J.; Annis, D. A.; Manning, A. M.; Fotouhi, N.; Nash, H.; Vassilev, L. T.; Sawyer, T. K., Stapled α -helical peptide drug development: A potent dual inhibitor of MDM2 and MDMX for p53-dependent cancer therapy. *Proc. Natl. Acad. Sci.* **2013**, *110* (36), E3445-E3454.

73. Matijasevic, Z.; Krzywicka-Racka, A.; Sluder, G.; Jones, S. N., MdmX regulates transformation and chromosomal stability in p53-deficient cells. *Cell Cycle* **2008**, *7* (19), 2967-2973.

74. Marine, J. C. W.; Dyer, M. A.; Jochemsen, A. G., MDMX: From bench to bedside. *Journal of Cell Science* **2007**, *120* (3), 371-378.

75. Lee, J. T.; Gu, W., The multiple levels of regulation by p53 ubiquitination. *Cell Death Differ.* **2009**, *17* (1), 86-92.

76. Popowicz, G. M.; Czarna, A.; Holak, T. A., Structure of the human Mdmx protein bound to the p53 tumor suppressor transactivation domain. *Cell Cycle* **2008**, *7* (15), 2441-2443.

77. Popowicz, G. M.; Dömling, A.; Holak, T. A., The structure-based design of Mdm2/Mdmx-p53 inhibitors gets serious. *Angew. Chem. Int. Ed.* **2011**, *50* (12), 2680-2688.

78. Hu, B.; Gilkes, D. M.; Chen, J., Efficient p53 activation and apoptosis by simultaneous disruption of binding to MDM2 and MDMX. *Cancer Res.* **2007**, *67* (18), 8810-8817.
79. Pazgier, M.; Liu, M.; Zou, G.; Yuan, W.; Li, C.; Li, C.; Li, J.; Monbo, J.; Zella, D.; Tarasov, S. G.; Lu, W., Structural basis for high-affinity peptide inhibition of p53 interactions with MDM2 and MDMX. *Proc. Natl. Acad. Sci. USA* **2009**, *106* (12), 4665-4670.
80. Verdine, G. L.; Hilinski, G. J., Stapled peptides for intracellular drug targets. 2012; Vol. 503, pp 3-33.
81. Bernal, F.; Wade, M.; Godes, M.; Davis, T. N.; Whitehead, D. G.; Kung, A. L.; Wahl, G. M.; Walensky, L. D., A Stapled p53 Helix Overcomes HDMX-Mediated Suppression of p53. *Cancer Cell* **2010**, *18* (5), 411-422.
82. Reed, D.; Shen, Y.; Shelat, A. A.; Arnold, L. A.; Ferreira, A. M.; Zhu, F.; Mills, N.; Smithson, D. C.; Regni, C. A.; Bashford, D.; Cicero, S. A.; Schulman, B. A.; Jochemsen, A. G.; Guy, R. K.; Dyer, M. A., Identification and characterization of the first small molecule inhibitor of MDMX. *J. Biol. Chem.* **2010**, *285* (14), 10786-10796.
83. Bista, M.; Smithson, D.; Pecak, A.; Salinas, G.; Pustelny, K.; Min, J.; Pirog, A.; Finch, K.; Zdzalik, M.; Waddell, B.; Wladyka, B.; Kedracka-Krok, S.; Dyer, M. A.; Dubin, G.; Guy, R. K., On the mechanism of action of SJ-172550 in inhibiting the interaction of MDM4 and p53. *PLoS ONE* **2012**, *7* (6).
84. Boettcher, A.; Buschmann, N.; Furet, P.; Groell, J. M.; Kallen, J.; Hergovich, L. J.; Masuya, K.; Mayr, L.; Vaupel, A., 3-imidazolyl-indoles for the treatment of proliferative diseases. Google Patents: 2008.
85. Neochoritis, C. G.; Wang, K.; Estrada-Ortiz, N.; Herdtweck, E.; Kubica, K.; Twarda, A.; Zak, K. M.; Holak, T. A.; Dömling, A., 2,3'-Bis(1'H-indole) heterocycles: New p53/MDM2/MDMX antagonists. *Bioorg. Med. Chem. Lett.* **2015**, *25* (24), 5661-5666.
86. Popowicz, G. M.; Czarna, A.; Wolf, S.; Wang, K.; Wang, W.; Dömling, A.; Holak, T. A., Structures of low molecular weight inhibitors bound to MDMX and MDM2 reveal new approaches for p53-MDMX/MDM2 antagonist drug discovery. *Cell Cycle* **2010**, *9* (6), 1104-1111.
87. Zhuang, C.; Miao, Z.; Zhu, L.; Dong, G.; Guo, Z.; Wang, S.; Zhang, Y.; Wu, Y.; Yao, J.; Sheng, C.; Zhang, W., Discovery, synthesis, and biological evaluation of orally active pyrrolidone derivatives as novel inhibitors of p53-MDM2 protein-protein interaction. *J. Med. Chem.* **2012**, *55* (22), 9630-9642.
88. Qin, L.; Yang, F.; Zhou, C.; Chen, Y.; Zhang, H.; Su, Z., Efficient Reactivation of p53 in Cancer Cells by a Dual MdmX/Mdm2 Inhibitor. *J. Am. Chem. Soc.* **2014**, *136* (52), 18023-18033.

89. Qin, L.; Yang, F.; Zhou, C.; Chen, Y.; Zhang, H.; Su, Z., Retraction of "Efficient Reactivation of p53 in Cancer Cells by a Dual MdmX/Mdm2 Inhibitor". *J. Am. Chem. Soc.* **2015**, *137* (45), 14546-14546.
90. Blackburn, T. J.; Ahmed, S.; Coxon, C. R.; Liu, J.; Lu, X.; Golding, B. T.; Griffin, R. J.; Hutton, C.; Newell, D. R.; Ojo, S.; Watson, A. F.; Zaytzev, A.; Zhao, Y.; Lunec, J.; Hardcastle, I. R., Diaryl- and triaryl-pyrrole derivatives: inhibitors of the MDM2-p53 and MDMX-p53 protein-protein interactions. *MedChemComm* **2013**, *4* (9), 1297-1304.
91. Baell, J. B.; Holloway, G. A., New Substructure Filters for Removal of Pan Assay Interference Compounds (PAINS) from Screening Libraries and for Their Exclusion in Bioassays. *J. Med. Chem.* **2010**, *53* (7), 2719-2740.
92. Bulatov, E., Identification and validation of a series of p53-MDM2 and p53-MDMX protein-protein interaction inhibitors. MPhil thesis, Newcastle University, Newcastle-Upon-Tyne, UK. **2010**.
93. Molecular Operating Environment (MOE), 2013.08; Chemical Computing Group Inc., 1010 Sherbooke St. West, Suite #910, Montreal, QC, Canada, H3A 2R7, **2015**.
94. Minetto, G.; Raveglia, L. F.; Taddei, M., Microwave-Assisted Paal-Knorr Reaction. A Rapid Approach to Substituted Pyrroles and Furans. *Org. Lett.* **2004**, *6* (3), 389-392.
95. Berti, G.; Da Settimo, A.; Nannipieri, E., The reactions of some indole derivatives with benzoyl nitrate. Novel oxidative coupling reactions of 2-methylindoles. *J. Chem. Soc. C* **1968**, 2145-2151.
96. Pelkey, E. T.; Gribble, G. W., Synthesis and reactions of N-protected 3-nitroindoles. *Synthesis* **1999**, (7), 1117-1122.
97. Lee, H.; Kim, B. H., Indium-mediated one-pot pyrrole synthesis from nitrobenzenes and 1,4-diketones. *Tetrahedron* **2013**, *69* (32), 6698-6708.
98. Minetto, G.; Raveglia, L. F.; Sega, A.; Taddei, M., Microwave-assisted Paal-Knorr reaction - Three-step regiocontrolled synthesis of polysubstituted furans, pyrroles and thiophenes. *Eur. J. Org. Chem.* **2005**, (24), 5277-5288.
99. Chen, G.; Wang, Z.; Wu, J.; Ding, K., Facile preparation of α -aryl nitriles by direct cyanation of alcohols with TMSCN under the catalysis of InX₃. *Org. Lett.* **2008**, *10* (20), 4573-4576.
100. Cafiero, L. R.; Snowden, T. S., General and Practical Conversion of Aldehydes to Homologated Carboxylic Acids. *Org. Lett.* **2008**, *10* (17), 3853-3856.
101. Fraile, J. M.; Lafuente, G.; Mayoral, J. A.; Pallarés, A., Synthesis and reactivity of 5-methylenehydantoins. *Tetrahedron* **2011**, *67* (45), 8639-8647.

102. Patton, J. T.; Mayo, L. D.; Singhi, A. D.; Gudkov, A. V.; Stark, G. R.; Jackson, M. W., Levels of HdmX expression dictate the sensitivity of normal and transformed cells to Nutlin-3. *Cancer Res.* **2006**, *66* (6), 3169-3176.
103. Wang, H.; Ma, X.; Ren, S.; Buolamwini, J. K.; Yan, C., A small-molecule inhibitor of MDMX activates p53 and induces apoptosis. *Molecular Cancer Therapeutics* **2011**, *10* (1), 69-79.
104. Shouksmith, A. E., Design and synthesis of small-molecule inhibitors targeting the SCF^{SKP2} E3 ligase and the MDMX-p53 interaction for cancer therapy. PhD thesis, Newcastle University, Newcastle-Upon-Tyne, UK. **2014**.
105. Bertoli, A., Design and synthesis of anti-tumour agents targeting Sulf2 and MDMX:p53. PhD thesis, Newcastle University, Newcastle-Upon-Tyne, UK. **2015**.
106. Cully, S. J., Design and synthesis of isoindolinone MDM2-p53 inhibitors. PhD thesis, Newcastle University, Newcastle-Upon-Tyne, UK. **2014**.
107. GE Life Sciences; <http://www.gelifesciences.com/> (accessed August 2015).
108. Bista, M.; Petrovich, M.; Fersht, A. R., MDMX contains an autoinhibitory sequence element. *Proc. Natl. Acad. Sci. USA* **2013**, *110* (44), 17814-17819.
109. Chen, L.; Borchers, W.; Wu, S.; Becker, A.; Schonbrunn, E.; Daughdrill, G. W.; Chen, J., Autoinhibition of MDMX by intramolecular p53 mimicry. *Proc. Natl. Acad. Sci. USA* **2015**, *112* (15), 4624-4629.
110. Kolb, J. M.; Yamanaka, G.; Manly, S. P., Use of a novel homogeneous fluorescent technology in high throughput screening. *J. Biomol. Screen.* **1996**, *1* (4), 203-210.
111. Degorce, F.; Card, A.; Soh, S.; Trinquet, E.; Knapik, G. P.; Xie, B., HTRF: A technology tailored for drug discovery - A review of theoretical aspects and recent applications. *Curr. Chem. Genomics* **2009**, *3* (1), 22-32.
112. Bazin, H.; Trinquet, E.; Mathis, G., Time resolved amplification of cryptate emission: a versatile technology to trace biomolecular interactions. *Reviews in Molecular Biotechnology* **2002**, *82* (3), 233-250.
113. Böttger, V.; Böttger, A.; Howard, S. F.; Picksley, S. M.; Chène, P.; Garcia-Echeverria, C.; Hochkeppel, H. K.; Lane, D. P., Identification of novel mdm2 binding peptides by phage display. *Oncogene* **1996**, *13* (10), 2141-2147.
114. Reeks, J., Unpublished work.
115. Stapled peptides YSO1 and YSO2 were provided by Professor David Lane, p53 laboratory, A Star Biomedical Sciences Institutes, Singapore.
116. Bird, A., Perceptions of epigenetics. *Nature* **2007**, *447* (7143), 396-398.

117. Portela, A.; Esteller, M., Epigenetic modifications and human disease. *Nat Biotech* **2010**, *28* (10), 1057-1068.
118. Arrowsmith, C. H.; Bountra, C.; Fish, P. V.; Lee, K.; Schapira, M., Epigenetic protein families: A new frontier for drug discovery. *Nat. Rev. Drug Discov.* **2012**, *11* (5), 384-400.
119. Khorasanizadeh, S., The Nucleosome: From Genomic Organization to Genomic Regulation. *Cell* **2004**, *116* (2), 259-272.
120. Kornberg, R. D., Chromatin structure: a repeating unit of histones and DNA. *Science* **1974**, *184* (4139), 868-871.
121. Luger, K.; Dechassa, M. L.; Tremethick, D. J., New insights into nucleosome and chromatin structure: An ordered state or a disordered affair? *Nat. Rev. Mol. Cell Biol.* **2012**, *13* (7), 436-447.
122. Luger, K.; Mäder, A. W.; Richmond, R. K.; Sargent, D. F.; Richmond, T. J., Crystal structure of the nucleosome core particle at 2.8 Å resolution. *Nature* **1997**, *389* (6648), 251-260.
123. Richmond, T. J.; Davey, C. A., The structure of DNA in the nucleosome core. *Nature* **2003**, *423* (6936), 145-150.
124. Marx, V., Epigenetics: Reading the second genomic code. *Nature* **2012**, *491* (7422), 143-147.
125. Bannister, A. J.; Kouzarides, T., Regulation of chromatin by histone modifications. *Cell Res* **2011**, *21* (3), 381-395.
126. Filippakopoulos, P.; Knapp, S., Targeting bromodomains: Epigenetic readers of lysine acetylation. *Nat. Rev. Drug Discov.* **2014**, *13* (5), 337-356.
127. Simão-Riudalbas, L.; Esteller, M., Targeting the histone orthography of cancer: Drugs for writers, erasers and readers. *Br. J. Pharmacol.* **2015**, *172* (11), 2716-2732.
128. Struhl, K., Histone acetylation and transcriptional regulatory mechanisms. *Genes and Development* **1998**, *12* (5), 599-606.
129. Hong, L.; Schroth, G. P.; Matthews, H. R.; Yau, P.; Bradbury, E. M., Studies of the DNA binding properties of histone H4 amino terminus. Thermal denaturation studies reveal that acetylation markedly reduces the binding constant of the H4 "tail" to DNA. *Journal of Biological Chemistry* **1993**, *268* (1), 305-314.
130. Das, C.; Lucia, M. S.; Hansen, K. C.; Tyler, J. K., CBP/p300-mediated acetylation of histone H3 on lysine 56 (Nature (2009) 459, (113-117)). *Nature* **2009**, *460* (7259), 1164.
131. Bolden, J. E.; Peart, M. J.; Johnstone, R. W., Anticancer activities of histone deacetylase inhibitors. *Nat. Rev. Drug Discov.* **2006**, *5* (9), 769-784.

132. West, A. C.; Johnstone, R. W., New and emerging HDAC inhibitors for cancer treatment. *J. Clin. Invest.* **2014**, *124* (1), 30-39.
133. Guha, M., HDAC inhibitors still need a home run, despite recent approval. *Nat. Rev. Drug Discov.* **2015**, *14* (4), 225-226.
134. Tessarz, P.; Santos-Rosa, H.; Robson, S. C.; Sylvestersen, K. B.; Nelson, C. J.; Nielsen, M. L.; Kouzarides, T., Glutamine methylation in histone H2A is an RNA-polymerase-I-dedicated modification. *Nature* **2014**, *505* (7484), 564-568.
135. Gershey, E. L.; Haslett, G. W.; Vidali, G.; Allfrey, V. G., Chemical Studies of Histone Methylation: Evidence for the Occurrence of 3-Methylhistidine in Avian Erythrocyte Histone Fractions. *J. Biol. Chem.* **1969**, *244* (18), 4871-4877.
136. Lee, M. G.; Villa, R.; Trojer, P.; Norman, J.; Yan, K.-P.; Reinberg, D.; Di Croce, L.; Shiekhatar, R., Demethylation of H3K27 Regulates Polycomb Recruitment and H2A Ubiquitination. *Science* **2007**, *318* (5849), 447-450.
137. Lyons, D. B.; Lomvardas, S., Repressive histone methylation: A case study in deterministic versus stochastic gene regulation. *Biochimica et Biophysica Acta (BBA) - Gene Regulatory Mechanisms* **2014**, *1839* (12), 1373-1384.
138. Greer, E. L.; Shi, Y., Histone methylation: a dynamic mark in health, disease and inheritance. *Nat Rev Genet* **2012**, *13* (5), 343-357.
139. Yun, M.; Wu, J.; Workman, J. L.; Li, B., Readers of histone modifications. *Cell Res.* **2011**, *21* (4), 564-578.
140. Tamkun, J. W.; Deuring, R.; Scott, M. P.; Kissinger, M.; Pattatucci, A. M.; Kaufman, T. C.; Kennison, J. A., brahma: A regulator of Drosophila homeotic genes structurally related to the yeast transcriptional activator SNF2 SWI2. *Cell* **1992**, *68* (3), 561-572.
141. Filippakopoulos, P.; Picaud, S.; Mangos, M.; Keates, T.; Lambert, J. P.; Barsyte-Lovejoy, D.; Felletar, I.; Volkmer, R.; Müller, S.; Pawson, T.; Gingras, A. C.; Arrowsmith, C. H.; Knapp, S., Histone recognition and large-scale structural analysis of the human bromodomain family. *Cell* **2012**, *149* (1), 214-231.
142. Belkina, A. C.; Denis, G. V., BET domain co-regulators in obesity, inflammation and cancer. *Nat. Rev. Cancer* **2012**, *12* (7), 465-477.
143. Nicodeme, E.; Jeffrey, K. L.; Schaefer, U.; Beinke, S.; Dewell, S.; Chung, C. W.; Chandwani, R.; Marazzi, I.; Wilson, P.; Coste, H.; White, J.; Kirilovsky, J.; Rice, C. M.; Lora, J. M.; Prinjha, R. K.; Lee, K.; Tarakhovsky, A., Suppression of inflammation by a synthetic histone mimic. *Nature* **2010**, *468* (7327), 1119-1123.

144. Wang, X.; Helfer, C. M.; Pancholi, N.; Pancholi, J. E.; You, J., Recruitment of Brd4 to the human papillomavirus type 16 DNA replication complex is essential for replication of viral DNA. *J. Virol.* **2013**, *87* (7), 3871-3884.
145. Yan, J.; Li, Q.; Lievens, S.; Tavernier, J.; You, J., Abrogation of the Brd4-positive transcription elongation factor b complex by papillomavirus E2 protein contributes to viral oncogene repression. *J. Virol.* **2010**, *84* (1), 76-87.
146. Owen, D. J.; Ornaghi, P.; Yang, J. C.; Lowe, N.; Evans, P. R.; Ballario, P.; Neuhaus, D.; Filetici, P.; Travers, A. A., The structural basis for the recognition of acetylated histone H4 by the bromodomain of histone acetyltransferase Gcn5p. *EMBO Journal* **2000**, *19* (22), 6141-6149.
147. Gallenkamp, D.; Gelato, K. A.; Haendler, B.; Weinmann, H., Bromodomains and their pharmacological inhibitors. *ChemMedChem* **2014**, *9* (3), 438-464.
148. Zeng, L.; Li, J.; Muller, M.; Yan, S.; Mujtaba, S.; Pan, C.; Wang, Z.; Zhou, M. M., Selective small molecules blocking HIV-1 tat and coactivator PCAF association. *J. Am. Chem. Soc.* **2005**, *127* (8), 2376-2377.
149. Filippakopoulos, P.; Qi, J.; Picaud, S.; Shen, Y.; Smith, W. B.; Fedorov, O.; Morse, E. M.; Keates, T.; Hickman, T. T.; Felletar, I.; Philpott, M.; Munro, S.; McKeown, M. R.; Wang, Y.; Christie, A. L.; West, N.; Cameron, M. J.; Schwartz, B.; Heightman, T. D.; La Thangue, N.; French, C. A.; Wiest, O.; Kung, A. L.; Knapp, S.; Bradner, J. E., Selective inhibition of BET bromodomains. *Nature* **2010**, *468* (7327), 1067-1073.
150. Chung, C. W.; Coste, H.; White, J. H.; Mirguet, O.; Wilde, J.; Gosmini, R. L.; Delves, C.; Magny, S. M.; Woodward, R.; Hughes, S. A.; Boursier, E. V.; Flynn, H.; Bouillot, A. M.; Bamborough, P.; Brusq, J. M. G.; Gellibert, F. O. J.; Jones, E. J.; Riou, A. M.; Homes, P.; Martin, S. L.; Uings, I. J.; Toum, J.; Clément, C. A.; Boullay, A. B.; Grimley, R. L.; Blandel, F. M.; Prinjha, R. K.; Lee, K.; Kirilovsky, J.; Nicodeme, E., Discovery and characterization of small molecule inhibitors of the BET family bromodomains. *J. Med. Chem.* **2011**, *54* (11), 3827-3838.
151. Brand, M.; Measures, A. M.; Wilson, B. G.; Cortopassi, W. A.; Alexander, R.; Höss, M.; Hewings, D. S.; Rooney, T. P. C.; Paton, R. S.; Conway, S. J., Small molecule inhibitors of bromodomain - Acetyl-lysine interactions. *ACS Chem. Biol.* **2015**, *10* (1), 22-39.
152. www.scopus.com, 01/11/2015.
153. Ehara, S.; Kobayashi, H.; Komatsu, H.; Sueoka, H., Thienotriazolodiazepine compounds and medicinal uses thereof. Google Patents: 1998.

154. Adachi, K.; Endoh, J. I.; Fujie, N.; Hamada, M.; Hikawa, H.; Ishibuchi, S.; Murata, M.; Oshita, K.; Sugahara, K.; Tanaka, M., Thienotriazolodiazepine compound and a medicinal use thereof. Google Patents: 2006.
155. Mertz, J. A.; Conery, A. R.; Bryant, B. M.; Sandy, P.; Balasubramanian, S.; Mele, D. A.; Bergeron, L.; Sims Iii, R. J., Targeting MYC dependence in cancer by inhibiting BET bromodomains. *Proc. Natl. Acad. Sci. USA* **2011**, *108* (40), 16669-16674.
156. Herrmann, H.; Blatt, K.; Shi, J.; Gleixner, K. V.; Cerny-Reiterer, S.; Müllauer, L.; Vakoc, C. R.; Sperr, W. R.; Horny, H. P.; Bradner, J. E.; Zuber, J.; Valent, P., Small-molecule inhibition of BRD4 as a new potent approach to eliminate leukemic stem- and progenitor cells in acute myeloid leukemia (AML). *Oncotarget* **2012**, *3* (12), 1588-1599.
157. Fiskus, W.; Sharma, S.; Qi, J.; Valenta, J. A.; Schaub, L. J.; Shah, B.; Peth, K.; Portier, B. P.; Rodriguez, M.; Devaraj, S. G. T.; Zhan, M.; Sheng, J.; Iyer, S. P.; Bradner, J. E.; Bhalla, K. N., Highly active combination of BRD4 antagonist and histone deacetylase inhibitor against human acute myelogenous leukemia cells. *Molecular Cancer Therapeutics* **2014**, *13* (5), 1142-1154.
158. Ott, C. J.; Kopp, N.; Bird, L.; Paranal, R. M.; Qi, J.; Bowman, T.; Rodig, S. J.; Kung, A. L.; Bradner, J. E.; Weinstock, D. M., BET bromodomain inhibition targets both c-Myc and IL7R in high-risk acute lymphoblastic leukemia. *Blood* **2012**, *120* (14), 2843-2852.
159. Wyce, A.; Degenhardt, Y.; Bai, Y.; Le, B.; Korenchuk, S.; Crouthamel, M. C.; McHugh, C. F.; Vessella, R.; Creasy, C. L.; Tummino, P. J.; Barbash, O., Inhibition of BET bromodomain proteins as a therapeutic approach in prostate cancer. *Oncotarget* **2013**, *4* (12), 2419-2429.
160. Structural Genomics Consortium website. <http://www.thesgc.org/science/bromodomains> (accessed 06-11-2015).
161. Structural Genomics Consortium Bromosporine Webpage. <http://www.thesgc.org/chemical-probes/Bromosporine> (accessed 15-12-2015).
162. Hammitzsch, A.; Tallant, C.; Fedorov, O.; O'Mahony, A.; Brennan, P. E.; Hay, D. A.; Martinez, F. O.; Al-Mossawi, M. H.; de Wit, J.; Vecellio, M.; Wells, C.; Wordsworth, P.; Müller, S.; Knapp, S.; Bowness, P., CBP30, a selective CBP/p300 bromodomain inhibitor, suppresses human Th17 responses. *Proceedings of the National Academy of Sciences* **2015**, *112* (34), 10768-10773.
163. Chen, P.; Chaikuad, A.; Bamborough, P.; Bantscheff, M.; Bountra, C.; Chung, C.-w.; Fedorov, O.; Grandi, P.; Jung, D.; Lesniak, R.; Lindon, M.; Müller, S.; Philpott, M.; Prinjha, R.; Rogers, C.; Selenski, C.; Tallant, C.; Werner, T.; Willson, T. M.; Knapp, S.; Drewry, D. H., Discovery and Characterization of GSK2801, a Selective Chemical Probe for the Bromodomains BAZ2A and BAZ2B. *Journal of Medicinal Chemistry* **2015**.

164. Structural Genomics Consortium PFI-3 webpage. <http://www.thesgc.org/chemical-probes/PFI-3> (accessed on 06-11-2015).
165. Neuwald, A. F.; Aravind, L.; Spouge, J. L.; Koonin, E. V., AAA+: A class of chaperone-like ATPases associated with the assembly, operation, and disassembly of protein complexes. *Genome Res.* **1999**, *9* (1), 27-43.
166. Kalashnikova, E. V.; Revenko, A. S.; Gemo, A. T.; Andrews, N. P.; Tepper, C. G.; Zou, J. X.; Cardiff, R. D.; Borowsky, A. D.; Chen, H. W., ANCCA/ATAD2 overexpression identifies breast cancer patients with poor prognosis, acting to drive proliferation and survival of triple-negative cells through control of B-Myb and EZH2. *Cancer Res.* **2010**, *70* (22), 9402-9412.
167. Zou, J. X.; Guo, L.; Revenko, A. S.; Tepper, C. G.; Gemo, A. T.; Kung, H. J.; Chen, H. W., Androgen-Induced coactivator ANCCA mediates specific Androgen receptor signaling in prostate cancer. *Cancer Res.* **2009**, *69* (8), 3339-3346.
168. Zou, J. X.; Revenko, A. S.; Li, L. B.; Gemo, A. T.; Chen, H. W., ANCCA, an estrogen-regulated AAA+ ATPase coactivator for ER α , is required for coregulator occupancy and chromatin modification. *Proc. Natl. Acad. Sci. USA* **2007**, *104* (46), 18067-18072.
169. Chaikuad, A.; Petros, A. M.; Fedorov, O.; Xu, J.; Knapp, S., Structure-based approaches towards identification of fragments for the low-druggability ATAD2 bromodomain. *MedChemComm* **2014**, *5* (12), 1843-1848.
170. Caron, C.; Lestrat, C.; Marsal, S.; Escoffier, E.; Curtet, S.; Virolle, V.; Barbry, P.; Debernardi, A.; Brambilla, C.; Brambilla, E.; Rousseaux, S.; Khochbin, S., Functional characterization of ATAD2 as a new cancer/testis factor and a predictor of poor prognosis in breast and lung cancers. *Oncogene* **2010**, *29* (37), 5171-5181.
171. Ciró, M.; Prosperini, E.; Quarto, M.; Grazini, U.; Walfridsson, J.; McBlane, F.; Nucifero, P.; Pacchiana, G.; Capra, M.; Christensen, J.; Helin, K., ATAD2 is a novel cofactor for MYC, overexpressed and amplified in aggressive tumors. *Cancer Res.* **2009**, *69* (21), 8491-8498.
172. Raeder, M. B.; Birkeland, E.; Trovik, J.; Krakstad, C.; Shehata, S.; Schumacher, S.; Zack, T. I.; Krohn, A.; Werner, H. M. J.; Moody, S. E.; Wik, E.; Stefansson, I. M.; Holst, F.; Oyan, A. M.; Tamayo, P.; Mesirov, J. P.; Kalland, K. H.; Akslen, L. A.; Simon, R.; Beroukhim, R.; Salvesen, H. B., Integrated Genomic Analysis of the 8q24 Amplification in Endometrial Cancers Identifies ATAD2 as Essential to MYC-Dependent Cancers. *PLoS ONE* **2013**, *8* (2).
173. Poncet-Montange, G.; Zhan, Y.; Bardenhagen, J. P.; Petrocchi, A.; Leo, E.; Shi, X.; Lee, G. R. I.; Leonard, P. G.; Geck Do, M. K.; Cardozo, M. G.; Andersen, J. N.; Palmer, W. S.;

- Jones, P.; Ladbury, J. E., Observed bromodomain flexibility reveals histone peptide- and small molecule ligand-compatible forms of ATAD2. *Biochem. J.* **2015**, *466*, 337-346.
174. Vidler, L. R.; Brown, N.; Knapp, S.; Hoelder, S., Druggability Analysis and Structural Classification of Bromodomain Acetyl-lysine Binding Sites. *J. Med. Chem.* **2012**, *55* (17), 7346-7359.
175. Bamborough, P.; Chung, C. W.; Furze, R. C.; Grandi, P.; Michon, A. M.; Sheppard, R. J.; Barnett, H.; Diallo, H.; Dixon, D. P.; Douault, C.; Jones, E. J.; Karamshi, B.; Mitchell, D. J.; Prinjha, R. K.; Rau, C.; Watson, R. J.; Werner, T.; Demont, E. H., Structure-Based Optimization of Naphthyridones into Potent ATAD2 Bromodomain Inhibitors. *J. Med. Chem.* **2015**, *58* (15), 6151-6178.
176. Harner, M. J.; Chauder, B. A.; Phan, J.; Fesik, S. W., Fragment-based screening of the bromodomain of ATAD2. *J. Med. Chem.* **2014**, *57* (22), 9687-9692.
177. Demont, E. H.; Chung, C. W.; Furze, R. C.; Grandi, P.; Michon, A. M.; Wellaway, C.; Barrett, N.; Bridges, A. M.; Craggs, P. D.; Diallo, H.; Dixon, D. P.; Douault, C.; Emmons, A. J.; Jones, E. J.; Karamshi, B. V.; Locke, K.; Mitchell, D. J.; Mouzon, B. H.; Prinjha, R. K.; Roberts, A. D.; Sheppard, R. J.; Watson, R. J.; Bamborough, P., Fragment-Based Discovery of Low-Micromolar ATAD2 Bromodomain Inhibitors. *J. Med. Chem.* **2015**, *58* (14), 5649-5673.
178. Hofsløkken, N. U.; Skattebøl, L., Convenient Method for the ortho-Formylation of Phenols. *Acta Chem. Scand.* **1999**, *53* (4), 258-262.
179. Chen, A.; Campeau, L.-C.; Cauchon, E.; Chefson, A.; Ducharme, Y.; Dubé, D.; Falgoutyret, J.-P.; Fournier, P.-A.; Gagné, S.; Grimm, E.; Han, Y.; Houle, R.; Huang, J.-Q.; Lacombe, P.; Laliberté, S.; Lévesque, J.-F.; Liu, S.; MacDonald, D.; Mackay, B.; McKay, D.; Percival, M. D.; Regan, C.; Regan, H.; St-Jacques, R.; Toulmond, S., Renin inhibitors for the treatment of hypertension: Design and optimization of a novel series of pyridone-substituted piperidines. *Bioorg. Med. Chem. Lett.* **2011**, *21* (13), 3970-3975.
180. Campeau, L.-C.; Dolman, S. J.; Gauvreau, D.; Corley, E.; Liu, J.; Guidry, E. N.; Ouellet, S. G.; Steinhuebel, D.; Weisel, M.; O'Shea, P. D., Convergent Kilo-Scale Synthesis of a Potent Renin Inhibitor for the Treatment of Hypertension. *Organic Process Research & Development* **2011**, *15* (5), 1138-1148.
181. Haidle, A. M.; Knowles, S. L.; Kattar, S. D.; Deschenes, D.; Burch, J.; Robichaud, J.; Christopher, M.; Altman, M. D.; Jewell, J. P.; Northrup, A. B., SUBSTITUTED PYRIDINE SPLEEN TYROSINE KINASE (Syk) INHIBITORS. Google Patents: 2013.
182. Morales-Ramos, Á. I.; Li, Y. H.; Hilfiker, M.; Mecom, J. S.; Eidam, P.; Shi, D.; Tseng, P.-S.; Brooks, C.; Zhang, D.; Wang, N.; Jaworski, J.-P.; Morrow, D.; Fries, H.; Edwards, R.; Jin, J., Structure-activity relationship studies of novel 3-oxazolidinedione-6-naphthyl-2-

- pyridinones as potent and orally bioavailable EP3 receptor antagonists. *Bioorg. Med. Chem. Lett.* **2011**, *21* (10), 2806-2811.
183. DeMarinis, R. M.; Hall, R. F.; Franz, R. G.; Webster, C.; Huffman, W. F.; Schwartz, M. S.; Kaiser, C.; Ross, S. T.; Gallagher, G., Syntheses and in vitro evaluation of 4-(2-aminoethyl)-2(3H)-indolones and related compounds as peripheral prejunctional dopamine receptor agonists. *J. Med. Chem.* **1986**, *29* (6), 939-947.
184. Volk, B.; Mezei, T.; Simig, G., Raney nickel-induced 3-alkylation of oxindole with alcohols and diols. *Synthesis* **2002**, (5), 595-597.
185. Trost, B. M.; Zhang, Y.; Zhang, T., Direct N-Carbamoylation of 3-Monosubstituted Oxindoles with Alkyl Imidazole Carboxylates. *J. Org. Chem.* **2009**, *74* (14), 5115-5117.
186. Petronijevic, F. R.; Wipf, P., Total Synthesis of (±)-Cycloclavine and (±)-5-epi-Cycloclavine. *J. Am. Chem. Soc.* **2011**, *133* (20), 7704-7707.
187. Theodoulou, N. H.; Bamborough, P.; Bannister, A. J.; Becher, I.; Bit, R. A.; Che, K. H.; Chung, C.-w.; Dittmann, A.; Drewes, G.; Drewry, D. H.; Gordon, L.; Grandi, P.; Leveridge, M.; Lindon, M.; Michon, A.-M.; Molnar, J.; Robson, S. C.; Tomkinson, N. C. O.; Kouzarides, T.; Prinjha, R. K.; Humphreys, P. G., Discovery of I-BRD9, a Selective Cell Active Chemical Probe for Bromodomain Containing Protein 9 Inhibition. *J. Med. Chem.* **2015**.
188. Hewings, D. S.; Rooney, T. P. C.; Jennings, L. E.; Hay, D. A.; Schofield, C. J.; Brennan, P. E.; Knapp, S.; Conway, S. J., Progress in the Development and Application of Small Molecule Inhibitors of Bromodomain–Acetyl-lysine Interactions. *J. Med. Chem.* **2012**, *55* (22), 9393-9413.
189. Jossang, A.; Jossang, P.; Hadi, H. A.; Sevenet, T.; Bodo, B., Horsfiline, an oxindole alkaloid from *Horsfieldia superba*. *J. Org. Chem.* **1991**, *56* (23), 6527-6530.
190. Scholl, M.; Ding, S.; Lee, C. W.; Grubbs, R. H., Synthesis and Activity of a New Generation of Ruthenium-Based Olefin Metathesis Catalysts Coordinated with 1,3-Dimesityl-4,5-dihydroimidazol-2-ylidene Ligands. *Org. Lett.* **1999**, *1* (6), 953-956.
191. Vougioukalakis, G. C.; Grubbs, R. H., Ruthenium-Based Heterocyclic Carbene-Coordinated Olefin Metathesis Catalysts. *Chem. Rev.* **2010**, *110* (3), 1746-1787.
192. Fischer, C.; Meyers, C.; Carreira, E. M., Efficient Synthesis of (±)-Horsfiline through the MgI₂-Catalyzed Ring-Expansion Reaction of a Spiro[cyclopropane-1,3'-indol]-2'-one. *Helv. Chim. Acta.* **2000**, *83* (6), 1175-1181.
193. Jasiński, M.; Mlostoń, G.; Heimgartner, H., Synthesis of 2,3-dihydroimidazo[2,1-b]thiazole derivatives viacyclization of N-allylimidazoline-2-thiones. *J. Heterocycl. Chem.* **2010**, *47* (6), 1287-1293.

194. Garro-Helion, F.; Merzouk, A.; Guibe, F., Mild and selective palladium(0)-catalyzed deallylation of allylic amines. Allylamine and diallylamine as very convenient ammonia equivalents for the synthesis of primary amines. *J. Org. Chem.* **1993**, *58* (22), 6109-6113.
195. Lee, H. J.; Lim, J. W.; Yu, J.; Kim, J. N., An expedient synthesis of 3-alkylideneoxindoles by Ti(OiPr)₄/pyridine-mediated Knoevenagel condensation. *Tetrahedron Lett.* **2014**, *55* (6), 1183-1187.
196. Trost, B. M.; Frederiksen, M. U., Palladium-Catalyzed Asymmetric Allylation of Prochiral Nucleophiles: Synthesis of 3-Allyl-3-Aryl Oxindoles. *Angew. Chem. Int. Ed.* **2005**, *44* (2), 308-310.
197. Loreto, M. A.; Migliorini, A.; Tardella, P. A.; Gambacorta, A., Novel spiroheterocycles by aziridination of α -methylene- γ - and δ -lactams. *Eur. J. Org. Chem.* **2007**, (14), 2365-2371.
198. Galley, G.; Stalder, H.; Goergler, A.; Hoener, M. C.; Norcross, R. D., Optimisation of imidazole compounds as selective TAAR1 agonists: Discovery of RO5073012. *Bioorg. Med. Chem. Lett.* **2012**, *22* (16), 5244-5248.
199. Chadwick, D. J.; Ngochindo, R. I., 2,5-Dilithiation of N-protected imidazoles. Syntheses of 2,5-disubstituted derivatives of 1-methoxymethyl-, 1-triphenylmethyl-, and 1-(N,N-dimethylsulphonamido)-imidazole. *J. Chem. Soc., Perkin Trans. 1* **1984**, (0), 481-486.
200. Anil, B.; Riedinger, C.; Endicott, J. A.; Noble, M. E. M., The structure of an MDM2-Nutlin-3a complex solved by the use of a validated MDM2 surface-entropy reduction mutant. *Acta Crystallogr. Sect. D Biol. Crystallogr.* **2013**, *69* (8), 1358-1366.
201. Hardcastle, I. R.; Ahmed, S. U.; Atkins, H.; Farnie, G.; Golding, B. T.; Griffin, R. J.; Guyenne, S.; Hutton, C.; Källblad, P.; Kemp, S. J.; Kitching, M. S.; Newell, D. R.; Norbedo, S.; Northen, J. S.; Reid, R. J.; Saravanan, K.; Willems, H. M. G.; Lunec, J., Small-Molecule Inhibitors of the MDM2-p53 Protein-Protein Interaction Based on an Isoindolinone Scaffold. *J. Med. Chem.* **2006**, *49* (21), 6209-6221.
202. Kyne, R. E.; Ryan, M. C.; Kliman, L. T.; Morken, J. P., Allylation of Nitrosobenzene with Pinacol Allylboronates. A Regioselective Complement to Peroxide Oxidation. *Org. Lett.* **2010**, *12* (17), 3796-3799.
203. Ogasawara, M.; Ge, Y.; Uetake, K.; Takahashi, T., Vinyl ketones to allenes: Preparation of 1,3-dien-2-yl triflates and their application in Pd-catalyzed reactions with soft nucleophiles. *Org. Lett.* **2005**, *7* (25), 5697-5700.
204. Satoh, T.; Kumagawa, T.; Sugimoto, A.; Yamakawa, K., α,β -Epoxy Sulfoxides as Useful Intermediates in Organic Synthesis. IX. A Novel Synthesis of Alkyl Vinyl Ketones and Divinyl Ketones from Carbonyl Compounds and 1-Chloro-3-phenylthiopropyl Phenyl

Sulfoxide as a Three-Carbon Homologating Agent. *Bull. Chem. Soc. Jpn.* **1987**, *60* (1), 301-310.

205. Li, A.; Ouyang, Y.; Wang, Z.; Cao, Y.; Liu, X.; Ran, L.; Li, C.; Li, L.; Zhang, L.; Qiao, K.; Xu, W.; Huang, Y.; Zhang, Z.; Tian, C.; Liu, Z.; Jiang, S.; Shao, Y.; Du, Y.; Ma, L.; Wang, X.; Liu, J., Novel Pyridinone Derivatives As Non-Nucleoside Reverse Transcriptase Inhibitors (NNRTIs) with High Potency against NNRTI-Resistant HIV-1 Strains. *J. Med. Chem.* **2013**, *56* (9), 3593-3608.